Journal of Oil Palm Research

REVIEW ARTICLE

Championing Sustainable Treatment
of Oil Palm Basal Stem Rot Disease
Via Biological Control Agents

Association of Dietary Fats with
Gut Microbiota Profile:
How does Palm Oil Fit in?

MPOB

JOURNAL OF OIL PALM RESEARCH

Vol. 34 (3) September 2022

C O N T E N T S

Cover picture: 1. *Ganoderma* spp., the fungal pathogen of basal stem rot (BSR) disease in oil palm
2. Gut bacterial profiles are correlated with fat intake.

CHAMPIONING SUSTAINABLE TREATMENT OF OIL PALM BASAL STEM ROT DISEASE VIA BIOLOGICAL CONTROL AGENTS

LAI KIM YEN[1] and NUSAIBAH SYD ALI[1]*

ABSTRACT

Oil palm is the most important commodity crop for Malaysia and Indonesia. However, it is being threatened by a disease identified as basal stem rot (BSR) caused by Ganoderma *spp. Common approaches such as chemical and cultural control have failed to demonstrate total effectiveness in controlling BSR disease. Nevertheless, these practices cause detrimental effects on the environment. Therefore, the attention on adopting biological control agents (BCA) as one of the sustainable methods to eradicate and control BSR disease is on the rise. The current review highlights on the attempts and outcome of applying various BCA such as fungi, bacteria and actinomycetes as single or mixed application to control BSR disease in oil palm.*

INTRODUCTION

Oil palm is the most important commodity crop being planted across Malaysia including Peninsular, Sarawak and Sabah. Planted area of oil palm has reached 5.85 million hectares in 2018 and utilised 60% of the agricultural lands in Malaysia (Kamarudin *et al.*, 2019). Malaysia's palm oil export was recorded with a rise of 6% in January-June 2020 with an approximate export value of USD5.50 billion compared to the first half of 2019 (MPOC, 2020). Malaysia is the second major palm oil producer after Indonesia with the forecast of total planted areas of mature palms at 11.75 million hectares in 2019/2020 (Mcdonald and Rahmanulloh, 2019). Oil palm is a golden commodity crop producing versatile raw materials for food industry and non-food industries such as biodiesel and oleochemical.

Regardless of whether large or small scale oil palm planters, Malaysian planters are challenged by the most destructive oil palm disease called basal stem rot (BSR) disease. This devastating disease

is caused by *Ganoderma* spp., white rot fungi that could be seen visibly at the bole of an infected palm tree if the infection is at the advanced stages. There are three species reported to be associated with BSR disease, they are *Ganoderma boninense*, *Ganoderma zonatum* and *Ganoderma miniatocinctum* (Idris *et al.*, 2000; Moncalvo, 2000). However, *G. boninense* has been identified as the most aggressive major causal pathogen of BSR disease in Peninsular Malaysia (Idris *et al.*, 2000; Wong *et al.*, 2012). Conversely, the most dominant virulent species in Sarawak state particularly in Betong and Miri areas has been identified as *G. zonatum* causing BSR disease and upper stem rot (USR) (Rakib *et al.*, 2017).

The pathogen causes rotting of the roots, bole and subsequently the stem leading to the failure in delivering water and nutritions from the root to the aerial parts of the palm (Chong *et al.*, 2017). Symptoms observed on mature palms include multiple unopened leaflets, flattening of the crown, pale coloured leaf canopy, presence of basidiocarps at the bottom of the stem (Turner, 1981) and collapse of the palm at the final stages of infection. Early detection of this disease is tough as the palms display noticeable symptoms at advanced stages when the disease severity reaches approximately 60%-70% (Chong *et al.*, 2017).

[1] Department of Plant Protection,
   Faculty of Agriculture, Universiti Putra Malaysia,
   43400 UPM, Serdang, Selangor, Malaysia.

* *Corresponding author e-mail: nusaibah@upm.edu.my*

In addition, all these symptoms could occur as single or in combination depending on the environmental conditions and care given to the palms. No absolute pattern of disease progression has been reported to date (Chong *et al.*, 2017).

The BSR disease is able to cause direct loss (death of the palm) or indirect loss causing reduction in the number of fresh fruit brunches (FFB) leading to yield losses. For the year 2020, BSR disease infection of planted areas is forecasted to touch 443 430 ha or affecting 65.6 million palm trees (Roslan and Idris, 2012). Hence, it is crucial to eradicate this devastating disease to prevent any further direct or indirect loss of productive palms.

There are many approaches that could be adopted to mitigate BSR. The most common is via chemical control by application of fungicide. Hexaconazole has been the typical fungicide used to control BSR. It is applied to symptomatic palms via trunk injection, soil drenching, or a combination of these two methods (Halimah *et al.*, 2012; Idris *et al.*, 2002). Even though hexaconazole fungicide application was proven to increase the productive life-span of an infected palm, the residue and non-targeted beneficial microorganism is of concern. In addition, by the end of 2019, all Malaysian oil palm planters and millers are required to obtain sustainability certification, such as the Malaysian Sustainable Palm Oil (MSPO) or the Roundtable on Sustainable Palm Oil (RSPO) by complying with the sustainability standard requirements in order to export certified palm oil to international markets (Kamarudin *et al.*, 2019). Requirement on the sustainability certification, urges the planters to adopt good agricultural practices (GAP). This could be achieved by minimising the usage of synthetic chemical fertilisers, pesticides, fungicides and weedicides.

Biocontrol could be the best alternative to adopt in controlling the disease without causing any environmental harmfulness (Aboutorabi, 2018; O'Brien, 2017). In addition, it is also lower in cost compared to the cultural and chemical control methods (Aboutorabi *et al.*, 2018).

AN OVERVIEW: BIOCONTROL OF BASAL STEM ROT (BSR) DISEASE

The term 'biocontrol' is defined as the incorporation of one or multiple microorganisms such as fungi, bacteria, virus and actinomycetes to suppress the population of disease-causing pathogens; either applied onto the soil or to the plants. These incorporated microorganisms are recognised as biological control agents (BCA) which exhibit antagonistic reaction towards the pathogen. Thus, BCA exhibit the potential to prevent the establishment of the disease or its severity. The

BCA is also highly specific towards the targeted pathogen without affecting the normal flora.

Over the past years, there have been extensive studies on the identification of effective BCA for controlling BSR disease (Musa *et al.*, 2018; Muniroh *et al.*, 2019; Naidu *et al.*, 2018). Their potentials have been investigated initially via various *in vitro* studies for screening and better understanding purpose prior to greenhouse and field trials. The basic method used to evaluate the efficacy of BCA are through dual culture (Naher *et al.*, 2015; Shariffah-Muzaimah *et al.*, 2015), poison agar (Marzuki *et al.*, 2015; Shariffah-Muzaimah *et al.*, 2015) and culture filtrate assay (Ramli *et al.*, 2016; Shariffah-Muzaimah *et al.*, 2015). The higher percentage of inhibition of radial growth (PIRG) value displays higher suppression efficacy the BCA towards the pathogen. The inhibition effect could be due to the ability of the BCA to suppress the growth performance of the pathogen through various mechanisms such as competition for nutrient and space, antibiosis, production of cell wall degrading enzymes (CWDE), and production of secondary or defence metabolites (Chong *et al.*, 2017; Heydari and Pessarakli, 2010; O'Brien, 2017). The BCA may utilise a single or an array of mechanisms in inhibiting a pathogen. In many BCA studies, plant growth promotion (PGP) was one of the benefits demonstrated apart from disease suppression (Muniroh *et al.*, 2019; Nur Azura *et al.*, 2016). In some cases, the degree of suppression by BCA towards plant pathogens tends to be lower when tested in field compared with the result achieved on agar plate for the same BCA. This could reflect the diversity of environment (O'Brien, 2017) and complexity of interaction between microbes in the soil. Hence, it is crucial to evaluate the suppression of BCA towards the pathogen not only *in vitro* but also *in vivo* (Nusaibah *et al.*, 2017). Various genera of BCA will be discussed in this article. Recent studies utilising BCA to control BSR disease of oil palm is summarised in *Table 1*.

Biocontrol Agent- Fungi

The most common fungi applied as BCA for pathogen eradication across variety of crops are *Trichoderma* spp. In Malaysia, the most common *Trichoderma* spp. proven to be antagonist towards *G. boninense* are *Trichoderma asperellum*, *Trichoderma harzianum* and *Trichoderma virens* (Angel *et al.*, 2018; Ho *et al.*, 2018; Musa *et al.*, 2018; Naher *et al.*, 2012; Nusaibah *et al.*, 2017; Sundram, 2013). A study conducted by Naher *et al.* (2015) determined the antagonistic and growth performance of *T. harzianum* T32 strain against *G. boninense* on different types of media namely potato dextrose agar (PDA), potato sucrose agar (PSA) and malt extract agar (MEA). Cultural morphology of

TABLE 1. SUMMARY OF RESEARCH FINDINGS IN THE PAST FIVE YEARS (2015-2019)

Year	Location	Biocontrol agent	Type of study	Source
2015	Peninsular Malaysia	*Actinomycetes*	*In vitro*	Shariffah-Muzaimah *et al.* (2015)
		Trichoderma harzianum T32	*In vitro*	Naher *et al.* (2015)
		Arbuscular mycorrhizal fungi with *Pseudomonas aeruginosa* UPMP3	*In vitro* and *in vivo* (nursery and bait seedling)	Sundram *et al.* (2015)
		Cladobotryum semicirculare	*In vitro* (dual culture, mycoparasitism test, poison agar)	Marzuki *et al.* (2015)
	Sabah	Multiple strains of *Bacillus* spp. and *Trichoderma* spp.	*In vitro* (agar well diffusion assay, SEM, PIRG)	Alexander *et al.* (2015)
2016	Peninsular Malaysia	*Scytalidium parasiticum*	*In vitro* and *in vivo* (nursery)	Goh *et al.* (2016)
		Pseudomonas aeruginosa GanoEB1, *Burkholderia cepacia* GanoEB2, *Pseudomonas syringae* GanoEB3	*In vitro* and *in vivo* (nursery)	Ramli *et al.* (2016)
		Streptomyces sanglieri	*In vitro*	Nur Azura *et al.* (2016)
2017	Peninsular Malaysia	*Trichoderma harzianum* and *Bacillus cereus*	*In vitro* and *in vivo* (nursery)	Nusaibah *et al.* (2017)
	Sabah	Multiple strains of *Bacillus* spp. and *Trichoderma* spp.	*In vitro* and *in vivo* (field)	Alexander *et al.* (2017)
	Indonesia	*Trichoderma harzianum*, *Trichoderma longibrachiatum*, *Lasiodiplodia venezuelensis*, *Dothidiomycetes* sp.	*In vitro* (chitinase analysis)	Esyanti *et al.* (2017)
2018	Indonesia	*Bacillus methylotrophicus*	*In vitro* (antifungal cyclic lipopeptides)	Pramudito *et al.* (2018)
	Peninsular Malaysia	*Trichoderma virens* 159C	*In vitro*	Angel *et al.* (2018)
	Sabah	*Streptomyces* spp.	*In vitro*	Lim *et al.* (2018)
	Peninsular Malaysia	*Trichoderma harzianum*	*In vitro*	Ho *et al.* (2018)
		Trichoderma asperellum, *Trichoderma harzianum*, *Trichiderma virens*	*In vivo* (nursery)	Musa *et al.* (2018)
		Hymenomycetes	*In vitro* and *in vivo* (nursery)	Naidu *et al.* (2018)
		Streptomyces spp.	*In vitro* and *in vivo* (nursery)	Shariffah-Muzaimah *et al.* (2018)
2019	Peninsular Malaysia	*Pseudomonas aeruginosa* UPMP3 and *Trichoderma asperellum* UPM16	*In vitro*	Muniroh *et al.* (2019)
	Indonesia	*Trichoderma* sp., *Aspergillus* sp. and *Mucor* sp.	*In vitro* (screening)	Puspita *et al.* (2019)

Note: SEM – scanning electron microscopy; PIRG – percentage of inhabitation of radial growth.

T. harzianum T32 exhibited concentric ring in all media with greenish colony observed on PDA and PSA while yellowish green colony on MEA. The study concluded that, biocontrol activity of *T. harzianum* T32 against *G. boninense* varied on different types of media in which the highest PIRG rate (70%) was recorded on PDA (Naher *et al.*, 2015).

To further understand the mechanism adopted by *T. harzianum*, Ho *et al.* (2018) identified the transcripts involved during induced systemic resistance (ISR) of oil palm by analysing the root transcriptomes of oil palm seedlings inoculated simultaneously with both *G. boninense* and *T. harzianum* compared with either pathogen only

or BCA only inoculated seedlings. The *in vivo* study showed that *T. harzianum* was able to delay or inhibit the development of BSR disease symptoms in BCA treated infected seedlings by modulating genes in the host that are involved in the biosynthesis of phytohormones methyljasmonate (MeJA), methylsalicylate (MeSA) and ethylene antioxidant (L-ascorbate and myo-inositol) and few unique secondary metabolites (Ho *et al.*, 2018).

Naher *et al.* (2015) also concluded that the inoculation of fungal cell wall suspension of endophytes (*T. harzianum*, *T. longibrachiatum*, *Dothidiomycetes* sp., *Lasiodiplodia venezuelensis*) into oil palm plantlets in Murashige and Skoog (MS) medium and broth was able to induce plant defence mechanism against *G. boninense* by synthesising one of the pathogenesis related protein namely chitinase (Naher *et al.*, 2015).

Recently, new biocontrol candidates' namely ascomycetous mycoparasitic and mycophilic fungi such as *Cladobotryum semicirculare* (Marzuki *et al.*, 2015) and *Scytalidium parasiticum* (Goh *et al.*, 2016) were reported with potential suppression of BSR disease. *Cladobotryum semicirculare* is a type of fungicolous fungus from *Hypocreales* under ascomycetes genus which consists of the biggest group of sporocarp or fruiting body-inhabiting fungi. *Cladobotryum* sp. was reported to cause disease outbreaks on mushroom production (McKay *et al.*, 1999) and severe losses in *Ganoderma tsugae* production in a mushroom farm in Taiwan (Kirschner *et al.*, 2007). This had driven Marzuki *et al.* (2015) to study their antagonistic or parasitic interaction on *G. boninense*. In this study, *Cladobotryum*-liked isolates were isolated from fruiting bodies of *G. boninense* and identified as *C. semicirculare*. Dual culture test demonstrated that *C. semicirculare* was able to suppress radial mycelial growth of various *Ganoderma* spp. (Marzuki *et al.*, 2015). *Ganoderma lucidum* (G32) and *G. boninense* G37 were the most suppressed with PIRG rate of 74.8% and 74.7%, respectively (Marzuki *et al.*, 2015). Poison agar test showed that *C. semicirculare* was able to inhibit the growth of *G. lucidum* (G32) with 25%-49% inhibition rate and *G. boninense* (G14) with 35%-55% with 50% or 100% filtrate concentration, respectively (Marzuki *et al.*, 2015). In mycoparasitism test (*in vitro*), melanised structures were observed on *Ganoderma* mycelia which served as protective organs to protect *Ganoderma* against antagonist effects of *C. semicirculare* (Marzuki *et al.*, 2015). Marzuki *et al.* (2015) was the first report to conclude *G. boninense* as the potential host of *C. semicirculare*. *Cladobotryum semicirculare* has the ability in reducing the regeneration or recovery of *Ganoderma* mycelia in mycoparasitism test. Field evaluation on its potential for disease suppression is obligatory. Another ascomycetes fungus, *Scytalidium parasiticum* AAX0113 isolated from the

basidiocarp of *G. boninense* was studied on its disease suppression efficacy on oil palm seedlings (Goh *et al.*, 2016). *Scytalidium parasiticum* was recognised as necrotrophic mycoparasite of *G. boninense* when hyphae coiling, short lateral hyphal branch enlarged contact structures and appressorium-like organs were observed in mycoparasitism test. Comparable to *C. semicirculare*, *S. parasiticum* could also suppress *G. boninense* fruiting bodies regeneration. In the nursery study, *S. parasiticum* was proven as non-pathogenic to oil palm seedlings. *Scytalidium parasiticum* could suppress BSR disease by reducing disease severity to 76.6% on treatment of *Ganoderma* G10 with *S. parasiticum*. Nonetheless, *S. parasiticum* has been proven to contribute in improving the seedlings growth performance with greater leaf area observed in treatments compared to control (Goh *et al.*, 2016).

In a study published by Naidu *et al.* (2015), a total of seven white rot hymenomycetes were isolated from fruiting bodies of healthy palms and all the isolates were tested for their antagonistic efficacy against *G. boninense* as well as biodegradation properties. Out of seven isolates, *Pycnoporus sanguineus*, *Trametes lactinea* and *Grammothele fuligo* showed high PIRG values ranging from 81%-84% in dual culture study with *G. boninense*. In biodegradation assessment, *G. fuligo*, *P. sanguineus*, *Rigidoporus* sp., *T. lactinea* and *Lentinus tigrinus* showed great mass losses in between 19.33%-32.50% due to the ability in producing one or more lignocellulolytic enzymes. *Grammothele fuligo* and *P. sanguineus* isolates demonstrated the best biodegradation activity and were further evaluated on their biodegradation performance on both colonised and uncolonised woods with *G. boninense* mycelium (Naidu *et al.*, 2017). This advanced study has demonstrated that both *G. fuligo* and *P. sanguineus* could efficiently degrade diseased oil palm wood waste in an ecologically friendly manner (Naidu *et al.*, 2017). Moreover, pathogenicity and growth promoting properties of these seven hymenomycetes isolates were also determined by Naidu *et al.* (2018). Naidu *et al.* (2018) found that all these isolates were non-pathogenic to oil palm and enhanced vegetative growth of seedlings under greenhouse condition. However, up to date, there is no further report on these hymenomycetes against *G. boninense*. It would be advantageous if a more thorough assessment is conducted based on the response of plant defence enzymes, gene expression and metabolites induced via treatment with these hymenomycetes.

Biocontrol Agent-Bacteria

Numerous endophytic bacteria have been reported on their antagonistic activity against *G. boninense* including *Burkholderia cepacia* (Buana *et al.*, 2014; Ramli *et al.*, 2016) and *Pseudomonas*

aeruginosa (Muniroh *et al.*, 2019; Ramli *et al.*, 2016; Zaiton *et al.*, 2006). In the recent research conducted by Lim *et al.* (2019), *P. aeruginosa* was successfully isolated from soil of a virgin and undisturbed forest area of Crocker Range. *P. aeruginosa* in this study caused distortion on hyphae of *G. boninense* and lowered its density of mycelium (Lim *et al.*, 2019). In ethyl acetate crude extract of this endobacteria, the best inhibitory effect against *G. boninense* with minimum inhibitory concentration (MIC) recorded as low as 0.04 mg mL^{-1}. The compound which may have contributed to the antagonistic effect was identified as 3-demethylubiquinone-9 using Liquid Chromatography-Mass Spectrometry (LC-MS) (Lim *et al.*, 2019).

Ramli *et al.* (2016) successfully isolated endophytic bacteria from symptomless oil palm root tissues. The isolates were identified as *P. aeruginosa* GanoEB1, *Pseudomonas syringae* GanoEB3 and *B. cepacia* GanoEB2. These endophytic bacteria were tested in nursery trial using pre and post treatment against BSR disease infected seedlings. In the study, it was concluded that *P. aeruginosa* GanoEB1 was the best potential BCA among other endobacteria to control BSR disease (Ramli *et al.*, 2016). It was also noted that pre-treated oil palm seedlings have better disease endurance than non-treated seedlings when challenged with *G. boninense* (Ramli *et al.*, 2016). Further evaluation in the field was emphasised by the authors to verify its effectiveness in suppressing BSR disease (Ramli *et al.*, 2016).

Although *P. aeruginosa* demonstrated great potential in suppressing BSR disease in many studies, *P. aeruginosa* has the disadvantage of being incapable to produce spores. This switches researchers to pay attention to spore bearing bacteria namely *Bacillus* spp. (Aboutorabi, 2018). *Bacillus* spp. have been proven to have disease suppression on *G. boninense* over the years (Nusaibah *et al.*, 2017; Suryanto *et al.*, 2012; Susanto *et al.*, 2005). A novel fengycin (antifungal cyclic lipopeptides) produced by *Bacillus methylotrophicus* HC51 was detected and exhibited strong inhibition on growth of *G. boninense* (Pramudito *et al.*, 2018). This new fengycin was characterised with substitution of L-ornithine into lysine (Pramudito *et al.*, 2018). Potential of *Bacillus* sp. was further evaluated on the possibility of formulating into biofungicide (Puspita *et al.*, 2019). In this study, *Bacillus subtilis* was formulated into different biofungicide tablets to control *G. boninense* in oil palm nurseries (Puspita *et al.*, 2019). The best formulation established in this research contained spores of endophytic *Bacillus* sp., solid waste, talc and tapioca flour in which it successfully delayed the disease incubation period and reduced the disease intensity to 0% within 140 days. Substantial growth improvement was observed on seedlings compared to the control treatment (Puspita *et al.*, 2019).

Multiple Biocontrol Agents

Considerable number of research has been done to evaluate the antagonist efficacy of BCA against *G. boninense*. However, one of the problems associated with biocontrol is the lack of consistency in suppressing disease by application of a single BCA (O'Brien, 2017). Effectiveness of disease suppression of BCA is largely affected by environmental factors (Guetsky *et al.*, 2001). To enhance efficacy and consistency of BCA in suppressing *G. boninense*, several researches have been identifying efficacy of using multiple BCA in controlling BSR disease. This would allow various BCA to provide synergistic effects for disease suppression by adopting different modes of biocontrol mechanism and survive in broader range of environmental conditions (Chong *et al.*, 2017). However, selection of compatible BCA would be challenging. Combination of BCA must have synergistic relationship in complementing each other to enhance their feasibility on disease suppression as well as promoting plant growth.

A cocktail of *Trichoderma* spp. including *T. virens*, *T. asperellum* and *T. harzianum* were used by Musa *et al.* (2018) in evaluating the efficacy of antagonistic activity against *G. boninense* on oil palm seedlings. In the *in vivo* study, cocktail treatment exhibited disease reduction in infected seedlings at 83.03% on foliar symptoms and 89.16% on bole symptoms compared to other single treatments (Musa *et al.*, 2018).

Muniroh *et al.* (2019) studied proficiency of *P. aeruginosa* and *T. asperellum* as a mixture of BCA to suppress BSR disease in oil palm. Both microbes demonstrated synergistic relationship that led to a successful biocontrol attempt against *G. boninense* (Muniroh *et al.*, 2019). Nevertheless, both BCA have demonstrated positive phosphate solubilising activity and indole acetic (IAA) production. However, siderophore was only observed in *T. asperellum* in which all these traits could improve plant growth of the palms. Ability to excrete various cell wall degrading enzymes including chitinase, cellulase and β-1,3-glucanase were also detected; which could be responsible for the growth inhibition of *G. boninense* in both dual culture and culture filtrate studies.

Furthermore, the consortium of *Trichoderma* spp. and *Bacillus* spp. tested by Alexander *et al.* (2015) had induced the stripping of *G. boninense* hyphal structure by destroying the cellular structure and highly disrupted, disaggregated, shrivelled and lysis of *G. boninense* hyphal were observed under scanning electron microscopy (SEM). Production of cell wall degrading enzymes (CWDE) could be the factor associated on their antagonist activity in suppressing mycelia growth of *G. boninense* up to 70% (Alexander *et al.*, 2015).

According to Nusaibah *et al.* (2017), a nursery trial was performed to determine disease suppression efficacy on the mixture of *T. harzianum* and *Bacillus cereus*. The seedlings were inoculated with *G. boninense* with a novel disease inoculation technique namely dip, place and drench (DPD) (Nusaibah *et al.*, 2017) which differed from the existing method using Rubber Wood Blocks (RWB) (Idris *et al.*, 2006). The result had concluded that single application of *B. cereus* was found to be the most effective treatment in suppressing BSR disease. It had achieved the highest, 94.75% of disease reduction followed by single applications of *T. harzianum* (78.98%) and a mixture of both *T. harzianum* and *B. cereus* (68.49%). This validates the importance of *in vivo* trial to verify the efficacy on disease suppression achieved in *in vitro* test. Results achieved in *in vitro* test may be in contrary with the *in vivo* trial result (Nusaibah *et al.*, 2017). This is because microbes may behave differently in the natural environment compared to the controlled laboratory environment (Nusaibah *et al.*, 2017). Based on the reviewed studies above, it could be concluded that *Bacillus* spp. may perform better as a stand-alone application than as a consortium of BCA with other genera.

The Potential of Actinomycetes as Biocontrol Agent to Suppress Oil Palm Basal Stem Rot

Compared to endophytic fungi and bacteria, endophytic actinomycetes obtain much lesser attention on the biocontrol efficacy. Actinomycetes are a group of Gram-positive bacteria with fungal liked morphology due to their branched, filamentous or hyphae-type elongated cells (Singh *et al.*, 2018). It is widely known for the ability to produce a wide range of antibiotics including actinomycetin, micromonosporin, mycetin, actinomyces lysozyme, actinomycin, streptothricin, proactinomycin and streptomycin (Waksman *et al.*, 2010). Most of the actinomycetes are isolated from the genus *Streptomyces* (Kumari *et al.*, 2013). Actinomycetes are proven to have the ability to promote plant growth contributed by the secretion of siderophores and IAA (Gopalakrishnan *et al.*, 2014). Therefore, *Streptomyces* could be a potential biocontrol candidate towards various soil borne pathogens. A study has proven the biocontrol ability of a marine isolated *Streptomyces vinaceusdrappus* in controlling a root rot disease in tomatoes, caused by *Rhizoctonia solani* (Yandigeri *et al.*, 2015). Besides displaying superior disease reduction in tomatoes plants, treatment plants with respective *Streptomyces* also have shown significant growth performance advantage (Yandigeri *et al.*, 2015). Besides that, actinomycetes from *Streptomyces* spp. also demonstrated biocontrol efficacy against various soil borne disease caused by *Phytophthora*

cinnamomic on avocado (You *et al.*, 1996). *Pythium aphanidermatum* on cucumber (El-Tarabily *et al.*, 2009) and *Fusarium oxysporum* f. sp. *ciceris* on chickpea (Amini *et al.*, 2016). However, not many reports on actinomycetes against BSR disease were documented.

The first report in screening potential of actinomycetes against *G. boninense* was documented by Tan *et al.* (2002). In their research, few *Streptomyces* spp. were found relatively more effective than *Micromonospora* spp. in controlling *G. boninense*. Another *in vitro* screening of actinomycetes from rhizosphere of oil palm was done by Shariffah-Muzaimah *et al.* (2015) where four isolates (AGA 043, AGA 048, AGA 347, AGA 506) were highlighted for their ability to inhibit *G. boninense*. A continuation study on these four isolates was performed and their efficacy of biocontrol against *G. boninense* in powder form after fermentation was tested in BSR disease infected oil palm seedlings (Shariffah-Muzaimah *et al.*, 2018). Isolate AGA347 was reported as the best formulation with 73.1% of disease reduction compared to other isolates (30.1%-54.8%). Isolate AGA347 was then identified as *Streptomyces hygroscopicus* subspecies *hygroscopicus* (Shariffah-Muzaimah *et al.*, 2018).

In vitro antagonistic efficacy of *Streptomyces sanglieri* was reported by Nur Azura *et al.* (2016) in suppressing *G. boninense*. The antifungal compounds identified from *S. sanglieri* were cycloheximide and actiphenol (Nur Azura *et al.*, 2016). To further study colonisation and potential as a BCA in the oil palm roots, *S. sanglieri* strain was inoculated into pre-germinated oil palm seeds and observed for six months period. Results showed that *S. sanglieri* could enhance the plant growth performance including root development, plant height, root length, number of secondary roots and wet weight (Nur Azura *et al.*, 2016). Colonisation of this strain in root area of oil palm seedlings was studied by re-isolating from the root segments one- and six-month after inoculation and observed under SEM. *Streptomyces sanglieri* was found to grow on the root epidermal surface after one-month inoculation and later penetrating the epidermal cell junctions after six-month of inoculation. Both *in vitro* and *in vivo* results had recommended *S. sanglieri* as a potential BCA towards BSR disease control (Nur Azura *et al.*, 2016).

In Sabah, a total of 20 soil samples collected from Crocker Range forest was used to isolate potential actinomycetes which have biocontrol ability towards to *G. boninense* (Lim *et al.*, 2019). Out of 72 types of actinomycetes isolates, A19 was reported to have the highest PIRG value with 80% and causing hyphae damage on *G. boninense* under SEM. Besides that, ethyl acetate extract of *Steptomyces* spp. A19 recorded a minimum inhibitory concentration (MIC) at 0.18 mg mL^{-1}. Several anti-fungal compounds were

also detected via LC-MS including ribostamycin, benzylmatic acid, landomycin B and salinomycin which may contribute to suppress BSR disease in oil palm (Lim *et al.*, 2019).

CONCLUSION

Efficacy of fungi, bacteria and actinomycetes as potential BCA in suppressing oil palm BSR disease were proven and documented in many studies. Most of these studies only performed the *in vitro* assessment and a few reported on the *in vivo* studies in the greenhouse. However, field trial was lacking, it is crucial to assess efficiency of these BCA in the field environment as BCA may behave differently in the field environment compared to agar plate or controlled environment (greenhouse trial). The interaction of BCA with the complexity of abiotic and biotic factors in the field may affect their efficacy as potent BCA in the controlled environment. In addition, assessment on carrier material for BCA is vital to be studied as there is potential of commercialisation of BCA into bio-fertiliser or bio-fungicide. Exploration of other potential microorganisms is also desirable in expanding the insight of potential BCA in controlling BSR disease. Little concern was placed on the *Streptomycetes* and more study should be attempted in evaluating their efficacy either as single application or as a consortium with different genera for greater disease suppression through adoption of altered mechanisms. A strict and reliable control measure is necessary to eradicate and prevent further spreading of the disease. The urge to explore natural controlling mechanism will not only be beneficial as it is also sustainable and could be a reliable substitute to synthetic chemical fungicides.

ACKNOWLEDGEMENT

REFERENCES

Aboutorabi, M (2018). A review on the biological control of plant diseases using various microorganisms. *J. Research in Medical and Dental Science, 6(4)*: 30-35.

Alexander, A; Dayou, J and Chong, K P (2015). Morphological changes of *Ganoderma boninense* mycelia after challenged by *Trichoderma* and *Bacillus*. *AIP Conference Proceedings, 1669(1)*: 20075.

Alexander, A; Abdullah, S; Rossall, S and Chong, K P (2017). Evaluation of the efficacy and mode of action of biological control for suppression of *Ganoderma boninense* in oil palm. *Pakistan J. Botany, 49*: 1193-1199.

Amini, J; Agapoor, Z and Ashengroph, M (2016). Evaluation of *Streptomyces* spp. against *Fusarium oxysporum* f. sp. ciceris for the management of chickpea wilt. *J. Plant Protection Research, 56(3)*: 257-264.

Angel, L; Sundram, S; Ping, B T Y; Yusof, M T and Ismail, I S (2018). Profiling of antifungal activity of *Trichoderma virens* 159C involved in biocontrol assay of *Ganoderma boninense*. *J. Oil Palm Res., 30(1)*: 83-93.

Buana, R F N; Wahyudi, A T and Mathius, N T (2014). Control activity of potential antifungal-producing *Burkholderia* sp. in suppressing *Ganoderma boninense* growth in oil palm. *Asian J. Agric. Res., 8(5)*: 259-268.

Chong, K P; Dayou, J and Alexander, A (2017). Detection and control of *Ganoderma boninense* in oil palm crop. *Springer Briefs in Agriculture*. DOI 10.1007/978-3-319-54969-9.

El-Tarabily, K A; Nassar, A H; Hardy, G S J and Sivasithamparam, K (2009). Plant growth promotion and biological control of *Pythium aphanidermatum*, a pathogen of cucumber by endophytic actinomycetes. *J. Applied Microbiology, 106(1)*: 13-26.

Goh, Y K; Marzuki, N F; Goh, T K; Tan, S Y; Goh, Y K and Goh, K J (2016). Mycoparasitic *Scytalidium parasiticum* as a potential biocontrol agent against *Ganoderma boninense* basal stem rot in oil palm. *Biocontrol Science and Technology, 26(10)*: 1352-1365. DOI: 10.1080/09583157.2016.1202192.

Gopalakrishnan, S; Vadlamudi, S and Bandikinda, P (2014). Evaluation of *Streptomyces* strains isolated from herbal vermicompost for their plant growth-promotion traits in rice. *Microbiological Research, 169(1)*: 40-48. DOI: 10.1016/j.micres.2013.09.008.

Guetsky, R; Shtienberg, D; Elad, Y and Dinoor, A (2001). Combining biocontrol agents to reduce the variability of biological control. *Phytopathology, 91(7)*: 621-627.

Halimah, M; Mazinah, Z; Ismail, S and Idris, A S (2012). Determination of hexaconazole in field samples of an oil palm plantation. *Drug Testing and Analysis, 4(S1)*: 112-117.

Heydari, A and Pessarakli, M (2010). A review on biological control of fungal plant pathogens using microbial antagonists. *J. Biological Sciences, 10(4)*: 273-290. DOI: 10.3923/jbs.2010.273.290.

Ho, C L; Tan, Y C; Yeoh, K A; Lee, W K; Ghazali, A K; Yee, W Y and Hoh, C C (2018). Transcriptional response of oil palm (*Elaeis guineensis* Jacq.) inoculated simultaneously with both *Ganoderma boninense* and *Trichoderma harzianum*. *Plant Gene, 13(January): 56-63.* DOI: 10.1016/j.plgene.2018.01.003.

Idris, A S; Ariffin, D; Swinburne, T R and Watt, T A (2000). The identity of *Ganoderma* species responsible for BSR disease of oil palm in Malaysia-pathogenicity test. *MPOB Information Series No. 77.*

Idris, A S; Ismail, S; Ariffin, D and Ahmad, H (2002). Control of *Ganoderma* infected palm-development of pressure injection and field applications. *MPOB Information Series No. 131.*

Idris, A S; Kushairi, D; Ariffin, D and Basri, M W (2006). Technique for inoculation of oil palm germinated seeds with *Ganoderma*. *MPOB Information Series No. 314.*

Kamarudin, N; Seman, I A and Masri, M M M (2019). Prospects in sustainable control of oil palm pests and diseases through the enhancement of ecosystem services – The way forward. *J. Oil Palm Res., 31(3)*: 381-393. DOI: 10.21894/jopr.2019.0030.

Kirschner, R; Arnold, G R W and Chen, C J (2007). *Cladobotryum semicirculare* sp. nov. (Hyphomycetes) from commercially grown *Ganoderma tsugae* in Taiwan and other Basidiomycota in Cuba. *SYDOWIA-HORN-, 59(1)*: 114-124.

Kumari, M; Myagmarjav, B E; Prasad, B and Choudhary, M (2013). Identification and characterization of antibiotic-producing actinomycetes isolates. *Amer. J. Microbiology, 4(1)*: 24 pp.

Lim, P H; Gansau, J A and Chong, K P (2018). *Streptomyces* spp. a potential biocontrol agent against *Ganoderma boninense* of basal stem rot. *J. Oil Palm Res., 30(2)*: 265-275. DOI: 10.21894/jopr.2018.0024.

Lim, P H; Gansau, J A and Chong, K P (2019). Biocontrol of basal stem rot pathogen *Ganoderma boninense* by *Pseudomonas aeruginosa*. *Bangladesh J., Bot., 48(2)*: 209-215.

Marzuki, N F; Goh, Y K; Tung, H J; Goh, Y K and Goh, K J (2015). Evaluation on the cultural characteristics and antagonistic activities of *Cladobotryum semicirculare* against *Ganoderma boninense in vitro*. *J. Oil Palm Res., 27(4)*: 326-338.

Mcdonald, G and Rahmanulloh, A (2019). Indonesia Oilseeds and Products Annual 2019. USDA Foreign Agricultural Service.

McKay, G J; Egan, D; Morris, E; Scott, C and Brown, A E (1999). Genetic and morphological characterization of *Cladobotryum* species causing cobweb disease of mushrooms. *Appl. Environ. Microbiol., 65(2)*: 606-610.

Moncalvo, J M (2000). Systematics of *Ganoderma*. *Ganoderma Diseases of Perennial Crops* (Flood, J; Bridge, P D and Holderness, M eds.). p. 23-45.

Muniroh, M S; Nusaibah, S A; Vadamalai, G and Siddique, Y (2019). Proficiency of biocontrol agents as plant growth promoters and hydrolytic enzyme producers in *Ganoderma boninense* infected oil palm seedlings. *Current Plant Biology, 20*: 100116. DOI: 10.1016/j.cpb.2019.100116.

Musa, H; Nusaibah, S A and Khairulmazmi, A (2018). Assessment on *Trichoderma* spp. mixture as a potential biocontrol agent of *Ganoderma boninense* infected oil palm seedlings. *J. Oil Palm Res., 30(3)*: 403-415. DOI: 10.21894/jopr.2018.0035.

Naher, L; Tan, S G; Yusuf, U K; Ho, C L and Siddiquee, S (2012). Activities of chitinase enzymes in the oil palm (*Elaeis guineensis* Jacq.) in interactions with pathogenic and non-pathogenic fungi. *Plant Omics, 5(4)*: 333.

Naher, L; Intan, S; Mokhtar, B and Sidek, N (2015). *Trichoderma harzianum* T32 growth and antagonistic performance against *Ganoderma boninense* on different culture media. *The 3rd International Conference on Biological, Chemical and Environmental Sciences* (BCES-2015): 21-23. DOI: 10.15242/iicbe.c0915047.

Naidu, Y; Idris, A S; Nusaibah, S A; Norman, K and Siddiqui, Y (2015). *In vitro* screening of biocontrol and biodegradation potential of selected hymenomycetes against *Ganoderma boninense* and infected oil palm waste. *Forest Pathology, 45(6)*: 474-483.

Naidu, Y; Siddiqui, Y; Rafii, M Y; Saud, H M and Idris, A S (2017). Investigating the effect of white-rot hymenomycetes biodegradation on basal stem rot infected oil palm wood blocks: Biochemical and anatomical characterization. *Industrial Crops and Products, 108*: 872-882.

Naidu, Y; Siddiqui, Y; Rafii, M Y; Saud, H M and Idris, A S (2018). Inoculation of oil palm seedlings in Malaysia with white-rot hymenomycetes: Assessment of pathogenicity and vegetative

growth. *Crop Protection, 110(February)*: 146-154. DOI: 10.1016/j.cropro.2018.02.018.

Nur Azura, A B; Yusoff, M; Tan, G Y A; Jegadeesh, R; Appleton, D R and Vikineswary, S (2016). *Streptomyces sanglieri* which colonised and enhanced the growth of *Elaeis guineensis* Jacq. seedlings was antagonistic to *Ganoderma boninense* in *in vitro* studies. *J. Industrial Microbiology and Biotechnology, Springer Berlin Heidelberg, 43(4)*: 485-493. DOI: 10.1007/s10295-015-1724-4.

Nusaibah, S A; Saad, G and Hun, T G (2017). Antagonistic efficacy of *Trichoderma harzianum* and *Bacillus cereus* against *Ganoderma* disease of oil palm via dip, place and drench (DPD) artificial inoculation technique. *Int. J. Agriculture and Biology, 19(2)*: 299-306. DOI: 10.17957/IJAB/15.0280.

O'Brien, P A (2017). Biological control of plant diseases. *Australasian Plant Pathology, 46(4)*: 293-304. DOI: 10.1007/s13313-017-0481-4.

Pramudito, T E; Agustina, D; Nguyen, T K N and Suwanto, A (2018). A novel variant of narrow-spectrum antifungal bacterial lipopeptides that strongly inhibit *Ganoderma boninense*. *Probiotics and Antimicrobial Proteins, 10(1)*: 110-117. DOI: 10.1007/s12602-017-9334-2.

Puspita, F; Dini, I R and Sari, D (2019). Screening of fungi from oil palm rhizosphere in peat soils and the potential as biological agents against *Ganoderma* sp. *Indonesian J. Agricultural Research, 2(2)*: 37-49.

Rakib, M R M; Khairulmazmi, A; Idris, A S; Jalloh, M B and Wahida, N H (2017). *Ganoderma* species of basal and upper stem rots in oil palm (*Elaeis guineensis*) in Sarawak, Malaysia. *J. Acad. UiTM Negeri Sembilan, 5*: 27-35.

Ramli, N R; Mohamed, M S; Seman, I A; Zairun, M A and Mohamad, N (2016). The potential of endophytic bacteria as a biological control agent for *Ganoderma* disease in oil palm. *Sains Malaysiana, 45(3)*: 401-409.

Roslan, A and Idris, A S (2012). Economic impact of *Ganoderma* incidence on Malaysian oil palm plantation – A case study in Johor. *Oil Palm Industry Economic J., 12(1)*: 24-30.

Shariffah-Muzaimah, S A; Idris, A S; Madihah, A Z; Dzolkhifli, O; Kamaruzzaman, S and Cheong, P C H (2015). Isolation of actinomycetes from rhizosphere of oil palm (*Elaeis guineensis* Jacq.) for antagonism against *Ganoderma boninense*. *J. Oil Palm Res., 27(1)*: 19-29.

Shariffah-Muzaimah, S A; Idris, A S; Madihah, A Z; Dzolkhifli, O; Kamaruzzaman, S and Maizatul-Suriza, M (2018). Characterization of *Streptomyces* spp. isolated from the rhizosphere of oil palm and evaluation of their ability to suppress basal stem rot disease in oil palm seedlings when applied as powder formulations in a glasshouse trial. *World J. Microbiology and Biotechnology, 34(1)*: 15.

Singh, D P; Patil, H J; Prabha, R; Yandigeri, M S; Prasad, S R; Susanto, A and Lai, H (2018). Evaluation of *Streptomyces* spp. against *Fusarium oxysporum* f. sp. ciceris for the management of chickpea wilt. *Plant Gene, 159(1)*: 264-274. DOI: 10.1515/jppr-2016-0038.

Sundram, S (2013). First report: Isolation of endophytic *Trichoderma* from oil palm (*Elaeis guineensis* Jacq.) and their *in vitro* antagonistic assessment on *Ganoderma boninense*. *J. Oil Palm Res., 25(3)*: 368-372.

Sundram, S; Meon, S; Seman, I A and Othman, R (2015). Application of arbuscular mycorrhizal fungi with *Pseudomonas aeruginosa* UPMP3 reduces the development of *Ganoderma* basal stem rot disease in oil palm seedlings. *Mycorrhiza, 25(5)*: 387-397. DOI: 10.1007/s00572-014-0620-5.

Suryanto, D; Wibowo, R H; Siregar, E B M and Munir, E (2012). A possibility of chitinolytic bacteria utilization to control basal stems disease caused by *Ganoderma boninense* in oil palm seedling. *African J. Microbiology Research, 6(9)*: 2053-2059.

Susanto, A; Sudharto, P S and Purba, R Y (2005). Enhancing biological control of basal stem rot disease (*Ganoderma boninense*) in oil palm plantations. *Mycopathologia, 159(1)*: 153-157. DOI: 10.1007/s11046-004-4438-0.

Tan, C J; How, K C; Loh-Mia, P P; Ismet, A; Getha, K; Seki, T and Vikineswary, S (2002). Bioactivity of selected actinomycetes against *Ganoderma boninense*. *Asia Pacific J. Molecular Biology and Biotechenology, 10(2)*: 119-125.

Turner, P D (1981). *Oil Palm Disease and Disorders*. Oxford University Press.

Waksman, S A; Schatz, A and Reynolds, D M (2010). Production of antibiotic substances by actinomycetes. *Annals of the New York Academy of Sciences, 1213(1)*: 112-124.

Wong, L C; Bong, C F J and Idris, A S (2012). *Ganoderma* species associated with basal stem rot disease of oil palm. *J. Applied Sciences, 9(6)*: 879-885.

Yandigeri, M S; Malviya, N; Solanki, M K; Shrivastava, P and Sivakumar, G (2015). Chitinolytic *Streptomyces vinaceusdrappus* S5MW2 isolated from Chilika lake, India enhances plant growth and biocontrol efficacy through chitin supplementation against *Rhizoctonia solani*. *World J. Microbiology and Biotechnology, 31(8)*: 1217-1225. DOI: 10.1007/s11274-015-1870-x.

You, M P; Sivasithamparam, K and Kurtböke, D I (1996). Actinomycetes in organic mulch used in avocado plantations and their ability to suppress *Phytophthora cinnamomi*. *Biology and Fertility of Soils, 22(3)*: 237-242. DOI: 10.1007/BF00382518.

Zaiton, S; Sariah, M and Zainal, A (2006). Isolation and characterization of microbial endophytes from oil palm roots: Implication as biological control agents against *Ganoderma*. *Planter, 82(966)*: 587-597.

ASSOCIATION OF DIETARY FATS WITH GUT MICROBIOTA PROFILE: HOW DOES PALM OIL FIT IN?

S Y YAP[1]*; P T VOON[1]; Y K CHEAH[2]; V K M LEE[3] and SELVADURAY, K R[1]

ABSTRACT

Diet manipulation alters the gut microbiota composition. Gut dysbiosis is characterised by imbalanced bacteria composition that has been associated with high fat diet. Diets containing high animal fat induce pathogenic bacteria growth and similar bacterial profiles have been identified in obese adults and chronic disease patients. Conversely, diets containing high plant fat increase the abundance of beneficial bacteria. Habitual fat intakes modulate the bacterial species and their metabolites in different geographical locations and ethnicities. Dietary interventions using various degrees of fatty acid saturation reported reduced bacterial diversity in high saturated fatty acid (SFA) diet and increased in high monounsaturated fatty acid (MUFA) diet. However, high polyunsaturated fatty acid (PUFA) diet demonstrated a wide variation in bacterial diversity. These results suggested that the effects of dietary fats on gut microbiota composition are not fully established. Palm oil has almost balanced proportions of saturated and unsaturated fatty acids coupled with unique stereo-specificity fatty acids compositions and nutritional properties, making it the main vegetable oil in the Malaysian diet. However, its effect on the gut microbiota profile is still unknown. This review highlights the abundance of specific bacteria after consuming various dietary fats and proposes potential bacteria profile following the palm oil diet.

INTRODUCTION

The bacterial composition inhabiting the intestine is highly affected by the diet of the human host. The fractions of carbohydrate, fat, and protein in food residue affect the survival of different population of colonic bacteria. These bacteria degrade and ferment colonic food residue to synthesise a wide range of metabolites that affect the health of the host. The prevalence of a specific type of bacteria could serve as a potential dietary biomarker for diagnosing intestinal health and related systemic health of the host (Mokkala *et al.*, 2019).

In healthy adults, the colonic bacterial composition is dominated by the phyla *Firmicutes* (60%-80%) and *Bacteroidetes* (20%-40%); while only a small amount of *Actinobacteria*, *Proteobacteria*, *Verrucomicrobia* and *Fusobacteria* are present among others (Clavel *et al.*, 2014). The compositions are stable over time and any change in gut environment such as diet modification, and ingestion of probiotics or drugs will result in 'gut dysbiosis' (Leeming *et al.*, 2019). Gut dysbiosis is characterised by the imbalance in the bacteria composition (Kriss *et al.*, 2018), low bacteria diversity as indicated by lower total bacteria counts and Chao number which represents bacteria richness (Tsuji *et al.*, 2018).

[1] Malaysian Palm Oil Board,
  6 Persiaran Institusi, Bandar Baru Bangi,
  43000 Kajang, Selangor, Malaysia.

[2] Department of Biomedical Sciences,
  Faculty of Medicine and Health Sciences,
  Universiti Putra Malaysia, 43400 UPM Serdang,
  Selangor, Malaysia.

[3] Department of Family Medicine,
  School of Medicine, International Medical University,
  Kuala Lumpur, Malaysia.

* Corresponding author e-mail: syyap@mpob.gov.my

Diets alter gut microbiota composition as shown in urban and rural populations (*Figure 1*). Individuals living in urban cities with a diet that is high in animal fat and low in fibre have a significantly ($p<0.05$) lower abundance of butyrate-producing bacteria compared to individuals living in rural villages that have diet high in fibre and plant-based fats (De Filippo *et al.*, 2010; Ou *et al.*, 2013; Yatsunenko *et al.*, 2012). Animal fat enriched diet induces gut perturbation by promoting opportunistic pathogenic bile-tolerant bacteria (*Figure 1*) such as *Alistipes* and *Bilophila* even in a short-term four days dietary intervention (David *et al.*, 2014). This finding agrees with Muegge *et al.* (2011) who had concluded that animal-based fat diets have a very similar gut microbiota profile that is found in carnivorous mammals (Muegge *et al.*, 2011).

Gut microbiota composition of high animal fat intake is correlated with the profile of individuals that are obese and/or have chronic diseases such as Type 2 diabetes, digestion disorder, cardiovascular disease and cancer (Illiano *et al.*, 2020; Murphy *et al.*, 2015; Requena *et al.*, 2018). Hence, bacteria species that overgrows or depletes significantly are proposed as dietary biomarkers for early disease diagnosis.

Cohort studies have attempted to generalise the bacteria profile from constituents adopted different habitual diet. A distinguish variation in gut profile was identified in population depending on various geographical location and ethnicities (Gupta *et al.*, 2017; Jain *et al.*, 2018; Yasir *et al.*, 2015) suggesting that individuals gut microbiota profiles are strongly associated with the host's geographical location. Therefore, extrapolated data collected from different nations is simply too general to be used in the diagnosis of diseases. Researchers should instead use small-scale interpolated data to accurately identify dietary biomarkers and predict metabolic risk (He *et al.*, 2018).

The effect of a high fat diet on the composition of gut microbiome is well known, but there exists little information on the type of geographically-based habitual fat intake on the profile of gut microbiota. Briefly, edible MUFA such as olive oil and PUFA such as fish oils are a staple in the diet of Mediterranean region (Pauwels, 2011). High PUFA soybean oil is extensively used by America, Argentina, Brazil, Russia and China (Jia *et al.*, 2020), whereas sunflower oil is mainly used in European diet (Pilorgé, 2020). Palm oil which is balanced in saturated and unsaturated fats has become an increasingly important edible oil in the India, China, European Union, United Arab Emirates and Southeast Asian regions (Parveez *et al.*, 2020).

To date, very few human clinical studies have focused on the effects of positional distribution of fatty acids varying in degree of saturation on the human gut microbiota profile. Therefore, this review highlights the association of dietary fat intakes with the composition of gut microbiota and their metabolites at different geographical locations. Moreover, we also propose a prospective palm oil nutritional research to identify specific genus or species and establish a baseline of gut microbiota profile in the Malaysian diet, which may be a potential dietary biomarker for predicting metabolic health.

THE LINK OF DIETARY FAT SOURCE WITH GUT MICROBIOTA COMPOSITION AND HEALTH

The bioavailability of dietary fats influences the composition of gut microbiota. A plant-based Mediterranean, vegetarian and vegan diets contain a variety of grains, nuts, vegetables, and fruits that provide a variable range of plant fats, phytonutrients and polyphenols (Muralidharan *et al.*, 2019). In contrast, modern diet has been associated with high intake of energy dense- and highly processed foods coupled with red meat consumption (Mozaffarian, 2016).

Effects of high plant-based or animal-based fats on gut microbiota compositions have been summarised into two general pathways (Valdes *et al.*, 2018). High intake of plant-based diet

Animal-based fats diet

↑ *Firmicutes, Proteobacteria*
↑ Secondary bile acids
↑ Pathogenic bile-tolerant bacteria

Plant-based fats diet

↓ *Bacteroidetes, Verrucomicrobia*
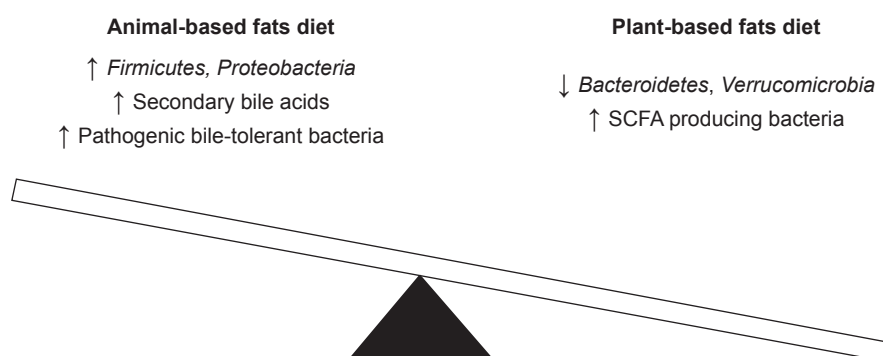↑ SCFA producing bacteria

Figure 1. Gut dysbiosis and effects of dietary fat.

stimulates butyrate-producing bacteria (De Filippo *et al.*, 2010) which have been reported to reduce the risk of non-communicable chronic diseases such as hypertension (Silveira-Nunes *et al.*, 2020) and cardiovascular diseases (Ganesan *et al.*, 2018). Animal-based fat intake increases the abundance of pathogenic bile acid-tolerant bacteria (De Filippo *et al.*, 2010) and leads to accumulation of toxins such as deconjugated bile acids and lipopolysaccharides (Requena *et al.*, 2018) in the systematic circulation.

Animal fat promotes the growth of detrimental bile acids tolerant species such as *Clostridium, Helicobacter, Catenibacterium, Fusobacterium, Enterobacterium, Bacteroides, Bilophila* and *Alistipes* (Murphy *et al.*, 2015; Shortt *et al.*, 2018; Tomova *et al.*, 2019; Yang *et al.*, 2020b). These bacteria secrete toxic metabolites such as trimethylamine N-oxide (TMAO) which is derived from dietary choline or L-carnitine, a component of proteins. Bacteria ferment the trimethylamine (TMA) in these proteins to TMAO via flavin-containing monooxygenase 3 (FMO3) enzyme and secrete it into the gut. High concentrations of TMAO in the circulating plasma activates the NF-kappa B pathway and increases the secretion of inflammatory cytokines such as IL-18 and IL-1β (Yang *et al.*, 2019). These inflammatory markers are found to be elevated in the plasma of insulin-resistant obese adult subjects (Moreno-Indias *et al.*, 2016). Similarly, elevated TMAO levels inhibit the synthesis of bile acid and trigger platelet hyper-reactivity which increases the risk of thrombosis and cardiovascular diseases (CVD) (Yang *et al.*, 2019).

A high fat diet alters the profile of gut microbiota and induces permeability of the intestinal barrier structure in the systematic circulation (Ghosh *et al.*, 2020) and increases the expression of Paneth Cell-Antimicrobial Peptides which trigger intestinal inflammation followed by activation of circulating inflammatory cytokines (IFN-γ and TNF-α) (Guo *et al.*, 2017). This finding sheds light on the importance of gut microbiota profile and metabolites in preventing intestinal tumorigenesis. Overgrowth of detrimental bile acids tolerant bacteria also produces deconjugated bile acid when accumulated and increases the rate of colonic cell proliferation and the risk of colon cancer (Fava *et al.*, 2013; O'Keefe, 2016).

Plant-based fats are generally associated with short-chain fatty acid (SCFA) production. Among the SCFA, acetate and propionate are fatty acids which activate the G-protein coupled receptors 43 (GPR43) in the colon enterocytes and adipocyte. The GPR43 activates cellular signalling events and inhibits colonocytes proliferation (O'Keefe, 2016) as indicated by low Ki-67 proliferation and apoptotic indices. The *ffar2* (*grp43*) and *ffar3* (*gpr41*), receptors of SCFA on glucagon-like peptide 1 (GLP-1) L cells, stimulate the GLP-1 secretion to regulate plasma glucose concentration and maintain glucose homeostasis (Tolhurst *et al.*, 2012). Hence, SCFA that

bind to these receptors may serve as therapeutic treatment for diabetes.

SCFA also demonstrate anti-inflammatory effect by suppressing the production of cytokines and inhibiting actions of the toll-like receptor (TLR) 4 (Mirmonsef *et al.*, 2012). Therefore, SCFA-producing bacteria such as *Prevotella, Bifidobacterium* spp. and *Lactobacillus* (Tomova *et al.*, 2019) may have a protective effect against colon cancer as reported in the study on native Africans (Ou *et al.*, 2013).

DIVERSITY OF GUT MICROBIOTA IN DIFFERENT HABITUAL DIETS

High dietary fat intake is associated with a decrease in the *Firmicutes* and *Proteobacteria* phylum but with an increase in *Bacteroidetes* and *Actinobacteria* (Senghor *et al.*, 2018), however contradictory results have also been documented. These contradictory results are likely due to the different ethnicity and lifestyle of populations from different geographical locations (Fontana *et al.*, 2004; Gupta *et al.*, 2017). Later, He *et al.* (2018) observed that variations in bacterial lineages occurred in different locations within the same ethnic group. Following this observation, they recommended establishing a localised baseline to identify gut microbial as dietary biomarkers (He *et al.*, 2018).

The type of food, meal preparation, drinks, and other socio-cultural rituals co-influence the gut microbiota profile of people in different regions (Senghor *et al.*, 2018). The typical gut microbiota profile in urban European and American population, and rural African population have been extensively reviewed (Almeida *et al.*, 2019; Snijder *et al.*, 2017). Therefore, this review focuses on the gut microbiota profile of Asians in geographically different locations (*Table 1*).

Comparison of Gut Microbiota Profile within Same Country but on Different Diets

Gut microbiota profile differs across geographical locations in urban and rural populations in Asian countries (*Table 1*). Generally, individuals from rural areas have diverse bacteria species as a result of variety of unprocessed plant-based diet intake; whereas the gut microbiome of urban population is dominated by *Bacteroides, Faecalibacterium* and *Ruminococcus* as a consequence of high modern processed food intake (*Table 1*).

Dietary patterns segregate the gut microbiota profile from different parts in the countries, particularly in Indian and Chinese populations (*Table 1*). Similar observation was also reported in South Korea, where Jeju Islanders who typically consume more animal lipid have high abundance of *Butyricimonas* than people who lived in Seoul city (Nam *et al.*, 2011).

TABLE 1. GUT MICROBIOTA DIVERSITY IN INDIVIDUALS FROM DIFFERENT GEOGRAPHICAL REGIONS

Country	Region	Study population; Sample size	Diets/ lifestyle	Sequencing method	Gut microbiota compositions	Reference
Saudi Arabia	• Urban	• adults • n=18	• limited food variety, low fruits and vegetables intake compared to French	• 16S rRNA Illumina MiSeq (V3-V4)	• Arabic: ↑ Proteobacteria, *Blautia wexlerae*, ↓ *Verrucomicrobia*, *Bifidobacterium* breve compared to French	Yasir *et al.* (2015)
	• Jeddah (Urban)	• healthy males • n=18	• limited food variety, fruit, vegetables, fast food and snacks	• 16S rRNA Illumina MiSeq (V3-V4)	• ↑ *Bacteroidetes*	Angelakis *et al.* (2016)
	• Bedouins (rural)	• healthy males • n=10	• vegetables, chicken, dairy products, fermented food and rice	• 16S rRNA Illumina MiSeq (V3-V4)	• ↑ *Verrucomicrobia* • ↑ *Spirochaetae Treponema berlinense*, *T. succinifaciens* due to fermented food intake	
	• Arabian Peninsula	• healthy native Arab Kuwaitis • n=25	• meats, dairy products, grains, legumes, nuts, vegetables (leafy greens, herbs), fruits and nuts	• 16S rRNA Illumina MiSeq (V3-V4)	• ↑ *Bacteroides dorei/ vulgatus*	Plummer *et al.* (2020)
India	• North (Bhopal, Ludhiana, Lucknow, New Delhi	• n=247	• Details dietary records were not provided	• 16S rRNA Ion Torrent (V3-V4)	• Eastern and Western: ↑ *Bacteroidetes* • Northern and Southern: ↑ *Spirochaetes* • ↑ *Faecalibacterium* and *Prevotella* genus across the geographic landscape	Shetty (2018)
	• East (Guwahati, Kolkata, Patna	• n=250				
	• West (Ahmedabad, Ajmer, Mumbai, Nagpur	• n=263				
	• South (Chennai, Cochin, Mangalore	• n=226				
	• Ahmedabad (Western India)	• healthy adults • n=80	• fruits, vegetables, wheat, millet, sorghum, dairy products, sprouts, leafy vegetables, rice, pulses, low meat and fish intake	• 16S rRNA Illumina MiSeq (V3-V4)	• ↑ *Prevotella*, *Sutterella* and *Succinivibrio* phylum *Proteobacteria*	Tandon *et al.* (2018)
	• Ballabhgarh, Faridabad district, sea level	• healthy adults • rural (n=25) • urban (n=24)	• vegetarian, eggetarian, non-vegetarian • mustard oil, soyabean oil and ghee	• 16S rRNA pyro-sequencing (V1-V5)	• Urban: ↑ *Lactobacillus* • Rural: ↑ *Parabacteroides, Blautia, Brevundimonas, Pelomonas* and *Megamonas* • Leh: ↑ *Prevotella copri*, uncharacterised species of *Faecalibacterium* and *Lachnospiraceae* • High ghee intake: ↑ *Collinsella* • High sunflower oil: ↑ *Roseburia* and *Sporobacter*	Das *et al.* (2018)
	• Leh, Ladakh district, high altitude	• n=35	• lack of dairy intake, high consumption of sunflower oil			
	• Central India (Bhopal) • Southern India (Kerela)	• n=110	• plant-based diet • omnivorous diet	• 16S rRNA sequencing, whole genome shotgun	• Central region: ↑ *Prevotella* • Southern region: ↑ *Bacteroides, Ruminococcus* and *Faecalibacterium*	Dhakan *et al.* (2019)

Country	Region	Study population; Sample size	Diets/ lifestyle	Sequencing method	Gut microbiota compositions	Reference
	• Ladakh (cold desert)	• healthy adults • n=31	• noodle, whole wheat bread, yak butter, barley, alcoholic beverage	• whole genome sequencing Illumina HiSeq-2500	• Ladakh: ↑ *Prevotella* • Jaisalmer: ↑ *Bifidobacterium*	Kaur *et al.* (2020)
	• Jaisalmer (hot-and semi-arid)		• whole wheat bread, spicy curries, lentils, grains and butter milk			
	• Khargone (subtropical to tropical climate)		• lentils, grains, rice, whole wheat bread, vegetables, spices, tea and milk			
Russia	• Saint Petersburg, Saratov, Rostov-on-Don and Novosibirsk (urban) • Tatarstan, Omsk, Tyva and Khakassia (rural)	• healthy adults • n=96	• urban: high processed food intake • rural: high unprocessed natural food intake	• 16S rRNA SOLiD sequencing	• Overall: ↑ *Bifidobacterium*, *Megamonas*, *Phascolarctobacterium*, *Lactobacillus* or *Akkermansia* • Omsk: ↑ *Prevotella*, *Lachnospiraceae*, *Coprococcus* and *Faecalibacterium* • Tatarstan: ↑ *Roseburia*, *Coprococcus*, *Faecalibacterium* and *Ruminococcus* genera • Tyva: ↑ *Bifidobacterium*	Tyakht *et al.* (2013)
China	Five locations • Northeast (Harbin) • Central (Zhengzhou) • East (Wuxi) • Southwest (Chengdu) • Ürümqi	• young healthy adults • n=314	• details dietary records were not provided but individuals from rural area of each locations practiced typical farming or pastoral lifestyle	• 16S rRNA pyro-sequencing (V5-V6)	• Overall: *Phascolarctobacterium* of *Firmicutes* most predominant • Core genera: *Roseburia*, *Bacteroides*, *Blautia*, *Faecalibacterium*, *Clostridium*, *Subdoligranulum*, *Ruminococcus*, and *Coprococcus* from SCFA-producing lineages • Tibetan group has most unique genera compared to all others ethnics • Rural areas: ↑ *Prevotella* and *Xylanibacter*	Zhang *et al.* (2015)
	• Babu district, He Zhou (Southern China)	• healthy • n=134 (Han, n=47; Zhuang, n=28;Yao, n=59)	• frequencies of 21 types regular food intakes	• 16S rRNA Illumina MiSeq (V3-V4)	• Overall: ↑ *Bacteroides* and *Prevotella* • Hans: ↑ *Megamonas* significantly (p <0.05) due to high intake of beans	Liao *et al.* (2018)
	• Beijing (Northern) • Jinan (Eastern) • Zigong (Southwest)	• healthy adults • n=131	• details dietary records was not provided except fruits, yogurt and drink intakes	• 16S rRNA Illumina MiSeq (V3-V4)	• Overall: ↑ *Bacteroides* • Core genera: *Alistipes*, *Bacteroides*, *Blautia*, *Clostridium*, *Coprococcus*, *Escherichia/Shigella*, *Faecalibacterium*, *Gemmiger*, *Parasutterella*, *Roseburia* and *Ruminococcuscore*	Zhang *et al.* (2019)
	• Zhejiang (Eastern China)	• healthy • n=10	• details dietary records were not provided	• 16S rRNA pyro-sequencing (V3)	• Overall: ↑ *Faecalibacterium*	Ling *et al.* (2013)
	• Shanghai, Jiangyin (Eastern China)	• healthy, native • n=29	• high fat diet (≥40% of dietary calories were from fat) • low fat diet (>40%) • fats were mainly from cooking oil, data of oil types were not provided	• 16S rRNA Illumina MiSeq (V3-V4)	• Faecal samples: ↑ *Prevotella* and *Abiotrophia* • Colon mucosa tissue ↑ unclassified genus of S24-7 from HDF compared to LFD	Qian *et al.* (2018)

Country	Region	Study population; Sample size	Diets/ lifestyle	Sequencing method	Gut microbiota compositions	Reference
South Korea	• Seoul (inland) • Jeju Island	• healthy, elderly • n=9 • healthy, elderly • n=10	• 24 hr diet recall • subjects from Jeju Island consumed significantly (p<0.05) more animal lipid than those from Seoul	• 16S rRNA Ion Torrent (V1-V2)	• ↑ *Catenibacterium* • ↑ *Butyricimonas*	Shin *et al.* (2016)
Korea	NA	• healthy • n=20	• details dietary records were not provided	• 16S rRNA pyro-sequencing (V1-V3)	• Overall: ↑ *Faecalibacterium, Prevotella* and *Bacteroides* • Core gut microbiota: *Bacteroides, Parabacteroides, Provotella, Clostridium, Eubacterium, Facalibacterium, Lachnospira, Oscillibacter, Roseburia, Ruminococcus, Subdoligranulum,* uncultivated human intestinal clones and *Fusobacterium*	Nam *et al.* (2011)
Japan	• Sendai city	• healthy adults • n=32	• traditional Japanese diet: soya products, fishes, vegetables, fruit, green tea, seaweed, mushrooms, rice, condiments, soup stock 'Dashi', fermented seasoning (soya sauce, miso, vinegar, mirin and sake) • modern Japanese diet contains deep fried dishes, grilled fishes added salts, soya sauce, butter, chesses, sugars	• 16S rRNA Illumina MiSeq (V3-V4)	• Traditional Japanese diet: ↑ *Sutterella,* ↓ unclassified *Lachnospiraceae, Parabacteroides,* unclassified *Rikenellaceae*	Kushida *et al.* (2019)
	• Azabu University (Eastern Japan)	• healthy adults • n=106	• details dietary records were not provided	• 16S rRNA Ion Torrent, pyro-sequencing, Illumina MiSeq (V1-V2)	• ↑ *Bifidobacterium* • ↓ *Methanobrevibacter smithii*	Nishijima *et al.* (2016)
Thailand	• NA	• healthy adults • vegetarian • non-vegetarian	• santi-Asoke vegetarian diets: vegetables, fruits • ovo-lacto, ovo, lacto vegetarian diets: include eggs, milk, and yoghurt • non-vegetarian diet: pork, fish and chicken, eggs, yoghurt, milk, fruits	• 16S rRNA pyro-sequencing (V6-V8)	• Overall: ↑ *Faecalibacterium prausnitzii* and *Gemmiger formicilis* • Vegetarian diets: ↑ *Clostridium nexile, Eubacterium eligens,* and *Prevotella copri* • Non-vegetarian diets: ↑ *Collinsella aerofaciens, Ruminococcus torques,* various species of *Bacteroides, Parabacteroides, Escherichia, Clostridium* and *Eubacterium*	Ruengsomwong *et al.* (2016)
Indonesia	• Bali	• healthy adults • n=41	• white rice, bread, fried tofu, chicken, palm oil, tempeh, egg, pork, fish, soto, milk and papaya	• 16S rRNA Illumina MiSeq (V4)	• Overall: ↑ *Prevotella*-rich (type-P) and *Bacteroides*-rich (type-B)	Febinia *et al.* (2020)

Note: n - number of subjects; FFQ - food frequency questionnaire; V - variable region; HFD - high fat diet; LDF - low fat diet; NA - not available; SCFA - short-chain fatty acids; 16S rRNA - 16S ribosomal RNA.

China and India have varying geographical locations and thus, create diverse dietary habits in their people and compositions of gut microbiota. In China, the predominated core genus was *Phascolarctobacterium* from the phylum of *Firmicutes* (Zhang *et al.*, 2015), which is also in high abundance in Russian population (Tyakht *et al.*, 2013). Other core genera in Chinese population include *Roseburia, Bacteroides, Faecalibacterium* and other bacteria from SCFA-producing lineages (*Table 1*).

Contrary in India, *Prevotella copri* and *Faecalibacterium prausnitzii* (Pulipati *et al.*, 2020) from the butyrate producing bacteria lineages (Kaur *et al.*, 2020), are the most predominant core bacterial genera as identified in the 'Landscape of Gut Microbiome-Pan India Exploration' (LogMPIE) study results suggesting that the majority of Indian populations are still adhering to the whole grains, legumes and plant-based diet (Kaur *et al.*, 2020). However, this result was not in agreement with the smaller cohort study conducted in unique geographical locations (Das *et al.*, 2018).

Das *et al.* (2018) reported that gut microbiota compositions of non-vegetarian adults in high altitude areas of Leh was predominated by *Provetella* compared with vegetarian or ovo-vegetarian diet from sea level Ballabhgarh urban region (Das *et al.*, 2018). These results suggest that *Provetella* has distinct oligo types that mediate the carbohydrate-enzyme activities in different diets (Das *et al.*, 2018; Kaur *et al.*, 2020).

The diversity of gut microbiota in Leh and Ballabhgarh populations was significantly associated with the types of dietary fat consumption, especially from cooking oils, butter and milk (*Table 1*). Individuals from Leh has high sunflower oil intake but low in dairy intake. Hence, *Roseburia* (Devillard *et al.*, 2007) and *Sporobacter* (Pu *et al.*, 2016) which are able to degrade PUFA oil, especially linoleic acids, were identified as the predominated gut bacteria in Leh individuals; but genera such as *Pseudomonas* and *Bifidobacterium* which have been associated with dairy products were rare. Furthermore, *Collinsella* was identified as the most abundant genus in Ballabhgarh subjects who have high ghee consumption (Das *et al.*, 2018).

Comparison of Gut Microbiota Profile between Countries but on Similar Diets

Although *Prevotella* has been related with high plant-based diet intake, but the core genera of individuals from different countries following the same diet are different (*Table 1*). For instance, vegetarian groups from Thailand were high in abundance of *Clostridium nexile, Eubacterium eligens* and *Prevotella copri* which was different from residence in Leh, India that made up of *Prevotella, Coprococcus, Clostridium, Ruminococcus,*

Howardella, Erysopelotrichaceae and *Peptococcus* (*Table 1*). Similarly, *Spirochaetae* was enriched in Arabs who consumed fermented foods made from pearl millet flour with starter culture (Angelakis *et al.*, 2016) but absent in Japanese who were also on high fermented food intake from soya (Kushida *et al.*, 2019).

Megamonas was the predominant bacteria in Hans population who have high bean intake (Liao *et al.*, 2018) which is rich with unsaturated fats. *Megamonas* was also of the core species in Russian (Tyakht *et al.*, 2013) and in Ballabhgarh, Indian populations (Das *et al.*, 2018). Linear discriminant analysis (LDA) effect size (Lefse) analysis could be used to cluster and identify the potential biomarkers from profile of these gut bacteria of distinct populations (Jain *et al.*, 2018).

These studies provided a good foundation of gut microbiota profile to establish localised baseline from complex dietary patterns in Asia and to predict metabolic disorder in niche community. In Southeast Asia, studies regarding the microbial diversity of healthy adults related to the gut health is limited, but effect of dietary pattern on gut microbiota profile in Bali (Febinia *et al.*, 2020) and a comparison on effects of vegetarian diet on gut microbiota on healthy adults in Thailand (Ruengsomwong *et al.*, 2016) are among the few reported works of healthy adults on habitual diet. More comprehensive studies should be conducted to establish the baseline of gut microbiota profile in this region.

SIGNIFICANCE OF SFA, MUFA AND PUFA ON COMPOSITIONS OF GUT MICROBIOTA COMPOSITION

Dietary fat is composed of 90% triglycerides (TG) that are made up of three fatty acid chains linked to a glycerol backbone. A substantial amount of the fatty acid is released by cleavage of the TG by the lingual lipase in the mouth and gastric lipases in the stomach (Mu and Høy, 2004). The remaining TG are almost completely hydrolysed in the proximal small intestine by the *sn*-1, 3 stereospecific pancreatic lipase and yield two free fatty acids (FFA) and a 2-monoacylglycerol (2-MG) (Rogalska *et al.*, 1990). The ionised FFA and 2-MG mix with the bile acid to form mixed micelles with phospholipids and up to 95% of these fatty acids are absorbed by the epithelial cells in the small intestine. These fatty acids are then randomly re-esterified and re-synthesised through a predominant 2-MG pathway to form new TG in the distal small intestine. These plasma TG are then packed with cholesterol, phospholipids, apoproteins to form chylomicrons and absorbed into the lymphatic and blood circulation systems. The remaining fatty acids reach the colon, where they are metabolised by the community of gut microbiota (Bauer *et al.*, 2005).

Dietary Fats Saturation

Dietary fats have fatty acids that vary in chain length, saturation, and positional distribution of fatty acids. Fatty acids are classified into SFA, MUFA, or PUFA based on their degree of saturation. Population or intervention studies of the effects of SFA, MUFA and PUFA rich diets on gut microbiota composition have either been reviewed systematically and extensively (Mokkala *et al.*, 2019; Yang *et al.*, 2020b).

SFA Rich Diet

Generally, a high SFA intake (18E% of SFA, >35E% of total fat) is inversely correlated with bacteria diversity and richness indices (Fava *et al.*, 2013), and higher *Firmicutes* to *Bacteroidetes* (F/B) ratio (David *et al.*, 2014). High F/B ratio has been associated with obese individuals (Kasai *et al.*, 2015). A study involving monozygotic twins shows that habitual SFA intake resulted in similar *Bacteroides* spp. profiles (Simões *et al.*, 2013) but a higher number of *Faecalibacterium prausnitzii* was demonstrated to reduce intestinal inflammation by inducing goblet cell proliferation and mucus production (Fava *et al.*, 2013) to maintain the epithelial integrity (Wrzosek *et al.*, 2013). Although SFA is frequently correlated with increased incidences of CVD and colon cancer, meta-analysis and systematic reviews do not support this claim (Dehghan *et al.*, 2017; Kang *et al.*, 2020; Kim and Park, 2018).

MUFA Rich Diet

A 24 weeks MUFA rich diet did not result in any significant changes in body mass index (BMI), waist circumference, body fat percentage, blood pressure or insulin resistant in 88 adults with metabolic syndrome (Fava *et al.*, 2013). High MUFA consumption also did not significantly affect bacteria richness as measured by Shannon, Chao1 and abundance based coverage (ACE) indices, the phylum distribution or F/B ratio (Pu *et al.*, 2016).

After a year of adhering to a MUFA-rich Mediterranean diet, 20 obese patients with coronary heart disease showed no significant difference in plasma glucose, and insulin and lipoprotein profile but enhanced significant growth in colonic *Roseburia, Oscillospira, Faecalibacterium prausnitzii* and *Parabacteroides distasonis* compared to the baseline using 16S rRNA pyrosequencing (454 Roche) (Haro *et al.*, 2016). However, another study reported that a MUFA-rich Mediterranean diet reduced the number of colonic *Prevotella* in obese healthy adults but increased it in adults with metabolic syndrome (Pu *et al.*, 2016). Individuals who had highly adhered

to the Mediterranean diet demonstrated lower *Escherichia coli* counts and increased commercial *Bifodobacteria* to *E. coli* ratio, which is an established healthy gut indicator (Mitsou *et al.*, 2017). The enrichment of these SCFA-producing and beneficial bacteria could also be related to the Mediterranean diet which consists of a high concentration of polyphenols and other phytochemicals found in vegetables and fruits (Muralidharan *et al.*, 2019).

PUFA Rich Diet

PUFA-based diets showed inconsistent results on gut microbiota compositions. Randomised controlled trials have demonstrated that high *n*-3 long-chain PUFA diets did not significantly alter bacterial diversity, richness, or phylum distribution compared to the control diet. The study duration varied from 30 days for adults with metabolic syndrome (Pu *et al.*, 2016), to 42 days for healthy overweight individuals (Rajkumar *et al.*, 2014), and to six months for patients with Type 2 diabetes (Balfegó *et al.*, 2016). A high dose of eicosapentaenoic acid (EPA) and docosahexaenoic acid (DHA) supplements failed to demonstrate any significant impact on the composition of gut bacteria (Watson *et al.*, 2017), although these fatty acids have been associated with lower plasma inflammatory markers such as C-creative protein (CRP) (Yang *et al.*, 2020a).

The effect of PUFA diet demonstrated contradictory results on the compositions of gut microbiota. High habitual intake of PUFA resulted in an increase in bacteria diversity in overweight middle-aged adults (Menni *et al.*, 2017) and this diet also promoted the abundance of *Actinobacteria* but lowered *Firmicutes* in the gut of postpartum women (Mandal *et al.*, 2016). Diets enriched with *n*-3 long-chain PUFA was positively associated with the *Lactobacillus* group, whereas *n*-6 long-chain PUFA was negatively correlated with the abundance of *Bifidobacteria* in 11 healthy and 29 overweight or obese monozygotic twin (Simões *et al.*, 2013). Reyes *et al.* (2016) reported that high habitual intake of unsaturated fatty acid and fibre diet increased the content of *Bifidobacterium longum* in young adults, with the increase being higher in lean participants than in overweight or obese participants (Reyes *et al.*, 2016). In men, the abundance of the genus *Blautia* in serum was negatively associated with *n*-3 and *n*-6 PUFA content (Org *et al.*, 2017). The abundance of *Blautia* was increased in participants with higher BMI (Liu *et al.*, 2019; Org *et al.*, 2017), or higher levels of low-density lipoprotein (LDL) and waist circumference in Chinese adults (Zeng *et al.*, 2014), but inversely associated with visceral fat accumulation in Japanese adults (Ozato *et al.*, 2019).

The discrepancy in PUFA diet studies is probably related to the study duration, variation in

the amount and sources of fats, and the pre-existing health condition of the subjects. This is proven in a study on premature infants that were fed with a mixture of fish oil and safflower oil via enterostomies for nine weeks, and the outcomes were compared to that of infants who had received standard treatment (Young *et al.*, 2017). The fish oil-enriched diet yielded varying gut microbial communities at different points in time between the study groups (Young *et al.*, 2017). Different functional pathways were inferred using microbial gene function analysis, and it revealed that the changes in the diversity of microbiota are associated with pathways related to lipid metabolism, followed by pathways related to butyrate and also specific amino acids metabolism between the intervention groups (Young *et al.*, 2017).

These studies showed inconsistent effects of fatty acid saturation on the diversity of gut microbiota and this could be due to the effect of stereo-specificity of fatty acid chains on TG, the sequencing and bioinformatic analysis methods.

EFFECTS OF STEREOSPECIFICITY ON TG OF PALM OIL AND GUT MICROBIOTA

Recently, palm oil has been identified as one of the most affordable EAT-Lancet diets along with transformation toward sustainable global food system (Hirvonen *et al.*, 2019). Palm oil is a unique oil, in which it has almost equal percentages of saturated and unsaturated fatty acids compositions (Koushki *et al.*, 2015) on the TG backbone. Similar to other vegetable oils, the *sn*-2 position in the TG of palm oil is mainly occupied by unsaturated fatty acids (May and Nesaretnam, 2014; Ong and Goh, 2002). However, in certain animal fats, particularly in lard, the *sn*-2 position is occupied by SFA (*Table 2*).

Increasing evidence demonstrates that the stereospecificity of fatty acids in TG molecules affect its absorbability (Ramíreza *et al.*, 2001). Differing from other vegetable oils, the *sn*-1,3 position of palm oil is predominated by long-chain SFA, C18:0 and C16:0. This is evidenced by a study in which high fat palm oil diet was fed to mice and it was found that a high palm oil diet (45% E fat) resulted in overflow of palm oil into the distal intestine, probably due to lack of absorptivity of long-chain fatty acids which then trigger dysbiosis (Wit *et al.*, 2012) rather than the type of diet itself. Therefore, clinical human study using palm oil at recommended dietary intake level should be conducted to avoid pre-mature claim.

The longer fatty acid chains at *sn*-1,3 position have a low tendency of fat deposition in the adipose tissue compared to high PUFA oils in animal studies (Gouk *et al.*, 2013; 2014). It is hypothesised that at certain threshold concentration, long-chain SFA at the *sn*-1,3 position are poorly absorbed in the small intestine due to these fatty acids having a higher melting point than the core human body temperature and therefore are more prone to form insoluble calcium soap in the high pH small intestinal environment. However, the effect of fatty acid positional distribution on palm oil intake from the habitual diet composition of gut microbiota in humans is unknown.

FUTURE PROSPECTIVES

Dietary fats alter certain species of gut microbiota and their metabolites following regular diet intake. If dietary fat could alter the gut microbiota compositions alone, the bacteria profile in Malaysians may have similar relative abundance to SFA and MUFA diets, but a lower similarity to PUFA diet. The simplified bacteria profile may consist of high abundance of *Bacteroides* spp. (phylum of *Bacteroidetes*) as identified in high SFA; *Roseburia, Oscillospira, Faecalibacterium prausnitzii* (phylum of *Firmicutes*), and *Parabacteroides distasonis* (phylum of *Bacteroidetes*) from MUFA diet; and *Actinobacteria,* and *Lactobacillus (Firmicutes)* as identified in high PUFA diet. However, more complex bacteria composition is anticipated as Malaysia is a multiracial country comprising of different ethnicities and cultures, each having their unique heritage food, which is also influenced by culinary attributes within Malaysia and neighbouring countries. Diversity in food, ethnicities and culture may give rise to a unique gut microbiota profile in Malaysians. Moreover, palm oil remains the most widely consumed oil in Malaysia (Kushairi *et al.*, 2019), although other imported vegetable oils are available in the Malaysian market. Therefore, the effects of fatty acids saturation and stereo-specificity of various cooking oils on Malaysian population's gut microbiota profiles might be of interest to explore.

High throughput sequencing and analytical technologies coupled with extensive bioinformatics database using analytical software (Onywera and Meiring, 2020; Zhao *et al.*, 2018) had accelerated the process of identifying colonic bacteria and predicting the functional profiles of metabolites in establishing the baseline of gut bacteria profile of Malaysian. The hope is that changes of the identified species or metabolite from the baseline could be used as a non-invasive biomarker for clinical diagnosis of diet-related cardio-metabolic or non-communicable diseases in the early stage.

TABLE 2. STEREOSPECIFIC POSITIONING OF FATTY ACID (MOL %) IN TRIACYL-*SN*-GLYCEROLS OF PLANT-BASED OIL AND ANIMAL-BASED FAT

Oil/ Fat	Position	Fatty acid (mol %)							
		14:0	16:0	16:1	18:0	18:1	18:2	18:3	20-24
Peanut	TG		9		3	58	23		7
	1		14		5	59	19		4
	2		2		trace	59	39		1
	3		11		5	57	10		15
Soybean	TG		3		2	26	17	10	43
	1		4		2	23	11		53
	2		1			37	36	6	6
	3		4		3	17	4	20	70
Linseed	TG		9		4	24	54	8	
	1		14		6	23	48	9	
	2		1		trace	22	70	7	
	3		13		6	28	45	9	
Corn	TG	11		2	29	57	1		
	1	1		3	28	50	1		
	2	18		trace	27	70	1		
	3	2		3	31	52	1		
Olive	TG		10		2	76	10	1	
	1		13		3	72	10	1	
	2		1			83	14	1	
	3		17		4	74	5		
Palm	TG		48		4	36	10		
	1		60		3	27	9		
	2		13		trace	68	18		
	3		72		8	14	3		
Cacao butter	TG		24		35	36	3	trace	1
	1		34		50	12	1	1	1
	2		2		2	87	9		
	3		37		53	9	trace		2
Beef	TG	5	27	6	17	33	5	1	
	1	4	41	6	177	20	4	1	
	2	9	17	6	9	41	5	1	
	3	1	22	6	24	37	5	1	
Lard	TG	2	27	3	13	45	9		
	1	1	10	2	30	51	6		
	2	4	72	5	2	13	3		
	3	-	trace	2	7	70	18		
Chicken	TG	1	30	6	6	45	11	1	
	1	1	47	7	8	31	5	1	
	2	trace	13	5	6	55	19	1	
	3	1	31	7	3	49	8	1	
Mutton#	TG	3	22	2	35	36	2		
	1	1	35	2	47	4	-		
	2	4	14	2	15	52	5		
	3	3	16	1	42	26	2		

Note: Trace = <0.5%, TG = intact triacylglycerols, #Results are listed for *cis*-18:1 isomers only; *trans*-18:1 was present in positions *sn*-1, *sn*-2 and *sn*-3 as 5%, 2% and 6%, respectively.

Source: Brockerhoff and Yurkowski (1991); Brockerhoff *et al.* (1966); Christie and Moore (1971).

REFERENCES

Almeida, A; Mitchell, A L; Boland, M; Forster, S C; Gloor, G B; Tarkowska, A; Lawley, T D and Finn, R D (2019). A new genomic blueprint of the human gut microbiota. *Nature, 568*: 499-504.

Angelakis, E; Yasir, M; Bachar, D; Azhar, E I; Lagier, J C; Bibi, F; Jiman-Fatani, A A; Alawi, M; Bakarman, M A; Robert, C and Raoult, D (2016). Gut microbiome and dietary patterns in different Saudi populations and monkeys. *Sci. Rep., 6*: 32191.

Balfegó, M; Canivell, S; Hanzu, F A; Sala-Vila, A; Martínez-Medina, M; Murillo, S; Mur, T; Ruano, E G; Linares, F; Porras, N; Valladares, S; Fontalba, M; Roura, E; Novials, A; Hernández, C; Aranda, G; Sisó-Almirall, A; Rojo-Martínez, G; Simó, R and Gomis, R (2016). Effects of sardine-enriched diet on metabolic control, inflammation and gut microbiota in drug-naïve patients with Type 2 diabetes: A pilot randomized trial. *Lipids Health Dis., 18*: 78.

Bauer, E; Jakob, S and Mosenthin, R (2005). Principles of physiology of lipid digestion. *Asian-Aust J. Anim Sci., 18*: 282-295.

Brockerhoff, H and Yurkowshi, M (1991). Stereospecific analyses of several vegetable fats. *J. Lipid Res., 7*: 62-64.

Brockerhoff, H; Hoyle, R J and Wolmark, N (1966). Positional distribution of fatty acids in triglycerides of animal depot fats. *Biochim. Biophys. Acta - Lipids Lipid Metab., 116*: 67-72.

Christie, W W and Moore, J H (1971). Structures of triglycerides isolated from various sheep tissues. *J. Sci. Food Agric., 22*: 120-124.

Clavel, T; Desmarchelier, C; Haller, D; Gérard, P; Rohn, S; Lepage, P and Daniel, H (2014). Intestinal microbiota in metabolic diseases. *Gut Microbes., 5*: 544-551.

Das, B; Ghosh, T S; Kedia, S; Rampal, R; Saxena, S; Bag, S; Mitra, R; Dayal, M; Mehta, O; Surendranath, A; Travis, S P L; Tripathi, P; Nair, G B and Ahuja, V (2018). Analysis of the gut microbiome of rural and urban healthy Indians living in sea level and high-altitude areas. *Sci. Rep., 8*: 10104.

David, L A; Maurice, C F; Carmody, R N; Gootenberg, D B; Button, J E; Wolfe, B E; Ling, A V; Devlin, A S; Varma, Y; Fischbach, M A; Biddinger, S B; Dutton, R J and Turnbaugh, P J (2014). Diet rapidly and reproducibly alters the human gut microbiome. *Nature, 505*: 559-563.

De Filippo, C; Cavalieri, D; Paola, M D; Ramazzotti, M; Poullet, J B; Massart, S; Collini, S; Pieraccini, G and Lionetti, P (2010). Impact of diet in shaping gut microbiota revealed by a comparative study in children from Europe and rural Africa. *Africa Proc. Natl. Acad. Sci. USA., 107*: 14691-14696.

Dehghan, M; Mente, A; Zhang, X H; Swaminathan, S; Li, W; Mohan, V; Iqbal, R; Kumar, R; Wentzel-Viljoen, E; Rosengren, A; Amma, L I; Avezum, A; Chifamba, J; Diaz, R; Khatib, R; Lear, S; Lopez-Jaramillo, P; Liu, X Y; Gupta, R; Mohammadifard, N; Gao, N; Oguz, A; Ramli, A S; Seron, P; Sun, Y; Uba, A; Tsolekile, L; Wielgosz, A; Yusuf, R; Yusufali, A H; Teo, K K; Rangarajan, S; Dagenais, G; Bangdiwala, S I; Islam, S; Anand, S S; Yusuf, S and Investigators, P U R E P S (2017). Associations of fats and carbohydrate intake with cardiovascular disease and mortality in 18 countries from five continents (PURE): A prospective cohort study. *The Lancet, 390*: 2050-2062.

Devillard, E; Mcintosh, F M; Duncan, S H and Wallace, R J (2007). Metabolism of linoleic acid by human gut bacteria: Different routes for biosynthesis of conjugated linoleic acid. *J. Bacteriol Res., 189*: 2566-2570.

Dhakan, D B; Maji, A; Sharma, A K; Saxena, R; Pulikkan, J; Grace, T; Gomez, A; Scaria, J; Amato, K R and Sharma, V K (2019). The unique composition of Indian gut microbiome, gene catalogue, and associated fecal metabolome deciphered using multi-omics approaches. *GigaScience, 8*: 1-20.

Fava, F; Gitau, R; Griffin, B A; Gibson, G R; Tuohy, K M and Lovegrove, J A (2013). The type and quantity of dietary fat and carbohydrate alter faecal microbiome and short-chain fatty acid excretion in a metabolic syndrome 'at-risk' population. *Int. J. Obes., 37*: 216-223.

Febinia, C; Malik, S; Djuwita, R; Weta, I; Wihandani, D; Maulida, R; Sudoyo, H and Holmes, A (2020). Population stratification in the gut microbiota of Bali is associated with transitional lifestyle. *Research Square General Microbiol.* DOI: 10.21203/rs.3.rs-40341/v1.

Fontana, L; Meyer, T E; Klein, S and Holloszy, J O (2004). Long-term calorie restriction is highly effective in reducing the risk for atherosclerosis in humans. *Proc. Natl. Acad. Sci. USA., 101*: 6659-6663.

Ganesan, K; Chung, S K; Vanamala, J and Xu, B (2018). Causal relationship between diet-induced gut microbiota changes and diabetes: A novel strategy to transplant *Faecalibacterium prausnitzii* in preventing diabetes. *Int. J. Mol. Sci., 19*: 3720.

Ghosh, S S; Wang, J; Yannie, P J and Ghosh, S (2020). Intestinal barrier dysfunction, LPS translocation and disease development. *J. Endocrine Soc., 4*: 1-15.

Gouk, S W; Cheng, S F; Mok, J S L; Ong, A S H and Chuah, C H (2013). Long-chain SFA at the *sn*-1, 3 positions of TAG reduce body fat deposition in C57BL/6 mice. *Br. J. Nutr., 110*: 1987-1995.

Gouk, S W; Cheng, S F; Ong, A S H and Chuah, C H (2014). Stearic acids at *sn*-1, 3 positions of TAG are more efficient at limiting fat deposition than palmitic and oleic acids in C57BL/6 mice. *Br. J. Nutr., 111*: 1174-1180.

Guo, X; Li, J; Tang, R; Zhang, G; Zeng, H; Wood, R J and Liu, Z (2017). High fat diet alters gut microbiota and the expression of paneth cell-antimicrobial peptides preceding changes of circulating inflammatory cytokines. *Mediators of Inflammation, 2017*: 9474896.

Gupta, V K; Paul, S and Dutta, C (2017). Geography, ethnicity or subsistence-specific variations in human microbiome composition and diversity. *Front Microbiol., 8*: 1162-1162.

Haro, C; Rangel-Zúñiga, O A; Alcalá-Díaz, J F; Gómez-Delgado, F; Pérez-Martínez, P; Delgado-Lista, J; Quintana-Navarro, G M; Landa, B B; Navas-Cortés, J A; Tena-Sempere, M; Clemente, J C; López-Miranda, J; Pérez-Jiménez, F and Camargo, A (2016). Intestinal microbiota is influenced by gender and body mass index. *PLoS ONE, 11*: e0154090.

He, Y; Wu, W; Zheng, H M; Li, P; Mcdonald, D; Sheng, H F; Chen, M X; Chen, Z H; Ji, G Y; Zheng, Z D X; Mujagond, P; Chen, X J; Rong, Z H; Chen, P; Lyu, L Y; Wang, X; Wu, C B; Yu, N; Xu, Y J; Yin, J; Raes, J; Knight, R; Ma, W J and Zhou, H W (2018). Regional variation limits applications of healthy gut microbiome reference ranges and disease models. *Nature Med., 24*: 1532-1535.

Hirvonen, K; Bai, Y; Headey, D and Masters, W A (2019). Affordability of the EAT–Lancet reference diet: A global analysis. *Lancet Glob Health, 7*: 1-8.

Illiano, P; Brambilla, R and Parolini, C (2020). The mutual interplay of gut microbiota, diet and human disease. *FEBS Journal, 287*: 833-855.

Jia, F; Peng, S; Green, J; Koh, L; Chen, X and Chen, X (2020). Soybean supply chain management and sustainability: A systematic literature review. *J. Clean Prod., 255*: 120254.

Jain, A; Li, X H and Chen, W N (2018). Similarities and differences in gut microbiome composition correlate with dietary patterns of Indian and Chinese adults. *AMB Expr., 8*: 104.

Kang, Z Q; Yang, Y and Xiao, B (2020). Dietary saturated fat intake and risk of stroke: Systematic review and dose – response meta-analysis of prospective cohort studies. *Nutr. Metab Cardiovas Dis., 30*: 179-189.

Kasai, C; Sugimoto, K; Moritani, I; Tanaka, J; Oya, Y; Inoue, H; Tameda, M; Shiraki, K; Ito, M; Takei, Y and Takase, K (2015). Comparison of the gut microbiota composition between obese and non-obese individuals in a Japanese population, as analysed by terminal restriction fragment length polymorphism and next-generation sequencing. *BMC Gastroenterol., 15*: 100.

Kaur, K; Khatri, I; Akhtar, A; Subramanian, S and Ramya, T N C (2020). Metagenomics analysis reveals features unique to Indian distal gut microbiota. *PLoS ONE, 15*: e0231197.

Kushairi, A; Abdullah, M O; Nambiappan, B; Hishamuddin, E; Zanal Bidin, M N I; Ghazali, R; Subramaniam, V; Sundram, S and Parveez, G K A (2019). Oil palm economic performance in Malaysia and R&D progress in 2018. *J. Oil Palm Res., 31*: 165-194.

Kim, M and Park, K (2018). Dietary fat intake and risk of colorectal cancer: A systematic review and meta-analysis of prospective studies. *Nutrients, 10*: 1963.

Koushki, M; Nahidi, M and Cheraghali, F (2015). Physico-chemical properties, fatty acid profile and nutrition in palm oil. *Arch. Adv. Biosci., 6*: 117-134.

Kriss, M; Hazleton, K Z; Nusbacher, N M; Martin, C G and Catherine, A L (2018). Low diversity gut microbiota dysbiosis: Drivers, functional implications and recovery. *Curr. Opin Microbiol., 44*: 34-40.

Kushida, M; Sugawara, S; Asano, M; Yamamoto, K; Fukuda, S and Tsuduki, T (2019). Effects of the 1975 Japanese diet on the gut microbiota in younger adults. *J. Nutr. Biochem., 64*: 121-127.

Leeming, E R; Johnson, A J; Spector, T D and Roy, C L (2019). Effect of diet on the gut microbiota: Rethinking intervention duration. *Nutrients, 11*: 2862.

Liao, M; Xie, Y; Mao, Y; Lu, Z; Tan, A; Wu, C; Zhang, Z; Chen, Y; Li, T; Ye, Y; Yao, Z; Jiang, Y; Li, H; Li, X; Yang, X; Wang, Q and Mo, Z (2018). Comparative analyses of fecal microbiota in Chinese isolated Yao

population, minority Zhuang and rural Han by 16S rRNA sequencing. *Sci. Rep., 8*: 1142.

Ling, Z; Liu, X; Luo, Y; Yuan, L; Nelson, K E; Wang, Y; Xiang, C and Li, L (2013). Pyrosequencing analysis of the human microbiota of healthy Chinese undergraduates. *BMC Genomics, 14*: 390.

Liu, Y; Qin, S T; Song, Y L; Feng, Y; Lv, N; Xue, Y; Liu, F; Wang, S X; Zhu, B L; Ma, J M and Yang, H X (2019). The perturbation of infant gut microbiota caused by cesarean delivery is partially restored by exclusive breastfeeding. *Front Microbiol., 10*: 598.

Mandal, S; Godfrey, K M; Mcdonald, D; Treuren, W V; Bjørnholt, J V; Midtvedt, T; Moen, B; Rudi, K; Knight, R; Brantsæter, A L; Peddada, S D and Eggesbø, M (2016). Fat and vitamin intakes during pregnancy have stronger relations with a pro-inflammatory maternal microbiota than does carbohydrate intake. *Microbiome, 4*: 55.

May, C Y and Nesaretnam, K (2014). Research advancements in palm oil nutrition. *Eur. J. Lipid Sci. Tech., 116*: 1301-1315.

Menni, C; Jackson, M A; Pallister, T; Steves, C J; Spector, T D and Valdes, A M (2017). Gut microbiome diversity and high-fibre intake are related to lower long-term weight gain. *Int. J. Obes., 41:* 1099-1105.

Mirmonsef, P; Zariffard, M R; Gilbert, D; Makinde, H; Landay, A L and Spear, G T (2012). Short-chain fatty acids induce pro-inflammatory cytokine production alone and in combination with Toll-like receptor ligands. *Am. J. Reprod. Immunol., 67*: 391-400.

Mitsou, E K; Kakali, A; Antonopoulou, S; Mountzouris, K C; Yannakoulia, M; Panagiotakos, D B and Kyriacou, A (2017). Adherence to the Mediterranean diet is associated with the gut microbiota pattern and gastrointestinal characteristics in an adult population. *Br. J. Nutr., 117*: 1645-1655.

Mokkala, K; Houttu, N; Cansev, T and Laitinen, K (2019). Interactions of dietary fat with the gut microbiota: Evaluation of mechanisms and metabolic consequences. *Clin. Nutr., 39*: 994-1018.

Moreno-Indias, I; Sánchez-Alcoholado, L; García-Fuentes, E; Cardona, F; Queipo-Ortuño, M I and Tinahones, F J (2016). Insulin resistance is associated with specific gut microbiota in appendix samples from morbidly obese patients. *Am. J. Transl Res., 8*: 5672-5684.

Mozaffarian, D (2016). Dietary and policy priorities for cardiovascular disease, diabetes, and obesity: A comprehensive review. *Circulation, 133*: 187-225.

Mu, H and Høy, C E (2004). The digestion of dietary triacylglycerols. *Prog. Lipid Res., 43*: 105-133.

Muegge, B D; Kuczynski, J; Knights, D; Clemente, J C; González, A; Fontana, L; Henrissat, B; Knight, R and Gordon, J I (2011). Diet drives convergence in gut microbiome functions across mammalian phylogeny and within humans. *Science, 332*: 970-974.

Muralidharan, J; Galiè, S; Hernández-Alonso, P; Bulló, M and Salas-Salvadó, J (2019). Plant based fat, dietary patterns rich in vegetable fat and gut microbiota modulation. *Front Nutr., 6*: 157.

Murphy, E A; Velazquez, K T and Herbert, K M (2015). Influence of high-fat diet on gut microbiota. *Curr. Opin Clin. Nutr. Metab. Care, 18*: 515-520.

Nam, Y D; Jung, M J; Roh, S W; Kim, M S and Bae, J W (2011). Comparative analysis of Korean human gut microbiota by barcoded pyrosequencing. *PLoS ONE, 6*: e22109-e22109.

Nishijima, S; Suda, W; Oshima, K; Kim, S W; Hirose, Y; Morita, H and Hattori, M (2016). The gut microbiome of healthy Japanese and its microbial and functional uniqueness. *DNA Res., 23*: 125-133.

O'Keefe, S J (2016). Diet, microorganisms and their metabolites, and colon cancer. *Nat. Rev. Gastroenterol Hepatol., 13*: 691-706.

Ong, S H A and Goh, S H (2002). Palm oil: A healthful and cost-effective dietary component. *Food Nutr. Bull., 23*: 11-22.

Onywera, H and Meiring, T L (2020). Comparative analyses of Ion Torrent V4 and Illumina V3-V4 16S rRNA gene metabarcoding methods for characterization of cervical microbiota: Taxonomic and functional profiling. *Sci. African, 7*: e00278.

Org, E; Blum, Y; Kasela, S; Mehrabian, M; Kuusisto, J; Kangas, A J; Soininen, P; Wang, Z; Ala-Korpela, M; Hazen, S L; Laakso, M and Lusis, A J (2017). Relationships between gut microbiota, plasma metabolites and metabolic syndrome traits in the METSIM cohort. *Genome Biol., 18*: 70.

Ou, J; Carbonero, F; Zoetendal, E G; Delany, J P; Wang, M; Newton, K; Gaskins, H R and O'keefe, S J (2013). Diet, microbiota, and microbial metabolites in colon cancer risk in rural Africans and African Americans. *Am. J. Clin. Nutr., 98*: 111-120.

Ozato, N; Saito, S; Yamaguchi, T; Katashima, M; Tokuda, I; Sawada, K; Katsuragi, Y; Imoto, S; Ihara, K and Nakaji, S (2019). Association between nutrients

and visceral fat in healthy Japanese adults: A 2-year longitudinal study brief title: Micronutrients associated with visceral fat accumulation. *Nutrients, 11*: 2698.

Parveez, G K A; Hishamuddin, E; Loh, S K; Abdullah, M O; Salleh, K M; Zanal Bidin, M N I; Sundram, S; Azizul Hassan, Z A and Idris, Z (2020). Oil palm economic performance in Malaysia and R&D progress in 2019. *J. Oil Palm Res., 32*: 159-190.

Pauwels, E K J (2011). The protective effect of the Mediterranean diet: Focus on cancer and cardiovascular risk. *Med. Princ. Pract., 20*: 103-111.

Pilorgé, E (2020). Sunflower in the global vegetable oil system: Situation, specificities and perspectives. *OCL, 27*: 34.

Plummer, E; Bulach, D; Carter, G and Albert, M J (2020). Gut microbiome of native Arab Kuwaitis. *Gut Pathogens, 12*: 10.

Pu, S; Khazanehei, H; Jones, P J and Khafipour, E (2016). Interactions between obesity status and dietary intake of monounsaturated and polyunsaturated oils on human gut microbiome profiles in the Canola Oil Multicenter Intervention Trial (COMIT). *Front in Microbiol., 7*: 1-14.

Pulipati, P; Sarkar, P; Jakkampudi, A; Kaila, V; Sarkar, S; Unnisa, M; Reddy, D N; Khan, M and Talukdar, R (2020). The Indian gut microbiota-Is it unique? *Indian J. Gastroenterol., 39*: 133-140.

Qian, L; Gao, R; Hong, L; Pan, C; Li, H; Huang, J and Qin, H (2018). Association analysis of dietary habits with gut microbiota of a native Chinese community. *Exp. Ther. Med., 16*: 856-866.

Rajkumar, H; Mahmood, N; Kumar, M; Varikuti, S R; Challa, H R and Myakala, S P (2014). Effect of probiotic (VSL#3) and omega-3 on lipid profile, insulin sensitivity, inflammatory markers, and gut colonization in overweight adults: A randomized, controlled trial. *Mediat Inflamm., 2014*: 348959.

Ramíreza, M; Amatea, L and Gilb, A (2001). Absorption and distribution of dietary fatty acids from different sources. *Early Hum. Dev., 65*: S95-S101.

Requena, T; Martínez-Cuesta, M C and Peláez, C (2018). Diet and microbiota linked in health and disease. *Food Funct., 9*: 688-704.

Reyes, L M; Vázquez, R G; Arroyo, S M C; Avalos, A M; Castillo, P A R; Pérez, D A C; Terrones, I R; Ibáñez, N R; Magallanes, M M R; Langella, P; Humarán, L B and Espinosa, A A (2016). Correlation between diet and gut bacteria in a population of young adults. *Int. J. Food Sci Nutr., 67*: 470-478.

Rogalska, E; Ransac, R and Verger, R (1990). Stereoselectivity of lipases II. Stereoselective hydrolysis of triglycerides by gastric and pancreatic lipases. *J. Biol. Chem., 33*: 20271-20276.

Ruengsomwong, S; La-Ongkham, O; Jiang, J; Wannissorn, B; Nakayama, J and Nitisinprasert, S (2016). Microbial community of healthy Thai vegetarians and non-vegetarians, their core gut microbiota, and pathogen risk. *J. Microbiol Biotechnol., 26*: 1723-1735.

Senghor, B; Sokhna, C; Ruimy, R and Lagier, J C (2018). Gut microbiota diversity according to dietary habits and geographical provenance. *Human Microbiome J., 8*: 1-9.

Shetty, S A (2018). Gut microbiota features of the geographically diverse Indian population. *BioRxiv*, 478586. DOI: 10.1101/478586.

Shin, J H; Sim, M; Lee, J Y and Shin, D M (2016). Lifestyle and geographic insights into the distinct gut microbiota in elderly women from two different geographic locations. *J. Physiol. Anthropol., 35*: 31.

Shortt, C; Hasselwander, O; Meynier, A; Nauta, A; Fernández, E N; Putz, P; Rowland, I; Swann, J; Türk, J; Vermeiren, J and Antoine, J M (2018). Systematic review of the effects of the intestinal microbiota on selected nutrients and non-nutrients. *Eur. J. Nutr., 57*: 25-49.

Silveira-Nunes, G; Durso, D F; De Oliveira, L R A; Cunha, E H M; Maioli, T U; Vieira, A T; Speziali, E; Corrêa-Oliveira, R; Martins-Filho, O A; Teixeira-Carvalho, A; Franceschi, C; Rampelli, S; Turroni, S; Brigidi, P and Faria, A M C (2020). Hypertension is associated with intestinal microbiota dysbiosis and inflammation in a Brazilian population. *Front Pharmacol., 11*: 258

Simões, C D; Maukonen, J; Kaprio, J; Rissanen, A; Pietiläinen, K H and Saarela, M (2013). Habitual dietary intake is associated with stool microbiota composition in monozygotic twins. *J. Nutr., 143*: 417-423.

Snijder, M B; Galenkamp, H; Prins, M; Derks, E M; Peters, R J G; Zwinderman, A H and Stronks, K (2017). Cohort profile: The healthy life in an urban setting (HELIUS) study in Amsterdam, The Netherlands. *BMJ Open, 7*: e017873-e017873.

Tandon, D; Haque, M M R S; Shaikh, S P S; Dubey, A K and Mande, S S (2018). A snapshot of gut microbiota

of an adult urban population from Western region of India. *PLoS ONE, 13*: e0195643.

Tolhurst, G; Heffron, H; Lam, Y S; Parker, H E; Habib, A M; Diakogiannaki, E; Cameron, J; Grosse, J; Reimann, F and Gribble, F M (2012). Short-chain fatty acids stimulate glucagon-like peptide-1 secretion via the G-protein-coupled receptor FFAR2. *Diabetes, 61*: 364-371.

Tomova, A; Bukovsky, I; Rembert, E; Yonas, W; Alwarith, J; Barnard, N and Kahleova, N (2019). Review article: The effects of vegetarian and vegan diets on gut microbiota. *Front in Nutr., 6*: 157.

Tsuji, H; Matsuda, K and Nomoto, K (2018). Counting the countless: Bacterial quantification by targeting rRNA molecules to explore the human gut microbiota in health and disease. *Front Microbiol., 9*: 1417.

Tyakht, A V; Kostryukova, E S; Popenko, A S; Belenikin, M S; Pavlenko, A V; Larin, A K; Karpova, I Y; Selezneva, O V; Semashko, T A; Ospanova, E A; Babenko, V V; Maev, I V; Cheremushkin, S V; Kucheryavyy, Y A; Shcherbakov, P L; Grinevich, V B; Efimov, O I; Sas, E I; Abdulkhakov, R A; Abdulkhakov, S R; Lyalyukova, E A; Livzan, M A; Vlassov, V V; Sagdeev, R Z; Tsukanov, V V; Osipenko, M F; Kozlova, I V; Tkachev, A V; Sergienko, V I; Alexeev, D G and Govorun, V M (2013). Human gut microbiota community structures in urban and rural populations in Russia. *Nat. Commun., 4*: 2469.

Valdes, A; Walter, J; Segal, E and Spector, T (2018). Role of the gut microbiota in nutrition and health. *BMJ, 361*: k2179.

Watson, H; Mitra, S; Croden, F C; Taylor, M; Wood, H M; Perry, S L; Spencer, J A; Quirke, P; Toogood, G J; Lawton, C L; Dye, L; Loadman, P M and Hull, M A (2017). A randomised trial of the effect of omega-3 polyunsaturated fatty acid supplements on the human intestinal microbiota. *Gut, 67*: 314968.

Wit, N D; Oosterink, E; Bosch-Vermeulen, H; Keshtkar, S; Duval, C N C; Vogel-Van B N J D; Muller, M and Meer, R V D (2012). Saturated fat stimulates obesity and hepatic steatosis and affects gut microbiota composition by an enhanced overflow of dietary fat to the distal intestine. *Mucosal Biol., 303*: G589-G599.

Wrzosek, L; Miquel, S; Noordine, M L; Bouet, S; Chevalier-Curt, M J; Robert, V; Philippe, C; Bridonneau, C; Cherbuy, C; Robbe-Masselot, C; Langella, P and Thomas, M (2013). *Bacteroides thetaiotaomicron* and *Faecalibacterium prausnitzii* influence the production of mucus glycans and the development of goblet cells in the colonic epithelium of a gnotobiotic model rodent. *BMC Biol., 11*: 61.

Yang, B; Ren, X L; Li, Z H; Shi, M Q; Ding, F; Su, K P; Guo, X J and Li, D (2020a). Lowering effects of fish oil supplementation on proinflammatory markers in hypertension: Results from a randomized controlled trial. *Food Funct., 11*: 1779-1789.

Yang, Q; Liang, Q; Balakrishnan, B; Belobrajdic, D P; Feng, Q J and Zhang, W (2020b). Role of dietary nutrients in the modulation of gut microbiota: A narrative review. *Nutrients, 12*: 381.

Yang, S J; Li, X Y; Yang, F; Zhao, R; Pan, X D; Liang, J Q; Tian, L; Li, X Y; Liu, L T; Xing, Y W and Wu, M (2019). Gut microbiota-dependent marker TMAO in promoting cardiovascular disease: Inflammation mechanism, clinical prognostic, and potential as a therapeutic target. *Front Pharmacol., 10*: 1360.

Yasir, M; Angelakis, E; Bibi, F; Azhar, E; Bachar, D; Lagier, J C; Gaborit, B; Hassan, A M; Jiman-Fatani, A A; Alshali, K Z; Robert, C; Dutour, A and Raoult, D (2015). Comparison of the gut microbiota of people in France and Saudi Arabia. *Nutr. Diabetes, 5*: e153.

Yatsunenko, T; Rey, F E; Manary, M J; Trehan, I; Dominguez-Bello, M G; Contreras, M; Magris, M; Hidalgo, G; Baldassano, R N; Anokhin, A P; Heath, A C; Warner, B; Reeder, J; Kuczynski, J; Caporaso, J G; Lozupone, C A; Lauber, C; Clemente, J C; Knights, D; Knight, R and Gordon, J I (2012). Human gut microbiome viewed across age and geography. *Nature, 486*: 222-227.

Young, A J; Marriott, B P; Champagne, C M; Hawes, M R; Montain, S J; Johannsen, N M; Berry, K and Hibbeln, J R (2017). Blood fatty acid changes in healthy young Americans in response to a 10-week diet that increased n-3 and reduced n-6 fatty acid consumption: A randomised controlled trial. *Br. J. Nutr., 23*: 1-13.

Zeng, Q; He, Y; Dong, S Y; Zhao, X L; Chen, Z H; Song, Z Y; Chang, G; Yang, F and Wang, Y J (2014). Optimal cut-off values of BMI, waist circumference and waist: Height ratio for defining obesity in Chinese adults. *Br. J. Nutr., 112*: 1735-1744.

Zhang, J; Guo, Z; Xue, Z; Sun, Z; Zhang, M; Wang, L; Wang, G; Wang, F; Xu, J; Cao, H; Xu, H; Lv, Q; Zhong, Z; Chen, Y; Qimuge, S; Menghe, B; Zheng, Y; Zhao, L; Chen, W and Zhang, H (2015). A phylo-functional core of gut microbiota in healthy young Chinese cohorts across lifestyles, geography and ethnicities. *The ISME J., 9*: 1979-1990.

Zhang, W; Li, J; Lu, S; Han, N; Miao, J; Zhang, T; Qiang, Y; Kong, Y; Wang, H; Gao, T; Liu, Y; Li, X; Peng, X; Chen, X; Zhao, X; Che, J; Zhang, L; Chen, X; Zhang, Q; Hu, M; Li, Q and Kan, B (2019). Gut

microbiota community characteristics and disease-related microorganism pattern in a population of healthy Chinese people. *Sci. Rep., 9*: 1594.

Zhao, D Y; Yuan, B; Carry, E; Pasinetti, G M; Ho, L; Faith, J; Mogno, I; Simon, J and Wu, Q L (2018). Development and validation of an ultra-high performance liquid chromatography/triple quadrupole mass spectrometry method for analyzing microbial-derived grape polyphenol metabolites. *J. Chromatogr. B. Analyt. Technol. Biomed Life Sci., 1*: 34-45.

NEW INSIGHTS INTO THE PHYLOGEOGRAPHY OF THE OIL PALM PEST, *Metisa plana* TOWARDS ITS MANAGEMENT CONTROL

AQILAH SAKINAH BADRULISHAM[1]; DAISUKE KAGEYAMA[2]; MADIHAH HALIM[1];
AMEYRA AMAN-ZUKI[1]; MOHAMED MAZMIRA MASRI[3]; SITI NURULHIDAYAH AHMAD[3];
BADRUL MUNIR MD-ZAIN[4] and SALMAH YAAKOP[1]*

ABSTRACT

Metisa plana *Walker, has contributed as an important pest in the palm oil industry. Even though various studies have been conducted on* M. plana *there is still insufficient information on the relationships among the populations to illustrate the distribution of this species. We aim to investigate the phylogeography of the* M. plana *populations by combining data of cytochrome c oxidase subunit I (COI), cytochrome b (Cytb), and 28S markers. The* M. plana *specimens have been sampled from 10 heavily infested oil palm plantations in Peninsular Malaysia. A total of 145 sequences of three markers were combined and implemented for the phylogenetic analyses, Neighbour-Joining (NJ) and Bayesian Inference (BI). Both phylogenetic trees showed mixing of individuals of the* M. plana *inter-populations, despite a very distinct geographical isolation. Based on findings from the haplotype analyses; haplotype diversity (Hd= 0.96089), haplotype number (27), haplotype network, and haplotype tree; all supported the genetic exchange, indicating the possibility of gene flow. The genetic exchange occurs probably due to the flying ability of the male moth or caused by the human activities between the various plantations that accidently resulted in the transportation and movement of the pest larvae. Interestingly, the haplotype network has also been visualised in estimating the origin of the infestation, which most probably originated from three different plantations, resulting in the rapid outbreaks of the* M. plana *infestation. These fundamental data are very crucial and informative in the effort to strategise the management control of the* M. plana.

[1] Centre for Insect Systematics,
Department of Biological Science and Biotechnology,
Faculty of Science and Technology,
Universiti Kebangsaan Malaysia,
43600 Bangi, Selangor, Malaysia.

[2] Institute of Agrobiological Sciences,
National Agriculture and Food Research Organization
(NARO), Owashi, Tsukuba, Ibaraki, 308-0851, Japan.

[3] Malaysian Palm Oil Board,
6 Persiaran Institusi, Bandar Baru Bangi,
43000 Kajang, Selangor, Malaysia.

[4] Department of Biological Science and Biotechnology,
Faculty of Science and Technology,
Universiti Kebangsaan Malaysia,
43600 Bangi, Selangor, Malaysia.

* Corresponding author e-mail: salmah78@ukm.edu.my

INTRODUCTION

Bagworms (Lepidoptera: Psychidae) are among some of the most notorious pests of oil palm (*Elaeis guineensis* Jacquin) in palm oil-producing countries. *Pteroma pendula* and *Metisa plana* Walker are two species of bagworms that have been reported to attack oil palm plantations in Peninsular Malaysia. Outbreaks of *M. plana* have been reported in Malaysia in the 1960s due to excessive application of insecticides (Wood and Kamaruddin, 2019). The attacks had also occurred in other countries such as Indonesia (Sudarsono *et al.*, 2011) and India (Potineni and Saravanan, 2013) which had led to a reduction of yields. According to Rahmat *et al.* (2021), outbreaks

of *M. plana* could cause up to 40% of yield loss if it remained uncontrolled over two consecutive years, due to serious defoliation of palm leaves by the larvae of *M. plana* (Ahmad *et al.*, 2017; Ho *et al.*, 2011). This issue is still becoming a concern today although various control methods are available.

Chemical control has been used widely to manage bagworms outbreak in most plantations (Ahmad *et al.*, 2017). It is the fastest and most effective way to suppress outbreaks of *M. plana*. However, it leads to other problems such as resistance of pests towards the treatments, abundance of harmful chemical residues in the environment and interference of the natural enemy populations (Kamarudin *et al.*, 2017). Currently, biological control using natural enemies has become a preferable method to suppress *M. plana* infestations. Previous studies have explored the use of pheromone trapping and biopesticides to control *M. plana*, resulting in decreased crop damage (Ahmad *et al.*, 2017; Kamarudin *et al.*, 2017; Salim *et al.*, 2015). In addition, several parasitoid species were recorded attacking *M. plana* and have the potential as the dominant biological agents in controlling the infestation of bagworms naturally (Halim *et al.*, 2018; Kamarudin and Arshad, 2016; 2019; Thaer *et al.*, 2021).

The most outstanding feature of *M. plana* is that the pupal bag is sub-cylindrical, 9-13 mm long with a hook-shaped attachment on the leaf (Loong and Chong, 2012). The portable bag is constructed from silk, plastered with the debris of palm leaves, stalks and flowers during the larval and pupal stages of the pest (Rhainds *et al.*, 2002; 2008; 2009). This feature becomes a problem in managing the infestation because of the difficulty of chemical insecticides to penetrate and have direct contact with the insects inside the bag. Sexual dimorphisms occur in *M. plana*, where the flightless adult female is sessile and stays in the bag for its entire life, attracting the males by secreting sex pheromones while the male would emerge from the bag upon reaching the adult stage and would fly towards the female to mate (Ali *et al.*, 2007). This behavioural feature is crucial in understanding the dispersal of the species, which leads to outbreaks.

Phylogeography is an analysis for investigating the dispersal distribution of a pest species in order to understand its niche divergence (Godefroid *et al.*, 2016). Thus, a comprehensive study on the biology of the *M. plana* is required to understand the dispersal habit of the insect species, *e.g.,* to study the maximum distance of its flying ability, what are the contributing factors that facilitate their movement, and other possible physical factors that would contribute to the movement. Such questions could be answered by implementing specific analysis using molecular data and studies with similar objectives have been conducted by Silva-Brandao *et al.* (2015) and Zhang *et al.* (2018), among others. The mitochondrial deoxyribonucleic acid (mtDNA), cytochrome *c* oxidase subunit I (*COI*) and cytochrome *b* (*Cytb*) have a higher mutation rate, and are more effective in genetic population studies compared to the use of nuclear genome (Jiang *et al.*, 2016). Besides, the mtDNA is also essential when constructing the lower classification level (Patwardhan *et al.*, 2014).

The distribution status of individuals among inter-populations of *M. plana* has never been investigated and is the crux of the hypothesis in this study. The question of whether *M. plana* can fly for long distances or if it is transported across inter-populations due to human activities becomes our main research objective. To date, little is known about the current relationships between the various populations of *M. plana* in Peninsular Malaysia in terms of molecular proof of their relationships. Despite its economic importance, information on the distribution of the dominant oil palm pest, *M. plana* is very limited and rarely discussed in Malaysia. By understanding the phylogeography of the *M. plana* populations, the distribution of the species may be interpreted, which is important in planning control strategies. Thus, in the present study, we aim to investigate the phylogeography of the *M. plana* populations from 10 heavily infested oil palm plantations, using mtDNA (*COI* and *Cytb*), and nuclear [28S ribosomal ribonucleic acid (rRNA)] markers.

MATERIALS AND METHODS

Insect Sampling

Specimens of *M. plana* were collected from 10 highly infested areas in Peninsular Malaysia, namely the northern zone (Tapah1, Tapah2, Sungkai and Slim River), the middle zone (Shah Alam and Banting) and the southern zone (Kluang, Muar, Yong Peng and Sri Medan) (*Table 1*, *Figure 1*). *Metisa plana* has been identified and differentiated from the other bagworm species in the field based on Loong and Chong (2012). Samplings were conducted on two occasions, from December 2015 to June 2016 and from January 2017 to December 2018, by handpicking from the upper and bottom parts of the oil palm fronds. A total of five trees were sampled randomly in 1000 m² area to collect a total of 100 individuals per tree. However, in this study, only one individual was chosen per tree for molecular work. The sampling sites were chosen based on several outbreak reports of high infestations of bagworms by the oil palm planters (Muhammad Adhni Rusli, 2018). Larval bagworms were differentiated from the adult females by their morphological bag design and the length of the bag following Kok *et al.* (2011). The collected samples were stored in 70% alcohol and at -20°C prior to DNA extraction.

TABLE 1. SAMPLING LOCATIONS OF *Metisa plana* AND ITS GLOBAL POSITIONING SYSTEM (GPS) COORDINATES

Study location	GPS coordinate
Perak: Tapah1	4°10'46.2"N 101°11'36.5"E
Perak: Tapah2	4°09'23.2"N 101°16'22.5"E
Perak: Sungkai	3°50'54.0"N 101°17'19.0"E
Perak: Slim River	3°48'23.8"N 101°22'56.8"E
Selangor: Shah Alam	3°13'57.5"N 101°22'36.6"E
Selangor: Banting	2°48'10.9"N 101°27'26.8"E
Johor: Kluang	1°57'20.0"N 103°22'15.1"E
Johor: Muar	2°03'28.1"N 102°36'24.6"E
Johor: Yong Peng	2°08'37.8"N 103°02'23.3"E
Johor: Sri Medan	1°58'45.0"N 102°57'25.0"E

Figure 1. Sampling sites of M. plana *in Peninsular Malaysia.*

DNA Extraction

Five individual larvae from each locality were used for molecular work with a total of 50 larvae (*Table 2*). Each specimen was cut into half to expose the tissues and then submerged in the buffer MG and proteinase K for the lysis process (Halim *et al.*, 2018). Total DNA was extracted using the NucleoSpin® DNA Insect (Macherey-Nagel, Germany) according to the manufacturer's protocol. The DNA samples were stored at -20°C.

Polymerase Chain Reaction (PCR) Amplification

A partial sequence of *COI* (646 bp) was amplified using a pair of primers from Folmer *et al.* (1994), while *Cytb* (417 bp) from Simmons and Weller (2001) and 28S rRNA gene (486 bp) was amplified using a forward primer from Belshaw and Quick (1997), whereas reverse primer was from Campbell *et al.* (1994). The PCR mixture and conditions followed the method by Halim *et al.* (2017; 2018), while the annealing temperatures used for *M. plana* were 45°C for *COI*, 50°C for *Cytb* and 48.7°C for 28S rRNA, respectively. The successful PCR products were purified using QIAquick Purification Kit (Qiagen) and sequenced by Apical Scientific Sdn. Bhd. (Selangor, Malaysia).

DNA Sequence Data and Analysis

All the sequences obtained were edited using Sequencher v4 (GeneCodes Corporation). Each sequence was subjected to Basic Local Alignment Search Tool (BLAST) in National Center for Biotechnology Information (NCBI) (https://blast.ncbi.nlm.nih.gov/) for the reliability of the results (Benson *et al.*, 2013) based on the percentage of similarity, evenness and probability values (E) with the data in GenBank (Krauthammer *et al.*, 2000). The dataset was

aligned with the outgroup, *Pteroma pendula* for *COI* and *Cytb*, while *Celastrina argiolus* (AY556547) for 28S using ClustalW multiple alignments (Thompson *et al.*, 1994) in MEGA7 software (Kumar *et al.*, 2016).

Incongruence Length Differences (ILD) Test

A total of 145 sequences of *M. plana* had been concatenated (28S, *COI* and *Cytb*) into a single data set by using MacClade ver. 3 software. ILD test was then conducted using PAUP version 4.0b10 (Swofford, 2002) to test the homogeneity of *COI*, *Cytb* and 28S rRNA region in order to combine for further phylogenetics analysis.

Phylogenetic Analysis

Phylogenetic analysis was conducted on the combined data using Neighbour-Joining (NJ) and Bayesian Inference (BI) analysis. The NJ tree was generated by using distance criterion and 1000 replications following Kimura 2-Parameter substitution model, where the robustness of the tree was estimated using bootstrap analysis of 1000 replications. For Bayesian analysis, the best-fit model was selected using jModeltest 3.7 based on Akaike Information Criterion (AIC). BI tree was generated using two chains of Monte Carlo Markov Chain (MCMC) with the sample frequency of 100 Hz. Both NJ and MP analysis were performed using PAUP version 4.0b10 (Swofford, 2002), while BI analysis was conducted using MrBayes version 3.1.2 (Ronquist *et al.*, 2012). NJ tree of combined data for 20 individuals of *M. plana* were also conducted using PAUP software.

TABLE 2. LIST OF DNA SAMPLES USED IN THIS STUDY

Code	Region	Locality	*COI* accession no.	*Cytb* accession no.	28S accession no.
OP04-3			KX055456	KY448251	MN661304
OP04-4			KX055457	KY448252	MN661305
OP04-5		Tapah1	KX055458	KY448253	MN661306
OP04-6			KX055455	KY448250	MN661307
OP04-7			KX055459	KY448254	n.e.
BT1			MK548624	MK804468	MN661287
BT2			MK548625	MK804469	MN661288
BT3		Tapah2	MK548626	MK804470	MN661289
BT4			MK548627	MK804471	MN661290
BT5	Northern		MK548628	MK804472	MN661291
BS1			MK548634	MK548604	n.e.
BS2			MK548635	MK548605	MN661296
BS3		Sungkai	MK548636	MK548606	MN661297
BS4			MK548637	MK548607	MN661298
BS5			MK548638	MK548608	MN661323
BR1			MK548639	MK548609	MN661299
BR2			MK548640	MK548610	MN661300
BR3		Slim River	MK548641	MK548611	MN661321
BR4			MK548642	MK548612	MN661322
BR5			MK548643	MK548614	MN661301
OP06-1			KX055460	KY448260	MN661308
OP06-2			KX055461	KY448261	MN661309
OP06-3		Shah Alam	KX055462	KY448262	MN661310
OP06-4			KX055463	KY448263	MN661311
OP06-5	Middle		KX055464	KY448264	MN661312
BB1			MK548614	MK548589	MN661318
BB2			MK548615	MK548590	MN661284
BB3		Banting	MK548616	MK548591	MN661319
BB4			MK548617	MK548592	MN661285
BB5			n.e.	MK548583	MN661286
OP16-1			KX055470	KY448270	MN661313
OP16-2			KX055471	KY448271	MN661314
OP16-3		Muar	KX055472	KY448272	MN661315
OP16-4			KX055473	KY448273	MN661316
OP16-5			KX055474	KY448274	MN661317
BM1			MK548619	MK548594	MN661280
BM2			MK548620	MK548595	MN661281
BM3		Sri Medan	MK548621	MK548596	MN661282
BM4			MK548622	MK548597	MN661283
BM5	Southern		MK548623	MK548598	MN661320
BY1			MK548629	MK548599	MN661292
BY2			MK548630	MK548600	MN661293
BY3		Yong Peng	MK548631	MK548601	MN661324
BY4			MK548632	MK548602	MN661294
BY5			MK548633	MK548603	MN661295
OP08-1			KX055465	KY448265	MN661325
OP08-2			KX055466	KY448266	MN661302
OP08-3		Kluang	KX055467	KY448267	n.e.
OP08-4			KX055468	KY448268	MN661303
OP08-5			KX055469	KY448269	n.e.

Haplotype Analysis

Haplotype number (n) was calculated on for the *M. plana* using DNA Sequence Polymorphism (DnaSP), version 5.10.01 (Librado and Rozas, 2009), as well as haplotype diversity, the Tajima's D and Fu's Fs values.

Haplotype Network Analysis

The haplotype network analysis was conducted using the software Network 5.0 (Fluxus Technology Ltd.) to visualise the relationships among haplotypes from different populations. For the haplotype tree, MEGA7 software (Kumar *et al.*, 2016) was used to perform maximum likelihood (ML) analysis in which the robustness of the tree was assessed by 1000 bootstrap replicates.

RESULTS

Sequence Analysis

The sequences analysis of *COI* resulted in 637/646, 3, 6, 0.46%; *Cytb* 406/417, 8, 3, 1.91%, and 28S rRNA 451/533, 16, 20, 3.00% of conserved sites, parsimony informative, parsimony uninformative characters, and variation percentage, respectively. A value of 1510/1550 for conserved sites, 11

for parsimony informative characters, 27 for uninformative characters, and 0.71% variation percentage were measured from the combined datasets.

ILD Test and Phylogenetic Trees

A total of 1596 bp of combining data of *COI*, *Cytb* and 28S, with the ILD test has shown *p*=0.14 that indicates the significance of combining the datasets. The phylogenetic trees using NJ and BI analyses also have shown the mixing of individuals in inter-populations in all analyses (*Figure 2*).

Haplotype Analysis Data

Based on the results of haplotype analysis (diversity and haplotype number), networks and tree have shown mixing of individuals among inter-populations (*Table 3*, *Figures 3-4*). The haplotype analysis has presented haplotype diversity, Hd= 0.96089. A total of 27 haplotypes had been observed from the combined data of *COI*, *Cytb* and 28S rRNA of the *M. plana* under 51 characters. Almost 74%, 20 haplotypes were found to be unique and represented only in single populations. Several haplotypes (Hap1, Hap5, Hap7, Hap14, Hap20, Hap24 and Hap26) were shared between populations, whereas Hap20 showed the highest frequency. The Hap20 was presented by the largest size of network, which
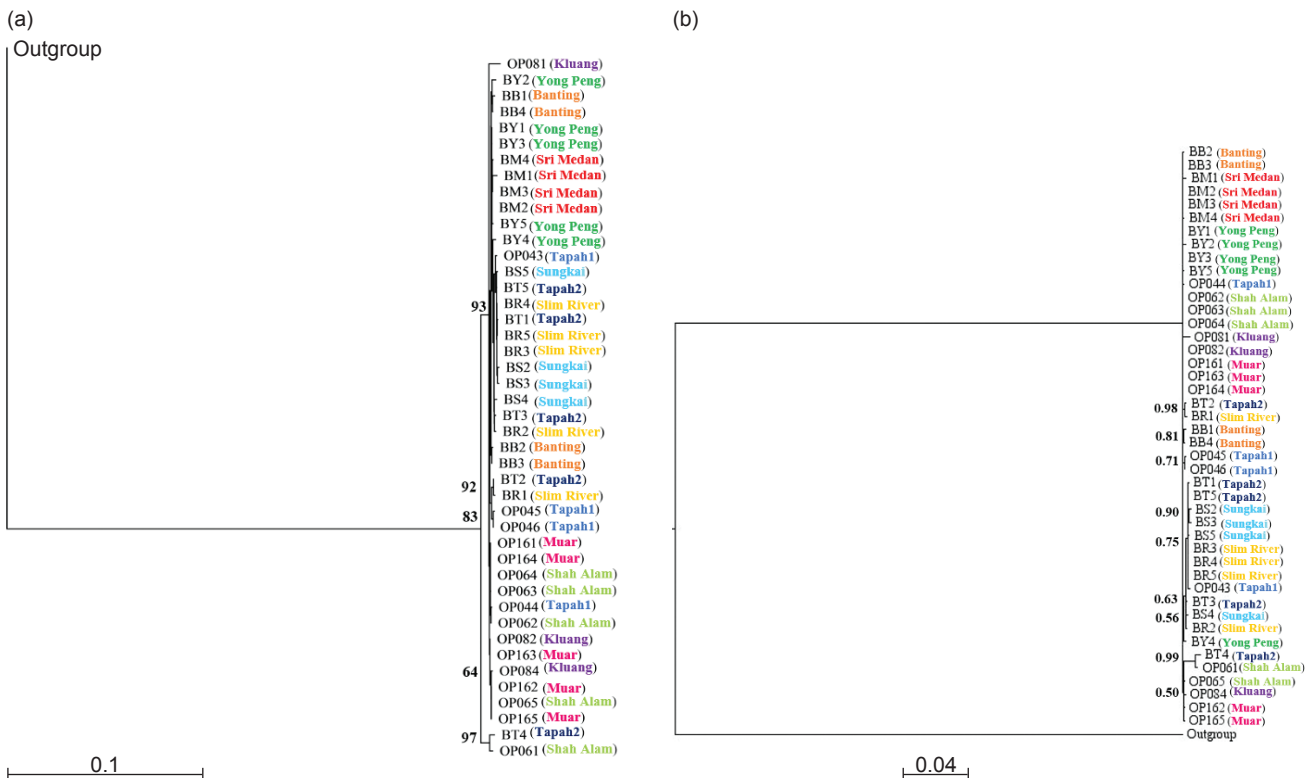
Figure 2. Phylogeography of 10 populations of M. plana *based on combining three markers (*COI, Cytb *and 28S).*
(a) Neighbour-Joining (NJ) tree, and (b) Bayesian (BI) tree.

TABLE 3. THE LIST OF SAMPLES, LOCATIONS AND THE HAPLOTYPE NUMBER

	Sample	Location	Haplotype
1	OP04-3	Perak: Tapah1	Hap19
2	OP04-4	Perak: Tapah1	Hap20
3	OP04-5	Perak: Tapah1	Hap21
4	OP04-6	Perak: Tapah1	Hap22
5	BT1	Perak: Tapah2	Hap7
6	BT2	Perak: Tapah2	Hap8
7	BT3	Perak: Tapah2	Hap9
8	BT4	Perak: Tapah2	Hap10
9	BT5	Perak: Tapah2	Hap7
10	BS2	Perak: Sungkai	Hap14
11	BS3	Perak: Sungkai	Hap14
12	BS4	Perak: Sungkai	Hap15
13	BS5	Perak: Sungkai	Hap16
14	BR1	Perak: Slim River	Hap17
15	BR2	Perak: Slim River	Hap18
16	BR3	Perak: Slim River	Hap7
17	BR4	Perak: Slim River	Hap7
18	BR5	Perak: Slim River	Hap7
19	OP06-1	Selangor: Shah Alam	Hap23
20	OP06-2	Selangor: Shah Alam	Hap20
21	OP06-3	Selangor: Shah Alam	Hap20
22	OP06-4	Selangor: Shah Alam	Hap20
23	OP06-5	Selangor: Shah Alam	Hap24
24	BB1	Selangor: Banting	Hap1
25	BB2	Selangor: Banting	Hap2
26	BB3	Selangor: Banting	Hap3
27	BB4	Selangor: Banting	Hap1
28	OP16-1	Johor: Muar	Hap20
29	OP16-2	Johor: Muar	Hap24
30	OP16-3	Johor: Muar	Hap26
31	OP16-4	Johor: Muar	Hap20
32	OP16-5	Johor: Muar	Hap24
33	BM1	Johor: Sri Medan	Hap4
34	BM2	Johor: Sri Medan	Hap5
35	BM3	Johor: Sri Medan	Hap5
36	BM4	Johor: Sri Medan	Hap6
37	BY1	Johor: Yong Peng	Hap5
38	BY2	Johor: Yong Peng	Hap11
39	BY3	Johor: Yong Peng	Hap5
40	BY4	Johor: Yong Peng	Hap12
41	BY5	Johor: Yong Peng	Hap13
42	OP08-1	Johor: Kluang	Hap25
43	OP08-2	Johor: Kluang	Hap26
44	OP08-4	Johor: Kluang	Hap27
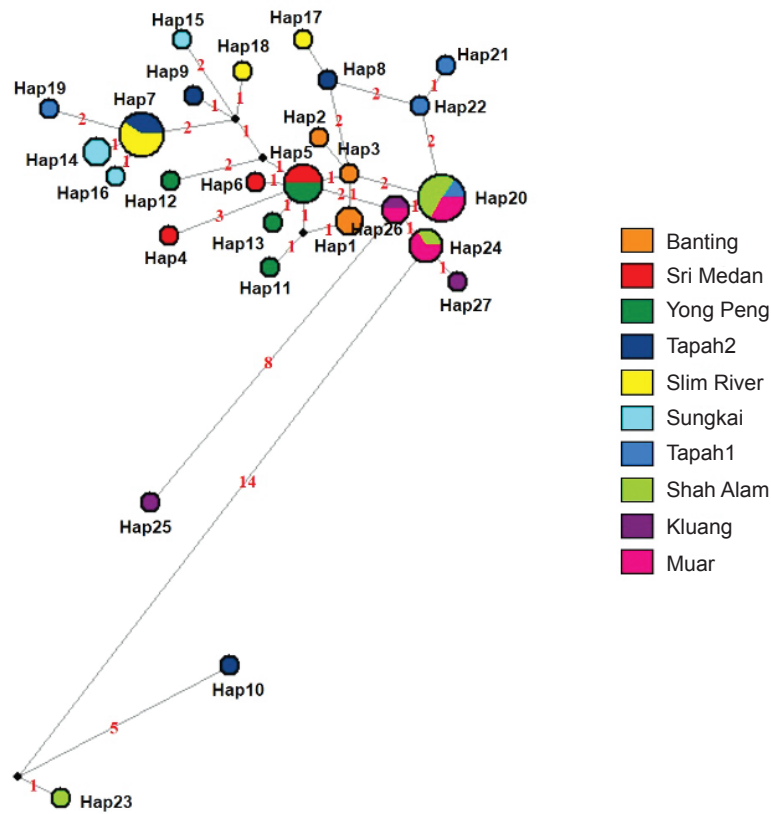
Figure 3. Haplotype network based on the combined data (COI, Cytb *and 28S) of* M. plana *collected from 10 populations of the pest.*
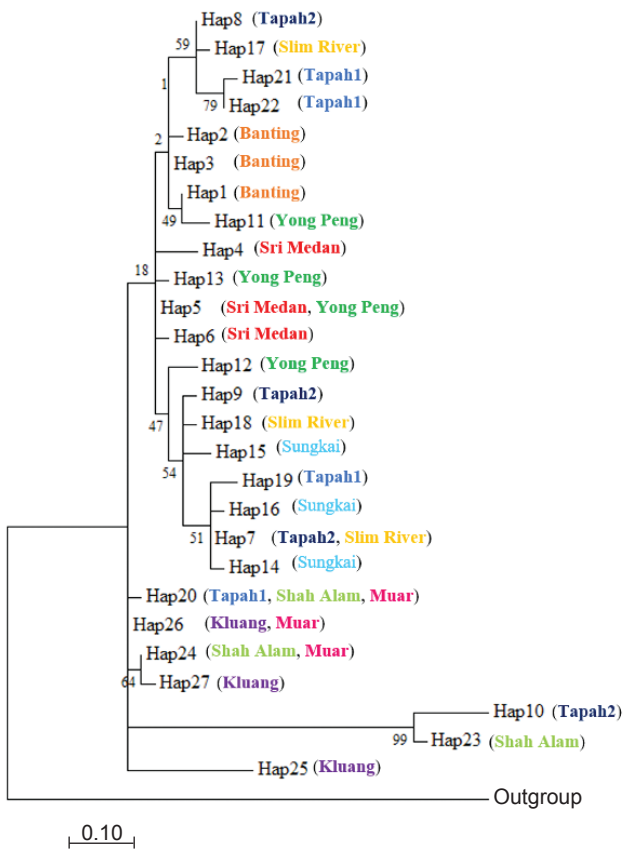
Figure 4. Haplotype tree of the combined data of COI, Cytb *and 28S based on ML analysis on 10 populations of* M. plana. *Numbers over the branches are bootstrap values based on 1000 replicates.*

contributed to the highest frequency (six sequences) in three populations, followed by Hap1 (2), Hap5 (4), Hap7 (5), Hap14 (2), Hap 24 (3), and Hap 26 (2). Putative relationships among the haplotypes are not resolved, in which several clades are collapsed due to unsupported bootstrap values (less than 50%). The haplotype tree also shows the mixing of haplotypes being represented and has occurred in several localities (*Figure 4*).

Haplotype Network

From the network above, the dispersal of the haplotypes was found as a mixture among and between populations, with no significant correlation between haplotypes and the mutation sites, supported by Tajima's D: -1.64644 and large negative value of Fu's Fs statistic: -12.51 with no significant values, $0.10 > p > 0.05$ in both analyses.

DISCUSSION

This study has successfully visualise the distribution of the *M. plana* based on the phylogeographical analysis (*Figure 2*) as well as haplotype analyses (haplotype number, haplotype network and haplotype tree) (*Figures 3-4*). This approach of study was more or less similar to the study conducted by Zhang *et al.* (2017) and Kang *et al.* (2021), but

with different objectives and samples of study. A combination of the mtDNA (*COI* and *Cytb*) and nuclear data (28S) has been used for phylogenetic analysis. The large subunit 28S ribosomal RNA gene (28S rRNA) is coded on the nuclear genome and is used as an additional data to comprehend the differences between winged males and apterous females at the nuclear level. Moreover, the different coalescent times in both mitochondrial and nuclear data also are feasible to reveal the biogeographical events at different periods (Templeton, 2002). For more robust phylogeny, the combined data has been formed into one dataset to obtain more informative characters for phylogenetic analyses (Vogler and Welsh, 1997). This is likely because a combination of three markers in this study has resulted in a total of 27 informative characters, compared to 3, 8 and 16 in *COI*, *Cytb* and 28S, respectively. In order to obtain more support values for the nodes on the phylogenetic trees (Wortley *et al.*, 2005), combination markers are suggested and this was supported by Aman-Zuki *et al.* (2019) who had proven that by combining mitochondrial and nuclear datasets, more robust phylogeny of the parasitic wasp, the *Apanteles* group was observed. In addition, Meemongkolkiat *et al.* (2019) and Baird *et al.* (2017) also presented more resolved phylogeography and phylogeny in both species of study by implementing nuclear and mtDNA.

The *M. plana* had been sampled from 10 infested oil palm plantations in Peninsular Malaysia. The identified *M. plana* DNA was isolated, sequenced and confirmed through the BLAST analysis. The same method has been performed in this study to reconfirm the species status in order to avoid including the sibling species in the analysis. It has been reported in Peninsular Malaysia that *M. plana* and *P. pendula* are primary pests and classified as siblings (Ho *et al.*, 2011). Misidentification of those as sibling species could happen due to the resemblance in their pupal bag structure. However, Loong and Chong (2012) have extensively explained the biology of both species based on the structure of the bag when attached to the frond and also the differences in their body size. In addition, the status of the sibling larvae of the *M. plana* was also avoided based on the sampling method used in collecting the samples, in which only a single individual larva was collected from a single tree in this study.

The *M. plana* species has been found to be distributed only on the west coast of the Peninsular Malaysia, but not on the east coast (Ho *et al.*, 2011). So far, there has been no report on the infestation of *M. plana* along the east coast of Peninsular Malaysia from the stakeholders and oil palm management. The east coast is physically separated from the west coast by the Titiwangsa Range (2183 km) that forms the backbone of Peninsular Malaysia (Tan *et al.*, 2011), and the poor ability of *M. plana* to fly far

across the great mountain barrier could escalate the separation of the *M. plana* populations. Even though physical barriers such as mountains, long rivers, *etc.*, (Elameen *et al.*, 2016) could become the main factors in population separation in insects and other animal species, however, this is not likely to be the case for distinct separation among populations of the *M. plana* in our study areas.

In this study, the 10 plantations that are highly infested by the *M. plana* extend ~420 km (south-Kluang to north- Tapah) on the west coast of the Peninsular Malaysia. The geographical isolation is posed by several geographical barriers, namely the ranges of Gunung Ledang (1276 m) at the south, and Gunung Angsi (825 m) at the middle, and the tributaries of Sungai Perak (400 km) at the northern part of west Peninsular Malaysia. However, based on the phylogenetic trees (*Figure 2*), the mixing of individuals between populations is apparently neither in line nor collaborated with the geographical isolation, thus, the physical barriers can be discounted. Therefore, there could be other possible factors contributing to the dispersal distribution apart from those of physical barriers, and most likely, the species behaviour, human and abiotic factors are the more significant contributing factors (Basoalto *et al.*, 2020; Zhang *et al.*, 2017).

In this study, based on the phylogeographic trees among the *M. plana* populations it is possible to estimate their relationships to facilitate in comprehending and illustrating their flying and dispersal abilities. To date, no specific study on the flying ability of *M. plana* has been comprehensively conducted. Therefore, the capability of *M. plana* to fly over long or short distances has never been described properly. However, in their studies, Abdullah *et al.* (2012) had briefly noted that *M. plana* was able to fly from one palm frond to another within 100 cm distance, while Rhainds *et al.* (2002) postulated that the ballooning event of the larvae was the dispersal mechanism that could contribute to only minimal dispersal. Nevertheless, such information would not reveal much regarding the relationships between populations, nor the mechanism and dispersal distribution status. Based on the phylogeographic trees (*Figure 2*), we could see that several individuals of the *M. plana* in one location had mixed with other populations. This could either be due to their ability to fly further afield or that the larvae of the *M. plana* were accidentally transported and dispersed by human activities between plantations.

Based on the phylogenetic analysis of each marker (gene tree), we have found that there was a mixture between populations in all trees (28S, *COI* and *Cytb*). However, the single-gene trees are not presented in this article. At first, we estimated the isolation in the population using the *COI* and *Cytb* sequences data due to the high mutation rate in the

mitochondrial markers (Patwardhan *et al.*, 2014). This, however, does not happen in the mtDNA in our study due to low variation detected in the sequences of *COI* and *Cytb*. Finally, the mixture between individuals from different populations was observed in both mitochondrial and nuclear data in this study.

Referring to the sequence analysis, 28S rRNA showed 3.00% variation, while 0.46% and 1.91% in *COI* and *Cytb*, respectively. In this study, the similar sequences in 28S were not sequenced in all the samples. A more detailed look into the mixing of individuals in the tree topologies would reveal that some individuals would remain static within their bags on the host fronds during their entire life, particularly those females known as flightless, wingless or apterous females. However, all the males can fly and disperse for mating and survival of the species and these males are the ones that could create the gene flow between populations (Abdullah *et al.*, 2012). This might contribute to the differences in the sequences that were derived from different male parents' information. Furthermore, the larvae of the *M. plana* might also be dispersed by wind, animals or human activities across plantations due to the unique structure of the larval bags, which were hung in an upright position on their long silken threads (Kok *et al.*, 2011; Thaer *et al.*, 2021) which could also lead to the mixture between populations in all markers.

The bagworm *M. plana* is known as a polyphagous insect and may feed on other plant materials within the vicinity of the oil palm plantation (Kamarudin *et al.*, 2017). This type of feeding behaviour and food range may contribute to the minimal dispersal activity of this bagworm species. During our sampling process, the gender of the larval stages (between 5-7 instars) has not been determined and predicted, but this can be accomplished by experienced field technicians or researchers. The gender of the male larvae during that stage may be identified by the blackish head colouration for the males, and pale colour for the females. Thus, our samplings have involved the collection of both male and female specimens.

The high application of chemical insecticides to control the population of *M. plana* would not change the genetic information of the species due to the thickness of the bag which was not affected much by the chemical residues (Loong and Chong, 2012). We also tried to reduce and minimise the mistakes in identifying the pseudogenes through the proper alignment with the parent sequences to make sure all had translated to the functional protein (Harrison *et al.*, 2005). It indicated a sign of pseudogenes in two *COI* samples (OP06-1 and BT4), however, we had reconfirmed that no pseudogenes appeared, and that both were referred to the *M. plana* after multiple checking.

The haplotype diversity based on both mitochondrial and nuclear data for all samples showed high value of 0.96089, indicating a high number of sequence variation in the population (Liu *et al.*, 2006), and also high genetic similarity between populations (Tan *et al.*, 2016). In our work, 27 haplotypes were observed, while 20 haplotypes were single and seven haplotypes were shared. Even though the 20 haplotypes are found in single frequency, it has proven that the genetic information is not shared between populations (Mohd-Yusof *et al.*, 2019), but is able to support the mixing between populations only for seven haplotypes. Hap 20 was the most shared between the *M. plana* populations under six frequencies. The distribution of haplotypes was also correlated with geographical factors which supported the mixing between individuals from different populations as shown in the phylogenetic tree (*Figure 2*). Even though the *M. plana* has minimal dispersal ability, human activities might have contributed to the sharing of haplotypes between the northern, middle and southern populations. The haplotype network and tree (*Figures 3-4*) are the two indicators to determine the variations in the nucleotide sequences for haplotype data (Paradis, 2018). In this study the origins of the infestation had occurred simultaneously from three different plantations (*i.e.,* Tapah2, Shah Alam and Muar under Hap20), which had made the outbreak of infestation worse and difficult to control. According to a study by Silva-Brandao *et al.* (2013), two mtDNA data showed a higher number of shared haplotypes for estimating the origin of infestation from the southern region in Brazil. However, in this study the origin of infestation could not be estimated but had occurred simultaneously.

CONCLUSION

In this study, the phylogeography of the *M. plana* as determined by combining nuclear and mtDNA data in Peninsular Malaysia has shown the mixing of individuals among inter-populations, despite the distinct differences in geographic location. The mixing of individuals between populations had been supported by the haplotype analyses by presenting the high haplotype diversity (Hd= 0.96089), 27 haplotype numbers, haplotype network, and haplotype tree that indicated the possibility of gene flow between populations. These results suggest the occurrence of genetic exchange of the *M. plana* between plantations, which is possibly mediated by human activities such as translocation of plants to which the larvae of *M. plana* are attached, while the workers are visiting the various plantations, or it could be due to the ability of male *M. plana* to fly far across physical barriers and facilitated by winds. Here, we estimated that the infestation could

have originated from three different plantations simultaneously, which then spread outwards as outbreaks of infestation which were difficult to control. However, further behavioural experiments need to be conducted before any solid conclusion can be derived regarding dispersal factors in *M. plana*. Consequently, the standard operating procedure and contingency measures should be continuously updated and implemented for the oil palm production sector to contain, control and therefore prevent the dispersal of this serious pest in the future.

ACKNOWLEDGEMENT

REFERENCES

Abdullah, F; Sabri, M S M; Sina, I; Fauzee, F and Isa, S M (2012). Response of the male bagworm moth (*Metisa plana* Walker, Lepidoptera: Psychidae) towards female bagworm pheromone lure in wind tunnel bioassays. *Asia Life Sci., 21(2)*: 375-389.

Ahmad, M N; Kamarudin, N; Ahmad, S N; Arshad, O; Masri, M M M; Moslim, R and Kushairi, A (2017). Efficacy of pheromone trapping and aerial spraying of *Bacillus thuringiensis* (Bt) for controlling bagworm, *Metisa plana* Walker (Lepidoptera: Psychidae) in Yong Peng, Johor, Malaysia. *J. Oil Palm Res., 29(1)*: 55-65.

Ali, S R R; Kamarudin, N; Wahid, M B; Ahmad, M N; Masri, M M M and Din, A K (2007). *Sistem Pengurusan Perosak Bersepadu bagi Kawalan Ulat Bungkus di Ladang Sawit*. MPOB, Bangi.

Aman-Zuki, A; Mohammed, M A; Md. Zain, B M and Yaakop, S (2019). Phylogenetic relationships of five oriental *Apanteles* species-groups (Hymenoptera: Braconidae: Microgastrinae) by concatenating four molecular markers. *J. Asia-Pac. Entomol., 22(1)*: 341-352.

Baird, A B; Braun, J K; Engstrom, M D; Holbert, A C; Huerta, M G; Lim, B K; Mares, M A; Patton, J C and Bickham, J (2017). Nuclear and mtDNA phylogenetic analyses clarify the evolutionary history of two species of native Hawaiian bats and the taxonomy of Lasiurini (Mammalia: Chiroptera). *PLoS ONE, 12(10)*: e0186085. DOI: 10.1371/journal.pone.0186085.

Basoalto, A; Ramírez, C C; Lavandero, B; Devotto, L; Curkovic, T; Franck, P and Fuentes-Contreras, E (2020). Population genetic structure of codling moth, *Cydia pomonella* (L.) (Lepidoptera: Tortricidae), in different localities and host plants in Chile. *Insects, 11*: 285.

Belshaw, R and Quicke, D L (1997). A molecular phylogeny of the Aphidiinae (Hymenoptera: Braconidae). *Mol. Phylogenet. Evol., 7(3)*: 281-293. DOI: 10.1006/mpev.1996.0400.

Benson, D A; Cavanaugh, M; Clark, K; Karsch-Mizrachi, I; Lipman, D J; Ostell, J and Sayers, E W (2013). GenBank. *Nucleic Acids Res., 41*: D36-D42. DOI: 10.1093/nar/gks1195.

Campbell, B C; Steffen-Campbell, J D and Werren, J H (1994). Phylogeny of the *Nasonia* species complex (Hymenoptera: Pteromalidae) inferred from an internal transcribed spacer (ITS2) and 28S rDNA sequences. *Insect Mol. Biol., 2(4)*: 225-237. DOI: 10.1111/j.1365-2583.1994.tb00142.x.

Elameen, A; Eiken, H G and Knudsen, G K (2016). Genetic diversity in apple fruit moth indicate different clusters in the two most important apple growing regions of Norway. *Diversity, 8(2)*: 10.

Folmer, O; Black, M; Hoeh, W; Lutz, R and Vrijenhoek, R (1994). DNA primers for amplification of mitochondrial cytochrome c oxidase subunit I from diverse metazoan invertebrates. *Mol. Mar. Biol. Biotechnol., 3(5)*: 294-299.

Godefroid, M; Rasplus, J Y and Rossi, J P (2016). Is phylogeography helpful for invasive species risk assessment? The case study of the bark beetle genus *Dendroctonus*. *Ecography, 39(12)*: 1197-1209.

Halim, M; Aman-Zuki, A; Syed Ahmad, S Z; Mohammad Din, A M; Abdul Rahim, A; Mohd Masri, M M; Md Zain, B M and Yaakop, S (2018). Exploring the abundance and DNA barcode information of eight parasitoid wasps species (Hymenoptera), the natural enemies of the important pest of oil palm, bagworm, *Metisa plana* (Lepidoptera: Psychidae) toward the biocontrol approach and its application in Malaysia. *J. Asia-Pac. Entomol., 21(4)*: 1359-1365.

Halim, M; Muhaimin, A M D; Syarifah Zulaikha, S A; Nor Atikah, A R; Masri, M M M and Yaakop, S (2017). Evaluation of infestation in parasitoids on *Metisa plana* Walker (Lepidoptera: Psychidae) in

three oil palm plantations in Peninsular Malaysia. *Serangga, 22(2)*: 135-149.

Halim, M; Syed Ahmad, S Z; Muhammad Din, A M and Yaakop, S (2019). The diversity and abundance of potential hymenopteran parasitoids assemblage associated with *Metisa plana* (Lepidoptera: Psychidae) in three infested oil palm plantations in Peninsular Malaysia. *AIP Conf. Proc., 2111*: 060024. DOI: 10.1063/1.5111286.

Harrison, P M; Zheng, D; Zhang, Z; Carriero, N and Gerstein, M (2005). Transcribed processed pseudogenes in the human genome: An intermediate form of expressed retro sequence lacking protein-coding ability. *Nucleic Acids Res., 33(8)*: 2374-2383.

Ho, C T; Yusof, I and Khoo, K C (2011). Infestation by the bagworms *Metisa plana* and *Pteroma pendula* for the period 1986-2000 in major oil palm estates managed by Golden Hope Plantations Berhad in Peninsular Malaysia. *J. Oil Palm Res., 23*: 1040-1050.

Jiang, J; Yu, J; Li, J; Li, P; Fan, Z; Niu, L; Deng, J; Yue, B and Li, J (2016). Mitochondrial genome and nuclear markers provide new insight into the evolutionary history of macaques. *PLoS ONE, 11(5)*: e0154665. DOI: 10.1371/journal.pone.0154665.

Kamarudin, N and Arshad, O (2016). Diversity and activity of insect natural enemies of the bagworm (Lepidoptera: Psychidae) within an oil palm plantation in Perak, Malaysia. *J. Oil Palm Res., 28(3)*: 296-307.

Kamarudin, N; Ali, S R A; Masri, M M M; Ahmad, M N; Manan, C A H C and Kamarudin, N (2017). Controlling *Metisa plana* Walker (Lepidoptera: Psychidae) outbreak using *Bacillus thuringiensis* at an oil palm plantation in Slim River, Perak, Malaysia. *J. Oil Palm Res., 29(1)*: 47-54.

Kang, J H; Yi, D A; Kuprin, A V; Han, C and Bae, Y J (2021). Phylogeographic investigation of an endangered longhorn beetle, *Callipogon relictus* (Coleoptera: Cerambycidae), in Northeast Asia: Implications for future restoration in Korea. *Insects, 12*: 555.

Kok, C C; Eng, O K; Razak, A R and Arshad, A M (2011). Microstructure and life cycle of *Metisa plana* (Lepidoptera: Psychidae). *J. Sustain. Sci. Manag., 6(1)*: 51-59.

Krauthammer, M; Rzhetsky, A; Morozov, P and Friedman, C (2000). Using BLAST for identifying gene and protein names in journal articles. *Gene, 259(1-2)*: 245-252. DOI: 10.1016/S0378-1119(00)00431-5.

Kumar, S; Stecher, G and Tamura, K (2016). MEGA7: Molecular evolutionary genetics analysis version 7.0 for bigger datasets. *Mol. Biol. Evol., 33(7)*: 1870-1874.

Librado, P and Rozas, J (2009). DnaSP v5: A software for comprehensive analysis of DNA polymorphism data. *Bioinformatics, 25(11)*: 1451-1452. DOI: 10.1093/bioinformatics/btp187.

Liu, R Y; Yang, G S and Lei, C Z (2006). The genetic diversity of mtDNA D-loop and the origin of Chinese goats. *Acta Genet. Sin., 33(5)*: 420-428.

Loong, C Y and Chong, T C (2012). Understanding pest biology and behavior for effective control of oil palm bagworms. *Planter, 88(1039)*: 699-715.

Meemongkolkiat, T; Rattanawannee, A and Chanchao, C (2019). Genetic diversity of *Apis* spp. in Thailand inferred from 28S rRNA nuclear and cytochrome b mitochondrial gene sequences. *Psyche*. p. 1-11.

Mohd-Yusof, N S; Senawi, J; Nor, S M and Md-Zain, B M (2020). Haplotype and network analysis of island flying fox (*Pteropus hypomelanus*) using D-loop region of mitochondrial DNA to confirm subspecies designation. *Mamm. Res., 65(2)*: 375-385.

Muhammad Adhni Rusli (2018). Personal communication. Malaysian Palm Oil Board, Bangi, Selangor, Malaysia.

Paradis, E (2018). Analysis of haplotype networks: The randomized minimum spanning tree method. *Methods Ecol. Evol., 9(5)*: 1308-1317.

Patwardhan, A; Ray, S and Roy, A (2014). Molecular markers in phylogenetic studies - A review. *J. Phylogenetics Evol. Biol., 2(2)*: 1-9.

Potineni, K and Saravanan, L (2013). Natural enemies of oil palm defoliators and their impact on pest population. *Pest Manag. Hortic. Ecosyst., 19(2)*: 179-184.

Rahmat, N L; Zifruddin, A N; Zainal Abidin, C M R; Nor Muhammad, N and Hassan, M (2021). The developmental transcriptome of bagworm, *Metisa plana* (Lepidoptera: Psychidae) and insights into chitin biosynthesis genes. *Genes, 12(1)*: 7.

Rhainds, M; Davis, D R and Price, P W (2009). Bionomics of bagworms (Lepidoptera: Psychidae). *Annu. Rev. Entomol., 54*: 209-226. DOI: 10.1146/annurev.ento.54.110807.090448.

Rhainds, M; Gries, G; Ho, C T and Chew, P S (2002). Dispersal by bagworm larvae, *Metisa plana*:

Effects of population density, larval sex, and host plant attributes. *Ecol. Entomol., 27(2)*: 204-212. DOI: 10.1046/j.1365-2311.2002.00389.x.

Rhainds, M; Leather, S R and Sadof, C (2008). Polyphagy, flightlessness, and reproductive output of females: A case study with bagworms (Lepidoptera: Psychidae). *Ecol. Entomol., 33(5)*: 663-672. DOI: 10.1111/j.1365-2311.2008.01027.x.

Ronquist, F; Teslenko, M; van der Mark, P; Ayres, D L; Darling, A; Höhna, S; Larget, B; Liu, L; Suchard, M A and Huelsenbeck, J P (2012). MrBayes 3.2: Efficient Bayesian phylogenetic inference and model choice across a large model space. *Syst. Biol., 61(3)*: 539-542.

Salim, H; Md. Rawi, C S; Ahmad, A H and Abdo Al-Shami, S (2015). Efficacy of insecticide and bioinsecticide ground sprays to control *Metisa plana* Walker (Lepidoptera: Psychidae) in oil palm plantations, Malaysia. *Trop. Life Sci. Res., 26(2)*: 73-83.

Silva-Brandao, K L; Almeida, L C; Moraes, S S and Cônsoli, F L (2013). Using population genetic methods to identify the origin of an invasive population and to diagnose cryptic subspecies of *Telchin licus* (Lepidoptera: Castniidae). *Bull. Entomol. Res., 103(1)*: 89-97.

Simmons, R B and Weller, S J (2001). Utility and evolution of cytochrome b in insects. *Mol. Phylogenet. Evol., 20*: 196-210. DOI: 10.1006/mpev.2001.0958.

Sudarsono, H; Purnomo, P and Hariri, A M (2011). Population assessment and appropriate spraying technique to control the bagworm (*Metisa plana* Walker) in North Sumatra and Lampung. *Agrivita J. Agric. Sci., 33(2)*: 188-198. DOI: 10.17503/agrivita. v33i2.62.

Swofford, D L (2002). PAUP*: *Phylogenetic Analysis Using Parsimony (*and Other Methods)*. Sinauer Associates, Massachusetts.

Tan, F; San-Lim, H and Abdullah, K (2011). The impact of the typhoon to Peninsular Malaysia on orographic effects. *2011 IEEE Symposium on Business, Engineering and Industrial Applications (ISBEIA)*, Langkawi, Malaysia. p. 286-291. DOI: 10.1109/ISBEIA.2011.6088822.

Tan, K; Qu, Y; Wang, Z; Liu, Z and Engel, M S (2016). Haplotype diversity and genetic similarity among populations of the Eastern honey bee from Himalaya - Southwest China and Nepal (Hymenoptera: Apidae). *Apidologie, 47(2)*: 197-205.

Templeton, A (2002). Out of Africa again and again. *Nature, 416*: 45-51. DOI: 10.1038/416045a.

Thaer, S; Kassim, F A; Hasbullah, N A and Al-Obaidi, J R (2021). Evaluation of bagworm, *Metisa plana* (Lepidoptera: Psychidae) infestation and beneficial parasitoid in an oil palm plantation, Perak, Malaysia. *J. Sci. Math. Lett., 9(1)*: 19-35.

Thompson, J D; Higgins, D G and Gibson, T J (1994). CLUSTAL W: Improving the sensitivity of progressive multiple sequence alignment through sequence weighting, position-specific gap penalties and weight matrix choice. *Nucleic Acids Res., 22(22)*: 4673-4680. DOI: 10.1093/nar/22.22.4673.

Vogler, A P and Welsh, A (1997). Phylogeny of North American *Cicindela* tiger beetles inferred from multiple mitochondrial DNA. *Mol. Phylogenet. Evol., 8(2)*: 225-235.

Wood, B J and Kamarudin, N (2019). Bagworm (Lepidoptera: Psychidae) infestation in the centennial of the Malaysian oil palm industry - A review of causes and control. *J. Oil Palm Res., 31(3)*: 364-380.

Wortley, A H; Rudall, P J; Harris, D J and Scotland, R W (2005). How much data are needed to resolve a difficult phylogeny? Case study in Lamiales. *Syst. Biol., 54(5)*: 697-709.

Zhang, L; Cai, W; Luo, J; Zhang, S; Li, W; Wang, C; Lv, L and Cui, J (2018). Population genetic structure and expansion patterns of the cotton pest *Adelphocoris fasciaticollis*. *J. Pest Sci., 91*: 539-550.

Zhang, L J; Cai, W Z; Luo, J Y; Zhang, S; Wang, C Y; Lv, L M; Zhu X Z; Wang, L and Cui, J J (2017). Phylogeographic patterns of *Lygus pratensis* (Hemiptera: Miridae): Evidence for weak genetic structure and recent expansion in Northwest China. *PLoS ONE, 12(4)*: e0174712.

DETERMINATION OF RELIABLE REFERENCE GENES FOR REVERSE TRANSCRIPTION QUANTITATIVE REAL-TIME PCR FROM OIL PALM TRANSCRIPTOMES

NADZIRAH AMIRUDDIN[1]; PEK-LAN CHAN[1]; KUANG-LIM CHAN[1]; PEI-WEN ONG[1]; PRISCILLA ELIZABETH MORRIS[1]; MEILINA ONG-ABDULLAH[1]; SUBHI SITI MASURA[1] and ENG-TI LESLIE LOW[1]*

ABSTRACT

A set of reliable reference genes is essential for accurate quantification and interpretation of gene expression data using reverse transcription quantitative real-time polymerase chain reaction (RT-qPCR). In this study, Roche-454 RNA-seq reads from 27 libraries of various oil palm tissues were systematically analysed to identify a set of potential reference genes. Eleven candidate reference genes were identified from the transcriptome data. These genes, together with three oil palm reference genes previously identified for tissue culture samples (PD000380, PD00569, pOP-EA01332) and five classical housekeeping genes [glyceraldehyde-3-phosphate dehydrogenase (GAPDH), NAD5, TUBULIN, UBIQUITIN, ACTIN] were analysed across samples collected from various tissues from mature oil palm (leaf, root, endosperm, mesocarp, female flowers) and stages of tissue culture (non-embryogenic callus, embryogenic callus, polyembryoids, and shoots from polyembryoids). The expression levels of these genes were compared and evaluated using geNorm. Three genes (EgREF_5, EgREF_7 and EgREF_11) were found to be appropriate reference genes for normalising gene expression data from both mature plant and tissue culture samples.

INTRODUCTION

Gene expression analysis or the study of transcript abundance is essential in molecular biology research, especially in understanding the role of gene expression patterns in different biological processes (Dussert *et al.*, 2013; Kong *et al.*, 2021; Tranbarger *et al.*, 2011). It furthers our understanding and provides insights on the genetic and molecular mechanisms underlying developmental and cellular processes.

Reverse transcription quantitative real-time polymerase chain reaction (RT-qPCR) is one of the most powerful and sensitive techniques to quantify gene expression levels and has been recognised as a key driver of gene expression analysis in numerous molecular biology applications (Kozera and Rapacz, 2013; VanGuilder *et al.*, 2008). It is still considered the method of choice to validate high-throughput gene expression data (Everaert *et al.*, 2017). This technique is sensitive enough to detect gene expression changes, for even low transcript levels (Bustin *et al.*, 2005; Nolan *et al.*, 2006).

Nevertheless, it is important to note that substantial experimental variability, such as initial material quality, different inhibitors in samples, primer design and reverse transcription efficiencies should be taken into account to accurately quantify gene expression (Ginzinger, 2002; Mahoney *et al.*, 2004). Technical variability could be added to

1 Malaysian Palm Oil Board,
   6 Persiaran Institusi, Bandar Baru Bangi,
   43000 Kajang, Selangor, Malaysia.

* *Corresponding author e-mail: lowengti@mpob.gov.my*

the data by random pipetting errors (Bustin and Nolan, 2004; Fleige and Pfaffl, 2006). These factors can cause unreliability in the quantifications of gene transcripts. Despite being considered highly sensitive, accurate, and reproducible (Kubista *et al.*, 2006), this approach needs normalisation of the expression data to reduce the effects of variability in experimental data. Selection of an appropriate normalisation strategy is critical to acquire biologically meaningful data. Commonly, the level of gene expression is normalised by comparing messenger ribonucleic acid (mRNA) levels of target genes to endogenous controls, known as reference genes.

Reliable reference genes are required to interpret quantification data from RT-qPCR and compensate for any differences in the studied tissues or cells. An ideal reference gene is expressed at a constant level across various conditions and unaffected by experimental parameters (Guénin *et al.*, 2009; Schmittgen and Zakrajsek, 2000; Thellin *et al.*, 1999; Zhu *et al.*, 2013). In addition, they should not be co-regulated with the target gene but must be expressed in abundance with minimal variability (Radonic *et al.*, 2004). The reference and target genes should also have similar ranges of expression in the samples to be analysed (Cappelli *et al.*, 2008). The use of one or more reference genes is preferred for optimum normalisation (Bustin *et al.*, 2009; Chandna *et al.*, 2012; Guénin *et al.*, 2009; Vandesompele *et al.*, 2002; 2009). However, expression levels of reference genes can vary in response to changes in experimental conditions and/or tissue types, and that using unstable reference genes in the relative quantification of gene expression will lead to biases and inappropriate biological data interpretation (Artico *et al.*, 2010; Czechowski *et al.*, 2005; Dheda *et al.*, 2005; Li *et al.*, 2020; Thellin *et al.*, 1999).

The expression of classical housekeeping genes such as *glyceraldehyde-3-phosphate dehydrogenase* (GAPDH), *actin*, *tubulin* and *18S ribosomal RNA* were presumed to have constant levels of expression, being involved in basal cell metabolism, cytoskeleton or intracellular functions. These genes are widely used as reference genes. However, their expression levels have been demonstrated to vary under different experimental conditions (Barsalobres-Cavallari *et al.*, 2009; Exposito-Rodriguez *et al.*, 2008; Jian *et al.*, 2008; Karuppaiya *et al.*, 2017; Li *et al.*, 2020; Mallona *et al.*, 2010; Qi *et al.*, 2010; Reid *et al.*, 2006; Tang *et al.*, 2021).

Meta-analysis of transcript data has been shown to be an efficient method to survey for novel stably expressed genes from high-throughput technologies as an alternative to mine for reference genes. For example, microarray datasets have enabled the identification of novel reference genes from a variety of plants, including *Arabidopsis thaliana*, *Eucalyptus*, soybean and rice, as well as in human samples and cynomolgus monkeys (Chan *et al.*, 2014; Chang *et al.*, 2011; Cheng *et al.*, 2011; Czechowski *et al.*, 2005; de Oliveira *et al.*, 2012; Garrido *et al.*, 2020; Libault *et al.*, 2008; Narsai *et al.*, 2010; Park *et al.*, 2013).

Another high-throughput analysis method which uses deep-sequencing technologies known as RNA-seq, has provided an additional resource to microarrays. It is widely used for quantitative mRNA expression studies and sensitive enough to detect very low transcript expressions and their isoforms (Marioni *et al.*, 2008; Wang *et al.*, 2009). Furthermore, it also has the ability to identify novel transcripts and splice variants (Trapnell *et al.*, 2010). The technique is fast and generates replicated data with minimal variations (Marioni *et al.*, 2008; Mortazavi *et al.*, 2008; Nagalakshmi *et al.*, 2008; Wang *et al.*, 2009). Thus, RNA-seq is a feasible whole-transcriptome method for mining of stably expressed genes and the identification of novel reference genes for RT-qPCR normalisation. In recent findings, combinations of suitable reference genes for abiotic stresses in potato (Tang *et al.*, 2017) and *Arabidopsis pumila* (Jin *et al.*, 2019) were identified from transcriptome data.

RNA-seq derived transcriptome data has been widely explored in a number of oil palm studies (Beulé *et al.*, 2011; Bourgis *et al.*, 2011; Dussert *et al.*, 2013; Kong *et al.*, 2021; Shearman *et al.*, 2013). In oil palm, RNA-seq data was generated in studies on lipid accumulation (Tranbarger *et al.*, 2011) and carbon partitioning (Bourgis *et al.*, 2011) in mesocarp, response to *Ganoderma boninense* infection (Tee *et al.*, 2013), normal or mantled flowers and fruits (Shearman *et al.*, 2013), and phosphorus starvation in roots (Kong *et al.*, 2021). More researches were also conducted with the availability and increasing volume of African oil palm sequence data (Adam *et al.*, 2007; Bourgis *et al.*, 2011; Chan *et al.*, 2017; Jaligot *et al.*, 2011; Low *et al.*, 2008; 2014; Singh *et al.*, 2013). These datasets as a whole provide an invaluable pool of information that can be utilised to identify stably expressed genes that would greatly contribute to accurate and reliable quantification of RT-qPCR data. In oil palm, a number of reference genes for normalisation of gene expression has been identified in specific developmental stages, such as tissue culture (Chan *et al.*, 2014), stress-treated samples (Xia *et al.*, 2014), diverse sets of biological samples (vegetative and reproductive tissues, and developmental stages of mesocarp tissues) (Yeap *et al.*, 2014), as well as from young plantlets (Muhammad Afiq *et al.*, 2019). Nevertheless, improving the collection of reference genes would certainly help expedite validation of newly discovered genes involved in various tissues and developmental stages.

In this study, Roche-454 RNA-seq transcriptome libraries comprising 27 oil palm tissue samples were utilised to identify a set of novel reference

genes for normalisation of RT-qPCR expression data in oil palm. Nineteen candidate reference genes including three oil palm reference genes (*PD00380, PD00569, pOP-EA01332*) previously identified for tissue culture samples (Chan *et al.*, 2014), five classical housekeeping genes (*GAPDH, NAD5, TUBULIN, UBIQUITIN, ACTIN*), and 11 genes from the transcriptome data were evaluated. Statistical analysis using geNorm identified the three most stable reference genes in combination, *EgREF_5, EgREF_7* and *EgREF_11*. This result demonstrates that stably expressed reference genes could be identified from mining and utilisation of transcriptome datasets.

MATERIALS AND METHODS

Plant Materials

Leaf (spear and mature), endosperm [10 weeks after anthesis (WAA) and 15WAA], mesocarp (10WAA and 15WAA) and female inflorescence (frond number F13: 8.5 cm in length and F17: 20.0 cm) were sampled from Malaysian Palm Oil Board (MPOB) Research Station, Kluang, Johor, Malaysia. White root from seedlings in polybags, primary root (10 months nursery palms) and lateral root (10 months nursery palms) were sampled from the oil palm nursery in MPOB, Bangi, Selangor, Malaysia. Embryogenic callus, non-embryogenic callus, polyembryoids, and shoots from polyembryoids were collected from the tissue culture laboratory at the Advanced Biotechnology and Breeding Centre, MPOB, Bangi, Selangor, Malaysia. All samples were frozen in liquid nitrogen and stored at -80ºC prior to RNA extraction.

Ribonucleic Acid (RNA) Extraction, Purification and Quality Assessment

Total RNA was extracted according to the method by Ong *et al.* (2019). The total RNA was purified using RNeasy Mini Kit with on-column RNase free DNase I treatment according to the manufacturer's instructions (Qiagen, USA, Valencia, CA, USA). The concentration and purity of total RNA were determined using Nanodrop ND-1000 UV-Vis Spectrophotometer (Thermo Fisher Scientific Inc.), and the integrity was assessed by electrophoretic fractionation on an Agilent 2100 Bioanalyser using RNA 6000 Nano LabChip (Agilent Technologies, CA, USA).

Identification of Candidate Reference Genes in Oil Palm Transcriptome Data Sets

Candidate reference genes in oil palm were identified by performing differential expression analysis of Roche-454 RNA-seq reads from 27 libraries of various oil palm tissues from PRJNA201497 (leaf, root, seedling white root, pollen, mesocarp, endosperm) (Singh *et al.*, 2013) and PRJNA345530 [pith (one day after anthesis, DAA), sepal (1DAA), fruit (1DAA), spikelet (1DAA), stalk (1DAA)] (Chan *et al.*, 2017). Reads of each tissue were mapped to the published oil palm EG5 reference genome (Singh *et al.*, 2013) using TopHat2 (Kim *et al.*, 2013). Gene expression data was generated by cuffdiff (part of TopHat2 package) and normalised using the Fragments Per Kilobase per Million Reads method (FPKM). The average expression of genes expressed in each tissue was calculated and genes with a minimum FPKM of 40 in all tissues were selected as putative stably expressed genes. These identified genes were compared to the protein database using BLASTX (https://blast.ncbi.nlm.nih.gov) with default parameter 1 e^{-5}.

Primer Design and Efficiency Test

Primer pairs for candidate reference genes were designed using Primer3Plus software (http://www.bioinformatics.nl/primer3plus) (Untergasser *et al.*, 2007) with melting temperatures between 60°C and 67°C, primer lengths 20-27 bases, GC content 40%-60%, and amplicon lengths of 100-150 bp (Chan *et al.*, 2014). The transcript sequences of candidate reference genes used for primer design were aligned to the oil palm EG5 genome sequence to predict intron positions using Exonerate program (Slater and Birney, 2005). Primer pairs were designed on either different exons or spanning exon-exon junctions of the complementary deoxyribonucleic acid (cDNA) (Hu *et al.*, 2009) to avoid co-amplification of the genes from genomic DNA. Primer search against the oil palm genome was performed to check the specificity of each designed primer. The HPLC-purified primers were purchased from Bio Basic Canada Inc. All primer pairs were tested for polymerase chain reaction (PCR) amplification efficiencies (Ex) and to check for the specificity of the amplicon.

Reverse Transcription Quantitative Real-time PCR (RT-qPCR)

First-strand cDNA synthesis was carried out using 2 µg of total RNA using the High-capacity cDNA Reverse-Transcription Kit according to the manufacturer's instructions (Applied Biosystems, Foster City, CA, USA). The synthesised cDNA strands were used as templates in a SYBR Green based RT-qPCR using the Eppendorf Mastercycler® ep *realplex* (Eppendorf, Germany). RT-qPCR was performed according to the method described by Chan *et al.* (2014). A 'no reverse transcriptase' (NRT) control and a 'non-template control' (NTC) were assigned as negative controls.

Data Analysis

Cycle threshold (Ct) values were retrieved using Realplex software version 2.2 (Eppendorf, Germany). Results were imported into Microsoft Excel and data analysis was carried out by calculating the average Ct values for three replicates. Subsequently, the results were transformed into expression quantities using the method described by Vandesompele *et al.* (2002), Ex^(minCt - sampleCt), (Ex = [10$^{(-1/\text{slope})}$-1] × 100%, slope = slope of linear regression). The most stable reference genes across all samples were selected based on geNorm v3.4 using log-transformed data as input (Vandesompele *et al.*, 2002).

RESULTS

Selection of Candidate Reference Genes and Expression Analysis

A total of 11 putative stably expressed genes were identified through differential gene expression analysis of 27 oil palm transcriptome libraries. These genes are involved in various functions, such as DNA binding protein, macrophage migration inhibitory factor family protein, histone, deleted in split hand/splt foot protein, MKI67 FHA domain-interacting nucleolar phosphoprotein-like, NADH-ubiquinone oxidoreductase 13 kDa-B subunit, ribosomal protein, OB-fold nucleic acid binding domain-containing protein and ubiquitin. Of all the 11 genes, *EgREF_10*, which is a ubiquitin family protein (*Table 1*), showed the highest level of variation, with the highest expression in pollen and floret after anthesis (*Figure 1*). The difference between the highest and lowest was ~2.2 fold difference in expression while the average difference for the other genes was ~1.6 fold. Primer pairs were designed for the 11 genes from the transcriptome data, five classical housekeeping genes and three oil palm tissue culture samples reference genes (Chan *et al.*, 2014). Efficiency of designed primer pairs was evaluated by the presence of a single peak in the melting curve obtained after 40 cycles of amplification. Only primer pairs which showed a single amplified product were selected for further studies. Thirteen candidate genes were thus selected for further analysis (*Table 2*). The Ex of the selected primers ranged from 82% to 100%, and correlation coefficient (R^2) ranged from 0.979 to 0.999. Subsequently, SYBR Green detection-based RT-qPCR assay was carried out for transcript profiling of these genes. As shown in *Figure 2*, the genes have an average Ct value of 22.79. Most of the genes have expression values between 20 and 24. *UBIQUITIN* was the most abundant gene of the set (mean Ct: 20.18), whereas *PD00380* and *pOP-EA01332* were the least abundant genes (mean Ct: *PD00380* = 25.58, *pOP-EA01332* = 25.98). *PD00380* showed highest level of Ct variation, with a range between 33.91 and 22.23, of which the difference between 25th and 75th percentile is ~5 Ct.

Selection of Potential Reference Genes for Oil Palm

GeNorm analysis executed using a Visual Basic Application in Microsoft Excel (Vandesompele *et al.*, 2002) was used to select the most stably expressed reference gene across various oil palm tissues. Gene expression stability measure (M) of each reference gene was calculated using the relative expression values for each cDNA sample as input for the geNorm algorithm. The threshold proposed for stably expressed genes was M≤0.5 (Vandesompele *et al.*, 2002). Genes with the lowest M value are deemed to have the most stable expression. Two most stably expressed genes were obtained by eliminating the least stable gene in a stepwise manner. The algorithm ranked the potential reference genes based on their expression stability (*Figure 3*). *EgREF_5* and *EgREF_7* were the most stable genes having M≤0.5, while other genes (*EgREF_11*, *pOP-EA01332*, *PD00569*, *EgREF_1*, *ACTIN*, *GAPDH*, *EgREF_2*, *EgREF_5*, *UBIQUITIN*) had an M value between 0.5 and 1. The least stable genes, *TUBULIN* and *PD00380*, had M values of more than 1.

GeNorm was also used to determine the optimal number of reference genes required for accurate and reliable normalisation of expression data in the tested sample sets. Parameter V, defined as the pairwise variation (V_n/V_{n+1}) was calculated by geNorm between the two sequential normalisation factors (NF) of n and n + 1 genes of consecutively ranked reference genes. The purpose is to measure the effect of adding further reference genes on the normalisation factor. A cut-off threshold parameter V of 0.15 was recommended by Vandesompele *et al.* (2002), below which the addition of more reference genes is not required. As shown in *Figure 4*, the analysis showed that V3/V4 was 0.129, suggesting that the optimum number of reference genes is three. Hence, the best combination of reference genes is *EgREF_5*, *EgREF_7* and *EgREF_11*. The data also indicates that the new reference genes have greater expression stability than the conventionally used housekeeping genes, and can therefore provide more reliable normalised expression data.

DISCUSSION

RT-qPCR is one of the most sensitive tools that is commonly used to achieve rapid and reliable quantification of gene expression levels. However,

TABLE 1. SELECTED CANDIDATE REFERENCE GENES FROM TRANSCRIPTOME DATA

Query	Acc. num.	Annotation	E-value
EgREF_1	NP_001147321	DNA binding protein (*Zea mays*)	2.00E-11
EgREF_2	NP_195785	Macrophage migration inhibitory factor family protein (*Arabidopsis thaliana*)	2.00E-51
EgREF_3	XP_002319269	Histone 2 (*Populus trichocarpa*)	1.00E-43
EgREF_4	XP_002870907	Macrophage migration inhibitory factor family protein (*Arabidopsis lyrata* subsp. *Lyrate*)	3.00E-52
EgREF_5	NM_001153724	Deleted in split hand/splt foot protein (*Zea mays*)	1.00E-26
EgREF_6	NP_001241759	MKI67 FHA domain-interacting nucleolar phosphoprotein-like (*Zea mays*)	2.00E-66
EgREF_7	NP_001151372	NADH-ubiquinone oxidoreductase 13 kDa-B subunit (*Zea mays*)	9.00E-64
EgREF_8	NP_001146947	60S ribosomal protein L27 (*Zea mays*)	8.00E-59
EgREF_9	NP_178531	OB-fold nucleic acid binding domain-containing protein (*Arabidopsis thaliana*)	1.00E-35
EgREF_10	XP_002863802	Ubiquitin family protein (*Arabidopsis lyrata* subsp. *Lyrate*)	1.00E-33
EgREF_11	NP_001152653	40S ribosomal protein S14 (*Zea mays*)	2.00E-63
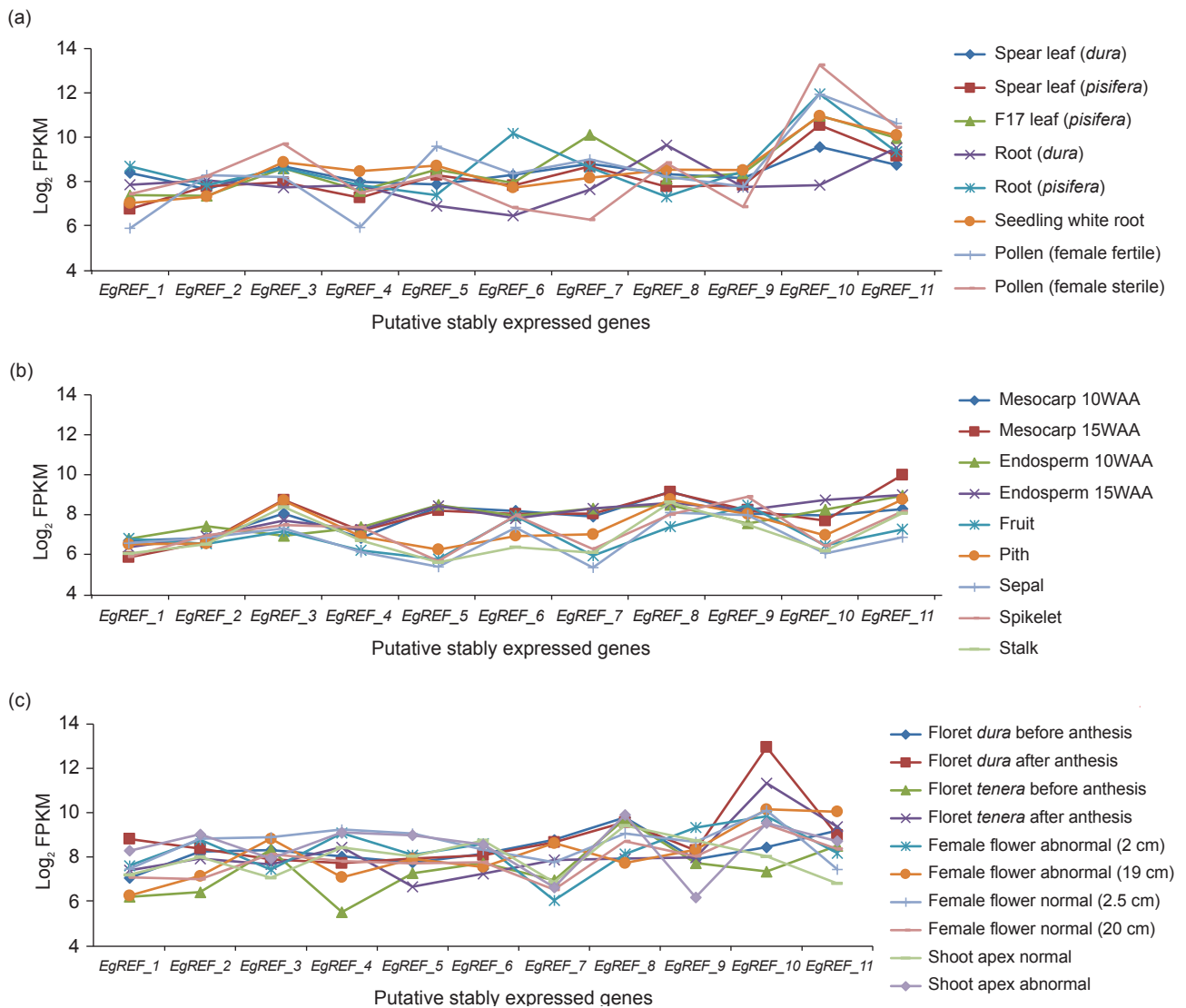
*Figure 1. Expression of putative stably expressed genes in various oil palm tissues based on transcriptome data. (a) spear leaf (*dura*), spear leaf (*pisifera*), F17 leaf (*pisifera*), root (*dura*), root (*pisifera*), seedling white root, pollen (female fertile), pollen (female sterile) (b) mesocarp 10WAA, mesocarp 15WAA, endosperm 10WAA, endosperm 15WAA, fruit, pith, sepal, spikelet, stalk, and (c) floret *dura* after anthesis, floret *dura* after anthesis, floret tenera before anthesis, floret tenera after anthesis, female flower abnormal (2 cm), female flower abnormal (19 cm), female flower normal (2.5 cm), female flower normal (20 cm), shoot apex normal, shoot apex abnormal.*

TABLE 2. PRIMERS AND AMPLICON CHARACTERISTICS OF SELECTED REFERENCE GENES

Gene abbreviation	Gene description	GenBank ID	Primer sequences (F/R) (5'-3')	Amplicon length (bp)	Annealing temperature (°C)	Amplification efficiency (%)	R^2
EgREF_3	Histone 2	Pr032825864	ATTTCTCAAGGCCGGCAAGTACG TGCCTCGGGACAATCCTAGTCTT	150	60	85	0.996
EgREF_4	Macrophage migration inhibitory factor family protein	Pr032825863	CCAAGACTGTCGCCAAGCTCATA GCCTCCAATGGAAACCAATTCGC	131	60	92	0.998
EgREF_5	Deleted in split hand/splt foot protein 1	Pr032825865	AGGACGCGAAGATCGACCTCTTT ATCATCCTCCCACTGCTGCATGA	116	60	87	0.997
EgREF_7	NADH-ubiquinone oxidoreductase 13 kDa-B subunit	Pr032825866	GCCAAGATGATCGAATGGGACCC GTCGGTGTTGGGGAACGTGTTTC	103	60	82	0.998
EgREF_10	Ubiquitin family protein	Pr032825867	ACAAGATCCGCATCCAGAAGTGGT GCTGTATTCTGATCAACCAGCC AACC	135	60	83	0.997
EgREF_11	40S ribosomal protein S17	Pr032825868	TCTCCCTCAAGCTTCAGGAGGAG GCATCTCGATGGTCTCCTTGTCG	111	60	87	0.995
PD00380	Predicted 40S ribosomal protein S27-2	EY397675	GATGGTTCTTCCGAACGATATTGA TCACATCCATGAAGAATGAGTTCG	113	60	87	0.995
PD00569	Manganese superoxide dismutase	EL682210	CACCACCAGACGTACATCACAAA GATATGACCTCCGCCATTGAACT	129	63	87	0.999
pOP-EA01332	Predicted protein IFH-1 like	EY406625	AAACGAAGGTACGGCAAGTACA AG CTTAGCACATGCAGAGCAGATGTT	111	63	100	0.979
GAPDH	Glyceraldehyde 3-phosphate dehydrogenase	DQ267444	GATCGAGAAATCAGCCACGTATG GTCACCAATAAAGTCGGTGGACA	124	63	87	0.998
TUBULIN	Alpha-tubulin 1	EL685625	CATGGCTTGCTGCCTTATGTATC AGGACACCAGTCAACAAACTGGA	109	63	95	0.999
UBIQUITIN	Polyubiquitin	EL689143	CCAGGCCAATCTCTCAGGATG GGGGGATGCCCTCTTTATCC	130	63	93	0.998
ACTIN	Actin	AY550991	TGCTGATCGTATGAGCAAGGAAA GAAATCCACATCTGCTGGAAGGT	147	60	83	0.999
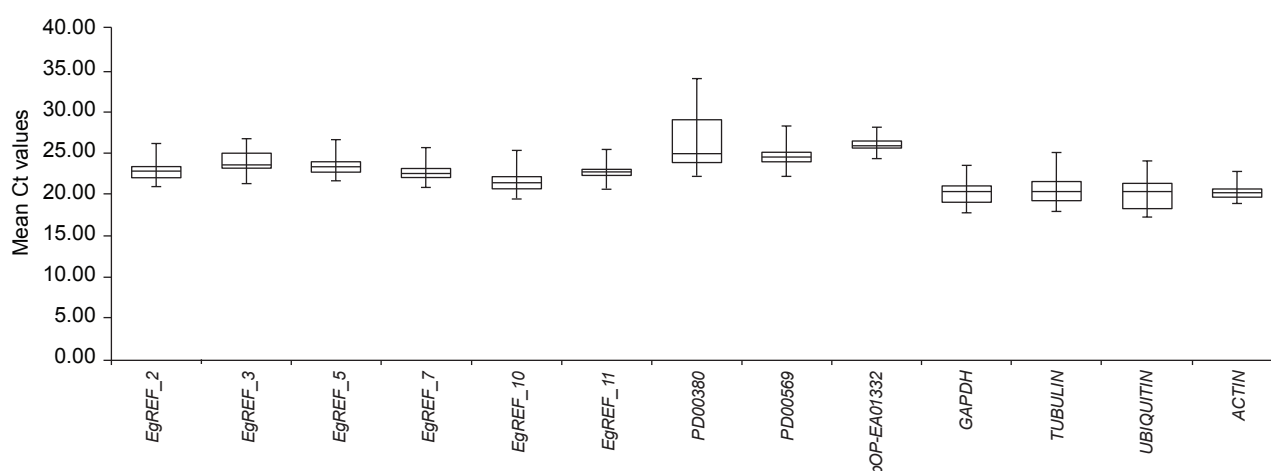
Figure 2. Mean Ct values of candidate reference genes across various oil palm tissues. The range of Ct values was exhibited in boxplot. The box indicates the 25th and 75th percentiles. Horizontal line inside the box is the median. Whiskers below and above the box represent minimum and maximum values. The 15 oil palm tissues tested are spear leaf, mature leaf, white root, lateral root, primary root, 10WAA kernel, 15WAA kernel, 10WAA mesocarp, 15WAA mesocarp, F17 inflorescence (20 cm), F13 inflorescence (8.5 cm), non-embryogenic callus, embryogenic callus, polyembryoids and shoots from the polyembryoids.
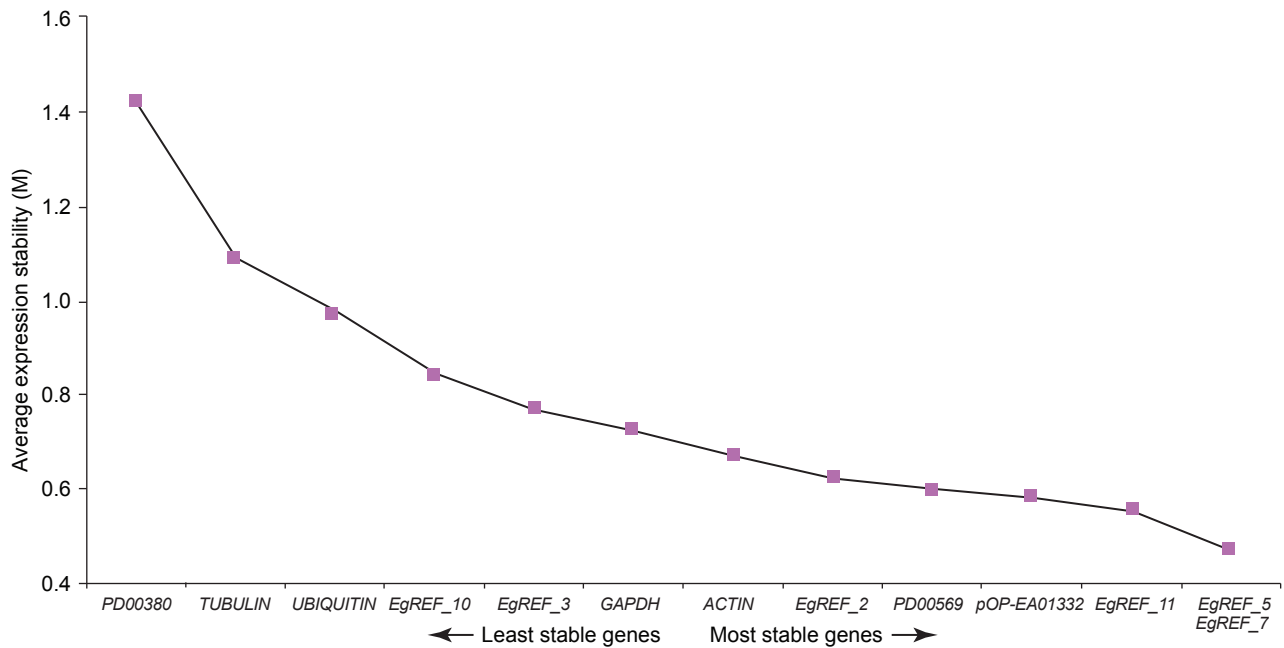
Figure 3. Determination of the most stably expressed reference genes using GeNorm software. Average expression stability values (M) were calculated for each candidate reference gene. Two most stable reference genes were obtained by excluding the least stable genes with higher M values in a stepwise manner.
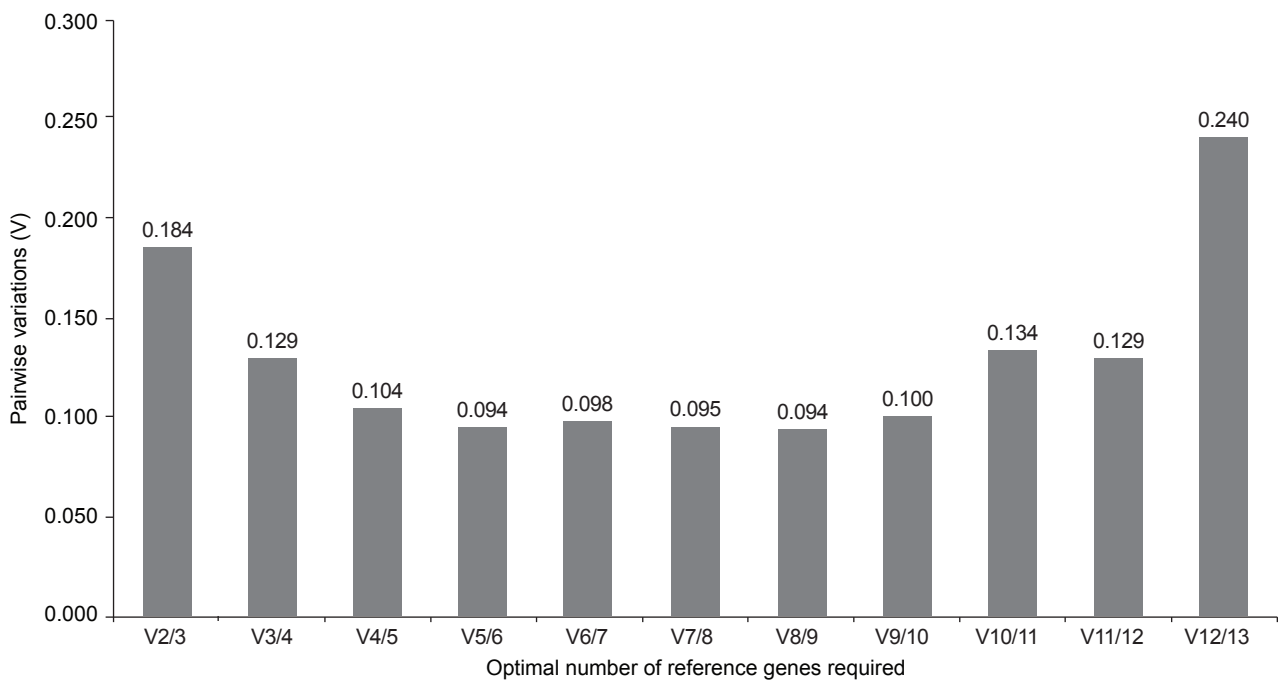
Figure 4. Determination of the optimal number of reference genes for accurate RT-qPCR data normalisation. Thirteen candidate reference genes were tested across 15 oil palm mature plant and tissue culture samples. Pairwise variation, $V_{n/n+1}$ were calculated between the normalisation factors (NF) of n and n + 1 genes by GeNorm. Additional reference gene is not required if V is lower than the cut-off value of 0.15.

this approach is potentially affected by the quantity and quality of initial materials, first strand cDNA synthesis efficiency, primer performance and statistical analysis methods chosen (Maroufi *et al.*, 2010). Thus, there is a need to normalise raw expression data with stably expressed reference genes for accurate and reliable results.

Normalisation is a critical step to compensate for technical variability caused by various steps of the experimental procedures which can affect interpretation of data from RT-qPCR. For this reason, it has become common practice to perform relative quantification by normalising RT-qPCR data to reference genes, as compared to absolute

quantification in which the input copy number is determined by relating the PCR signal to a standard curve for the particular genes of interest. It is also essential to understand that measurement of gene expression patterns may vary under different experimental conditions. Therefore, validation of reference genes should be done according to the panel that is specific for the chosen experimental conditions and tissue types under which the target gene is studied (Ruan and Lai, 2007; Selvey *et al.*, 2001; Song *et al.*, 2020; Suzuki *et al.*, 2000; Thellin *et al.*, 1999; Thorrez *et al.*, 2008; Zhao *et al.*, 2021).

In this study, we analysed transcriptome data from 27 libraries of various oil palm tissues to identify genes with low levels of variation in expression. A total of 11 genes with stable expression across all of the tissues tested were identified. From these genes, *EgREF_10*, annotated as ubiquitin, exhibited the highest level of variation, with highest levels of expression in pollen and floret. Ubiquitins, one of the most commonly used reference genes, are constitutively expressed to maintain cellular function. They are known as housekeeping genes whose protein products are involved in basic cellular processes (Bustin, 2002; Czechowski *et al.*, 2005; Dheda *et al.*, 2004; Hugget *et al.*, 2005). Ubiquitin and small ubiquitin-related modifiers are reported to be involved in post-translational protein modifications by attaching to target proteins to alter their functions (Smalle and Vierstra, 2004). Other functions include protein regulatory activity known as ubiquitination, and ubiquitin-proteasome system, which involves 5% of *Arabidopsis* proteins (Hellman and Estelle, 2002).

In theory, housekeeping genes are assumed to have a constant level of expression and classical housekeeping genes are frequently used and utilised as reference genes for normalisation in RT-qPCR. A number of frequently used classical housekeeping genes that have been validated as suitable reference genes in many plants includes *ACTIN, TUBULIN, UBIQUITIN* and *GAPDH* (Garg *et al.*, 2010; Gu *et al.*, 2011; Hu *et al.*, 2009; Maroufi *et al.*, 2010; Nicot *et al.*, 2005). *ACTIN*, a widely used reference gene, was selected as the most stable reference gene for normalisation of gene expression data in grapevine leaves (Gutha *et al.*, 2010). In papaya, a number of gene expression studies using RT-qPCR had used *ACTIN* as a reference gene (Hernandez *et al.*, 2007; Kouzaki *et al.*, 2009; Yu *et al.*, 2005; 2008).

TUBULIN was also deemed as an appropriate reference gene in banana (Podevin *et al.*, 2012). This gene was also identified to be the most suitable reference gene for normalisation across various developmental stages of somatic embryos in two representative conifer species, *Pinus pinaster* and *Picea abies* (De Vega-Bartol *et al.*, 2013). As for *UBIQUITIN*, it was found to have stable expression in *A. thaliana* and *Brachypodium* sp. (Czechowski

et al., 2005; Hong *et al.*, 2008). It was also considered a suitable reference gene in sugarcane leaf samples (de Andrade *et al.*, 2017) and bioenergy plants (Cheng *et al.*, 2019). *GAPDH* on the other hand has been used as a reference gene in citrus, Chinese wolfberry, cotton, chickpea, peanut, grapevine, coffee and sugarcane (Barsalobres-Cavallari *et al.*, 2009; de Andrade *et al.*, 2017; Garg *et al.*, 2010; Mafra *et al.*, 2012; Morgante *et al.*, 2011; Reid *et al.*, 2006; Wang *et al.*, 2013a; 2013b).

Among the four classical housekeeping genes, the ranking from the most stable to the least stable gene was: *ACTIN > GAPDH > UBIQUITIN > TUBULIN*. *TUBULIN* and *UBIQUITIN* are two of the five frequently used classical housekeeping genes. However, in our range of samples, these genes performed poorly as well as in tissue culture materials evaluated by Chan *et al.* (2014). It has been reported that *TUBULIN* was found poorly ranked in bamboo, peanut, grape, potato and soybean (Chi *et al.*, 2012; Fan *et al.*, 2013; Jian *et al.*, 2008; Nicot *et al.*, 2005; Reid *et al.*, 2006), while *UBIQUITIN* performed poorly as a reference gene in soybean (Jian *et al.*, 2008) and grape (Reid *et al.*, 2006).

In this study, *GAPDH* was ranked in the middle amongst the classical housekeeping genes. However, it had unstable expression across papaya fruit samples (Zhu *et al.*, 2012), and was considered the least stably expressed gene during leaf and flower development in petunia (Mallona *et al.*, 2010). It also displayed the biggest variation in leaves and roots of *Boehmeria nivea* L. (Yu *et al.*, 2020). Based on EST data analysis, this gene was also identified as poorly ranked reference gene in tomato (Coker and Davis, 2003).

In our range of samples, *ACTIN* was observed to be the most stable gene among all classical housekeeping genes studied. However, two published reference genes and four genes identified from transcriptome data were found to be more stably expressed than *ACTIN*. Furthermore, expression stability of *ACTIN* gene family members was observed to differ in peanut in specific conditions (Chi *et al.*, 2012; Morgante *et al.*, 2011; Reddy *et al.*, 2013). These results showed that the transcripts of housekeeping genes can vary in response to experimental conditions and tissue types. Thus, it is important to validate the expression stability of these genes prior to their use in normalisation for RT-qPCR.

Our results showed that three reference genes, *EgREF_5*, *EgREF_7* and *EgREF_11*, are suitable for normalisation of gene expression data from oil palm tissues. As reported by Szabo *et al.* (2004), valuable reference genes are expressed in several tissues with minimal variation in transcript level across experimental conditions. Genes with low variation in expression with coefficient variation of normalised relative quantities of less than 0.5

are suitable reference gene candidates (Hellemans *et al.*, 2007). The results suggest that it is possible to identify reliable candidate reference genes from multiple transcriptome datasets. *EgREF_5* was annotated as deleted in split hand/splt foot protein 1A, while the other two are NADH-ubiquinone oxidoreductase 13 kDa-B subunit (*EgREF_7*) and 40S ribosomal protein S17 (*EgREF_11*). Expression of these genes were found to be more stable than previously determined reference genes (Chan *et al.*, 2014) and classical housekeeping genes, in the set of diverse oil palm tissues within this study. In recent publications on oil palm reference genes, four genes namely *elF1, elF2, APT* and *cyc*, were identified from transcriptome datasets by Xia *et al.* (2014), of which *elF1* and *elF2* were selected as reference genes for cold, drought and salinity treatments. While *APT* and *cyc* were deemed stable reference genes for drought and salinity stress samples, two genes (*PD00380, PD00569*) were selected as reference genes for tissue culture samples (Chan *et al.*, 2014). These genes were also determined to be good reference genes for oil palm cultured leaf explants (Ooi *et al.*, 2012) and tissue culture samples (Chan *et al.*, 2010). However, in our range of samples, *PD00380* was observed to be the least stable expressed gene. Nevertheless, *pOP-EA01332* and *PD00569* were observed to have more stable expression and were ranked amongst the top five stably expressed genes. Other oil palm reference genes that have also been identified include *GRAS, Glutaredoxin, Cyp2* and *SLU7*, where *GRAS* and *Glutaredoxin* are suitable for reproductive tissues, vegetative tissues (*GRAS, Cyp2, SLU7*) and fruit development (*GRAS, Cyp2*) (Yeap *et al.*, 2014). Thus, validation of candidate reference genes is best done under specific experimental conditions and tissue types, as supported by the results of all of these studies.

CONCLUSION

This study shows that systematic analysis of transcriptome data can successfully guide the selection of reference genes for gene expression studies in oil palm, resulting in three housekeeping genes that can be used for RT-qPCR experiment on a wide range of mature plant and tissue culture samples. GeNorm statistical algorithm, identified a combination of three genes, *EgREF_5, EgREF_7* and *EgREF_11* as suitable reference genes for accurate and reliable normalisation across a diverse range of oil palm samples that consist of leaf, root, endosperm, mesocarp, female flowers, non-embryogenic callus, embryogenic callus, polyembryoids and shoots from polyembryoids. Hence, reference genes identified in this study could be used to generate reliable gene expression profile for a wide variety of tissues in oil palm.

REFERENCES

Adam, H; Jouannic, S; Orieux, Y; Morcillo, F; Richaud, F; Duval, Y and Tregear, J W (2007). Functional characterization of MADS box genes involved in the determination of oil palm flower structure. *J. Exp. Bot., 58*: 1245-1259.

Artico, S; Nardeli, S M; Brihante, O; Grossi-de-sa, M F and Alves-Ferreira, M (2010). Identification and evaluation of new reference genes in *Gossypium hirsutum* for accurate normalization of real-time quantitative RT-PCR data. *BMC Plant Biol., 10*: 49.

Barsalobres-Cavallari, C F; Severino, F E; Maluf, M P and Maia, I G (2009). Identification of suitable internal control genes for expression studies in *Coffea arabica* under different experimental conditions. *BMC Mol. Biol., 10*: 1.

Beulé, T; Camps, C; Debiesse, S; Tranchant, C; Dussert, S; Sabau, X; Jaligot, E; Alwee, S and Tregear, J W (2011). Transcriptome analysis reveals differentially expressed genes associated with mantled homeotic flowering abnormality in oil palm (*Elaeis guineensis*). *Tree Genet. Genomes, 7*: 169-182.

Bustin, S A (2002). Quantification of mRNA using real-time reverse transcription PCR (RT-PCR): Trends and problems. *J. Mol. Endocrinol., 29(1)*: 23-29.

Bustin, S A and Nolan, T (2004). Pitfalls of quantitative real-time reverse transcription polymerase chain reaction. *J. Biomol. Tech., 15*: 155-566.

Bustin, S A; Benes, V; Nolan, T and Pfaffl, M W (2005). Quantitative real-time RT-PCR – A perspective. *J. Mol. Endocrinol., 34*: 597-601.

Bustin, S A; Benes, V; Garson, J A; Hellemans, J; Hugget, J; Kubista, M; Mueller, R; Nolan, T; Pfaffl, M W; Shipley, G L; Vandesompele, J and Wittwer, C T (2009). The MIQE Guidelines: Minimum information for publication of quantitative real-time PCR experiments. *Clin. Chem., 55*: 611-622.

Bourgis, F; Kilaru, A; Cao, X; Ngando Ebongue, G F; Drira, N; Ohlrogge, J B and Arondel, V (2011).

Comparative transcriptome and metabolite analysis of oil palm and date palm mesocarp that differ dramatically in carbon partitioning. *Proc. Natl. Acad. Sci., 108*: 12527-12532.

Cappelli, K; Felicetti, M; Capomaccio, S; Spinsanti, G; Silvestrelli, M and Supplizi, A V (2008). Exercise induced stress in horses: Selection of the most stable reference genes for quantitative RT-PCR normalization. *BMC Mol. Biol., 9*: 1.

Chan, K L; Tatarinova, T V; Rosli, R; Amiruddin, N; Azizi, N; Ab Halim, M A; Sanusi, N S N M; Jayanthi, N; Ponomarenko, P; Triska, M; Solovyev, V; Firdaus-Raih, M; Sambanthamurthi, R; Murphy, D and Low, E T L (2017). Evidence-based gene models for structural and functional annotations of the oil palm genome. *Biol. Direct, 12*: 21.

Chan, P L; Ma, L S; Low, E T L; Shariff, E M; Ooi, L C L; Cheah, S C and Singh, R (2010). Normalized embryoid cDNA library of oil palm (*Elaeis guineensis*). *Electron. J. Biotechnol., 13*: 1-17.

Chan, P L; Rose, R J; Abdul Murad, A M; Zainal, Z; Low, E T L; Ooi, C L L; Ooi, S E; Yahya, S and Singh, R (2014). Evaluation of reference genes for quantitative real-time PCR in oil palm elite planting materials propagated by tissue culture. *PLoS ONE, 9(6)*: e99774.

Chandna, R; Augustine, R and Bisht, N C (2012). Evaluation of candidate reference genes for gene expression normalization in *Brassica juncea* using real-time quantitative RT-PCR. *PLoS ONE, 7*: e36918.

Chang, C W; Cheng, W C; Chen, C R; Shu, W Y; Tsai, M L; Huang, C L and Hsu, I C (2011). Identification of human housekeeping genes and tissue-selective genes by microarray meta-analysis. *PLoS ONE, 6*: e22859.

Cheng, T; Zhu, F; Sheng, J; Zhao, L; Zhou, F; Hu, Z; Diao, Y and Jin, S (2019). Selection of suitable reference genes for quantitative real-time PCR normalization in *Miscanthus lutarioriparia*. *Mol. Biol. Rep., 46*: 4545-4553.

Cheng, W C; Chang, C W; Chen, C R; Tsai, M L; Shu, W Y; Li, C Y and Hsu, I C (2011). Identification of reference genes across physiological states for qRT-PCR through microarray meta-analysis. *PLoS ONE, 6*: e17347.

Chi, X Y; Hu, R B; Yang, Q L; Zhang, X W; Pan, L J; Chen, N; Chen, M; Yang, Z; Wang, T; He, Y and Yu, S (2012). Validation of reference genes for gene expression studies in peanut by quantitative real-time RT-PCR. *Mol. Genet. Genomics, 287*: 167-176.

Coker, J S and Davies, E (2003). Selection of candidate housekeeping controls in tomato plants using EST data. *Biotechniques, 35*: 740-749.

Czechowski, T; Stitt, M; Altmann, T; Udvardi, M K and Scheible, W R (2005). Genome-wide identification and testing of superior reference genes for transcript normalization in *Arabidopsis*. *Plant Physiol., 139*: 5-17.

Dheda, K; Hugget, J F; Bustin, S A; Johnson, M A; Rook, G and Zumla, A (2004). Validation of housekeeping genes for transcript normalizing RNA expression real-time PCR. *Biotechniques, 37(1)*: 112-114, 116, 118-119.

Dheda, K; Hugget, J F; Chang, J S; Kim, L U; Bustin, S A; Johnson, M A; Rook, J A W and Zumla, A (2005). The implications of using an inappropriate reference gene for real-time reverse transcription PCR data normalization. *Anal. Biochem., 344*: 141-143.

De Andrade, L M; dos Santos Brito, M; Fávero Peixoto Junior, R; Marchiori, P E R; Nóbile, P M; Martins, A P B; Ribeiro, R V and Creste, S (2017). Reference genes for normalization of qPCR assays in sugarcane plants under water deficit. *Plant Methods, 13*: 28.

De Oliveira, L A; Breton, M C; Bastolla, F M; Camargo, S D; Margis, R; Frazzon, J and Pasquali, G (2012). Reference genes for the normalization of gene expression *Eucalyptus* species. *Plant Cell Physiol., 53(2)*: 405-422.

De Vega-Bartol, J J; Santos, R R; Simões, M and Miguel, C M (2013). Normalizing gene expression by quantitative PCR during somatic embryogenesis in two representative conifer species: *Pinus pinaster* and *Picea abies*. *Plant Cell Rep., 32*: 715-729.

Dussert, S; Guerin, C; Andersson, M; Joët, T; Tranbarger, T J; Pizot, M; Sarah, G; Omore, A; Durand-Gasselin, T and Morcillo, F (2013). Comparative transcriptome analysis of three oil palm fruit and seed tissues that differ in oil content and fatty acid composition. *Plant Physiol., 162*: 1337-1358.

Exposito-Rodriguez, M; Borges, A A; Borges-Perez, A and Perez, J A (2008). Selection of internal control genes for quantitative real-time PCR studies during tomato development process. *BMC Plant Biol., 8*: 131.

Everaert, C; Luypaert, M; Maag, J L V; Cheng, Q X; Dinger, M E; Hellemans, J and Mestdagh, P (2017). Benchmarking of RNA-sequencing analysis workflows using whole-transcriptome RT-qPCR expression data. *Sci. Rep., 7(1)*: 1559.

Fan, C; Ma, J; Guo, Q; Li, X; Wang, H and Lu, M (2013). Selection of reference genes for quantitative real-time PCR in bamboo (*Phyllostachys edulis*). *PLoS ONE, 8*: e56573.

Fleige, S and Pfaffl, M W (2006). RNA integrity and the effect on the real-time qRT-PCR performance. *Mol. Aspects of Med., 27*: 126-139.

Garg, R; Sahoo, A; Tyagi, A K and Jain, M (2010). Validation of internal control gene for quantitative gene expression studies in chickpea. *Biochem. Biophys. Res. Commun., 396*: 283-288.

Garrido, J; Aguilar, M and Prieto, P (2020). Identification and validation of reference genes for RT-qPCR normalization in wheat meiosis. *Sci. Rep., 10*: 2726.

Ginzinger, D G (2002). Gene quantification using real-time quantitative PCR: An emerging technology hits the mainstream. *Exp. Hematol., 30*: 503-512.

Gu, C; Chen, S; Liu, Z; Shan, H; Luo, H; Guan, Z and Chen, F (2011). Reference gene selection for quantitative real-time PCR in *Chrysanthemum* subjected to biotic and abiotic stress. *Mol. Biotechnol., 49*: 192.

Guénin, S; Mauriat, M; Pelloux, J; Wuytswinkle, O V; Bellini, C and Gutierrez, L (2009). Normalization of qRT-PCR data: The necessity of adopting a systematics, experimental conditions-specific, validation of references. *J. Exp. Bot., 60*: 487-493.

Gutha, L R; Casassa, L F; Harbertson, J F and Naidu, R A (2010). Modulation of flavonoid biosynthetic pathway genes and anthocyanins due to virus infection in grapevine (*Vitis vinifera L.*) leaves. *BMC Plant Biol., 10*: 187.

Hellman, H and Estelle, M (2002). Plant development: Regulation by protein degradation. *Science, 297(5582)*: 793-797.

Hellemans, J; Mortier, G; de Paepe, A; Speleman, F and Vandesompele, J (2007). qBase relative quantification framework and software for management and automated analysis of real-time quantitative PCR data. *Genome Biol., 8(2)*: R19.

Hernandez, M; Cabrera-Ponce, J L; Fragoso, G; Lopez-Casilla, F; Guevara-Garsia, A; Rosas, G; León-Ramírez, C; Juárez, P; Sánchez-García, G; Cervantes, J; Acero, G; Toledo, A; Cruz, C; Bojalil, R; Herrera-Estrella, L and Sciutto, E (2007). A new highly effective anticysticercosis vaccine expressed in transgenic papaya. *Vaccine, 25*: 4252-4260.

Hu, R B; Fan, C M; Li, H Y; Zhang, Q Z and Fu, Y F (2009). Evaluation of putative reference genes for gene expression normalization in soybean by quantitative real-time RT-PCR. *BMC Mol. Biol., 10*: 93.

Hugget, J; Dheda, K; Bustin, S and Zumla, A (2005). Real-time RT-PCR normalization: Strategies and considerations. *Genes Immun., 6(4)*: 279-284.

Hong, S Y; Seo, P J; Yang, M S; Xiang, F and Park, C M (2008). Exploring valid reference genes for gene expression studies in *Brachypodium distachyon* by real-time PCR. *BMC Plant Biol., 8*: 112.

Jaligot, E; Adler, S; Debladis, E; Beule, T; Richaud, F; Ilbert, P; Finnegan, E J and Rival, A (2011). Epigenetic imbalance and the floral development abnormality of the *in vitro*-regenerated oil palm *Elaeis guineensis*. *Ann. Bot., 108*: 1453-1462.

Jian, B; Liu, B; Bi, Y; Hou, W; Wu, C and Han, T (2008). Validation of internal control for gene expression study in soybean by quantitative real-time PCR. *BMC Mol. Biol., 9*: 59.

Jin, Y; Liu, F; Huang, W; Sun, Q and Huang, X (2019). Identification of reliable reference genes for qRT-PCR in the ephemeral plant *Arabidopsis pumila* based on full-length transcriptome data. *Sci. Rep., 9*: 8408.

Karuppaiya, P; Yan, X X; Liao, W; Wu, J; Chen, F and Tang, L (2017). Identification and validation of superior reference gene for gene expression normalization via RT-qPCR in staminate and pistillate flowers of *Jatropha curcas* – A biodiesel plant. *PLoS ONE, 12(5)*: e0177039.

Kim, D; Pertea, G; Trapnell, C; Pimentel, H; Kelley, R and Salzberg, S L (2013). TopHat2: Accurate alignment of transcriptomes in the presence of insertions, deletions and gene fusions. *Genome Biol., 14(4)*: R36.

Kong, S L; Abdullah, S N A; Ho, C L; Musa, M H and Yeap, W C (2021). Comparative transcriptome analysis reveals novel insights into transcriptional responses to phosphorus starvation in oil palm (*Elaeis guineensis*) root. *BMC Genom Data, 22*: 6.

Kouzaki, H; O'Grandy, S M; Lawrence, C B and Kita, H (2009). Proteases induce production of thymic stromal lymphopoietin by airway epithelial cells through protease-activated receptor-2. *J. Immunol., 183*: 1427.

Kozera, B and Rapcz, M (2013). Reference genes in real-time PCR. *J. Appl. Genetics, 54*: 391-406.

Kubista, M; Andrade, J M; Bengstsson, M; Forootan, A; Jonák, J; Lind, K; Sindelka, R; Sjöback, R; Sjögreen, B; Ståhlberg, A and Zoric, N (2006). The real-time polymerase chain reaction. *Mol. Aspects Med., 27(2-3)*: 95-125.

Li, Y; Liang, X; Zhou, X; Wu, Z; Yuan, L; Wang, Y and Li, Y (2020). Selection of reference genes for qRT-PCR analysis in medicinal plant *Glycyrrhiza* under abiotic stresses and hormonal treatments. *Plants, 9*: 1441.

Libault, M; Thibivilliers, S; Bilgin, D; Radwan, O; Benitez, M; Clough, S J and Stacey, G (2008). Identification of four soybean reference genes for gene expression normalization. *Plant Genome, 1*: 44-54.

Low, E T L; Alias, H; Boon, S H; Shariff, E M; Tan, C Y A; Ooi, L C L; Cheah, S C; Raha, A R; Wan, K L and Singh, R (2008). Oil palm (*Elaeis guineensis* Jacq.) tissue culture ESTs: Identifying genes associated with callogenesis and embryogenesis. *BMC Plant Biol., 8*: 62.

Low, E T L; Rosli, R; Jayanthi, N; Mohd-Amin, A H; Azizi, N; Chan, K L; Maqbool, N J; Maclean, P; Brauning, R; McCulloch, A; Moraga, R; Ong-Abdullah, M and Singh, R (2014). Analyses of hypomethylated oil palm gene space. *PLoS ONE, 9(1)*: e86728.

Mafra, V; Kubo, K S; Alves-Ferreira, M; Ribeiro-Alves, M; Stuart, R M; Boava, L P; Rodrigues, C M and Machado, M A (2012). Reference genes for accurate transcript normalization in Citrus genotypes under different experimental conditions. *PLoS ONE, 7*: e31263.

Mahoney, D J; Carey, K; Fu, M H; Snow, R; Cameron-Smith, D; Parise, G and Tarnopolsky, M A (2004). Real-time RT-PCR analysis of housekeeping genes in human skeletal muscle following acute exercise. *Physiol. Genomics, 18*: 226-231.

Mallona, I; Lischewski, S; Weiss, J; Hause, B and Egea-Cortines, M (2010). Validation of reference genes for quantitative real-time PCR during leaf and flower development in Petunia hybrid. *BMC Plant Biol., 10*: 4.

Maroufi, A; Bockstaele, E V and Loose, M D (2010). Validation of reference genes for gene expression analysis in chicory (*Cichorium intybus*) using quantitative real-time PCR. *BMC Mol. Biol., 11*: 15.

Marioni, J C; Mason, C E; Mane, S M; Stephens, M and Gilad, Y (2008). RNA-seq: An assessment of technical reproducibility and comparison with gene expression arrays. *Genome Res., 18(9)*: 1509-1517.

Morgante, C V; Guimarães, P M; Martins, A C Q; Araújo, A C G; Leal-Bertioli, S C M; Bertioli, D J and Brasileiro, A C (2011). Reference genes for quantitative reverse transcription-polymerase chain reaction expression studies in wild and cultivated peanut. *BMC Res. Notes, 4*: 339-350.

Mortazavi, A; Williams, B A; McCue, K; Schaeffer, L and Wold, B (2008). Mapping and quantifying mammalian transcriptomes by RNA-seq. *Nat. Methods, 5(7)*: 621-628.

Muhammad Afiq, A H; Shaharuddin, N A and Zubaidah, R (2019). Identification of reliable reference genes for gene expression studies of oil pam plantlets using NormFinder and BestKeeper algorithms. *J. Oil Palm Res., 31*: 204-211.

Nagalakshmi, U; Wang, Z; Waern, K; Shou, C; Raha, D; Gerstein, M and Snyder, M (2008). The transcriptional landscape of the yeast genome defined by RNA sequencing. *Science, 320(5881)*: 1344-1349.

Narsai, R; Ivanova, A; Ng, S and Whelan, J (2010). Defining reference genes in *Oryza sativa* using organ development, biotic and abiotic transcriptome datasets. *BMC Plant Biol., 10*: 56.

Nicot, N; Hausman, J F; Hoffman, L and Evers, D (2005). Housekeeping gene selection for real-time RT-PCR normalization in potato during biotic and abiotic stress. *J. Exp. Bot., 56(421)*: 2907-2914.

Nolan, T; Hands, R E and Bustin, S A (2006). Quantification of mRNA using real-time RT-PCR. *Nat. Protoc., 1*: 1559-1582.

Ong, P W; Chan, P L and Singh, R (2019). Isolation of high quality total RNA from various tissues of oil palm (*Elaeis guineensis*) for reverse transcription quantitative real-time PCR (RT-qPCR). *J. Oil Palm Res., 31*: 195-203.

Ooi, S E; Choo, C N; Ishak, Z and Ong Abdullah, M (2012). A candidate auxin-responsive expression marker gene, *Eg*IAA9, for somatic embryogenesis in oil palm (*Elaeis guineensis* Jacq.). *Plant Cell Tiss. Organ Cult., 110*: 201-212.

Park, S J; Kim, Y H; Huh, J W; Lee, S R; Kim, S H; Kim, S U; Kim, J S; Jeong, K J; Kim, K M; Kim, H S and Chang, K T (2013). Selection of new appropriate reference genes for RT-qPCR analysis via transcriptome sequencing of cynomolgus monkeys (*Macaca fascicularis*). *PLoS ONE, 8*: e60758.

Podevin, N; Krauss, A; Henri, I; Swennen, R and Remy, S (2012). Selection and validation of reference genes for quantitative RT-PCR expression studies of the non-model crop *Musa*. *Mol. Breeding, 30*: 1237-1252.

Qi, J; Yu, S; Zhang, F; Shen, X; Zhao, X; Yu, Y and Zhang, D (2010). Reference gene selection for real-time quantitative polymerase chain reaction of mRNA transcript levels in Chinese cabbage (*Brassica rapa* L. ssp. pikenensis). *Plant Mol. Biol. Rep., 28*: 597-604.

Radonic, A; Thulke, S; Mackay, I M; Landt, O; Siegert, W and Nitsche, A (2004). Guideline to reference gene selection for quantitative real-time PCR. *Biochem. Biophy. Res. Commun., 313*: 856-862.

Reddy, D S; Bhatnagar-Mathur, P; Cindhuri, K S and Sharma, K K (2013). Evaluation and validation of reference genes for normalization of quantitative real-time PCR based gene expression studies in peanut. *PLoS ONE, 8(10)*: e78555.

Reid, K E; Olsson, N; Schlosser, J; Peng, F and Lund, S T (2006). An optimized grapevine RNA isolation procedure and statistical determination of reference genes for real-time RT-PCR during berry development. *BMC Plant Biol., 6*: 27.

Ruan, W and Lai, M (2007). Actin, a reliable marker of internal control? *Clin. Chim. Acta, 385(1-2)*: 1-5.

Schmittgen, T D and Zakrajsek, B A (2000). Effect of experimental treatment on housekeeping gene expression: Validation by real-time, quantitative RT-PCR. *J. Biochem. Biophys. Methods, 46*: 69-81.

Selvey, S; Thompson, E W; Matthaei, K; Lea, R A; Irving, M G and Griffiths, L R (2001). Beta-actin an unsuitable internal control for RT-PCR. *Mol. Cell. Probes, 15(5)*: 307-311.

Shearman, J R; Jantasurirayat, C; Sangsrakru, D; Yoocha, T; Vannavichit, A; Tragoonrung, S and Tangphatsornruang (2013). Trancriptome analysis of normal and mantled developing oil palm flower and fruit. *Genomics, 101*: 306-312.

Singh, R; Ong-Abdullah, M; Low, E T L; Abdul Manaf, M A; Rosli, R; Nookiah, R; Ooi, C L L; Ooi, S E; Chan, K L; Halim, M A; Azizi, N; Nagappan, J; Bacher, B; Lakey, N; Smith, S W; He, D; Hogan, M; Budiman, M A; Lee, E K; DeSalle, R; Kudrna, D; Goicoechea, J L; Wing, R A; Wilson, R K; Fulton, R S; Ordway, J M; Martienssen, R A and Sambanthamurthi, R (2013). Oil palm genome sequence reveals divergence of infertile species in old and new worlds. *Nature, 500*: 335-339.

Slater, G S C and Birney, E (2005). Automated generation of heuristics for biological sequence comparison. *BMC Bioinformatics, 6*: 31.

Smalle, J and Vierstra, R D (2004). The ubiquitin 26S proteasome proteolytic pathway. *Annu. Rev. Plant Biol., 55*: 555-590.

Song, H; Mao, W; Duan, Z; Que, Q; Zhou, W; Chen, X and Li, P (2020). Selection and validation of reference genes for measuring gene expression in *Toona ciliata* under different experimental conditions by quantitative real-time PCR analysis. *BMC Plant Biol., 20*: 450.

Suzuki, T; Higgins, P J and Crawford, D R (2000). Control selection for RNA quantification. *Biotechniques, 29(2)*: 332-337.

Szabo, A; Perou, C M; Karaca, M; Perreard, L; Quackenbush, J F and Bernard, P S (2004). Statistical modeling for selecting housekeeper genes. *Genome Biol., 5*: R59.

Tang, N; Zhang, W; Chen, L; Wang, Y and Tang, D (2021). Reference gene selection for real-time quantitative reverse-transcription polymerase chain reaction in flower buds of marigold. *J. Amer. Soc. Hortic. Sci., 146(5)*: DOI: 10.21273/JASHS05074-21.

Tang, X; Zhang, N; Si, H and Calderón-Urrea, A (2017). Selection and validation of reference genes for RT-qPCR analysis in potato under abiotic stress. *Plant Methods, 13*: 85.

Tee, S S; Tan, Y C; Abdullah, F; Ong-Abdullah, M and Ho, C L (2013). Transcriptome of oil palm (*Elaeis guineensis* Jacq.) roots treated with *Ganoderma boninense*. *Tree Genetics and Genomes, 9*: 377-386.

Thellin, O; Zorzi, W; Lakaye, B; De Borman, B; Coumans, B; Henne, G; Grisar, T; Igout, A and Heinen, E (1999). Housekeeping genes as internal standards: Use and limits. *J. Biotechnol., 75*: 291-295.

Thorrez, L; Van Deun, K; Tranchevent, L C; Van Lommel, L; Engelen, K; Marchal, K; Moreau, Y; Mechelen, I V and Schuit, F (2008). Using ribosomal protein genes as reference: A tale of caution. *PLoS ONE, 3(3)*: e1854.

Tranbarger, T J; Dussert, S; Joët, T; Argout, X; Summo, M; Champion, A; Cros, D; Omore, A; Nouy, B and Morcillo, F (2011). Regulatory mechanisms underlying oil palm fruit mesocarp maturation, ripening, and functional specialization in lipid and carotenoid metabolism. *Plant Physiol., 156*: 564-584.

Trapnell, C; Williams, B A; Pertea, G; Mortazavi, A; Kwan, G; van Baren, M J; Salzberg, S L; Wold, B J and Pachter, L (2010). Transcript assembly and quantification by RNA-seq reveals unannotated transcripts and isoform switching during cell differentiation. *Nature Biotechnol., 28(5)*: 511-515.

Untergasser, A; Nijveen, H; Rao, X; Biselling, T; Geurts, R and Leunissen, J A M (2007). Primer3Plus, an enhanced web interface to Primer3. *Nucleic Acids Res., 35* (Web Server issue): W71-W74.

Vandesompele, J; De Preter, K; Pattyn, F; Poppe, B; Van Roy, N; De Paepe, A and Speleman, F (2002). Accurate normalization of real-time quantitative RT-PCR data by geometric averaging of multiple internal control genes. *Genome Biol., 3*: research0034.1-0034.11.

Vandesompele, J; Kubista, M and Pfaffl, M W (2009). Reference gene validation software for improved normalization. *Real-time PCR: Current Technology and Applications* (Logan, J; Edward, S K and Saunders, N eds.). Caister Academic Press, London. p. 47-64.

VanGuilder, H D; Vrana, K E and Freeman, W M (2008). Twenty-five years of quantitative PCR for gene expression analysis. *Biotechniques, 44(5)*: 619-626.

Wang, L; Wang, Y and Zhou, P (2013a). Validation of reference genes for quantitative real-time PCR during Chinese wolfberry fruit development. *Plant Physiol. Biochem., 70*: 304-310.

Wang, M; Wang, Q and Zhang, B (2013b). Evaluation and selection of reliable reference genes for gene expression under abiotic stress in cotton (*Gossypium hirsutum* L.). *Gene, 530*: 44-50.

Wang, Z; Gerstein, M and Snyder, M (2009). RNA-seq: A revolutionary tool for transcriptomics. *Nat. Rev. Genet., 10*: 57-63.

Xia, W; Mason, A S; Xiao, Y; Liu, Z; Yang, Y; Lei, X; Wu, X; Ma, Z and Peng, M (2014). Analysis of multiple transcriptomes of the African oil palm (*Elaeis guineensis*) to identify reference genes for RT-qPCR. *J. Biotechnol., 184*: 63-73.

Yeap, W C; Loo, J M; Wong, Y C and Kulaveerasingam, H (2014). Evaluation of suitable reference genes for qRT-PCR gene expression normalization in reproductive, vegetative tissues and during fruit development in oil palm. *Plant Cell Tiss. Organ Cult., 116*: 55-66.

Yu, Q; Hou, S; Feltus, F A; Jones, M R; Murray, J E; Veatch, O; Lemke, C; Saw, J H; Moore, R C; Thimmapuram, J; Liu, L; Moore, P H; Alam, M; Jiang, J; Paterson, A H and Ming, R (2008). Low X/Y divergence in four pairs of papaya sex-linked genes. *Plant J., 53*: 124-132.

Yu, Q; Moore, P H; Albert, H H; Roader, A H K and Ming, R (2005). Cloning and characterization of a FLORICAULA/LEAFY ortholog, PFL, in polygamous papaya. *Cell Res., 15*: 576-584.

Yu, Y; Zhang, G; Chen, Y; Bai, Q; Gao, C; Zeng, L; Li, Z; Cheng, Y; Chen, J; Sun, X; Guo, L; Xu, J and Yan, Z (2020). Selection of reference genes for qPCR analyses of gene expression in ramie leaves and roots across eleven abiotic/biotic treatments. *Sci. Rep., 9*: 20004.

Zhao, Z; Zhou H; Nie, Z; Wang, X; Luo, B; Yi, Z; Li, X; Hu, X and Yang, T (2021). Appropriate reference genes for RT-qPCR normalization in various organs of *Anemone flaccida* Fr. Schmidt at different growing stages. *Genes, 12*: 459.

Zhu, J; Zhang, L; Li, W; Han, S; Yang, W and Chen, F (2013). Reference gene selection for quantitative real-time PCR normalization in *Caragana intermedia* under different abiotic stress conditions. *PLoS ONE, 8*: e53196.

Zhu, X; Li, X; Chen, W; Chen, J; Lu, W; Chen, L and Fu, D (2012). Evaluation of new reference genes in papaya for accurate transcript normalization under different experimental conditions. *PLoS ONE, 7*: e44405.

ANTIFUNGAL AND ANTIOXIDANT PEPTIDES FROM OIL PALM MESOCARPS

BENJAMIN LAU YII CHUNG[1]*; ABRIZAH OTHMAN[1] and UMI SALAMAH RAMLI[1]

ABSTRACT

Phytochemicals and bioactive peptides have been discovered in oil palm organs such as kernel and leaf, but there is no documented study in isolating peptides with bioactivities from fruit mesocarps. In this work, we aimed to determine the bioactivity of the peptides derived from hydrolysis of oil palm fruit mesocarps. The fruit mesocarps were subjected to enzyme hydrolysis using trypsin and pepsin, followed by separation of these peptides through liquid chromatography-tandem mass spectrometry (LC-MS/MS) and database searching. Analysis of bioactivity from 25% and 30% fractions (trypsinised), and 10% and 30% fractions (pepsinised) showed inhibitory effect towards the growth of Ganoderma boninense. *In antioxidant assay, only non-fractionated protein hydrolysate with trypsin and pepsin showed a scavenging activity of 17.7%-22.3% for 2,2-diphenyl-1-picrylhydrazyl. We further determined the possible occurrence of antimicrobial activity* in silico *by matching the experimental peptide sequences to known bioactive peptides. Four antimicrobial peptides were found in fractionated mesocarp hydrolysates using trypsin and pepsin. These bioactive peptides had molecular masses of less than 4-5 kiloDalton (kDa) and made of 11-39 amino acid residues. A total of 23%-54% hydrophobic amino acids were found within these sequences. The results showed that the oil palm mesocarps contained peptides with various bioactivities that could be bioprospected into functional constituents with health and crop protection benefits.*

INTRODUCTION

Crude palm oil (CPO) extraction from fruit bunches in palm oil mills around Malaysia generate waste by-products in the form of solid (palm kernel shells, mesocarp fibres and empty fruit bunches-EFB) and liquid (palm oil mill effluent). In 2019, there were 452 palm oil mills in operation throughout Malaysia, capable to produce 112.91 million tonnes of fresh fruit bunches (FFB) annually (Kushairi and Mohd Din, 2020). Chavalparit (2006) reported that an average value of waste generation rate per tonne FFB from palm oil mill in Thailand were 140 kg of fibre, 60 kg of shells, 240 kg of EFB and 42 kg of decanter cake. Abas *et al.* (2011) reported that these by-products could reach 70-80 million tonnes per year. Irvan (2018) also stated that for every tonne of CPO produced, 0.90 t of EFB, 0.60 t of mesocarp fibres and 0.27 t of palm kernel shells are generated. This huge amount of waste by-products must be treated efficiently or used as biomass to reduce their undesired impacts to the environment.

Mesocarp fibres are generated from mesocarp pressed cake after the removal of nuts and pulp oil (Sabil *et al.*, 2013; Sreekala *et al.*, 1997). Together with EFB and palm kernel shells, the fruit fibres can be considered harmful waste to the surrounding environment, if released untreated. These fibres are

---

1   Malaysian Palm Oil Board,
    6 Persiaran Institusi, Bandar Baru Bangi,
    43000 Kajang, Selangor, Malaysia.

*   *Corresponding author e-mail: benjamin@mpob.gov.my*

harder to dispose and normally discarded in the palm oil mills as wastes or used as boiler fuel to produce steam and generating power due to their low moisture content compared to other biomass residues such as EFB. However, mesocarp fibres have low carbon content and therefore, require a remarkably high load to generate power energy, compared to coal. Mesocarp fibres also have low heating value, rendering it difficult to be utilised (Pereira *et al.*, 2020).

Bio-based products are a growing trend in industrial crops. The increasing need for these products is the driving force for the growth of functional food market. Bioactive peptides with antioxidant properties have been indicated as one of the key ingredients in health-promoting foods. The peptides work to lessen the effects of oxidative stress and lipid peroxidation caused by free radicals in human body and food products (Tadesse and Emire, 2020). A demand for less detrimental agricultural pesticides with reduced detrimental effects for crop protection is also pushing for the emergence of the peptide-based biopesticide industry. Biopesticides work similarly with chemical pesticides but not toxic and damaging to the environment. The oil palm industry is currently being threatened by *Ganoderma boninense*-induced basal stem rot disease. Biofungicides could provide an alternative to the management of this disease without the use of chemical-based control agents.

Mesocarp pressed cake and fibres are readily available raw materials for the extraction of bioactive peptides with antioxidant and antifungal properties. Through this technology, a downstream processing technology to convert mesocarp-based materials into value added natural product can be developed. Bioactive peptides represent specific sequences of amino acids that possess biological activity with several health effects and potential applications in nutraceutical industry. These peptides can be obtained from a chain of procedures, including cell lysis and protein extraction and enzymatic hydrolysis. Mesocarp fibres can have economic values as they can be used as sources of these biomaterials. Protein hydrolysates from palm kernel cake had been found to exhibit good angiotensin converting enzyme (ACE)-inhibitory activity between 22.9% and 70.9% (Zarei *et al.*, 2015), antiradical capacity (Ng *et al.*, 2013) and antibacterial activity (Tan *et al.*, 2013). It is therefore rationale to investigate if mesocarp tissues also contain other natural occurring peptides to be developed as bioactive defense against harmful environments. The current process using fruit mesocarp could be adapted to produce bioactive peptides from the abundant mesocarp pressed cake and fibres. To our best knowledge, there is no reported use of oil palm fruit mesocarp as raw material to produce protein hydrolysate, nor is there any published work on the bioactive properties of the protein hydrolysate from this important oil crop.

MATERIALS AND METHODS

Plant Materials

Ripe *Elaeis guineensis* (oil palm) fruitlets (20th week after anthesis) were used as the source of proteins for enzyme hydrolysis. The fruit mesocarps from the fruitlets were sliced to about 2 cm in length, snap frozen in liquid nitrogen and stored at -80°C.

Protein Extraction

Protein extraction was performed according to Lau *et al*. (2015). Five g of sliced fruit mesocarps were ground in 15 mL of acetone containing 10% trichloroacetic acid and 1 mM dithiothreitol. The slurry was then centrifuged at 13 000 g for 10 min at 4°C (RA-300 rotor, Kubota 7820, Kubota Corporation, Tokyo, Japan). The washing step was repeated prior to addition of 15 mL of 80% methanol containing 0.1 M ammonium acetate. The slurry was mixed and centrifuged as before. The precipitated mesocarp pellet was washed with 15 mL of 80% acetone. The mixture was centrifuged at 13 000 g for 10 min at 4°C. Pellet was re-suspended in 15 mL of extraction buffer containing 0.7 M sucrose, 1 M Tris-HCl, pH 8.3, 5 M NaCl, 50 mM DTT, and a tablet of Roche protease inhibitors. The resuspension was sonicated in ultrasonic bath for 15 min (Townson Mercer Ltd., Stretford, United Kingdom). The mixture was then sieved through two layers of Miracloth (Calbiochem, EMD Millipore Corporation, Billerica, MA, USA) to isolate the non-macerated plant materials. An equal volume of fresh 50 mM, pH 8.0 Tris-saturated phenol (15 mL) was added to the mixture, mixed, and centrifuged at 15 000 g for 15 min at 4°C. Proteins in the upper phase were precipitated by adding 5 volumes of cold ammonium acetate-saturated methanol and incubated at -20°C overnight before being centrifuged at 15 000 g for 15 min at 4°C. The protein pellet was rinsed with ammonium acetate-saturated methanol and washed twice with 10 mL of 80% acetone. The protein pellet was air-dried.

Protein Hydrolysis and Fractionation

Pellet was solubilised in 50 mM Tris-HCl, pH 8.0 (for trypsin) or 50 mM KCl, pH 2.0 (for pepsin). A 1 mg of trypsin or pepsin was added to 50 mg of proteins. The mixture was incubated for 24 hr with agitation rate of 300 rpm (Innova 42, New Brunswick Scientific Co. Inc., CT, USA). Reaction

was stopped by heating at 100°C for 10 min. The hydrolysed peptides were filtered with 10 kDa centrifugal filters (Amicon Ultra, Merck Millipore Ltd., County Cork, Ireland), purified with C18 disk and fractionated through sequential elution with 5%-80% acetonitrile.

2,2-Diphenyl-1-Picrylhydrazyl (DPPH) Free Radical Scavenging Activity Assay

A volume of 50 mL of DPPH solution was prepared using 1.25 mg of 2,2-diphenyl-1-picrylhydrazyl and 50% methanol. An assay standard of 1 mL was prepared using 25 mg gallic acid and 5 mL of double-distilled water (ddH$_2$O). A volume of 15 µL of assay standard or sample was mixed with 975 µL DPPH solution. Absorbance at 515 nm was read every 20 s for 12 cycles (Infinite M200, Tecan, Mannedorf, Switzerland). The antioxidant activity was expressed as percentage of DPPH free radical scavenging activity (%DPPH$_{SC}$) and calculated using the Equation (1):

$$\%DPPH_{SC} = (ABS_{blank} - ABS_{sample}) / (ABS_{blank} \times 100\%) \qquad (1)$$

where ABS$_{blank}$ is the absorbance value of blank at t=195 s and ABS$_{sample}$ is the absorbance value of protein hydrolysate. Gallic acid at a concentration of 0-10 µg mL^{-1} was used as the assay standard.

Antifungal Assay

A volume of 100 µL of potato dextrose broth was added into the well of a 96-well microtiter plate. The potato dextrose broth was mixed with 10 µL of sample in the well. A plug of the *G. boninense* fungus, with a diameter of 5 mm, was added into the well. In this assay, well with a plug of the *G. boninense* fungus without the sample was used as a positive control. The well containing just the potato dextrose broth was used as a negative control. The plate was incubated in dark at 27°C. Growth was observed until day 7.

Liquid Chromatography-tandem Mass Spectrometry

Separation and spectra acquisition of the peptides was conducted with a Thermo EASY-nano liquid chromatography 1200 System, coupled to a Thermo Q Exactive Plus mass spectrometer (Thermo Scientific, MA, USA). The dried peptide digests were reconstituted in 30 µL of 0.1% formic acid and 5% acetonitrile. A digest volume of 2 µL was injected into an Acclaim PepMap 100 C18 reversed phase column (3 µm, 0.075 x 250 mm) (Thermo Scientific, MA, USA). The column was equilibrated with 0.1% formic acid (Mobile phase A) and 80% acetonitrile containing 0.1% formic acid (Mobile phase B). Gradient of 5%-35% in 90 min was applied at a flow rate of 300 nL min^{-1}. Peptide ions were generated by electrospray ionisation using a spray voltage of 1900 V. Peptide precursor survey scan with a mass ranged from *m/z* 310-1800 and resolving power of 70 000 was acquired. Only peptide precursors with charge state of 2-7 were chosen for tandem MS. Tandem MS conditions consisted of rapid scan rate using a resolving power of 17 500 and 0.7 *m/z* isolation window. Precursors were fragmented using collision induced and high-energy collision induced at normalised collision energy of 28%, respectively. Mass range scanned was from *m/z* 110-1800.

Data Analysis

Data acquisitions in positive mode were executed with Thermo Scientific Tune. Generated raw data was processed with Thermo Scientific Proteome Discoverer, version 2.2 (Thermo Scientific, MA, USA). Tandem mass spectra were searched with SEQUEST HT engine against antimicrobial peptide FASTA sequences obtained from the Antimicrobial Peptide Database (APD) (Wang *et al.*, 2016) to determine peptide with bioactivity. Mass tolerances for peptide and product ions were set to 20 ppm and 0.5 Da. Trypsin or pepsin with customised cleavage sites was designated as the protease with two missing cleavages was allowed. Carbamidomethylation on cysteine was set as the static modification while oxidation of methionine, deamidation of asparagine and glutamine, and acetyl N-terminal modifications were searched as dynamic modifications. All peptide spectral matches were validated using the Percolator (component of Proteome Discoverer) based on q-value at a 1% false discovery rate.

RESULTS

The process to convert the oil palm mesocarps to produce bioactive peptides comprised of a series of steps from protein extraction to fractionate the obtained protein hydrolysates using enzymatic hydrolysis (*Figure 1*). The subsequent search for other bioactive peptides involves generating the sequence of the fractionated peptides and matched them to existing antimicrobial databases to identify possible antimicrobial peptides (Odintsova *et al.*, 2009).

Antifungal Assay

Fractionated peptides were qualitatively tested for their antifungal bioactivity, specifically towards *G. boninense* using a microtiter plate-based assay. As indicated in *Figure 2*, 25% and 30% fractions of the trypsin hydrolysate showed inhibition of the fungus *G. boninense* at day 2 to day 3. Eluted fractions 10%

and 30% of the pepsin hydrolysate also demonstrated inhibition against *G. boninense* from day 2 to day 3. In this antifungal activity assay, we had monitored the inhibition behaviour until day 7 of the *G. boninense* growth. At day 7, *G. boninense* growth no longer show any inhibition by the peptide (for both trypsin and pepsinised) hydrolysates as the fungal growth reached saturation at day 7. It was postulated that the dosage of the peptide hydrolysates (10 µL) was enough to suppress the growth until day 3.

2,2-Diphenyl-1-Picrylhydrazyl (DPPH) Free Radical Scavenging Activity Assay

Only non-fractionated mesocarp protein hydrolysates were assayed for their scavenging activity towards DPPH. *Figure 3* shows the $DPPH_{SC}$ of the trypsin and pepsin hydrolysates. Presence of peptides with scavenging activity of 22.3% was found in pepsin-treated mesocarp proteins after 3 min. Trypsin-digested mesocarp
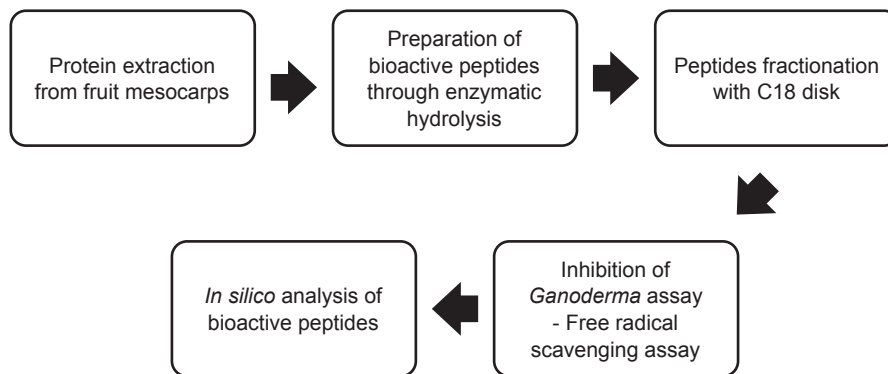

Figure 1. Overall process to generate bioactive peptides from oil palm mesocarps. The protein was extracted from the oil palm fruit mesocarps before being treated with trypsin and pepsin for enzyme hydrolysis. Then, the peptides were fractionated with C18 disk for antifungal, while the non-fractionated hydrolysates were used for antioxidant assay. The acquired peptides were further matched to the antimicrobial peptide database (APD) to determine the existence of bioactivity.
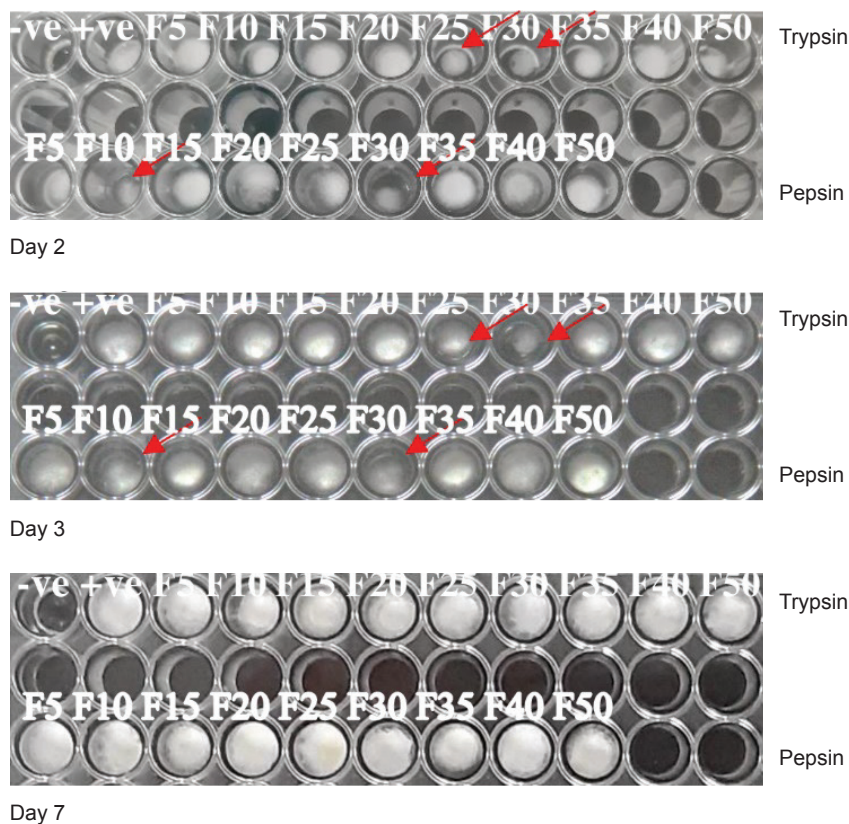
Figure 2. Antifungal bioactivity of the fractionated peptide hydrolysates towards Ganoderma boninense until day 7 of the fungal growth. The fractionated trypsin and peptide hydrolysates (F5, F10, F15, F20, F25, F30, F35, F40 and F50) were tested for their inhibition against the Ganoderma boninense fungus. F25 and F30 of the trypsin hydrolysate showed inhibition at day 2 to day 3. F10 and F30 of the pepsin hydrolysate also showed inhibition from day 2 to day 3.
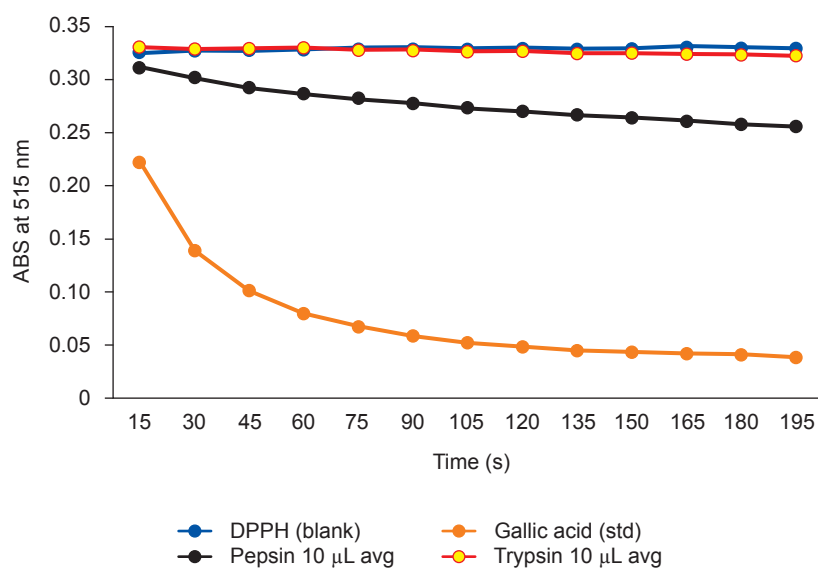
Figure 3. Free radical-scavenging activity assays of trypsin- and pepsin-treated mesocarp proteins. Gallic acid was the assay standard used and DPPH was the assay blank. Pepsin hydrolysate showed 22.3% of scavenging activity and trypsin hydrolysate exhibited a lower scavenging activity of 17.7%.

proteins showed lower $DPPH_{SC}$ of 17.7% after 3 min. Digestion with pepsin clearly exposed more amino acid residues that could act as hydrogen donor to enhance the scavenging capability of the peptides. Digestion with trypsin resulted in peptides with higher hydrophilicity that render them inaccessible to DPPH free radicals (Bamdad *et al.*, 2011). Both hydrolysates were filtered and supposed to comprise of peptides with masses of less than 10 kDa. Low mass peptides are normally more effective as antioxidants (Hong *et al.*, 2014; Liu *et al.*, 2015; Zhao *et al.*, 2007).

### *In Silico* Identification of Peptide with Antimicrobial Bioactivity

Sequence of the fractionated peptides was determined using shotgun proteomics strategy. *Figures 4* and *5* displayed the representative peptide fragment spectra from the fractionated hydrolysates corresponding to trypsin and pepsin hydrolysis. The peptide sequences were searched against the antimicrobial database to identify peptides with bioactivities. The *in silico* analysis found four peptides with mass of less than 4 kDa (MH+) obtained from the trypsin digestion matched (82%-100%) to known antimicrobial peptides deposited in the database. Their sequences contained 11-39 amino acid residues per peptide. Three of these peptides identified to PG-K111, Peptide 5 and lactococcin Q, possess anti-gram positive and negative activities while peptide NKGCAICSIGAACLVDGPIPDFEIAGATGLFGLWG (identified to subtilosin A1) from fraction 15% has anti-gram positive property only. All these

peptides have high amount of hydrophobic amino acids (23%-54%). The increment of these hydrophobic residues explained the higher concentration of acetonitrile to elute these bioactive peptides and their solubility in lipid. This could help in enhancing the lipid inhibitory activity by facilitating the interaction between peptides and radical species (Siow and Gan, 2013). Hydrophobic amino acid could also help to exhibit higher antihypertensive potential (Cheung *et al.*, 1980; Ghribi *et al.*, 2015).

Peptide sequences identified from 5% peptide fraction of pepsin digestion were found matched to the known antimicrobial and antifungal peptides. All these peptides have mass of less than 5 kDa (MH+). All the matched peptides identified to human drosomycin-like defensin, MiAMP2c and MiAMP2d, have antifungal properties except peptide RMRRSKSGKGSGGSKGSGSKGSKGSKGS GSKGSGSKGGSRPGGGSSIAGGGSKGKGGT QTA, identified to ayu cathelicidin (aCATH) peptide in the APD. Less than 25% of the peptides are made of hydrophobic amino acids and these explained the poor retention by the hydrophobic column. The *in silico* analysis also showed that these peptides are very long, from 48-68 amino acid residues per peptide. The peptide sequences were observed to possess a high amount of repeating amino acid residues. Many reported dipeptides from plant proteins were found to exhibit *in vitro* antioxidant effects (Samaraweera *et al.*, 2011). These di- and tri-peptides have exhibited better biological activity if compared to their constituent amino acids (Kawashima *et al.*, 1979). They are also absorbed more rapidly than free amino acid (Silk *et al.*, 1980).
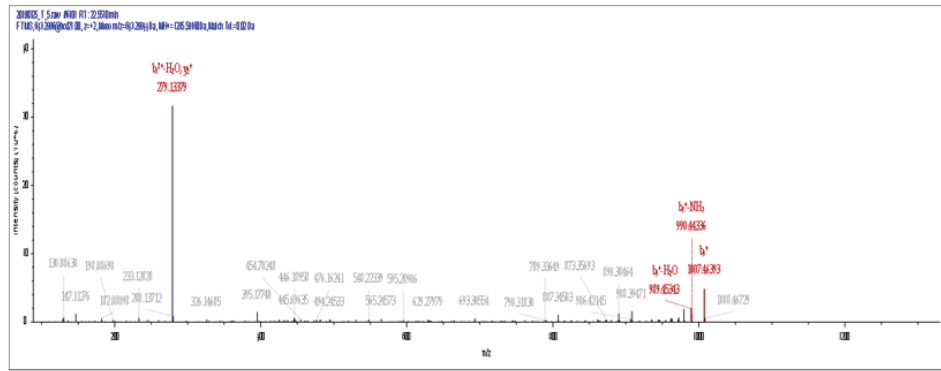
EPHPNEFVGLM (MH+: 1285.58815 Da, Fraction 5% and 20%)
36% hydrophobic residue, length: 11 amino acid
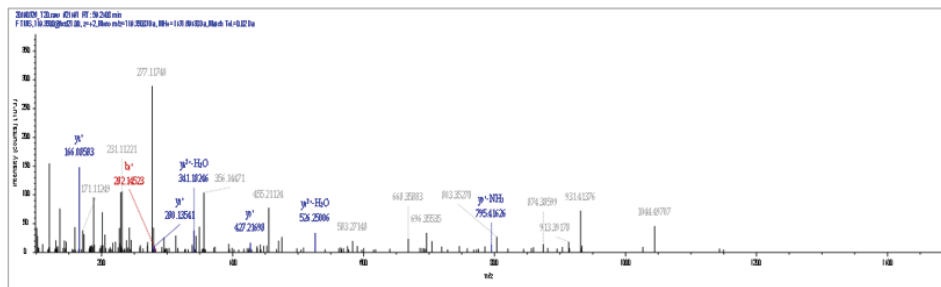
SPPSEQLGKSFNF (MH+: 1437.70087 Da, Fraction 10%)
23% hydrophobic residue, length: 13 amino acid
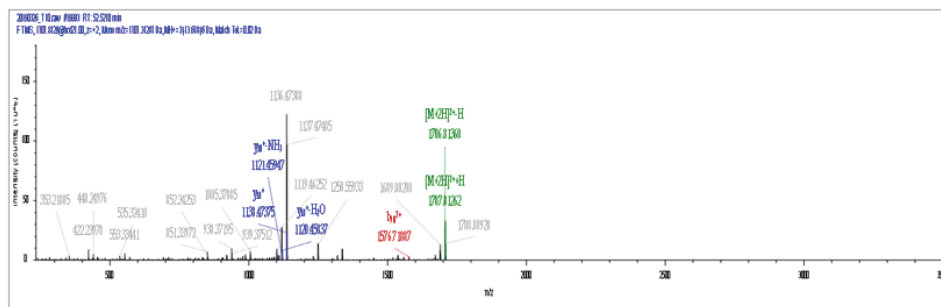
SIWGDIGQGVGKAAYWVGKAMGNMSDVNQASEINRKKKH (MH+: 3413.58890 Da, Fraction 10%)
35% hydrophobic residue, length: 39 amino acid
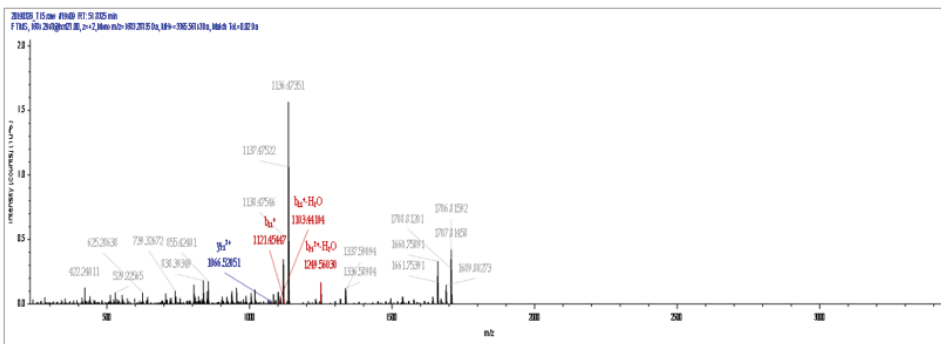
NK**GCAICSIGAACLVDGPIPDFEIAGATGLFGLWG** (MH+: 3365.60032 Da, Fraction 15%)
54% hydrophobic residue, length: 35 amino acid

Figure 4. Peptide spectra identified as bioactive peptide from 5%, 10%, 15% and 20% fraction of trypsin hydrolysate. The peptide sequences determined from this work were matched to known bioactive peptide sequences in Antimicrobial Peptide Database (APD). Sequence matched is in red font and underlined. The peptides were identified to PG-K111, Peptide 5, lactococcin Q and subtilosin A1.
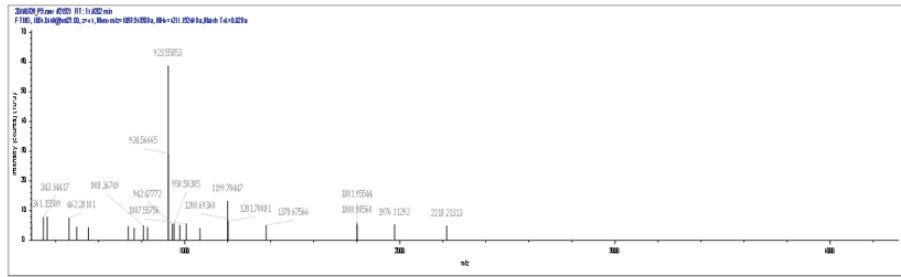
RMRRSKSGKGS**GGSKGSGSKGSKGSKGSGSKGSGSKGGSRPGGGSIAGGGSKGKGGTQTA**
(MH+: 4211.11075 Da, Fraction 5%)
6% hydrophobic residue, length: 61 amino acid
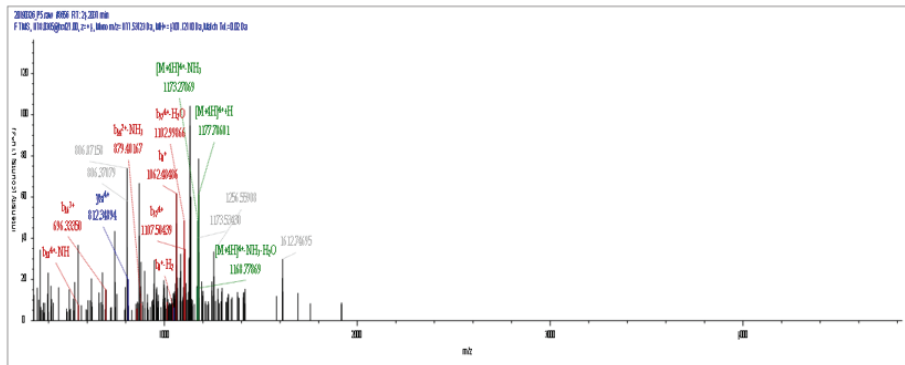
CLAG**RLDKQCTCRRSQPSRRSGHEVGRPSPHCGPSRQCGCHMD** (MH+: 4707.09939 Da,
Fraction 5%)
25% hydrophobic residue, length: 43 amino acid
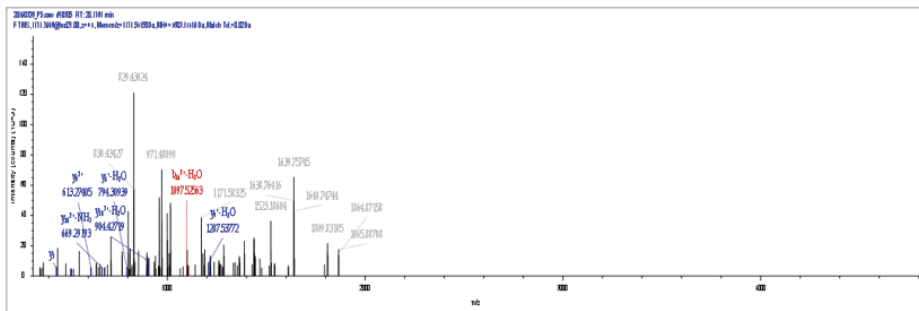
RQ**RDPQQQYEQCQKHCQRRETEPRH**MQTCQQRCERRYEKEKRKQQKRYEEQQREDEEKY
(MH+: 4683.18453 Da, Fraction 5%)
8% hydrophobic residue, length: 68 amino acid
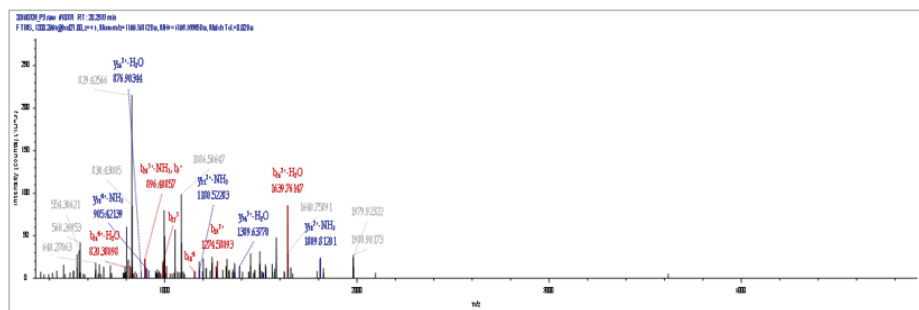
KRDPQQ**REYEDCRRRC**EQQEPRQQHQCQLRCREQQRQHGRGGDMMNPQRGGSGRY
EEGEEEQS (MH+: 4796.17269 Da, Fraction 5%)
11% hydrophobic residue, length: 63 amino acid

Figure 5. Peptide spectra identified as bioactive peptide from 5% fraction of pepsin hydrolysate. The peptide sequences determined from this work were matched to known bioactive peptide sequences in Antimicrobial Peptide Database (APD). Sequence matched is in red font and underlined. The peptides were identified to aCATH, human drosomycin-like defensin, MiAMP2c and MiAMP2d.

459

DISCUSSION

This study described the isolation of peptides with validated antifungal towards *G. boninense* and antioxidant bioactivities from oil palm fruit mesocarp. *In silico* analysis also revealed the presence of antimicrobial peptides after tryptic and peptic hydrolysis of the oil palm fruit mesocarp. There is no reported study that examined the conversion of oil palm mesocarp to generate these bioactive peptides. The nearest oil palm related materials that were used to produce peptides with bioactivity were extracted from palm kernel cake and pulp (Chee *et al.*, 2012; Ng *et al.*, 2013; Tan *et al.*, 2013; Zarei *et al.*, 2015; Zheng *et al.*, 2017).

In this work, the 25% and 30% fractions of trypsin hydrolysate were observed to suppress the growth of *G. boninense*. However, *in silico* analysis found four antimicrobial peptides in 5%-20% fractions of trypsin hydrolysate, instead. Similarly, the 10% and 30% fractions of the pepsin hydrolysate were found to suppress the fungal growth until day 3 before the effect wore out by day 7. *In silico* analysis identified four peptides with reported antifungal and antimicrobial activity from 5% fraction of the pepsin hydrolysate only. The results indicated that the peptide with antifungal activity towards *G. boninense* could be novel and has not been reported previously. Antimicrobial and antifungal peptides are amphipathic naturally and they are made up of both hydrophilic and hydrophobic domains (Tang *et al.*, 2018). The possible routes for the inhibition range from disintegration of cell membranes (binding to lipid bilayer structure and phospholipid groups) (Brogden, 2005; De Cesare *et al.*, 2020; Shai, 2002) to inhibit certain key pathways in the cell such as protein synthesis (Le *et al.*, 2017).

In the *in silico* analysis, peptides with antimicrobial peptides against gram-positive and gram-negative bacteria were identified from the fractionated trypsin and pepsin hydrolysates. Generally, peptides corresponding to different enzymatic hydrolysis exhibited different characteristics, in terms of their hydrophobic amino acid contents and the length of amino acid residues per peptide (Karami and Akbari-adergani, 2019). In our study, using the trypsin hydrolysis, the generated peptides were identified to PG-K111, Peptide 5, lactococcin Q and subtilosin A1 in the Antimicrobial Peptide Database (APD). PG-K111 is a neuropeptide from the tachykinin family and related to kassinin, which is involved in Kassina frog's neuropeptide signaling in a defense response (Grace *et al.*, 2001; Simmaco *et al.*, 1990). Tachykinin-related peptides were also known to have antimicrobial activity as reported in studies on *Triatoma infestans* hemolymph (Diniz

et al., 2020). Meanwhile, Peptide 5, a proline-rich peptide, was found to inhibit *Staphylococcus aureus* (Gram-positive bacteria) and *Klebsiella pneumoniae* (Gram-negative bacteria) (Dolashka *et al.*, 2011). Lactococcin Q, a bacteriocin, was originally demonstrated to inhibit *Lactococcus lactis* strains only (Zendo *et al.*, 2006). Later, the antimicrobial peptide was found to show high gene sequence cluster similarity to that of lactococcin G (Ishibashi *et al.*, 2015). Subtilosin A1 is an anionic bacteriocin that showed antibacterial activity towards certain gram-positive bacteria. Subtilosin A1 was an enhanced antimicrobial peptide by substituting the threonine with isoleucine at position 6 (Huang *et al.*, 2009). These antimicrobial peptides are believed to protect plants from invasive fungal and bacterial species. Their mode of action are believed to involve adhesion to microbial cells and penetrate the phospholipid membranes since the peptides are small in size (less than 10 kDa) and charge, and capable to alter hydrophobic and hydrophilic properties (Dicks *et al.*, 2018; Meade *et al.*, 2020). For example, studies on the mode of action by lactococcin G postulated that the peptide form a membrane-penetrating helix-helix structure which interacts with the membrane receptor of bacteria (Rogne *et al.*, 2008). Lactococci was also revealed to possess antifungal by producing novel antibiotic complex against food-borne pathogens, including fungi (Stoyanova *et al.*, 2010). Subtilosin is also found to inhibit various phytopathogenic fungi in a study on autochthonous *Bacilllus subtilis* isolated from *Prosopis juliflora* (Abdelmoteleb *et al.*, 2017).

The enzymatic hydrolysis of oil palm fruit mesocarps with pepsin yielded four peptides identified to *Plecoglossus altivelis* or aCATH, human drosomycin-like defensin, MiAMP2c and MiAMP2d. Initially aCATH was found to exhibit antimicrobial activity in fish (Lu *et al.*, 2011). A more recent studies found that cathelicidin peptides are effective against *Candida* species (Rapala-Kozik *et al.*, 2015; Scarsini *et al.*, 2015). Cathelicidins is generally thought to exhibit the antifungal activity through membrane destabilisation and internalisation (Ordonez *et al.*, 2014). Peptide acquired from our works also matched to human drosomycin-like defensin. Defensin is known for its antifungal properties (Lacerda *et al.*, 2014; Stotz *et al.*, 2009). The human drosomycin-like defensin from the APD matches was found to display fungal inhibition towards *Aspergillus* spp. and other clinically relevant filamentous fungi (Simon *et al.*, 2008). Similar to cathelicidins, drosomycin-like defensin, or defensin itself, interacts with the fungal target, either the cell membrane and/or the fungal cell wall (Struyfs *et al.*, 2021). Both vicilin-like macadamia antimicrobial peptides (MiAMP2c and MiAMP2d) were found to be inhibiting

various plant pathogenic fungi (Marcus *et al.*, 1999), though their inhibitory mechanism is still not clear.

Many antimicrobial peptides are known to exert antioxidant bioactivity as well (Memarpoor-Yazdi *et al.*, 2012). The presence of dipeptides and tripeptides in pepsin hydrolysate seemed to contribute to their antioxidant bioactivity as reported previously (Kawashima *et al.*, 1979; Samaraweera *et al.*, 2011; Wu *et al.*, 2020). The result of the *in silico* analysis was in agreement with their free radical-scavenging activity. Non-fractionated mesocarp pepsin hydrolysate showed a DPPH$_{SC}$ of 22.3%. The hydrophobicity of peptide is also considered as the key determinant in its antioxidant property, possibly due to the aromatic and sulphur containing structures that make them sequester radicals (Nwachukwu and Aluko, 2019; Zou *et al.*, 2016). The high amount of hydrophobic amino acid presence in the peptides confers to better antioxidant activity. However, this was not the case with pepsin hydrolysates as the identified peptides were found to have low quantity of hydrophobic amino acid residues. This suggests that there are novel antioxidant peptides present in the pepsin hydrolysate but was not being identified through the *in silico* analysis.

CONCLUSION

Confirmation of the presence of bioactive peptides from oil palm fruit mesocarps indirectly indicates that the oil palm by-product wastes such as pressed mesocarp fibres, generated after the oil extraction, could potentially serve as a promising source of bioactive peptides for a sustainable and eco-friendly management of the oil palm wastes. The conversion of these mesocarp wastes to peptides with antifungal bioactivities towards *G. boninense* also presents a more direct way to control the onset of basal stem rot disease caused by *G. boninense*. Results from this works also suggest that protein hydrolysates from oil palm fruit mesocarps could serve as valuable functional agents in healthy diets to manage metabolic diseases that arise from excessive levels of free radicals. However, *in vivo* antioxidant activity of these peptides and the mechanism underlying their protection of cellular oxidative stress protection need to be explored further. In the meantime, inhibition of *G. boninense* growth by higher concentration of the fractionated hydrolysates and the potential inhibitory or control mechanisms would also be established. These peptides could be utilised to develop novel agent with biologically active component in agriculture as natural and sustainable crop protection agents.

REFERENCES

Abas, R; Kamarudin, M F; Nordin, A B A and Simeh, M A (2011). A study on the Malaysian oil palm biomass sector - Supply and perception of palm oil millers. *Oil Palm Industry Economic J., 11*: 28-41.

Abdelmoteleb, A; Troncoso-Rojas, R; Gonzalez-Soto, T and Gonzalez-Mendoza, D (2017). Antifungical activity of autochthonous *Bacillus subtilis* isolated from *Prosopis juliflora* against phytopathogenic fungi. *Mycobiol., 45*: 385-391.

Bamdad, F; Wu, J and Chen, L (2011). Effects of enzymatic hydrolysis on molecular structure and antioxidant activity of barley hordein. *J. Cereal Sci., 54*: 20-28.

Brogden, K A (2005). Antimicrobial peptides: Pore formers or metabolic inhibitors in bacteria? *Nat. Rev. Microbiol., 3*: 238-250.

De Cesare, G B; Cristy, S A; Garsin, D A and Lorenz, M C (2020). Antimicrobial peptides: A new frontier in antifungal therapy. *mBio, 11*: e02123-20.

Chavalparit, O (2006). *Clean technology for the crude palm oil industry in Thailand.* Ph.D thesis, Wageningen University.

Chee, K L; Ling, H K and Ayob, M K (2012). Optimization of trypsin-assisted extraction, physico-chemical characterization, nutritional qualities and functionalities of palm kernel cake protein. *LWT - Food Sci. Technol., 46*: 419-427.

Cheung, H S; Wang, F L; Ondetti, M A; Sabo, E F and Cushman, D W (1980). Binding of peptide substrates and inhibitors of angiotensin-converting enzyme. Importance of the COOH-terminal dipeptide sequence. *J. Biol. Chem., 255*: 401-407.

Dicks, L M T; Dreyer, L; Smith, C and Van Staden, A D (2018). A review: The fate of bacteriocins in the human gastro-intestinal tract: Do they cross the gut-blood barrier? *Front. Microbiol.*, *9*: 2297.

Diniz, L C L; Alves, F L; Miranda, A and Da Silva Junior, P I (2020). Two tachykinin-related peptides with antimicrobial activity isolated from *Triatoma infestans* hemolymph. *Microbiol. Insights*, *13*: 1178636120933635.

Dolashka, P; Moshtanska, V; Borisova, V; Dolashki, A; Stevanovic, S; Dimanov, T and Voelter, W (2011). Antimicrobial proline-rich peptides from the hemolymph of marine snail *Rapana venosa. Peptides,* *32*: 1477-1483.

Ghribi, A M; Sila, A; Przybylski, R; Nedjar-Arroume, N; Makhlouf, I; Blecker, C; Attia, H; Dhulster, P; Bougatef, A and Besbes, S (2015). Purification and identification of novel antioxidant peptides from enzymatic hydrolysate of chickpea (*Cicer arietinum* L.) protein concentrate. *J. Funct. Foods*, *12*: 516-525.

Grace, R C R; Lynn, A M and Cowsik, S M (2001). Lipid induced conformation of the tachykinin peptide Kassinin. *J. Biomol. Struct. Dyn.*, *18*: 611-625.

Hong, J; Chen, T T; Hu, P; Yang, J and Wang, S Y (2014). Purification and characterization of an antioxidant peptide (GSQ) from Chinese leek (*Allium tuberosum* Rottler) seeds. *J. Funct. Foods*, *10*: 144-153.

Huang, T; Geng, H; Miyyapuram, V R; Sit, C S; Vederas, J C and Nakano, M M (2009). Isolation of a variant of subtilosin A with hemolytic activity. *J. Bacteriol.*, *191*: 5690-5696.

Irvan (2018). Processing of palm oil mill wastes based on zero waste technology. *IOP Conf. Ser.: Mater. Sci. Eng., 2018*. Sumatera Utara, Indonesia. IOP Publishing Ltd. p. 012136.

Ishibashi, N; Zendo, T; Koga, S; Shigeri, Y and Sonomoto, K (2015). Molecular characterization of the genes involved in the secretion and immunity of lactococcin Q, a two-peptide bacteriocin produced by *Lactococcus lactis* QU 4. *Microbiology (Reading), 161*: 2069-2078.

Karami, Z and Akbari-Adergani, B (2019). Bioactive food derived peptides: A review on correlation between structure of bioactive peptides and their functional properties. *J. Food Sci. Technol.*, *56*: 535-547.

Kawashima, K; Itoh, H; Miyoshi, M and Chibata, I (1979). Antioxidant properties of branched-chain amino acid derivatives. *Chem. Pharm. Bull. (Tokyo)*, *27*: 1912-1916.

Kushairi, A and Mohd Din, A (2020). Development of new oil palm cultivars in Malaysia. *J. Oil Palm Res.*, *32*: 420-426.

Lacerda, A F; Vasconcelos, E A R; Pelegrini, P B and Grossi De Sa, M F (2014). Antifungal defensins and their role in plant defense. *Front. Microbiol.*, *5*: 116.

Lau, B Y C; Deb-Choudhury, S; Morton, J D; Clerens, S; Dyer, J M and Ramli, U S (2015). Method developments to extract proteins from oil palm chromoplast for proteomic analysis. *SpringerPlus,* *4*: 791.

Le, C F; Fang, C M and Sekaran, S D (2017). Intracellular targeting mechanisms by antimicrobial peptides. *Antimicrob. Agents Chemother.*, *61*: e02340-16.

Liu, K; Zhao, Y; Chen, F and Fang, Y (2015). Purification and identification of Se-containing antioxidative peptides from enzymatic hydrolysates of Se-enriched brown rice protein. *Food Chem.*, *187*: 424-430.

Lu, X J; Chen, J; Huang, Z A; Shi, Y H and Lu¨, J N (2011). Identification and characterization of a novel cathelicidin from ayu, *Plecoglossus altivelis. Fish Shellfish Immunol.*, *31*: 52-57.

Marcus, J P; Green, J L; Goulter, K C and Manners, J M (1999). A family of antimicrobial peptides is produced by processing of a 7S globulin protein in *Macadamia integrifolia* kernels. *Plant J.*, *19*: 699-710.

Meade, E; Slattery, M A and Garvey, M (2020). Bacteriocins, potent antimicrobial peptides and the fight against multi drug resistant species: Resistance is futile? *Antibiotics (Basel)*, *9*: 32.

Memarpoor-Yazdi, M; Asoodeh, A and Chamani, J (2012). A novel antioxidant and antimicrobial peptide from hen egg white lysozyme hydrolysates. *J. Funct. Foods*, *4*: 278-286.

Ng, K L; Ayob, M K; Said, M; Osman, M A and Ismail, A (2013). Optimization of enzymatic hydrolysis of palm kernel cake protein (PKCP) for producing hydrolysates with antiradical capacity. *Ind. Crops Prod.*, *43*: 725-731.

Nwachukwu, I D and Aluko, R E (2019). Structural and functional properties of food protein-derived antioxidant peptides. *J. Food Biochem.*, *43*: e12761.

Odintsova, T I; Vassilevski, A A; Slavokhotova, A A; Musolyamov, A K; Finkina, E I; Khadeeva, N V; Rogozhin, E A; Korostyleva, T V; Pukhalsky, V

A; Grishin, E V and Egorov, T A (2009). A novel antifungal hevein-type peptide from *Triticum kiharae* seeds with a unique 10-cysteine motif. *FEBS J.*, *276*: 4266-4275.

Ordonez, S R; Amarullah, I H; Wubbolts, R W; Veldhuizen, E J and Haagsman, H P (2014). Fungicidal mechanisms of cathelicidins LL-37 and CATH-2 revealed by live-cell imaging. *Antimicrob. Agents Chemother.*, *58*: 2240-2248.

Pereira, P H F; Souza, N F; Ornaghi Jr, H L and De Freitas, M R (2020). Comparative analysis of different chlorine-free extraction on oil palm mesocarp fiber. *Ind. Crops Prod.*, *150*: 112305.

Rapala-Kozik, M; Bochenska, O; Zawrotniak, M; Wolak, N; Trebacz, G; Gogol, M; Ostrowska, D; Aoki, W; Ueda, M and Kozik, A (2015). Inactivation of the antifungal and immunomodulatory properties of human cathelicidin LL-37 by aspartic proteases produced by the pathogenic yeast *Candida albicans. Infect. Immun.*, *83*: 2518-2530.

Rogne, P; Fimland, G; Nissen-Meyer, J and Kristiansen, P E (2008). Three-dimensional structure of the two peptides that constitute the two-peptide bacteriocin lactococcin G. *Biochim. Biophys. Acta*, *1784*: 543-554.

Sabil, K M; Aziz, M A; Lal, B and Uemura, Y (2013). Effects of torrefaction on the physiochemical properties of oil palm empty fruit bunches, mesocarp fiber and kernel shell. *Biomass Bioenergy*, *56*: 351-360.

Samaraweera, H; Zhang, W G; Lee, E J and Ahn, D U (2011). Egg yolk phosvitin and functional phosphopeptides-Review. *J. Food Sci.*, *76*: R143-150.

Scarsini, M; Tomasinsig, L; Arzese, A; D'este, F; Oro, D and Skerlavaj, B (2015). Antifungal activity of cathelicidin peptides against planktonic and biofilm cultures of *Candida* species isolated from vaginal infections. *Peptides*, *71*: 211-221.

Shai, Y (2002). Mode of action of membrane active antimicrobial peptides. *Biopolymers*, *66*: 236-248.

Silk, D B; Fairclough, P D; Clark, M L; Hegarty, J E; Marrs, T C; Addison, J M; Burston, D; Clegg, K M and Matthews, D M (1980). Use of a peptide rather than free amino acid nitrogen source in chemically defined 'elemental' diets. *JPEN J. Parenter. Enteral Nutr.*, *4*: 548-553.

Simmaco, M; Severini, C; De Biase, D; Barra, D; Bossa, F; Roberts, J D; Melchiorri, P and Erspamer, V (1990). Six novel tachykinin- and bombesin-related peptides from the skin of the Australian frog *Pseudophryne güntheri*. *Peptides*, 11: 299-304.

Simon, A; Kullberg, B J; Tripet, B; Boerman, O C; Zeeuwen, P; Van Der Ven-Jongekrijg, J; Verweij, P; Schalkwijk, J; Hodges, R; Van Der Meer, J W and Netea, M G (2008). Drosomycin-like defensin, a human homologue of *Drosophila melanogaster* drosomycin with antifungal activity. *Antimicrob. Agents Chemother.*, *52*: 1407-1412.

Siow, H L and Gan, C Y (2013). Extraction of antioxidative and antihypertensive bioactive peptides from *Parkia speciosa* seeds. *Food Chem.*, *141*: 3435-3442.

Sreekala, M S; Kumaran, M G and Thomas, S (1997). Oil palm fibers: Morphology, chemical composition, surface modification, and mechanical properties. *J. Appl. Polym. Sci.*, *66*: 821-835.

Stotz, H U; Thomson, J G and Wang, Y (2009). Plant defensins: Defense, development and application. *Plant Signal. Behav.*, *4*: 1010-1012.

Stoyanova, L G; Ustyugova, E A; Sultimova, T D; Bilanenko, E N; Fedorova, G B; Khatrukha, G S and Netrusov, A I (2010). New antifungal bacteriocin-synthesizing strains of *Lactococcus lactis* ssp. *lactis* as the perspective biopreservatives for protection of raw smoked sausages. *Amer. J. Agric. Biol. Sci.*, *5*: 477-485.

Struyfs, C; Cammue, B P A and Thevissen, K (2021). Membrane-interacting antifungal peptides. *Front. Cell Dev. Biol.*, *9*: 649875.

Tadesse, S A and Emire, S A (2020). Production and processing of antioxidant bioactive peptides: A driving force for the functional food market. *Heliyon, 6*: e04765.

Tan, Y N; Ayob, M K and Wan Yaacob, W A (2013). Purification and characterisation of antibacterial peptide-containing compound derived from palm kernel cake. *Food Chem.*, *136*: 279-284.

Tang, S S; Prodhan, Z H; Biswas, S K; Le, C F and Sekaran, S D (2018). Antimicrobial peptides from different plant sources: Isolation, characterisation, and purification. *Phytochemistry*, *154*: 94-105.

Wang, G; Li, X and Wang, Z (2016). APD3: The antimicrobial peptide database as a tool for research and education. *Nucleic Acids Res.*, *44*: D1087-1093.

Wu, M; Zhu, Z; Li, S; Cai, J; Cong, X; Yu, T; Yang, W; He, J and Cheng, S (2020). Green recovery of Se-rich

protein and antioxidant peptides from *Cardamine violifolia*: Composition and bioactivity. *Food Biosci.*, *38*: 100743.

Zarei, M; Forghani, B; Ebrahimpour, A; Abdul-Hamid, A; Anwar, F and Saari, N (2015). *In vitro* and *in vivo* antihypertensive activity of palm kernel cake protein hydrolysates: Sequencing and characterization of potent bioactive peptides. *Ind. Crops Prod.*, *76*: 112-120.

Zendo, T; Koga, S; Shigeri, Y; Nakayama, J and Sonomoto, K (2006). Lactococcin Q, a novel two-peptide bacteriocin produced by *Lactococcus lactis* QU 4. *Appl. Environ. Microbiol.*, *72*: 3383-3389.

Zhao, Y; Li, B; Liu, Z; Dong, S; Zhao, X and Zeng, M (2007). Antihypertensive effect and purification of an ACE inhibitory peptide from sea cucumber gelatin hydrolysate. *Process Biochem.*, *42*: 1586-1591.

Zheng, Y; Li, Y; Zhang, Y; Ruan, X and Zhang, R (2017). Purification, characterization, synthesis, *in vitro* ACE inhibition and *in vivo* antihypertensive activity of bioactive peptides derived from oil palm kernel glutelin-2 hydrolysates. *J. Funct. Foods*, *28*: 48-58.

Zou, T B; He, T P; Li, H B; Tang, H W and Xia, E Q (2016). The structure-activity relationship of the antioxidant peptides from natural proteins. *Molecules, 21*: 72.

EFFECTS OF *Phoma herbarum* AS A BIOLOGICAL CONTROL AGENT OF GLYPHOSATE RESISTANT *Eleusine indica*

RUSLI, M H[1]*; SHARIFFAH MUZAIMAH, S A[1]; MAIZATUL, S M[1] and IDRIS, A S[1]

ABSTRACT

Goosegrass (Eleusine indica) *is one of the weeds that has a problem of herbicide resistance to glyphosate. This study investigated the potential use of* Phoma herbarum *as a biological control agent of glyphosate resistant* E. indica*. Nursery and field experiments showed that the application of 10^6 conidial suspension of* P. herbarum *demonstrated biofungicidal activity whereby 91.70% of treated* E. indica *died whilst for field experiment the mortality rate was recorded at 80.00%. The effect of* P. herbarum *was noticeable at 14 days after treatment and continued to increase at 21 days and 28 days after application. This study also investigated the direct effects of a few common herbicides that were used to control* E. indica *in oil palm plantations. The study found that the* P. herbarum *was compatible with herbicide diuron and was able to cause 80.00% mortality to* E. indica *when diuron was applied at full strength. The percentage mortality of* E. indica *increased to 91.67% when half strength diuron was applied. Thus, this study was to report the effectiveness of* P. herbarum *as a potential biological control agent against resistant* E. indica *and compatible with herbicide diuron.*

INTRODUCTION

Goosegrass (*Eleusine indica*) is a noxious weed in oil palm and fruit trees cultivations in Malaysia (Barnes and Chan, 1990). *Eleusine* is a member of the tribe Eragrosteae, family Poaceae (Bisht and Mukai, 2002). Goosegrass is an all-season prolific grass that is widely distributed in the tropics, particularly in Asia, Africa, South America, and the southern parts of North America (Holm *et al.*, 1977). *Eleusine indica* was reported as one of the five most troublesome weeds in the world and caused problems to 46 different crop species in more than 60 countries (Chuah and Lim, 2015).

In Malaysia, *E. indica* was found to be the most occurred grass (82.2%) followed by *Imperata cylindrical* (81.2%), *Ishaemum muticum* (71.8%) and *Pennisetum polystachion* (67.1%) in immature oil palm plantation (Maizatul-Suriza and Idris, 2012).

The only practical way to control *E. indica* is by using herbicide. However, excessive and repeated use of herbicide such as glyphosate to control *E. indica* has caused the weed to become resistant. Glyphosate resistance in *E. indica* has been reported in many countries and could seriously affect future control of this weed if the resistance problem is left unsolved (Chen *et al.*, 2017; Lim and Ngim, 2000; Teng and Teo, 1999; Tran *et al.*, 1999).

Due to the repeated use of herbicides with the same mode of action, populations of *E. indica* have evolved resistance to acetolactate synthase inhibitors (Valverde *et al.*, 2000), acetyl CoA carboxylase inhibitors (Leach *et al.*, 1995), bipyridiliums, glycines (Lim and Ngim, 2000),

---

1   Malaysian Palm Oil Board,
    6 Persiaran Institusi, Bandar Baru Bangi,
    43000 Kajang, Selangor, Malaysia.

*   *Corresponding author e-mail: mohd.hefni@mpob.gov.my*

and dinitroaniline herbicides (Mudge *et al.*, 1984), all of which are important herbicides for controlling *E. indica* in crops. In Malaysia, the first case of glyphosate-resistant annual grassy weed *E. indica* was reported in an orchard at Teluk Intan, Perak, Malaysia in 1998, where glyphosate failed to give adequate control of goosegrass in a four-year-old orchard (Lim and Ngim, 2000).

Thus, an alternative method such as using a biological control formulation, which is environmental-friendly for controlling weed species and reducing environmental pollution compared to using herbicide formulations that can affect soil microorganisms is sought after (Savita, 2019). Nevertheless, an effective microbial formulation plays a significant role in order to work as an alternative to chemical application (Lacey *et al.*, 2001). Biological control of weeds is seen as an economical, effective and environmentally sound method of weed control. Many phytopathogenic fungi such as *Fusarium oxysporum* and *Puccinia komarovii* var. *glanduliferae* have been found to effectively control weeds (Currie *et al.*, 2020; Dutta and Ray 2017).

Phoma herbarum Westend is an ubiquitous saprobe and toxigenic pathogen to plants and animals (Hamayun *et al.*, 2009). Previous study has reported that three species of *Phoma* have been identified as potential biological control agents to various weeds (Harding and Raizada, 2015). Previous studies showed *P. chenopodia* could control weeds such as *Chenopodium album, Cirsium arvense, Setaria viridis*, and *Mercurialis annua* (Cimmino *et al.*, 2013) whilst *P. macrostoma* was reported as biological control agent of many wide host range predominantly dicot plants (Bailey *et al.*, 2011). Zhou *et al.* (2004) also isolated a number of *P. macrostoma* strains from necrotic lesions on Canada thistle [*Cirsium arvense* (L.) Scop.] plants collected from fields and roadside ditches.

It was reported that disease symptoms known as photobleaching whereby chlorosis and bleaching on the leaf tissues occurred on broadleaved weed species such as dandelion (*Taraxacum officinale* Weber ex F.H. Wigg.) when applied with mycelial fragments of *P. macrostoma* strain (Bailey *et al.*, 2011). Todero *et al.* (2018) found out that culture filtrate of *Phoma* sp. showed significant phytotoxic efficiency against three weeds namely *Bidens pilosa, Amaranthus retroflexus* and *Conyza canadensis* when combined with specific adjuvants. Furthermore, Zhao and Shamoun (2005) reported that *Phoma exigua* can control salal (*Gaultheria shallon*), a perennial evergreen shrub.

Whilst, *P. herbarum* was reported as a biological control agent of dandelion weed *Taraxacum officinale* and *Trianthema portulacastrum* (Ray and Vijayachandran, 2013). *P. herbarum* also was reported to possess strong adaptability to diverse environments, including salty and chilly surroundings (Yang *et al.* 2005), and that it is also a versatile producer of many potent natural products (Cruz *et al.*, 2003). To date, there is no report on the utilisation or application of *P. herbarum* as a biological control agent of *E. indica*. The potential of *P. herbarum* for biological control of weeds such as on turfgrass (Hahn *et al.*, 2020) and other species of *P. dimorpha* on *Echinochloa* sp., *Amaranthus cruentus, Senna obtusifolia* and *Bidens Pilosa* (Neto *et al.*, 2021) have made it as a promising candidate to control *E. indica*, consequently could be a key to solve the herbicide resistant problems in the field. Therefore, this study aimed to investigate *P. herbarum* as a potential biological control agent of resistant *E. indica* and its sequential application with herbicides.

MATERIALS AND METHODS

The resistant goosegrass seeds (Rusli *et al.*, 2014) were collected from MPOB nursery in Section 15, Bandar Baru Bangi, Selangor, Malaysia and pre-germinated in trays containing a mixture of 3:2:1 (top soil: peat: sand) with a total weight of 3.0 kg. After two weeks, the one seedling of goosegrass was transferred into each of the terracotta plant pots (20 × 8 inches). The soil medium was made up of sandy loam topsoil in a proportion of 2:1 (top soil: sand). Ten g of rock phosphate was added to the soil medium in each pot to enhance and promote healthy plant growth and approximately 1.5 kg of soil medium was added to the pots, which were placed in the nursery with 50% polyethylene shading net. They were watered from below on alternate days. Other weeds were removed manually when necessary. Every month, approximately 5 g of N.P.K Green 15: 15: 15 (Nifosk Green) was applied to each pot.

Preparation of *P. herbarum* (PH81) Inoculum

Single spore isolates of *P. herbarum* (PH81) isolated from diseased *E. indica* from Malaysian Palm Oil Board (MPOB) nursery in Section 15, Bandar Baru Bangi, Selangor were used in the pathogenicity experiments. Isolates were stored at -80°C in 20% glycerol and were then cultured on potato dextrose agar (PDA) and incubated at 28°C for five days. Three plugs of five-day-old fungus were inoculated onto solid media containing 50 g of semi-fine corns (0.1-0.2 cm), 1% starch, 1% sucrose and 30% water solutions (containing 0.01% Tween 20 and 0.1% glycerol). After 14 days of incubation at room temperature, the *P. herbarum* (PH81) spores were subjected to harvesting through filtration and counted using a haemocytometer. The *P. herbarum* (PH81) spore concentrations were adjusted to 10^6 conidia per mL upon spraying.

Standard Inoculation Procedure for *P. herbarum* (PH81)

Ten mL of conidial suspension was applied to the leaves and around the base of each *E. indica*. The inoculated *E. indica* were watered with sterile distilled water (SDW) for two weeks. Un-inoculated *E. indica* served as controls. *Eleusine indica* seedlings were inoculated at one month of age.

Colonisation of *P. herbarum* (PH81) on *E. indica*

Re-isolation of *P. herbarum* (PH81) from the plant leaves and roots of each inoculated and un-inoculated *E. indica* was attempted. For qualitative re-isolation, 3-cm fragments of plant materials (leaves and roots) were surface sterilised in 2% (v/v) sodium hypochlorite for 10 min (5 min for tissue cores) before rinsing twice in SDW. The materials were then plated onto PDA and incubated for four days at 28°C.

Deoxyribonucleic Acid (DNA) Extraction

Phoma herbarum (PH81) DNA was isolated using a modified cetyltrimethylammonium bromide (CTAB) method described by Manicom *et al.* (1987). First, 500 µL of isolate suspension (10^6 spores/mL) and 10-15 glass beads were vortexed in 1.5 mL Eppendorf tubes for 45 s to disrupt the cells. Then, 500 µL of CTAB buffer (2% w/v CTAB, 1 M Tris-hydrochloric acid (Tris-HCl) pH 8, 5 M sodium chloride (NaCl) and 0.5 M EDTA pH 8 was added to the suspension and vortexed again before incubating the samples at 65°C for 40 min. An equal volume of phenol: chloroform: isoamyl alcohol (25: 24: 1) was added to extract the DNA. The suspension was vortexed thoroughly to mix the layers and centrifuged at 4000 rpm for 10 min. The aqueous supernatant was transferred to a clean Eppendorf tube, and 500 µL of cold isopropanol was added to precipitate nucleic acids overnight at -20°C. The DNA was pelleted at 13 000 rpm for 30 min, washed with 100 µL of cold 70% ethanol by centrifuging twice and taken up in 100 µL of sterile MilliQ water. DNA purity and concentration were determined using the ND-100 Nanodrop Spectrophotometer (Thermo Scientific) according to the manufacturer's protocol.

Polymerase Chain Reaction (PCR) for Target Sequence Amplification

The PCR was performed with a PTC-100™ (MJ Research Cycling) in reaction volumes of 25 µL. Each reaction consisted of >20 ng genomic DNA (or a 2.5 µL culture suspension), 0.2 µM of each primer, 0.4 mM dNTP mix (10 mM, Promega), 0.5× GoTaq buffer (5× GoTaq buffer, Promega), 2.5 mM MgCl$_2$ (25 mM, Promega), 0.02 u/µL GoTaq® DNA polymerase (5 u/µL, Promega), and sterile Milli-Q water. The PCR cycle conditions were as follows: one cycle at 94°C for 5 min, followed by 40 amplification cycles at 94°C for 0.05 s, 57°C for 0.05 s, and 72°C for 0.05 s. A final extension at 72°C for 2 min was done after 40 cycles followed by cooling at 14°C until recovery of the sample. Amplification products were assessed on a 1% w/v agarose gel stained with ethidium bromide run for 20 min at 80 volts and visualised under ultraviolet (UV) illumination.

Nursery Trial

The nursery trial was carried out in Bandar Baru Bangi, Selangor, Malaysia (2° 57' 56.4120" N and 101° 45' 3.2688" E). The experiment comprised of two treatments (treated and untreated) carried out where each treatment consisted of 20 pots with three replicates using a randomised complete block design (RCBD). Each plant was inoculated with 10 mL of 3×10^6 *P. herbarum* (PH81) conidia/mL. The determinations of weed mortality were carried out at 7, 14, 21 and 28 days post-inoculation, and sample re-isolation was performed at the end of the experiment, after 28 days.

Field Trial

A field trial was conducted in Bandar Baru Bangi, Selangor, Malaysia (2° 57' 56.4120" N and 101° 45' 3.2688" E). This experiment made use of the available *E. indica* to simulate the real weed conditions in the field. It was set up in plots (2 m × 5 m) with approximately 20 *E. indica* aged between 1-2 months old (based on the last cycle of herbicide application) in each plot. Two treatments were replicated in five RCBD plots whereby the first treatment consisted of 200 mL of 10^6 *P. herbarum* (PH81) conidial/mL suspensions sprayed in each plot using a hand-operated sprayer (a knapsack hand pump) with a cone (green) nozzle and the second treatment was a control plot (*E. indica* sprayed with water). The determinations of weed mortality were carried out at 7, 14, 21, 28 and 35 days post-inoculation and *P. herbarum* (PH81) sample re-isolation was performed at the end of the experiment after 35 days.

The Percentage of Weed Mortality in Nursery and Field Trials

The weed mortality percentage was taken at one, two, three and four weeks after treatment (WAT) by counting plants with all tissues completely dead from the point of growing to the surface of soil using a non-destructive sampling method.

Eleusine indica Dry Weight

The growth parameters and dry weight were assessed. The weeds planted in the pots were washed twice with tap water before constant dry weight (g) of the whole plant (roots and aerial parts) were determined, following ≥72 hr at 80°C in a drying oven (Rusli *et al.*, 2014).

Sequential Application of Herbicide and Bioherbicide on Goosegrass Mortality

The experiment was conducted in an open nursery area in Bandar Baru Bangi, Selangor, Malaysia (2° 57' 56.4120" N and 101° 45' 3.2688" E). Five commonly used herbicides to control *E. indica* and a stock solution of each herbicide was made based the product's field recommendation (*Table 1*). Each treatment consisted of 20 pots with three replicates using a RCBD. Each plant was inoculated with 10 mL of 3×10^6 *P. herbarum* (PH81) conidia/mL, 12 hr after application of herbicide at full strength and half strength. The determinations of weed mortality were carried out at 7, 14, 21 and 28 days post-inoculation.

Statistical Analysis

The data collected in the nursery and field studies were subjected to Fisher's exact test. Means were separated using a significance level of *p*<0.05. Comparisons between the treatment means were made using Tukey's HSD test.

RESULTS

Efficacy of *P. herbarum* (PH81) on *E. indica* in the Nursery Trial

Based on the nursery trials, the effects of *P. herbarum* (PH81) application were noticeable after 14 days with 30% mortality and continued to increase significantly with mortality rate at 80% after 21 days post application. It was noticeable

that formation of *P. herbarum* (PH81) mycelia on the treated *E. indica* leaves. Overtime, it was observed that *P. herbarum* (PH81) incite photobleaching on the infected leaves and gradually became chlorotic before eventually die (*Figure 1*). The same symptoms was observed when *Conyza canadensis* was treated with mycoherbicides derived from *Phoma* sp. (Todero *et al.*, 2018). At the end of the experiment, 90% of the *E. indica* treated with *P. herbarum* (PH81) was dead 28 days after treatment, whereas no dead signs were observed in the control treatment during the same period (*Table 2*). Twenty fungal isolations from samples that showed black spot discolourations and dried and colonised roots of *E. indica* were carried out at the end of the experiment. The samples were subjected to PCR amplifications using universal primers (White *et al.*, 1990) and were sent out for sequence analysis. Based on the Basic Local Alignment Search Tool (BLAST) sequence analysis, it was found that the isolated fungus was *P. herbarum*. This showed that a stable formulation of *P. herbarum* that can sustain the viability of a potential biocontrol agent has been developed and can be delivered to the target weed.

Field Efficacy Test of *P. herbarum* (PH81) on *E. indica*

Seven days after treatment, no mortality was observed in all treated quadrats. However, the mortality of *E. indica* increased significantly 14 days after treatment to 30% (*Table 3*). The mortality pattern was similar to the previous nursery trial. It was also observed that from day 14 to day 21, a sharp trend of *E. indica* mortality was recorded whereby the percentage of mortality jumped from 30%-70%. The mortality rate of *E. indica* continued until 28 days and stabilised at 80% (*Table 3*). This shows that *E. indica* are susceptible to *P. herbarum* (PH81) infections. The treated *E. indica* showed black spot discolourations and dried in all quadrats. These are typical symptoms of *Phoma* infections which range from necrotic spots, chlorotic halos and wilting (Deb *et al.*, 2020). The study also recorded that 10% of the untreated *E. indica* died due to ageing

TABLE 1. SELECTION OF HERBICIDES WITH DIFFERENT ACTIVE INGREDIENTS AND MODE OF ACTIONS USED IN EXPERIMENTAL STUDIES

Herbicide active ingredient	Mode of action	Product rate per ha (L/ha) Full strength	Product rate per ha (L/ha) Half strength
Glyphosate isopropylammonium (41% w/w)	Systemic	3.0	1.50
Glyphosate monoamonium (52% w/w)	Systemic	5.0	2.50
Diuron (42% w/w)	Systemic	0.9	0.45
Gluphosinate – ammonium (13.5 w/w)	Contact	3.3	1.65
Paraquat dichloride (13% w/w)	Contact	6.0	3.00

TABLE 2. PERCENTAGE OF *Eleusine indica* MORTALITY DUE TO *Phoma herbarum* (PH81) INFECTION AT 7, 14, 21 AND 28 DAYS AFTER TREATMENT IN NURSERY TRIAL

Treatment	% of dead *E. indica*			
	7 days	14 days	21 days	28 days
T1 – *E. indica* treated with *P. herbarum* (PH81) (10^6 conidia/mL)	0a	30a	80a	91.7a
T2 – Untreated *E. indica* (control)	0a	0b	0b	0b

Note: Different letters denote a significance ($p<0.05$) between different treatments on *E. indica* analysed by Fisher's exact test. n - 20; replicate - 3; experimental design - RCBD.

TABLE 3. THE EFFICACY OF *Phoma herbarum* (PH81) ON RESISTANT *Eleusine indica* IN A FIELD TRIAL

Treatment	Mortality of *E. indica* (%)				
	7 days	14 days	21 days	28 days	35 days
T1 – *P. herbarum* (PH81) at 10^6 conidia/mL	0	30a	70a	80a	80a
T2 – Untreated *E. indica* (control)	0	0b	0b	0b	10b

Note: Different letters denote a significance ($p<0.05$) between different treatments on *E. indica* analysed by Fisher's exact test. n - 5; replicate - 3; experimental design - RCBD.

Figure 1. The photobleaching and chlorosis effects of P. herbarum *application at seven days interval in field trial.*

factors. Further investigation found that the weed's root system were still active and regenerated after 42 days post treatments in all quadrat. Figliola *et al.* (1988) also reported similar findings when two leaf-spotting pathogens, *Bipolaris setariae* (Saw.) and *Pyricularia grisea* (Cke.) Sacc., were applied to *E. indica*. In comparison, *E. indica* regeneration was recorded 21 days after treatment when conventional herbicide mixtures were used (Rusli *et al.*, 2014).

This experiment exhibited significantly reduced dry weight compared to the control treatment as shown in *Table 4*. Field efficacy treatments of *P. herbarum* as a potential biological control agent on *E. indica* have been repeated on a number of occasions

TABLE 4. THE EFFECT OF *Phoma herbarum* (PH81) TREATMENT ON *Eleusine indica* DRY WEIGHT 35 DAYS AFTER APPLICATIONS

Treatment	Dry weight (g)
T1 – *P. herbarum* (PH81) at 10^6 conidia/mL	115a
T2 – Untreated *E. indica* (control)	250b

Note: Different letters denote a significance ($p<0.05$) between different treatments on *E. indica* analysed by Fisher's exact test. n - 5; replicate - 3; experimental design - RCBD.

and giving similar results. The effectiveness of *P. herbarum* treatment indicated the fungus is a potential biological control agent whereby it could suppress the weed growth compared to control.

Sequential Herbicide Application and Bioherbicide (PH81) on Goosegrass

The bio herbicide fungus, *P. herbarum* (PH81) was tested alone and 12 hr after full strength or half strength selected herbicides application. Based on the results obtained, treatment with *P. herbarum* (PH81) and full strength gluphosinate ammonium (T4) recorded the highest *E. indica* mortality as early as seven days post application (*Table 5*). The weed mortality continued to increase at day 14 (93.33%), day 21 (98.33%) and day 28 (100.00%). Treatment of *P. herbarum* (PH81) with half strength gluphosinate ammonium recorded a lower mortality rate at 43.33% during the whole course of the experiment. The treated *E. indica* was then sampled and fungal re-isolation was carried out in order to confirm the presence of *P. herbarum* (PH81). Nevertheless, no *P. herbarum* can be re-isolated from *E. indica* in T4.

It was also recorded that the *E. indica* mortality in T3 also high with treatment *P. herbarum* (PH81) and full strength diuron shows 71.67% mortality after seven days post application before stagnated at 80.00%. However, treatment *P. herbarum* (PH81) and half strength diuron killed 50.00% of treated *E. indica* and the mortality rate increased to 60.00% (day 14) and 91.67% at day 21 dan 28. This was the highest percentage of mortality recorded compared to other treatments. Based on fungal re-isolation and sequence analysis, the presence of *P. herbarum* (PH81)

was identified and confirmed. It was recorded that, weed mortality was significantly improved when *P. herbarum* (PH81) was applied with reduced diuron rate.

For T5, no *P. herbarum* could be re-isolated from treatment with paraquat although 80.00% weed killed was achieved with full strength paraquat application. This could probably due to the herbicide toxicity that inhibited or killed *P. herbarum* (PH81). Nevertheless, *P. herbarum* (PH81) could be isolated from T1 and T2 when the herbicides were applied at half strength though the percentage of mortality were low. T1 recorded weed mortality at 11.67% at full strength glyphosate isopropylammonium in combination with *P. herbarum* (PH81) while half strength application recorded weed mortality at 28.33%. T2 also showed low weed control whereby full strength application of glyphosate monoammonium with *P. herbarum* (PH81) only showed 20.00% mortality whilst 10% weed mortality was recorded with half strength application of the herbicide. Treatment with full strength *P. herbarum* (PH81) (T6) showed similar pattern as observed in previous field trial whereby 28.33% *E. indica* mortality due to PH81 infection was recorded. The highest *E. indica* mortality rate was recorded at 21 days post inoculation at 80.00% and maintained when assessment was carried out at 28 days. Nevertheless, half strength application of PH81 was only able to kill 50.00% of the resistant *E. indica*.

TABLE 5. BIOHERBICIDAL ACTIVITY OF *P. herbarum* (PH81) IN COMBINATION WITH FULL STRENGTH AND HALF STRENGTH OF SELECTED HERBICIDES AGAINST *E. indica*

Treatment	Active ingredient	Percentage of *E. indica* killed (%)							
		7 days		14 days		21 days		28 days	
		FS	HS	FS	HS	FS	HS	FS	HS
T1	*P. herbarum* (PH81) + Glyphosate isopropylammonium	11.67bC	25.0aBC	11.67bCD	25.0aC	11.67bCD	28.33aBC	11.67b	28.33aC
T2	*P. herbarum* (PH81) + Glyphosate monoammonium	13.33aC	10.0aC	20.0aC	10.0bD	20.0aC	10.0bD	20.0b	10.0aD
T3	*P. herbarum* (PH81) + Diuron	71.67aB	50.0bA	80.0aAB	60.0bA	80.0bB	91.67aA	80.0b	91.67aA
T4	*P. herbarum* (PH81) + Gluphosinate–ammonium	91.67aA	43.33bA	93.33aA	43.33bB	98.33aA	43.33bB	100.0a	43.33bBC
T5	*P. herbarum* (PH81) + Paraquat dichloride	80.0aAB	35.0bAB	80.0aAB	35.0bBC	80.0aB	35.0bB	80.0a	35.0bC
T6	*P. herbarum* (PH81) (positive control)	0aD	0aD	28.33aC	0bF	80.0aB	35.0bB	80.0a	50.0bB
T7	Control (water only; negative control)	0aD	0aD	0aE	0aF	0aF	0aE	0a	0aE

Note: *FS - Full strength of herbicide rate application; HS - Half strength of herbicide rate application. Different lowercase letters denote a significance (*p*<0.05) between different treatments strength of each herbicides (between columns) and between treatment (between rows) on *E. indica* analysed by Fisher's exact test. Different uppercase letters denote a significance (*p*<0.05) between treatment 1 to treatment 6 by Fisher's exact test. n - 20; replicate - 3; experimental design - RCBD.

DISCUSSION AND CONCLUSION

Chemical control represents an effective way to control weeds for many decades. In Malaysia, the agriculture sectors remains reliant on herbicides despite some efforts to integrate with physical, mechanical and biological methods (Dilipkumar *et al.*, 2020). The heavy dependence to herbicides has affected the environment, people, animal and furthermore causing weeds to evolve and become resistant; hence higher use rate is needed for control.

In this study, a stable formulation of *P. herbarum* (PH81) that is able to sustain the viability of potential biocontrol agent and can be delivered to the target weed has been developed for both nursery and field applications. According to the nursery trials, *P. herbarum* (PH81) showed an effective potential as a biological agent to control goosegrass (*E. indica*) with 91.7% efficacy while the mortality rate of *E. indica* recorded in the field trials was 80.00% and recorded the lowest dry weight which showed the effectiveness of the treatment. It is interesting to note that wild *E. indica* around the field trial was reported to be resistant to glyphosate (Rusli *et al.*, 2014). This suggested that application of *P. herbarum* (PH81) could be a feasible alternative to control glyphosate resistant *E. indica*.

For both the nursery and field trials, the infection began 14 days after *P. herbarum* application. This result agrees with that of Bailey *et al.* (2011), who also recorded *Phoma* sp. colonisation and mycelial growth on the epidermis of barley roots and root hair seven days and 28 days after treatment, respectively. *Phoma* sp. was recently reported to significantly reduced *Verticillium* wilt of olive disease severity caused by *Verticillium dahlia* 12 weeks post application (Ana López-Moral *et al.*, 2021).

Hynes (2018) stated that the ubiquitous genus of *Phoma* had been widely reported as the fungus that was responsible for saprophytic, phytopathogenic and recently bio herbicidal activity, therefore it was not surprising that the *P. herbarum* could also control resistant *E. indica*. This is the first report of *P. herbarum* as a potential biological control agent of resistant *E. indica*. Vikrant *et al.* (2006) identified one particular toxin 3-nitro-1,2-benzenedi-carboxylic acid (3-natrophthalic acid) from *P. herbarum* that can be applied as a phytotoxin against target weed *Parthenium hysterophorus*.

Phoma species have also previously been linked as biological control agents for many invasive weeds such as Canada thistle (Guske *et al.*, 2004), and dandelion (Neumann and Boland, 2002). This study recorded that photo-bleaching and chlorosis symptoms appeared 14 days after inoculation. Similarly, Hynes (2018) reported that *Phoma* sp. causes photo-bleaching, significantly reduced the overall weed biomass and weed death whilst Johnston (1981) reported root inhibition by *Phoma*

sp. in susceptible plants when broadcast onto the soil as granules.

The delivery of the product formulation of *P. herbarum* through soil application further enhanced its ability to infect the target weed. Pedrasand Yu (2008) stated that *Phoma* affected the target weed by secreting macrocidins that was able to deteriorate the weed's cortex. The application of the fungus at or below soil surface was also found effective and thought to overcome environment detrimental caused by the application of foliar bioherbicides (Boyette *et al.*, 1991); the persistent and survival of the biological agent was also found to be increased and therefore provide longer term weed control (Boyette *et al.*, 1984). Previous study also reported that soil application of *P. macrostoma's* mycelium was more effective in controlling dandelion compared to using its spores (Bailey *et al.*, 2011).

Nevertheless, it is important to note that many of the previous bioherbicides restricted in their use (Jones and Hancock, 1990). Host range studies have shown that the use of *Phoma* sp. as bioherbicide affects several plant species in the Asteraceae, Brassicaceae, and Leguminosae (Bailey *et al.*, 2011). Hynes (2018) continued to report that no *Phoma* spp. infection was observed on species from the plant families Poaceae, Pinaceae and Lamiaceae, such as *Agrostis palustris* (bentgrass), *Poa pratensis* (Kentucky bluegrass), *Picea mariana* (black spruce), *Pinus* spp. (pine), *Salvia coccinea* (Crimson sage). Bailey *et al.* (2009) stated that it was vital to demonstrate that the potential bioherbicide does not pose risk to non-target species particularly in the surrounding area of the targeted weeds. It is important to note that *P. herbarum* (PH81) was also inoculated on various crops such as oil palm, maize, chilli and okra and the study (unpublished) found that no infection occurred on these crops that are usually used in oil palm integration.

The incompatibility between mycoherbicide and chemical herbicides is still under study, but herbicides are known to interfere with disease development, either because of a direct toxicity to the pathogen or indirectly by triggering defence responses in the plants (Sanogo *et al.*, 2000). The negative effect of gluphosinate ammonium, paraquat dichloride, glyphosate isopropylammonium and glyphosate monoammonium towards *P. herbarum* showed that herbicides can inhibit disease progress because of their direct toxicity to the fungus. Therefore, it is not recommended to use these herbicides in combination with the application of *P. herbarum* since the herbicides will have a tendency to kill the fungus. Moreover, in the field, the fungus exists as a weak, opportunistic, or wound pathogen occurring mostly on woody hosts, especially on members of the Rosaceae (Farr *et al.*, 1989). However, the combination of *P. herbarum* with diuron could yield encouraging results for the potential of fungus-

herbicide combinations. Nevertheless, a field trial needs to be conducted to verify this assumption about fungus-herbicide combinations.

Lastly, it was also noted that the application of *P. herbarum* was effective when weeds were at the pre-emergence stages, then it became difficult to control over time as the weeds become persistent and well established. Indeed, one of the most important aspects for successful biocontrol is an even distribution of the bioherbicides. Therefore, the application of bioherbicide at the pre-emergence stages is crucial and essential in order to control this noxious weed.

ACKNOWLEDGEMENT

REFERENCES

Ana López-Moral, A; Agustí-Brisach, C and Trapero, A (2021). Plant biostimulants: New insights into the biological control of verticillium wilt of olive. *Front. Plant Sci., 2*: 662178. DOI: 10.3389/fpls.2021.662178.

Bailey, K L; Boyetchko, S M; Peng, G; Hynes, R K; Taylor, W G and Pitt, W M (2009). Developing weed control technologies with fungi. *Current Advances in Fungal Biotechnology* (Rai, M ed.). I.K. International Pvt. Ltd., New Delhi, India. p. 1-44.

Bailey, K L; Pitt, W M; Falk, S and Derby, J (2011). The effects of *Phoma macrostoma* on non-target plant and target weed species. *Biol. Control, 58*: 379-386. DOI: 10.1016/j.biocontrol.2011.06.001.

Barnes, D E and Chan, L G (1990). *Common Weeds of Malaysia and Their Control*. Ancom Berhad. Kuala Lumpur, Malaysia. 349 pp.

Bisht, M S and Mukai, Y (2002). Genome organization and polyploid evolution in the genus *Eleusine* (Poaceae). *Plant Syst. Evol., 233*: 243-258. DOI: 10.1007/s00606-002-0201-5.

Boyette, C D; Templeton, G E and Oliver, L R (1984). Texas gourd (*Cucurbita texana*) control with *Fusarium solani* f.sp.cucurbitae. *Weed Sci., 32*: 649-657. DOI: 10.1017/S0043174500059737.

Boyette, C D; Quimby, JR P C; Connick, JR W J; Daigle, D J and Fulgham, F E (1991). Progress in the production, formulation and application of mycoherbicides. *Microbial Control of Weeds* (TeBeest, D O ed.). Chapman and Hall Inc., New York. p. 209-224.

Chen, J; Huang, H; Wei, S; Huang, Z; Wang, X and Zhang, C (2017). Investigating the mechanism of glyphosate (*Eleusine indica* (L.) Gaertn.) by RNA sequencing technology. *Plant J., 89*: 407-415. DOI: 10.1111/tpj.13395.

Chuah, T S and Lim, W K (2015). Assessment of phytotoxic potential of oil palm leaflet, rachis and frond extracts and powders on goosegrass [*Eleusine indica* (L.) Gaertn.] germination, emergence and seedling growth. *Malays. Appl. Biol., 44*: 75-84.

Cimmino, A; Andolfi, A; Zonno, M C; Avolio, F; Santini, A; Tuzi, A; Berestetskyi, A; Vurro, M and Antonio, E (2013). Chenopodolin: A phytotoxic unrearranged ent-pimaradienediterpene produced by *Phoma chenopodicola*, a fungal pathogen for *Chenopodium album* biocontrol. *J. Nat. Prod., 76*: 1291-1297. DOI: 10.1021/np400218z.

Cruz, J F R; Macias, M; Rojas, C M C G and Mata, R (2003). A new phytotoxic nonenolide from *Phoma herbarum*. *J. Nat. Prod., 66*: 511-514. DOI: 10.1021/np020501t.

Currie, A F; Gange, A C; Ab Razak, N; Ellison, C A; Maczey, N and Wood, S V (2020). Endophytic fungi in the invasive weed *Impatiens glandulifera*: A barrier to classical biological control? *Weed Res., 60*: 50-59. DOI: 10.1111/wre.12396.

Deb, D; Khan, A and Dey, N (2020). *Phoma* diseases: Epidemiology and control. *Plant Pathol., 69*: 1203-1217. DOI: 10.1111/ppa.13221.

Dilipkumar, M; Chuah, T S; Hoh, S H and Sahid, I (2020). Weed management issues, challenges and opportunities in Malaysia. *Crop Prot., 134*: 104347. DOI: 10.1016/j.cropro.2017.08.027.

Dutta, W and Ray, P (2017). A glimpse into the compatibilities and conflicts between arthrods and fungal biological control agents of aquatic weed waterhyacinth. *Phytoparasitica, 45*: 429-437. DOI: 10.1007/s12600-017-0605-y.

Farr, D F; Bills, G F; Chamuris, G P and Rossman, A Y (1989). *Fungi on Plants and Plant Products in the United States. VIII, 1252 S*. The American Phytopathological Society (APS) Press, St. Paul, Minnesota. 1252 pp.

Figliola, S S; Camper, N D and Ridings, W H (1988). Potential biological control agents for goosegrass

Eleusine indica. *Weed Sci., 36*: 830-835. DOI: 10.1017/ S0043174500075913.

Guske, S; Schulz, B and Boyle, C (2004). Biocontrol options for *Cirsium arvense* with indigenous fungal pathogens. *Weed Res., 44*: 107-116. DOI: 10.1111/j.1365-3180.2003.00378.x.

Hamayun, M; Khan, S A; Khan, A L; Rehman, G; Sohn, E Y; Shah, A A; Kim, S K; Joo, G J and Lee, I J (2009). *Phoma herbarum* as new gibberellin-producing and plant growth promoting fungus. *J. Microbiol. Biotech., 19*: 1224-1249. DOI: 10.4014/ jmb.0901.030.

Harding, D P and Raizada, M N (2015). Controlling weeds with fungi, bacteria and viruses: A review. *Front. Plant Sci., 6*: 659. DOI: 10.3389/ fpls.2015.00659.

Hahn, D; Sallenave, R; Pornaro, C and Leinauer, B (2020). Managing cool-season turfgrass without herbicides: Optimizing maintenance practices to control weeds. *Crop Sci., 60*: 2204-2220. DOI: 10.1002/csc2.20175.

Hynes, R K (2018). *Phoma macrostoma*: As a broad spectrum bioherbicide for turfgrass and agricultural applications. *CAB Reviews, 13*: 5. DOI: 10.1079/PAVSNNR201813005.

Holm, L G; Plucknett, D L; Pancho, J V and Herberner, J P (1977). *The World's Worst Weeds*. University Press of Hawaii, Honolulu. 609 pp.

Jones, R W and Hancock, J G (1990). Soilborne fungi for biological control of weeds. *Microbes and Microbial Products as Herbicides* (Hoagland, R E ed.). ACS Symposium Series, Vol. 439. American Chemical Society, Washington, DC. p. 276-286.

Johnston, P R (1981). *Phoma* on New Zealand grasses and pasture legumes. *N. Z. J. Bot., 19*: 173-186. DOI: 10.1080/0028825X.1981.10425118.

Lacey, L A; Frutos, R; Kaya, H K and Vail, P (2001). Insect pathogens as biological control agents: Do they have a future? *Biol. Control, 21*: 230-248. DOI: 10.1006/bcon.2001.0938.

Leach, G E; Devine, M D; Kirkwood, R C and Marshall, G (1995). Target enzyme-based resistance to acetyl-coenzyme A carboxylase in-hibitors in *Eleusine indica*. *Pestic. Biochem. Phys., 51*: 129-136. DOI: 10.1006/pest.1995.1013.

Lee, L J and Ngim, J (2000). A first report of glyphosate-resistant goosegrass [*Eleusine indica* (L.) Gaertn] in Malaysia. *Pest Manag. Sci., 56*:

336-339. DOI: 10.1002/(SICI)1526-4998(200004) 56:4<336::AID-PS123>3.0.CO;2-8.

Maizatul-Suriza, M and Idris, A S (2012). Occurrence of common weeds in mature plantings of oil palm plantations in Malaysia. *The Planter, 88*: 537-547.

Manicom, B Q; Bar-Joseph, M; Rosner, A; Vigodsky-Haas, H and Kotze, J M (1987). Potential applications of random DNA probes and restriction fragment length polymorphisms in the taxonomy of the Fusaria. *Phytopathology, 77*: 669-672. DOI: 10.1094/Phyto-77-669.

Mudge, L C; Gosset, T B J and Murphy, T R (1984). Resistance of goosegrass (*Eleusine indica*) to dinitroaniline herbicides. *Weed Sci., 32*: 591-594. DOI: 10.1017/S0043174500059610.

Neumann, S and Boland, G J (2002). Influence of host and pathogen variables on the efficacy of *Phoma herbarum*, a potential biological control agent of Taraxacum officinale. *Can. J. Bot., 80*: 425-429. DOI: 10.1139/b02-024.

Neto, J R C; dos Santos, M S N; Mazutti, M A; Zabot, G L and Tres, M V (2021). *Phoma dimorpha* phytotoxic activity potentialization of bioherbicide production. *Biocatal. Agric. Biotechnol., 33*: 101986. DOI: 10.1016/j.bcab.2021.101986.

Pedras, M S C and Yu, Y (2008). Structural and biological activity of maculansin A, a phytotoxin from the phytopathogenic fungus *Leptosphaeria maculans*. *Phytopathol, 69*: 2966-2971. DOI: 10.1016/j. phytochem.2008.09.015.

Ray, P and Vijayachandran, L S (2013). Evaluation of indigenous fungal pathogens from horse purslane (*Trianthema portulacastrum*) for their relative virulence and host range assessments to select a potential mycoherbicidal agent. *Weed Sci., 61*: 580-585. DOI: 10.1614/WS-D-12-00076.1.

Rusli, M H; Idris, A S; Norman, K and Sim, K C (2014). The combination effect of MSMA and Diuron in controlling glyphosate resistant *Eleusine indica* in oil palm plantation. *The Planter, 90*: 801-815.

Sanogo, S; Yang, X B and Scherm, H (2000). Effects of herbicides on *Fusarium solani* f.sp. *glycines* and development of sudden death syndrome in glyphosate-tolerant soybean. *Phytopathology, 90*: 57-66. DOI: 10.1094/PHYTO.2000.90.1.57.

Savita, S A (2019). Fungi as biological control agents. *Biofertilizers for Sustainable Agriculture and*

Environment (Giri, B; Prasad, R; Wu, Q S and Varma, A eds.). Soil Biology Springer, Cham. 55 pp. DOI: 10.1007/978-3-030-18933-4.

Teng, Y T and Teo, K C (1999). Weed control and management of resistant goose grass (*Eleusine indica*) in Malaysia. *Proc. of the 17th Asian-Pacific Weed Science Society Conference*. 22-27 November 1999. Bangkok, Thailand. p. 753-758.

Todero, I; Confortin, T C; Luft, L; Brun, T; Ugalde, G A; De Almeida, T C; Arnemann, J A; Zabot, G L and Mazutti, M A (2018). Formulation of a bioherbicide with metabolite from *Phoma* sp. *Sci. Hortic., 241*: 285-292. DOI: 10.1016/j.scienta.2018.07.009.

Tran, M; Baerson, S; Brinkler, R; Casagrande, L; Falletti, M and Feng, Y (1999). Characterization of glyphosate resistant *Eleusine indica* biotypes from Malaysia. *Proc. of the 17th Asian-Pacific Weed Science Society Conference*. 22-27 November 1999. Bangkok, Thailand. p. 527-536.

Valverde, B E; Riches, C R and Caseley, J C (2000). Prevention and Management of Herbicide Resistant Weed in Rice: Experiances from Central America with *Echinochloa colona*. Camara de Insumos Agropecuarios, Costa Rica's. http://www.weedscience.org/EBooks/RiceBookIntro.aspx., accessed on 1 May 2020.

Vikrant, P; Verma, K K; Rajak, R C and Pandey, A K (2006). Characterization of a phytotoxin from *Phoma herbarum* for management of *Parthenium hysterophorus* L. *J. Phytopathol.,154*: 461-468. DOI: 10.1111/j.1439-0434.2006.01129.x.

White, T J; Bruns, T; Lee, S and Taylor, J W (1990). Amplification and direct sequencing of fungal ribosomal RNA genes for phylogenetics. PCR protocols. *A Guide to Methods and Applications* (Innis, M A; Gelfand, D H; Sninsky, J J and White, T J eds.). Academic Press, San Diego, CA, USA. p. 315-322.

Yang, X B; Gao, X D; Han, F B and Tan, R X (2005). Sulfation of a polysaccharide produced by a marine filamentous fungus *Phoma herbarum* (YS4108) alters its antioxidant properties *in vitro*. *Biochim Biophys Acta, 1725*: 120-127. DOI: 10.1016/j.bbagen.2005.06.013.

Zhou, L; Bailey, K L and Derby, J (2004). Plant colonization and environmental fate of the biocontrol fungus *Phoma macrostoma. Biol. Control, 30*: 634-644. DOI: 10.1016/j.biocontrol.2004.03.002.

Zhao, S and Shamoun, S F (2005). Effects of potato dextrose broth and gelatin on germination and efficacy of *Phoma exigua*, a potential biocontrol agent for salal (*Gaultheria shallon*). *Can. J. Plant Pathol., 27*: 234-244. DOI: 10.1080/07060660509507221.

NUTRITIONAL POTENTIAL OF SUPERCRITICAL FLUID-EXTRACTED PALM FRUIT

SOEK SIN TEH[1]*; NATALIE VIVIEN GUNTER[1,2] and HARRISON LIK NANG LAU[1]

ABSTRACT

Supercritical-fluid extraction (SFE) has been suggested to be highly suitable method for food processing due to its greener approach and use of readily available and safe solvents. The palm fruit fibres (PFF) have limited food applications and are often regarded as waste despite being a potential source of dietary fibre. Therefore, the aims of the study were to analyse the nutritional attributes and chemical composition of SFE-extracted palm oil (SFE-O) and fibre (SFE-F). Results showed that SFE-O has comparable phytonutrients and oil quality with hexane-(HEX-O) and commercial mechanical pressing (MP-O)-extracted crude palm oils. Although SFE-O contains lower concentrations of phytonutrients (total of carotenoids, vitamin E, squalene and sterols) than the two oils, it exhibited higher antioxidant effects than MP-O as showed in 2,2-diphenyl-1-picrylhdrazyl (DPPH) radical scavenging, hydrogen peroxide (H_2O_2) scavenging and ferric ion chelating assays, whereas SFE-O also exhibited higher ferric ion chelating activity than HEX-O, postulating its protective health benefits. Meanwhile, both SFE-fibre and HEX-fibre contain comparable dietary fibre with existing food products, suggesting the potential of PFF as a source of dietary fibre and other food applications. The beneficial effects of SFE-O and PFF also suggested that recovery of both would potentially generate additional revenue for palm oil mills.

INTRODUCTION

Palm oil is commonly used in the food industry and known for its balanced ratio of saturated and unsaturated fatty acids, zero content of *trans* fatty acids and a variety of beneficial active compounds including phenolic compounds, phytosterols and squalene. The presence of tocopherols, tocotrienols and carotenoids in palm oil with notable antioxidant activities which enhances its nutritional value and dietary benefits when incorporated in our daily diet (Kushairi *et al.*, 2019). However, active compounds such as polyphenols are commonly sensitive to processing conditions during the oil extraction and refining, rendering it susceptible to degradation (Ruiz-Marcial *et al.*, 2007). This becomes one of the driving factors to find alternative methods of oil extraction with milder conditions in order to preserve these antioxidants.

The conventional extraction of oil from palm fruits using mechanical screw-press generally involves sterilisation, digestion, clarification and drying. Another common extraction method is by using organic solvents, most commonly hexane, which is widely implemented within the industry of seed oil extraction and fractionations, owing to its high oil recovery capacity. Nonetheless, the extracted oil via this solvent extraction has been criticised for its use in the food industry as the resulting residual solvent could be harmful to both human health and the environment (Galle *et al.*, 2003). While the simple process and generally lower cost are attractive, however, the arising limitations combined with the demand for high quality oil have prompted the search for environmentally-friendly

[1] Malaysian Palm Oil Board,
6 Persiaran Institusi, Bandar Baru Bangi,
43000 Kajang, Selangor, Malaysia.

[2] School of Biosciences,
Taylor's University, Lakeside Campus,
47500 Subang Jaya, Selangor, Malaysia.

* Corresponding author e-mail: ssteh@mpob.gov.my

alternative extraction methods that pose minimal risk to the human health (Ialenti *et al.*, 1992). The supercritical fluid extraction (SFE) now, emerges as a potential alternative extraction process and has since been received as a safe method. Carbon dioxide (CO_2), the most commonly used solvent for SFE, is an inert, inexpensive solvent which has low critical temperature and pressure. These characteristics allow extraction using gentler conditions while leaving no solvent residues and thermally degraded active compounds in the extract. Thus, SFE-CO_2 has been suggested to be highly suitable for the extraction of thermally labile products. Furthermore, SFE-CO_2 extracts have been accepted for the processing of food products as they are generally recognised as safe, attributed to its non-toxic and non-flammable character of CO_2. In fact, the use of SFE-CO_2 for palm oil extraction has thus, been previously studied and published in literature (Ialenti *et al.*, 1992; Lau *et al.*, 2006).

In Malaysia, about 5.8 million hectares of land has been used to cultivate oil palm (Kushairi *et al.*, 2019). Generally, oil palm produces approximately 10% of oil and the remaining 90% is oil palm biomass (OPB) in the form of oil palm frond (36.9%), palm oil mill effluent (27.1%), empty fruit bunches (10.4%), palm fruit fibres (PFF) (5.4%), oil palm trunk (4.5%) and palm kernel shell (3.1%) (Loh, 2017; Yeo *et al.*, 2020). The biomass can be obtained from oil palm plantations and palm oil milling activities. In general, pre-treatment of OPB can be achieved by biological, physical, chemical, or physiochemical methods. All these methods resulted in either chemical or physical changes of the biomass. Physical pre-treatment involves grinding (Barakat *et al.*, 2015), steaming and steam extrusion (Duque *et al.*, 2016; Hendriks and Zeeman, 2009; Lin *et al.*, 2012), thermal-mechanical extrusion (Lin *et al.*, 2012) or ultrasonication (Subhedar and Gogate, 2016), whereas chemical pre-treatment involves the utilisation of acids (Noparat *et al.*, 2015), alkali (Chen *et al.*, 2013), organic solvents (Park *et al.*, 2017) or ionic liquids (Elgharbawy *et al.*, 2016), as well as oxidation reaction (Li *et al.*, 2013). Physicochemical methods include steam (Pielhop *et al.*, 2016), supercritical CO_2 (SC-CO_2) explosion (Zheng *et al.*, 1995) and ammonia fibre explosion (AFEX) (Alizadeh *et al.*, 2005). On the other hand, biological method involves the utilisation of microbial communities (Amin *et al.*, 2017). Nevertheless, there are challenges associated with the pre-treatment methods, primarily due to the energy intensive processes such as high temperature and high pressure, along with expensive chemical reagents involved. Therefore, finding alternative methods that can prevail over these limitations are crucial.

Meanwhile, the use of the remaining PFF, after palm oil extraction is still limited. The fibres mixed with palm shells are most commonly recycled as boiler fuel for steam and electricity production (Kwong *et al.*, 2017). Several studies highlighted the main utilisation of the biomass for solid biofuel and bio-composite production.

Nonetheless, the functional and economic potential of the fibres have yet to be realised with very little information on its nutritional value. In its original form, the major fibre components of palm fruit *i.e.*, cellulose, hemicellulose and lignin are determined as insoluble fibre (Abdul Aziz *et al.*, 2011). Numerous benefits of dietary fibre (DF) on human metabolism and physiology have been established in literature over the past years. For example, the intake of DF has been associated with the reduced risk of diabetes, cardiovascular diseases, certain gastrointestinal disorders and improve immune function (Anderson *et al.*, 2009). Thus, this preliminary characterisation of the fibre content of PFF, including the total dietary fibre (TDF), insoluble dietary fibre (IDF) and soluble dietary fibre (SDF) should initially be done which would subsequently shed light on its potential for downstream applications in the food industry.

In the present study, SFE-CO_2 and hexane extractions were carried out to extract crude palm oil (CPO) from palm fruits. The two extracted CPO are termed SFE-extracted palm oil (SFE-O) and hexane- (HEX-O), respectively. These two oils and commercial mechanically pressed CPO termed MP-O, were characterised and analysed for their oil compositions and quality, including free fatty acid (FFA) content, peroxide value (PV), phosphorus content, fatty acid composition (FAC), total carotenoid content, vitamin E content, squalene and sterols contents, total phenolic content (TPC) and total flavonoid content (TFC). This was followed by evaluation of antioxidant activities using various antioxidant assays, including 2,2-diphenyl-1-picrylhdrazyl (DPPH) radical scavenging, hydrogen peroxide (H_2O_2) scavenging, ferrous ion chelating (FIC) and ferric reducing antioxidant power (FRAP) assays. The chemical composition and DF content of the extractive-free PFF were evaluated on its potential nutritional applications.

MATERIALS AND METHODS

Materials

The sterilised palm fruits were collected from a local palm oil mill (Labu, Negeri sembilan, Malaysia). The fruits were separated into two batches for the hexane and supercritical extraction methods.

The sterilised palm fruits were peeled and dried in an oven, followed by grinding to break up the fibres. The palm fruits were then subjected

to Soxhlet extraction with hexane at 70°C for 8 hr. Hexane was evaporated using a rotary evaporator until a constant weight of oil was achieved. PFF was collected from the extraction thimble and was left to dry overnight in a fume hood at room temperature. The hexane-extracted CPO is denoted as HEX-O while the fibre is marked as HEX-F.

Meanwhile, the sterilised palm fruits were subjected to SFE-CO_2 system as described by Lau *et al.* (2006) with some modifications. In brief, it was subjected into a 100-mL extraction vessel and extracted with SC-CO_2 with the flow rate of 5 mL min^{-1}. SC-CO_2 was pumped continuously from the top through the vertical extraction vessel. The extraction condition was set at 60°C, 30 MPa and 8 hr. Next, the oil-laden stream was depressurised by expanding through a heated needle valve to atmospheric pressure, and the oil was collected in a receiver. The flow diagram of SC-CO_2 system is as shown in *Figure 1*. The extracted CPO and the PFF after extraction were denoted as SFE-O and SFE-F, respectively.

On the other hand, MP-O was collected from Labu Palm Oil Mill. Generally, the palm fruits were sterilised at 140°C for 70-90 min (Akhbari *et al.*, 2020) where the sterilised palm fruits above were also obtained at this stage, subsequently subjected to a steam-heated vessels, also known as digester. Next, the oil mixture from the digester was heated to 90°C for 20 min (Yosri *et al.*, 2019) and allowed to separate in the clarification tank, and subsequently subjected to continuous vacuum dryer to remove water (Akhbari *et al.*, 2020). All the palm oil samples were stored at 4°C and room temperature, respectively prior to analyses.

Total DF assay kit was purchased from Megazyme (Bray, Ireland). Potassium iodine and sodium thiosulphate were purchased from R&M Sdn. Bhd. (Selangor, Malaysia). CP-grade CO_2 of 99.995% purity was purchased from Malaysia Oxygen Berhad (Selangor, Malaysia). Myristic acid (C14:0), palmitic acid (C16:0), stearic acid (C18:0), oleic acid (C18:1), p-anisidine, DPPH, hydrogen peroxide, ferrous (II) chloride, potassium ferricyanide, ferric (III) chloride as well as all solvents of chromatographic and analytical grades were purchased from Merck (Darmstadt, Germany).

Methods

All the tests were carried out in triplicate for each sample. Results were expressed as mean value ± standard deviation.

Quality assessment of extracted oils

Determination of free fatty acid (FFA) content. FFA content of oil samples was determined according to Malaysian Palm Oil Board (MPOB) test method p2.5:2004 (MPOB, 2004). Approximately 3 g of oil sample was weighed in a conical flask and 50 mL of isopropanol was added. About 10 drops of 1 g mL^{-1} phenolphthalein in ethanol was dripped into the flask and the solution was mixed. The mixture was then titrated with 0.1 N sodium hydroxide (NaOH) until the colour changed from colourless to pink. The percentage content of FFA [as weight (wt)% of palmitic acid] was calculated as (25.6 N V)/W, where N is the normality of NaOH used, V is the volume of titrant and W is the weight of the oil sample.
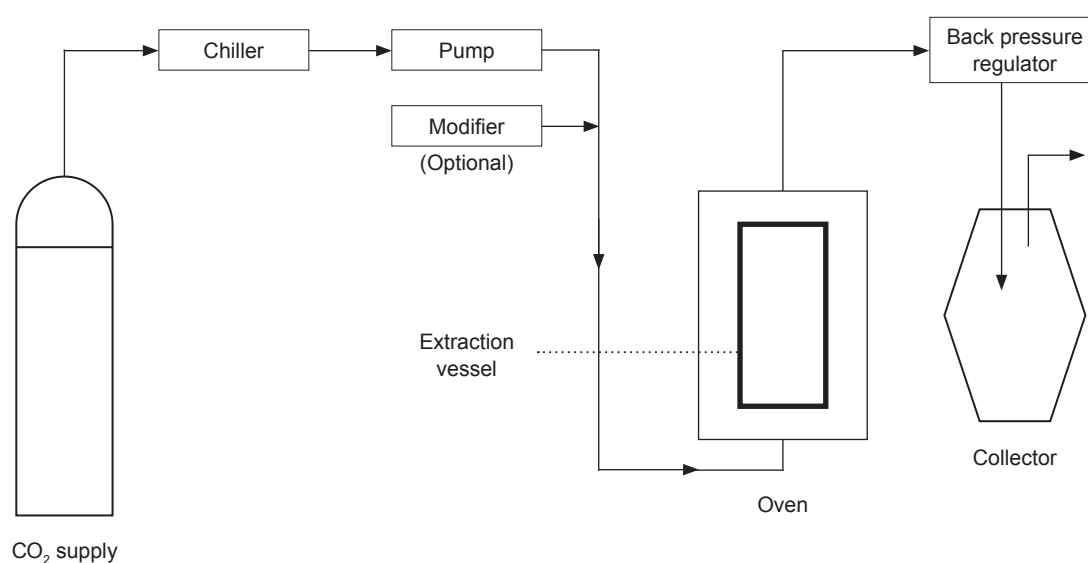

Figure 1. Flow diagram of the supercritical fluid-extracted CO_2 (SFE-CO_2) system.

Peroxide value (PV). PV of oil samples was determined from titration of the sample with sodium thiosulphate solution according to MPOB Test Method p2.3:2004 (MPOB, 2004). A starch indicator was freshly prepared by weighing 0.5 g of starch, followed by sequential addition of 3 mL of distilled water and then 100 mL of boiling water. The starch indicator was left to stand for 3 min before use. Approximately 5 g of oil sample was aliquoted into a conical flask. A blank was run alongside the sample. Then, 30 mL of acetic acid:chloroform (3:2 v/v) solution and 0.5 mL of saturated potassium iodide, potassium iodide (KI) solution were added into the conical flask. The solution was slowly mixed for 1 min, followed by the addition of 30 mL of distilled water. Starch indicator was added until the solution turned to a grey-blue colour. The mixture was then titrated with 0.01 N sodium thiosulphate solution until the grey-blue colour faded. PV (meq O_2 kg^{-1}) was calculated as $[(V_S - V_0)$ N 1000]/W, where V_S is the volume of sodium thiosulphate solution used for titration with the oil sample, V_0 is the volume of titrant used for the blank, N is the normality of sodium thiosulphate solution used and W is the sample weight of oil.

Phosphorus content. Phosphorus content of oil samples was determined according to MPOB Test Method Part 1b, p2.8:2004 (MPOB, 2004). Firstly, 5 g of the oil was weighed in a crucible and then 0.1 g of magnesium oxide (MgO) was added. The mixture was charred until no more smoke was produced and was burnt in the furnace at 900°C for 2 hr. Once cooled to room temperature, the ash in the crucible was dissolved in 5 mL of 6N nitric acid (HNO$_3$), followed by the addition of 10 mL of ammonium vanadate solution and 10 mL of ammonium molybdate solution into the crucible. The mixture was left to stand at room temperature for 20 min. The solution was then transferred into a quartz cuvette and the absorbance of the cell was measured at 400 nm against a blank containing HNO$_3$, ammonium vanadate and ammonium molybdate in a ratio of 1:2:2. A calibration curve with potassium dihydrogen phosphate (KH$_2$PO$_4$) was constructed by plotting a graph of concentration against absorbance. Briefly, the concentrations of 4, 8, 12 and 16 μg mL^{-1} of the standard and their corresponding absorbances were determined by first reacting respectively with 1, 2, 3 and 4 mL of 0.1N KH$_2$PO$_4$ solution, followed by 10 mL of ammonium vanadate and 10 mL of ammonium molybdate. The solution was then marked up to 25 mL with 6N HNO$_3$ and the absorbance was measured at 400 nm.

The phosphorus content, in ppm, was calculated as (C 25 A)/W, where C is the slope of the KH$_2$PO$_4$ calibration curve, A is the absorbance of the sample at 400 nm and W is the weight of the oil sample.

Characterisation of Extracted Oils

Fatty acid composition (FAC). FAC of the oil samples were analysed using gas chromatography equipped with a flame ionisation detector (GC-FID; Perkin Elmer, USA). Oil samples were prepared by aliquoting three drops of oil into a 1.5-mL autosampler vial. The same volume of 0.5 M of sodium methoxide solution was added. The sample was topped up to 1.5 mL with hexane and was then shaken well. Samples were injected at a volume of 1 μl into the system, fitted with a BPX70 column (25 m length (L), 0.22 mm internal diameter (D) and 0.25 μm film thickness). The oven temperature program was initially started at 140°C and then ramped up to 220°C at a rate of 8.0°C min^{-1} and held for 2 min. The injector and detector temperatures were both set to 250°C. Each sample was run for 12 min using purified compressed air, purified hydrogen and purified helium as carrier gases.

Total carotenoid content. The total carotenoid content of the oils was determined following MPOB Test Method p2.6:2004 (MPOB, 2004). Approximately 0.1 g of oil was dissolved in 250 mL of n-hexane. The absorbance of the oil extract was then measured at 446 nm using a UV spectrometer (U-2001, Hitachi Instruments Inc., Tokyo, Japan). The total carotenoid content was calculated as $(383 \, E)/(I \, c)$, where E is the observed difference in absorption between the oil and hexane, I is the path length of the cell (cm), and c is the concentration used for the absorption measurement g (100 mL^{-1}).

Vitamin E composition. Tocopherol and tocotrienol content of the oils were determined according to the method of Che et al. (2015). The vitamin E composition was analysed using HPLC (Agilent 1100 series, Agilent Technologies, USA), equipped with a normal phase Supelco Ascentis® Si column [(150 mm (L) x 4.6 mm (D) x 5 μm particle size)]. The HPLC system was coupled to a fluorescence detector with the detection wavelengths for excitation and emission set at 270 nm and 315 nm, respectively. A mixture of n-heptane and ethyl acetate at 97:3% (v/v) was used as the mobile phase.

Sterol composition and squalene content. The sterol composition and squalene content were concurrently determined according to the method by Lau et al. (2006). A gas chromatograph (GC, 7890B Agilent, Agilent Technologies, USA) with a CP9078 – select biodiesel for glycerides, UM + 2 m RG column [15 m (L) x 320 μm (D) x 0.1 μm (film)] coupled to a flame ionisation detector was used. Helium was used as the carrier gas with a flow rate of 5 mL min^{-1}. The temperatures of the injector, detector and oven were set at 50°C, 380°C and 370°C, respectively. Identification of sterol

composition and squalene content in the oils was done *via* comparison of their retention times with commercial standards, cholesterol and squalene.

Antioxidant Assays

Extraction of polar compounds from oils. The extraction of polar compounds from oil samples was performed following the method described by Radhia *et al*. (2017) with some modifications. Approximately 1 g of oil sample was weighed in a 2 mL microcentrifuge tube, followed by addition of 1 mL of methanol:water (80:20 v/v) which was used as the extraction solvent. Herewith, the methanol:water (80:20 v/v) was referred to as 'extraction solvent'.

The oil-solvent mixture was vortexed for 10 min and was then left to stand until two layers separated (~1 hr). The upper methanolic layer was collected *via* careful pipetting. The extraction process was repeated twice. The oil extracts were combined and stored in a scintillation vial at 4°C for subsequent assays. The concentration of the extracts was noted as 0.33 g mL^{-1}. For DPPH radical scavenging assay, the extracts used were collected from a single extraction (concentration of 1.0 g mL^{-1}) and was diluted accordingly. The extracts were named according to the oils (*e.g.* SFE-O extract, HEX-O extract or MP-O extract), or otherwise referred to as 'oil extracts'.

Total phenolic content (TPC). Determination of TPC in the oil extracts was done using the Folin-Ciocalteu (FC) method as described by Abdullah *et al*. (2018).

Total flavonoid content (TFC). TFC of the oil extracts was determined following the aluminum chloride (AlCl$_3$) colorimetric method described by Radhia *et al*. (2017) where rutin hydrate was used as the standard.

2,2-diphenyl-1-picrylhdrazyl (DPPH) radical scavenging assay. DPPH radical scavenging assay was conducted following the method described by Teh *et al*. (2013) using ascorbic acid as the standard drug.

Hydrogen peroxide (H$_2$O$_2$) scavenging assay. H$_2$O$_2$ scavenging activity of the phenolic extracts was determined according to the method of Keser *et al*. (2012).

Ferrous ion chelating (FIC) assay. FIC activity of the extracts was determined according to the method described by Mah *et al.* (2017).

Ferric reducing antioxidant power (FRAP) assay. FRAP of the extracts was performed following the protocol by Mah *et al.* (2017) using ascorbic acid as the standard drug.

Fibre Compositional Analysis

Compositional analysis of holocellulose was performed according to the method described by Then *et al*. (2014). The α-cellulose content was then determined following the ASTM D1103-60 (1978) method. The hemicellulose content of the fibre was calculated as the difference between the content of holocellulose and α-cellulose. Lignin content of fibre samples was determined according to ASTM D1106-96 (2007).

Dietary Fibre (DF) Analysis

Determination of TDF, IDF and SDF contents was performed according to AOAC Official Method 991.43.

Statistical Analysis

Statistical analyses were performed using GraphPad Prism 7. Statistical tests such as Student's t test, one-way analysis of variance (ANOVA) and Tukey *post-hoc* tests were performed to compare data at 5% significance level ($p<0.05$).

RESULTS AND DISCUSSION

Evaluation of physical and chemical properties of palm oil such as its FFA content, PV, phosphorus content and FAC provides fundamental information on the quality of the oil. These aspects are particularly important to gauge market acceptability, usefulness in downstream technological processes, shelf life, and the overall value of palm oil (Ji *et al*., 2011). The FFA, PV and phosphorus contents of the HEX-O, SFE-O and MP-O are summarised in *Table 1* while the FAC of the oil samples is recorded in *Table 2*.

Among various quality parameters, FFA content is an excellent indicator of oil deterioration, where at high levels of FFA, sensory characteristics and nutritional benefits of the edible oil are altered due to oil rancidity. Triglycerides (TG) are composed of a glycerol molecule bound to three fatty acids molecules where TG has been reported to be prone to hydrolyse in an autocatalytic oxidation reaction to release the FFA and therefore, FFA content generally increases with time and storage period of the oil (Mizushima and Kobayashi, 1968). Consequently, FFA are considered to be pro-oxidants and is commonly correlated to the economic value of edible oils, often representative of the quality index for storage length, marketing and production of palm oil (Akihisa *et al*., 2000). The FFA content of SFE-O and HEX-O was below 1% at 0.59 ± 0.09% and 0.56 ± 0.04%, respectively, while the FFA content of MP-O was significantly higher at 3.39 ± 0.09% ($p<0.05$) (*Table 1*). Experimental FFA values for SFE-O

and HEX-O were also comparable to the published literature where SFE-O and HEX-O were reported to have an average of 0.61% and 0.37%, respectively (Lau *et al.*, 2006). The FFA content of MP-O, on the other hand, was significantly higher than SFE-O and HEX-O where the former was comparable to reported values that range from 3.15% to 4.60% (Lau *et al.*, 2006). Hence, it is possible to infer that hexane extraction or SFE produce better quality palm oil compared to the conventional mechanical pressing. The FFA content for all samples is satisfactory as they are below the maximum acceptable FFA content of 5%, as specified by Palm Oil Refiners Association of Malaysia (PORAM) Specification. When FFA levels exceed 5%, the oil becomes unfit for applications in the food industry and human consumption. The FFA content range of 0.5%-0.8% is normally encountered for edible oils especially for those used in frying. The FFA content of SFE-O and HEX-O fall within this common range, suggesting suitability of the oils to be used directly without further refining for edible purpose. CPO with low FFA content of about 0.65% has also been reported to display good physicochemical properties with high industrial applicability (Akihisa *et al.*, 2000).

PV is a quality parameter that provides information on the oxidation state of the oil based on the measurement of primary oxidation products. The main primary oxidation products are hydroperoxides which are highly unstable and will subsequently break down into mixtures of secondary oxidation products such as aldehydes, ketones, and fatty acids. Classification of the oxidation level of vegetable oils has been proposed based on PV, as follows: 3-5 meq O_2 kg^{-1} (low), 10-12 meq O_2 kg^{-1} (moderate), and 16-18 meq O_2 kg^{-1} (high) oxidation levels, respectively (Zhou *et al.*, 2008). PV of 10 meq O_2 kg^{-1} is specified to be the maximum acceptable value where vegetable oils with PV below this value is considered to be suitable for consumption whereas oil will be considered rancid if PV is greater than 30 meq O_2 kg^{-1}. PV of HEX-O and MP-O are 1.67 ± 0.30 and 1.67 ± 0.31 meq O_2 kg^{-1} oil, respectively (*Table 1*) while PV of SFE-O is higher at 3.24 ± 1.07 meq O_2 kg^{-1} oil, which is higher than that previously extracted via similar method with an average PV of 1.68 meq O_2 kg^{-1} oil (Lau *et al.*, 2006). Nevertheless, statistical analyses showed no significant differences (*p*>0.05) between the PV of SFE-O, HEX-O and MP-O; thus, the difference in PV between samples may be considered as negligible. The low PV may be associated with the presence of antioxidants in palm oils such as carotenoids and vitamin E (*Table 4*). Based on classification by Zhou *et al.* (2008), the three oil samples fall under the category of low oxidation level (between 3-5 meq O_2 kg^{-1}), indicating good oxidative stability.

Total phosphorus content in CPO represents the total phosphatides content. Phosphatides, in turn, comprises of phospholipids or gums, and inorganic phosphates. Numerous issues have been attributed to the high content of phosphorus in palm oil. Researchers have linked phosphorus content to the oxidative stability of palm oil, suggesting the contribution of oxidation of the oil by either inorganic phosphates or phospholipids and thus, negatively affecting oil quality. Goh *et al.* (1984) reported that problems occur during refining of palm oil such as reduced yield of oil and the diminished bleaching power of bleaching earth. Therefore, these undesired components are usually removed by degumming process during refining of palm oil in order to obtain oxidative stable edible oils. SFE-O was found to have the lowest phosphorus content of 22.09 ± 1.55 ppm among the samples, followed by MP-O (45.32 ± 5.24 ppm) and HEX-O (66.60 ± 4.17 ppm), where the phosphorus content of the three oil samples was significantly different (*p*<0.05). The lowest phosphorus content of SFE-O (26 ppm) might attribute to the insolubility of polar phospholipids in the non-polar CO_2 solvent. Meanwhile, phosphorus content of HEX-O was significantly higher than MP-O, which may be related to the affinity of phospholipids for hexane used in solvent extraction, resulting in the higher content when compared to extraction with physical means as that did not disrupt the membrane layer. A similar relationship was observed where the hexane-extracted CPO from residual palm-pressed fibre possessed higher phosphorus content than that in the commercial CPO (Safari *et al.*, 2015).

The FAC of an oil is particularly important for product development and subsequent product marketing as the composition strongly influences the oxidative stability of the oil. This is because the structure of TG, in terms of the proportion and arrangement of fatty acids on the glycerol backbone, affects the physicochemical properties of the oil. Oils containing fatty acids with higher degrees of unsaturation are more prone to oxidation, resulting in alterations in taste, aroma and colour of the oil, subsequently reducing the shelf life of the oil (Ji *et al.*, 2011). One of the unique characteristics of palm oil is having equal amounts of saturated and unsaturated fatty acids as many vegetable oils have higher content of unsaturated fatty acid. SFE-O, HEX-O and MP-O have similar ratios of saturated (SFA), monounsaturated (MUFA) and polyunsaturated (PUFA) fatty acids content with about 5:4:1. Statistical analyses showed significant differences (*p*<0.05) for SFA and MUFA between SFE-O and HEX-O with MP-O, while there were no significant differences for PUFA. The outcome indicates that the polarity of the extractive solvents *i.e.*, CO_2 and hexane had affected FAC of the oils as more non-polar fatty acids (SFA) were extracted.

TABLE 1. QUALITY ASSESSMENT OF OIL SAMPLES

Oil sample	FFA (%)	PV (meq O_2 kg^{-1} oil)	Phosphorus (ppm)
SFE-O	0.59 ± 0.09^a	3.24 ± 1.07^a	22.09 ± 1.55^a
HEX-O	0.56 ± 0.04^a	1.67 ± 0.30^a	66.60 ± 4.17^c
MP-O	3.39 ± 0.09^b	1.67 ± 0.31^a	45.32 ± 5.24^b

Note: Each data represents the mean ± SD of three independent experiments where means with different letters in the same column indicate significant differences ($p<0.05$) among the samples. SFE-O - supercritical fluid-extracted crude palm oil; HEX-O - hexane-extracted crude palm oil; MP-O - mechanically pressed crude palm oil; FFA - free fatty acid; PV - peroxide value.

TABLE 2. FATTY ACID COMPOSITION (FAC) OF OIL SAMPLES

Fatty acid		Composition (wt. %)		
	Name	SFE-O	HEX-O	MP-O
C10:0	Capric acid	0.29 ± 0.02	0.06 ± 0.04	0.40 ± 0.11
C12:0	Lauric acid	0.05 ± 0.04	0.03 ± 0.00	0.07 ± 0.02
C14:0	Myristic acid	1.17 ± 0.11	1.03 ± 0.00	0.82 ± 0.02
C16:0	Palmitic acid	45.34 ± 0.56	45.77 ± 0.16	43.16 ± 0.15
C16:1	Palmitoleic acid	0.47 ± 0.12	0.53 ± 0.18	0.23 ± 0.04
C18:0	Stearic acid	3.25 ± 0.12	3.32 ± 0.05	3.98 ± 0.06
C18:1	Oleic acid	39.51 ± 0.21	39.56 ± 0.21	41.06 ± 0.15
C18:2	Linoleic acid	9.12 ± 0.13	9.07 ± 0.13	9.57 ± 0.13
C18:3	Linolenic acid	0.74 ± 0.46	0.60 ± 0.06	0.66 ± 0.13
C20:0	Arachidic acid	0.06 ± 0.07	0.02 ± 0.07	0.03 ± 0.02

Note: Each data represents the mean ± SD of three independent experiments. SFE-O - supercritical fluid-extracted crude palm oil; HEX-O - hexane-extracted crude palm oil; MP-O - mechanically pressed crude palm oil.

Palm oil contains various important minor components such as phenolic compounds, flavonoids, vitamin E and carotene contents that contribute to oil stability as well as health and nutritional properties (Choo *et al.*, 1996; Teh *et al.*, 2020). These compounds offer a wide range of biological activities due to their potential activities in free radical scavenging, chelation of divalent cations and as antioxidants (Abdullah *et al.*, 2018).

In the present study, TPC and TFC analyses were carried out using the FC and $AlCl_3$ colorimetric methods, respectively. Both HEX-O and MP-O were observed to have very similar TPC and TFC profiles with about 75.5 μg GAE g^{-1} oil and 10.7 μg RE g^{-1} oil, respectively, with no significant difference ($p>0.05$) (*Table 3*). In contrast, the TPC and TFC of SFE-O are comparably lower than both HEX-O and MP-O. As flavonoids are phenolic compounds, it can be inferred that 12.13%, 14.15% and 14.26% of TPC of SFE-O, HEX-O and MP-O, respectively, are flavonoids. There were no significant differences between TFC of all samples, which suggest that oil extraction methods did not substantially affect the extraction of flavonoids. Meanwhile, the difference of TPC between samples may be associated with the ability of the oil extraction systems *i.e.*, hexane extraction, SFE or mechanical pressing, to simultaneously extract different types of phenolic components from the palm fruit. Furthermore, the source of the palm oil may also affect the TPC as described in a recent study which reported that CPO contains 31.20-70.18 ppm of phenolics depending on the palm oil mill where the oil sample was collected from (Abdullah *et al.*, 2018).

The content of minor components in palm oil, namely vitamin E and carotenes, as well as squalene and sterols content were also analysed and presented in *Table 4*. The MP-O had the highest (1868.9 ppm) minor components, followed by HEX-O (1360.2 ppm) and SFE-O (1299.0 ppm). The results are in line with the literature reported that palm oil contains an average of 500-700 ppm of carotenoids (Choo *et al.*, 1996). However, in term of vitamin E, squalene and sterols, the concentrations were remarkably low compared to the literature data which were 600-1000 ppm of vitamin E, 421-979 ppm of squalene and 250-650 ppm of sterols (Choo *et al.*, 1996; Lau *et al.*, 2006). The differences in the concentrations might be attributed to the growth conditions, maturity and source of the palm fruits used (El Sayed, 2000).

The presence of the above phytonutrients in the oil is crucial to maintain oil stability, prolong shelf-life, and to provide health benefits from its dietary consumption although its proportion in

palm oil is less than 1%. The synergistic antioxidant action of vitamin E and carotenoids has also been documented in literature where the combination of both compounds produce an improved overall antioxidant effect by the inhibition of lipid oxidation (Morel *et al.*, 2002). Moreover, as the presence of antioxidants can affect the oxidative stability of the oil, the relatively lower average phytonutrient concentration of SFE-O may also explain the higher PV of the oil compared to HEX-O and MP-O (Ji *et al.*, 2011).

The DPPH radical scavenging activity of the oil extracts increase in a dose-dependent relationship. The standard compound, ascorbic acid, demonstrated significant radical scavenging activity with an EC_{50} of 0.02 mg mL^{-1} which is much lower compared to the EC_{50} of 242.67, 214.67 and 348.33 mg mL^{-1} for the extracts of SFE-O, HEX-O and MP-O, respectively (*Table 5*). Among the oil samples, the HEX-O extract displayed the lowest EC_{50} which means the highest DPPH radical scavenging activity, followed by SFE-O and MP-O. These results highlighted the hydrogen donating ability of the phenolic compounds in the extracts. Surprisingly, MP-O which had the highest content of vitamin E among the three samples was found to have the lowest DPPH radical scavenging activity despite vitamin E exhibiting effective free radical scavenging activity, while HEX-O with the lowest vitamin E content displayed highest radical scavenging activity. This contradicting finding may be linked to the nature of vitamin E as lipid-soluble compounds. Consequently, vitamin E is not maximally extracted from the oil using the polar

extraction solvent which were methanol:water (80:20 v/v), in this case and therefore had minimal contribution to antioxidant activity. A similar inference may be extended to the lipophilic squalene which is extracted by the polar extraction solvent. The outcome postulates that both SFE-O and HEX-O contain similar profile of methanolic extract of carotenoids, vitamin, squalene and sterols but different from MP-O.

H_2O_2 is classified as a non-radical reactive oxygen species where scavenging activity is important to curb the generation of reactive hydroxyl radicals that occur via the Fenton reaction: $Fe^{2+} + H_2O_2 \rightarrow Fe^{3+} + OH^- + OH\bullet$ (Balasundram *et al.*, 2005). The scavenging ability has been correlated to the electron-donating capacity of phenolic compounds which removes the odd number of electrons of the hydroxyl radical (Balasundram *et al.*, 2005). The standard compound, α-tocopherol, had H_2O_2 scavenging activity of 52.42 ± 3.45% at 1 mg mL^{-1} (*Table 5*) which is comparable to the value reported by Keser *et al.* (2012) of 44.58%. The H_2O_2 scavenging activity of the oil extracts can be ranked as follows: HEX-O > SFE-O > MP-O at a concentration of 1 mg mL^{-1}, with no significant differences between the scavenging activities of the three oil extracts ($p>0.05$). In contrast to previous publications by Mah *et al.* (2017) and Abdullah *et al.* (2018) that highlighted positive correlations between TPC and antioxidant activity, no direct relationship can be observed between TPC and TFC with the scavenging activity of the extracts. Different active compounds may exhibit antioxidant activities *via* various mechanisms of action. Thus, combination

TABLE 3. TOTAL PHENOLIC CONTENT (TPC) AND TOTAL FLAVONOID CONTENT (TFC) OF OIL EXTRACTS

Oil extract	TPC (µg GAE g^{-1} oil)	TFC (µg RE g^{-1} oil)
SFE-O	64.97 ± 1.12[a]	7.88 ± 0.78[a]
HEX-O	75.98 ± 1.28[b]	10.75 ± 3.80[a]
MP-O	75.11 ± 4.08[b]	10.71 ± 0.31[a]

Note: Each data represents the mean ± SD of three independent experiments where means with different letters in the same column indicate significant differences ($p<0.05$) among the samples. SFE-O - supercritical fluid-extracted crude palm oil; HEX-O - hexane-extracted crude palm oil; MP-O - mechanically pressed crude palm oil; GAE - gallic acid equivalent; RE - rutin hydrate equivalent.

TABLE 4. CAROTENOID, VITAMIN E, SQUALENE AND STEROLS CONTENTS OF OIL SAMPLES

Oil samples	Carotenoids (ppm)	Vitamin E (ppm)	Squalene (ppm)	Sterols (ppm)
SFE-O	540.0 ± 21.0[a]	495.0 ± 7.9[b]	129.3 ± 1.5[a]	134.7 ± 3.2[a]
HEX-O	583.3 ± 13.0[a]	471.3 ± 8.1[a]	171.3 ± 15.8[b]	134.3 ± 1.2[a]
MP-O	633.3 ± 7.2[b]	931.3 ± 2.5[c]	130.0 ±10.0[a]	174.3 ± 15.9[b]

Note: Each data represents the mean ± SD of three independent experiments where means with different letters in the same column indicate significant differences ($p<0.05$) among the samples. SFE-O - supercritical fluid-extracted crude palm oil; HEX-O - hexane-extracted crude palm oil; MP-O - mechanically pressed crude palm oil.

of antioxidant assays gives better insights on the antioxidant reactions, especially when compounds are present as a mixture.

Iron in its ferrous form, Fe^{2+} is capable of initiating and propagating numerous radical reactions, such as the generation of hydroxyl radicals via the Fenton reaction as described earlier. Iron may be released from storage and iron-binding proteins during altered physiological states which may contribute to the damage and development of more serious disease states due to the activity of radicals. Thus, iron chelators are essential to prevent and halt radical and reactive oxygen species generation and propagation. The standard compound ethylenediaminetetraacetic acid (EDTA), known for its chelating activity, was found to have an EC_{50} of 54.33 ± 1.53 µg mL^{-1} which is higher than the literature data which was 10 µg mL^{-1} (Chai *et al.*, 2014). SFE-O extracts displayed the highest chelation activity of $47.96 \pm 1.24\%$ at sample concentration of 0.33 g mL^{-1}. In contrast, MP-O and HEX-O showed lower activity of $32.35 \pm 1.80\%$ and $17.48 \pm 2.43\%$, respectively, where the latter had the lowest chelating power among the three oil extracts. The FIC of SFE-O, HEX-O and MP-O are significantly different from one another ($p<0.05$). Previous research on carotenoids identify these compounds to possess chelating capacities (Sen Gupta and Ghosh, 2013), however, the outcome is not in good agreement with the literature. Vitamin E, squalene and sterols have not been associated with significant chelating activity. The distinct chelating activity of the oil extracts could hence be correlated to the synergistic and antagonistic effects on varying amount and types of compounds present as the consequence of using different oil extraction methods.

FRAP assay is based on the reducing power of active compounds to reduce the Fe^{3+}-ferricyanide complex to the ferrous state. This assay evaluates the ability of compounds to maintain the redox status in the physiological body (FDA Food Code, 2013). FRAP of the palm oil extracts was expressed as ascorbic acid equivalents (AE), determined from the plotted ascorbic acid calibration curve. The highest antioxidant capacity was shown by HEX-O extract (1072.66 ± 1.58 µg AE g^{-1} oil), followed closely by MP-O (1043.33 ± 9.06 µg AE g^{-1} oil). On the other hand, SFE-O exhibited the weakest antioxidant capacity of 960.79 ± 1.10 µg AE g^{-1} oil. The total antioxidant capacities of the oil extracts are significantly different from each other ($p<0.05$). A relationship between TPC-TFC and FRAP of the oils can be observed, contrary to results from other antioxidant assays. For example, HEX-O with the highest TPC and TFC demonstrated the highest total antioxidant capacity. This trend was also observed for MP-O and SFE-O which is in accordance with a previous study demonstrating the positive linear relationship of TPC-TFC and FRAP where a higher TPC and TFC is associated with higher antioxidant capacity (FDA Food Code, 2013).

Although SFE-O, HEX-O and MP-O extracts had similar TPC and TFC, the differences in activity from the various antioxidant assays conducted suggest varying concentrations or the presence of different types of phenolic compounds in the palm oils which may be due to the different extraction methods. The biological activities as antioxidants, free radical scavengers and ion chelators of the oils are the result of the combined action of all phenolic compounds in the extracts; consequently, distinct composition of compounds in the oil extracts of SFE-O, HEX-O and MP-O had resulted in the exhibition of different antioxidant activities (Balasundram *et al.*, 2005). This explanation could also be extended to SFE-O, which was found to possess different TPC, TFC and antioxidant activities compared to HEX-O and MP-O. For example, despite SFE-O having the lowest TPC and TFC content compared to HEX-O and MP-O, it demonstrated higher FIC ability ($47.96 \pm 1.24\%$) and had the second highest DPPH and H_2O_2 radical scavenging activity. Comparing the antioxidant activities of the oil extracts across the various assays performed, it may be hypothesised that extraction method influences the type and composition of phenolic compounds present in the oil. Regardless, the palm oils evidently exhibit antioxidant activities through different mechanisms. The generation of free radicals may overwhelm the body's natural protective defense and cause oxidative stress despite the human body being capable of producing its own endogenous antioxidants where oxidative stress has been implicated in the development of various diseases including cancer, atherosclerosis and diabetes (Gopalakrishnan *et al.*, 1980). Thus, incorporation of antioxidant-rich food products such as palm oil into the daily diet offers nutritional and health benefits such as the protection against free radicals and oxidative stress (Soundararajan and Sasidharan, 2012).

The fibre composition of SFE-F and HEX-F is similar where the major components in both fibres are hemicellulose (23.83%-24.10%), followed by lignin (22.63%-24.52%) and α-cellulose (16.24%-16.78%). This is not surprising as oil palm biomass is often referred to as lignocellulosic material. The lignin content of the fibres is similar to published data for PFF with the range of 22.0%-25.7% (Abdul Aziz *et al.*, 2011; Yasim-Anuar *et al.*, 2016). On the other hand, literature data showed that hemicellulose content in PFF ranged from 31.80% to 33.10% (Abdul Aziz *et al.*, 2011; Nordin *et al.*, 2013; Yasim-Anuar *et al.*, 2016) while cellulose content in PFF ranged from 34.5% to 43.00% (Abdul Aziz *et al.*, 2011; Nordin *et al.*, 2013; Yasim-Anuar *et al.*, 2016) which is two to three folds higher than

in SFE-F and HEX-F. These published findings were comparably higher compared to SFE-F and HEX-F. Various publications highlighted the discrepancies and contrasting findings of fibre composition despite being from the same plant source. Factors such as plant age, geography, soil and other climate variations may alter the fibre composition which may explain the lower cellulose and hemicellulose content in SFE-F and HEX-F compared to the reported data. In addition, the sum of fibre constituents may not necessarily add up to 100%, as observed in the present study, as some components were not traced to a measurable quantity (Komuraiah *et al.*, 2014).

The high composition of lignocellulosic components *i.e.,* cellulose, hemicellulose and lignin in PFF suggests a potential source of DF. Analysis of DF content in PFF after oil extraction revealed a relatively high TDF content of SFE-F and HEX-F of 59.26 ± 0.54% and 55.32 ± 1.90%, respectively. Results from this analysis is highly comparable with the fibre compositional analyses which identified SFE-F and HEX-F to contain 64.59% and 63.51% of IDF (cellulose, hemicellulose and lignin), respectively (*Table 6*). Functional and sensorial

properties of food products are most commonly described with the ratio of IDF to SDF (Shen *et al.*, 2005). The IDF:SDF ratio of HEX-F is 22.09 whereas the ratio for SFE-F is significantly higher by at least five-fold at 114.78 (*Table 6*) where the ratios imply a higher content of IDF in the latter. The IDF:SDF ratio of HEX-F is comparable to those of several food items such as beans, vegetables and fruits that are popular and established sources of DF. For example, IDF:SDF ratio of mung beans, cooked yellow corn, organically grown wheat cereal and mooth Cayenne pineapple is in the range of 22.17 to 35.5 (Kanterman *et al.*, 2012; Safari *et al.*, 2015; Shen *et al.*, 2005). Meanwhile, the IDF:SDF ratio of SFE-F is comparable to the ratio of split peas which is 117.3 (Safari *et al.*, 2015).

Overall, this characterisation study of PFF highlighted the potential of PFF as a source of DF. As the daily intake of DF is still below recommended levels, incorporation of PFF into human diet combats this problem while concurrently maximising the functional and economic potential of OPB. Further investigation is therefore recommended to continue this effort for the comprehensive utilisation of the PFF in the field of nutrition.

TABLE 5. ANTIOXIDANT PROPERTIES OF OIL EXTRACTS

| Oil extracts | EC_{50} towards DPPH radicals (mg mL^{-1}) | Concentrations | | |
| | | 1 mg mL^{-1} | 0.33 g mL^{-1} | |
		H_2O_2 scavenging activity (%)	Ferrous ion chelating activity (%)	Total antioxidant capacity (μg ascorbic acid equivalent g^{-1} oil)
SFE-O	242.67 ± 6.81[c]	40.32 ± 2.49[a]	47.96 ± 1.24[c]	960.79 ± 1.10[a]
HEX-O	214.67 ± 4.62[b]	40.55 ± 1.46[a]	17.48 ± 2.43[a]	1072.66 ± 1.58[c]
MP-O	348.33 ± 2.89[d]	35.65 ± 3.33[a]	32.35 ± 1.80[b]	1043.33 ± 9.06[b]
Ascorbic acid	0.02 ± 0.01[a]	-	-	-
α-tocopherol	-	52.42 ± 3.45[b]	-	-
EDTA	-	-	100	-

Note: Each data represents the mean ± SD of three independent experiments where means with different letters in the same column indicate significant differences (*p*<0.05) among the samples. SFE-O - supercritical fluid-extracted crude palm oil; HEX-O - hexane-extracted crude palm oil; MP-O - mechanically pressed crude palm oil. EDTA - ethylenediaminetetraacetic acid.

TABLE 6. DIETARY FIBRE (DF) CONTENT OF OIL PALM FRUIT FIBRES (PFF)

| Component | Percentage content (wt%) | |
	SFE-F	HEX-F
TDF	59.26 ± 0.54	55.32 ± 1.90
IDF	56.24 ± 1.40	52.58 ± 2.25
SDF	0.49 ± 0.12	2.38 ± 0.10
IDF:SDF ratio	114.78	22.09

Note: Values are expressed as mean ± SD from three independent experiments. Values have been corrected for ash and protein content. SFE-F - PFF after oil extraction using supercritical fluid; HEX-F - PFF after oil extraction using hexane; TDF - total dietary fibre; IDF - insoluble dietary fibre; SDF - soluble dietary fibre.

CONCLUSION

SFE-O has good oil quality and stability where all tested quality parameters were within acceptance limit and were highly comparable to HEX-O and MP-O. SFE is thus, highly advantageous and is also a greener extraction alternative for the extraction of high-quality palm oil. Furthermore, the antioxidant activity of SFE-O extracts was akin to HEX-O and MP-O. Phenolic and flavonoid compounds, as well as vitamin E, carotenoids and squalene exist as minor components in oil with considerable antioxidant activity which are beneficial to health while also contributing to the oxidative stability of the oil. The lignocellulosic PFF remaining after CPO extraction is rich in IDF with small amounts of SDF, suggesting the potential use of PFF in nutrition. The complete utilisation of palm fruit as palm oil and fibre source is promising; thus, further studies for the incorporation of PFF in the daily diet is recommended.

REFERENCES

Abdul Aziz, M; Uemura, Y and Sabil, K (2011). Characterization of oil palm biomass as feed for torrefaction process. Paper presented at the 2011 National Postgraduate Conference. Perak. p. 1-6.

Abdullah, F; Ismail, R; Ghazali, R and Idris, Z (2018). Total phenolic contents and antioxidant activity of palm oils and palm kernel oils at various refining processes. *J. Oil Palm Res.*, *30*: 682-692.

Akhbari, A; Kutty, P K; Chuen, O C and Ibrahim, S (2020). A study of palm oil mill processing and environmental assessment of palm oil mill effluent treatment. *Environ. Eng. Res.*, *25*: 212-221.

Akihisa, T; Yasukawa, K; Yamaura, M; Ukiya, M; Kimura, Y; Shimizu, N and Arai, K (2000). Triterpene alcohol and sterol ferulates from rice bran and their anti-inflammatory effects. *J. Agric. Food Chem.*, *48*: 2313-2319.

Alizadeh, H; Teymouri, F; Gilbert, T I and Dale, B E (2005). Pretreatment of switchgrass by ammonia fibre explosion (AFEX). *Appl. Biochem. Biotechnol.*, *124*: 1133-1141.

Amin, F R; Khalid, H; Zhang, H; Rahman, S U; Zhang, R; Liu, G and Chen, C (2017). Pretreatment methods of lignocellulosic biomass for anaerobic digestion. *AMB Expr.*, *7*: 72-83.

Anderson, J W; Baird, P; Davis, R H, Jr; Ferreri, S; Knudtson, M; Koraym, A; Waters, V and Williams, C L (2009). Health benefits of dietary fibre. *Nutr. Rev.*, *67*: 188-205.

Balasundram, N; Ai, T; Sambanthamurthi, R; Sundram, K and Samman, S (2005). Antioxidant properties of palm fruit extracts. *Asia Pac. J. Clin. Nutr.*, *14*: 319-324.

Barakat, A; Monlau, F; Solhy, A and Carrere, H (2015). Mechanical dissociation and fragmentation of lignocellulosic biomass: Effect of initial moisture, biochemical and structural proprieties on energy requirement. *Appl. Energy*, *142*: 240-246.

Chai, T; Mohan, M; Ong, H and Wong, F (2014). Antioxidant, iron-chelating and anti-glucosidase activities of *Typha domingensis* Pers (Typhaceae). *Trop. J. Pharm. Res.*, *13*: 67-72.

Che, H L; Tan, D M Y; Meganathan, P; Gan, Y L; Razak, G A and Fu, J Y (2015). Validation of a HPLC/FLD method for quantification of tocotrienols in human plasma. *Int. J. Anal. Chem.*, *2015*: 1-7.

Chen, Y; Stevens, M A; Zhu, Y; Holmes, J and Xu, H (2013). Understanding of alkaline pretreatment parameters for corn stover enzymatic saccharification. *Biotechnol. Biofuels*, *6*: 1-10.

Choo, Y M; Yap, S C; Ooi, C K; Ma, A N; Goh, S H and Ong, A S H (1996). Recovered oil from palm-pressed fibre: A good source of natural carotenoids, vitamin E and sterols. *J. Am. Oil Chem. Soc.*, *73*: 599-602.

Comalada, M; Camuesco, D; Sierra, S; Ballester, I; Xaus, J; Galvez, J and Zarzuelo, A (2005). *In vivo* quercitrin anti-inflammatory effect involves release of quercetin, which inhibits inflammation through down-regulation of the NF-kappaB pathway. *Eur. J. Immunol*, *35*: 584-592.

Duque, A; Manzanares, P; Ballesteros, I and Ballesteros, M (2016). Chapter 15 - Steam explosion as lignocellulosic biomass pretreatment. *Biomass Fractionation Technologies for a Lignocellulosic Feedstock Based Biorefinery* (Mussatto, S I ed.). Elsevier, Amsterdam. p. 349-368.

El Sayed, K A 2000. Natural Products as Antiviral Agents. (Atta Ur, R ed). *Studies in Natural Products Chemistry.* Elsevier, Amsterdam. 279 pp.

Elgharbawy, A A; Alam, M Z; Moniruzzaman, M and Goto, M (2016). Ionic liquid pretreatment as emerging approaches for enhanced enzymatic hydrolysis of lignocellulosic biomass. *Biochem. Eng. J., 109*: 252-267.

FDA Food Code (2013). Recommendations of the United States Public Health Service Food and Drug Administration. United States Public Health Service. Food and Drug Administration.

Galle, J; Quaschning, T; Seibold, S and Wanner, C (2003). Endothelial dysfunction and inflammation: what is the link? *Kidney Int. Suppl., 63:* S45-S49.

Goh, S H; Tong, S L and Gee, P T (1984). Inorganic phosphate in crude palm oil: Quantitative analysis and correlations with oil quality parameters. *J. Am. Oil Chem. Soc., 61(10)*: 1601-1604.

Gopalakrishnan, C; Shankaranarayanan, D; Nazimudeen, S K; Viswanathan, S and Kameswaran, L (1980). Anti-inflammatory and CNS depressant activities of xanthones from *Calophyllum inophyllum* and *Mesua ferrea. Indian J. Pharmacol., 12*: 181-191.

Hendriks, A T W M and Zeeman, G (2009). Pretreatments to enhance the digestibility of lignocellulosic biomass. *Bioresour. Technol., 100*: 10-18.

Ialenti, A; Ianaro, A; Moncada, S and Di Rosa, M (1992). Modulation of acute inflammation by endogenous nitric oxide. *Eur. J. Pharmacol., 211*: 177-182.

Ji, G; Yang, Q; Hao, J; Guo, L; Chen, X; Hu, J; Leng, L and Jiang, Z (2011). Anti-inflammatory effect of genistein on non-alcoholic steatohepatitis rats induced by high fat diet and its potential mechanisms. *Int. Immunopharmacol., 11*: 762-768.

Kanterman, J; Sade-Feldman, M and Baniyash, M (2012). New insights into chronic inflammation-induced immunosuppression. *Semin. Cancer Biol., 22*: 307-318.

Keser, S; Celik, S; Turkoglu, S; Yilmaz, O and Turkoglu, I (2012). Hydrogen peroxide radical scavenging and total antioxidant activity of hawthorn. *Chem. J., 2*: 9-12.

Komuraiah, A; Shyam Kumar, N and Durga Prasad, B (2014). Chemical composition of natural fibres and its influence on their mechanical properties. *Mech. Compos. Mater., 50*: 359-376.

Kushairi, A; Ong-Abdullah, M; Nambiappan, B; Hishamuddin, E; Izuddin, Z; Ghazali, R;

Subramaniam, V; Sundram, S and Ghulam Kadir, A P (2019). Oil palm economic performance in Malaysia and R&D progress in 2018. *J. Oil Palm Res., 31*: 165-194.

Kwong, H C; Chidan Kumar, C S; Mah, S H; Chia, T S; Quah, C K; Loh, Z H; Chandraju, S and Lim, G K (2017). Novel biphenyl ester derivatives as tyrosinase inhibitors: Synthesis, crystallographic, spectral analysis and molecular docking studies. *PLoS ONE, 12*: e0170117.

Lau, H L N; Choo, Y M; Ma, A N and Chuah, C H (2006). Quality of residual oil from palm-pressed mesocarp fibre (*Elaies guineensis*) using supercritical CO_2 with and without ethanol. *J. Am. Oil Chem. Soc., 83*: 893-898.

Li, Z; Chen, C H; Hegg, E L and Hodge, D B (2013). Rapid and effective oxidative pretreatment of woody biomass at mild reaction conditions and low oxidant loadings. *Biotechnol. Biofuels, 6*: 119-127.

Lin, Z; Liu, L; Li, R and Shi, J (2012). Screw extrusion pretreatments to enhance the hydrolysis of lignocellulosic biomass. *J. Microb. Biochem. Technol., S12*: 1-5.

Loh, S K (2017). The potential of the Malaysian oil palm biomass as a renewable energy source. *Energy Convers. Manag., 141*: 285-298.

Mah, S H; Teh, S S and Ee, G C L (2017). Anti-inflammatory, anti-cholinergic and cytotoxic effects of *Sida rhombifolia. Pharm. Biol., 55*: 920-928.

Mahesar, S A; Sherazi, S T H; Khaskheli, A R; Kandhro, A A and Uddin, S (2014). Analytical approaches for the assessment of free fatty acids in oils and fats. *Anal. Methods, 6*: 4956-4963.

Mizushima, Y and Kobayashi, M (1968). Interaction of anti-inflammatory drugs with serum proteins, especially with some biologically active proteins. *J. Pharm. Pharmacol., 20*: 169-173.

Morel, C; Seraphin, D; Teyrouz, A; Larcher, G; Bouchara, J P; Litaudon, M; Richomme, P and Bruneton, J (2002). New and antifungal xanthones from *Calophyllum caledonicum. Planta Med., 68*: 41-44.

MPOB (2004). *MPOB Test Methods – A Compendium of Test on Palm Oil Products, Palm Kernel Products, Fatty Acids, Food Related Products and Others* (Kuntom, A; Siew, W L; Tan, Y A; Idris, N A; Yusof, M; Tang, T S and Amri, N eds.). MPOB, Bangi.

Noparat, P; Prasertsan, P; O-Thong, S and Pan, X (2015). Dilute acid pretreatment of oil palm

trunk biomass at high temperature for enzymatic hydrolysis. *Energy Procedia*, 79: 924-929.

Nordin, N I A; Ariffin, H; Andou, Y; Hassan, M A; Shirai, Y; Nishida, H; Yunus, W M Z W; Karuppuchamy, S and Ibrahim, N A (2013). Modification of oil palm mesocarp fibre characteristics using superheated steam treatment. *Molecules (Basel, Switzerland)*, 18: 9132-9146.

Park, Y C; Kim, T H and Kim, J S (2017). Effect of organosolv pretreatment on mechanically pretreated biomass by use of concentrated ethanol as the solvent. *Biotechnol. Bioprocess Eng.*, 22: 431-439.

Pielhop, T; Amgarten, J; von Rohr, P R and Studer, M H (2016). Steam explosion pretreatment of softwood: the effect of the explosive decompression on enzymatic digestibility. *Biotechnol. Biofuels*, 9: 152-163.

Radhia, F; Lekbir, A; Ouadah, H; Kahoul, M A; Khlalfa, L; Laroui, S and Alloui-Lombarkia, O (2017). Effect of extraction solvent on total phenolic content, total flavonoid content, and antioxidant activities of Algerian pomace olive oil. *Int. Food Res. J.*, 24: 2295-2303.

Ruiz-Marcial, C; Reyes Chilpa, R; Estrada, E; Reyes-Esparza, J; Farina, G G and Rodriguez-Fragoso, L (2007). Antiproliferative, cytotoxic and antitumour activity of coumarins isolated from *Calophyllum brasiliense*. *J. Pharm. Pharmacol.*, 59: 719-725.

Safari, F; Tavasoli, A; Ataei, A and Choi, J K (2015). Hydrogen and syngas production from gasification of lignocellulosic biomass in supercritical water media. *Int. J. Recycl. Org. Waste Agricult.*, 4: 121-125.

Sen Gupta, S and Ghosh, M (2013). *In vitro* antioxidative evaluation of *α*- and *β*-carotene isolated from crude palm oil. *J. Anal. Methods Chem.*, 2013: 351671-351671.

Shen, Y C; Wang, L T; Khalil, A T; Chiang, L C and Cheng, P W (2005). Bioactive pyranoxanthones from the roots of *Calophyllum blancoi*. *Chem. Pharm. Bull. (Tokyo)*, 53: 244-247.

Soundararajan, V and Sasidharan, S (2012). Antioxidant activity of *Elaeis guineensis* leaf extract: An alternative nutraceutical approach in impeding aging. *APCBEE Procedia*, 2: 153-159.

Souza, M do C; Beserra, A M S; Martins, D C; Real, V V; Santos, R A; Rao, V S; Silva, R M and Martins, D T (2009). *In vitro* and *in vivo* anti-helicobacter pylori activity of *Calophyllum brasiliense* camb. *J. Ethnopharmacol.*, 123: 452-458.

Subhedar, P B and Gogate, P R (2016). Chapter 6 - Use of ultrasound for pretreatment of biomass and subsequent hydrolysis and fermentation. *Biomass Fractionation Technologies for a Lignocellulosic Feedstock Based Biorefinery* (Mussatto, S I ed.). Elsevier, Amsterdam.

Teh, S S; Ee, G C L; Mah, S H; Yong, Y K; Lim, Y M; Rahmani, M and Ahmad, Z (2013). *In vitro* cytotoxic, antioxidant, and antimicrobial activities of *Mesua beccariana* (Baill.) kosterm., *Mesua ferrea* Linn., and *Mesua congestiflora* extracts. *BioMed Res. Int.*, 2013: 1-9.

Teh, S S; Mah, S H and Razak, R A A (2020). Oxidative stability and physicochemical properties of palm olein. *J. Oil Palm Res.*, 32: 518-525.

Then, Y Y; Ibrahim, N A; Zainuddin, N; Ariffin, H; Wan Yunus, W M Z and Chieng, B W (2014). Surface modifications of oil palm mesocarp fiber by superheated steam, alkali, and superheated steam-alkali for biocomposite applications. *BioResources, 9 (4)*: 7467-7483.

Yasim-Anuar, T A T; Ariffin, H; Norrrahim, M N F and Hassan, M A (2016). Factors affecting spinnability of oil palm mesocarp fibre cellulose solution for the production of microfibre. *BioResources*, *12(1)*: 715-734.

Yeo, J Y J; How, B S; Teng, S Y; Leong, W D; Ng, W P Q; Lim, C H; Ngan, S L; Sunarso, J and Lam, H L (2020). Synthesis of sustainable circular economy in palm oil industry using graph-theoretic method. *Sustainability*, 12: 8081.

Yosri, M S; Syahril Anuar, M R; Nik Suhaimi, M H; Muhammad Zaidy, A; Mohammed Faisal, M Y and Ahmad Jaril, A (2019). Screw press operation optimisation for oil and kernel recovery enhancement. *Palm Oil Engineering Bulletin*, 130. p. 18-26.

Zheng, Y; Lin, H M; Wen, J; Cao, N; Yu, X and T Tsao, G (1995). Supercritical carbon dioxide explosion as a pretreatment for cellulose hydrolysis. *Biotechnol. Lett.*, 17: 845-850.

Zhou, H Y; Shin, E M; Guo, L Y; Youn, U J; Bae, K; Kang, S S; Zou, L B and Kim, Y S (2008). Anti-inflammatory activity of 4-methoxyhonokiol is a function of the inhibition of iNOS and COX-2 expression in RAW 264.7 macrophages via NF-kappaB, JNK and p38 MAPK inactivation. *Eur. J. Pharmacol.*, 586: 340-349.

FEASIBILITY STUDY OF OIL PALM HARVESTING USING PULSE FIBRE LASER SYSTEM WITH DIFFERENT LENSES

MOHD IKMAL HAFIZI AZAMAN[1]*; AHMAD SYAZWAN RAMLI[1]; MOHD KHAIRUL FADZLY MDRADZI[1]; MOHD RIZAL AHMAD[1]; MOHD RAMDHAN MOHD KHALID[1]; MOHD AZWAN MOHD BAKRI[1]; YASMIN MUSTAPHA KAMIL[1] and MOHD ADZIR MAHDI[2]

ABSTRACT

Malaysia is currently experiencing a labour shortage in oil palm plantations, estimated to account for 46% of the total industrial workforce. The industry is striving to increase worker productivity by adopting new technologies using a variety of work methods. Increment of fresh fruit bunch (FFB) production in oil palm plantations has created a demand for improved harvesting technique. Some of the technologies that have been developed are practical, yet they impose several technical issues that must be solved. The potential of oil palm frond cutting using pulse fibre laser was explored. The optimisation of the laser cutting system was made using a 250 mm and 63 mm focus lens. A better cutting rate was achieved using 63 mm focus lens due to its shorter focal length (compared to the 250 mm focus lens) and capability to retain stability at a higher pulse laser frequency. The same lens was able to perform complete cuts on oil palm fronds with power and speed of 50 Watt at 500 kHz and 1 mm/s, respectively. Good consistency was also exhibited with an average cutting rate of 0.1024 mm/s. Perhaps with further investigation and optimisation, such technique can be a viable alternative to the FFB harvesting methods that the industry is practicing today.

INTRODUCTION

In 2018, the oil palm was grown over 5.85 million hectares of land in Malaysia. In return, Malaysia became the world's second-largest producer and exporter of palm oil after Indonesia, and the industry contributed RM67.50 billion to the country's export earnings in 2019 (Kushairi *et al.*, 2019). The keys to

[1] Malaysian Palm Oil Board,
6 Persiaran Institusi, Bandar Baru Bangi,
43000 Kajang, Selangor, Malaysia.

[2] Department of Computer and Communication System Engineering, Faculty of Engineering,
Universiti Putra Malaysia, 43400 Serdang,
Selangor, Malaysia.

* Corresponding author e-mail: ikmalhafizi@mpob.gov.my

retain premium quality, increased productivity and maximised profit are appropriate management and operating harvesting schemes of the oil palm fresh fruit bunch (FFB) (Jelani *et al.*, 2018). Several decades ago, harvesting by using bamboo as a harvesting pole has been used, and then currently replaced by aluminium with either sickle or chisel attached to it. The development of technology is parallel to the increase of oil palm plantation in Malaysia with many harvesting technologies developed to date. Harvesting is an important activity in oil palm plantation and is estimated for about 60% of the total labour force. The efficiency of harvesting FFB plays a big role in improving the quality of harvested fruits (Jelani *et al.*, 2003). In the past decade, the oil palm industry has adopted modern mechanisation for harvesting, mainly to increase labour productivity (Jelani *et al.*, 2018). Over the

years, several technologies for cutting oil palm fronds and FFB have been designed, developed and tested. Many inventions have been commercialised and introduced to the industry. The use of the Oil Palm Motorised Cutter known as *Cantas* has been proven to increase the productivity of harvesting FFB and reduce workers' fatigue. This machine conserves the energy of workers during the cutting operation, thus, prolonging their working hours. It can effectively harvest palm trees below 4.5 m (Jelani *et al.*, 2003). For the tall palm, a mechanical harvester was invented and is able to perform all the necessary functions for harvesting activity effectively. The important role of the mechanical harvester's grapple in holding and bringing down the bunch has shown that the machine can be operated effectively (Mohd and Abd Rahim, 2014). Although some of the technologies developed are practical, several technical and capital issues as well as high maintenance costs have prompted the industry to look into new approaches (Ismail *et al.*, 2015).

One of the many cutting technologies worth exploring is laser cutting. Laser application has been widely used in various fields especially in state-of-the-art machinery and equipment (Ali *et al.*, 2020; Singh *et al.*, 2020). Laser, in general, is a device that emits light through an optical amplification process based on the stimulated emission of electromagnetic radiation. When this high intensity light beam hits the surface of a particular material, the material absorbs the radiation that will increase its internal energy, causing heat to be generated. Consequently, the heat created will partially melt or completely vapourise the material depending on the focal spot size, wavelength and power of the emitted light (Yuliansyah and Hirajima, 2012). The affected area on the surface which has lost a certain mass from the interaction with the laser beam creates the desired cut. The type of lasers that have been used for cutting are classified as carbon dioxide (CO_2) laser, solid state laser, and pulse fibre laser. Among the various laser types, fibre lasers have been deemed to be very efficient at both low and high-output power levels despite being less complex compared to other lasers (Niyibizi *et al.*, 2014). More specifically, pulse fibre lasers are known to generate better laser beam quality at high efficiency with zero to minimal maintenance (Westphäling, 2010). The pulse regime segments the light emission into periodic impulses, delivering smaller heat-affected-zones and high spatial resolution. The pulse fibre laser is suitable for cutting biomaterials. The reason for selecting pulse laser is that energy is channelled via a temporal pulse profile different from a continuous wave (CW) beam, resulting in frond burning due to continuous energy being channelled (*Figure 1*). Not only that, it has the capability to cut almost any material, from textiles and bio materials to composites and leather (Caprino and Tagliaferri, 1988; Cenna and Mathew,

2002; Eltawahni *et al.*, 2013; Steen and Mazumder, 2010). With these advantages, cutting with pulse fibre lasers is considered as one of the fastest and most versatile cutting techniques implemented across various industries (Chen *et al.*, 2004; Ottemer and Colton, 2002).

Findings from previous investigation described the possibility of cutting plant stalks using a laser beam in contrast to mechanical cutting (Liu *et al.*, 2011). The biomass of the plants after a certain period under standard greenhouse conditions was used to measure the effect of partial or complete cutting with a laser. The effect of laser irradiation at 1064 nm is less pronounced, but at this wavelength, the regrowth or continuous growth were able to be reduced (Schou *et al.*, 2002). The laser technology has the potential to improve the oil palm harvesting, but many parameters must be considered and assessed before it can be applied in oil palm plantation (Azaman *et al.*, 2019).

The oil palm industry is among the few industries that guarantees the nation a high rate of return on capital investment, especially for an oil palm producing country like Malaysia (Kushairi *et al.*, 2019). Thus, seeing labour shortage as a potential critical hindrance to the continuation of oil palm production, there is a dire need of finding appropriate technology to compensate the labour loss and maintain production rate and efficiency. Success of this work will offer the industry an alternative that is capable of harvesting, as well as reduced workforce and energy usage which would boost production efficiency. It also requires less mechanical parts thus, leading to less maintenance. Besides, this will promote the advancement of conventional semi-automated harvesting techniques towards yielding optimum production without the hassle of frequent maintenance nor dependence on hard manual labour. Hence, the
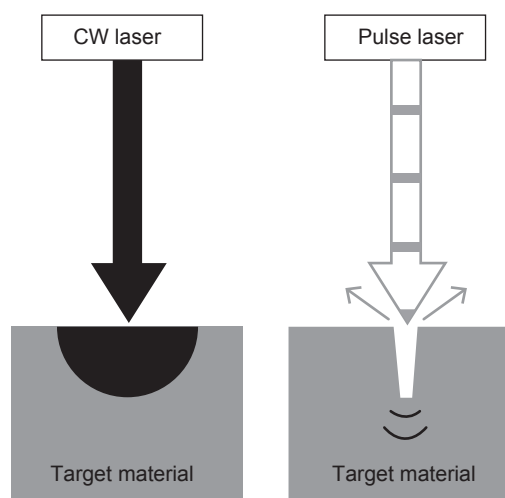

Figure 1. The difference between continuous wave (CW) laser and pulse laser cutting.

work is worth exploring and may contribute greatly to the advancement of oil palm harvesting technology. In this study, pulse fibre laser was explored as a potential mechanism to cut oil palm fronds. Two lenses with focal lengths of 250 mm and 63 mm, respectively, were tested and cutting performance was compared based on cutting rate.

MATERIALS AND METHODS

Optical Characterisation of Oil Palm Fronds

Laser cutting efficiency depends on the overlap between the wavelength of emitted laser light and the absorption wavelength of the material. In this work, the absorption spectrum of the oil palm fronds was recorded using the experimental setup shown in *Figure 2*. With a supercontinuum laser (450-2400 nm), the laser beam was emitted towards a slice of oil palm frond sample and the remaining transmitted light was directed to an Optical Spectrum Analyser

(OSA). The size of each slice was an average of 0.3-1.0 mm of the samples.

Based on the findings in *Figure 3*, the absorption spectrum ranged from 900 nm to 1600 nm. This is mainly contributed by the high amount of cellulose, hemicellulose and lignin within the frond. The flat absorption spectrum from 900 nm to 1300 nm refers to the cell structure as previously reported (Quintero *et al.*, 2011). The peaks within 1400-1500 nm indicate water absorption which also coincides with the previous report (Quintero *et al.*, 2011). As previously reported, the investigated optical properties and characteristics of the oil palm fronds are similar to other leafy vegetables with high moisture (Dawson *et al.*, 1998). The understanding of the cellulose absorption spectrum will play a huge part in determining the optimum laser operation wavelength for laser cutting (Heiderscheit *et al.*, 2019; Parvin *et al.*, 2012). Based on the experimental findings, a working wavelength of 1064 nm was selected which coincided with the emission wavelength of ytterbium-doped fibre laser.
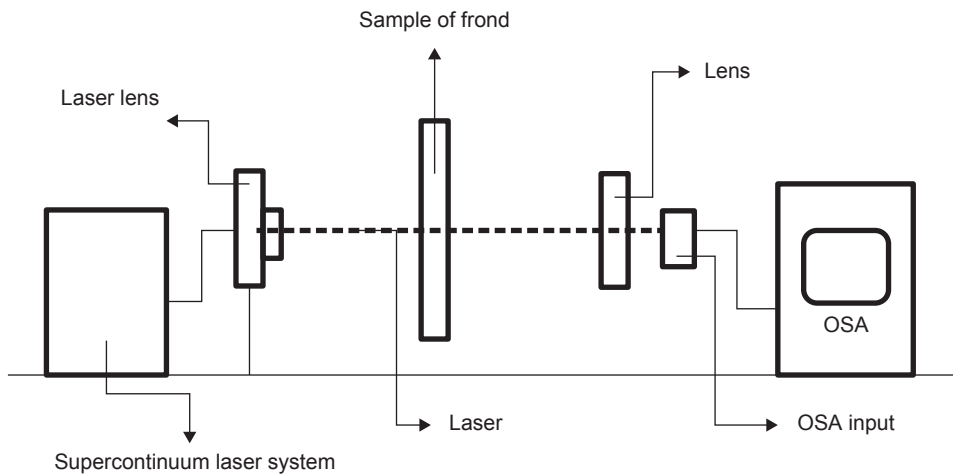

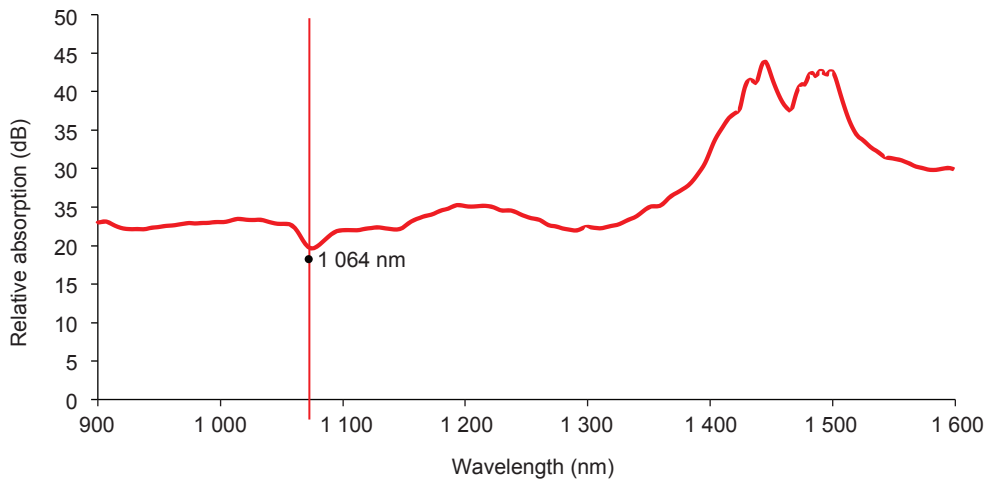*Figure 2. Diagram of absorption characteristic experimental setup.*

Figure 3. Relative absorption of palm oil frond sample at 1064 nm wavelength.

Sample Collection for Cutting of Oil Palm Frond

Samples of oil palm frond were randomly taken fresh within the same oil palm plantation. Preserving the freshness of the fronds was important as to mimic the moisture condition at the field for the cutting process in the laboratory. The size of the fronds was approximately 30 cm in length with average width of 55-66 mm and thickness of 35-45 mm. These dimensions were chosen to ease sample placement onto the limited space of the test platform at the motorised stage.

Experimental Setup

The experimental configuration of oil palm frond cutting using pulsed fibre laser at 1064 nm is depicted in *Figure 4*. Two focus lenses were used: 63-mm and 250-mm focus lenses. Theoretically, by using a short focal length lens (63 mm), the focusing will be tighter, resulting in smaller spot size. However, the tighter the focusing gradient, the faster the beam was defocused. Therefore, the tolerance was much shorter as compared to the longer focal length lens (250 mm). Due to the different focal lengths, the intensity profile of the two lenses was different from each other. The distance between the target material and the lens was adjusted using a motorised vertical movement stage to ensure ablation at the focal point. The system was operated using an EZCAD programme with a central processing unit that allowed users to monitor key laser marking parameters, such as speed, frequency and power. The pulse fibre laser employed for this experiment had an emission wavelength of 1064 nm, an average power capacity of 50 Watt, and maximum pulse energy of 1 mJ. The sample was mounted on a test platform underneath the lens to evaluate the cutting characteristics of the laser.

RESULTS AND DISCUSSION

Performance of Cutting Rate using Pulse Fibre Laser

Figure 5a shows one of the frond samples during the laser cutting process. The working principle of lasers on oil palm fronds is by initiating a laser beam on the surface of the material and linear movement of the laser. The frond was horizontally placed on the motorised stage in which its distance from lens was optimised beforehand. A stop-watch was employed to record the time taken for this cutting process. The laser pulse frequency was varied to obtain different pulse energy at maximum average optical power. By selecting different operating frequency, the difference in depth of cutting could be observed on the frond *Figure 5b*.

The depth of cutting could be observed and estimated at the cross-section (*Figure 6*). The resulting energy per pulse was determined by dividing the average power, P_{AV} (Watts) by the repetition rate, R_{Rate} in pulse per second (Hz). The energy was measured as shown in Equation (1). The resultant quantity was the energy, in Joules, contained in each laser pulse. The result was compared with others biomaterials (*Figure 7*).

$$E = \frac{P_{AV}}{R_{Rate}} \quad (1)$$

The comparative energy of laser cutting to palm fronds with other materials such as Oak and Birch (Aniszewska *et al.*, 2020) was to ensure that the study was carried out in accordance with the trend of laser energy that operated at the predetermined specific parameters throughout the test conducted.
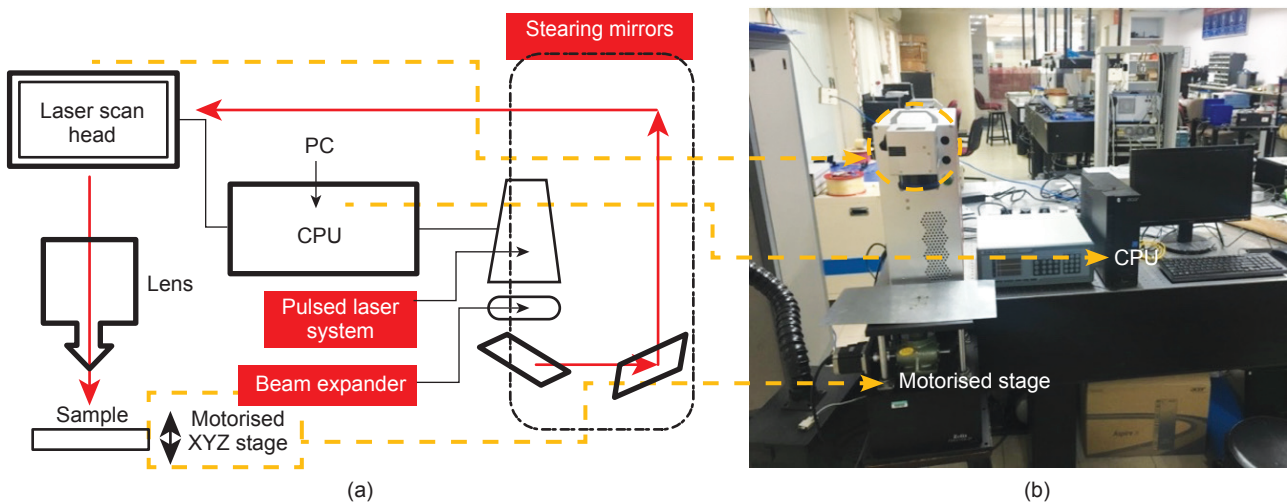

Figure 4. (a) Diagram of experimental setup of laser system, and (b) the setting of a pulsed laser system.
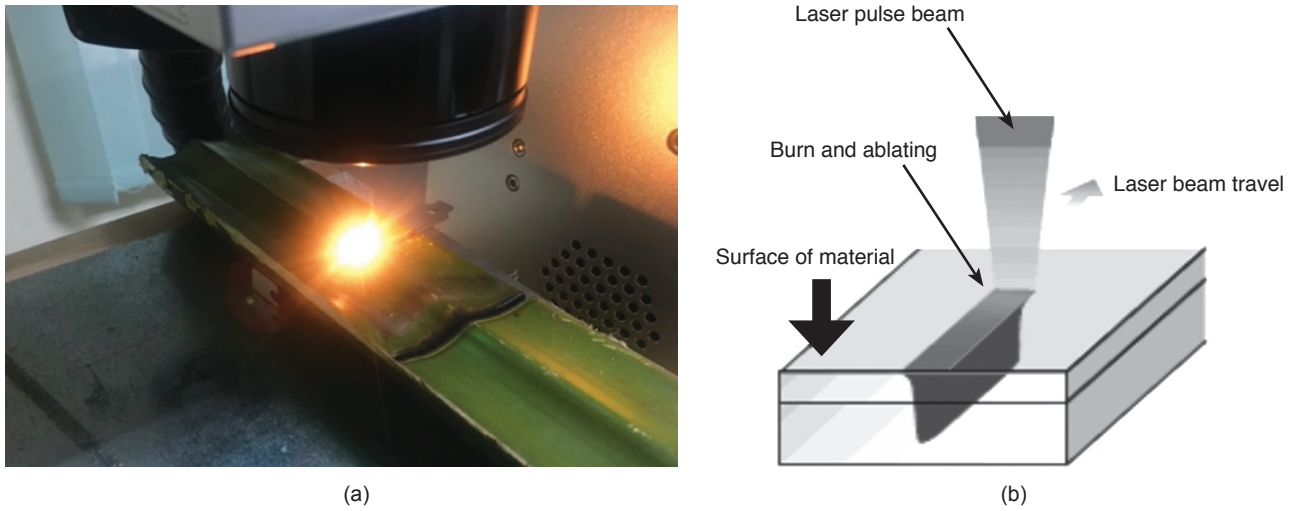
(a)

(b)

Figure 5. (a) The laser cutting process to the sample of frond and (b) three parameters; frequency power and speed; play critical roles in determining the quality and efficiency of the laser cutting.

The cutting performance of the two lenses was determined through their respective cutting rate. The cutting rate was measured by dividing the cutting depth with the total time taken as shown in Equation (2):

$$R = \frac{L_C}{t_C} \qquad (2)$$

where R is the cutting rate, L_c is the depth of cutting (mm), and t_c is the time taken for cutting (s). The resulting cutting rates for each laser cutting at certain depths were measured in mm/s. In this work, cutting depth was measured using a standard ruler and by dividing the fringe crossed into sliced parts.

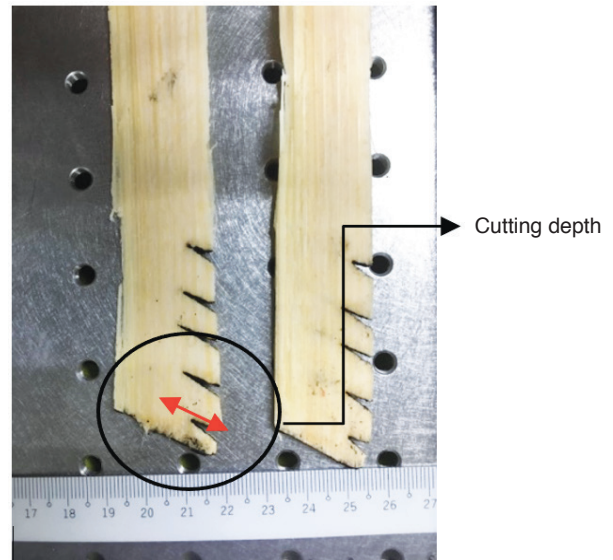Twelve frond samples were selected to assess the cutting rate. A total of three cutting tests per sample

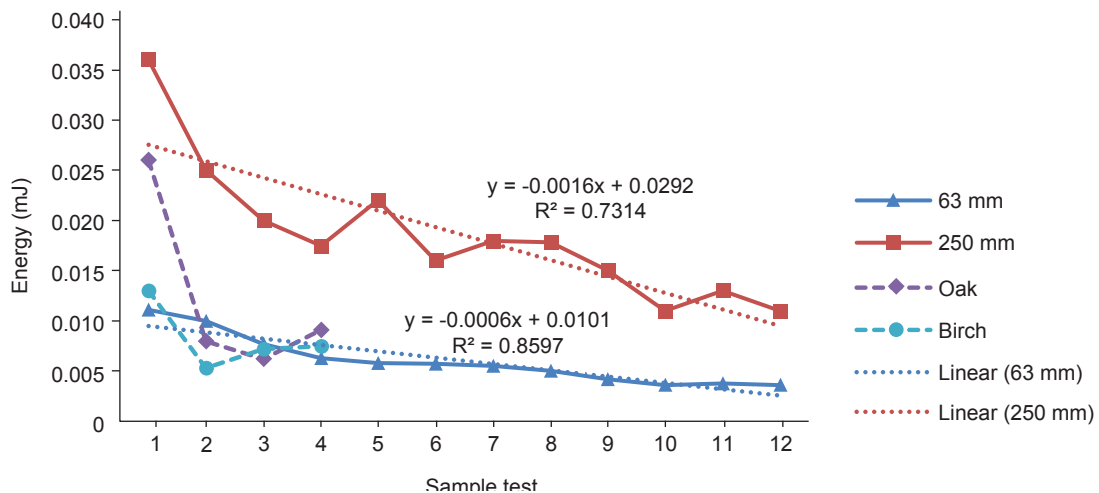*Figure 6. The slice of fronds with cutting depth.*

Figure 7. The energy of the laser cutting trend in sample of palm fronds compared to other biomaterials.

492

of oil palm frond were conducted and an average of three cutting depths were measured for the cutting rate analysis (*Table 1*). The cross-section of the palm slice of the sample was examined to identify the depth of cutting as represented by the red arrow (*Figure 8*).

The laser's applied frequency during the test was within the range of 10-600 kHz. However, after running some preliminary tests, it was found that the frequency above 700 kHz produced an instable emission and thus, the upper frequency limit was capped at 600 kHz. In this experiment, 12 frond samples were tested by each focus lens with cutting time fixed at 60 s. For each repetition of rate frequency, the frond was cut three times at different locations and the average cutting rate was derived based on these three reading values. *Figure 8* depicts the average cutting rate at different repetition rate frequency for 63 mm and 250 mm focus lens.

Based on *Figure 8*, the 63 mm focus lens yielded a higher cutting rate as compared to 250 mm despite the variation in pulse energy. The highest cutting rate achieved using the 63 mm focus lens was 0.47 mm/s with an operating frequency of 500 kHz while the 250 mm lens only managed a cutting rate of only 0.15 mm/s at 600 kHz. This observation was due to the shorter focal length of 63 mm focal lens that led to a smaller laser spot beam, in which the intensity per unit area was greater by a factor of ~60. By comparing the cutting rate, the 63 mm focus lens was concluded to be more efficient in cutting oil palm. Another observation worth noting was that the cutting rate was significantly reduced beyond 500 kHz for both lenses (indicated within the red boxed in *Figure 7*. This could be due to the heating effect on the focusing lens as no active cooling was applied, thus, disrupting the effective focal length of the lens.

TABLE 1. THE MEASUREMENT OF CUTTING PERFORMANCE

| No.	Frequency (kHz)	Power (Watt)	Focus lens (250 mm)		Focus lens (63 mm)		Time taken (s)
			CD (mm)	CR (mm/s)	CD (mm)	CR (mm/s)	
1	50	50	1.4	0.046	4.5	0.150	30
2	100	50	2.0	0.067	5.0	0.166	30
3	150	50	2.5	0.083	6.5	0.216	30
4	200	50	2.7	0.090	8.0	0.266	30
5	250	50	2.3	0.076	8.5	0.283	30
6	300	50	3.0	0.100	8.8	0.293	30
7	350	50	2.75	0.092	9.0	0.300	30
8	400	50	2.80	0.093	10.0	0.333	30
9	450	50	3.25	0.108	12.0	0.400	30
10	500	50	4.25	0.142	14.0	0.466	30
11	550	50	3.75	0.125	13.0	0.433	30
12	600	50	4.50	0.150	13.8	0.460	30

Note: CD - cutting depth; CR - cutting rate.
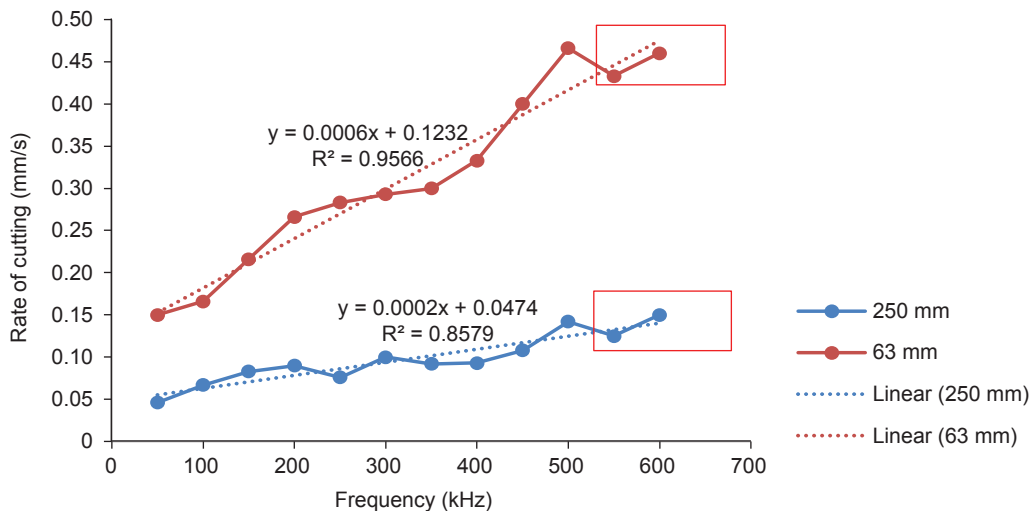
Figure 8. Performance of pulse fibre laser system with 63 mm and 250 mm focus lenses.

Performance of Complete Frond Cutting with 63 mm Focus Lens

Further assessment of the oil palm frond laser cutting performance using the 63 mm focus lens was carried out by investigating its capability in making complete frond cuts. With the same laser parameters previously applied, the experiment was replicated to cut through another sample of oil palm frond with a width of 55 mm and 35 mm thickness. *Figure 9* shows the oil palm fronds that have been completely cut through using a pulse fibre laser system. The total time taken for one complete cut is summarised in *Table 2*.

As listed in *Table 2*, the cutting time with applied energy of 0.01 mJ/pulse was consistent with an average cutting time of 342 ± 10.4 s, and the average cutting rate was 0.1024 mm/s. The cutting time recorded varied from one another due to the shape of the oil palm fronds which tapered from the base to both ends. Despite the natural tapering thickness, the cutting rate was constant for each of the test. The consistency of the cutting rate on several frond samples proved that the system was reliable and predictable, making it feasible to be integrated in a harvesting mechanism.

A small scale of combustion and ignition of fire on the surface of the palm fronds was observed during laser operation at higher frequencies beyond 400 kHz. However, at lower frequency operation with maximum pulse energy, no such ignition of fire was observed. Such occurrence happens as the pulsed laser has smaller 'heat affected zones' as compared with a CW laser. The energy of the pulsed laser was effectively involved in the cutting process and thus, not much residual energy was left to transfer to the surrounding. From the results discussed, the laser cutting method has the potential to cut the oil palm fronds, and the potential to be developed as harvesting tools. Cutting speed is important to be considered as the main factor for the purpose of harvesting.

In this study, the assumption is that the weight of palm fronds helps the laser cutting process. The cutting force may come from the energy per pulse when hitting the surface of the sample. The frequent energy hitting the biomaterial surface makes the engraving and cutting processes easier due to the help of gravitational weight of oil palm fronds. From this research, in conclusion, laser cutting on palm fronds is possible but at the current available setup, there are limitations to the laser power. Further scaling up the laser power will allow a better and faster cutting performance. Given the speed of development of laser technology currently, it is envisaged that a smaller and compact, yet highly efficient high power laser system will be available for laser cutting palm fronds and will be possibly more effective against the current conventional methods. The time taken for the cutting task using motorised cutter attached with either sickle or chisel for example is within 6-10 s depending on the skills of the labour (Jelani *et al.*, 2018). *Table 3* shows the comparison of cutting time by using different methods of harvesting.

The pulsed laser system operating at 1064 nm was capable to cut oil palm fronds using a 63 mm focus lens and these parameters determined the intensity of the laser at a given time and also time taken to cut through the fronds. Based on the results obtained, higher power and frequency at low speed will give better laser cutting performance. With a shorter focal distance, lesser loss was experienced by the focused beam from laser. However, the cutting time of this pulsed fibre laser is still too slow compared to

Figure 9. The sample of cut oil palm fronds.

TABLE 2. THE AVERAGE TIME OF COMPLETELY CUTTING AN OIL PALM FROND

No. of test	Time (s)	R (mm/s)
1	320	0.109
2	340	0.103
3	360	0.097
4	350	0.100
5	340	0.103

Note: Average - 342 ± 10.4 s; average rate of cutting - 0.1024; energy - 0.01 mJ/pulse.

TABLE 3. THE COMPARISON OF CUTTING TIME USING LASER WITH OTHER HARVESTING METHODS

Harvesting methods	Average cutting time (s)	
	Cut palm bunch	Cut palm fronds
Manual*	55	65
Motorised cutter**	10	6
Mechanical harvester***	35	30
Laser (lab test)	-	342

Note: * (Saibani *et al.*, 2015); ** (Jelani *et al.*, 2018) and *** (Mohd and Abd Rahim, 2014).

conventional methods of cutting oil palm fronds. As shown in *Table 3*, the laser cutting method took the longest amount of time for cut a frond, which was around five times longer in comparison with manual harvesting method. Among the harvesting methods listed, laser harvesting is far behind compared to the others in terms of cutting time. However, this study was still at the preliminary stage, and the main objective of this study which was to find out whether laser cutting has the potential to be used in oil palm harvesting. The fact that the frond was able to be cut has shown a promising potential of this technology and achieved the objective of the study at this current stage. The next step of this study is to try and cut a palm bunch and further optimise the laser setting so that the frond cutting time can be reduced and thus increase its efficiency.

Hence there are many technical issues that need to be further explored, before it can be pushed as an alternative harvesting technology. It was also found that, the enhancement of laser cutting system via power amplification must be increased from the current 50 Watt or 1 mJ of energy and it is therefore suggested to increase the power up to 100 Watt or above, so that faster cutting time can be achieved.

CONCLUSION

The main focus of this work is to assess the ability and potential of using pulsed fibre laser technology in cutting oil palm fronds. This was achieved by assessing the effects of power, speed, and frequency on time taken to cut through a frond sample. Two focus lenses were investigated: 63 mm and 250 mm. The cutting performance of both lenses was evaluated based on cutting rate. Two different focal length lenses have been tested, with 63 mm lens giving significant improvement of cutting results in terms of precision, sharpness and depth of cutting. With the 63 mm focus lens, better cutting rate was achieved with power, speed and frequency of 100%, 1 mm/s, and 500 kHz, respectively. Due to the shorter focal length, the 63 mm focus lens was able to uphold laser energy intensity and stability at higher frequencies. The same lens was also tested to perform complete oil frond cuts, yielding consistent results with an average cutting rate of 0.1024 mm/s. Despite the good potential for laser cutting, the cutting time achieved was still too slow compared to conventional methods. Thus, further experiments are encouraged to look into better ways to enhance the speed of the laser cutting.

ACKNOWLEDGEMENT

REFERENCES

Ali, M M; Hashim, N and Hamid, A S A (2020). Combination of laser-light backscattering imaging and computer vision for rapid determination of oil palm fresh fruit bunches maturity. *Comput. Electron. Agric., 169*: 105235.

Aniszewska, M; Maciak, A; Zychowicz, W; Zowczak, W; Mühlke, T; Christoph, B; Lamrini, S and Sujecki, S (2020). Infrared laser application to wood cutting. *Materials (Basel), 13(22)*: 5222.

Azaman, M I H; Mahdi, M A; Jelani, A R; Ahmad, M R and Shuib, A R (2019). The potentials of laser cutting technologies for oil palm harvesting. *Oil Palm Bulletin, 77*: 19-25.

Caprino, G and Tagliaferri, V (1988). Maximum cutting speed in laser cutting of fibre reinforced plastics. *Int. J. Mach. Tools Manuf., 28(4)*: 389-398.

Cenna, A A and Mathew, P (2002). Analysis and prediction of laser cutting parameters of fibre reinforced plastics (FRP) composite materials. *Int. J. Mach. Tools Manuf., 42(1)*: 105-113.

Chen, J K; Beraun, J E and Tham, C L (2004). Ultrafast thermoelasticity for short-pulse laser heating. *Int. J. Eng. Sci., 42(8-9)*: 793-807.

Dawson, T P; Curran, P J and Plummer, S E (1998). Liberty-Modeling the effects of leaf biochemical concentration on reflectance spectra. *Remote Sens. Environ., 65(1)*: 50-60.

Eltawahni, H A; Rossini, N S; Dassisti, M; Alrashed, K; Aldaham, T A; Benyounis, K Y and Olabi, A G (2013). Evalaution and optimization of laser cutting parametersfor plywood materials. *Opt. Lasers Eng., 51(9)*: 1029-1043.

Heiderscheit, T; Shen, N; Wang, Q; Samanta, A; Wu, B and Ding, H (2019). Keyhole cutting of carbon fiber reinforced polymer using a long-duration nanosecond pulse laser. *Opt. Lasers Eng., 120*: 101-109.

Ismail, A; Ahmad, S M and Sharudin, S Z (2015). Labour productivity in the Malaysian oil palm plantation sector. *Oil Palm Industry Economic J., 15(2)*: 1-10.

Jelani, A R; Shuib, A R; Hitam, A; Jamak, J and Noor, M M (2003). Hand-held mechanical cutter. *MPOB Information Series No. 180*.

Jelani, A R; Ahmad, M R; Azaman, M I H; Gono, Y; Mohamed, Z; Sukawai, S; Aduka, A; Aziz, A; Bakri, A; Mohamed, A and Selamat, M B (2018). Development and evaluation of a new generation oil palm motorised cutter (*Cantas Evo*). *J. Oil Palm Res., 30(2)*: 276-288.

Kushairi, A; Ong-Abdullah, M; Nambiappan, B; Hishamuddin, E; Bidin, M; Ghazali, R; Subramaniam, V; Sundram, S and Parveez, G K A (2019). Oil palm economic performance in Malaysia and R&D progress in 2018. *J. Oil Palm Res., 31(2)*: 165-194.

Liu, J; Hu, Y; Xu, X and Li, P (2011). Feasibility and influencing factors of laser cutting of tomato peduncles for robotic harvesting. *Afr. J. Biotechnol., 10(69)*: 15552-15563.

Mohd, R K and Abd Rahim, S (2014). Field evaluation of harvesting machines for tall oil palms. *J. Oil Palm Res., 26(2)*: 125-132.

Niyibizi, A; Kioni, P N and Ikua, B G (2014). Recent developments in laser sources for industrial applications. *Proc. of the 2013 Mech. Eng. Conf. Sust. Res. Innov., 5*: 24-26.

Ottemer, X and Colton, J S (2002). Effects of aging on epoxy-based rapid tooling materials. *Rapid Prototyp. J., 8(4)*: 215-223.

Parvin, P; Shoursheini, S Z; Khalilinejad, F; Bavali, A; Gosha, M M and Mansouri, B (2012). Simultaneous fluorescence and breakdown spectroscopy of fresh and aging transformer oil immersed in paper using ArF excimer laser. *Opt. Lasers Eng., 50(11)*: 1672-1676.

Quintero, F; Riveiro, A; Lusquiños, F; Comesaña, R and Pou, J (2011). Feasibility study on laser cutting of phenolic resin boards. *Phys. Procedia, 12*: 578-583.

Saibani, N; Muhamed, A A; Maliami, M F and Ahmad, R (2015). Time and motion studies of manual harvesting methods for oil palm fruit bunches: A Malaysian case study. *J. Teknol., 74(3)*. DOI: 10.11113/jt.v74.4555.

Schou, J; Heisel, T; Nordskov, A; Christensen, S; Jensen, P S; Thestrup, B and Toftmann, B (2002). Quantitative laser cutting of plants. *In High-Power Laser Ablation IV. International Society for Optics and Photonics*. p. 734-742.

Singh, P; Chatterjee, A; Bhatia, V and Prakash, S (2020). Application of laser biospeckle analysis for assessment of seed priming treatments. *Comput. Electron. Agric., 169*: 105212.

Steen, W M and Mazumder, J (2010). Laser welding. *Laser Material Processing*. 4th Edition. Springer, London. p. 199-249.

Westphäling, T (2010). Pulsed fiber lasers from NS to MS range and their applications. *Phys. Procedia, 5*: 125-136.

Yuliansyah, A T and Hirajima, T (2012). Efficacy of hydrothermal treatment for production of solid fuel from oil palm wastes. *Resource Management for Sustainable Agriculture* (Abrol, A and Sharma, P eds.). *IntechOpen*. p. 296.

CELLULOSE NANOCRYSTALS DERIVED FROM OIL PALM EMPTY FRUIT BUNCH REINFORCED NATURAL RUBBER LATEX NANOCOMPOSITES

**INTAN SYAHIERA AZLI[1]; AFKAR RABBANI HIDAYATULLAH HIPENI[2]
and KHAIRATUN NAJWA MOHD AMIN[2]***

ABSTRACT

Natural rubber latex (NRL) has long been used in lots of application in elastomer industry. However, finished products may develop pinholes or tear easily while being used. Thus, cellulose nanocrystal (CNC) was used as reinforcing filler in NRL to overcome this problem. CNC from cellulose derived from oil palm empty fruit bunch (EFB) was isolated via sulphuric acid hydrolysis method. The CNC concentration added to the NRL was varied at 1, 3 and 5 wt.%. The effect of CNC addition and curing temperature of 70°C and 100°C of NRL on the mechanical properties, functional group presence, glass transition temperature (T_g) and swelling behaviour of CNC/NRL nanocomposite were studied. The morphology of CNC with needle-like shape, length of 672 ± 445 nm, and diameter of 103 ± 39 nm was determined by using field emission scanning electron microscopy (FESEM). The best nanocomposites performance with low CNC loading of 1 wt.% has successfully increased the tensile strength and elongation at break with 20% and 14% of improvement, respectively at 70°C of curing temperature.

INTRODUCTION

One of the most significant elastomers with interesting strength, elasticity, durability, resilience, and abrasion resistance is natural rubber latex (NRL). NRL refers to the white sap that comes from the tree of *Hevea brasiliensis* and has low intensity, softens in warm weather and brittle in cold weather and is almost limited in use in its original uncured form (Vandenplas and Raulf, 2017). NRL will undergo vulcanisation, a chemical process where long chains of rubber molecules are cross-linked, transform the soft, weak plastic-like material into a strong elastic product with high and reversible deformability and good mechanical properties (Visakh *et al.*, 2012). There are some latex products that have been carried into finished products by inadequate manufacturing processes that will result into pinholes or tear easily during the application of latex products in their field of work. The mechanical properties of NRL can be improved and tailored by crosslinking and addition of reinforcing fillers (Gopalan Nair and Dufresne, 2003).

It is proven that cellulose nanocrystal (CNC) have a distinct advantage for improving the mechanical properties of nanocomposites. Favier *et al.* (1995) first reported on the use of CNC as reinforcing agents in polymer composites which enhanced the mechanical properties of poly(styrene-co-butyl acrylate) prepared via solvent casting processing of the corresponding latex. Their

[1] Department of Chemical Engineering,
  College of Engineering, Universiti Malaysia Pahang,
  Lebuhraya Tun Razak, 26300 Gambang,
  Kuantan, Pahang, Malaysia.

[2] Faculty of Chemical and Process Engineering Technology,
  College of Engineering Technology,
  Universiti Malaysia Pahang, Lebuhraya Tun Razak,
  26300 Gambang, Kuantan, Pahang, Malaysia.

* Corresponding author e-mail: knajwa@ump.edu.my

reinforcing effect, remarkable mechanical, chemical, and biocompatible properties as well as non-toxicity, biologically inertness, low density, biodegradability, surface functional groups, *etc.*, could facilitate the application of CNC-filled nanocomposites as advanced materials. To enhance its mechanical properties, various polymer matrixes have been strengthened by CNC including NRL. CNC reinforced from various sources like wood (Mariano *et al.*, 2016), cotton (Tian *et al.*, 2017) and tunicate (Cao *et al.*, 2018) were used to reinforce NRL.

Biomass such as empty fruit bunch (EFB) was also used a lot as a source to produce CNC (Gan *et al.*, 2020; Shanmugarajah *et al.*, 2015; Zulnazri *et al.*, 2017). EFB is a good potential raw material for the CNC as the lignocellulosic constituents in EFB consist of high cellulose (24-65 wt.%) (Chang, 2014). In our previous work (Supian *et al.*, 2020), EFB was used to produce cellulose nanofibre (CNF) and it has shown promising characteristics. It is likely that similar potential can be expected with CNC produced from EFB. Up to this date, there is no work yet that reported on CNC derived from EFB as reinforcing filler for NRL as well as investigation on the effect of curing temperature towards NRL nanocomposite.

In this work, CNC isolated using sulphuric acid hydrolysis from EFB was used as reinforcing filler. The CNC with volume fraction of 1, 3 and 5 wt.% were incorporated with NRL. The curing temperature effect at 70°C and 100°C were also investigated. The CNC size and dimension were measured and the performance of CNC/NRL nanocomposites was evaluated by the thermal, mechanical and swelling properties accordingly.

MATERIALS AND METHODS

Materials

High ammonia natural rubber was bought from Kinetic Chemicals (M) Sdn. Bhd., Malaysia while CNC were extracted from EFB's cellulose (Supian *et al.*, 2020). Sulphuric acid (H_2SO_4) 98% was purchased from Sigma Aldrich. The chemicals for rubber compounding which are zinc oxide (ZnO), zinc dithiocaramate (ZDC), zinc mercapto benzothiazole (ZMBT), potassium hydroxide (KOH) and sulphur were bought from Sigma Aldrich.

Isolation of CNC

The isolation process using H_2SO_4 is adapted from Amin *et al.* (2017). Cellulose from EFB was stirred with deionised water. The solid to liquid ratio for this isolation process was 1:75. The H_2SO_4 was added slowly under vigorous mechanical stirring to cellulose until the final solution reached

an acid concentration of 32%. The ice bath was used to keep the temperature below 20°C while adding the acid. The mixture was heated for 3.5 hr at 50°C. The CNC suspension was cooled and centrifuged at 4750 rpm four to five times until turbid. The suspension of CNC was dialysed against deionised water until the suspension reached the neutral state (pH~7). The CNC suspension was then subjected to ultrasonic using high intensity ultrasonic (QSonica ultrasonicator) for 30 min with an output of 500 W, a frequency of 20 kHz and amplitude of 20%. Finally, the suspension of cellulose was lyophilised then dried using vacuum freeze dryer.

Preparation of NRL Nanocomposites

The NRL was stirred with other chemicals simultaneously as listed in *Table 1*. Neat NRL (without CNC) compounding was stirred within 30 min with speed of 35 rpm. NRL was poured into the beaker and stirred for 6 hr at 12 rpm until deaerated. Then, the steps were repeated for NRL nanocomposite by adding CNC with concentrations of 1, 3 and 5 wt.% and was stirred for another 30 min.

CNC/NRL mixture was casted into flat glass mould and dried overnight at room temperature. Then, the dried film was dusted with calcium carbonate powder subsequently was leached for 10 min in distilled water, followed by being cured at two different temperatures, 70°C and 100°C in a convection oven under gentle purge of dry nitrogen for at least 4 hr. NRL films were rested at least 48 hr at room temperature and 50% humidity before any further characterisation (Hosseinmardi *et al.*, 2017). All the samples were labelled as CNC/NRL XY where X was for curing temperature and Y was for wt.% of CNC.

Characterisation

Field emission scanning electron microscopy (FESEM) by JSM-7800F Schottky which operated up to 30 kV and spot of 1.3 nm was employed to

TABLE 1. FORMULATION OF CNC/NRL NANOCOMPOSITE

Item	Weight % in nanocomposite			
CNC weight (%)	0	1	3	5
High ammonia NRL	96.5	95.5	93.5	91.5
Potassium hydroxide solution	0.35	0.35	0.35	0.35
Sulphur	1.5	1.5	1.5	1.5
ZDC	0.75	0.75	0.75	0.75
ZMBT	0.6	0.6	0.6	0.6
ZnO	0.3	0.3	0.3	0.3

analyse morphology and dimension of CNC. The sample was prepared in powdery form and coated with platinum. The thermal stability of CNC was studied using a Mettler Toledo TGA/DSC1 using aluminium crucible standard 40 μL. A heating rate of 10°C min^{-1} from 30°C to 700°C in air atmospheric condition was used. The N$_2$ flow rate was 20 mL min^{-1}. Thermal degradation behaviour was then evaluated based on the weight loss against temperature. FT-IR was conducted on Spectrum 100 FT-IR to observe the changes in chemical bonding in NRL before and after the incorporation of CNC. The experiments were conducted with resolution being 4 cm^{-1} and the spectra was collected from 4000 to 500 cm^{-1}.

The tensile testing of the composites was performed at room temperature using an Instron model 5543 universal testing equipped with 500 N load cell. The sample was cut into dumbbell shapes specimens according to ASTM D-412 (Varghese *et al.*, 2004). The specimens of 40 mm length and 5 mm width were tested at a crosshead speed of 50 mm min^{-1}, which corresponded to an initial strain rate of 10% min^{-1}. A differential scanning calorimeter (DSC) Model Q1000 from TA Instruments was used to determine the thermal behaviour of CNC/NRL nanocomposite. All samples were analysed from -80°C to 500°C, at heating rate of 10°C min^{-1} (Hajji *et al.*, 1996). The toluene-swelling behaviour of the nanocomposites was conducted in toluene at ambient condition. The samples were weighed, immersed in toluene and removed every hour, gently blotted with paper towel, weighed, and immersed in toluene again immediately. Toluene-swelling behaviour was carried out for 8 hr and was

conducted in triplicate for each sample. The toluene uptake (SI) was determined from the Equation (1):

$$SI = \frac{W_F - W_0}{W_0} \times 100\% \tag{1}$$

where W_0 and W_F are masses of the sample before immersion and immersed for a certain period (t), respectively.

RESULTS AND DISCUSSION

Morphology and Dimension of CNC

Figure 1 shows a rod like shape of CNC was obtained via sulphuric acid hydrolysis. The size of CNC was calculated based on the average length and diameter of 100 random CNC particles using Image J software. *Table 2* summarises the length, diameter, aspect ratio and the production yield of CNC based on the FESEM images. The value and shape obtained is in agreement with other CNC from different cellulose sources like corn husk (Kampeerapappun, 2015) and sugarcane bagasse (Kumar *et al.*, 2014). However, CNC from EFB as reported by Gray *et al.* (2018) showed a slightly different result due to higher acid concentration (62%) used in acid hydrolysis process.

Thermal Stability of CNC

Thermal degradation of cellulose materials or the reduction in mechanical properties at elevated temperatures is one of the major issues that limit their applications. The thermal stability of CNC
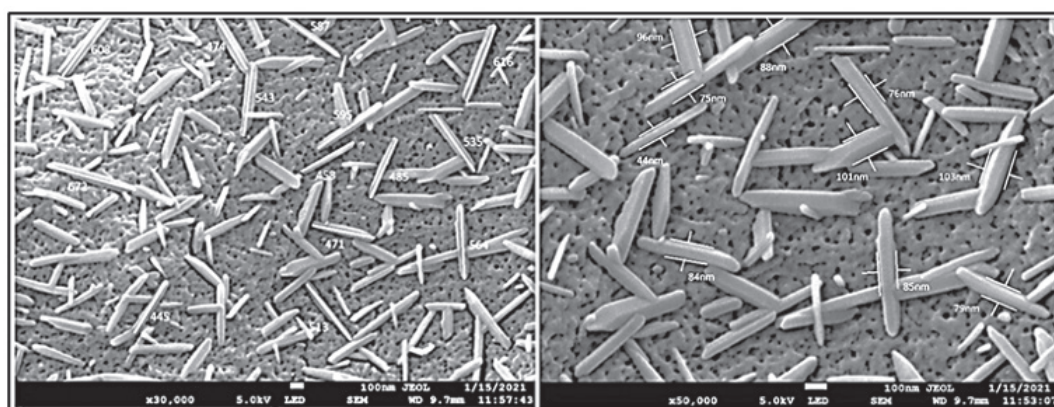

Figure 1. FESEM image of CNC from empty fruit bunch (EFB) via sulphuric acid hydrolysis at magnification of 15kX and 50kX.

TABLE 2. DIMENSION AND PRODUCTION YIELD OF CNC ISOLATED FROM EFB

Sample	Length (nm)	Diameter (nm)	Aspect ratio (L/D)	Production yield (%)
CNC	672 ± 445	103 ± 39	11.4 ± 6.5	86

was determined using TGA and the associated thermograms are shown in *Figure 2*. The CNC started to degrade at 180°C with maximum decomposition at around 300°C. This degradation temperature was lower compared to the degradation temperature via phosphoric acid hydrolysis and mechanical method where recorded degradation temperatures were at 255°C and 258°C, respectively (Amin *et al.*, 2017). However, isolation of CNC by using sulphuric acid is well-known for giving advantages in terms of stable aqueous colloidal stability despite its poor thermal stability (Mao *et al.*, 2017). In fact, in this work, the maximum processing temperature used was at 100°C (curing temperature), which was under degradation temperature of CNC, thus, it would not disrupt the properties of CNC.

CNC obtained from other various biomass resources were also found to have lower thermal stability than the CNC obtained from EFB. In studies conducted by Neto *et al.* (2013) and Song *et al.* (2019), CNC that was extracted from soy hulls and *Calotropis procera* (fruit) biomass recorded the degradation temperature of 160°C and 170°C, respectively. Hence, the thermal stability of CNC from EFB in this work is verified to be much better than other nanocellulose from other biomass sources.

Fourier-transform Infrared Spectroscopy (FTIR) Analysis

The FTIR spectra of NRL and CNC/NRL nanocomposites are shown in *Figure 3* for both curing temperature of 70°C and 100°C. The absorbance peaks recorded approximately between 3000 cm^{-1} and 3500 cm^{-1} are attributed to the stretching vibrations of -OH of CNC. The adsorbed water has also some contribution to the

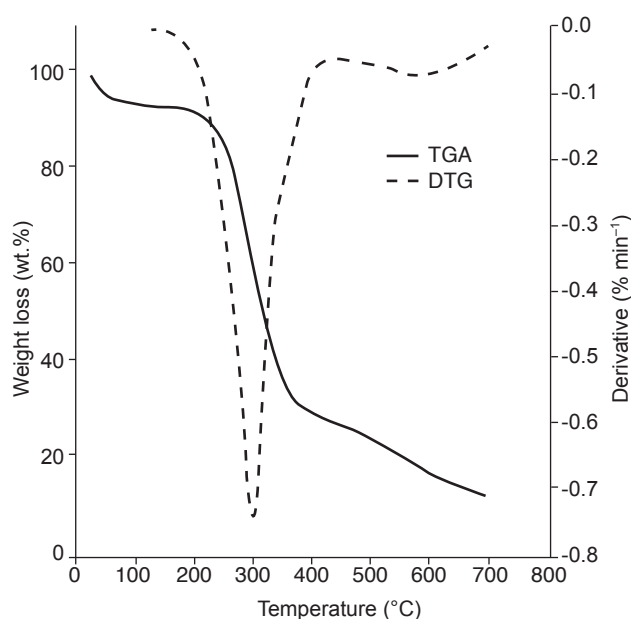corresponding peak and its intensity is attributed to the hydroxyl group present in each cellulosic unit, similar result was shown by Xu *et al.* (2013). For both curing temperatures of nanocomposites, the peak intensity was increased with increasing CNC contents, indicating the incorporation of the CNC in NRL.

FTIR spectra of nanocomposites with 70°C and 100°C of curing temperature, the peaks are between 2850 to 2851 cm^{-1}, 1640 to 1662 cm^{-1} and 2959 cm^{-1} which are assigned to -CH3, -C-H and =C-H stretching, respectively, and the peaks that show for -C-H bending is between 1425.96 to 1447.22 cm^{-1}. There are peaks of -OH stretching between 3330.89 to 3394.64 cm^{-1} and C-O stretching between 1079.55 to 1084.49 cm^{-1}.

These results of CNC/NRL nanocomposites show similar pattern as Abraham *et al.* (2013) and Jailudin and Amin (2020). In order for cross-linking of the rubber chains to occur, there has to be cleavage on some of the double bonds of the =C-H groups and the appearance of -C-H groups must be observed (Blanchard *et al.*, 2020) and these peak can be seen in *Figure 3* (marked in red circle). A slight increase in the peak intensity of -C-H groups after the incorporation of CNC was also observed. In addition, the peak centered at 3380-3390 cm^{-1} and 1600-1500 cm^{-1} corresponding to the -OH stretching modes are much sharper and stronger, indicating higher densities of the hydroxyl groups on the surfaces of CNC (Agrebi *et al.*, 2019). Other than that, there was no significant difference of peaks between the two curing temperatures at 70°C and 100°C.

Tensile Properties of CNC/NRL Nanocomposites

The tensile properties of the CNC/NRL nanocomposites, as well as the pure NRL films, were characterised at room temperature. Tensile properties of CNC/NRL nanocomposites at two different curing temperatures are reported in *Table 3*. *Figure 4* shows the stress *vs.* strain curves for these materials at 70°C and 100°C.

At 70°C of curing temperature, the maximum tensile strength was achieved at 1 wt.% of CNC with 20% of improvement at 7.2 MPa. Meanwhile, the elongation at break and modulus recorded were 14% and 16% of improvement, respectively. Whereas for sample with 100°C of curing temperature, the maximum tensile strength, elongation at break and modulus were also achieved at 1 wt.% of CNC as well. Nevertheless, the value was slightly lower than curing temperature at 70°C.

These significant improvements might be due to the reinforcing effect of CNC and its interaction with NRL on the molecular chain which became a good stress transfer agent that could provide higher strength (Blanchard *et al.*, 2020). According to Thomas *et al.* (2015), CNC addition formed
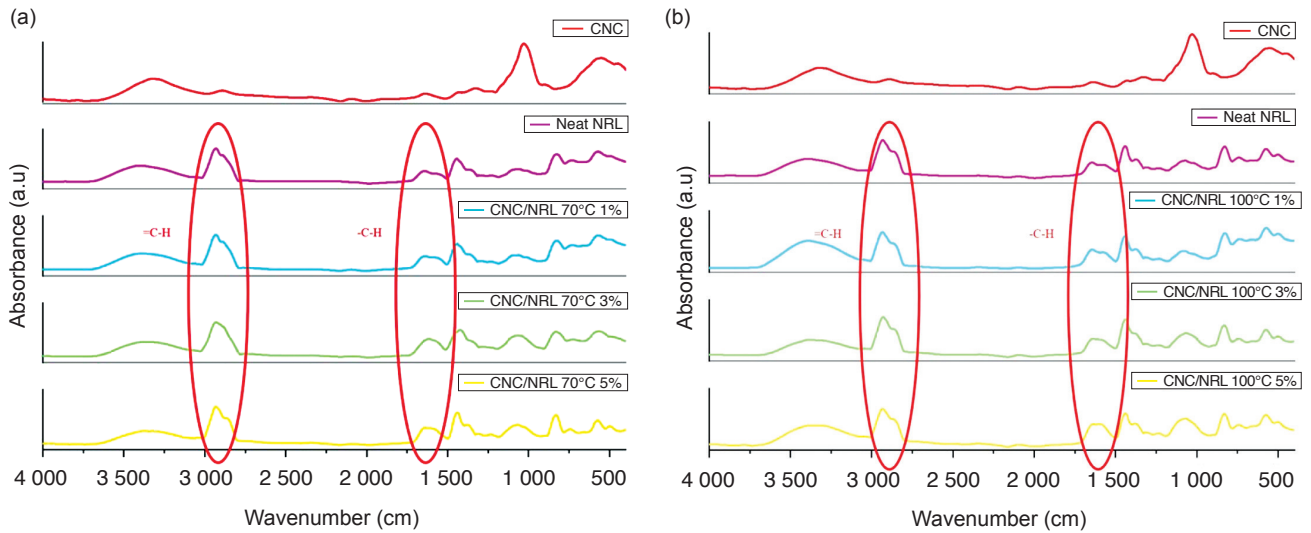

Figure 2. TGA and DTG curve of CNC.

Figure 3. FTIR spectra of CNC and CNC/NRL nanocomposites at curing temperature of (a) 70°C, and (b) 100°C.

TABLE 3. TENSILE PROPERTIES OF NEAT NRL AND CNC/NRL NANOCOMPOSITES

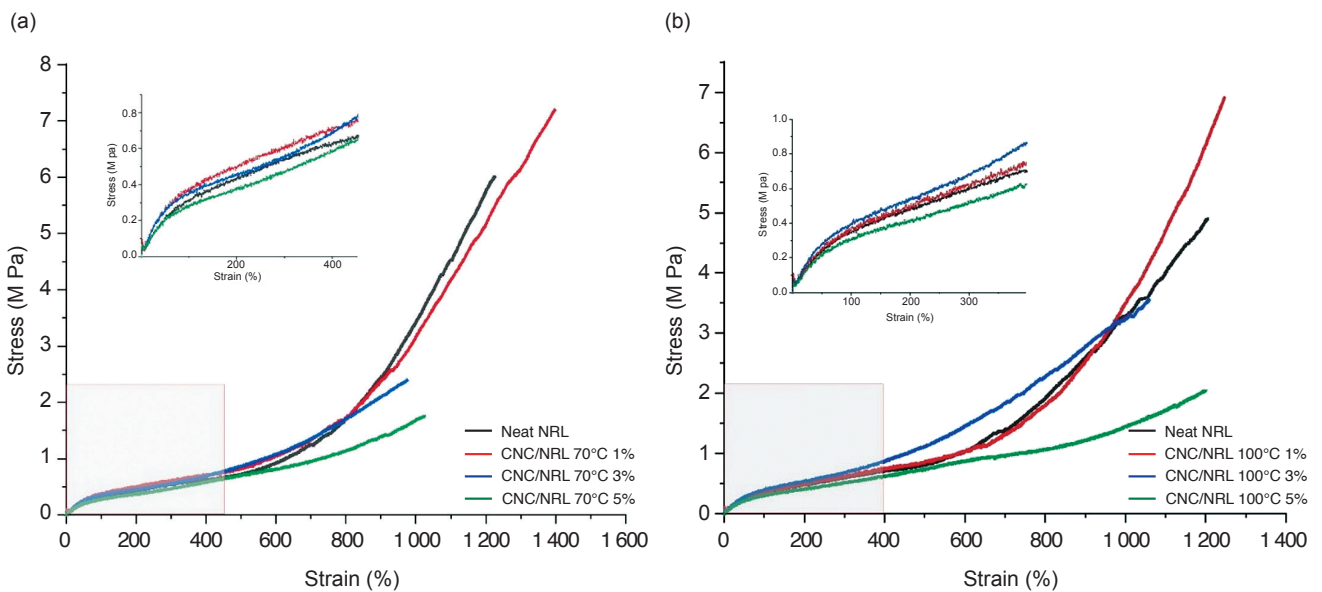| Curing temperature	Sample (%)	Tensile strength (MPa)	Elongation at break (%)	Young modulus, E (kPa)
70°C	Neat NRL	6.0 ± 0.2	1 225 ± 29.0	3.1
	1	7.2 ± 0.2	1 398 ± 50.4	3.6
	3	2.4 ± 0.4	976 ± 29.0	3.4
	5	1.8 ± 0.3	1 025 ± 66.0	2.7
100°C	Neat NRL	4.9 ± 0.3	1 206 ± 76.0	3.4
	1	6.9 ± 1.4	1 247 ± 77.0	3.9
	3	3.6 ± 0.5	1 059 ± 47.0	3.6
	5	2.0 ± 0.6	1 200 ± 57.0	3.0

Figure 4. Stress-strain curve of CNC/NRL nanocomposites at curing temperature of (a) 70°C, and (b) 100°C.

percolation network within the polymer matrix and the interfacial interaction between matrix and CNC. Thus, the CNC-CNC and NRL-CNC

reactions are both responsible to the mechanical enhancement of the resulting nanocomposites. Notably, for both curing temperatures, at 3% and

5% CNC addition decreased the tensile strength by more than 20%. These results might be attributed by the possible restriction of polymer chain mobility in the vicinity of nanocrystal or due to agglomeration and its hydrophilicity characters (Zhang *et al.*, 2014).

Table 4 shows the comparison of mechanical properties of CNC/NRL nanocomposites from different types of cellulose sources. All nanocomposites show significant tensile strength improvement due to addition of additives or surface modification of CNC. However, the elongation at break results displayed significant reduction which sacrificed the ductility of NRL. This might be due to high loading of CNC in NRL matrix. Nonetheless, in this work, tensile strength was improved significantly as well as the elongation at break of the nanocomposite with only 1 wt.% of CNC loading and without any CNC modification or additives.

Thermal Behaviour of CNC/NRL Nanocomposites

The thermal behaviour of CNC/NRL nanocomposite was studied by DSC. *Figure 5* displays the DSC curve for samples of NRL and CNC/NRL 1 wt.% nanocomposites at 70°C and 100°C of curing temperatures.

Based on *Figure 5*, the glass transition temperature (T_g) at 70°C of curing temperature recorded -65.60°C and -64.90°C for neat NRL and 1 wt.% CNC filled nanocomposite, respectively. Melting temperature (T_m) for each film was around -60°C whereas at 100°C curing temperature were at -60.31°C and -59.87°C for neat NRL and 1 wt.% CNC filled NRL, respectively. Bendahou *et al.* (2010) reported that no significant variation of T_g upon increasing content of CNC. In this study, similar results were also found for both curing temperatures of 70°C and 100°C displayed a T_g around -60°C. Hence, the results are in agreement with previous observations on CNC-filled nanocomposites where no modification on T_g values was reported when increasing the CNC content regardless of the nature of the polymeric matric (Anglès and Dufresne, 2001). This also may indicate that CNC acted as reinforcing filler with only physical interaction/bonding with NRL and in agreement with the result from FTIR

which also showed no change in terms of chemical bond after the addition of CNC in the NRL.

The value of T_g will also affect the usage of the composite material, where polymers that have T_g value below than 25°C will result in a soft, flexible polymer at ambient temperature. This statement is verified in this study where NRL and its nanocomposite recorded T_g around -60°C resulted in a rubbery-like texture which can be considered as soft and flexible polymer. Thus, in this study the CNC was not disrupting the molecular structure of the NRL and was able to retain the rubbery properties and improved the ductility of NRL.

Swelling Behaviour of NRL Nanocomposites

The toluene-swelling behaviour of neat NRL and CNC/NRL nanocomposite was also studied to observe the interaction of toluene with the rubber nanocomposite films, and the results are shown in *Figure 6*.

From the results, the toluene uptake at equilibrium state for both nanocomposites decreased gradually with increasing CNC content and this could be attributed by the higher interfacial interaction between CNC and NRL matrix (Colom *et al.*, 2018) or possibility by the increase in crosslinking density (Blanchard *et al.*, 2020) which can be seen in FTIR result. This is in agreement with the results that recorded the best tensile strength was at 1 wt.% of CNC. Meanwhile, CNC addition at 3 and 5 wt.% reduced the swelling index and might be due to the increase of crosslink density of rubber which is not necessarily good. When heavily crosslinked, the rubber chain mobility becomes highly restricted and the chains are unable to dissipate heat generated by deformation through molecular motion, resulting in easy and brittle rapture at low elongation (Mok and Eng, 2018).

However, it cannot distinguish between the effect of chemical crosslinks or other factors such as entanglement as no significant changes can be seen from DSC result (Flink *et al.*, 1988). It might also be that the swelling test affected by the area occupied by CNC molecules which is hydrophilic as well as strong matrix-filler interactions that can hinder

TABLE 4. MECHANICAL PROPERTIES OF CNC FROM DIFFERENT SOURCES

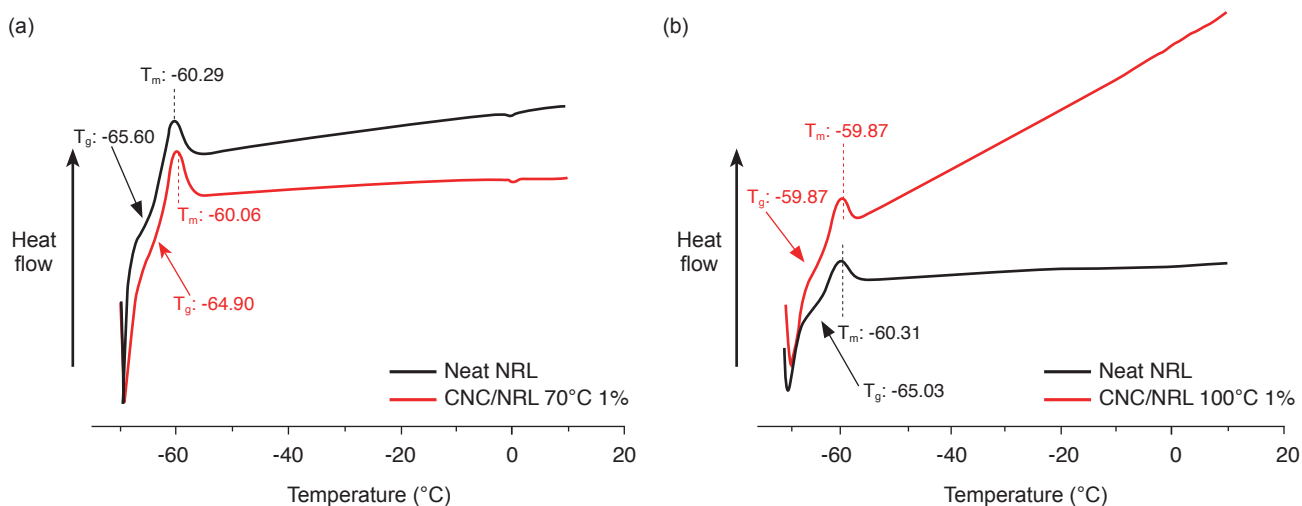| Sources of cellulose	Nanocellulose loading	Mechanical properties of nanocomposites		Reference
		Improvement of tensile strength (%)	Reduction of elongation at break (%)	
Potato starch	20 wt.%	300	65.0	Rajisha *et al.* (2014)
Peanut shell	3 wt.%	30	14.3	Chandra *et al.* (2020)
Wood	5 phr	200	33.0	Blanchard *et al.* (2020)
EFB	1 wt.%	20	Improved 14.0%	This work

Figure 5. DSC curve of CNC/NRL nanocomposites at curing temperature of (a) 70°C, and (b) 100°C.
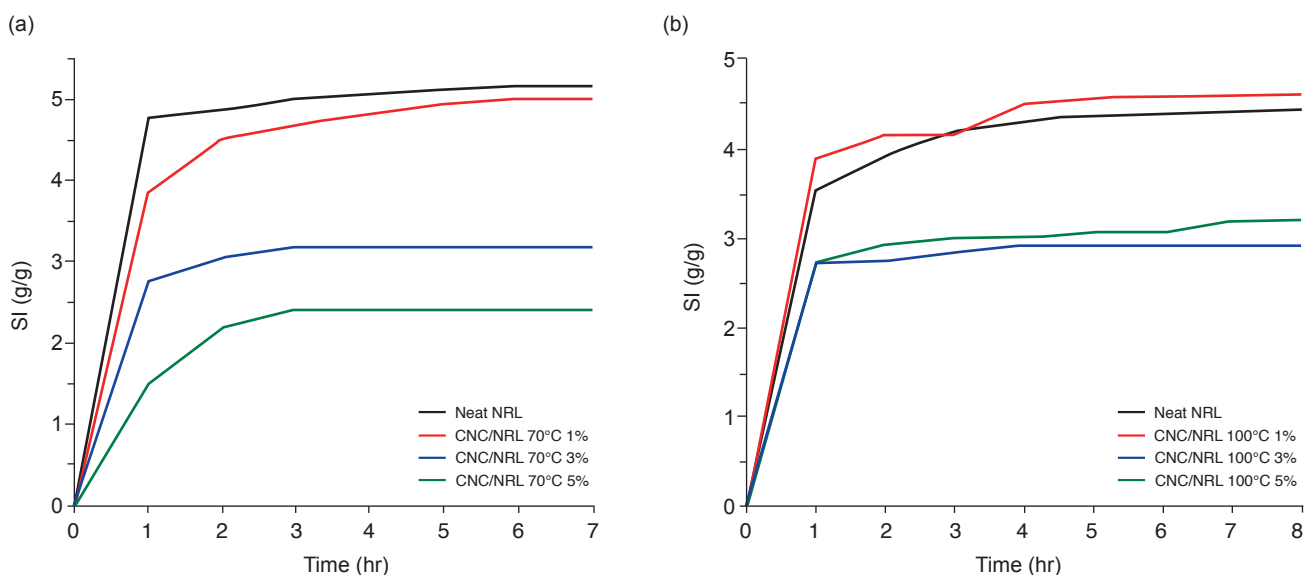

Figure 6. Swelling test OF CNC/NRL nanocomposites at curing temperature of (a) 70°C, and (b) 100°C.

solvent permeation in the rubber matrix, reducing the volume of the solvent absorbed (Cao *et al.*, 2018).

Meanwhile, as comparison for both curing temperatures of 70°C and 100°C, it showed similar swelling behaviour: toluene uptake increased in the first 4 hr and then increased slowly until reaching the equilibrium state in day one and remained constant. However, for sample with 1 wt.% of CNC, it reached the equilibrium state after day 4 for both curing temperatures.

with 20% of improvement at 70°C of curing temperature. Thermal behaviour of CNC/NRL nanocomposites also did not show any significant changes indicating no chemical bonding can be identified. The toluene-swelling behaviour of neat NRL and CNC/NRL nanocomposites for both curing temperatures at 70°C and 100°C showed similar swelling behaviour: toluene uptake went up rapidly in the first 4 hr and then increased slowly until reaching equilibrium state in one day. The swelling intake was reduced upon the CNC addition.

CONCLUSION

CNC in needle-like shape with an average length of 672 ± 445 nm and diameter of 103 ± 39 nm were successfully extracted from EFB cellulose via sulphuric acid hydrolysis. The best tensile strength was achieved at 1 wt.% of CNC loading in NRL

ACKNOWLEDGEMENT

REFERENCES

Abraham, E; Deepa, B; Pothan, L A; John, M; Narine, S S; Thomas, S and Anandjiwala, R (2013). Physicomechanical properties of nanocomposites based on cellulose nanofibre and natural rubber latex. *Cellulose, 20(1)*: 417-427. DOI: 10.1007/s10570-012-9830-1.

Agrebi, F; Ghorbel, N; Bresson, S; Abbas, O and Kallel, A (2019). Study of nanocomposites based on cellulose nanoparticles and natural rubber latex by ATR/FTIR spectroscopy: The impact of reinforcement. *Polym. Compos., 40(5)*: 2076-2087. DOI: 10.1002/pc.24989.

Amin, K N M; Annamalai, P K and Martin, D (2017). Cellulose nanocrystals with enhanced thermal stability reinforced thermoplastic polyurethane. *Malays. J. Anal. Sci., 21(3)*: 754-761.

Anglès, M N and Dufresne, A (2001). Plasticized starch/tunicin whiskers nanocomposite materials. 2. Mechanical behavior. *Macromolecules, 34(9)*: 2921-2931. DOI: 10.1021/ma001555h.

Bendahou, A; Kaddami, H and Dufresne, A (2010). Investigation on the effect of cellulosic nanoparticles' morphology on the properties of natural rubber based nanocomposites. *Eur. Polym. J., 46(4)*: 609-620. DOI: 10.1016/j.eurpolymj.2009.12.025.

Blanchard, R; Ogunsona, E O; Hojabr, S; Berry, R and Mekonnen, T H (2020). Synergistic cross-linking and reinforcing enhancement of rubber latex with cellulose nanocrystals for glove applications. *ACS Appl. Polym. Mater., 2(2)*: 887-898. DOI: 10.1021/acsapm.9b01117.

Cao, L; Yuan, D; Fu, X and Chen, Y (2018). Green method to reinforce natural rubber with tunicate cellulose nanocrystals via one-pot reaction. *Cellulose, 25(8)*: 4551-4563. DOI: 10.1007/s10570-018-1877-1.

Chandra, T; Harahap, H; Wangi, Y and Halimatuddahliana (2020). Physical and mechanical properties of natural rubber latex film (Rubber Dam) products with filler nanocrystal cellulose from peanut shell (*Arachis hypogea* L.) and synthetic dyes. *IOP Conf. Ser.: Mater. Sci. Eng., 801(1)*: 012091.

Chang, S H (2014). An overview of empty fruit bunch from oil palm as feedstock for bio-oil production. *Biomass Bioenergy, 62*: 174-181. DOI: /10.1016/j.biombioe.2014.01.002.

Colom, X; Marín-Genescà, M; Mujal, R; Formela, K and Cañavate, J (2018). Structural and physico-mechanical properties of natural rubber/GTR composites devulcanized by microwaves: Influence of GTR source and irradiation time. *J. Compos. Mater., 52(22)*: 3099-3108. DOI: 10.1177/0021998318761554.

Favier, V; Canova, G R; Cavaillé, J Y; Chanzy, H; Dufresne, A and Gauthier, C (1995). Nanocomposite materials from latex and cellulose whiskers. *Polym. Adv. Technol., 6(5)*: 351-355. DOI: 10.1002/pat.1995.220060514.

Flink, P; Westerlind, B; Rigdahl, M and Stenberg, B (1988). Bonding of untreated cellulose fibers to natural rubber. *J. Appl. Polym. Sci., 35(8)*: 2155-2164.

Gan, P G; Sam, S T; Abdullah, M F; Omar, M F and Tan, L S (2020). An alkaline deep eutectic solvent based on potassium carbonate and glycerol as pretreatment for the isolation of cellulose nanocrystals from empty fruit bunch. *BioRes., 15(1)*: 1154-1170.

Gopalan Nair, K and Dufresne, A (2003). Crab shell chitin whisker reinforced natural rubber nanocomposites. 1. Processing and swelling behavior. *Biomacromolecules, 4(3)*: 657-665. DOI: 10.1021/bm020127b.

Gray, N; Hamzeh, Y; Kaboorani, A and Abdulkhani, A (2018). Influence of cellulose nanocrystal on strength and properties of low density polyethylene and thermoplastic starch composites. *Ind. Crops Prod., 115*: 298-305.

Hajji, P; Cavaillé, J Y; Favier, V; Gauthier, C and Vigier, G (1996). Tensile behavior of nanocomposites from latex and cellulose whiskers. *Polym. Compos., 17(4)*: 612-619. DOI: 10.1002/pc.10651.

Hosseinmardi, A; Annamalai, P K; Wang, L; Martin, D and Amiralian, N (2017). Reinforcement of natural rubber latex using lignocellulosic nanofibers isolated from spinifex grass. *Nanoscale, 9(27)*: 9510-9519. DOI: 10.1039/C7NR02632C.

Jailudin, N A H and Amin, K N M (2020). The effect of curing temperature on cellulose nanocrystal reinforced natural rubber latex. *J. Chem. Eng. Ind. Biotechnol., 6(1)*: 20-25. DOI: 10.15282/jceib.v6i1.4875.

Kampeerapappun, P (2015). Extraction and characterization of cellulose nanocrystals produced by acid hydrolysis from corn husk. *J. Metals, Materials Minerals, 25(1)*: 19-26.

Kumar, A; Negi, Y S; Choudhary, V and Bhardwaj, N K (2014). Characterization of cellulose nanocrystals produced by acid-hydrolysis from sugarcane bagasse as agro-waste. *J. Mater. Phys. Chem., 2(1)*: 1-8.

Mao, H; Gong, Y; Liu, Y; Wang, S; Du, L and Wei, C (2017). Progress in nanocellulose preparation and application. *Paper and Biomaterials, 2(4)*: 65-76.

Mariano, M; El Kissi, N and Dufresne, A (2016). Cellulose nanocrystal reinforced oxidized natural rubber nanocomposites. *Carbohydr. Polym., 137*: 174-183.

Mok, K L and Eng, A H (2018). Characterisation of crosslinks in vulcanised rubbers: From simple to advanced techniques. *Malays. J. Chem. (Mjchem), 20*: 118-127.

Neto, W P F; Silvério, H A; Dantas, N O and Pasquini, D (2013). Extraction and characterization of cellulose nanocrystals from agro-industrial residue - Soy hulls. *Ind. Crops Prod., 42*: 480-488.

Rajisha, K R; Maria, H J; Pothan, L A; Ahmad, Z and Thomas, S (2014). Preparation and characterization of potato starch nanocrystal reinforced natural rubber nanocomposites. *Int. J. Biol. Macromol., 67*: 147-153. DOI: 10.1016/j.ijbiomac.2014.03.013.

Shanmugarajah, B; Kiew, P L; Chew, I M L; Choong, T S Y and Tan, K W (2015). Isolation of nanocrystalline cellulose (NCC) from palm oil empty fruit bunch (EFB): Preliminary result on FTIR and DLS analysis. *Chem. Eng. Trans., 45*: 1705-1710.

Song, K; Zhu, X; Zhu, W and Li, X (2019). Preparation and characterization of cellulose nanocrystal extracted from *Calotropis procera* biomass. *Bioresour. Bioprocess., 6(1)*: 1-8.

Supian, M A F; Amin, K N M; Jamari, S S and Mohamad, S (2020). Production of cellulose nanofiber (CNF) from empty fruit bunch (EFB) via mechanical method. *J. Environ. Chem. Eng., 8(1)*: 103024. DOI: 10.1016/j.jece.2019.103024.

Thomas, M G; Abraham, E; Jyotishkumar, P; Maria, H J; Pothen, L A and Thomas, S (2015). Nanocelluloses from jute fibers and their nanocomposites with natural rubber: Preparation and characterization.

Int. J. Biol. Macromol., 81: 768-777. DOI: 10.1016/j.ijbiomac.2015.08.053.

Tian, M; Zhen, X; Wang, Z; Zou, H; Zhang, L and Ning, N (2017). Bioderived rubber-cellulose nanocrystal composites with tunable water-responsive adaptive mechanical behavior. *ACS Appl. Mater. Interfaces, 9(7)*: 6482-6487.

Vandenplas, O and Raulf, M (2017). Occupational latex allergy: The current state of affairs. *Curr. Allergy Asthma Rep., 17(3)*: 14. DOI: 10.1007/s11882-017-0682-5.

Varghese, S; Gatos, K G; Apostolov, A A and Karger-Kocsis, J (2004). Morphology and mechanical properties of layered silicate reinforced natural and polyurethane rubber blends produced by latex compounding. *J. Appl. Polym. Sci., 92(1)*: 543-551. DOI: 10.1002/app.20036.

Visakh, P M; Thomas, S; Oksman, K and Mathew, A P (2012). Crosslinked natural rubber nanocomposites reinforced with cellulose whiskers isolated from bamboo waste: Processing and mechanical/thermal properties. *Compos. Part A: Appl. Sci. Manuf., 43(4)*: 735-741. DOI: 10.1016/j.compositesa.2011.12.015.

Xu, X; Liu, F; Jiang, L; Zhu, J Y; Haagenson, D and Wiesenborn, D P (2013). Cellulose nanocrystals *vs.* cellulose nanofibrils: A comparative study on their microstructures and effects as polymer reinforcing agents. *ACS Appl. Mater. Interfaces, 5(8)*: 2999-3009. DOI: 10.1021/am302624t.

Zhang, C; Dan, Y; Peng, J; Turng, L S; Sabo, R and Clemons, C (2014). Thermal and mechanical properties of natural rubber composites reinforced with cellulose nanocrystals from Southern Pine. *Adv. Polym. Technol., 33(S1)*. DOI: 10.1002/adv.21448.

Zulnazri, Z; Anjana, F and Roesyadi, A (2017). Temperature effect of crystalinity in cellulose nanocrystal from oil palm empty fruit bunch (OPEFB) using sonication-hydrothermal methods. *J. Pure Appl. Chem. Res., 6(1)*: 14-21.

INVESTIGATING THE POTENTIAL ANTI-DIABETIC MECHANISMS OF WATER-SOLUBLE PALM FRUIT EXTRACT

**SOON-SEN LEOW[1]*; NORFAZLINA MOHD NAWI[1,2]; SYED FAIRUS[1]
and RAVIGADEVI SAMBANTHAMURTHI[1,3]**

ABSTRACT

Water-Soluble Palm Fruit Extract (WSPFE) obtained from the aqueous vegetation liquor of oil palm (Elaeis guineensis) *fruit milling demonstrated anti-diabetic effects in Nile rats, but the related mechanisms were unknown. Here, we investigated the potential effects of WSPFE samples on glucose uptake and enzymes involved in carbohydrate hydrolysis and incretin degradation. Glucose uptake assays were performed using spray dried (SD) WSPFE, freeze dried (FD) WSPFE, WSPFE ethyl acetate fraction (EAF) and seven individual WSPFE fractions obtained from WSPFE EAF on everted mouse intestinal sacs ex vivo and Caco-2 cell monolayers in vitro. α-glucosidase, α-amylase and dipeptidyl peptidase-4 (DPPIV) enzymatic assays were performed in vitro. Glucose uptake assays revealed that all the WSPFE samples tested did not inhibit glucose absorption. However, WSPFE EAF consistently had stronger inhibitory effects on α-glucosidase, α-amylase and DPPIV enzymes compared to SD WSPFE and FD WSPFE. SD WSPFE inhibited α-amylase better than FD WSPFE. In terms of individual fractions, F2 demonstrated the strongest inhibitory effects against α-glucosidase and DPPIV. Hence, although WSPFE samples did not inhibit glucose uptake, they showed inhibitory effects on the three enzymes tested, especially WSPFE EAF and F2. Further studies to investigate their effects on carbohydrate digestion and postprandial hyperglycaemia are warranted.*

INTRODUCTION

Rising physical inactivity, obesity and consumption of energy-dense diets have resulted in an unprecedented increase in the incidence and prevalence of type 2 diabetes mellitus (T2DM), with a projected increase to 642 million cases by 2040 (Chatterjee *et al.*, 2017). T2DM is characterised by insulin resistance, declining insulin production and pancreatic β-cell failure (Lyssenko *et al.*, 2008). In overcoming T2DM, plant phenolic compounds may influence glucose metabolism via different mechanisms (Cuervo *et al.*, 2014; Hanhineva *et al.*, 2010; Moco *et al.*, 2012). These include inhibition of intestinal carbohydrate digestion, inhibition of intestinal glucose absorption, stimulation of pancreatic insulin secretion, modulation of hepatic glucose release, as well as activation of insulin receptors and glucose uptake in insulin-sensitive tissues. Modulation of gut flora activities that effect changes in energy metabolism, as well as modulation of gene expression and intracellular signalling pathways may also occur. An important property of phenolic compounds identified is their preventive effects against long-term T2DM

[1] Malaysian Palm Oil Board,
6 Persiaran Institusi, Bandar Baru Bangi,
43000 Kajang, Selangor, Malaysia.

[2] University College London, 5, University Street London,
WC1E 6JF, United Kingdom.

[3] Academy of Sciences Malaysia, Level 20, West Wing,
MATRADE Tower, Jalan Sultan Ahmad Shah, off Jalan
Tuanku Abdul Halim, 50480 Kuala Lumpur, Malaysia.

* Corresponding author e-mail: ssleow@mpob.gov.my

complications, such as retinopathy, nephropathy and neuropathy, which may help improve quality of life in diabetic patients (Bahadoran *et al.*, 2013).

An extract obtained from the aqueous vegetation liquor produced from the milling of the oil palm (*Elaeis guineensis*) fruit, termed Water-Soluble Palm Fruit Extract (WSPFE), Palm Fruit Bioactives, palm fruit juice or oil palm phenolics (Sambanthamurthi *et al.*, 2011a), is rich in phenolic acids, including three caffeoylshikimic acid isomers, *p*-hydroxybenzoic acid and protocatechuic acid (Sambanthamurthi *et al.*, 2011a). It also contains an indoleacetic acid derivative (Sambanthamurthi *et al.*, 2014) and shikimic acid (Sambandan *et al.*, 2011). Pre-clinical *in vitro*, *ex vivo* and *in vivo* studies have shown that WSPFE has beneficial bioactive properties, while clinical studies in healthy volunteers have demonstrated that it is safe for human consumption and confers antioxidant as well as anti-inflammatory effects (Leow *et al.*, 2021a). We previously showed that WSPFE blocked T2DM progression in 12 week-old male Nile rats (*Arvicanthis niloticus*), with a significant decrease in blood glucose after 17 weeks of treatment (Sambanthamurthi *et al.*, 2011b). We also demonstrated that WSPFE delayed T2DM onset, completely prevented it and even reversed advancing T2DM in Nile rats (Bolsinger *et al.*, 2014). WSPFE thus, has excellent anti-diabetic effects. It would therefore be important to identify the potential mechanisms involved and the components which confer these effects, if possible, via bioactivity-guided fractionation. The underlying mechanism is not likely a rise in insulin secretion, as insulin levels were not significantly increased after WSPFE supplementation in Nile rats (Bolsinger *et al.*, 2014; Sambanthamurthi *et al.*, 2011b). This necessitates investigations into other possible mechanisms, which may include inhibition of glucose absorption, carbohydrate hydrolysis or incretin degradation.

In addition, different drying methods may have effects on the biological activities of polyphenols. For example, higher chokeberry polyphenol levels were present after drying at high temperatures as compared to after freeze drying (Horszwald *et al.*, 2013), while spray dried (SD) papaya products also retained higher levels of flavonoids and phenolic compounds as compared to freeze dried (FD) products (Gomes *et al.*, 2018). As such, investigating different drying methods would also be important for preparation of related products with optimal biological activities.

When compared to other routes of exposure, the gastrointestinal tract is highly relevant to the effects of phenolic compounds, as the areas of exposure of the gastrointestinal tract to these ingested compounds are extensive. *Ex vivo* everted intestinal sacs have been used in various drug pharmacokinetic and pharmacodynamic studies (Alam *et al.*, 2012). Caco-2 cell monolayers have also been used as an *in vitro* model of the intestinal barrier for studies on metabolism and transport kinetics of dietary phenolic compounds (Sambuy *et al.*, 2005).

In humans, dietary glucose intake primarily comes from the hydrolysis of carbohydrates, such as starch. Salivary and pancreatic α-amylases, as well as intestinal α-glucosidases, are the carbohydrate-hydrolysing enzymes involved in the generation of dietary glucose. Inhibition of these carbohydrate-hydrolysing enzymes can be an important concept for T2DM management (Apostolidis and Lee, 2010; Striegel *et al.*, 2015). In addition, the dipeptidyl peptidase-4 (DPPIV) enzyme is involved in the degradation of incretins, which are gut peptides that are secreted after nutrient intake and stimulate insulin secretion. Glucose-dependent insulinotropic polypeptide (GIP) and glucagon-like peptide-1 (GLP-1) are the known incretin hormones from the cells of the upper and lower gut, respectively. These two hormones are responsible for the incretin effect, a phenomenon where there is a two- to three-fold higher insulin secretory response to oral as compared to intravenous glucose administration. In subjects with T2DM, this incretin effect is diminished or no longer present (Nauck and Meier, 2018). The inhibition of DPPIV is thus, another possible anti-diabetic mechanism (Fan *et al.*, 2013).

In the present study, we were interested to find out the possible mechanisms by which WSPFE samples confer potential protection against T2DM. Thus, we sought to investigate whether they have inhibitory activities on glucose absorption, as well as their potential effects on enzymes involved in carbohydrate hydrolysis and incretin degradation. We compared the effects of WSPFE samples produced using two different drying methods and fractions prepared using preparative high-performance liquid chromatography (HPLC), so as to inform future studies on carbohydrate digestion and postprandial hyperglycaemia using WSPFE samples.

MATERIALS AND METHODS

Preparation of Water-Soluble Palm Fruit Extract (WSPFE) Samples

The solvents used were purchased from Merck KGaA (Darmstadt, Germany) unless otherwise stated. Liquid WSPFE was produced at the Malaysian Palm Oil Board (MPOB) Phenolic Antioxidant Pilot Plant as described by Sambanthamurthi *et al.* (2008) in Labu, Negeri Sembilan, Malaysia. Spray dried (SD) WSPFE

was obtained through the spray drying process carried out on liquid WSPFE at Biotropics Malaysia Berhad, Shah Alam, Selangor, Malaysia. This spray drying process was performed using the Agridon AG-10 spray dryer (Agridon Technologies, Sungai Buloh, Selangor, Malaysia), with the following conditions: inlet temperature of 185°C-200°C, outlet temperature of 110°C-130°C, aspirator value of 85%-100%, feed rate of 83-116 mL/min, air for drying and compressed air with a flow of 150-200 kPa for pneumatic liquid atomiser. Freeze dried (FD) WSPFE was obtained by freeze drying liquid WSPFE at MPOB using a FreeZone 2.5 L Benchtop Freeze Dry System (Labconco Corp., Kansas City, Missouri, United States of America) at -54°C. WSPFE ethyl acetate fraction (EAF) was obtained by extracting liquid WSPFE with ethyl acetate using a sample:solvent ratio of 1:3 and then collecting the upper solvent layer for rotary evaporation and freeze drying. Compared to using other solvents such as hexane, chloroform, methanol and water, extraction using ethyl acetate has been previously found to result in plant extracts containing high total phenolic content (Ooi *et al.*, 2016), as well as high carbohydrate-hydrolysing enzyme inhibitory activities (Ablat *et al.*, 2017; Nguyen *et al.*, 2020a) and anti-diabetic properties in animal models (Ablat *et al.*, 2017; Nguyen *et al.*, 2020b; Olatunji *et al.*, 2017; Ooi *et al.*, 2018).

Individual WSPFE fractions (F1-F7) were prepared by subjecting WSPFE EAF to preparative HPLC using a Waters Preparative AutoPurification HPLC System (Waters Corp., Milford, Massachusetts, United States of America) as described previously (Leow *et al.*, 2021b). Separation was achieved by using a reverse phase Waters Atlantis C18 5 μm column (Waters Corporation, Milford, Massachusetts, United States of America). A binary gradient system was used as the mobile phase, with phase A comprising 0.02% (v/v) trifluoroacetic acid in distilled water and phase B comprising 70%:30% (v/v) methanol-acetonitrile. A flow rate of 20 mL/min and a pressure limit of 2.76 x 10^4 kPa were used. The gradient elution with a total run time of 55 min was as follows: Started from 100% (v/v) phase A and 0% (v/v) phase B, increased to 32.5% (v/v) phase B over 40 min, then increased to 62.5% (v/v) phase B over 6 min and finally decreased to 0% (v/v) phase B over 9 min. Seven fractions (F1-F7) as characterised by ultraviolet/visible (UV/VIS) detection at 280 nm UV wavelength were collected. The identities of the major components in these fractions were confirmed by the retention times and UV/VIS spectra of the peaks which had already been identified in WSPFE previously. The related preparative HPLC chromatogram of these prepared fractions had been published previously (Leow *et al.*, 2021b).

Glucose Uptake of Everted Mouse Intestinal Sacs

Male, Institute of Cancer Research (ICR) mice aged between nine to 19 weeks (30 to 44 g) obtained from the Laboratory Animal Resources Unit, Universiti Kebangsaan Malaysia (UKM), Kuala Lumpur, Malaysia were maintained in a controlled environment of 25°C with a 12-hr/12-hr light/dark cycle. Twelve hours prior to the preparation of the everted intestinal sacs, the mice were only given access to water but not food. These animals were then euthanised using the cervical dislocation technique. Everted mouse intestinal sacs were prepared according to adapted protocols (Hamilton and Butt, 2013; Mary and Rao, 2002), with the relevant animal care and use protocols approved by the UKM Animal Ethics Committee with the approval number MPOB/2016/LEOW/23-MAR./735-APR.-2016-MAR.2019-AR-CAT2.

The chemicals used for glucose uptake experiments were purchased from Sigma-Aldrich (Saint Louis, Missouri, United States of America) unless otherwise stated. Ringer's solution was used as the buffer in the glucose uptake experiments on everted mouse intestinal sacs (Luz-Madrigal *et al.*, 2015). This buffer consisted of 123 mM sodium chloride (NaCl), 1.53 mM calcium chloride ($CaCl_2$), 5 mM potassium chloride (KCl), 0.8 mM disodium hydrogen phosphate (Na_2HPO_4) and 0.1 mM potassium dihydrogen phosphate (KH_2PO_4) [pH 7.4, adjusted with 0.1 M hydrochloric acid (HCl) and 0.1 M sodium hydroxide (NaOH)]. SD WSPFE samples for final concentrations between 0 to 500 μg/mL were prepared. Serial dilutions of phloretin (Cayman Chemical Company, Ann Arbor, Michigan, United States of America) and phloridzin (Cayman Chemical Company, Ann Arbor, Michigan, United States of America) were also prepared as positive controls. Glucose uptake assays were conducted by introducing Ringer's solution into everted mouse intestinal sacs (inner serosal sides) and immersing these sacs into Ringer's solution containing 10 mM of D-glucose as well as each prepared concentration of either one of the positive controls or SD WSPFE (outer mucosal sides) for 30 min. These assays were conducted in a 37°C oxygenated [95% v/v oxygen (O_2) and 5% v/v carbon dioxide (CO_2)] water bath (Memmert GmbH, Buchenbach, Germany). For the measurement of glucose, samples from the inner serosal sides were collected before and after the glucose uptake assays. Glucose measurement was performed using the Glucose Oxidase Assay Kit (Sigma-Aldrich, Saint Louis, Missouri, United States of America).

Glucose Uptake of Human Colonic Caco-2 Cell Monolayers

Human colonic Caco-2 cells (ATCC® HTB-37™) (passage numbers 20-60) were utilised for

the *in vitro* cell culture experiments. Appropriate aseptic mammalian cell culture techniques were applied throughout the cell culture experiments described in this study. The complete medium used for maintenance and subculturing of the cells was Dulbecco's Modified Eagles' Medium (DMEM) containing 10% v/v fetal bovine serum (FBS) and 1% v/v non-essential amino acids, obtained from Gibco (Thermo Fisher Scientific, Waltham, Massachusetts, United States of America). Dimethyl sulphoxide (DMSO) (Sigma-Aldrich, Saint Louis, Missouri, United States of America) was added at 5% v/v to the complete medium for cell cryopreservation.

For CellTiter-Glo (CTG) luminescent cell viability assays, Caco-2 cells grown to confluence were trypsinised with Gibco trypsin ethylenediaminetetraacetic acid (EDTA) (0.25% w/v) containing phenol red (Thermo Fisher Scientific, Waltham, Massachusetts, United States of America) and centrifuged at 130 x g for 5 min. Following cell counting, 75 μL of complete Gibco DMEM medium containing 2.5×10^4 cells was pipetted into each well of a 96-well white opaque tissue-culture treated microplate (SPL Life Sciences Co. Ltd., Pocheon-si, South Korea). The microplate was then incubated overnight at 37°C in a 5% v/v CO_2 incubator (NuAire, Inc., Plymouth, Minnesota, United States of America). Appropriate media controls were also prepared in other wells within the same plate. WSPFE samples were prepared the following day using complete Gibco DMEM medium containing 0.4% v/v DMSO as the vehicle. A total of 25 μL of each WSPFE sample was added into the wells of the 96-well microplates prepared previously, before being subjected to incubation at 37°C in 5% v/v CO_2 for 24 hr. WSPFE samples were tested at varying final concentrations between 0 to 2000 μg/mL to determine the half maximal inhibitory concentration (IC_{50}) values of the samples on Caco-2 cell viability. The CTG Luminescent Cell Viability Assay Kit (Promega Corp., Madison, Wisconsin, United States of America) was used for this purpose.

The protocols used to prepare Caco-2 monolayers were adapted from literature (Hubatsch *et al.*, 2007). Each sterile filter insert in 12-well plates (Corning, New York City, New York, United States of America) was coated with 250 μL of type I collagen solution from rat tail (Sigma-Aldrich, Saint Louis, Missouri, United States of America) prepared in 0.02 M acetic acid (Merck KGaA, Darmstadt, Germany) at a coating density of 10 μg cm^{-2}. This coating step was carried out at 37°C for 1 hr. Excess collagen solution was then pipetted out and 400 μL of complete Gibco DMEM medium containing 20% v/v FBS, 1% v/v non-essential amino acids and 1% v/v penicillin-streptomycin was then added to each well. The plates were then incubated at 37°C for 4 hr, after which the medium was removed prior to cell seeding.

Caco-2 cells grown to confluence were then trypsinised with Gibco trypsin-EDTA (0.25% w/v) containing phenol red and centrifuged at 130 x g for 5 min. Following cell counting, 500 μL of complete Gibco DMEM medium containing 3×10^5 cells was pipetted into each collagen-coated filter insert (apical layer). The bottom well (basolateral layer) was filled with 1500 μL of complete Gibco DMEM medium. Incubation was then carried out at 37°C in 5% v/v CO_2 overnight before the apical medium was replaced with fresh complete Gibco DMEM medium. Both apical and basolateral media were changed twice a week to allow cell monolayers to form and differentiate for three weeks. The integrity of the cell monolayers was assessed by measuring the transepithelial electrical resistance (TEER) using the Millicell® ERS-2 Voltohmmeter (Merck KGaA, Darmstadt, Germany). Caco-2 monolayers with TEER values >200 Ω cm^2 were used in the glucose uptake experiments.

The chemicals used for glucose uptake experiments were purchased from Sigma-Aldrich (Saint Louis, Missouri, United States of America) unless otherwise stated. One day before the glucose uptake experiments, both apical and basolateral media of the cell monolayers were discarded. The monolayers were then washed with Gibco phosphate buffered saline (Thermo Fisher Scientific, Waltham, Massachusetts, United States of America). Serum-free Gibco DMEM medium containing 1% v/v non-essential amino acids and 1% v/v penicillin-streptomycin was then added to the apical and basolateral sides. The plates were then incubated at 37°C in 5% v/v CO_2 overnight to increase glucose uptake.

The following day, WSPFE samples were dissolved in DMSO and added to serum-free Gibco DMEM medium containing 1% v/v non-essential amino acids and 1% v/v penicillin-streptomycin at a final 0.4% v/v DMSO concentration. The dissolved test compounds were then serially diluted to the concentrations required using serum-free Gibco DMEM medium containing 1% v/v non-essential amino acids, 1% v/v penicillin-streptomycin and 0.4% v/v DMSO. Serial dilutions of phloretin (Cayman Chemical Company, Ann Arbor, Michigan, United States of America) and phloridzin (Cayman Chemical Company, Ann Arbor, Michigan, United States of America) were also prepared as positive controls. Following this, the apical and basolateral media of the cell monolayers were discarded. The prepared test compounds were then added to the apical sides. Serum-free Gibco DMEM medium containing 1% v/v non-essential amino acids, 1% v/v penicillin-streptomycin and 0.4% v/v DMSO was then added to the basolateral sides. The plates were then incubated at 37°C in 5% v/v CO_2 for 1 hr in acute studies, or 20 hr in chronic studies.

Following the required incubation time, the test compounds were discarded. The apical and basolateral sides were then washed with glucose-free sodium uptake buffer, which contained 140 mM NaCl, 5 mM KCl, 2.5 mM $CaCl_2$, 1 mM magnesium sulphate ($MgSO_4$), 1 mM sodium dihydrogen phosphate (NaH_2PO_4), 10 mM 4-(2-hydroxyethyl)-1-piperazineethanesulphonic acid (HEPES), 1% v/v L-glutamine, 1% v/v non-essential amino acids and 1% v/v penicillin-streptomycin (pH 7.4, adjusted with 0.1 M HCl and 0.1 M NaOH). Following the wash step, 250 µL of 10 mM D-glucose solution prepared in glucose-free sodium uptake buffer was added to the apical sides, while 750 µL of the glucose-free sodium uptake buffer was added to the basolateral sides. The plates were then incubated at 37°C in 5% v/v CO_2 for 1 hr. Following this, samples from the basolateral sides were collected for glucose measurements. These glucose uptake experiments using human colonic Caco-2 cell monolayers were repeated using sodium-free uptake buffer, whereby NaCl was replaced with KCl and NaH_2PO_4 was replaced with KH_2PO_4. The Glucose Hexokinase Assay Kit (Sigma-Aldrich, Saint Louis, Missouri, United States of America) was used for glucose measurement of samples collected from the basolateral sides of the Caco-2 monolayers.

Assays on Carbohydrate Hydrolysis and Incretin Degradation Enzymes

The Alpha-Glucosidase Activity Assay Kit (Colorimetric) (ab174093) (Abcam PLC, Cambridge, United Kingdom) was utilised to perform assays on α-glucosidase, a carbohydrate-hydrolysing enzyme. Assays on another carbohydrate-hydrolysing enzyme, α-amylase, were carried out using the Alpha-Amylase Activity Assay Kit (Colorimetric) (ab102523) (Abcam PLC, Cambridge, United Kingdom). For the incretin degradation enzyme DPPIV, assays were performed using the DPPIV-Glo Protease Assay Kit (G8351) (Promega Corp., Madison, Wisconsin, United States of America) and the recombinant human DPPIV high purity dimer enzyme (R&D Systems, Inc., Minneapolis, Minnesota, United States of America).

WSPFE samples were tested at varying final concentrations between 0 to 500 µg/mL to determine the IC_{50} values of the samples on α-glucosidase, α-amylase and DPPIV. Negative control wells containing the substrate and enzyme without inhibitor samples, positive control wells containing the substrate, enzyme and the positive control inhibitor, as well as colour control samples which functioned as blanks for the corresponding samples were also prepared in these experiments. Acarbose (Sigma-Aldrich, Saint Louis, United States of America) was used as the positive

control inhibitor in the α-glucosidase and α-amylase assays, while sitagliptin phosphate (Cayman Chemical Company, Ann Arbor, Michigan, United States of America) was used as the positive control inhibitor in the DPPIV assays. Acarbose which is a pseudo-tetrasaccharide obtained from the fermentation processes of the microorganism *Actinoplanes utahensis* is commonly used as an oral reversible competitive inhibitor of α-glucosidase and α-amylase enzymes in T2DM patients (Rosak and Mertes, 2012; Yee and Fong, 1996). On the other hand, sitagliptin which is a synthesised beta-amino amide incorporating fused heterocycles called triazolopiperazines is an oral reversible DPPIV inhibitor that is generally well tolerated when administered in T2DM patients (Bergman *et al.*, 2007; Kim *et al.*, 2005).

Statistical Analyses

Measurements of all enzymatic assays were carried out using the Tecan Infinite M200 microplate reader (Tecan Group Ltd., Zurich, Switzerland). Raw data was exported into the Microsoft Excel software (Microsoft Corp., Redmond, Washington, United States of America) for analysis. Data were expressed as means ± standard error of the mean (SEM). Statistical analyses on the results obtained were performed using the SPSS Statistics software (IBM Corp., Armonk, New York, United States of America). One-way analysis of variance (ANOVA) with Tukey's honestly significant difference (HSD) *post-hoc* test or Dunnett's *post-hoc* test against Negative Control where appropriate was carried out. Differences were considered statistically significant at $p<0.05$. IC_{50} values were calculated using the Quest Graph™ IC_{50} Calculator (AAT Bioquest, Inc., Sunnyvale, California, United States of America) (AAT Bioquest, 2019).

RESULTS AND DISCUSSION

Glucose Uptake of Everted Mouse Intestinal Sacs

Ex vivo everted mouse intestinal sac preparation protocols from previous studies (Hamilton and Butt, 2013; Mary and Rao, 2002) were adapted to elucidate the possible effects of WSPFE samples on glucose transport, since this model is considered to be one of the efficient tools used for studying intestinal absorption (Alam *et al.*, 2012). However, initial experiments conducted on SD WSPFE samples using *ex vivo* everted mouse intestinal sacs showed that while positive controls phloretin and phloridzin inhibited glucose transport from the mucosal to the serosal sides of the everted mouse intestinal sacs, SD WSPFE did not have any glucose absorption inhibition effects up to
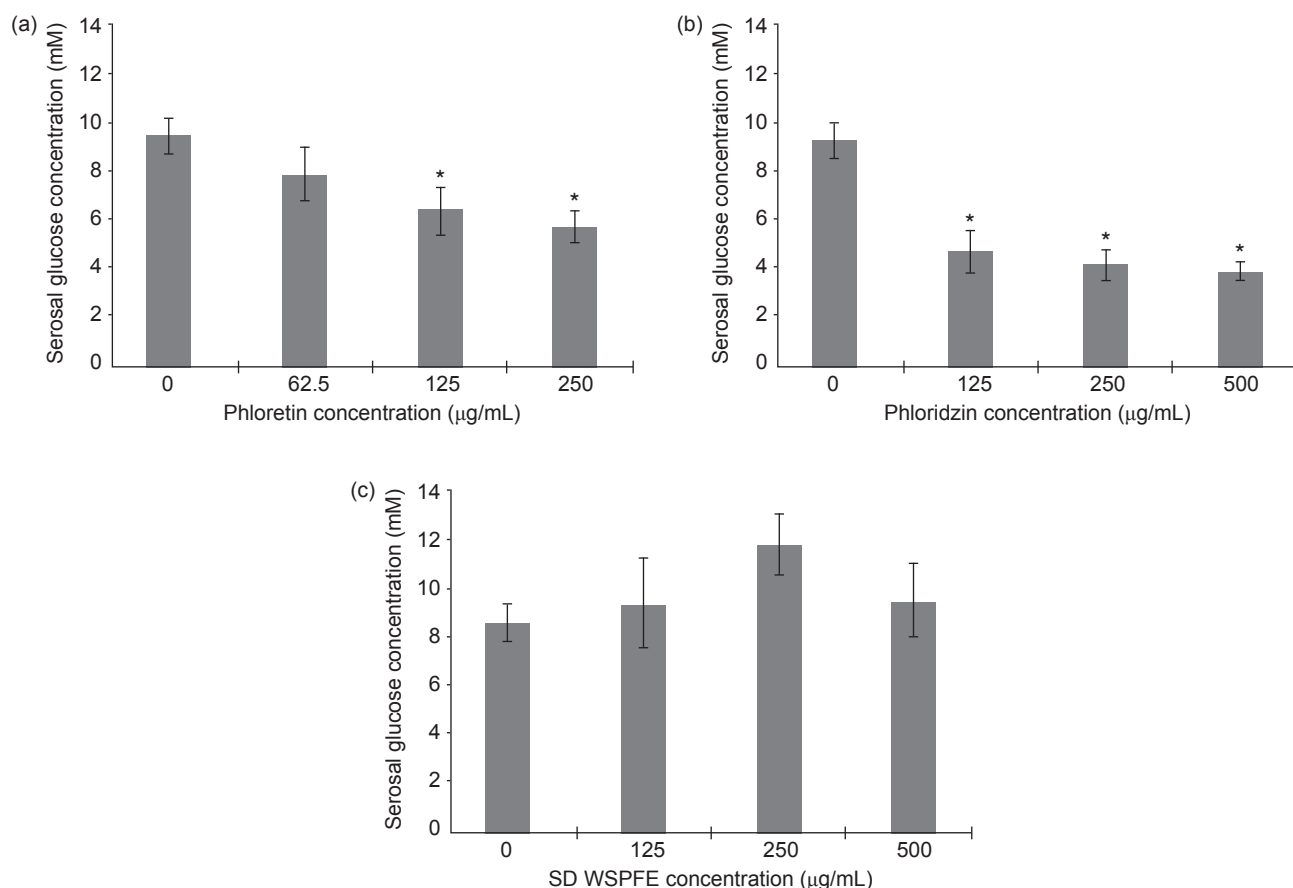
Note: Error bars indicate standard error of the mean (SEM); $n=5$ biological replicates; * $p<0.05$ by one-way analysis of variance (ANOVA) with Dunnett's *post-hoc* test against Negative Control (0 μg/mL). SD - spray dried; WSPFE - Water-Soluble Palm Fruit Extract.

Figure 1. Glucose uptake assay results on everted mouse intestinal sacs using positive controls and SD WSPFE of different doses as measured using the absorbance-based Glucose Oxidase Assay Kit over the assay time period of 30 min after incubation with the respective test samples for 30 min. (a) phloretin, (b) phloridzin, and (c) SD WSPFE.

500 μg/mL (*Figure 1*). This suggested that the anti-diabetic effects of SD WSPFE were not due to inhibition of glucose absorption in the intestines. To further confirm this and to reduce the use of animals, another model of the intestinal barrier, the *in vitro* Caco-2 cell monolayer model, was utilised for glucose uptake evaluation. In addition, the glucose hexokinase assay was subsequently used for glucose measurements in the present study, since previous investigations had demonstrated the sensitivity and accuracy of this assay, which results from reduction of colour interference by plant phenolic compounds (Xu *et al.*, 2012).

Preparation of WSPFE Fractions

Further glucose transport investigations were conducted using *in vitro* Caco-2 cell monolayers. In addition to SD WSPFE, additional WSPFE samples were tested in this set of experiments, including FD WSPFE, WSPFE EAF, as well as seven individual WSPFE fractions (F1-F7) isolated using preparative HPLC. These seven individual fractions were prepared as previously described (Leow *et al.*,

2021b) and identification of the major components of the fractions was based on information obtained from our previous published work on WSPFE. F1 contained shikimic acid (Sambandan *et al.*, 2011), F3 contained protocatechuic acid (Sambanthamurthi *et al.*, 2011a), F4 contained *p*-hydroxybenzoic acid (Sambanthamurthi *et al.*, 2011a), F5 contained an indoleacetic acid derivative (Sambanthamurthi *et al.*, 2014), while F6 contained three caffeoylshikimic acid isomers (Sambanthamurthi *et al.*, 2011a). The components of F2 and F7 are presently unknown.

Caco-2 Cell Viability Assays

In cell viability and cytotoxicity studies, the IC_{50} of a compound defines its maximum non-toxic dose (Neubig *et al.*, 2003). IC_{50} thus, acts as a parameter to determine the maximum concentration of a tested compound which could be used to produce desirable effects without exceeding the range of acceptable toxicity. The IC_{50} value of a tested compound on cell lines is determined by the concentration needed to inhibit half of the maximum viability of the cell lines.

In the present study, before carrying out glucose uptake assays on Caco-2 cell monolayers, the IC_{50} values of the WSPFE samples on the viability of the cell line were determined using the CTG Luminescent Cell Viability Assay Kit. The positive control phloridzin, SD WSPFE, FD WSPFE, WSPFE EAF and F1 were not cytotoxic to Caco-2 cells after incubation up to 2000 μg/mL for 24 hr (*Table 1*). On the other hand, the positive control phloretin and F2 to F7 showed cytotoxicity on the Caco-2 cells after incubation for 24 hr. F2 had an IC_{50} value of 1265 ± 107 μg/mL, while F3 had an IC_{50} value of 544 ± 48 μg/mL. The IC_{50} value of F4 was 1007 ± 99 μg/mL, while F5 had an IC_{50} value of 666 ± 107 μg/mL. F6 had an IC_{50} value of 571 ± 178 μg/mL, while the last fraction, F7, had an IC_{50} value of 737 ± 78 μg/mL. The positive control phloretin was most toxic to the Caco-2 cells, with an IC_{50} value of 131 ± 31 μg/mL.

As such, the levels of cytotoxicity of WSPFE samples on Caco-2 cells followed the order of SD WSPFE = FD WSPFE = WSPFE EAF = F1 < F2 < F4 < F7 < F5 < F6 < F3. The results obtained suggested that the concentrations of WSPFE samples to be used in the glucose uptake experiments should

TABLE 1. IC_{50} VALUES OF WSPFE SAMPLES AGAINST CACO-2 CELL VIABILITY

Sample	IC_{50} (μg/mL)
SD WSPFE	*
FD WSPFE	*
WSPFE EAF	*
F1	*
F2	1265 ± 107[a]
F3	544 ± 48[bc]
F4	1007 ± 99[ab]
F5	666 ± 107[b]
F6	571 ± 178[bc]
F7	737 ± 78[b]
Phloretin	131 ± 31[c]
Phloridzin	*

Note: IC_{50} indicates the dose that induced a 50% cell viability inhibition compared to Negative Control as measured using the luminescence-based CTG Luminescent Cell Viability Assay Kit over 10 min after incubation with the respective test samples up to 2000 μg/mL for 24 hr. These IC_{50} values were expressed as means ± standard error of the mean (SEM) from three biological replicates. Means in a column with different letters are significantly different ($p<0.05$) by one-way analysis of variance (ANOVA) with Tukey's honestly significant difference (HSD) *post-hoc* test. *indicates IC_{50} was not achieved at the highest concentration tested (2000 μg/mL). EAF - ethyl acetate fraction; F - fraction; FD - freeze dried; SD - spray dried; WSPFE - Water-Soluble Palm Fruit Extract.

be up to 500 μg/mL, as the IC_{50} value of the most cytotoxic WSPFE sample, F3, was 544 ± 48 μg/mL. This would help to determine the effects of these samples in influencing glucose absorption, by discounting their effects on cell viability. Caco-2 cell monolayers have been widely used to determine the effects of dietary phenolic compounds on glucose transport (Alzaid *et al.*, 2013; Farrell *et al.*, 2013; Johnston *et al.*, 2005; Manzano and Williamson, 2010), as these cells abundantly express the active sodium-dependent glucose transporter 1 (SGLT1) and facilitated glucose transporter 2 (GLUT2) proteins (Sambuy *et al.*, 2005). Nevertheless, it should be noted that Caco-2 is a human cell line derived from human colon adenocarcinoma cancer tissues, and thus, these immortalised cell lines may have their own characteristics which may not be typical of primary cultures.

It is also interesting to note that the toxicity effects of F2 to F7 at various concentrations suggest the potential use of these fractions against colon cancer. Many studies have shown that phenolic acids were able to inhibit cancer (Abotaleb *et al.*, 2020), including colon cancer (Rosa *et al.*, 2016). The cell viability results obtained in the present study showed that F3 containing protocatechuic acid was more cytotoxic to the Caco-2 cells as compared to fractions containing the caffeoylshikimic acid isomers, the indoleacetic acid derivative and *p*-hydroxybenzoic acid. Protocatechuic acid was shown to be a potential cancer chemopreventive agent (Tanaka *et al.*, 2011), as it exerted pro-apoptotic and anti-proliferative effects (Kakkar and Bais, 2014). 3-O-caffeoylshikimic acid and 5-O-caffeoylshikimic acid from the fruits of the Chinese fan or fountain palm (*Livistona chinensis*) were shown to have potent anti-proliferative activities against several cancer cell lines (Zeng *et al.*, 2012). Indoleacetic acid was also found to induce cancer cell death in combination with horseradish peroxidase (Wardman, 2002) or ultraviolet B irradiation (Kim *et al.*, 2010). Derivatives of *p*-hydroxybenzoic acid also exhibited anti-cancer activities (Seidel *et al.*, 2014).

Key structural motifs in phenolic acids responsible for anti-cancer activities include the aromatic ring, number and position of free hydroxyl groups and unsaturated fatty acid chains (Anantharaju *et al.*, 2016). The simpler structure of protocatechuic acid containing an aromatic ring attached with one free hydroxyl group might have contributed to the cytotoxicity effects of F3, but future *in silico* molecular docking experiments would be helpful to better explain the structure-activity relationships between the individual compounds present in WSPFE and potential anti-cancer molecular targets (Chen *et al.*, 2012). However, it would be important to note that F1-F7 used in the present study were not

pure compounds, but only fractions enriched in the compounds mentioned. Therefore, their effects might not only be attributable to the compounds, but also to unidentified non-phenolic compounds and/or the complex nature of these fractions and interactions between phytochemicals present in them.

The cytotoxic properties of the WSPFE samples demonstrated in the present study are also consistent with the anti-cancer effects of WSPFE previously identified, in which FD WSPFE exhibited inhibitory effects on human A549 lung carcinoma, human MCF7 breast adenocarcinoma and mouse J558 immunoglobulin A-secreting myeloma cell lines (Sekaran *et al.*, 2010) when tested up to 2000 μg/mL. Nevertheless, FD WSPFE did not have an effect on the cell viability of the Caco-2 cells used in the present study when tested up to 2000 μg/mL. This suggests that FD WSPFE may not be as effective against human colon adenocarcinoma cancer as compared to other types of cancer. As such, additional experiments in the future on other types of colon cancer cell lines and on normal colon cell lines would be required to further supplement the present findings.

Glucose Uptake of Human Colonic Caco-2 Cell Monolayers

The uptake of glucose in the gastrointestinal tract occurs via the enterocyte membrane transporters SGLT1 and GLUT2. SGLT1 is involved in active glucose transport from the apical side of the intestinal lumen into enterocytes, while GLUT2 is involved in facilitated glucose diffusion from the basolateral side of the intestinal lumen into the hepatic portal vein (Scheepers *et al.*, 2004).

In the present study, positive controls phloretin and phloridzin dose-dependently inhibited glucose transport from the apical sides to the basolateral sides of the Caco-2 monolayers when tested in both sodium uptake buffer (*Figure 2*) and sodium-free uptake buffer (*Figure 3*). When tested using sodium uptake buffer, the inhibitory effects of phloretin on glucose uptake were more pronounced during acute treatment (*Figure 2a*), while those of phloridzin were more pronounced during chronic treatment (*Figure 2b*). On the other hand, SD WSPFE and FD WSPFE did not show any glucose absorption inhibition effects up to 500 μg/mL during acute treatment (*Figure 2c*) or chronic treatment (*Figure 2d*). In addition, glucose uptake assays carried out using WSPFE EAF and F1-F7 up to 500 μg/mL also did not show any effects of the WSPFE fractions on glucose uptake during acute treatment (*Figure 2e*) or chronic treatment (*Figure 2f*). Similar results were obtained when glucose uptake assays were performed on the Caco-2 cell monolayers using sodium-free uptake buffer (*Figures 3a-f*). These results implied that the anti-diabetic effects of WSPFE were not due to glucose uptake inhibition, and hence other mechanisms might be involved instead.

Although phloretin is known to inhibit GLUT2 and phloridzin is known to inhibit SGLT1 (and also renal SGLT2) (Ehrenkranz *et al.*, 2005), we did not find any differences in terms of the inhibitory patterns of these positive controls when using sodium uptake buffer or sodium-free uptake buffer in the present study (*Figures 2a-b* and *3a-b*). The strong acute inhibitory effects of phloretin on glucose uptake compared to the strong chronic inhibitory effects of phloridzin observed in the present study would most likely be due to the degradation of phloridzin to its phloretin and glucose moieties (Ehrenkranz *et al.*, 2005), which increased the availability of phloretin in inhibiting glucose uptake of the Caco-2 cell monolayers.

Assays on Carbohydrate Hydrolysis and Incretin Degradation Enzymes

The IC_{50} results obtained from the α-glucosidase assays showed that F2, WSPFE EAF, F1, F5, F3 and F4 inhibited this enzyme more significantly than the positive control acarbose, while SD WSPFE, FD WSPFE, F6 and F7 did not (*Table 2*). F2 and WSPFE EAF inhibited α-glucosidase the most, with F2 having stronger inhibitory effects compared to WSPFE EAF, as indicated by their IC_{50} values of 162 ± 23 μg/mL and 179 ± 11 μg/mL, respectively.

The IC_{50} results obtained from the α-amylase assays showed that WSPFE EAF, SD WSPFE, F7, FD WSPFE and F5 inhibited this enzyme, but their inhibitory activities were significantly weaker than that of the positive control acarbose by several orders of magnitude. On the other hand, F1, F2, F3, F4 and F6 did not inhibit α-amylase (*Table 2*). Among the WSPFE samples which inhibited α-amylase, WSPFE EAF inhibited the enzyme the most, as indicated by its lowest IC_{50} value of 108 ± 13 μg/mL. This was followed by SD WSPFE and F7, as indicated by their IC_{50} values of 158 ± 1 μg/mL and 160 ± 2 μg/mL, respectively. As such, WSPFE EAF which contained all the seven individual WSPFE fractions had the strongest inhibitory effects on this enzyme, as compared to whole SD WSPFE and FD WSPFE samples. Nevertheless, SD WSPFE had stronger inhibitory effects on α-amylase as compared to FD WSPFE. In terms of individual fractions, F7 followed by F5 inhibited α-amylase the most, but their inhibitory effects were generally weaker than that of WSPFE EAF.

Acarbose is a known anti-hyperglycaemic agent which acts by inhibiting starch digestion enzymes and is widely used in combination with other anti-diabetic drugs (Derosa and Maffioli, 2012). Acarbose is known to inhibit α-amylase
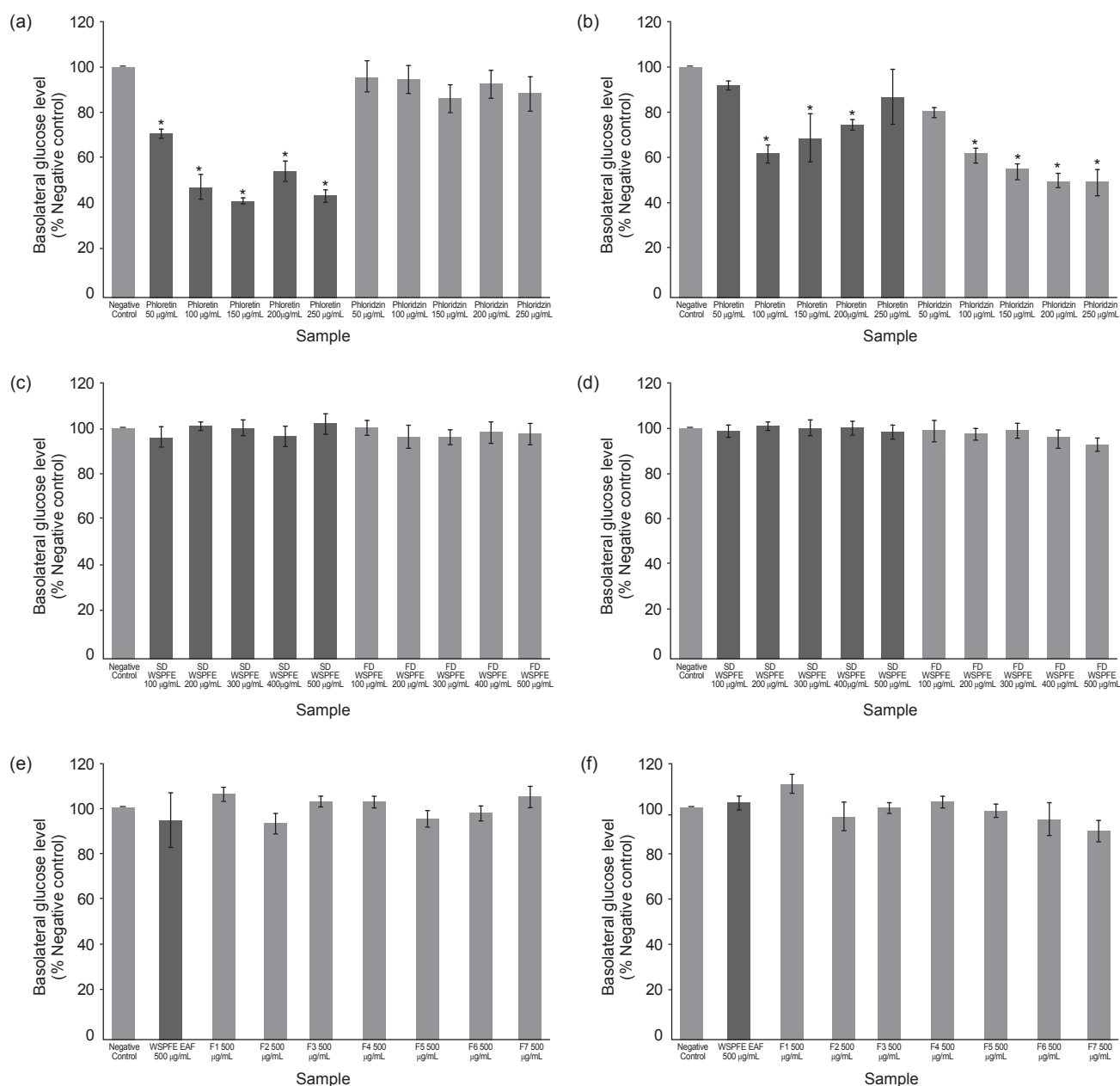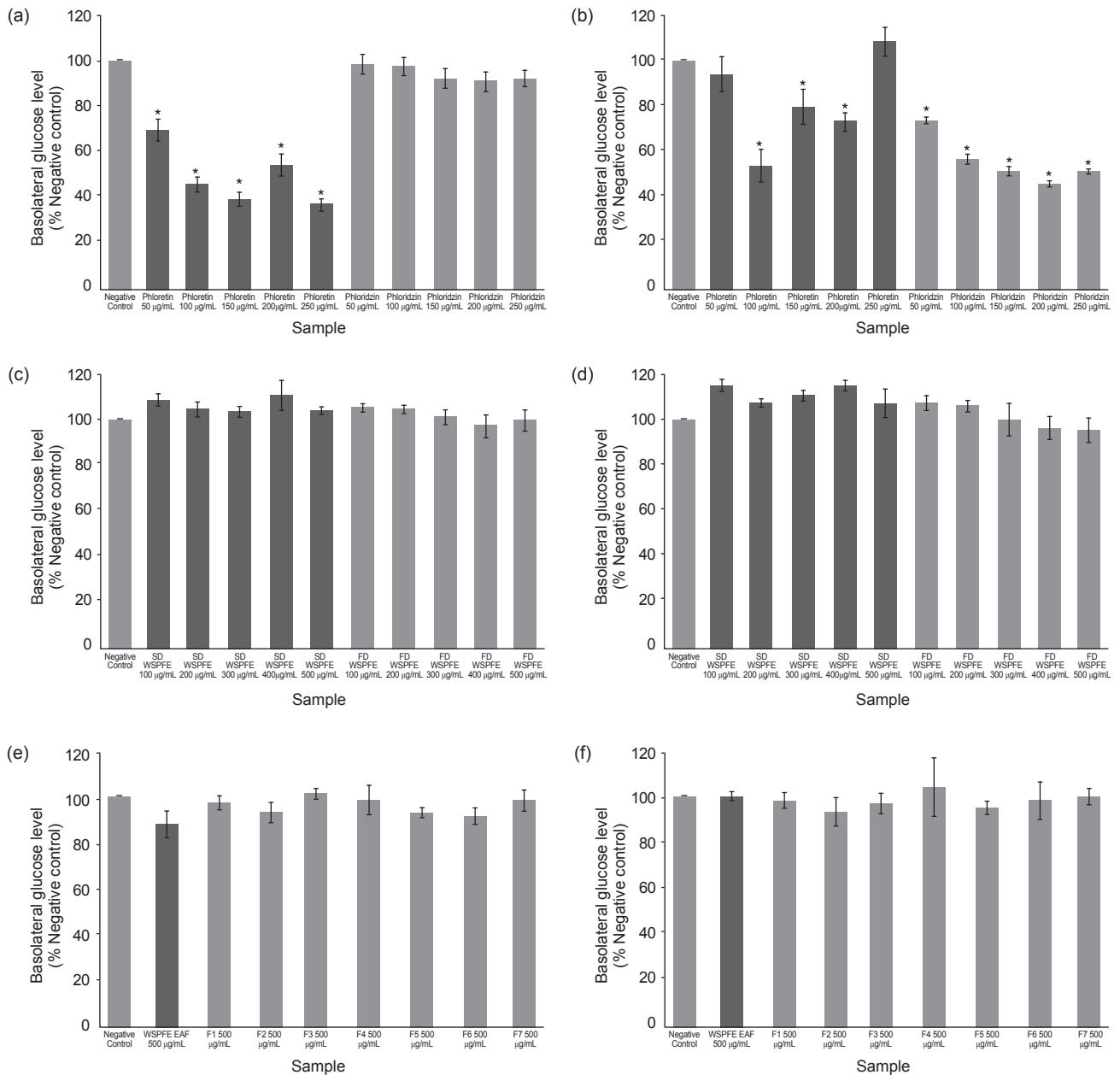
Note: Error bars indicate standard error of the mean (SEM); n=3 biological replicates; * p<0.05 by one-way analysis of variance (ANOVA) with Dunnett's *post-hoc* test against Negative Control. EAF - ethyl acetate fraction; F - fraction; FD - freeze dried; SD - spray dried; WSPFE - Water-Soluble Palm Fruit Extract.

Figure 2. Glucose uptake assay results on human colonic Caco-2 cell monolayers in sodium uptake buffer as measured using the absorbance-based Glucose Hexokinase Assay Kit over the assay time period of 30 min after incubation with the respective test samples. (a) Different doses of positive controls phloretin and phloridzin in 1-hr acute treatment, (b) different doses of positive controls phloretin and phloridzin in 20-hr chronic treatment, (c) different doses of SD WSPFE and FD WSPFE in 1-hr acute treatment, (d) different doses of SD WSPFE and FD WSPFE in 20-hr chronic treatment, (e) WSPFE EAF and F1-F7 (500 μg/mL) in 1-hr acute treatment, and (f) WSPFE EAF and F1-F7 (500 μg/mL) in 20-hr chronic treatment.

significantly more than it inhibits α-glucosidase (Oboh *et al.*, 2016). However, strong α-amylase inhibitors such as acarbose cause unpleasant side effects including flatulence, bloating and abdominal distention, due to suppression of starch digestion and bacterial fermentation in the gut (Yee and Fong, 1996). As such, anti-hyperglycaemic agents, drugs or phytochemicals should ideally have mild α-amylase inhibition but moderate α-glucosidase

inhibition, in order to minimise their side effects. In line with this, bound polyphenol fractions from date (*Phoenix dactylifera* L.) seeds for example, were found to have strong α-glucosidase inhibition but weak α-amylase inhibition (Sirisena *et al.*, 2016). Similar results were found for ethyl acetate extract from the roots of *Smilax glabra* Roxb, an Asian medicinal plant used for the treatment of various chronic diseases (Nguyen *et al.*, 2020b).

Note: Error bars indicate standard error of the mean (SEM); n=3 biological replicates; * $p<0.05$ by one-way analysis of variance (ANOVA) with Dunnett's *post-hoc* test against Negative Control. EAF - ethyl acetate fraction; F - fraction; FD - freeze dried; SD - spray dried; WSPFE - Water-Soluble Palm Fruit Extract.

Figure 3. Glucose uptake assay results on human colonic Caco-2 cell monolayers in sodium-free uptake buffer as measured using the absorbance-based Glucose Hexokinase Assay Kit over the assay time period of 30 min after incubation with the respective test samples. (a) Different doses of positive controls phloretin and phloridzin in 1-hr acute treatment, (b) different doses of positive controls phloretin and phloridzin in 20-hr chronic treatment, (c) different doses of SD WSPFE and FD WSPFE in 1-hr acute treatment, (d) different doses of SD WSPFE and FD WSPFE in 20-hr chronic treatment, (e) WSPFE EAF and F1-F7 (500 μg/mL) in 1-hr acute treatment, and (f) WSPFE EAF and F1-F7 (500 μg/mL) in 20-hr chronic treatment.

In the present study, SD WSPFE and FD WSPFE inhibited α-amylase but not α-glucosidase. These results indicate that the anti-diabetic effects of WSPFE may be due to α-amylase inhibition and not α-glucosidase inhibition, especially more so when SD WSPFE is supplemented. WSPFE EAF and most of the individual WSPFE fractions, as compared to the positive control acarbose, had stronger inhibitory effects on α-glucosidase but weaker inhibitory effects on α-amylase. Several

of the individual WSPFE fractions, *i.e.*, F1-F5, also preferably inhibited α-glucosidase than α-amylase, hence these fractions might be better anti-diabetic oral supplement candidates worthy of further investigations.

The IC_{50} results obtained from the DPPIV assays showed that F2, F5, F4, WSPFE EAF and F3 inhibited this enzyme, while SD WSPFE, FD WSPFE, F1, F6 and F7 did not (*Table 2*). F2 inhibited DPPIV the most, as indicated by its lowest IC_{50}

TABLE 2. IC$_{50}$ VALUES OF WSPFE SAMPLES AGAINST α-GLUCOSIDASE, α-AMYLASE AND DPPIV

Sample	IC$_{50}$ (μg/mL)		
	α-glucosidase	α-amylase	DPPIV
SD WSPFE	*	158 ± 1[b]	*
FD WSPFE	*	232 ± 13[a]	*
WSPFE EAF	179 ± 11[b]	108 ± 13[b]	224 ± 6[b]
F1	210 ± 10[b]	*	*
F2	162 ± 23[b]	*	162 ± 7[c]
F3	213 ± 18[b]	*	291 ± 16[a]
F4	214 ± 18[b]	*	196 ± 2[bc]
F5	210 ± 13[b]	239 ± 29[a]	185 ± 4[c]
F6	*	*	*
F7	*	160 ± 2[b]	*
Positive Control	440 ± 64[a]	0.324 ± 0.016[c]	0.006333 ± 0.000384[d]

Note: IC$_{50}$ indicates the dose that induced a 50% enzymatic inhibition compared to Negative Control as measured using the respective enzymatic assays kits over 60 min. These IC$_{50}$ values were expressed as means ± standard error of the mean (SEM) from three technical replicates. Means in a column with different letters are significantly different ($p<0.05$) by one-way analysis of variance (ANOVA) with Tukey's honestly significant difference (HSD) *post-hoc* test. * indicates IC$_{50}$ was not achieved at the highest concentration tested (500 μg/mL). Acarbose was used as the positive control for α-glucosidase and α-amylase assays, while sitagliptin was used as the positive control for DPPIV assays. DPPIV - dipeptidyl peptidase-4; EAF - ethyl acetate fraction; F - fraction; FD - freeze dried; SD - spray dried; WSPFE - Water-Soluble Palm Fruit Extract.

value of 162 ± 7 μg/mL. This was followed by F5 and F4, as indicated by their IC$_{50}$ values of 185 ± 4 μg/mL and 196 ± 2 μg/mL, respectively. WSPFE EAF which contained all the seven individual WSPFE fractions was also found to have better inhibitory effects on DPPIV, as compared to SD WSPFE and FD WSPFE. In terms of individual fractions, F2 followed by F5, F4 and F3 inhibited DPPIV the most with their inhibitory effects being generally stronger than those of WSPFE EAF, except for F3. However, the inhibitory effects of all the WSPFE samples towards DPPIV were several orders of magnitude less effective than that of the positive control sitagliptin, which had an IC$_{50}$ value of 0.006333 ± 0.000384 μg/mL.

The incretin effect, which refers to the amplification of insulin secretion after oral *vs.* intravenous glucose, is responsible for the disposal of most ingested glucose and is hence, essential for glucose tolerance. It is mainly due to the actions of the gut hormones GIP and GLP-1. GIP is essential for insulin secretion, while GLP-1 is important for inhibition of glucagon secretion (Holst, 2019). DPPIV inhibitors help to protect both GIP and GLP-1 from degradation, hence suppress postprandial glucagon release, delay gastric emptying and regulate satiety (Singh *et al.*, 2017). Natural phenolic compounds such as curcumin have been shown to reduce blood glucose via DPPIV inhibition as one of their mechanisms (Huang *et al.*, 2019).

In the present study, WSPFE EAF and most of the individual WSPFE fractions inhibited DPPIV, although their inhibitory effects were several orders of magnitude less effective than that of the positive control sitagliptin. Clinical studies to date indicate that DPPIV inhibitors increase native GLP-1 to effectively improve glucose control. These agents have low adverse effects and are well tolerated (Ling *et al.*, 2019), hence they could be better than α-glucosidase inhibitors for improved glycaemic control and lower gastrointestinal side effects in T2DM patients (Li *et al.*, 2019).

Among the individual WSPFE fractions, F2 demonstrated the strongest inhibitory effects against both DPPIV and α-glucosidase, but not α-amylase. However, the components in F2 are presently unknown. On the other hand, F7 only inhibited α-amylase, similar to SD WSPFE and FD WSPFE, but the components of F7 are also unknown. Further studies on the components in these two fractions are warranted.

F1 which contained shikimic acid was found to only inhibit α-glucosidase in the present study, although shikimic acid itself was found inactive as an α-glucosidase inhibitor in a previous study (Pham *et al.*, 2014). However, this discrepancy might be because a fraction, and not pure shikimic acid was used in the present study. In line with this, *Juniperus oxycedrus* subsp. *oxycedrus* berry extracts containing shikimic acid were previously shown to be hypoglycaemic (Orhan *et al.*, 2012).

F5 which contained an indoleacetic acid derivative was shown to inhibit all three α-glucosidase, α-amylase and DPPIV enzymes, in the present study. However, its quantity in WSPFE is the most limited. Indole compounds, which are aromatic nitrogen-containing heterocyclic organic compounds each consisting of a six-membered benzene ring fused to a five-membered pyrrole ring, have been found to a have potential anti-diabetic activities (Zhu *et al.*, 2021), including α-glucosidase and α-amylase inhibitory properties (Sravanthi *et al.*, 2017).

F4 containing *p*-hydroxybenzoic acid and F3 containing protocatechuic acid had lower α-glucosidase and DPPIV inhibitory activities compared to F5. These phenolic acids have two and one hydroxyl groups attached to benzoic acid, respectively. *p*-hydroxybenzoic acid was shown to possess α-glucosidase inhibitory activities in a previous study (Ablat *et al.*, 2017). On the other hand, protocatechuic acid was previously shown to inhibit α-amylase more than α-glucosidase (Adefegha *et al.*, 2015). But this might be because a fraction, and not pure protocatechuic acid was used in the present study.

For α-glucosidase inhibition, hydroxyl groups in phenolic compounds such as flavonoids play an important role in binding with α-glucosidase (Sun and Miao, 2020). On the other hand, methyl and acetate groups decrease this binding (Sarian *et al.*, 2017). For DPPIV inhibition, hydrogen bonding was found to be the main binding mode of all berry and citrus phenolic compounds tested in a previous study (Fan *et al.*, 2013). It would again be helpful to perform *in silico* molecular docking experiments in the future to identify the molecular mechanists of enzymatic inhibition by the major compounds in WSPFE, as well as the structure-activity relationships of individual compounds with these enzymes (Kim *et al.*, 2018; Rasouli *et al.*, 2017).

The α-amylase inhibitory activities of WSPFE samples found in the present study might be caused by non-phenolic rather than the phenolic compounds present in WSPFE samples, in line with a previous study on extracts obtained from bioprocessed pineapple and guava wastes, whereby α-amylase inhibition was caused by the presence of specific compounds, phenolic or not, rather than by the actual concentration of overall fruit phenolics (Sousa and Correia, 2012). Nevertheless, there might still be direct interactions between dietary plant phenolic compounds on starch properties and starch digestion (Sun and Miao, 2020). These might alter starch physical properties and micromolecular arrangements, such as its morphology, hydrogen bond intensity, crystalline structure, thermal stability and spatial configuration (Chen *et al.*, 2020).

F6 which contained three caffeoylshikimic acid isomers did not show inhibitory activities against α-glucosidase, α-amylase or DPPIV. This was in contrast with a previous study which showed that kitul palm (*Caryota urens* L.) inflorescence extract containing caffeoylshikimic acid isomers had significant α-glucosidase and α-amylase inhibitory properties (Ferreres *et al.*, 2021). However, these kitul extracts not only contained caffeoylshikimic acid isomers, but caffeoylquinic acid isomers as well, the latter of which have been shown to have inhibitory effects towards carbohydrate-hydrolysing enzymes (Nyambe-Silavwe and Williamson, 2018).

Bioactivity Comparison Summary of Various WSPFE Samples

Different forms of plant phenolic compounds may confer different anti-diabetic effects. These mechanisms may also vary from one extract or component to another and they may thus, be harnessed to maximise the anti-diabetic effects of these compounds. In the present study, all of the WSPFE samples tested did not inhibit glucose transport, but several had inhibitory effects on α-glucosidase, α-amylase and DPPIV. It is interesting to note that SD WSPFE had stronger inhibitory effects on α-amylase as compared to FD WSPFE. Drying is a major food processing operation to increase shelf life. The choice of drying method however influences product quality, as it is related to the retention of bioactive compounds and biological activities (Abascal *et al.*, 2005). In spray drying, moisture is removed by rapid evaporation on spray droplet under high temperature exposure using hot gas. It is the preferred drying method for thermally sensitive materials such as foods and pharmaceuticals (Verma and Singh, 2015). Conversely, freeze drying involves water removal by sublimation under low pressure (Santo *et al.*, 2013), where much water is removed. This makes a product lightweight, prevents the survival of yeast and bacteria in it, as well as retains its taste, shape and appearance when water is reintroduced. However, freeze drying equipment is expensive, while the process is very time-consuming and labour-intensive. The results obtained in the present study suggest that the spray drying technique is preferable compared to the freeze drying technique in order to retain the potential anti-diabetic bioactivities of WSPFE.

On the other hand, WSPFE EAF had stronger inhibitory effects in all three enzymatic assays carried out, as compared to both SD WSPFE and FD WSPFE. WSPFE contains various components including phenolic acids, indoleacetic acid derivative, shikimic acid, fibre, *etc.*, while its EAF had a higher phenolic content (Leow *et al.*, 2021b).

When compared to most individual WSPFE fractions, WSPFE EAF also consistently inhibited all the three enzymes tested, the other being F5. This suggests that the seven individual WSPFE fractions when given together as WSPFE EAF had additive or synergistic inhibitory effects against these enzymes and may work better in attenuating diabetes as compared to giving individual WSPFE fractions, or even whole WSPFE samples. It was also interesting to note that while WSPFE EAF consistently inhibited all three enzymes tested in the present study, it was not cytotoxic to the Caco-2 colon cancer cells, although additional experiments on normal colon cell lines would be useful to indicate the implied safety of WSPFE EAF.

In terms of individual WSPFE fractions, F2 demonstrated the strongest inhibitory effects towards α-glucosidase and DPPIV, but not α-amylase. This individual fraction should be explored further in future anti-diabetic studies, but its possible cytotoxic effects must be taken into account when designing future experiments. It is again important to emphasise here that F1-F7 were enriched in certain phenolic compounds as mentioned previously and that their effects might also be due to other compounds besides those described.

The anti-diabetic mechanisms investigated in the present study are only a fraction of what is possible. Hence, it would be important that other possible anti-diabetic mechanisms besides those explored in the present study, such as hormonal response to food and modulation of gut flora activities, be investigated as well (Cuervo *et al.*, 2014; Hanhineva *et al.*, 2010; Moco *et al.*, 2012). As such, further pre-clinical studies which investigate the effects of WSPFE using T2DM animal models such as the Nile rat would be useful to explore other *in vivo* anti-diabetic mechanisms. Human intervention clinical trials administering different forms of carbohydrates in healthy volunteers, such as starch, disaccharides and glucose, together with WSPFE, such as that done by Kerimi *et al.* (2019) using oleuropein from olives, would also be useful to confirm the inhibitory effects of WSPFE on carbohydrate-hydrolysing enzymes *in vivo*. It would also be important to carry out studies on postprandial absorption and bioavailability of WSPFE after human consumption *in vivo* to determine its potential anti-diabetic effects on other types of functional insulin-sensitive tissues post-absorption, such as liver, muscle and adipose tissues (Sun and Miao, 2020). Nevertheless, although direct measurements have not been done to confirm the bioavailability of WSPFE, various *in vivo* physiological effects previously observed in animal models and human volunteers as reviewed by Leow *et al.* (2021a) indicate that WSPFE is bioavailable to exert these health functions.

CONCLUSION

Our previous studies in Nile rats demonstrated the potential anti-diabetic properties of WSPFE, but the related mechanisms were unknown. The present study indicated that WSPFE samples did not inhibit glucose uptake, as shown through experiments using *ex vivo* everted mouse intestinal sacs and *in vitro* Caco-2 cell monolayers. The concentrations of WSPFE samples used in the glucose uptake experiments were only up to 500 μg/mL, as the IC_{50} value of the most cytotoxic WSPFE sample against Caco-2 cells, F3, was 544 $\pm$ 48 μg/mL. Further experiments on α-glucosidase, α-amylase and DPPIV enzymes showed that, WSPFE EAF which contained all seven individual WSPFE fractions, consistently had stronger inhibitory effects as compared to SD WSPFE and FD WSPFE. SD WSPFE had better α-amylase inhibitory effects than FD WSPFE. In terms of individual fractions, F2 demonstrated the strongest inhibitory effects against α-glucosidase and DPPIV. Future studies to investigate the effects of these WSPFE samples on carbohydrate digestion and postprandial hyperglycaemia are thus warranted.

ACKNOWLEDGEMENT

REFERENCES

AAT Bioquest (2019). Quest Graph™ IC_{50} calculator. https://www.aatbio.com/tools/ic50-calculator, accessed on 18 June 2021.

Abascal, K; Ganora, L and Yarnell, E (2005). The effect of freeze-drying and its implications for botanical medicine: A review. *Phytother. Res., 19(8)*: 655-660. DOI: 10.1002/ptr.1651.

Ablat, A; Halabi, M F; Mohamad, J; Hasnan, M H H; Hazni, H; Teh, S H; Shilpi, J A; Mohamed, Z and Awang, K (2017). Antidiabetic effects of

Brucea javanica seeds in type 2 diabetic rats. *BMC Complement. Altern. Med., 17(1)*: 94. DOI: 10.1186/s12906-017-1610-x.

Abotaleb, M; Liskova, A; Kubatka, P and Busselberg, D (2020). Therapeutic potential of plant phenolic acids in the treatment of cancer. *Biomolecules, 10(2)*: 221. DOI: 10.3390/biom10020221.

Adefegha, S A; Oboh, G; Ejakpovi, I I and Oyeleye, S I (2015). Antioxidant and antidiabetic effects of gallic and protocatechuic acids: A structure-function perspective. *Comp. Clin. Pathol., 24*: 1579-1585. DOI: 10.1007/s00580-015-2119-7.

Alam, M A; Al-Jenoobi, F I and Al-Mohizea, A M (2012). Everted gut sac model as a tool in pharmaceutical research: Limitations and applications. *J. Pharm. Pharmacol., 64(3)*: 326-336. DOI: 10.1111/j.2042-7158.2011.01391.x.

Alzaid, F; Cheung, H M; Preedy, V R and Sharp, P A (2013). Regulation of glucose transporter expression in human intestinal Caco-2 cells following exposure to an anthocyanin-rich berry extract. *PLoS ONE, 8(11)*: e78932. DOI: 10.1371/journal.pone.0078932.

Anantharaju, P G; Gowda, P C; Vimalambike, M G and Madhunapantula, S V (2016). An overview on the role of dietary phenolics for the treatment of cancers. *Nutr. J., 15(1)*: 99. DOI: 10.1186/s12937-016-0217-2.

Apostolidis, E and Lee, C M (2010). *In vitro* potential of *Ascophyllum nodosum* phenolic antioxidant-mediated α-glucosidase and α-amylase inhibition. *J. Food Sci., 75(3)*: H97-H102. DOI: 10.1111/j.1750-3841.2010.01544.x.

Bahadoran, Z; Mirmiran, P and Azizi, F (2013). Dietary polyphenols as potential nutraceuticals in management of diabetes: A review. *J. Diabetes Metab. Disord., 12(1)*: 43. DOI: 10.1186/2251-6581-12-43.

Bergman, A; Ebel, D; Liu, F; Stone, J; Wang, A; Zeng, W; Chen, L; Dilzer, S; Lasseter, K; Herman, G; Wagner, J and Krishna, R (2007). Absolute bioavailability of sitagliptin, an oral dipeptidyl peptidase-4 inhibitor, in healthy volunteers. *Biopharm. Drug Dispos., 28(6)*: 315-322. DOI: 10.1002/bdd.560.

Bolsinger, J; Pronczuk, A; Sambanthamurthi, R and Hayes, K C (2014). Anti-diabetic effects of palm fruit juice in the Nile rat (*Arvicanthis niloticus*). *J. Nutr. Sci., 3*: e5. DOI: 10.1017/jns.2014.3.

Chatterjee, S; Khunti, K and Davies, M J (2017). Type 2 diabetes. *Lancet, 389(10085)*: 2239-2251. DOI: 10.1016/S0140-6736(17)30058-2.

Chen, H; Yao, K; Nadas, J; Bode, A M; Malakhova, M; Oi, N; Li, H; Lubet, R A and Dong, Z (2012). Prediction of molecular targets of cancer preventing flavonoid compounds using computational methods. *PLoS ONE, 7(5)*: e38261. DOI: 10.1371/journal.pone.0038261.

Chen, N; Gao, H X; He, Q; Yu, Z L and Zeng, W C (2020). Interaction and action mechanism of starch with different phenolic compounds. *Int. J. Food Sci. Nutr., 71(6)*: 726-737. DOI: 10.1080/09637486.2020.1722074.

Cuervo, A; Valdes, L; Salazar, N; De Los Reyes-Gavilan, C G; Ruas-Madiedo, P; Gueimonde, M and Gonzalez, S (2014). Pilot study of diet and microbiota: Interactive associations of fibers and polyphenols with human intestinal bacteria. *J. Agric. Food Chem., 62(23)*: 5330-5336. DOI: 10.1021/jf501546a.

Derosa, G and Maffioli, P (2012). Efficacy and safety profile evaluation of acarbose alone and in association with other antidiabetic drugs: A systematic review. *Clin. Ther., 34(6)*: 1221-1236. DOI: 10.1016/j.clinthera.2012.04.012.

Ehrenkranz, J R L; Lewis, N G; Kahn, C R and Roth, J (2005). Phlorizin: A review. *Diabetes Metab. Res. Rev., 21(1)*: 31-38. DOI: 10.1002/dmrr.532.

Fan, J; Johnson, M H; Lila, M A; Yousef, G and De Mejia, E G (2013). Berry and citrus phenolic compounds inhibit dipeptidyl peptidase IV: Implications in diabetes management. *Evid. Based Complement. Alternat. Med., 2013*: 479505. DOI: 10.1155/2013/479505.

Farrell, T L; Ellam, S L; Forrelli, T and Williamson, G (2013). Attenuation of glucose transport across Caco-2 cell monolayers by a polyphenol-rich herbal extract: Interactions with SGLT1 and GLUT2 transporters. *BioFactors, 39(4)*: 448-456. DOI: 10.1002/biof.1090.

Ferreres, F; Andrade, C; Gomes, N G M; Andrade, P B; Gil-Izquierdo, A; Pereira, D M; Suksungworn, R; Duangsrisai, S; Videira, R A and Valentao, P (2021). Valorisation of kitul, an overlooked food plant: Phenolic profiling of fruits and inflorescences and assessment of their effects on diabetes-related targets. *Food Chem., 342*: 128323. DOI: 10.1016/j.foodchem.2020.128323.

Gomes, W F; Franca, F R M; Denadai, M; Andrade, J K S; Da Silva Oliveira, E M; De Brito, E S; Rodrigues, S and Narain, N (2018). Effect of freeze- and spray-drying on physico-chemical characteristics, phenolic compounds and antioxidant activity of papaya pulp.

J. Food Sci. Technol., 55(6): 2095-2102. DOI: 10.1007/s13197-018-3124-z.

Hamilton, K L and Butt, A G (2013). Glucose transport into everted sacs of the small intestine of mice. *Adv. Physiol. Educ., 37(4)*: 415-426. DOI: 10.1152/advan.00017.2013.

Hanhineva, K; Torronen, R; Bondia-Pons, I; Pekkinen, J; Kolehmainen, M; Mykkanen, H and Poutanen, K (2010). Impact of dietary polyphenols on carbohydrate metabolism. *Int. J. Mol. Sci., 11(4)*: 1365-1402. DOI: 10.3390/ijms11041365.

Holst, J J (2019). The incretin system in healthy humans: The role of GIP and GLP-1. *Metabolism, 96*: 46-55. DOI: 10.1016/j.metabol.2019.04.014.

Horszwald, A; Julien, H and Andlauer, W (2013). Characterisation of *Aronia* powders obtained by different drying processes. *Food Chem., 141(3)*: 2858-2863. DOI: 10.1016/j.foodchem.2013.05.103.

Huang, P K; Lin, S R; Chang, C H; Tsai, M J; Lee, D N and Weng, C F (2019). Natural phenolic compounds potentiate hypoglycemia via inhibition of dipeptidyl peptidase IV. *Sci. Rep., 9(1)*: 15585. DOI: 10.1038/s41598-019-52088-7.

Hubatsch, I; Ragnarsson, E G and Artursson, P (2007). Determination of drug permeability and prediction of drug absorption in Caco-2 monolayers. *Nat. Protoc., 2(9)*: 2111-2119. DOI: 10.1038/nprot.2007.303.

Johnston, K; Sharp, P; Clifford, M and Morgan, L (2005). Dietary polyphenols decrease glucose uptake by human intestinal Caco-2 cells. *FEBS Lett., 579(7)*: 1653-1657. DOI: 10.1016/j.febslet.2004.12.099.

Kakkar, S and Bais, S (2014). A review on protocatechuic acid and its pharmacological potential. *ISRN Pharmacol., 2014*: 952943. DOI: 10.1155/2014/952943.

Kerimi, A; Nyambe-Silavwe, H; Pyner, A; Oladele, E; Gauer, J S; Stevens, Y and Williamson, G (2019). Nutritional implications of olives and sugar: Attenuation of post-prandial glucose spikes in healthy volunteers by inhibition of sucrose hydrolysis and glucose transport by oleuropein. *Eur. J. Nutr., 58(3)*: 1315-1330. DOI: 10.1007/s00394-018-1662-9.

Kim, B R; Kim, H Y; Choi, I; Kim, J B; Jin, C H and Han, A R (2018). DPP-IV inhibitory potentials of flavonol glycosides isolated from the seeds of *Lens culinaris: In vitro* and molecular docking analyses. *Molecules, 23(8)*: 1998. DOI: 10.3390/molecules23081998.

Kim, D; Wang, L; Beconi, M; Eiermann, G J; Fisher, M H; He, H; Hickey, G J; Kowalchick, J E; Leiting, B; Lyons, K; Marsilio, F; Mccann, M E; Patel, R A; Petrov, A; Scapin, G; Patel, S B; Roy, R S; Wu, J K; Wyvratt, M J; Zhang, B B; Zhu, L; Thornberry, N A and Weber, A E (2005). (2R)-4-oxo-4-[3-(trifluoromethyl)-5,6-dihydro[1,2,4]triazolo[4,3-a]pyrazin-7(8H)- yl]-1-(2,4,5-trifluorophenyl)butan-2-amine: A potent, orally active dipeptidyl peptidase IV inhibitor for the treatment of type 2 diabetes. *J. Med. Chem., 48(1)*: 141-151. DOI: 10.1021/jm0493156.

Kim, S Y; Ryu, J S; Li, H; Park, W J; Yun, H Y; Baek, K J; Kwon, N S; Sohn, U D and Kim, D S (2010). UVB-activated indole-3-acetic acid induces apoptosis of PC-3 prostate cancer cells. *Anticancer Res., 30(11)*: 4607-4612.

Leow, S S; Fairus, S and Sambanthamurthi, R (2021a). Water-Soluble Palm Fruit Extract: Composition, biological properties, and molecular mechanisms for health and non-health applications. *Crit. Rev. Food Sci. Nutr*. DOI: 10.1080/10408398.2021.1939648.

Leow, S S; Fairus, S and Sambanthamurthi, R (2021b). Inhibition of cholinesterases by Water-Soluble Palm Fruit Extract. *J. Oil Palm Res*. DOI: 10.21894/jopr.2021.0028.

Li, Z; Zhao, L; Yu, L and Yang, J (2019). Head-to-head comparison of the hypoglycemic efficacy and safety between dipeptidyl peptidase-4 inhibitors and α-glucosidase inhibitors in patients with type 2 diabetes mellitus: A meta-analysis of randomized controlled trials. *Front. Pharmacol., 10*: 777. DOI: 10.3389/fphar.2019.00777.

Ling, J; Cheng, P; Ge, L; Zhang, D H; Shi, A C; Tian, J H; Chen, Y J; Li, X X; Zhang, J Y and Yang, K H (2019). The efficacy and safety of dipeptidyl peptidase-4 inhibitors for type 2 diabetes: A Bayesian network meta-analysis of 58 randomized controlled trials. *Acta Diabetol., 56(3)*: 249-272. DOI: 10.1007/s00592-018-1222-z.

Luz-Madrigal, A; Grajales-Esquivel, E and Del Rio-Tsonis, K (2015). Electroporation of embryonic chick eyes. *Bio. Protoc., 5(12)*: e1498. DOI: 10.21769/BioProtoc.1498.

Lyssenko, V; Jonsson, A; Almgren, P; Pulizzi, N; Isomaa, B; Tuomi, T; Berglund, G; Altshuler, D; Nilsson, P and Groop, L (2008). Clinical risk factors, DNA variants, and the development of type 2 diabetes. *N. Engl. J. Med., 359(21)*: 2220-2232. DOI: 10.1056/NEJMoa0801869.

Manzano, S and Williamson, G (2010). Polyphenols and phenolic acids from strawberry and apple

decrease glucose uptake and transport by human intestinal Caco-2 cells. *Mol. Nutr. Food Res., 54(12)*: 1773-1780. DOI: 10.1002/mnfr.201000019.

Mary, P L and Rao, J P (2002). Phenol red inhibits uptake of phosphate by the everted gut sacs of mice. *Kobe J. Med. Sci., 48(1-2)*: 59-62.

Moco, S; Martin, F P J and Rezzi, S (2012). Metabolomics view on gut microbiome modulation by polyphenol-rich foods. *J. Proteome Res., 11(10)*: 4781-4790. DOI: 10.1021/pr300581s.

Nauck, M A and Meier, J J (2018). Incretin hormones: Their role in health and disease. *Diabetes Obes. Metab., 20 Suppl 1*: 5-21. DOI: 10.1111/dom.13129.

Neubig, R R; Spedding, M; Kenakin, T and Christopoulos, A (2003). International Union of Pharmacology Committee on receptor nomenclature and drug classification. XXXVIII. Update on terms and symbols in quantitative pharmacology. *Pharmacol. Rev., 55(4)*: 597-606. DOI: 10.1124/pr.55.4.4.

Nguyen, P T M; Ngo, Q V; Nguyen, M T H; Maccarone, A T and Pyne, S G (2020a). α-Glucosidase inhibitory activity of the extracts and major phytochemical components of *Smilax glabra* Roxb. *Nat. Prod. J., 10(1)*: 26-32. DOI: 10.2174/2210315509666190124111435.

Nguyen, P T M; Ngo, Q V; Nguyen, M T H; Quach, L T and Pyne, S G (2020b). Hypoglycemic activity of the ethyl acetate extract from *Smilax glabra* Roxb in mice: Biochemical and histopathological studies. *Iran. J. Basic Med. Sci., 23(12)*: 1558-1564. DOI: 10.22038/ijbms.2020.46658.10763.

Nyambe-Silavwe, H and Williamson, G (2018). Chlorogenic and phenolic acids are only very weak inhibitors of human salivary α-amylase and rat intestinal maltase activities. *Food Res. Int., 113*: 452-455. DOI: 10.1016/j.foodres.2018.07.038.

Oboh, G; Ogunsuyi, O B; Ogunbadejo, M D and Adefegha, S A (2016). Influence of gallic acid on α-amylase and α-glucosidase inhibitory properties of acarbose. *J. Food Drug Anal., 24(3)*: 627-634. DOI: 10.1016/j.jfda.2016.03.003.

Olatunji, O J; Chen, H and Zhou, Y (2017). Effect of the polyphenol rich ethyl acetate fraction from the leaves of *Lycium chinense* Mill. on oxidative stress, dyslipidemia, and diabetes mellitus in streptozotocin-nicotinamide induced diabetic rats. *Chem. Biodiversity, 14(10)*: e1700277. DOI: 10.1002/cbdv.201700277.

Ooi, D J; Chan, K W; Sarega, N; Alitheen, N B; Ithnin, H and Ismail, M (2016). Bioprospecting the curculigoside-cinnamic acid-rich fraction from *Molineria latifolia* rhizome as a potential antioxidant therapeutic agent. *Molecules, 21(6)*: 682. DOI: 10.3390/molecules21060682.

Ooi, D J; Adamu, H A; Imam, M U; Ithnin, H and Ismail, M (2018). Polyphenol-rich ethyl acetate fraction isolated from *Molineria latifolia* ameliorates insulin resistance in experimental diabetic rats via IRS1/AKT activation. *Biomed. Pharmacother., 98*: 125-133. DOI: 10.1016/j.biopha.2017.12.002.

Orhan, N; Aslan, M; Pekcan, M; Orhan, D D; Bedir, E and Ergun, F (2012). Identification of hypoglycaemic compounds from berries of *Juniperus oxycedrus* subsp. *oxycedrus* through bioactivity guided isolation technique. *J. Ethnopharmacol., 139(1)*: 110-118. DOI: 10.1016/j.jep.2011.10.027.

Pham, A T; Malterud, K E; Paulsen, B S; Diallo, D and Wangensteen, H (2014). α-Glucosidase inhibition, 15-lipoxygenase inhibition, and brine shrimp toxicity of extracts and isolated compounds from *Terminalia macroptera* leaves. *Pharm. Biol., 52(9)*: 1166-1169. DOI: 10.3109/13880209.2014.880486.

Rasouli, H; Hosseini-Ghazvini, S M; Adibi, H and Khodarahmi, R (2017). Differential α-amylase/α-glucosidase inhibitory activities of plant-derived phenolic compounds: A virtual screening perspective for the treatment of obesity and diabetes. *Food Funct., 8(5)*: 1942-1954. DOI: 10.1039/c7fo00220c.

Rosa, L S; Silva, N J A; Soares, N C P; Monteiro, M C and Teodoro, A J (2016). Anticancer properties of phenolic acids in colon cancer - A review. *J. Nutr. Food Sci., 6*: 468. DOI: 10.4172/2155-9600.1000468.

Rosak, C and Mertes, G (2012). Critical evaluation of the role of acarbose in the treatment of diabetes: Patient considerations. *Diabetes Metab. Syndr. Obes., 5*: 357-367. DOI: 10.2147/DMSO.S28340.

Sambandan, T G; Rha, C K; Sambanthamurthi, R; Sinskey, A J; Tan, Y A; Sundram, K and Wahid, M B (2011). Compositions comprising shikimic acid obtained from oil palm based materials and method of producing thereof. Malaysian Palm Oil Board. *WIPO Patent Application WO 2011/159144*.

Sambanthamurthi, R; Tan, Y A and Sundram, K (2008). Treatment of vegetation liquors derived from oil-bearing fruit. Malaysian Palm Oil Board. *United States Patent US 7387802 B2*.

Sambanthamurthi, R; Tan, Y A; Sundram, K; Abeywardena, M; Sambandan, T G; Rha, C;

Sinskey, A J; Subramaniam, K; Leow, S S; Hayes, K C and Wahid, M B (2011a). Oil palm vegetation liquor: A new source of phenolic bioactives. *Br. J. Nutr., 106(11)*: 1655-1663. DOI: 10.1017/S0007114511002121.

Sambanthamurthi, R; Tan, Y A; Sundram, K; Hayes, K C; Abeywardena, M; Leow, S S; Sekaran, S D; Sambandan, T G; Rha, C; Sinskey, A J; Subramaniam, K; Fairus, S and Wahid, M B (2011b). Positive outcomes of oil palm phenolics on degenerative diseases in animal models. *Br. J. Nutr., 106(11)*: 1664-1675. DOI: 10.1017/S0007114511002133.

Sambanthamurthi, R; Tan, Y A; Omar, W S W; Ali, J M; Sambandan, T G; Yang, M F; Rha, C K and Sinskey, A J (2014). Isolation of a novel bioactive compound obtained from oil palm base materials. Malaysian Palm Oil Board. *WIPO Patent Application WO 2014/209100*.

Sambuy, Y; De Angelis, I; Ranaldi, G; Scarino, M L; Stammati, A and Zucco, F (2005). The Caco-2 cell line as a model of the intestinal barrier: Influence of cell and culture-related factors on Caco-2 cell functional characteristics. *Cell Biol. Toxicol., 21(1)*: 1-26. DOI: 10.1007/s10565-005-0085-6.

Santo, E F D E; Lima, L K F D; Torres, A P C; Oliveira, G D and Ponsano, E H G (2013). Comparison between freeze and spray drying to obtain powder *Rubrivivax gelatinosus* biomass. *Food Sci. Technol., 33*: 47-51. DOI: 10.1590/S0101-20612013005000008.

Sarian, M N; Ahmed, Q U; Mat So'ad, S Z; Alhassan, A M; Murugesu, S; Perumal, V; Syed Mohamad, S N A; Khatib, A and Latip, J (2017). Antioxidant and antidiabetic effects of flavonoids: A structure-activity relationship based study. *Biomed. Res. Int., 2017*: 8386065. DOI: 10.1155/2017/8386065.

Scheepers, A; Joost, H G and Schurmann, A (2004). The glucose transporter families SGLT and GLUT: Molecular basis of normal and aberrant function. *JPEN J. Parenter. Enteral Nutr., 28(5)*: 364-371. DOI: 10.1177/0148607104028005364.

Seidel, C; Schnekenburger, M; Dicato, M and Diederich, M (2014). Antiproliferative and proapoptotic activities of 4-hydroxybenzoic acid-based inhibitors of histone deacetylases. *Cancer Lett., 343(1)*: 134-146. DOI: 10.1016/j.canlet.2013.09.026.

Sekaran, S D; Leow, S S; Abobaker, N; Tee, K K; Sundram, K; Sambanthamurthi, R and Wahid, M B (2010). Effects of oil palm phenolics on tumor cells *in vitro* and *in vivo*. *Afri. J. Food Sci., 4(8)*: 495-502. DOI: 10.5897/AJFS.9000113.

Singh, A K; Jatwa, R; Purohit, A and Ram, H (2017). Synthetic and phytocompounds based dipeptidyl peptidase-IV (DPP-IV) inhibitors for therapeutics of diabetes. *J. Asian Nat. Prod. Res., 19(10)*: 1036-1045. DOI: 10.1080/10286020.2017.1307183.

Sirisena, S; Ng, K and Aljouni, S (2016). Antioxidant activities and inhibitory effects of free and bound polyphenols from date (*Phoenix dactylifera* L.) seeds on starch digestive enzymes. *Int. J. Food Stud., 5*: 212-223. DOI: 10.7455/ijfs/5.2.2016.a9.

Sousa, B A and Correia, R T P (2012). Phenolic content, antioxidant activity and antiamylolytic activity of extracts obtained from bioprocessed pineapple and guava wastes. *Braz. J. Chem. Eng., 29(1)*: 25-30. DOI: 10.1590/S0104-66322012000100003.

Sravanthi, T; Sajitha Lulu, S; Vino, S; Jayasri, M A; Mohanapriya, A and Manju, S L (2017). Synthesis, docking, and evaluation of novel thiazoles for potent antidiabetic activity. *Med. Chem. Res., 26*: 1306-1315. DOI: 10.1007/s00044-017-1851-8.

Striegel, L; Kang, B; Pilkenton, S J; Rychlik, M and Apostolidis, E (2015). Effect of black tea and black tea pomace polyphenols on α-glucosidase and α-amylase inhibition, relevant to type 2 diabetes prevention. *Front. Nutr., 2*: 3. DOI: 10.3389/fnut.2015.00003.

Sun, L and Miao, M (2020). Dietary polyphenols modulate starch digestion and glycaemic level: A review. *Crit. Rev. Food Sci. Nutr., 60(4)*: 541-555. DOI: 10.1080/10408398.2018.1544883.

Tanaka, T; Tanaka, T and Tanaka, M (2011). Potential cancer chemopreventive activity of protocatechuic acid. *J. Exp. Clin. Med., 3(1)*: 27-33. DOI: 10.1016/j.jecm.2010.12.005.

Verma, A and Singh, S V (2015). Spray drying of fruit and vegetable juices - A review. *Crit. Rev. Food Sci. Nutr., 55(5)*: 701-719. DOI: 10.1080/10408398.2012.672939.

Wardman, P (2002). Indole-3-acetic acids and horseradish peroxidase: A new prodrug/enzyme combination for targeted cancer therapy. *Curr. Pharm. Des., 8(15)*: 1363-1374. DOI: 10.2174/1381612023394610.

Xu, H; Leng, X; Wang, M and Zhang, G (2012). Glucose measurement in the presence of tea polyphenols. *Food Anal. Methods, 5*: 1027-1032. DOI: 10.1007/s12161-011-9335-9.

Yee, H S and Fong, N T (1996). A review of the safety and efficacy of acarbose in diabetes mellitus. *Pharmacotherapy, 16(5)*: 792-805. DOI: 10.1002/j.1875-9114.1996.tb02997.x.

Zeng, X; Wang, Y; Qiu, Q; Jiang, C; Jing, Y; Qiu, G and He, X (2012). Bioactive phenolics from the fruits of *Livistona chinensis. Fitoterapia, 83(1)*: 104-109. DOI: 10.1016/j.fitote.2011.09.020.

Zhu, Y; Zhao, J; Luo, L; Gao, Y; Bao, H; Li, P and Zhang, H (2021). Research progress of indole compounds with potential antidiabetic activity. *Eur. J. Med. Chem., 223*: 113665. DOI: 10.1016/j.ejmech.2021.113665.

OPTIMISATION OF REACTION PARAMETERS FOR THE SYNTHESIS OF SOLKETAL LEVULINATE AS POTENTIAL BIODIESEL ADDITIVE

NMD NIK SITI MARIAM[1]*; SENG SOI HOONG[1]; MOHD ZAN ARNIZA[1]; SRIHANUM ADNAN[1]; TUAN NOOR MAZNEE TUAN ISMAIL[1]; SHOOT KIAN YEONG[1] and MUHAMMAD RAHIMI YUSOP[2]

ABSTRACT

Glycerol is a major by-product of biodiesel production and finding new uses for glycerol is crucial to ensure the sustainability and continuance of the biodiesel industry. Thus, the transformation of glycerol into ketal compounds that have potential as additive to improve biodiesel properties, could be an option to provide an outlet for increasing glycerol stock. This study aims to optimise the transesterification reaction to afford solketal levulinate ester (SoLE) in highest yield by reacting solketal with methyl levulinate (ML). The reaction parameters varied are type of base catalyst, catalyst concentration, reaction temperature, reaction time and reactants molar ratio. Under optimised reaction conditions: 1.5% sodium carbonate (Na_2CO_3) catalyst loading, reaction temperature of 140°C, reaction time of 4 hr and molar ratio of 3:1 (solketal:ML), as high as 74.5% yield and 95.0% purity of SoLE was obtained.

INTRODUCTION

Glycerol (propane-1,2,3-triol) is the simplest alcohol with three hydroxyl (OH) group. It is also known as glycerin. Glycerol demonstrates versatile uses in numerous fields such as in food improver, pharmaceutical product, polymer industries, fuel and diesel additive (Anitha *et al.*, 2016). Glycerol (Gly) is made as a by-product commonly from biodiesel production where approximately 10% by volume for every tonne of biodiesel (Karinen and Krause, 2006).

The global growth of biodiesel production over the last decade had caused surplus of glycerol in the marketplace which resulted in decline of glycerol price, hence threaten the economic viability of biodiesel plants. Other than that, glycerol also comes from oleochemical plant. There are currently 19 oleochemical plants operating in Malaysia, which exported approximately 3.28 million tonnes of oleochemicals in 2019 (Parveez *et al.*, 2020). Therefore, new uses of glycerol are needed if the present and future glycerol stock is to be managed (Lapuerta *et al.*, 2015). Glycerol ketals and acetals are among interesting compounds to be explored, as they have been demonstrated as potential additive in the formulation of gasoline, diesel and biodiesel fuels to improve fuel properties (Nanda *et al.*, 2016). Solketal improves cold flow, ignition properties and cetane number of fuels (Kumar *et al.*, 2021), while the use of glycerol acetals in diesel fuels (biodiesel) reduces the viscosity, pour point and particles emission (Torres *et al.*, 2012). Solketal is derived from condensation of glycerol and acetone in the presence of acid catalysts (Deutsch *et al.*, 2007; Li *et al.*, 2012; Suriyaprapadilok and Kitiyanan, 2011). Solketal can be used as a fuel additive to reduce the particulate emission and to improve the cold flow properties of liquid

[1] Malaysian Palm Oil Board,
6 Persiaran Institusi, Bandar Baru Bangi,
43000 Kajang, Selangor, Malaysia.

[2] School of Chemical Sciences and Food Technology,
Faculty of Science and Technology,
Universiti Kebangsaan Malaysia,
43600 Bangi, Selangor, Malaysia.

* Corresponding author e-mail: nsmariam@mpob.gov.my

transportation fuels (Pariente *et al.*, 2009). It helps to reduce the gum formation, improves the oxidation stability, and enhances the octane number when added to gasoline (Mota *et al.*, 2010). Maksimov *et al.* (2011) reported its use as a versatile solvent and a plasticiser in the polymer industry and a solubilising and suspending agent in pharmaceutical preparations.

The free –OH in solketal can also be further reacted to give solketal fatty esters (SFE) via base-catalysed transesterification with fatty acid methyl esters (FAMEs) (Trifoi *et al.*, 2016). Solketal ester and their cyclic group family correspondingly have been reported as a useful fuel additive for enhancing octane number of gasoline (Lozano *et al.*, 2016). Other than that, biodiesels formulations based on mixtures of FAME and fatty acid glycerol formal esters (FAGE) have been described as very efficient for diesel engines. Biodiesel blends up to 20% volume fraction of FAGE, exhibited an excellent suitability as liquid fuel (*e.g.* viscosity, cetane number, adiabatic flame temperature, *etc.*), as it was demonstrated by testing in an automotive engine (Lozano *et al.*, 2016; Nanda *et al.*, 2016; Perosa *et al.*, 2016).

The oil palm industry generates a large quantity of oil palm biomass on yearly basis and it was estimated that in year 2016, the Malaysian palm oil industry generated 80 million tonnes of oil palm biomass (Din *et al.*, 2019). Levulinic acid (LA) is a value-added chemical that can be obtained from lignocellulosic biomass. LA and its derivatives have been used as building blocks for the preparation of new compounds such as levulinate esters, α-valerolactone, acrylic acid and 1,4-pentanediol (Bozell *et al.*, 2000; Girisuta and Heeres, 2017; Rackemann and Doherty, 2011).

The most highlighted LA derivatives are their esters (Adeleye *et al.*, 2019; Castro and Fernandes, 2021; Din *et al.*, 2019; Tiong *et al.*, 2019). The properties of levulinate esters such as methyl and ethyl levulinate (EL) have been investigated for application as gasoline and diesel additives (Liang *et al.*, 2020; Unlu *et al.*, 2018; Vázquez-Castillo *et al.*, 2019; Xu *et al.*, 2020). EL is considered as a bio-based cold flow improver for biodiesel, as it has shown to reduce cloud point of biodiesel and the resultant mixture of biodiesel and EL showed better cold flow properties. It also has additional excellent properties such as clean combustion and low toxicity for fuel additive (Joshi *et al.*, 2011).

High-efficiency process parameters is an inevitable topic of discussion in synthesis process for sustainable synthetic chemistry (Castro and Fernandes, 2021). The synthesis of levulinate ester using LA and short chain alcohol is reported to be conducted mostly via esterification reaction employing different mineral acid catalysts, such as sulphuric acid (H_2SO_4), hydrochloric acid (HCl) and phosphoric acid (H_3PO_4) (Bart *et al.*, 1994;

Liu *et al.*, 2006; Pileidis *et al.*, 2014), and various solid acids, such as sulphonic acid functionalised materials (Oliveira and Teixeira da Silva, 2014; Song *et al.*, 2015). However, we found that the esterification of solketal with LA in the presence of acid catalyst gave unsatisfactory yield of solketal levulinate ester (SoLE). This is due to possibility of hydrolysis of solketal under acidic condition forming undesirable side product. This is in agreement with the work reported by Pouilloux *et al.* (2000), where they reported utilisation of acid catalyst favours side reactions such as degradation of the fatty acid (oxidation, dimerisation) or from the glycerol (polymerisation, dehydration into acrolein, oxidation). Hence, we adopt based-catalysed transesterification of solketal with methyl levulinate (ML), where base catalyst and mL were utilised instead of acid catalyst and LA. Thus, this article reported the further optimisation of reaction parameters such as type of catalyst, effect of reaction duration, temperature and molar ratio of solketal/ML to attain maximum yield of solketal levulinate. To the best of authors' knowledge, no literature reported on the optimisation of transesterification reaction of solketal and levulinic ester for the synthesis of solketal levulinate, which potentially can be used as fuel additive in biodiesel.

MATERIALS AND METHODS

Materials

Refined solketal (99.8% purity) and mL (98.0%) were obtained from Sigma Aldrich, USA. Sodium carbonate (Na_2CO_3) and potassium carbonate (K_2CO_3) were obtained from Systerm, Malaysia. Sodium hydroxide (NaOH) was obtained from R&M Chemicals, Malaysia, and potassium hydroxide (KOH) was obtained from Chemiz, Malaysia. Magnesium oxide (MgO) and sodium methoxide (30% in MeOH, NaOMe) both were obtained from Sigma Aldrich, USA. All the reagents were used without further purification.

Methods

General procedure for the synthesis of solketal levulinate (SoLE). Reactions were carried out in a 50 mL one-neck round bottom flask equipped with a magnetic stirrer. A condenser was attached to the round bottom flask and connected to a vacuum pump to facilitate removal of methanol from the reaction system. Desired amount of solketal, mL and Na_2CO_3 (catalyst) were placed in the flask and heated to the desired temperature. An oil bath equipped with a thermometer was used to monitor the reaction temperature. *Figure 1* is the diagram of the reaction setup. The amount of reagents was

calculated according to the desired mole ratio. The reaction progress was monitored via thin-layer chromatography analysis. After the reaction was completed, the crude mixture was washed with distilled water to remove the basic catalyst, followed by addition of diethyl ether to extract SoLE. The organic layer was concentrated under vacuum using roto-evaporator. Thereafter, the product was evaluated using gas chromatography (GC), proton (^{1}H) and carbon (^{13}C) nuclear magnetic resonance (NMR) spectroscopy and Fourier transform infrared (FTIR) spectroscopy.

Analysis and Characterisation of SoLE

FTIR. A convenient analytical method for determining the functional groups of the SoLE was conducted using Perkin Elmer Spectrum 100 FT-IR Spectrometer equipment with attenuated total reflectance (ATR). Samples were scanned on ATR top plate between 4000 to 650 cm^{-1} wave number with 8 scans per sample at 4 cm^{-1} resolution.

GC analysis. Quantitative analysis of the reaction mixture was conducted using GC. The GC (Agilent System 6890N Network GC System) was equipped with a ZB-5HT INFERNO (30 m x 250 μm x 0.2 μm) capillary column and flame ionisation detector. The following temperature programming was used: oven temperature, 80°C; initial temperature, 80°C; heating rate at 10°C min^{-1}; final temperature, 315°C; injector temperature, 300°C; detector temperature, 325°C; carrier gas, helium at 40.0 mL min^{-1}. The composition of products was determined according to the percent area under the respective peak in the GC chromatogram.

^{1}H and ^{13}C NMR analysis. ^{1}H and ^{13}C NMR spectroscopy were recorded on JOEL JNM-ECZ600R at 600 MHz and 150 MHz, respectively at 298 K with approximately 10% w/v solutions in deuterated NMR solvents. Chemical shifts were quoted in ppm relative to internal standard tetramethylsilane (TMS) and reference to the residual solvent. All coupling constants were quoted in hertz (Hz).

RESULTS AND DISCUSSION

Effect of Reaction Parameters on the Yield of SoLE

Influence of different types of catalysts. SFE can be prepared by the catalytic esterification of fatty acids with solketal (Sankaranarayanan *et al.*, 2017). Acidic homogeneous catalysts, such as H_2SO_4, HCl, hydrogen fluoride (HF) and *p*-toluenesulphonic acid, can be applied for this process. Although the homogeneously acid catalysed processes give high conversion of solketal, they also generates a large amount of waste from the neutralisation and separation of the acidic catalyst (Ilgen *et al.*, 2017). Conversely, the use of base catalysts (*Figure 1*) has advantages that can overcome the drawbacks of acid catalyst. Therefore, in this study, the influences of base catalyst on transesterification of solketal with mL were studied. In this work, base catalysts were tested instead of the acidic catalyst in order to prevent several side reactions associated with acid catalyst such as cleavage of the acetonide of solketal. The following reaction parameters were fixed while several base catalysts were evaluated: mole ratio (ML:solketal) – 1:1.5; reaction temperature of 140ºC; reaction duration of 6 hr.
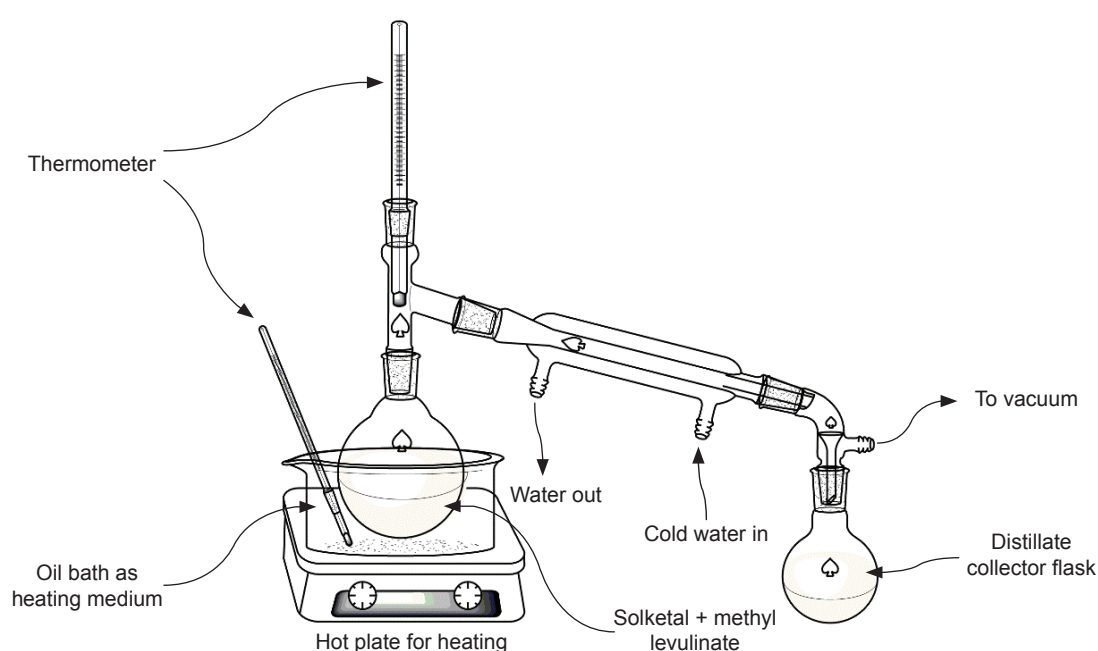

Figure 1. Reaction diagram of transesterification reaction of solketal with methyl levulinate (ML).

Application of base catalyst in transesterification reaction provides faster rate, nearly 4000 times faster than that catalysed by the same amount of an acid catalyst (Fukuda *et al.*, 2001). In this reaction, six homogeneous base catalysts were tested: Na_2CO_3, K_2CO_3, NaOH, KOH, MgO and NaOMe. The effect of different catalysts on the yield of SoLE is illustrated in *Figure 2*.

K_2CO_3 exhibited the best catalytic activity affording the highest yield of SoLE (57.29%), followed by Na_2CO_3 (49.88%) (*Figure 3*). On the other hand, both hydroxide and oxide bases gave low yield of SoLE between 3.80% and 17.36%, respectively. NaOMe was notable to be the paramount catalyst in transesterification of vegetable oil with methanol to produce methyl ester as biodiesel (Atadashi *et al.*, 2013). However, in this reaction, NaOMe generated only 29% yield of SoLE as shown in *Figure 3*. Therefore, we selected the two carbonate bases, K_2CO_3 and Na_2CO_3 as the catalysts for further optimisation.
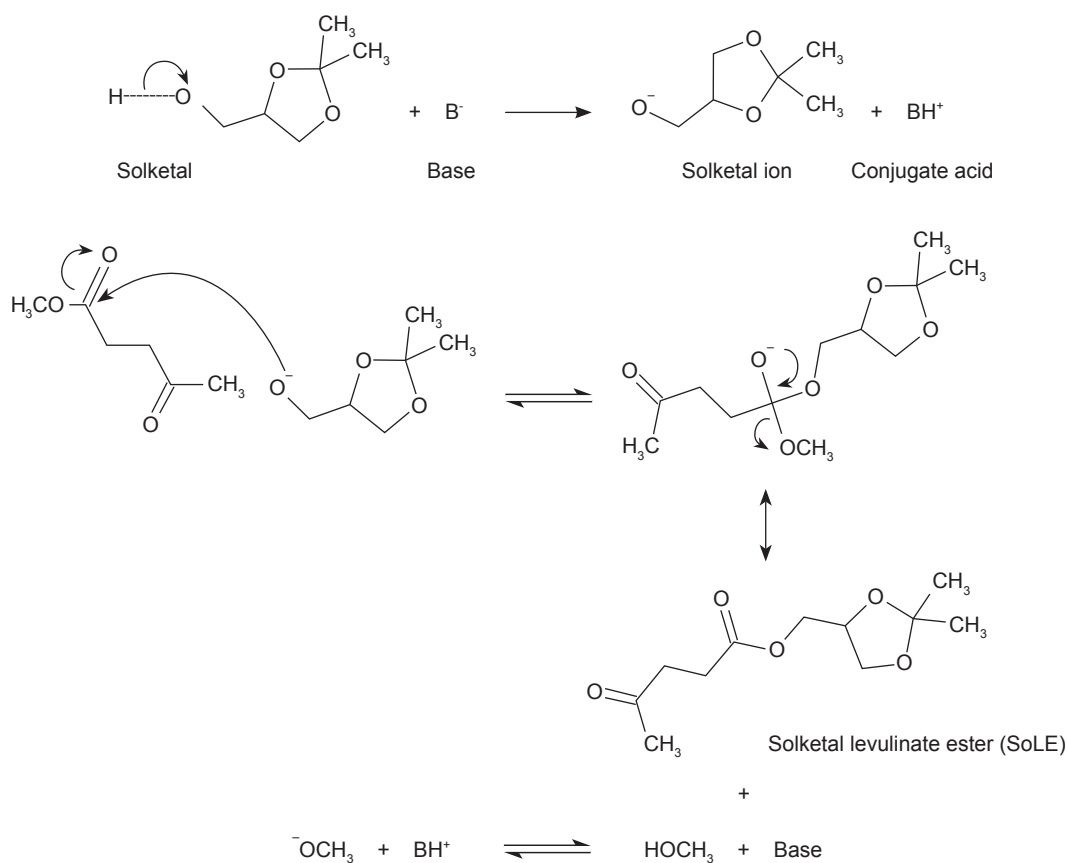
Figure 2. Reaction mechanism of based-catalysed transesterification reaction of solketal with methyl levulinate (ML).
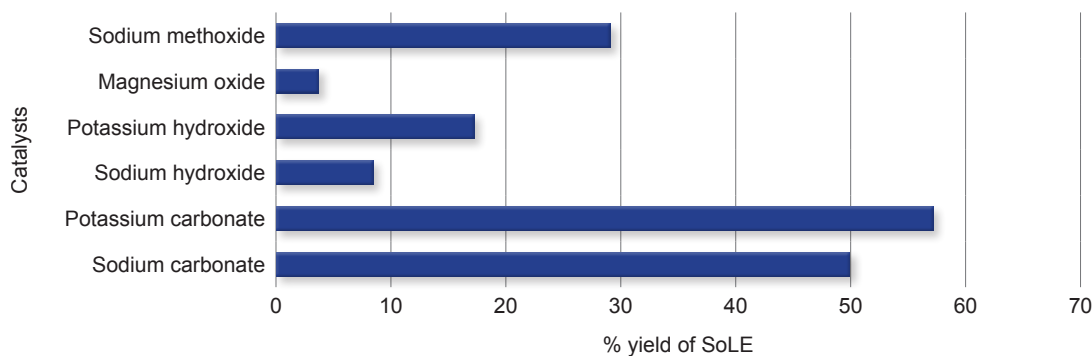

Figure 3. Effect of different type of base catalyst on the yield of SoLE.

527

Influence of Reaction Time on Yield of SoLE

We then investigated the effect of reaction time on the yield of SoLE, while keeping the following reaction parameters constant throughout this set of the experiments and two types of catalysts were used: molar ratio of ML:solketal = 1:3; reaction temperature of 140°C; 1% catalyst loading of K_2CO_3 and Na_2CO_3.

The reaction between solketal and mL was terminated at predetermined reaction duration, which were 2, 3, 4, 6 and 8 hr. The reaction mixture was stirred vigorously in order to achieve perfect contact between the reagents and the catalyst through the process (Ramadhas *et al.*, 2005). The effect of reaction time on the yield of SoLE is shown in *Figure 4*. The results essentially indicated that the yield of SoLE increased with longer reaction time. The result clearly showed that the maximum yield of SoLE was obtained after 4 hr of reaction for Na_2CO_3-catalysed reaction and 6 hr of reaction for K_2CO_3-catalysed reaction. Reaction time of 4 hr is more favourable due to time and cost effective of the reaction. Thus, Na_2CO_3 and reaction time of 4 hr were selected as the catalyst and optimum reaction time, respectively for the transesterification process. The selected catalyst is in agreement with a study reported by Yu *et al.* (2003) that employed Na_2CO_3 as the catalyst in transesterification of solketal with fatty acid such as stearic acid.
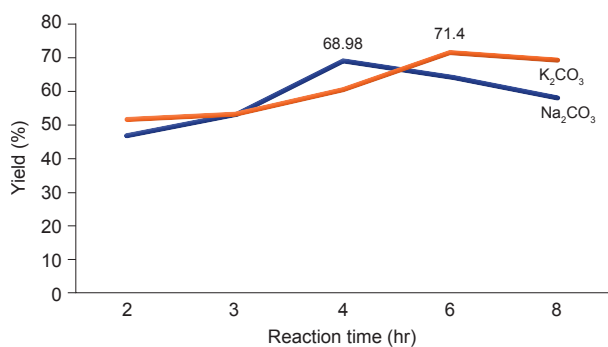

Figure 4. The effect of reaction time on the yield of SoLE.

Influence of Catalyst Loading

It is well documented that esterification/transesterification reactions require acid/base catalysts and the strength of the acid/base used is an important factor affecting the kinetics of the reaction (Rastegari and Ghaziaskar, 2015). The amount of catalyst in a reaction system will greatly influence the effectiveness of the catalyst. Therefore, in order to study the effect of catalyst loading on the yield of SoLE, the following reaction parameters were fixed as follow: molar ratio of ML:solketal = 1:3; reaction temperature of 140°C; reaction time of 4 hr.

The catalyst loading was varied from 1.0% to 3.0%. The change of yield of SoLE in respect to catalyst concentration is shown in *Figure 5*. The result showed that the yield of SoLE increased gradually with higher catalyst loading up to 1.5% and slightly decreased at catalyst loading higher than 1.5%. The highest yield of SoLE obtained with 1.5% catalyst was 74.6%. Other than that, excess addition of catalyst will lead to SoLE with darker colour. In the next stage of study, Na_2CO_3 loading amount of 1.5% will be used in subsequent sections of the study.
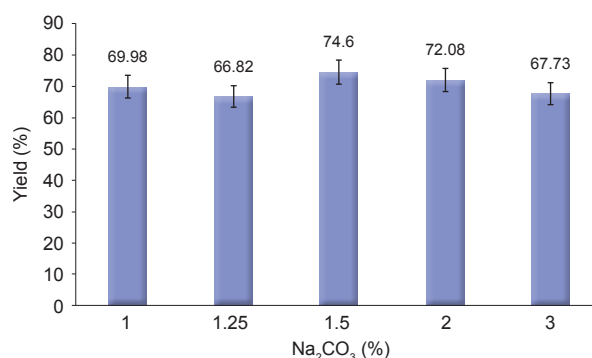

Figure 5. Effect of catalyst loading on the yield of solketal.

Influence of Molar Ratio of mL to Solketal

The mole ratio of mL to solketal is one of the most important variables affecting the yield of SoLE. Stoichiometrically, one mole of solketal is required per mole of ML, but in practice an excess of alcohol is employed in order to displace the equilibrium to produce more ester. The molar ratio of mL to solketal was varied from 1:2 to 1:4.5, while the other reaction parameters were kept constant as follow: Na_2CO_3 (1.5%); reaction temperature of 140°C; reaction duration of 4 hr. *Figure 6* shows the yield of SoLE against molar ratio of mL to solketal. Molar ratio of 1:3 (ML:solketal) was the optimum mole ratio that gave best yield of SoLE of 74.6%. When the amount of solketal was increased above or reduced below the optimal amount, the reaction condition did not increase the yield of SoLE. Hence, molar ratio of 1:3 will be used for the next section of the study.
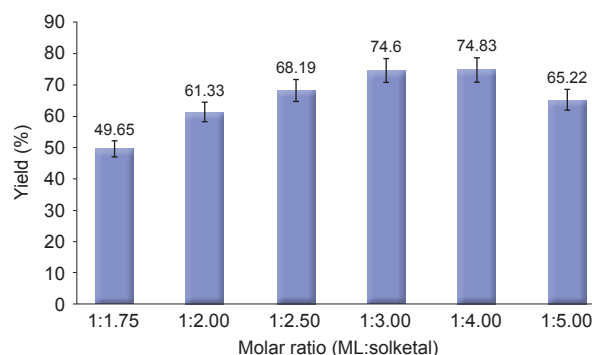

Figure 6. Effect of molar ratio (ML:solketal) on the yield of SoLE.

Effects of Reaction Temperature

Temperature is a significant factor that affects the transesterification reaction, where relatively it will influence the yield of product. To determine the effect of reaction temperature on the yield of SoLE, the reaction temperature was varied from 80°C to 160°C, while the other reaction parameters were kept constant as follow: molar ratio of ML:solketal = 1:3; Na_2CO_3 (1.5%); reaction time of 4 hr. *Figure 7* shows the yield of SoLE against reaction temperature. The figure shows that the yield of SoLE gradually increased until the reaction temperature of 140°C, giving 74.6% yield. As the reaction temperature continue to increase, the yield of SoLE slightly decreased. According to results, reaction temperature of 140°C gave the highest yield of SoLE and it was regarded to be the optimum value.
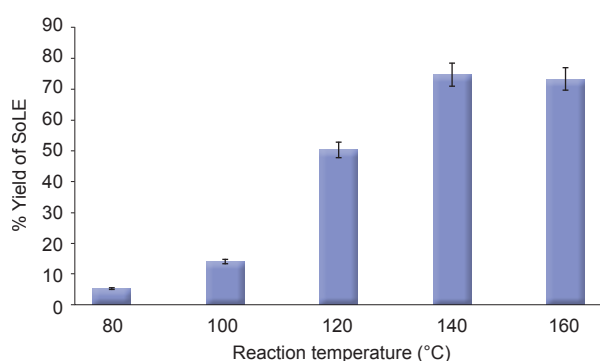
Figure 7. Effect of reaction temperature on the yield of SoLE.

Characterisation of SoLE

FTIR spectra. FTIR spectra of both solketal and mL were compared with the product in order to prove that the esterification reaction between solketal and mL had taken place. In the FTIR spectra (*Figure 8*), the absorption band at 3421 cm^{-1} assigned to C-OH stretching of hydroxyl group of solketal had almost flattened, indicating reaction had happened at the -OH group and SoLE was produced.

^{1}H and ^{13}C NMR analysis. *Figure 9* shows the ^{1}H- and ^{13}C-NMR spectra of SoLE. The chemical shift at 1.32 and 1.4 ppm in ^{1}H-NMR spectrum (*Figure 9a*) correspond to two prominent methyl groups (-CH$_3$) in solketal. The protons attached adjacent to ketone-carbonyl and ester-carbonyl in mL were featured at 2.16 (H), 2.58 (G) and 2.73 (F) ppm, respectively. Peaks between 3.70 (C) and 4.30 (D) ppm were related to the protons of –CH$_2$– and –CH– central carbon in the glyceride unit correspondingly. Lost of CH$_2$–OH protons peak in this region marked the occurance of transesterification reaction between mL and solketal. For the ^{13}C-NMR spectrum (*Figure 9b*), the prominent paired methyl group in solketal (B and A) appeared at 25.4 and 26.7 ppm, respectively. The glyceride carbons present in –CH$_2$– groups (C) and central carbon (D) can be observed at 64.9 to 73.6 ppm, correspondingly. In addition, peaks at 27.8 ppm and 37.9 ppm (F) correspond to the –CH$_2$– group adjacent to ester and ketone group, respectively. While peak at 29.9 ppm (H) relates to –CH$_3$ group of ML.
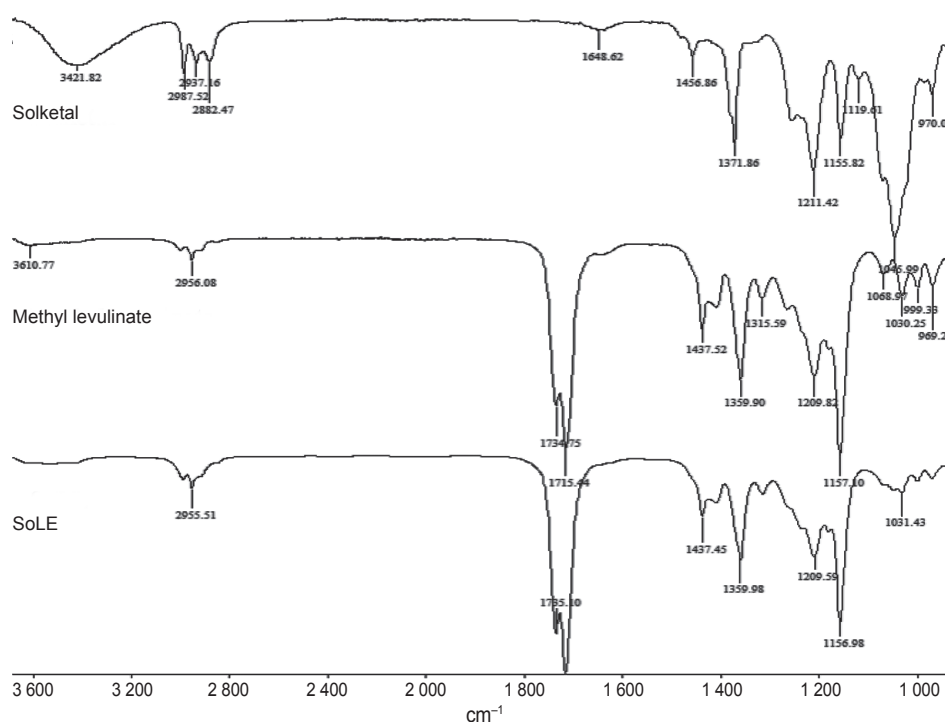
Figure 8. Fourier transform infrared (FTIR) spectrum of SoLE obtained from Na$_2$CO$_3$-catalysed transesterification between solketal and methyl levulinate (ML) at 1:3 molar ratios and at 140°C for 4 hr.
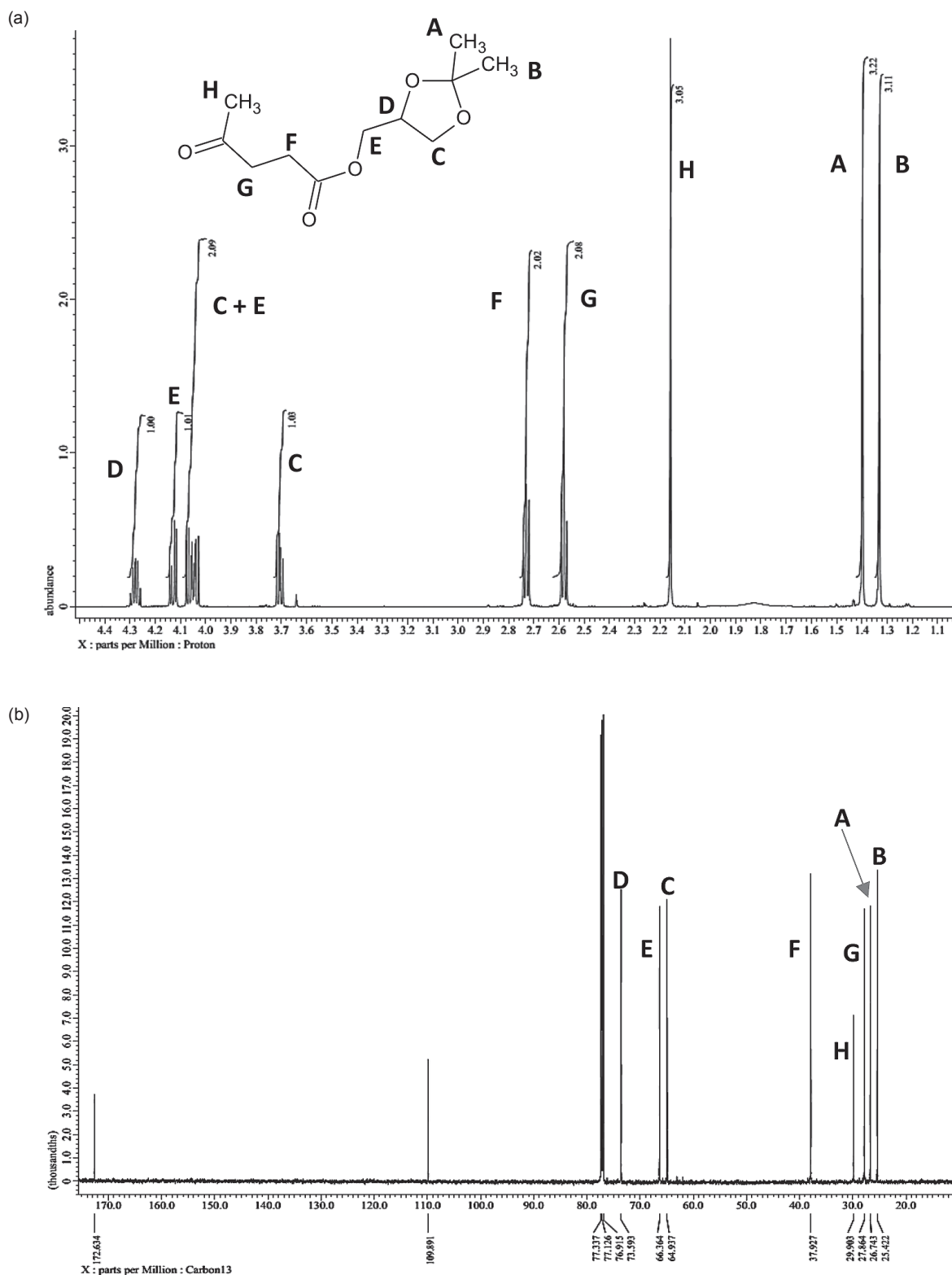
Figure 9. (a) The ¹H-NMR and (b) ¹³C-NMR spectrum of SoLE obtained from Na₂CO₃-catalysed transesterification between solketal and mL at 1:3 mole ratio, 140°C for 4 hr.

GC analysis of SoLE. The formation of SoLE was confirmed qualitatively via GC analysis. The GC chromatogram of the product confirmed that the synthesised product contains high percent composition of SoLE (95%) as represented by a peak at retention time at 11.79 min (*Figure 10*). The chromatogram also indicated the existence of two other minor products with low percent composition namely methly levulinate and solketal, which appeared at 4.63 min and 5.83 min, respectively.
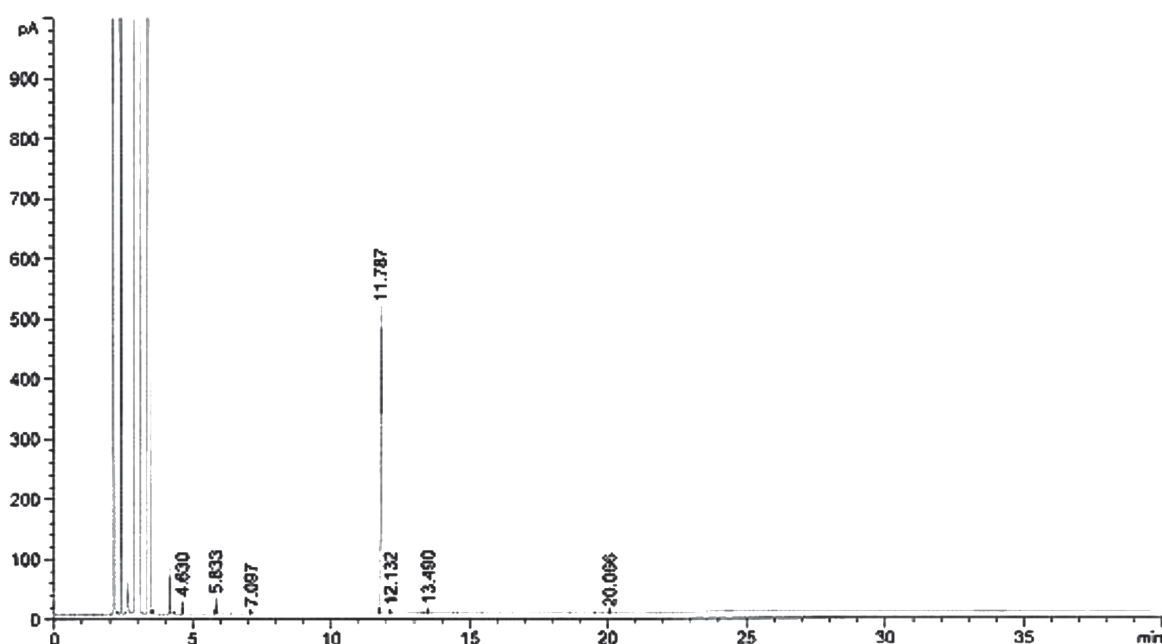
Figure 10. Gas chromatography (GC) chromatogram of solketal levulinate ester (SoLE) obtained from sodium carbonate (Na$_2$CO$_3$)-catalysed esterification between solketal (Sol) and methyl levulinate (ML) at 1:3 mole ratios and at 140°C for 4 hr.

Potential Uses of SoLE

Solketal esters has interesting properties that are between those of cyclic acetal and glycerol ester. While current uses of solketal ester are still limited, solketal ester is proposed as a promising bio-based alternative in both direct and indirect applications.

Solketal has been reported to be applied as a fuel improver. Solketal was showed to decrease the particulate emission and enhanced the cold flow properties of liquid transportation fuels (Pariente *et al.*, 2009). It helps to reduce the gum formation, improves the oxidation stability, and enhances the octane number when added to gasoline (Mota *et al.*, 2010). Maksimov *et al.* (2011) described its use as a multipurpose solvent and a plasticiser in the polymer industry and a solubilising and suspending agent in pharmaceutical preparations.

Solketal and their cyclic group members has been reported as a useful fuel additive for enhancing octane number of gasoline. It was reported to reduce the gum formation and increased the octane number of gasolin (Lozano *et al.*, 2016; Mota *et al.*, 2010; Nanda *et al.*, 2016). Lozano *et al.* (2016) has reported on producing oxygenated biofuels, based on FAME and fatty acid solketal ester mixtures, by lipase-catalysed transesterification of several vegetable oils or direct esterification of free fatty acid with methanol or solketal in ionic liquid. Other than that biodiesels formulations based on mixtures of FAME and FAGE have been described as very efficient for diesel engines. Biodiesel blends up to 20% volume fraction (vol.%) of FAGE, exhibitied an excellent suitability as liquid fuel (*e.g.*, viscosity, cetane number, adiabatic flame temperature, *etc.*),

as it was demonstrated by testing in an automotive engine (Lapuerta *et al.*, 2015; Lozano *et al.*, 2016; Nanda *et al.*, 2016; Perosa *et al.*, 2016).

Since solketal ester has attracted considerable attention in the fuel and biodiesel sector. We have evaluated the fuel properties of biodiesel blend with SoLE. The density of the mixture increased upon addition of SoLE. The blended biodiesel became slightly viscous with increasing SoLE amounts. The acid number of biodiesel increased upon blending with SoLE. The pour point of biodiesel was lowered to 14°C by the addition of 20 vol. % SoLE. The blending with SoLE had improved the cold flow performance of the biodiesel. The cloud point of biodiesel was also improved with the addition of 20 vol. % SoLE. This work will assist in further evaluation of SoLE as cold flow improver of biodiesel fuel.

On the other hand, solketal ester also has been reported to show potential as antimicrobial agent by Mendoza-Ortiz *et al.* (2020). In their study, they reported that solketal palmitate had showed antifungal activity against *Candida albicans* and *Candida parapsilosis*, with minimum inhibitory concentration (MIC) between 200 and 400 μg mL^{-1}.

CONCLUSION

In this study, SoLE was successfully synthesised in the presence of basic catalyst, Na$_2$CO$_3$ (1.5%). Optimum reaction temperature and reaction time to obtain high yield of SoLE were 140°C for 4 hr reaction. The best molar ratio to obtain high yield of SoLE was 1:3 of ML:solketal. Analysis by GC, FTIR

and NMR confirmed the structure and composition of SoLE. The highest yield of SoLE obtained using the optimised parameters was 75% with the purity of 95%. The optimised reaction procedure to synthesise SoLE may give opportunity to industrial players in specialty chemical for production at larger scale. As described in potential application of SoLE, this research prospective will increase the uses of glycerol and chemical derived from biomass, which can boost the momentum of green chemical usage in fuel industry.

ACKNOWLEDGEMENT

REFERENCES

Adeleye, A T; Louis, H; Akakuru, O U; Joseph, I; Enudi, O C and Michael, D P (2019). A review on the conversion of levulinic acid and its esters to various useful chemicals. *AIMS Energy, 7(2)*: 165-185. DOI: 10.3934/energy.2019.2.165.

Anitha, M; Kamarudin, S K and Kofli, N T (2016). The potential of glycerol as a value-added commodity. *Chem. Eng. J., 295*: 119-130. DOI: 10.1016/J.CEJ.2016.03.012.

Atadashi, I M; Aroua, M K; Sulaiman, N M N and Abdul Aziz, A R (2013). The effects of catalysts in biodiesel production - A review. *J. Ind. Eng. Chem., 19(1)*: 14-26. DOI: 10.1016/j.jiec.2012.07.009.

Bart, H J; Reidetschlager, J; Schatka, K and Lehmann, A (1994). Kinetics of esterification of levulinic acid with *n*-butanol by homogeneous catalysis. *Ind. Eng. Chem. Res., 33*: 21-25.

Bozell, J J; Moens, L; Elliott, D C; Wang, Y; Neuenscwander, G G; Fitzpatrick, S W; Bilski, R J and Jarnefeld, J L (2000). Production of levulinic acid and use as a platform chemical for derived products. *Resour. Conserv. Recycl., 28*: 227-239.

Castro, G A D and Fernandes, S A (2021). Microwave-assisted green synthesis of levulinate esters as biofuel precursors using calix[4]arene as an organocatalyst under solvent-free conditions. *Sustain. Energ. Fuels, 5*: 108-111. DOI: 10.1039/D0SE01257B.

Deutsch, J; Martin, A and Lieske, H (2007). Investigations on heterogeneously catalysed condensations of glycerol to cyclic acetals. *J. Catal., 245(2)*: 428-435. DOI: 10.1016/j.jcat.2006.11.006.

Din, N S M N M; Kian, Y S; Soi, H S; Zan, A M; Adnan, S and Yusop, R M (2019). Synthesis of glycerol trilevulinate ester: Effect of reaction parameters. *J. Oil Palm Res., 31*: 624-633.

Fukuda, H; Kondo, A and Noda, H (2001). Biodiesel fuel production by transesterification of oils. *J. Biosci. Bioeng., 92(5)*: 405-416. DOI: 10.1016/S1389-1723(01)80288-7.

Girisuta, B and Heeres, H J (2017). Levulinic acid from biomass: Synthesis and applications. *Production of Platform Chemicals from Sustainable Resources. Biofuels and Biorefineries* (Fang, Z; Smith, Jr. R and Qi X eds.). Springer, Singapore. p. 143-169.

Ilgen, O; Yerlikaya, S and Akyurek, F (2017). Synthesis of solketal from glycerol and acetone over amberlyst-46 to produce an oxygenated fuel additive. *Period. Polytech. Chem. Eng., 61(2)*: 144-148. DOI: 10.3311/PPch.8895.

Joshi, H; Moser, B; Toler, J; Smith, W and Walker, T (2011). Ethyl levulinate: A potential bio-based diluent for biodiesel which improves cold flow properties. *Biomass Bioenerg., 35(7)*: 3262-3266. DOI: 0.1016/j.biombioe.2011.04.020.

Karinen, R S and Krause, A O I (2006). New biocomponents from glycerol. *Appl. Catal. A Gen., 306*: 128-133. DOI: 10.1016/j.apcata.2006.03.047.

Kumar, P; Kumar, S; Shah, S and Kumar, S (2021). Study of performance parameters and emissions of four stroke ci engine using solketal-biodiesel blends. *SN Appl. Sci., 3(59)*. DOI: 10.1007/s42452-020-04073-3.

Lapuerta, M; Rodríguez-Fernández, J; Estevez, C and Bayarri, N (2015). Properties of fatty acid glycerol formal ester (FAGE) for use as a component in blends for diesel engines. *Biomass Bioenerg., 76*: 130-140. DOI: 10.1016/j.biombioe.2015.03.008.

Li, L; Korányi, T I; Sels, B F and Pescarmona, P P (2012). Highly-efficient conversion of glycerol to solketal over heterogeneous Lewis acid catalysts. *Green Chem., 14*: 1611-1619.

Liang, X; Fu, Y and Chang, J (2020). Sustainable production of methyl levulinate from biomass in ionic liquid-methanol system with biomass-based catalyst. *Fuel, 259*: 116246. DOI: 10.1016/j.fuel.2019.116246.

Liu, Y; Lotero, E and Goodwin Jr., J G (2006). A comparison of the esterification of acetic acid with methanol using heterogeneous versus homogeneous acid catalysis. *J. Catal., 242(2)*: 278-286. DOI: 10.1016/j.jcat.2006.05.026.

Lozano, P; Gomez, C; Nicolas, A; Polo, R; Nieto, S; Bernal, J M; García-Verdugo, E and Luis, S V (2016). Clean enzymatic preparation of oxygenated biofuels from vegetable and waste cooking oils by using spongelike ionic liquids technology. *ACS Sustainable Chem. Eng., 4*: 6125-6132. DOI: 10.1021/acssuschemeng.6b01570.

Maksimov, A L; Nekhaev, A I; Ramazanov, D N; Arinicheva, Y A; Dzyubenko, A A and Khadzhiev, S N (2011). Preparation of high-octane oxygenate fuel components from plant-derived polyols. *Pet. Chem., 51*: 61-69.

Mendoza-Ortiz, P A; Gama, R S; Gómez, O C; Luiz, J H H; Fernandez-Lafuente, R; Cren, E C and Mendes, A A (2020). Sustainable enzymatic synthesis of a solketal ester - Process optimization and evaluation of its antimicrobial activity. *Catalysts, 10(2)*: 218. DOI: 10.3390/catal10020218.

Mota, C J A; da Silva, C X A; Rosenbach, N; Costa, J and da Silva, F (2010). Glycerin derivatives as fuel additives: The addition of glycerol/acetone ketal (solketal) in gasolines. *Energy Fuels, 24*: 2733-2736. DOI: 10.1021/ef9015735.

Nanda, M R; Zhang, Y; Yuan, Z; Qin, W; Ghaziaskar, H S and Xu, C (2016). Catalytic conversion of glycerol for sustainable production of solketal as a fuel additive: A review. *Renew. Sust. Energ. Rev., 56*: 1022-1031. DOI: 10.1016/j.rser.2015.12.008.

Oliveira, B L and da Silva, V T (2014). Sulfonated carbon nanotubes as catalysts for the conversion of levulinic acid into ethyl levulinate. *Catalysis Today, 234*: 257-263. DOI: 10.1016/j.cattod.2013.11.028.

Pariente, S; Tanchoux, N and Fajula, F (2009). Etherification of glycerol with ethanol over solid acid catalysts. *Green Chem., 11*: 1256-1261. DOI: 10.1039/B905405G.

Parveez, G K A; Hishamuddin, E; Loh, S K; Ong-Abdullah, M; Salleh, K M; Bidin, M N I Z; Sundram, S; Hasan, Z A A and Idris, Z (2020). Oil palm economic performance in Malaysia and R&D progress in 2019. *J. Oil Palm Res., 32(2)*: 159-190. DOI: 10.21894/jopr.2020.0032.

Perosa, A; Moraschini, A; Selva, M and Noè, M (2016). Synthesis of the fatty esters of solketal and glycerol-formal: Biobased specialty chemicals. *Molecules, 21*: 170-178. DOI: 10.3390/molecules21020170.

Pileidis, F D; Tabassum, M; Coutts, S and Titirici, M M (2014). Esterification of levulinic acid into ethyl levulinate catalysed by sulfonated hydrothermal carbons. *Chinese J. Catalysis, 35*: 929-936. DOI: 10.1016/S1872-2067(14)60125-X.

Rackemann, D W and Doherty, W O (2011). The conversion of lignocellulosics to levulinic acid. *Biofuels, Bioprod. Bioref., 5(2)*: 198-214. DOI: 10.1002/bbb.267.

Ramadhas, A S; Jayaraj, S and Muraleedharan, C (2005). Characterization and effect of using rubber seed oil as fuel in the compression ignition engines. *Renew. Energy, 30*: 795-803. DOI: 10.1016/j.renene.2004.07.002.

Rastegari, H and Ghaziaskar, H S (2015). From glycerol as the by-product of biodiesel production to value-added monoacetin by continuous and selective esterification in acetic acid. *J. Ind. Eng. Chem., 21*: 856-861. DOI: 10.1016/j.jiec.2014.04.023.

Sankaranarayanan, S; Jindapon, W and Ngamcharussrivichai, C (2017). Valorization of biodiesel plant-derived products via preparation of solketal fatty esters over calcium-rich natural materials derived oxides. *J. Taiwan Inst. Chem. Eng., 81*: 57-64. DOI: 10.1016/j.jtice.2017.10.007.

Song, D; An, S; Lu, B; Guo, Y and Leng, J (2015). Arylsulfonic acid functionalized hollow mesoporous carbon spheres for efficient conversion of levulinic acid or furfuryl alcohol to ethyl levulinate. *Appl. Catal. B: Environ., 179*: 445-457. DOI: 10.1016/j.apcatb.2015.05.047.

Suriyaprapadilok, N and Kitiyanan, B (2011). Synthesis of solketal from glycerol and its reaction with benzyl alcohol. *Energy Procedia, 9*: 63-69. DOI: 10.1016/j.egypro.2011.09.008.

Tiong, Y W; Yap, C L; Gan, S and Yap, W S P (2019). Optimisation studies on the conversion of oil palm biomass to levulinic acid and ethyl levulinate via indium trichloride-ionic liquids: A response surface methodology approach. *Ind. Crops Prod., 128*: 221-234.

Torres, M; Jiménez-Osés, G; Mayoral, J A; Pires, E and de Los Santos, M (2012). Glycerol ketals: Synthesis and profits in biodiesel blends. *Fuel, 94*: 614-616. DOI: 10.1016/j.fuel.2011.11.062.

Trifoi, A R; Agachi, P Ş and Pap, T (2016). Glycerol acetals and ketals as possible diesel additives. A review of their synthesis protocols. *Renew. Sust. Energ. Rev., 62*: 804-814.

Unlu, D; Boz, N; Ilgen, O and Hilmioglu, N (2018). Improvement of fuel properties of biodiesel with

bioadditive ethyl levulinate. *Open Chem., 16*: 647-652. DOI: 10.1515/chem-2018-0070.

Vázquez-Castillo, J A; Contreras-Zarazúa, G; Segovia-Hernández, J G and Kiss, A A (2019). Optimally designed reactive distillation processes for eco-efficient production of ethyl levulinate. *J. Chem. Technol. Biotechnol., 94*: 2131-2140. DOI: 10.1002/jctb.6033.

Xu, Y; Guo, P; Chang, C; Li, P; Zhao, S and Xu, G (2020). Aluminum chloride-catalyzed conversion of levulinic acid to methyl levulinate: Optimization

and kinetics. *J. Chem. Technol. Biotechnol., 95(8)*: 2251-2260. DOI: 10.1002/jctb.6413.

Pouilloux, Y; Me´tayer, S and Barrault, J (2000). Synthesis of glycerol monooctadecanoate from octadecanoic acid and glycerol. Influence of solvent on the catalytic properties of basic oxides. *C. R. Acad. Sci. - Series IIC – Chem., 3*: 589-594.

Yu, C C; Lee, Y S; Cheon, B S and Lee, S H (2003). Synthesis of glycerol monostearate with high purity. *Bull. Korean Chem. Soc., 24(8)*: 1229-1231.

PALM-BASED CHOCOLATE SPREAD FOR WIDE RANGE TEMPERATURE APPLICATIONS USING SUNFLOWER WAX, CARNAUBA WAX AND BEES WAX

NORAZURA AILA MOHD HASSIM[1]*; SIVARUBY KANAGARATNAM[1]; NUR HAQIM ISMAIL[1]; NOOR LIDA HABI MAT DIAN[1]; WAN ROSNANI AWG ISA[1] and NOOR SOFFALINA SOFIAN SENG[2]

ABSTRACT

The study was conducted to produce chocolate spread (CS) with a wide range temperature applications (5°C-45°C) by using blended base oil [50% palm superolein (POOo) and 50% sunflower oil (SFO)] and different types of waxes [0%-3.5% sunflower wax (SFW), carnauba wax (CW) and bees wax (BW)]. The waxes were added to impart solid-like property to a low saturated fatty acids oil blend in the CS. The main analysis for the oil system without wax (OSWW) was solid fat content (SFC) while the analysis for CS using these oils was hardness and spreadability. Main analyses for the oil system with wax (OSW) were SFC as well as hardness, spreadability and stability of CS containing different percentage of OSW. POOo:SFO at 50:50 ratio was chosen as OSWW as its SFC was not affected by temperature, and its CS showed good spreadability at 5°C which provided lower significant hardness than commercial CS at 5°C. CS produced from OSW of 3.5% SFW and 3.5% CW showed promising outcome with no phase separation at 5°C-40°C after 24 hr of storage and good spreadability (hardness of 1636 g_f and 1492 g_f respectively) compared to commercial CS (hardness of 2105 g_f) which showed no spreadability at 5°C.

INTRODUCTION

Chocolate spread (CS) is a type of confectionery and is loved by all walks of life especially children. It is usually spread on bread, pancakes or used as filling in bakery products. CS contains oils and fats that provide desirable physical properties such as spreadability and structural stability to it. These physical properties depend on the chemical structure of the oils and fats, especially on the fatty acid (FAC) and triacylglycerols (TAG) compositions. Traditional or common CS uses oils and fats from partial hydrogenation process to obtain the desirable physical properties. However, partial hydrogenation product contains *trans* fatty acid that is detrimental to health in which United States of America (USA) Food and Drug Administration (FDA) has banned the use of this fat (Kushairi *et al.*, 2018). Alternatives to *trans* fatty acid have been sought after by manufacturers as well as researchers and some of the alternatives found are palm fractions [palm oil (PO), palm olein (POo), palm stearin (POs), as well as red POo] and butter fat or blended palm fractions with other vegetable oils (El-Hadad *et al.*, 2011; El-Kalyoubi *et al.*, 2011; Jeyarani *et al.*, 2013). Some food manufacturers used special processing techniques (*e.g.*, tailor-made fractionation) to minimise *trans* fatty acid (Roe *et al.*, 2013).

CS should be stable at room temperature for at least 6-12 months (Shamsudin, 2004). CS will show phase separation/oil out (instable) at higher temperature (especially summer of

[1] Malaysian Palm Oil Board,
6 Persiaran Institusi, Bandar Baru Bangi,
43000 Kajang, Selangor, Malaysia.

[2] Universiti Kebangsaan Malaysia,
43600 UKM Bangi, Selangor, Malaysia.

* Corresponding author email: azuraaila@mpob.gov.my

40°C and above) and solidify at low temperature (especially winter of 10°C and below). The oil out and solidification scenarios are common for a four-season country. These scenarios will eventually affect the stability of the CS especially during storage and transportation as in most cases air-conditioning is not provided during these two conditions. Therefore, there is a need to formulate a chocolate that is stable at a wide range of temperature (5°C-45°C).

In formulating a CS of good spreadability and structurally stable at wide temperature range (5°C-45°C), wax containing high percentage of wax ester might be suitable as they can act as gelling agent to the oil by trapping the oil in a three-dimensional (3D) network to mimic solid fat (Manzocco et al., 2017). For example, wax ester of sunflower wax (SFW) is 75.0%-85.0% (Endlein and Peleikis, 2011), carnauba wax (CW) is 96.0%-97.0% (Doan et al., 2017) and bees wax (BW) is 46.9%-82.0% (Aguilar et al., 2007). The percentage of wax ester might affect gelling process of the oil system without wax (OSWW) and consequently, affect hardness and spreadability of CS. Other wax components such as fatty acid, fatty alcohol and n-alkane are present in small amounts and will less influence the gelling process in producing CS. FDA has approved natural waxes as ingredient and additive in food (Rocha et al., 2013). Gelling of soft oil such as rice bran oil, soybean oil and rapeseed oil is common in current research (Doan et. al., 2015; Patel et al., 2014; Wolfer et al., 2018). However, gelling of POo or palm superolein (POOo) or its combination with other vegetable oils is not much studied. Saw et al. (2020) studied the gelling effect of POOo with many gellators and found that SFW oleogel with at least 1% SFW was stable for 90 days at 15°C, 20°C and 25°C. There was no literature found on the stability of CS at wide range of temperature by using POOo as the OSWW. However, Patel et al. (2014) reported that shellac oleogel (with rapeseed oil) was able to substitute 27% of PO in a CS formulation which was stable after four weeks of storage at 30°C. However, full substitution of wax oleogel having low saturated fatty acid oil was yet to be explored for CS especially for the wide temperature range application (5°C-45°C). Current commercial CS is only stable at 25°C (room temperature). Commercial CS hardened at low temperatures (5°C-10°C) and showed phase separation at high temperatures (40°C-45°C). In view of this, three types of wax namely SFW, CW and BW at 0.0%-3.5% were used to structure blended oil of 50.0% POOo and 50.0% sunflower oil (SFO) to produce CS that is spreadable and stable at wide range of temperatures (5°C-45°C). OSWW of low SFC was used to facilitate spreadability while addition of waxes could possibly hinder phase separation. In a nutshell, the waxes were added to impart solid-like property to a low saturated fatty acids oil blend to produce a CS with a wide temperature range (5°C-45°C).

MATERIALS AND METHODS

Materials

OSWW and oil system with wax (OSW) comprising POOo (iodine value of 62), SFW, CW and BW were bought from local suppliers while SFO was bought from local supermarket. Ingredients for producing CS namely sugar, flavouring and commercial CS were bought from a local supermarket while cocoa powder, protein powder, emulsifiers and milk powder were bought from local suppliers.

Experimental Design and Sample Preparation

Oil system without wax (OSWW). POOo and SFO were blended in six ratios as shown in *Table 1* and were known as OSWW. The OSWW were subjected to solid fat content (SFC) analysis. Raw ingredients according to Shamsudin et al. (2015) were used to produce CS with the OSWW with slight modification. CS was produced using method according to Shamsudin (2004) but without the aqueous phase. These CS were then stabilised at 25°C for 24 hr and then stored at experimental temperatures before conducting hardness and spreadability test.

TABLE 1. VARIOUS BASE OIL (OSWW) RATIO OF PALM SUPEROLEIN (POOo) AND SUNFLOWER OIL (SFO)

No.	Base oil/oil system without wax (OSWW) ratio (POOo:SFO)
1	0:100
2	40:60
3	50:50
4	60:40
5	80:20
6	100:0

Oil system with wax (OSW). As shown in *Table 2*, three types of waxes namely SFW, CW and BW at different percentages (0.0%-3.5%) were blended with the selected OSWW and was called OSW. This OSW was subjected to SFC analysis. Raw ingredients according to Shamsudin et al. (2015) was used to produce CS with OSW. These CS were stabilised at 25°C for 24 hr and then stored at experimental temperatures for three types of analyses namely hardness, spreadability and stability (oiling out).

TABLE 2. EXPERIMENTAL DESIGN OF OIL SYSTEM WITH WAX (OSW)

Oil	Type of wax	Percentage of wax
Selected oil	Sunflower wax (SFW)	0.0%
		0.5%
		1.0%
		1.5%
		2.0%
		2.5%
		3.0%
		3.5%
	Carnauba wax (CW)	0.0%
		0.5%
		1.0%
		1.5%
		2.0%
		2.5%
		3.0%
		3.5%
	Bees wax (BW)	0.0%
		0.5%
		1.0%
		1.5%
		2.0%
		2.5%
		3.0%
		3.5%

Methods

Solid fat content (SFC). SFC of selected OSWW and OSW as shown in *Tables 1* and *2* was measured according to AOCS Official Method Cd 16b-93 (AOCS, 2012) using pulsed nuclear magnetic resonance (NMS Minispec from Bruker, Germany). Samples (OSWW and OSW) were melted at 90°C for at least 1 hr and filled into NMR tubes of 0.8 cm (diameter) and 3.0 cm (height). Samples were placed at 0°C for 90 min and the SFC were measured at 5°C, 10°C, 15°C, 20°C, 25°C, 30°C, 35°C, 37°C, 40 °C and 45°C. Three measurements were taken for each experimental temperature.

Fatty acid composition (FAC). FAC of the selected OSWW and OSW was analysed using gas chromatography (GC) based on fatty acid methyl esters (FAME) by weighing 0.1 g samples and dissolving it in 1.8 mL hexane. Vortex mixer was used to mix the sample's solution. Methylation process was conducted by adding 100 µL of sodium methoxide solution to the samples followed by water addition. The sample's solution was leave for 1 hr to separate. The clear supernatant was transferred to another vial added with sodium sulphate anhydrous and kept for 15 min before complete clear supernatant (1.5 mL) was injected into GC (Agilent Technologies, Model 7890B). Flame

ionisation detector (FID) is equipped with this GC. The injector and detector temperature were set at 230°C. The column temperature was set at 185°C. The carrier (helium gas) having a flow rate of 1 mL/min was used. The peaks were identified by comparing retention times with FAME standards and quantified using peak area normalisation method.

Triacylglycerol composition (TAG). TAG composition of OSWW and OSW was performed according to AOCS Official Method Ce 5b-89 (AOCS, 2012) using Ultra High-Performance Liquid Chromatography (U-HPLC) system (1290 Infinity LC System, Agilent Technologies, USA) and Agilent 1260 RI detector (Waters Corp., USA). A Cortecs UPLC C18 column (2.1 mm x 150 mm length i.d; 1.6 µm particle size) (Waters Corp., Milford, Massachusetts, USA) maintained at 30°C was used. Mobile phase of a mixture of acetone-acetonitrile at ratio 63.5:36.5 (v/v) with a flow rate of 0.25 mL/min was used. Samples of 0.1 g were solubilised in 1 mL of acetone. HPLC grade chemicals and reagents were used. HPLC analysis was conducted in duplicate, and data was recorded as percent areas.

Hardness of chocolate spread (CS). CS of 110 g was placed in a 6 cm (diameter) x 6 cm (height) container. CS containing OSWW and OSW as shown in *Tables 1* and *2,* respectively were tempered at 25°C for 24 hr to assist crystallisation. Tempered samples were stored at 5°C, 10°C and 25°C (for OSW) and 5°C, 10°C, 25°C, 40°C and 45°C (for OSW) for another 24 hr. Hardness of CS was measured using Texture Analyser (TA.XT Plus, Stable Micro System, England) following method from the library of texture analyser regarding CS with modification. CS was penetrated by cylinder probe (5 mm) with depth of 23 mm with rate of 1 mm/min with trigger force of 1 g. Three replicates were conducted for hardness.

Spreadability of chocolate spread (CS) (by observation). The observation was based on whether the CS can be spread or not. CS of 110 g was placed in a 6 cm (diameter) x 6 cm (height) container. CS containing OSWW and OSW as shown in *Tables 1* and *2,* respectively were tempered at 25°C for 24 hr to assist crystallisation. Tempered samples were stored at 5°C for another 24 hr. Spreadability of the CS were observed on its ability to spread on white paper using butter knife before 30 s. Three replicates were conducted for spreadability.

Stability test (by observation). Stability test is the oiling out test for CS. The observation was categorised into three groups which were oil out, slightly oil out and no oil out. CS containing OSW as shown in *Table 2* were tempered at 25°C for 24 hr to assist crystallisation. About 20 g of tempered samples were placed in self-standing centrifuges.

Samples were then stored at 5°C, 10°C, 25°C, 40°C and 45°C for another 24 hr. Oiling out of the CS were observed after storage of 24 hr at temperatures of 5°C, 10°C, 25°C, 40°C and 45°C. Three replicates were conducted for stability.

Oil extraction from commercial chocolate spread (CS) sample. This analysis was to extract oil from commercial CS to further evaluate its SFC for negative control purpose. Oil from the commercial CS samples was extracted using freeze-thaw method according to El-Hadad *et al.* (2011) with some modifications. The samples were stored at 5°C for 24 hr and were left at room temperature for 24 hr to melt. The melted samples were filled in centrifuge tube. The samples were centrifuged at 9500 rpm for 30 min using Thermo Scientific Megafuge 8R. Oil was then pipetted out and mixed with sodium sulphate to eliminate moisture followed by filtration before it was used for other analysis.

Statistical analysis. Results were analysed with Minitab version 16.0 (Pennsylvania, USA) using one-way analysis of variance (ANOVA). Significance differences ($p \leq 0.05$) among the samples were analysed using the Tukey's *post-hoc* test. All tests were carried out in triplicates.

RESULTS AND DISCUSSION

Base Oil without Wax (OSWW)

Solid fat content (SFC). SFC of various oil ratios of OSWW and oil extracted from commercial CS was shown in *Figure 1*. All OSWW except for oil extracted from commercial product were observed to have 0% SFC at experimental temperature of 15°C and above. Oil extracted from commercial CS has the highest SFC at 5°C followed by CS having OSWW of 100% POOo:0% SFO, 80% POOo:20% SFO and 60% POOo:40% SFO. The commercial CS use palm fraction in the formulation based on its label on the packaging. These might include the use of PO and POo (El-Kalyoubi *et al.*, 2011) in its formulation as partially hydrogenated fat from liquid oil has been phased-out (Kushairi *et al.*, 2018). The palm fraction used in the commercial CS tested might be POo as no SFC was observed at 20°C. Gold *et al.* (2011) reported that POo has 0% SFC at 20°C. POo (IV 56.0-59.1) is rich in oleic and palmitic acid with values of 39.8%-43.9% and 38.2%-42.9%, respectively (MPOB, 2017). OSWW having 100% POOo:0% SFO and 80% POOo:20% SFO showed very minor deviation of SFC at all experimental temperatures. OSWW having 50% POOo and below were observed to have SFC of 0% or near 0% at all experimental temperatures. This can be explained by its FAC and TAG composition in each OSWW. The higher the content of POOo, the higher the saturated fatty acid which can be translated into solid fat and influence SFC of the OSWW. In terms of TAG, the higher the POOo, the higher the SUS (disaturated) TAG. In addition, SSS (trisaturated) TAG was detected at 100% POOo based on TAG study.

Decreasing trend of SFC at 5°C when percentage of POOo decreased in an OSWW was expected as this scenario was also related to their TAG composition. Spreadability is a challenge for producing stable CS across a broad temperature range with high SFC at low temperatures especially at 5°C. SFC of blends is important at different temperatures as this will influence the hardness and spreadability of the product. The authors were of the opinion that the ideal SFC for CS with OSW to be spreadable at 5°C-10°C is 0% or close to 0% as further addition of wax will increase its hardness. Therefore, the selection of OSWW was based on this requirement. Based on the results obtained, OSWW with 50% POOo:50% SFO and below are the most suitable to work with as it has 0% SFC at temperature of 5°C-45°C. In view that maximising POOo is a priority (more cost-effective compared to 100% SFO), 50% POOo:50%SFO was the best option for SFC justification. It was also important to note that using oil or oil blends having 0% SFC will work for spreadability only. Waxes were added to cater phase separation at high temperatures (40°C-45°C).

Hardness of chocolate spread (CS). Hardness of CS produced using various ratios of OSWW and commercial CS is shown in *Figure 2*. It can be observed that the hardness of all CS varied at temperatures of 5°C and 10°C. However, they began to plateau at 0% at 25°C. Prasanth Kumar *et al.* (2016) reported that hardness of selected CS made using 80% butterfat and 20% red POo was 88 g_f at 23°C. In this study, the hardness of CS using the OSWW was lower than the study by Prasanth Kumar *et al.* (2016) at 23°C. CS containing OSWW of 100% POOo:0%SFO and 80% POOo:0% SFO showed the highest hardness of 6717 g_f and 3386 g_f, respectively, followed by commercial product with hardness of 2105 g_f at 5°C. According to Prasanth Kumar *et al.* (2016), in general, higher SFC resulted to higher product's hardness. The hardness of CS at 5°C with 50% POOo:50% SFO (1041 g_f) was well below the hardness of commercial product (2105 g_f) and therefore, was able to be spread at 5°C.

Spreadability of chocolate spread (CS). Spreadability articulates acceptance of customers in CS and refers to ease of spreading of the CS and can be expressed in terms of hardness (firmness) (Aydın and Özdemir, 2017). All CS produced using various ratios of OSWW were spreadable at 5°C except for those containing 100% POOo:0% SFO, 80%
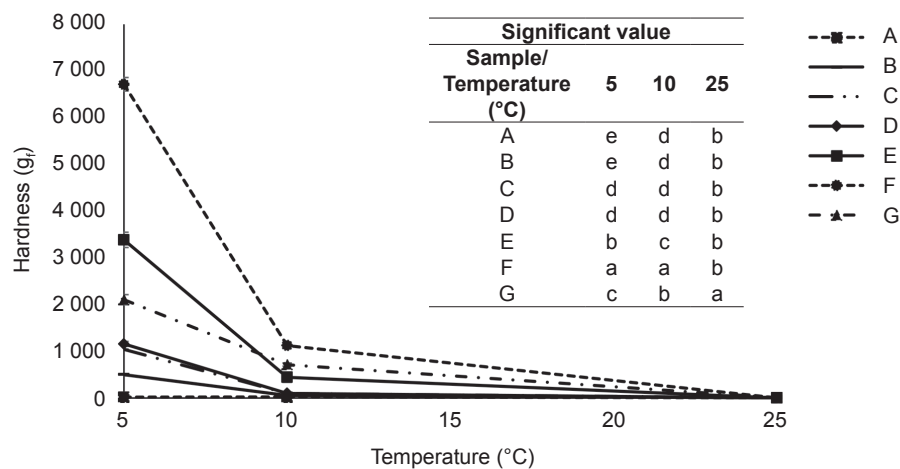
POOo:20% SFO and commercial product. Commercial product which was not able to spread at 5°C was used as negative control as it uses conventional oils and fats to structure the CS. 100% POOo:0% SFO contains 50.92% SUS TAG and 0.17% SSS TAG while 80% POOo:20% SFO contains 38.38% SUS TAG and 0% SSS TAG which can be translated into solid fat. 50% POOo:50% contains only 27.59% SUS TAG and 0% SSS TAG. Overall, 50% POOo:50% SFO contains 34.82% UUU TAG with 37.59% SUU TAG which make up to 72.41% of the total TAG. No literature review was found for spreadability of CS at 5°C. However, a study

by Samsudin (2006) reported that palm-based low-fat CS at 10°C and 20°C had spreadability below 90 g_f and 30 g_f, respectively at one week of storage. Although the spreadability of CS using OSWW was determined by visual observation, the findings can be correlated with hardness values shown in *Figure 2*. When hardness increase, spreadability will decrease (Aydın and Özdemir, 2017; Mohd Razalli *et al.*, 2016). As further addition of waxes is predicted to increase hardness of CS, CS with OSWW that can spread at 5°C is crucial for selection. In view of this, OSWW of 50% POOo:50% SFO that has been pre-selected based on SFC profile was still valid.
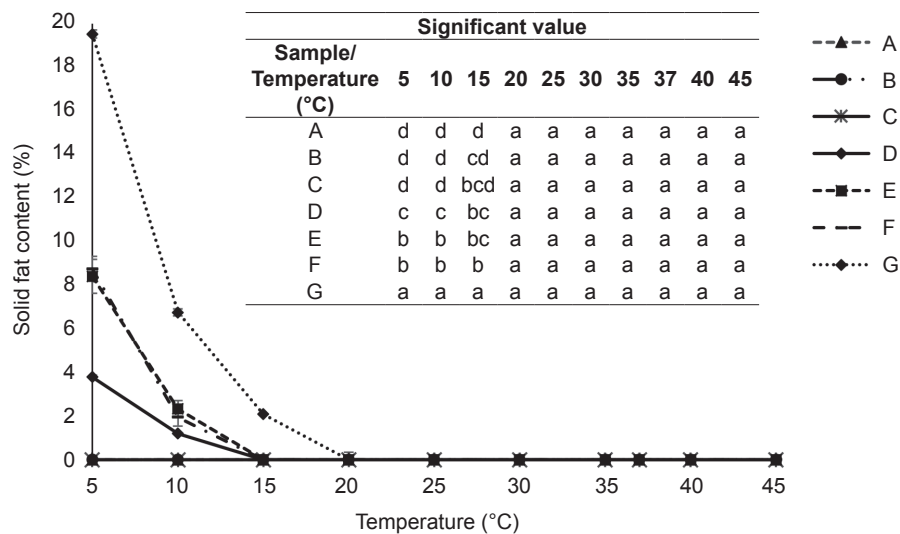
Note: Different small letters within each column in the table are significantly different (*p*<0.05).
A - 0% POOo: 100% SFO; B - 40% POOo: 60% SFO; C - 50% POOo: 50% SFO; D - 60% POOo: 40% SFO; E - 80% POOo: 20% SFO; F -100% POOo: 0% SFO; G - Oil extracted from commercial product.

Figure 1. Solid fat content (SFC) of various oil ratios of palm superolein (POOo) and sunflower oil (SFO) as well as extracted oil from commercial chocolate spread (CS).

Note: Different small letters within each column in the table are significantly different (*p*<0.05).
A - 0% POOo: 100% SFO; B - 40% POOo: 60% SFO; C - 50% POOo: 50% SFO; D - 60% POOo: 40% SFO; E - 80% POOo: 20% SFO; F - 100% POOo: 0% SFO; G - Oil extracted from commercial product.

Figure 2. Hardness of chocolate spread (CS) from various ratios of base oil (OSWW) from palm superolein (POOo) and sunflower oil (SFO) as well as commercial CS.

Oil System with Waxes (OSW)

Solid fat content (SFC). SFC of OSW with different types and percentages of waxes at experimental temperatures are shown in *Figures 3a* (SFW), *3b* (CW) and *3c* (BW). SFC of OSW with SFW (all percentages) predominantly recorded the lowest SFC compared to CW and BW. However, the SFC remains practically linear and constant trend with very slight variation across the experimental temperature used in the study (5°C-45°C). This trend indicated that the OSW with SFW system did not much affected by temperature. It was expected that SFC of OSW with 3.50% SFW will be higher than other experimental percentages of SFW due to its higher percentage of wax. However, the increment was minor and the SFC value was below 3.50%. Notwithstanding this, OSW with 3.50% SFW has quite similar value compared to OSW with 3.00% SFW. A study by Yılmaz and Öğütcü (2013) revealed that an OSW with 5.00% SFW and hazelnut oil had SFC of 3.64% at 20°C which was comparable to this study as they used higher percentage of SFW.

SFC of OSW containing CW (*Figure 3b*) showed a linear and constant trend at experimental temperature of 15°C-40°C. This was aligned with the findings by Kim *et al.* (2017) when they found that CW in carnauba oil system had constant SFC for temperature of 20°C-50°C. However, temperature of below 20°C was not conducted in this study. Similar to OSW with SFW, OSW with CW also demonstrated that 3.5% CW as having the highest SFC at all experimental temperatures. Yi *et al.* (2017) discovered that SFC in a fat system containing CW and BW increased with increasing concentration of waxes. This was also supported by Kim *et al.* (2017), who found that lesser percentage of wax in an OSW provided lesser SFC. The SFC showed inclination at temperatures of 5°C and 10°C for all OSW containing CW. However, the SFC was still below 7.0%.

The SFC of OSW with BW showed a declining trend at experimental temperature of 5°C-45°C. The SFC of OSW containing 3.5% BW was below 6.0% at 5°C. At 45°C, there was no crystalline phase as it was fully melted (Jung *et al.*, 2020). It can be deduced that the SFC of OSW with BW was strongly temperature-dependent. This was in line with the finding by Yi *et al.* (2017), who reported that OSW with BW showed a decreasing SFC trend from 10°C-60°C. This can be explained by low melting point of BW (35°C-41°C) compared to high melting point of CW (67°C-73°C) (Yi *et al.*, 2017). OSW with 3.5% BW exhibited the highest SFC, similar to OSW with SFW and CW. However, many SFC point for OSW 3.5% BW were very close to OSW 3.0% BW.

It was observed that the three types of OSW (SFW, CW and BW) at 3.5% showed different SFC trend. This might be due to different chemical composition of wax with the most consistent (less variation) SFC for all experimental temperatures being OSW with SFW while the most inconsistent (large variation) SFC for all experimental temperatures was BW. The addition of SFW, CW and BW at the maximum of 3.5% did not considerably increase the SFC (*Figure 3*) as they mainly consisted of wax ester (Doan *et al.*, 2018). In fact, SFC of oil extracted from commercial produc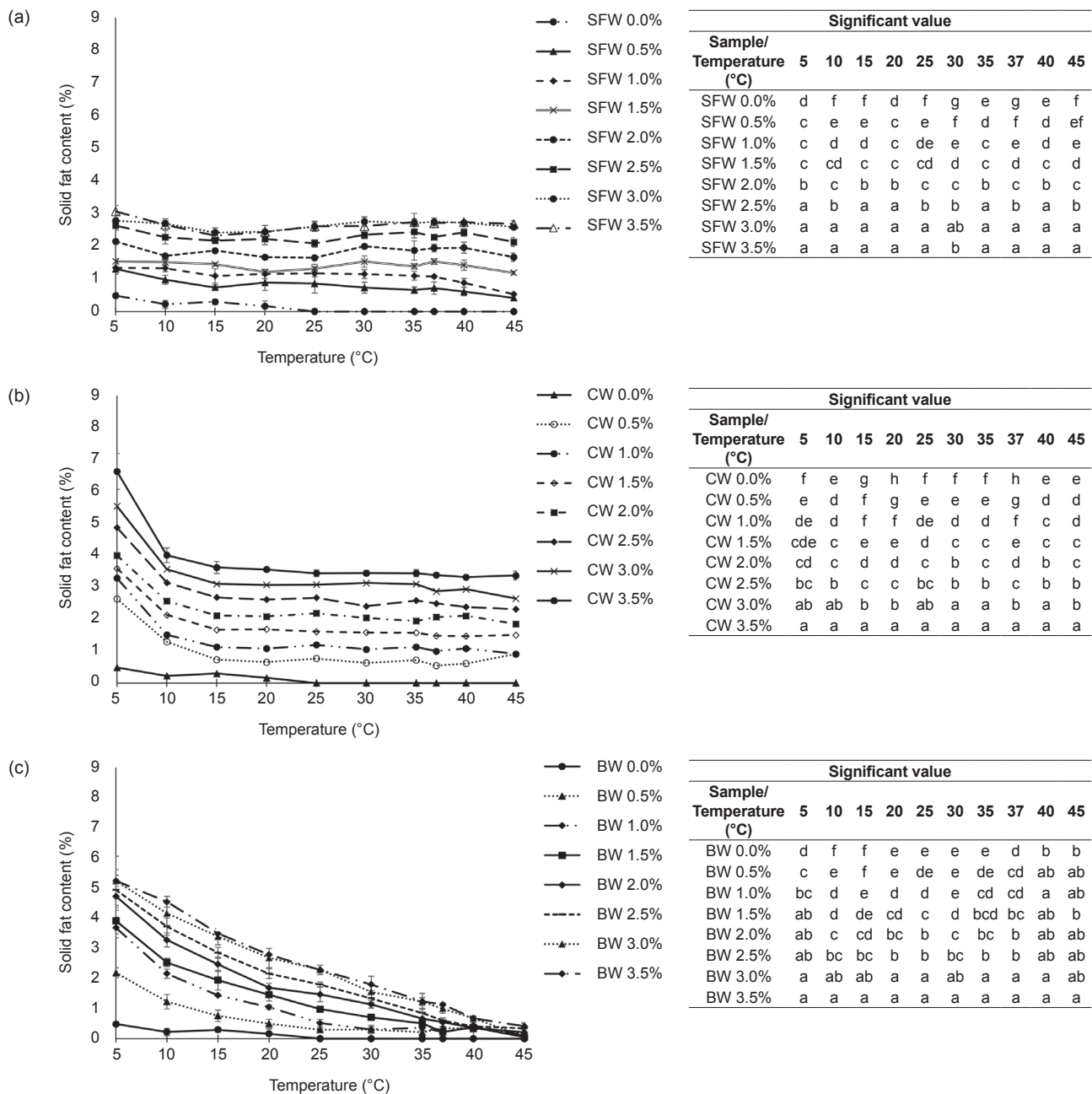t had higher value at 5°C and 10°C (*Figure 1*). The SFC of all 3.5% OSW was expected as waxes do not interfere in the saturation level of OSWW in which their TAG/ FAC levels did not change much (Marangoni and Garti, 2011). These waxes do contain trace or small amounts of fatty acid, fatty alcohol and n-alkane (Aguilar *et al.*, 2007; Doan *et al.*, 2018). Therefore, when waxes were added to the selected base oil, slight increases of SFC that reflected saturated fatty acid were observed (Mert and Demirkesen, 2016). OSW experienced similar steps of nucleation, crystal growth, aggregation and network formation as conventional oils and fats. However, their crystals formation is different in type and morphology, they have lower aggregation within the crystal formed and they have the tendency for unidirectional growth. This translated into high oil binding capacity network formation for a much lower crystal (Patel and Dewettinck, 2016). Oil trapping of OSW in 3D network linkages can be seen effectively through hardness, spreadability and oil stability of the end product which is the CS. In our study, it was found that all of the experimental OSW had low SFC between 35°C-45°C (especially OSW with BW) indicating low waxy taste which was common for OSW that had high melting properties (Patel *et al.*, 2014; 2013).

Hardness of chocolate spread (CS). Hardness of CS made with different types and percentages of waxes at experimental temperatures are shown in *Figures 4a* (SFW), *4b* (CW) and *4c* (BW), respectively. In general, hardness of CS at 35°C-45°C with OSW of SFW, CW and BW at all percentages was near to 0 g_f. Their hardness increased at 5°C but dropped significantly at 10°C. It was stated by Daniel and Marangoni (2012) that below the melting point of OSW, solubility of the system decreases, phase separation (microscopic) transpires, and nucleation occurs upon further supercooling. This might increase hardness of CS at low temperatures. In general, at 5°C, all CS containing 3.0% and 3.5% SFW, CW and BW showed the highest hardness among their own OSW system with CS containing 3.0% SFW displayed the highest hardness (1653 g_f) among all, while 3.5% SFW has hardness of 1636 g_f which was statistically similar to 3.0% SFW. However, this hardness was lower than the hardness of commercial CS at 5°C which was 2105 g_f.
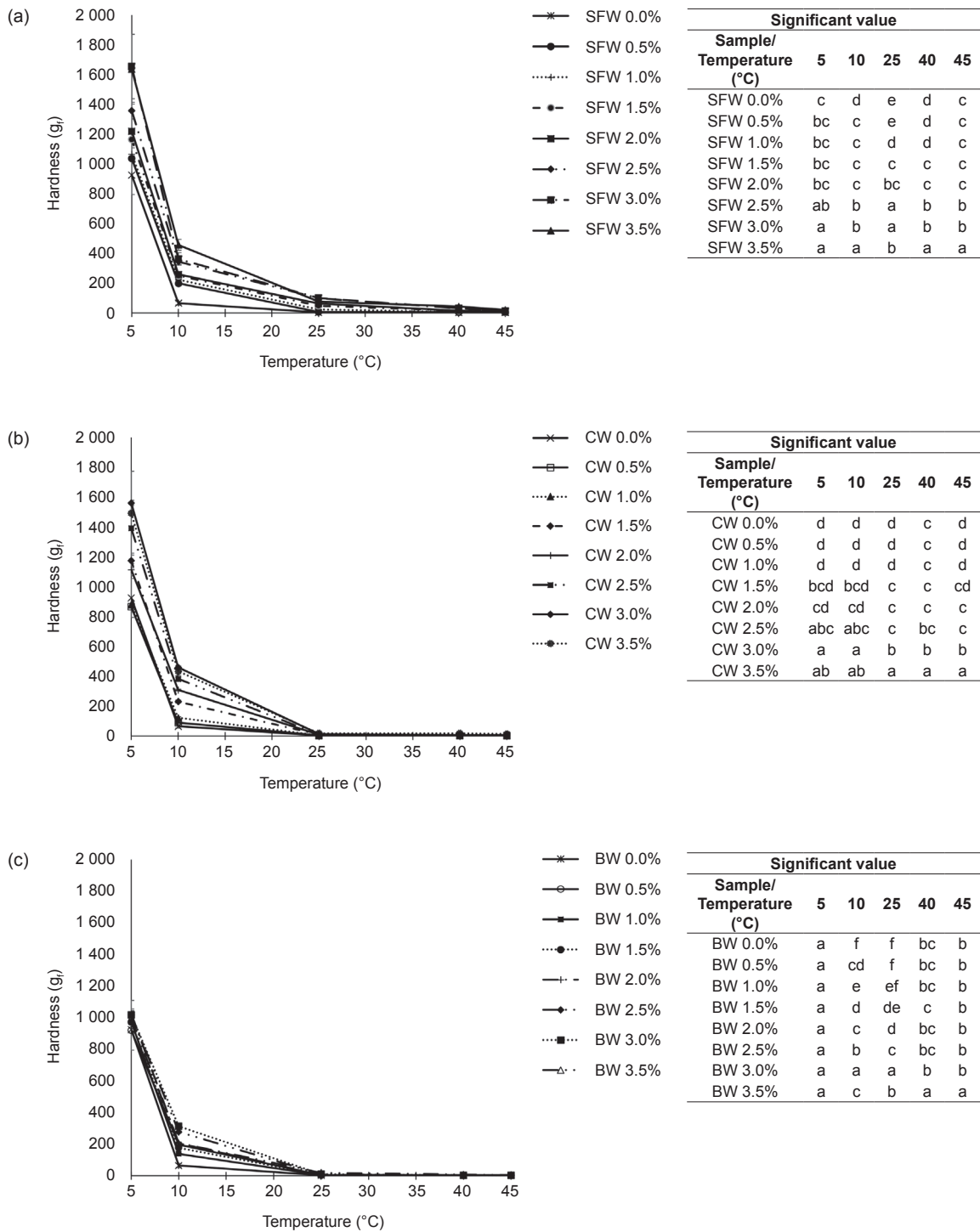
At 5°C and 10°C, hardness of CS containing SFW and CW increased with increasing levels of wax added. However, hardness of CS containing BW at all levels/percentages did not vary much at 5°C, but did vary in small percentages at 10°C. This was aligned with the finding by Lim *et al.* (2017) that CW in canola oil system was harder than BW in canola oil system. These figures concluded that CS with SFW displayed the largest gap in terms of hardness compared to CS without the addition of any waxes. Although SFC of OSW with SFW did not vary much with temperature, the hardness of CS produced with this OSW did affect by temperature variation especially below 25°C. OSW precipitate upon cooling resulted to the formation of solid nuclei while liquefy during heating (Doan *et al.*, 2018). This resulted to strong interactions of crystal as well as supramolecular entities development that trap liquid oil in 3D network when onset of crystal growth occurs (Yuping *et al.*, 2005). This scenario can also be related to study by Doan *et al.* (2016) who found that bees wax oleogel at 5°C has stronger gel strength than 20°C. This hardness can be observed through spreadability and stability (oiling out) of the CS.

(a)

	Significant value									
Sample/Temperature (°C)	5	10	15	20	25	30	35	37	40	45
SFW 0.0%	d	f	f	d	f	g	e	g	e	f
SFW 0.5%	c	e	e	c	e	f	d	f	d	ef
SFW 1.0%	c	d	d	c	de	e	c	e	d	e
SFW 1.5%	c	cd	c	c	cd	d	c	d	c	d
SFW 2.0%	b	c	b	b	c	c	b	c	b	c
SFW 2.5%	a	b	a	a	b	b	a	b	a	b
SFW 3.0%	a	a	a	a	a	ab	a	a	a	a
SFW 3.5%	a	a	a	a	a	b	a	a	a	a

(b)

	Significant value									
Sample/Temperature (°C)	5	10	15	20	25	30	35	37	40	45
CW 0.0%	f	e	g	h	f	f	f	h	e	e
CW 0.5%	e	d	f	g	e	e	e	g	d	d
CW 1.0%	de	d	f	f	de	d	d	f	c	d
CW 1.5%	cde	c	e	e	d	c	c	e	c	c
CW 2.0%	cd	c	d	d	c	b	c	d	b	c
CW 2.5%	bc	b	c	c	bc	b	b	c	b	b
CW 3.0%	ab	ab	b	b	ab	a	a	b	a	b
CW 3.5%	a	a	a	a	a	a	a	a	a	a

(c)

	Significant value									
Sample/Temperature (°C)	5	10	15	20	25	30	35	37	40	45
BW 0.0%	d	f	f	e	e	e	e	d	b	b
BW 0.5%	c	e	f	e	de	e	de	cd	ab	ab
BW 1.0%	bc	d	e	d	d	e	cd	cd	a	ab
BW 1.5%	ab	d	de	cd	c	d	bcd	bc	ab	b
BW 2.0%	ab	c	cd	bc	b	c	bc	b	ab	ab
BW 2.5%	ab	bc	bc	b	b	bc	b	b	ab	ab
BW 3.0%	a	ab	ab	a	a	ab	a	a	a	ab
BW 3.5%	a	a	a	a	a	a	a	a	a	a

Note: Different small letters within each column in the table are significantly different ($p < 0.05$).

Figure 3. Solid fat content (SFC) of oil system with wax (OSW) containing 0.0%, 0.5%, 1.0%, 1.5%, 2.0%, 2.5%, 3.0% and 3.5% (a) sunflower wax (SFW) (b) carnauba wax (CW), and (c) bees wax (BW).

(a)

	Significant value				
Sample/Temperature (°C)	**5**	**10**	**25**	**40**	**45**
SFW 0.0%	c	d	e	d	c
SFW 0.5%	bc	c	e	d	c
SFW 1.0%	bc	c	d	d	c
SFW 1.5%	bc	c	c	c	c
SFW 2.0%	bc	c	bc	c	c
SFW 2.5%	ab	b	a	b	b
SFW 3.0%	a	b	a	b	b
SFW 3.5%	a	a	b	a	a

(b)

	Significant value				
Sample/Temperature (°C)	**5**	**10**	**25**	**40**	**45**
CW 0.0%	d	d	d	c	d
CW 0.5%	d	d	d	c	d
CW 1.0%	d	d	d	c	d
CW 1.5%	bcd	bcd	c	c	cd
CW 2.0%	cd	cd	c	c	c
CW 2.5%	abc	abc	c	bc	c
CW 3.0%	a	a	b	b	b
CW 3.5%	ab	ab	a	a	a

(c)

	Significant value				
Sample/Temperature (°C)	**5**	**10**	**25**	**40**	**45**
BW 0.0%	a	f	f	bc	b
BW 0.5%	a	cd	f	bc	b
BW 1.0%	a	e	ef	bc	b
BW 1.5%	a	d	de	c	b
BW 2.0%	a	c	d	bc	b
BW 2.5%	a	b	c	bc	b
BW 3.0%	a	a	a	b	b
BW 3.5%	a	c	b	a	a

Note: Different small letters within each column in the table are significantly different (*p*<0.05).

Figure 4. Hardness of chocolate spread (CS) with oil system containing 0.0%, 0.5%, 1.0%, 1.5%, 2.0%, 2.5%, 3.0% and 3.5% (a) sunflower wax (SFW) (b) carnauba wax (CW) and (c) bees wax (BW) at different temperatures.

Spreadability of chocolate spread (CS). Spreadability was only conducted at 5°C as all CS were spreadable at other experimental temperatures (10°C, 25°C, 40°C and 45°C). It was observed that all CS were spreadable after 24 hr of storage at 5°C. This scenario indicated that the hardest CS (OSW of 3.0% and 3.5% SFW) with hardness value of 1653 g_f and 1636 g_f were still spreadable at 5°C after 24 hr of storage. However, commercial CS with hardness of 2104 g_f was not spreadable at 5°C. In this case, not spreadable referred to the inability of the butter knife to scoop the CS from the bottle. This might relate to the choice of fat that was used in the commercial CS as it comprised conventional oils and fats. Although

CS having 3.0% and 3.5% SFW was the hardest at 5°C after 24 hr of storage, it has less than 3.5% SFC at similar temperature. Our earlier study in *Figure 1* revealed that this commercial CS had 19% SFC at 5°C. In this study, the wax trapped the oil in a 3D network without altering its chemical composition. Such network made spreadability possible at lower temperatures.

Stability of chocolate spread (CS). CS containing OSW of 0.5%-1.0% SFW has started to oil out at 25°C while that with 1.5%-3.0% SFW started to oil out at 40°C after 24 hr of storage. The oiling out of CS with 3.0% SFW at 40°C and 45°C after 24 hr of storage was in small quantity. Oiling out is also known as phase separation or oil syneresis (Daniel and Marangoni, 2012). No oiling out was observed for CS containing 3.5% SFW at 40°C after 24 hr of storage. Therefore, CS containing 3.5% SFW was stable at wide range of temperatures (5°C-40°C) up to 24 hr of storage. However, this CS started to oil out at 45°C after 24 hr of storage. OSW and other types of oleogels have the ability to thicken food products and can be referred as oil migration inhibitors with the rationale that oil phase's thickening will restrict its movement through food matrix because of escalation of viscosity value (Daniel and Marangoni, 2012; Puşcaş *et al.*, 2020; Wendt *et al.*, 2017). This was the result of droplet coalescence (Mwangi *et al.*, 2016). Hwang *et al.* (2015) reported that SFW provided the most

promising results in terms of gelling due to its high percentage and long chain ester wax. In their study, SFW was able to form gel with soybean oil at low concentration (0.5%) and at low cooling rate. Endlein and Peleikis (2011) stated that SFW has 75%-85% wax ester in it.

CS containing 0.5% CW, started to oil out at 25°C. However, with more levels of CW (1.0%-3.0%) added, oiling out scenario was only observed at 40°C and 45°C. Higher levels of CW (3.5%) shifted the oiling out scenario (slight oiling out) to 45°C after 24 hr of storage. At 3.0% CW, oiling out has started at 40°C but the amount is small. Doan *et al.* (2017) stated that CW has wax ester of 96.0%-97.0% in which high content of wax ester produced strong gelling properties that can affect stability of its end product. According to Doan *et al.* (2016), BW crystallised earlier than PO due to its higher melting point compared to PO as crystallisation was referred as lowering the temperature from high to low. Therefore, it can be referenced that CW crystallised earlier than OSWW. As there is difference in waxes crystal microstructure and OSWW fatty acid organisation, the waxes' crystal will be the initial template for crystallisation (Doan *et al.*, 2016).

CS with OSW of 0.5%-2.0% BW oiled out even at 25°C. CS containing 2.5%-3.5% BW started to oil out at 40°C. Aguilar *et al.* (2007) stated that BW has wax ester of 46.9%-82.9%. The BW used for this study might have wax ester lesser than SFW and CW as it was not stable at 40°C and 45°C.

| SFW 3.5% | CW 3.5% | BW 3.5% |
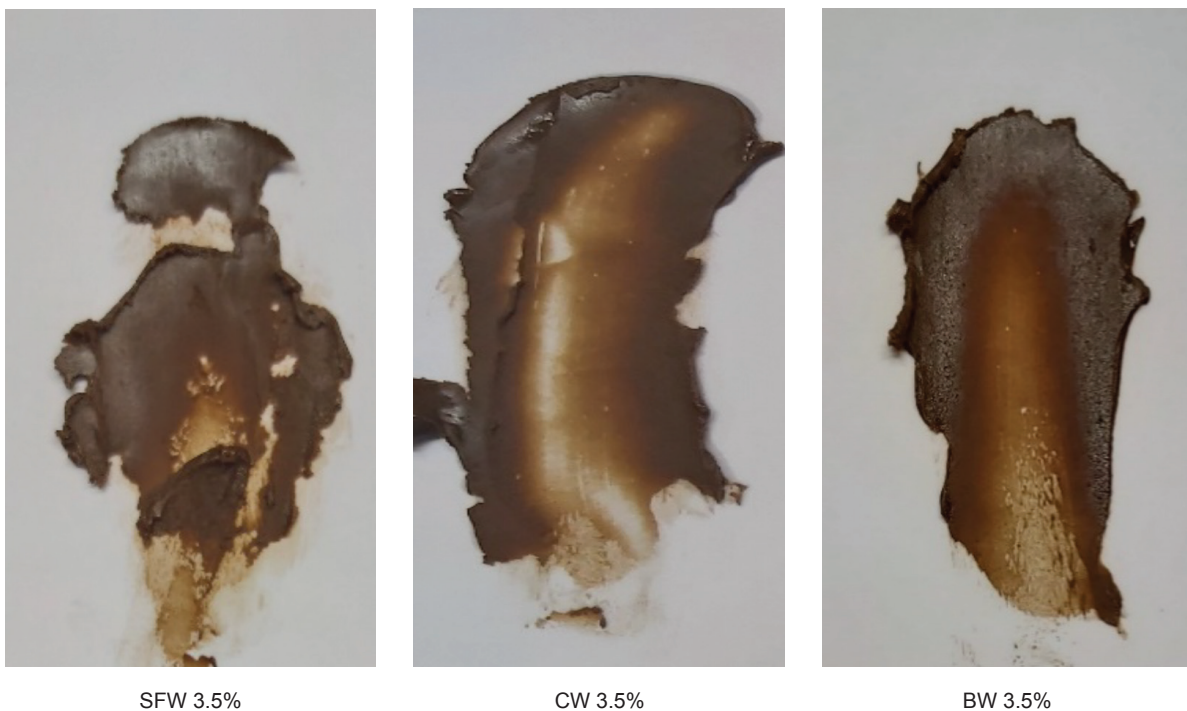
Figure 5. Examples of spreadability of chocolate spread (CS) at 3.5% sunflower wax (SFW), carnauba wax (CW) and bees wax (BW) after 24 hr of storage at 5°C.

CONCLUSION

In order to produce CS that can be spreadable at low temperatures (5°C-10°C) and hinder phase separation at high temperatures (40°C-45°C), waxes were added to a low saturated fatty acids oil blend. The waxes were added to impart solid-like property. Oil blend containing 50% POOo:50% SFO was selected as the OSWW because this oil blend showed 0.0% SFC at temperature range of 5°C-45°C. Notwithstanding this, CS from this oil blend was also spreadable at 5°C and has hardness value of 925 g_f, well below the commercial CS (2105 g_f). CS produced with OSWW (50% POOo:50% SFO) with 3.5% SFW and 3.5% CW have good spreadability at 5°C. These CS had hardness value of 1636 g_f and 1492 g_f, respectively, which were well below the hardness of commercial product. In addition, these CS showed no oiling out at 40°C after 24 hr of storage.

ACKNOWLEDGEMENT

REFERENCES

Aguilar, F; Autrup, H; Barlow, S; Castle, L; Crebelli, R; Engel, K; Gontard, N; Gott, D; Grilli, S; Gürtler, R; Larsen, C; Leclercq, C; Leblanc, J; Malcata, F X; Mennes, W; Milana, M R; Pratt, I; Rietjens, I; Tobback, P and Toldrá, F (2007). Bees wax (E901) as a glazing agent and as carrier for flavours. Scientific opinion of the panel on food additives, flavourings, processing aids and materials in contact with food (AFC). *EFSA J., 615*: 1-28.

Akoh, C C and Min, D B (2008). *Food lipids: Chemistry, Nutrition and Biotechnology*. 3rd edition. CRC Press, Boca Raton, USA. 1047 pp.

AOCS (2012). *Official Methods and Recommended Practices of the AOCS. Vol. 6*. Champaign.

Aydın, S and Özdemir, Y (2017). Development and characterization of carob flour based functional spread for increasing use as nutritious snack for children. *J. Food Qual., 2017*. DOI: 10.1155/2017/5028150.

Daniel, C E and Marangoni, A G (2012). Organogels: An alternative edible oil-structuring method. *J. Am. Oil Chem. Soc., 89*: 749-780.

Doan, C D; Patel, A R; Tavernier, I; De Clercq, N; Van Raemdonck, K; Van de Walle, D; Delbaere, C and Dewettinck, K (2016). The feasibility of wax-based oleogel as a potential co-structurant with palm oil in low-saturated fat confectionery fillings. *Eur. J. Lipid Sci. Technol., 118*: 1903-1914.

Doan, C D; Tavernier, I; Okuro, P K and Dewettinck, K (2018). Internal and external factors affecting the crystallization, gelation and applicability of wax-based oleogels in food industry. *Innov. Food Sci. Emerg. Technol., 45*: 42-52.

Doan, C D; To, C M; De Vrieze, M; Lynen, F; Danthine, S; Brown, A; Dewettinck, K and Patel, A R (2017). Chemical profiling of the major components in natural waxes to elucidate their role in liquid oil structuring. *Food Chem., 214*: 717-725.

Doan, C D; Van de Walle, D; Dewettinck, K and Patel, A R (2015). Evaluating the oil-gelling properties of natural waxes in rice bran oil: Rheological, thermal and microstructural study. *J. Am. Oil Chem. Soc., 92*: 801-811.

El-Hadad, N N M; Youssef, M M; Abd El-Aal, M H and Abou-Gharbia, H H (2011). Utilisation of red palm olein in formulating functional chocolate spread. *Food Chem., 124*: 285-290.

El-Kalyoubi, M; Khallaf, M F; Abdelrashid, A and Mostafa, E M (2011). Quality characteristics of chocolate - Containing some fat replacer. *Ann. Agric. Sci., 56*: 89-96.

Endlein, E and Peleikis, K H (2011). Natural waxes - Properties, composition and applications. *SOFW J., 137*: 1-8.

Gold, I L; Ukhun, M E and Akoh, C C (2011). Characteristics of eutectic compositions of restructured palm oil olein, palm kernel oil and their mixtures. *J. Am. Oil Chem. Soc., 88*: 1659-1667.

Hwang, H S; Kim, S; Evans, K O; Koga, C and Lee, Y (2015). Morphology and networks of sunflower wax crystals in soybean oil organogel. *Food Struct., 5*: 10-20.

Jeyarani, T; Banerjee, T; Ravi, R and Gopala Krishna, A G (2013). Omega-3 fatty acids enriched chocolate spreads using soybean and coconut oils. *J. Food Sci. Technol., 52*: 1082-1088.

Jung, D; Oh, I; Lee, J and Lee, S (2020). Utilization of butter and oleogel blends in sweet pan bread for saturated fat reduction: Dough rheology and baking performance. *LWT, 125*: 109194.

Kim, J Y; Lim, J; Lee, J H; Hwang, H S and Lee, S (2017). Utilization of oleogels as a replacement for

solid fat in aerated baked goods: Physicochemical, rheological, and tomographic characterization. *J. Food Sci., 82*: 445-452.

Kushairi, A; Loh, S K; Azman, I; Elina, H; Meilina, O A; Zanal Bidin, M N I; Razmah, G; Shamala, S and Ghulam, K A P (2018). Oil palm economic performance in Malaysia and R&D progress in 2017. *J. Oil Palm Res., 30*: 163-195.

Lim, J; Hwang, H S and Lee, S (2017). Oil-structuring characterization of natural waxes in canola oil oleogels: Rheological, thermal, and oxidative properties. *Appl. Biol. Chem., 60*: 17-22.

Manzocco, L; Valoppi, F; Calligaris, S; Andreatta, F; Spilimbergo, S and Nicoli, M C (2017). Exploitation of ƙ-carrageenan aerogels as template for edible oleogel preparation. *Food Hydrocoll., 71*: 68-75.

Marangoni, A and Garti, N (2011). *Edible Oleogels: Structure and Health Implications*. 2ⁿᵈ edition. AOCS Press, Urbana, USA.

Mert, B and Demirkesen, I (2016). Reducing saturated fat with oleogel/shortening blends in a baked product. *Food Chem., 199*: 809-816.

Mohd Razalli, N H; Chin, N L; Yusof, Y A and Mahyudin, N (2016). Quality changes of stabilizer-free natural peanut butter during storage. *J. Food Sci. Technol., 53*: 694-702.

MPOB (2017). Palm olein. *Pocketbook of Oil Palm Uses*. Sixth edition. MPOB, Bangi. 17 pp.

Mwangi, W W; Ho, K W; Tey, B T and Chan, E S (2016). Effects of environmental factors on the physical stability of pickering-emulsions stabilized by chitosan particles. *Food Hydrocoll., 60*: 543-550.

Patel, A R and Dewettinck, K (2016). Edible oil structuring: An overview and recent updates. *Food Funct., 7*: 20-29.

Patel, A R; Rajarethinem, P S; Grędowska, A; Turhan, O; Lesaffer, A; De Vos, W H; Van de Walle, D and Dewettinck, K (2014). Edible applications of shellac oleogels: Spreads, chocolate paste and cakes. *Food Funct., 5*: 645-652.

Patel, A R; Schatteman, D; De Vos, W H; Lesaffer, A and Dewettinck, K (2013). Preparation and rheological characterization of shellac oleogels and oleogel-based emulsions. *J. Colloid Interface Sci., 411*: 114-121.

Prasanth Kumar, P K P; Jeyarani, T and Gopala Krishna, A G G (2016). Physicochemical characteristics of phytonutrient retained red palm olein and butter-fat blends and its utilization for formulating CS. *J. Food Sci. Technol., 53*: 3060-3072.

Puşcaş, A; Mureşan, V; Socaciu, C and Muste, S (2020). Oleogels in food: A review of current and potential applications. *Foods, 9*: 70.

Rocha, J C B; Lopes, J D; Mascarenhas, M C N; Arellano, D B; Guerreiro, L M R and da Cunha, R L (2013). Thermal and rheological properties of organogels formed by sugarcane or candelilla wax in soybean oil. *Food Res. Int., 50*: 318-323.

Roe, M; Pinchen, H; Church, S; Elahi, S; Walker, M; Farron-Wilson, M; Buttriss, J and Finglas, P (2013). *Trans* fatty acids in a range of UK processed foods. *Food Chem., 140*: 427-431.

Samsudin, S Y (2006). Low-fat chocolate spread based on palm oil. *Palm Oil Developments, 45*: 27-30.

Saw, M H; Lim, W H; Badlishah, S B and Tan, C P (2020). Screening of organogelators for structuring palm superolein. *J. Oil Palm Res., 32*: 152-158.

Shamsudin, S Y (2004). *Trans* free palm based chocolate spread. *MPOB Information Series No. 251.*

Shamsudin, S Y; Abd Hamid, R and Kanagaratnam, S (2015). Chocolate spread with tocotrienol. *MPOB Information Series No. 584.*

Wendt, A; Abraham, K; Wernecke, C; Pfeiffer, J and Flöter, E (2017). Application of *β*-sitosterol + *γ*-oryzanol-structured organogel as migration barrier in filled chocolate products. *J. Am. Oil Chem. Soc., 94*: 1131-1140.

Wolfer, T L; Acevedo, N C; Prusa, K J; Sebranek, J G and Tarté, R (2018). Replacement of pork fat in frankfurter-type sausages by soybean oil oleogels structured with rice bran wax. *Meat Sci., 145*: 352-362.

Yi, B R; Kim, M J; Lee, S Y and Lee, J H (2017). Physicochemical properties and oxidative stability of oleogels made of carnauba wax with canola oil or beeswax with grapeseed oil. *Food Sci. Biotechnol., 26*: 79-87.

Yilmaz, E and Öğütcü, M (2013). The texture, sensory properties and stability of cookies prepared with wax oleogels. *Food Funct., 6*: 1194-1204.

Yuping, S H I; Baomin, L and Richard, H (2005). Crystal morphology, microstructure, and textural properties of model lipid systems. *J. Am. Oil Chem. Soc., 82*: 399-408.

TOPICAL APPLICATION OF THE PALM TOCOTRIENOL-RICH FRACTION (TRF) ENHANCES CUTANEOUS WOUND HEALING IN TYPE 2 DIABETIC MICE

ZAIZUHANA SHAHRIM[1,2]*; SUZANA MAKPOL[2]; GEOK CHIN TAN[3]; NURUL AISHAH MUHAMMAD[1] and ZAFARIZAL ALDRIN AZIZUL HASAN[1]

ABSTRACT

Type 2 diabetic (T2D) wounds are characterised by excessive, persistent inflammation and oxidative stress, resulting in delayed healing. The tocotrienol-rich fraction (TRF) has potential as a therapeutic agent in improving diabetic wounds due to its anti-inflammatory and antioxidative effects. Thus, we aimed to evaluate the effect of the TRF on diabetic cutaneous wounds using a T2D mouse model. Full-thickness wounds were made on the backs of mice, and the TRF formulation was topically applied. The effect of the TRF was evaluated by examining wound closure, histology, CD31 immunohistochemistry and collagen deposition with Masson's trichrome staining. Biochemical assessments of catalase (CAT), glutathione peroxidase (GPx), myeloperoxidase (MPO), protein levels, transforming growth factor beta-1 (TGF-β1), metalloproteinase-9 (MMP-9) and cytokine production were performed. The results showed that TRF treatment enhanced wound closure and healing in the T2D mouse wounds. The TRF increased CAT, GPx, protein, hydroxyproline and TGF-β1 levels but reduced MPO activity and MMP-9 production in diabetic wounds. Multiplex immunoassay revealed that the TRF modulated proinflammatory cytokine and chemokine production. However, it increased interleukin-4 (IL-4) and vascular endothelial growth factor (VEGF) production and reduced granulocyte-macrophage colony-stimulating factor (GM-CSF). Our data suggest that topical TRF application may enhance diabetic cutaneous wound healing.

[1]   Malaysian Palm Oil Board,
     6 Persiaran Institusi, Bandar Baru Bangi,
     43000 Kajang, Selangor, Malaysia.

[2]   Department of Biochemistry, Faculty of Medicine,
     Universiti Kebangsaan Malaysia, UKM Medical Center,
     Jalan Yaacob Latif, Bandar Tun Razak Cheras,
     56000 Kuala Lumpur, Malaysia.

[3]   Department of Pathology, Faculty of Medicine,
     Universiti Kebangsaan Malaysia, UKM Medical Center,
     Jalan Yaacob Latif, Bandar Tun Razak,
     56000 Kuala Lumpur, Malaysia.

*   *Corresponding author e-mail: zaizuhana@mpob.gov.my*

INTRODUCTION

The most common type of diabetes is type 2 diabetes (T2D) mellitus (Tsalamandris *et al.*, 2019). T2D patients have a greater risk of limb amputation than nondiabetic individuals due to impaired wound healing (Zheng *et al.*, 2018). Wound healing is multifactorial, and it requires homeostasis, inflammation, proliferation, and tissue remodelling (Rodrigues *et al.*, 2019; Thangavel *et al.*, 2018; Xiao *et al.*, 2020). However, wound healing is delayed in diabetic patients for many reasons, including persistent inflammatory and high oxidative stress states, resulting in abnormal angiogenesis and

neuropathy (Katsuhiro *et al.*, 2018; Strang *et al.*, 2020; Yuan *et al.*, 2018).

Although inflammation is an essential part of healing, disproportionate inflammation leads to disruptions in the normal healing cascade (Strang *et al.*, 2020; Zhao *et al.*, 2016), such as in the skin of diabetic mice (Brandt *et al.*, 2018). Inflammation and the immune system are modulated by cytokines and extracellular signalling proteins (Fields *et al.*, 2019). Dysregulated production of these proteins results in impaired diabetic wound healing (Strang *et al.*, 2020). Thus, regulating inflammation through its mediators and increasing antioxidant activities may improve cutaneous wound healing in diabetic patients (Zhao *et al.*, 2016).

A study performed on diabetic patients showed reductions in catalase (CAT) and glutathione peroxidase (GPx) activities and an overall decrease in antioxidant levels (Alghazeer *et al.*, 2018). The reduction in antioxidant defence, which is one of the detrimental effects of reactive oxygen species (ROS) on cellular homeostasis, often worsens redox imbalance (Cano Sanchez *et al.*, 2018). Diabetic complications mainly occur when ROS production induced by diabetes stimulates various pathological signalling pathways that lead to tissue injury (Deng *et al.*, 2021; Zhao *et al.*, 2016). Therefore, increasing antioxidant activity may enhance wound healing (Zhao *et al.*, 2016).

During inflammation or oxidative stress, neutrophils secrete a certain amount of myeloperoxidase (MPO) to help recover from tissue injury (Khan *et al.*, 2018). While excessive MPO activity is detrimental to tissue recovery, MPO is an important indicator of inflammation and the oxidative stress response (Khan *et al.*, 2018). The structural protein, collagen is essential for tissue regeneration and dermal reconstruction (Thangavel *et al.*, 2017), and collagen deposition in the wound can be indicated by hydroxyproline content (Hemmati *et al.*, 2018).

It was previously reported that low transforming growth factor beta (TGF-β) levels can predict the chronicity of diabetic wounds (Liarte *et al.*, 2020). Transforming growth factor beta-1 (TGF-β1) is known to stimulate collagen production in dermal fibroblasts to achieve wound contraction (Serra *et al.*, 2017) and closure. In contrast, metalloproteinase-9 (MMP-9) leads to excessive degradation of the extracellular matrix and reduces the tensile stress of the wound. MMP-9 is highly expressed in diabetic wounds (Ayuk *et al.*, 2016) and is considered the primary cause of diabetic foot ulcer recalcitrance in healing (Jones *et al.*, 2019). Thus, this proteinase would be an excellent candidate in a study regarding the treatment of diabetic wounds.

The tocotrienol-rich fraction (TRF) is a blend of tocotrienol (~70%) and alpha-tocopherol (~30%). It has been reported that the tocotrienol/tocopherol ratios in rice bran oil, barley, and palm oil are 1:1, 1.9:1, and 3:1, respectively (Cheng *et al.*, 2017). As a rich source of vitamin E, the TRF has an abundance of antioxidative (Khor *et al.*, 2017; Matough *et al.*, 2014; Shahidi and De Camargo, 2016) and anti-inflammatory (Nor Azman *et al.*, 2018; Yap, 2018) properties. No adverse skin reactions after the topical application of tocotrienols have been reported (Hasan *et al.*, 2018). Wound recovery in diabetic (streptozotocin-induced) and normal rats could be enhanced by the TRF (Elsy *et al.*, 2017; Musalmah *et al.*, 2005), and topical treatment with the TRF could also promote burn healing (Elsy *et al.*, 2017). Despite years of research, the pathogenesis of impaired cutaneous wounds in T2D patients remains incompletely understood, and there is still a need to identify therapeutic approaches and remedies for wounds. Furthermore, alternative therapeutic treatments using natural products are in high demand. In view of the background of the TRF and to the best of our knowledge, studies using the TRF in T2D skin wound healing are very limited. Therefore, the current study aimed to evaluate cutaneous wound healing in a T2D model that was topically treated with the TRF.

MATERIALS AND METHODS

Reagents

In this study, palm-based TRF Gold Tri E 70 was purchased from Sime Darby Food and Beverages Marketing Sdn. Bhd. (Selangor, Malaysia). The TRF (10%, w/w) was loaded in vehicle consisting of PEG-400 (85%, w/w, Sigma-Aldrich, USA, Cat No. 202398) with Tween® 80 (5% w/w, Polysorbate, Sigma-Aldrich, USA, Cat No. 59924).

Diabetic and Normal Mouse Models

Type 2 diabetic (T2D) and obese (B6. V-Lepob/objRj) male mice were obtained from Janvier Laboratory (France), and lean male mice (C57BL/6) were used as the normal control. The levels of fasting blood glucose and serum insulin were determined using an Accu-Chek device (Roche, GmbH, Mannheim, Germany) and ELISA (Rat/Mouse Insulin Kit; Millipore, St. Charles, MO, USA) to validate the development of diabetes in the mouse models. Mice with blood glucose exceeding 300 mg dL^{-1} were considered hyperglycaemic. The body weights of the mice were recorded at every postinjury time point. All procedures were strictly performed based on the approved protocols by the Universiti Kebangsaan Malaysia Animal Care and Use Committee (UKMAEC, procedure number: BIOK/PP2017/SUZANA/25-JAN./817-JAN.-2017-SEPT.-2018). The mice were subjected to a cutaneous

wounding experiment and randomly divided into three groups of 12 mice.

Group I: Normal control (wild-type, received vehicle only)
Group II: T2D control (received vehicle only)
Group III: T2D treated (received TRF in vehicle)

Cutaneous Wound Model with Full-thickness Skin Excision

Four full-thickness skin excision wounds were made on the dorsum of the mice using a sterile 5 mm punch biopsy (Kai Medical, Japan) under anaesthesia (sodium pentobarbital, 60 mg kg^{-1}). Subsequently, a silicone wound splint (Grace Bio-Labs Oregon, USA) was used to secure the wound perimeter and prevent contraction. Topical application of the TRF was performed twice daily, and the wounds were covered with a transparent dressing (Tegaderm, 3M Health Care, St. Paul, MN, USA Cat. No. 1624) after the treatment. All mice were kept in a controlled environment at a temperature of $21 \pm 0.5°C$, relative humidity of $50 \pm 10\%$, and a 12-hr alternating light and dark schedule. Water and food were provided *ad libitum*.

Measurement of Wound Closure Kinetics

Images of the wounds were captured on days 0, 1, 3, 7 and 14 using a digital camera beginning on the first day of skin excision until day 14. Images were examined using image processing software (ImageJ, version 1.5e, NIH, USA). The percentage of wound closure was calculated as follows:

$$\text{Wound closure (\%)} = \frac{\text{Initial wound area (day 0) - wound area at n}}{\text{Wound area day 0}} \times 100$$

where, n = number of days (0, 1, 3, 7 and 14 days) after skin excision.

Histopathological and Immunohistochemical Examination of Wound Tissues

Excised wound tissues were prepared for clinical pathology on the indicated days postinjury. The tissues were fixed with buffered formalin (10%)

obtained from Sigma-Aldrich (USA) and dehydrated before being converted into paraffin-embedded blocks. Tissue sections with a thickness of 4 μm were prepared and stained with haematoxylin and eosin (H&E) (Leica, Germany) to assess cellular responses to the treatments and stained with Masson's trichrome on day 14 to observe collagen deposition in the wound tissue according to the manufacturer's protocol. A semiquantitative method was used to examine the following processes: inflammatory cell infiltration, epidermal regeneration (re-epithelialisation), fibroblast proliferation and collagen deposition. Three stained sections in each group were evaluated and scored using a scale, as summarised in *Table 1*. To detect the presence of CD31, immunohistochemistry was conducted. Briefly, the sections were blocked with 3% BSA at 37°C for 30 min, followed by incubation with CD31 antibodies (1:100, goat, Servicebio, GB13063) at 4°C overnight. After being washed with phosphate buffered saline (PBS), a goat anti-rabbit secondary antibody (Servicebio, GB23204, 1:200) coupled with horseradish peroxidase was added. The samples were incubated at 37°C for 1 hr. The sections were stained with diaminobenzidine tetrahydrochloride (Servicebio, G1211) and lightly counterstained with haematoxylin. Positive immunohistochemical staining was observed as brown staining. The number of blood vessels in three tissue sections was assessed using the microvessel density (MVD) counting technique, whereby the average number of microvessels per high-power field (HPF) was estimated by counting CD31-stained cells. All sections were examined using a digital microscope (Eclipse 200, Nikon Instruments, Inc., Melville, NY) and evaluated by pathologists in a single-blind manner.

Determination of CAT, GPx and MPO Activities in Wound Tissues

CAT and GPx activities were assessed using kits from Cayman Chemical (Ann Arbor, MI, USA), whereas MPO was assessed using kits from (BioVision Inc., USA) according to the manufacturer's protocol.

Protein and Hydroxyproline Measurement

Protein and hydroxyproline levels in wound tissues were measured using commercial assay kits

TABLE 1. HISTOLOGICAL FEATURES AND SCORING

Histological score	0	1	2	3	4
Presence of inflammatory cells	Absent	Occasionally present	Light scattering	Abundant	Confluent
Fibroblast proliferation	Absent	Occasionally present	Light scattering	Abundant	-
Epidermal regeneration	None	Mild	Moderate	Complete	-
Collagen	None	Present	Mild	Moderate	Intense

from Cayman Chemical (Ann Arbor, MI, USA) and BioVision Inc. (USA), respectively, according to the manufacturer's instructions.

Measurement of MMP-9 and TGF-β1 Levels in Granulation Tissues

MMP-9 and TGF-β1 levels in wound tissues were examined using a Fine Test ELISA kit for mice from Wuhan Fine Biotech Co., Ltd. (Wuhan, China) per the manufacturer's protocols.

Multiplex Cytokine Analysis

A custom-made multiplex analysis was performed based on xMAP Luminex technology using a ProcartaPlex™ cytokine 36 plex assay from Thermo Fisher Scientific Inc. according to the manufacturer's protocol. Measurements were performed using Luminex 200 with xPONENT® software version 3.1, and the concentration of cytokines was determined using MasterPlex QT software version 2.0.0.59.

Statistical Analysis

All experiments were conducted in replicates. The data were subjected to statistical analysis using the Statistical Package for Social Sciences (SPSS) version 22. A p value less than 0.05 was considered significant.

RESULTS AND DISCUSSION

All diabetic mice had significantly higher ($p<0.01$) body weights throughout the study duration than those in the normal control group (*Figure 1a*). For example, the mean measurement for the T2D control group was 41.33 ± 0.84 g on day 1 and 43.06 ± 0.26 g on day 14 and that for the TRF-treated group was 41.75 ± 0.10 on day 1 and 42.98 ± 0.60 g on day 14. Moreover, normal control mice exhibited body

weights of 26.24 ± 0.60 g on day 1 and 27.33 ± 0.45 g on day 14 (*Figure 1a*). Blood glucose levels were significantly ($p<0.01$) higher in the T2D control group (362.67 ± 5.24 mg dL^{-1} (day 1) and 372.00 ± 4.16 mg dL^{-1} (day 14) and the TRF-treated group (355.00 ± 9.54 mg dL^{-1} (day 1) and 377.33 ± 5.80 mg dL^{-1} (day 14) than in the normal control group (120.00 ± 12.70 mg dL^{-1}, day 1 and 151.70 ± 13.70 mg dL^{-1}, day 14) (*Figure 1b*). The normal control group also exhibited significantly ($p<0.01$) lower serum insulin levels on day 1 (1.67 ± 0.03 ng mL^{-1}) and day 14 (1.54 ± 0.13 ng mL^{-1}) than the diabetic control group (3.62 ± 0.22 ng mL^{-1}) on days 1 and 14 (3.70 ± 0.03 ng mL^{-1}). TRF-treated mice also showed significantly lower ($p<0.01$) insulin levels on day 1 (3.66 ± 0.04 ng mL^{-1}) and day 14 (3.75 ± 0.02 ng mL^{-1}) than those in the normal control group (*Figure 1c*).

Wound Closure and Histological Effects of the TRF on Cutaneous Wound Healing

Wound kinetics and macroscopic assessments. Wound kinetic and macroscopic assessments of all mice were measured on days 0, 1, 3, 7 and 14, and the excised wound site was photographed as shown in *Figure 2*. Normal control mice showed the fastest wound closure rate, and the wounds were completely closed (100%) on day 14 with visible hair growth. In contrast, T2D controls showed significantly slower ($p<0.01$) rates at days 3, 7 and 14 than the normal controls. However, TRF-treated wounds showed significantly higher ($p<0.05$) wound closure rates on days 3, 7 and 14 than T2D control wounds (*Figure 2b*).

Histological assessments. Previous findings were consistent with the histological examination (*Figure 3a*). Wound sections in all groups showed the presence of inflammatory cells on day 3. These immune cells are the key regulators and players during acute wound healing and prevent infection (Peiseler and Kubes, 2019). Immune cell infiltration is followed by alterations from a proinflammatory to
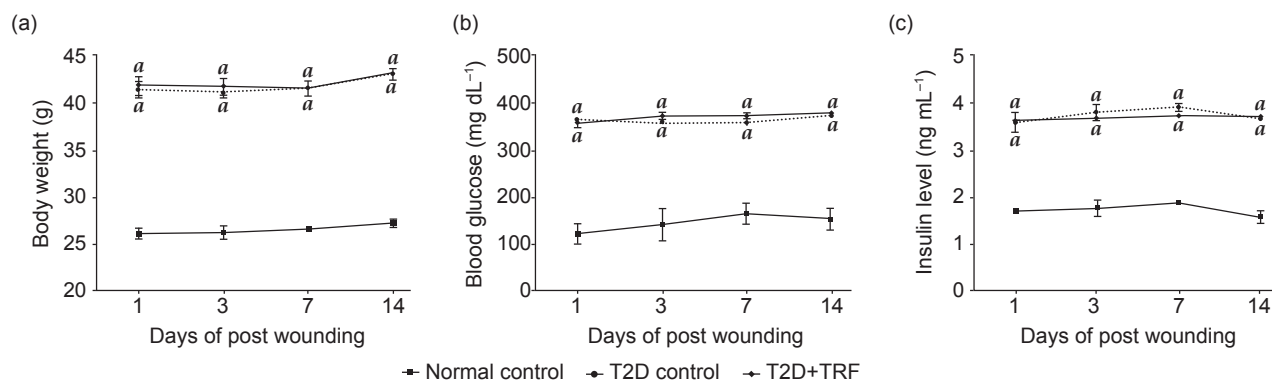
Figure 1. (a) Body weights, (b) blood glucose levels, and (c) insulin levels of the mice. The data are expressed as the mean ± SEM (n=3) and were analysed using two-way ANOVA with Tukey's multiple comparison test. [a]p<0.01 compared with the normal control group.
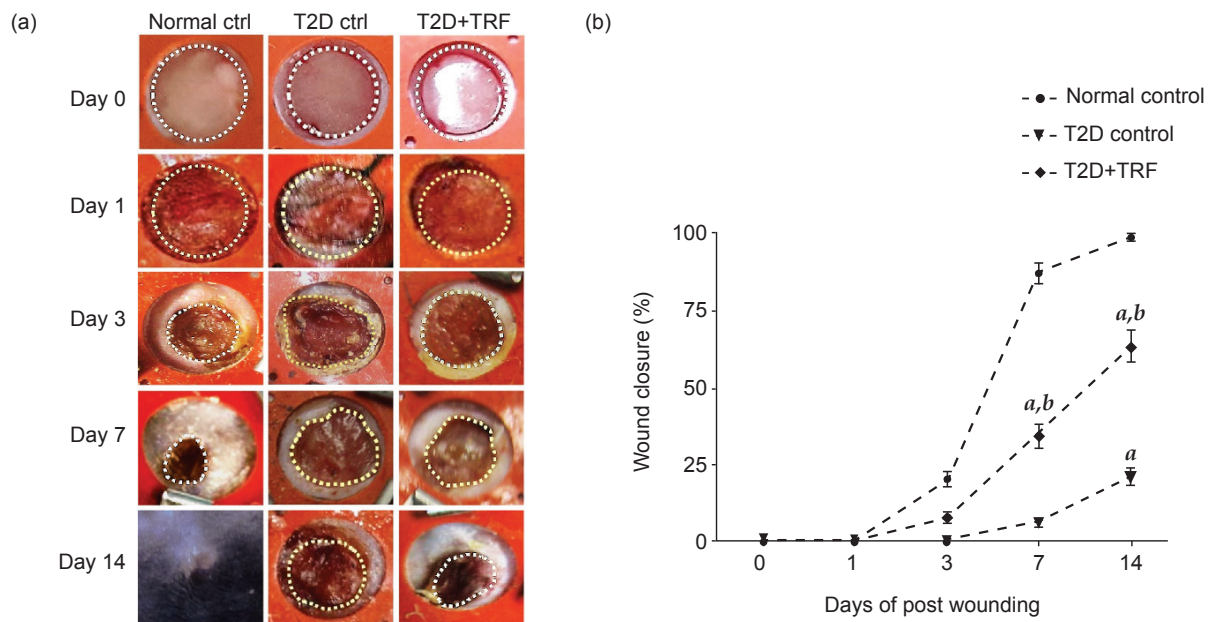
Figure 2. Effects of the TRF on wound closure. (a) Representative images of the gross appearance of wounds, and (b) the percentage of wound closure. The wound closure data are the mean ± SEM (n=3, 12 wounds/group) and were calculated by two-way ANOVA with Tukey's multiple comparison test. ^{a}p<0.01 vs. *the normal control,* ^{b}p<0.05 vs. *the T2D control.*

a healing immune response to inhibit inflammation and initiate the tissue remodelling process (Raziyeva *et al.*, 2021).

In the present study, the normal control wound exhibited standard healing stages, whereby thin re-epithelialisation was observed as early as day 3 after wounding and continued until day 7. The wound surface was also fully covered on day 14. In addition, the presence of more fibroblasts and blood vessels was also evident in the normal control group than in the other groups. In contrast, the T2D controls showed an abundance of inflammatory cells and disorganised structures, but TRF-treated wounds showed a moderate inflammatory response compared to diabetic controls.

On day 7, the T2D control group showed marked dominance of inflammatory cells with few fibroblasts, but in TRF-treated wounds, the inflammatory cells seemed to subside, and the wounds showed well-formed granulation tissue, which was covered by more blood vessels and fibroblasts with some collagen deposition than those in the T2D control. On day 14, the wound sections in the diabetic control group showed the presence of blood vessels and were dominated by inflammatory cells compared to TRF-treated wounds, whereby thicker granulation tissue was dominated by fibroblasts with adequate, more organised, and compact collagen deposition and a completely newly regenerated epithelial layer.

In addition, histological scoring of inflammation, fibroblast proliferation, re-epithelialisation and collagen deposition was performed (*Figure 3b*). The results showed that the proportion of inflammatory cells was significantly reduced at days 3 ($p<0.01$), 7 ($p<0.05$) and 14 ($p<0.05$) in TRF-treated wounds compared to T2D control wounds. Moreover, the rate of fibroblast proliferation was significantly increased in TRF-treated diabetic wounds on days 3 ($p<0.05$), 7 ($p<0.01$) and 14 ($p<0.001$) compared with diabetic wounds. The T2D control group demonstrated incomplete re-epithelialisation and poorly formed granulation tissue, but TRF-treated wounds showed significantly higher epidermal regeneration on days 3 ($p<0.05$), 7 ($p<0.001$) and 14 ($p<0.01$) with denser collagen deposition on days 7 ($p<0.01$) and 14 ($p<0.001$) than the diabetic control (*Figure 3b*). We showed that T2D wounds sustained production of inflammatory cells in the wound sites, which blocked the progression of healing, thus, impeding wound closure (Tan *et al.*, 2019). Dysfunctional fibroblasts and epidermal cells, failed angiogenesis and impaired tissue maturation (Daemi *et al.*, 2019; Manzouerh *et al.*, 2019; Thangavel *et al.*, 2017) were observed in this group.

Diabetic wound healing is impaired due to improper angiogenesis (Okonkwo and DiPietro, 2017). To understand the effect of the TRF on angiogenesis, the wound sections were stained with CD31 (*Figure 3c*) and quantified (*Figure 3d*). The diabetic controls showed a few immature blood vessels compared to normal controls and TRF-treated wounds on days 7 and 14. A few densely packed vessels were also observed. In comparison to the T2D control, TRF treatment significantly ($p<0.001$) increased the number of CD31-positive cells on days 7 and 14.

Collagen is the major component of the extracellular matrix, which is essential for wound closure. Collagen synthesis, deposition, remodelling

and maturation are crucial during tissue repair and regeneration (Thangavel *et al.*, 2017). Collagen biosynthesis in tissue sections was examined by Masson's trichrome staining (Daemi *et al.*, 2019; Zadeh Gharaboghaz *et al.*, 2020) on day 14 (*Figure 3e*). The results showed that granulation tissues in TRF-treated diabetic wounds exhibited collagen densities that were similar to those of normal wound healing. Treatment with the TRF induced significantly higher collagen synthesis and deposition than diabetic control wounds. This result suggests that topical application of the TRF may improve collagen synthesis, maturation and deposition.

Protein and Hydroxyproline Levels in Wound Tissues

Protein and hydroxyproline levels were measured on days 7 and 14 (*Table 2*). The level of protein indicates the cellular proliferation rate in the wound site (Lin *et al.*, 2012). The protein level in the T2D control group was significantly lower ($p<0.05$) than that in the normal control on days 7 and 14. However, TRF treatment significantly increased ($p<0.01$) the protein level on days 7 and 14 ($p<0.05$) compared to that in the T2D control. The hydroxyproline level was also significantly reduced ($p<0.001$) on days 7 and 14 in the T2D group compared to the normal control. However, TRF-treated wounds showed a significant ($p<0.001$) increase in hydroxyproline on days 7 and 14. The concentration of hydroxyproline reflects the collagen concentration in tissue, and a higher concentration indicates a faster rate of wound healing, providing the tissue matrix with integrity and strength (Dwivedi *et al.*, 2017). A high hydroxyproline level also indicates an increase in cellular proliferation and collagen synthesis (Dwivedi *et al.*, 2017).
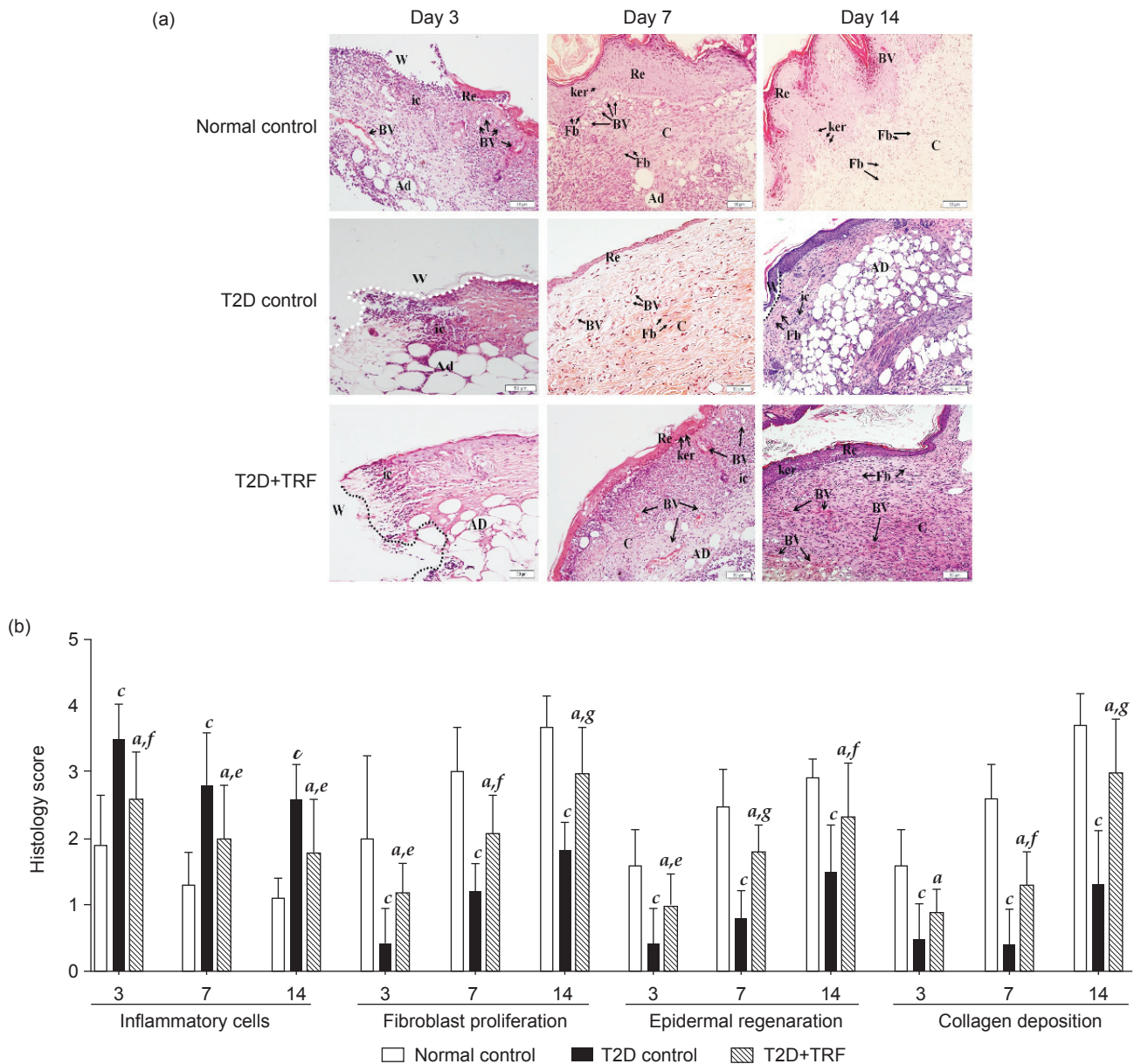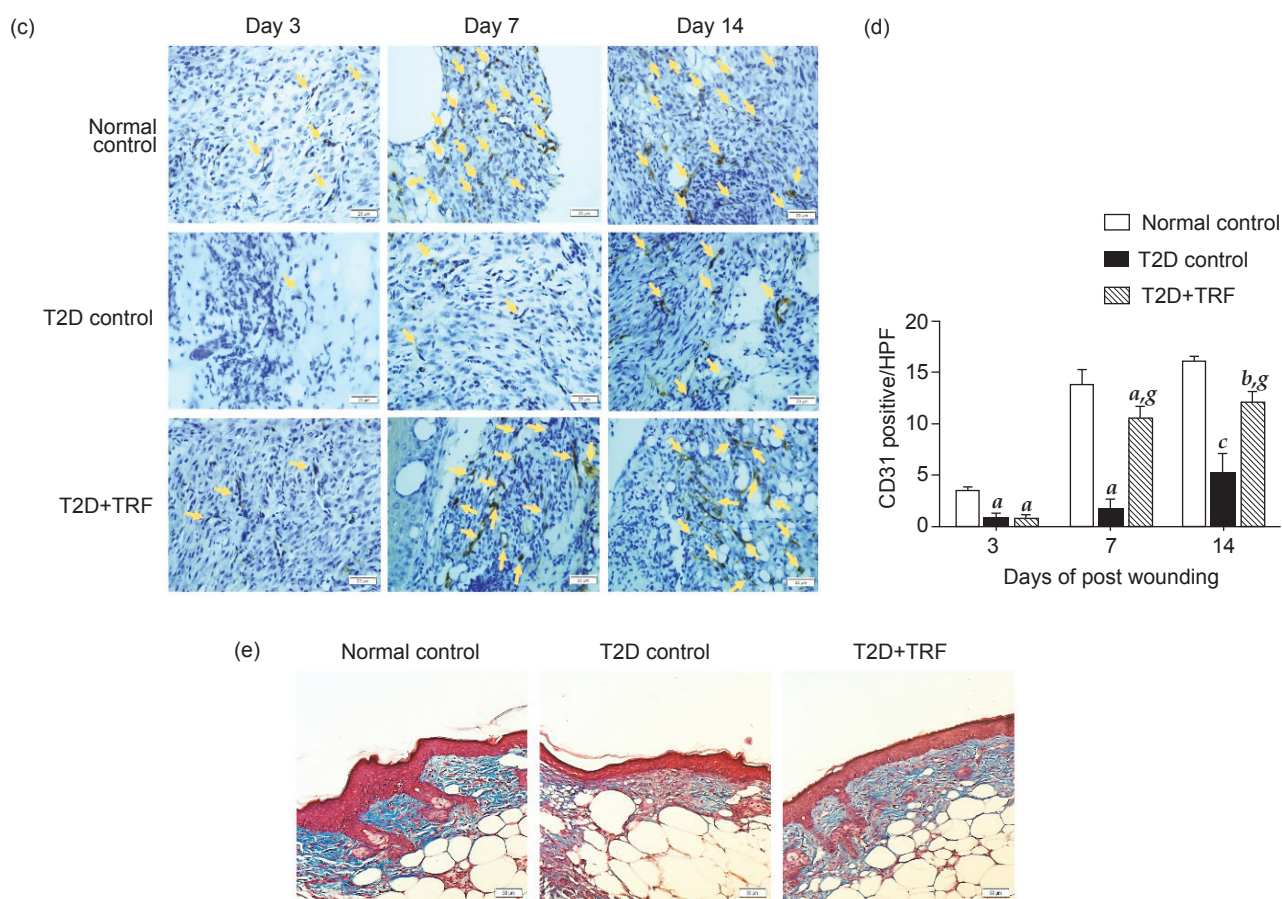
Figure 3. Representative photomicrographs showing the histological features of wounds using (a) H&E staining (n=3). Magnification (20×) with a scale bar of 50 μm; W, wound (dotted line); BV, blood vessel; AD adipose tissue; SC, subcutaneous; Fb, fibroblast; ic, inflammatory cell. (b) Histological score of inflammatory cell infiltration, fibroblast proliferation, epidermal regeneration and collagen deposition (n=3). (c) CD31-stained granulation tissues on days 3, 7 and 14. (d) Number of CD31-positive cells on days 3, 7 and 14 (n=3). Yellow arrows show the formation of blood vessels. (e) Masson's trichrome staining (n=3) on day 14. Blue staining represents collagen fibre deposition in the wounds. The data are the mean ± SEM (n=3) and were calculated using two-way ANOVA with Tukey's multiple comparison test. ^{a}p<0.05, ^{b}p<0.01, ^{c}p<0.001 vs. the normal control; ^{e}p<0.05, ^{f}p<0.01, ^{g}p<0.001 vs. the T2D control.

Effect of the TRF on TGF-β1 and MMP-9 Levels

TGF-β, a transforming growth factor, plays a critical role in each phase of wound healing by suppressing the inflammatory response and supporting granulation tissue development at the wound site (Wang *et al.*, 2017). A significant reduction ($p<0.001$) in TGF-β1 levels was observed in T2D control wound tissue compared to normal control wound tissue on days 7 and 14. However, TRF treatment significantly ($p<0.001$) increased the level of TGF-β1 on days 7 and 14 compared to that in the diabetic control.

High levels of MMP-9 in diabetic wounds often lead to excessive degradation of the extracellular matrix and reduced tensile strength of the wound (Ayuk *et al.*, 2016). Our data showed significantly higher ($p<0.001$) concentrations of MMP-9 in T2D control wounds than in normal control wounds on days 7 and 14. However, treatment with the TRF significantly decreased MMP-9 production on days 7 and 14 ($p<0.001$) compared to those in the diabetic control (*Table 2*).

The TRF Reduces Oxidative Stress in Diabetic Wounds

The first line of defence against oxidants during injury involves the antioxidants CAT and GPx (Ighodaro and Akinloye, 2018; Kurahasi and Fujii, 2015). In the present study, the T2D control group showed significantly lower ($p<0.05$) CAT activity on days 7 and 14 than the normal control group. However, TRF treatment significantly increased CAT activity on days 7 ($p<0.01$) and 14 ($p<0.05$) compared to that in the T2D control (*Figure 4a*). The T2D control group showed significantly ($p<0.05$) lower GPx activity on days 7 and 14 postinjury than the normal controls. In contrast, TRF-treated wounds showed significantly ($p<0.05$) higher GPx activity on day 14 than T2D control wounds (*Figure 4b*). The TRF has also been reported to increase other antioxidants, such as superoxide dismutase (SOD) and glutathione (GSH), but reduce lipid peroxidation in T2D wounds (Shahrim *et al.*, 2016; 2019).

Myeloperoxidase protects against infection during injury by killing pathogens. It also acts as

TABLE 2. EFFECT OF THE TRF ON PROTEIN, HYDROXYPROLINE, TGF-B1 AND MMP-9 LEVELS

Group	Protein content (µg 100 mg⁻¹ tissue)		Hydroxyproline (µg 100 mg⁻¹ tissue)		TGF-β1 (pg mL⁻¹)		MMP-9 (pg mL⁻¹)	
	Day 7	Day 14	Day 7	Day 14	Day 7	Day 14	Day 7	Day 14
Normal ctrl	69.23 ± 4.96	54.06 ± 5.96	234.03 ± 4.59	127.34 ± 0.653	183.54 ± 3.33	226.83 ± 20.09	25.88 ± 0.81	17.24 ± 1.50
T2D ctrl	48.78 ± 6.55^a	51.37 ± 5.91^a	47.42 ± 0.38^c	54.60 ± 0.38^c	43.01 ± 1.51^c	65.21 ± 1.97^c	70.33 ± 0.16^c	57.61 ± 0.44^c
T2D+TRF	63.76 ± 5.16^e	70.83 ± 3.95^{a,d}	185.40 ± 4.94^{c,f}	134.51 ± 5.32^{c,f}	145.46 ± 1.70^{c,f}	123.06 ± 1.11^{c,f}	29.21 ± 3.49^f	20.68 ± 0.30^f

Note: The values are expressed as the mean ± SEM (n=3) of the level of protein, hydroxyproline, TGF-β1, and MMP-9 and were analysed using two-way ANOVA with Tukey's multiple comparison test. $^a p<0.05$, $^b p<0.01$, $^c p<0.001$ *vs.* the normal control. $^d p<0.05$, $^e p<0.01$, $^f p<0.001$ *vs.* the T2D control.

an indicator of neutrophil infiltration in the wound site, which is the first sign of inflammation or injury to cells and tissues (Khan *et al.*, 2018). However, MPO could induce oxidative stress, inflammation, and tissue damage when its levels become too high (Ferdous *et al.*, 2020). MPO activity was significantly higher ($p<0.05$) on day 7 in the T2D control group than in the normal control group. However, the TRF significantly ($p<0.05$) attenuated MPO activity on day 7 compared to that in the T2D control (*Figure 4c*).

Cytokine Profile of T2D Wounds Treated with the TRF

A multiplex protein array was carried out to determine the effects of TRF on cytokine levels in tissue collected from wounds on days 1, 3, 7 and 14. This analysis included the proinflammatory interleukin family (IL-1α and IL-17A), leukaemia inhibitory factor (LIF) and interleukin-4 (IL-4), which are anti-inflammatory markers. The chemokines analysed included eotaxin, monocyte chemoattractant protein-1 (MCP-1), MCP-3, macrophage inflammatory proteins-1 alpha (MIP-1α), regulated upon activation, normal T cell expressed and presumably secreted (RANTES),

LIX/CXCL-5 (C-X-C motif chemokine 5), growth regulated oncogene (GRO-α), macrophage inflammatory protein-2 (MIP-2) and interferon gamma-induced protein 10 (IP-10). Growth factors such as granulocyte-macrophage colony-stimulating factor (GM-CSF) and vascular endothelial growth factor (VEGF) were also examined.

Inflammatory mediators are mostly synthesised *de novo* by activated cells in response to wounding (Chang *et al.*, 2018). Chronic wounds are in a persistent inflammatory state, as indicated by excessive inflammatory mediator release (Ligi *et al.*, 2016). Profound increases in proinflammatory cytokines (IL-1α, IL-17A, and LIF) were observed in T2D wounds compared to normal controls (*Figures 5a-c*). Our results showed that treatment with the TRF significantly abated proinflammatory cytokine production, particularly that of IL-1α, on day 1 ($p<0.001$), day 3 ($p<0.05$), day 7 ($p<0.05$), and day 14 ($p<0.01$) (*Figure 5a*). IL-17A was also reported to be involved in the pathogenesis of chronic wounds (Hadian *et al.*, 2019). This study showed that TRF treatment significantly mitigated IL-17A at day 7 ($p<0.05$) compared to that in the diabetic control (*Figure 5b*). Moreover, LIF, a cytokine belonging to the IL-6 family, was significantly increased in the T2D group; however, the TRF-treated group exhibited a
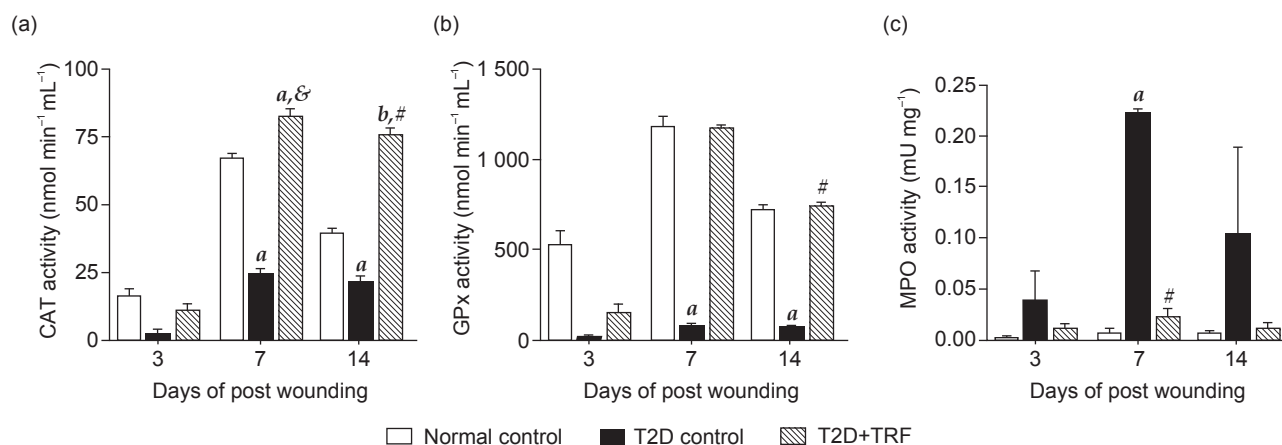

Figure 4. Effects of the TRF on (a) CAT, (b) GPx, and (c) MPO activities in wound tissues. The data are the mean ± SEM (n=3) and were calculated using two-way ANOVA with Tukey's multiple comparison test. $^a p<0.05$, $^b p<0.01$ vs. the normal control; $^\# p<0.05$, $^\& p<0.001$ vs. the T2D control.

reduction in LIF on day 1 ($p<0.05$), day 3 ($p<0.001$), and day 7 ($p<0.001$) compared to the diabetic control (*Figure 5c*).

IL-4 production was significantly increased in TRF-treated wounds on day 1 ($p<0.01$), day 3 ($p<0.05$), and day 7 ($p<0.05$) compared to that in T2D control wounds (*Figure 5d*). This anti-inflammatory marker significantly contributes to the healing process in wounds by promoting neuronal and glial survival by inhibiting the local response to inflammation, as well as signalling nerve growth factor production and GM-CSF, which are beneficial for diabetic peripheral neuropathy (Zhao *et al.*, 2016).

Our findings also showed a significant increase ($p<0.05$) in eotaxin in TRF-treated wounds on days 3, 7 and 14 compared to T2D control wounds (*Figure 6a*). This increase might be related to the function of eotaxin, a chemotactic protein that attracts eosinophils and promotes collagen deposition, angiogenesis, and mitogenesis during injury (Burns *et al.*, 2020). Eotaxin is a proinflammatory chemokine, is a small chemotactic cytokine that is secreted by a variety of cells in the wound (Ridiandries *et al.*, 2018) and functions to regulate the migration of cells to the injured area (Sokol and Luster, 2015). The chemokines MCP-1 and MIP-2 are known to

modulate postinfection inflammation and tissue lesions (Fan *et al.*, 2021). However, overexpression of these biomolecules in the wounds of diabetic patients may amplify tissue permeability and leucocyte intrusion, leading to chronic inflammation in the surrounding normal skin and subsequently hindering wound recovery (Fan *et al.*, 2021). Similarly, significant reductions in MCP-1 were observed on day 3 ($p<0.001$) compared to those in the T2D control (*Figure 6b*). MCP-3 has been reported to be a negative regulator of cutaneous inflammation, and its upregulation has been correlated with various inflammatory conditions, such as infection, the tumour microenvironment, and cardiovascular disease (Ford *et al.*, 2019). Our data showed that MCP-3 production was reduced by the TRF on day 3 ($p<0.05$), days 7 ($p<0.01$) and 14 ($p<0.05$) compared to the T2D control (*Figure 6c*). However, treatment with the TRF significantly ($p<0.05$) increased MIP-1α on days 1, 3 and 7 compared to that in the T2D control (*Figure 6d*). This chemokine is often found to be increased in foot ulcer patients (Van Asten *et al.*, 2017). Additionally, MIP-2 was significantly increased on day 1 ($p<0.05$), day 7 ($p<0.01$), and day 14 ($p<0.05$) compared to those in the T2D control (*Figure 6e*).
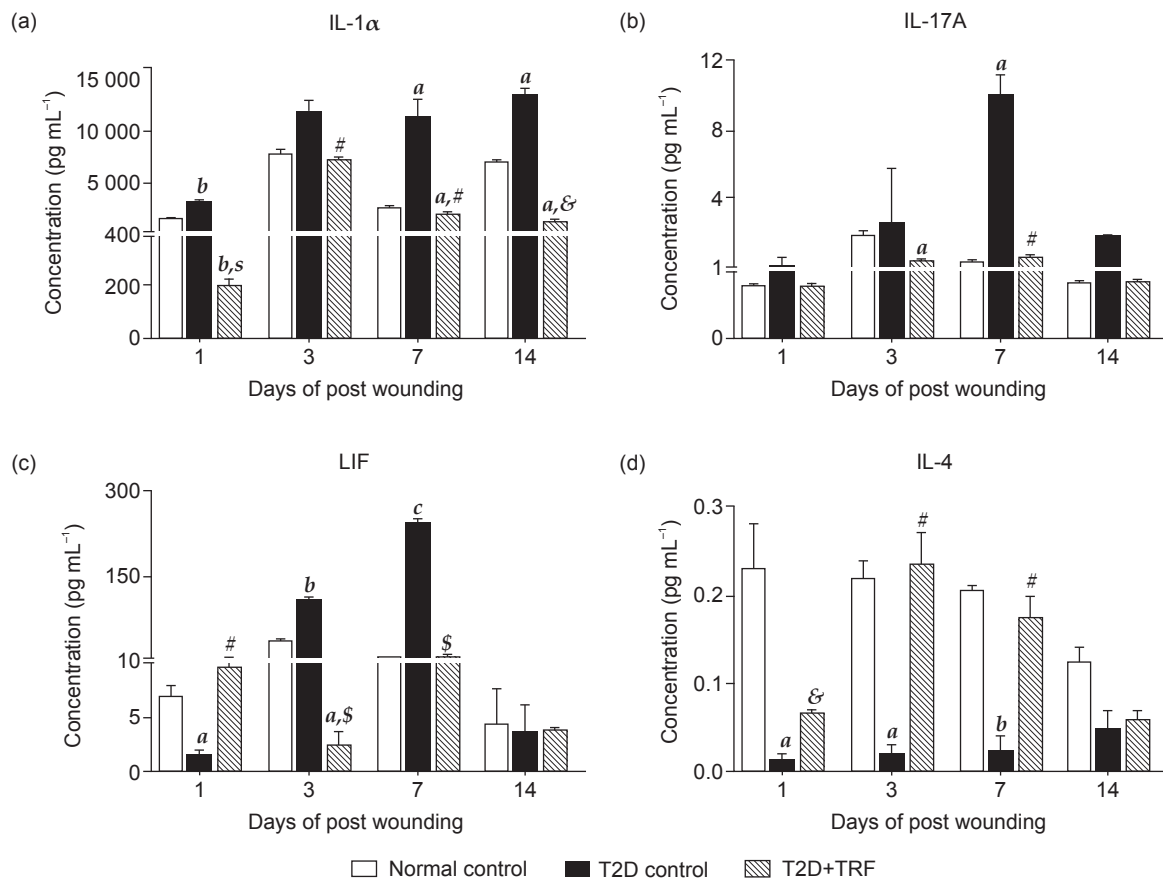
Figure 5. (a-c) Changes in proinflammatory, and (d) anti-inflammatory cytokines in wound tissues in response to TRF. The data are the mean ± SEM (n=3) and were calculated using two-way ANOVA with Tukey's multiple comparison test. [a]p<0.05, [b]p<0.01, [c]p<0.001 vs. the normal control; [#]p<0.05, [&]p<0.01, [$]p<0.001 vs. the T2D control.
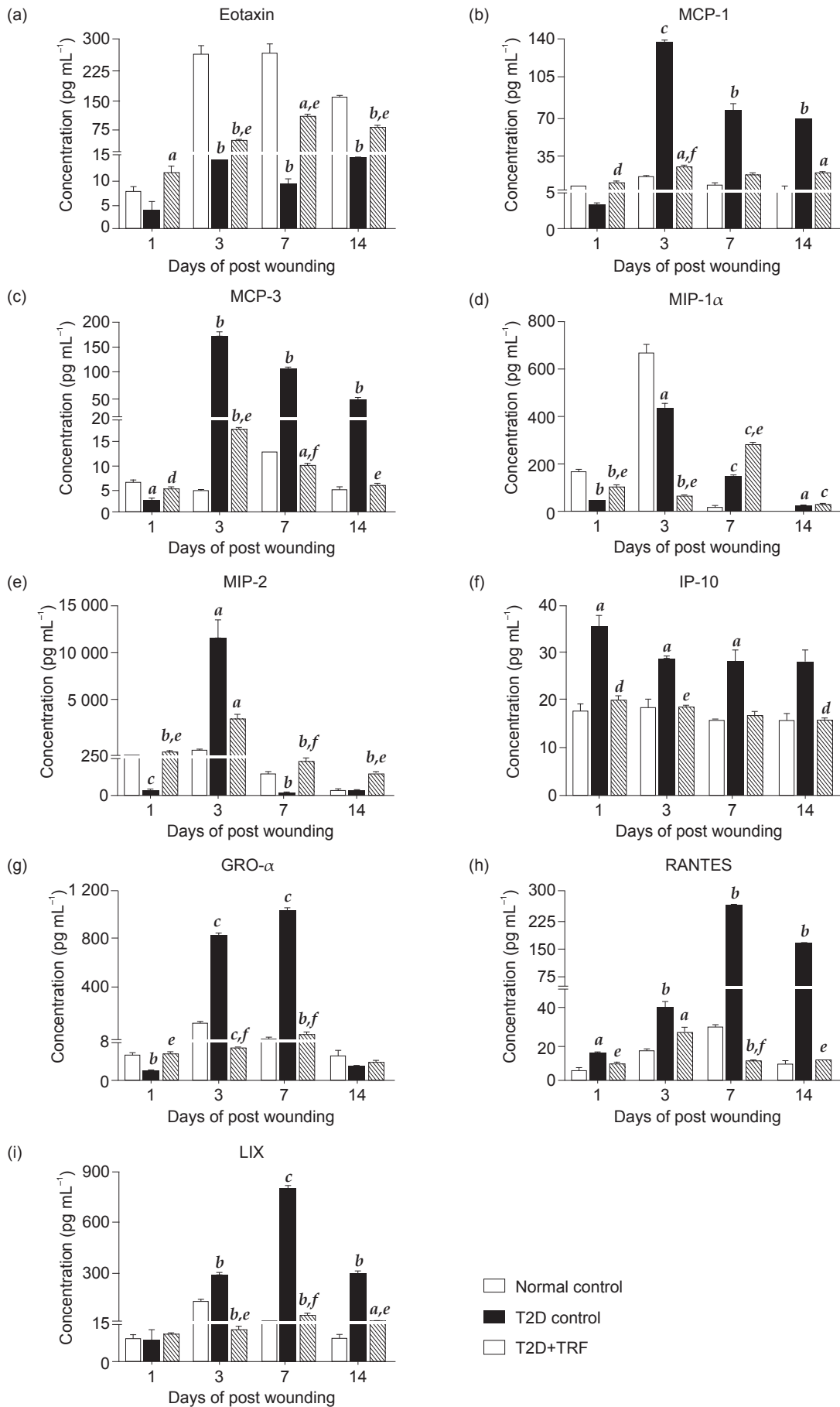
Figure 6. Changes in chemokines in skin wound tissues in response to TRF. The data are the mean ± SEM (n=3) and were calculated using two-way ANOVA with Tukey's multiple comparison test. [a]p<0.05, [b]p<0.01, [c]p<0.001, [d]p<0.0001 vs. the normal control; [e]p<0.05, [f]p<0.01 vs. the T2D control.

Moreover, the inflammatory chemokine IP-10 has been reported to be increased in diabetic patients due to inflammation induced by oxidative stress (Fatehi *et al.*, 2015). TRF treatment significantly reduced IP-10 ($p<0.05$) on day 3 compared to that in the T2D control (*Figure 6f*). Higher GRO-α production was observed on days 3 ($p<0.001$) and 7 ($p<0.001$) in T2D controls than in normal controls (*Figure 6g*). Interestingly, a significant reduction was observed in TRF-treated wounds on days 1 ($p<0.05$), 3 ($p<0.01$) and 7 ($p<0.01$) compared to diabetic control wounds.

RANTES and LIX have been reported to be crucially associated with impaired wound healing (Ligi *et al.*, 2016). Low levels of RANTES have been reported to enhance the inflammatory response in venous leg ulcers (VLUs) throughout the healing process in the wound (Ligi *et al.*, 2016). TRF treatment significantly decreased RANTES levels in diabetic mice on day 1 ($p<0.05$), day 7 ($p<0.01$), and day 14 ($p<0.05$) compared to the T2D control (*Figure 6h*). A significant decrease in LIX was observed in the TRF-treated group on day 3 ($p<0.05$), day 7 ($p<0.01$) and day 14 ($p<0.05$) compared to the T2D control (*Figure 6i*).

Activation of granulocyte and macrophage lineages is initiated by the pleiotropic cytokine GM-CSF (Rho *et al.*, 2015), which triggers the proliferation of monocytes and granulocytes (neutrophils, eosinophils and basophils) (Bhattacharya *et al.*, 2015; Weston *et al.*, 2018). Due to these effects, an imbalance in GM-CSF production/signalling through ERK1/2 and NFκB activation (Bhattacharya *et al.*, 2015) may lead to harmful inflammatory conditions (Lotfi *et al.*, 2019). Initially, this cytokine was low on day 1 ($p<0.01$) and then increased on day 3 ($p<0.001$) and day 7 ($p<0.01$) in T2D controls compared with normal controls (*Figure 7a*). Treatment with TRF elevated GM-CSF levels on day 1 ($p<0.01$), but these levels declined on day 3 ($p<0.01$) and increased again on days 7 and 14 ($p<0.05$) compared to those of the T2D controls (*Figure 7a*).

VEGF is known to initiate wound healing and promote expansion of the vascular network (DiPietro, 2016; Zhou *et al.*, 2017) throughout granulation tissue that is essential for providing oxygen, immune cells and nutrients to aid wound healing (Hutchings *et al.*, 2021). This study showed that the production of VEGF in diabetic group was significantly decreased on day 1 ($p<0.01$), day 3 ($p<0.001$), day 7 ($p<0.01$), and day 14 ($p<0.05$) compared to that in the normal control (*Figure 7b*). However, treatment with the TRF significantly increased VEGF production on day 1 ($p<0.05$), day 3 ($p<0.01$), day 7 ($p<0.05$) and day 14 ($p<0.05$) compared to that in the T2D control. The increase in VEGF production suggests its role in facilitating angiogenesis, thus, promoting the formation of more blood vessels and improving blood flow in the wound area (Johnson and Wilgus, 2014).

There have been several studies on the efficacy of the TRF mediated by a variety of pharmacological activities, including antioxidant (Ahsan *et al.*, 2014), anti-inflammatory and wound healing activities (Elsy *et al.*, 2017). In the present study on T2D diabetic mice, topical application resulted in the acceleration of wound closure, improved re-epithelialisation and increased formation of granulation tissue, which consists of various cells, vascular capillaries and loose connective tissues to fill the injured space (Karim *et al.*, 2021; Tan *et al.*, 2019). Moreover, marked collagen synthesis and deposition with high levels of hydroxyproline
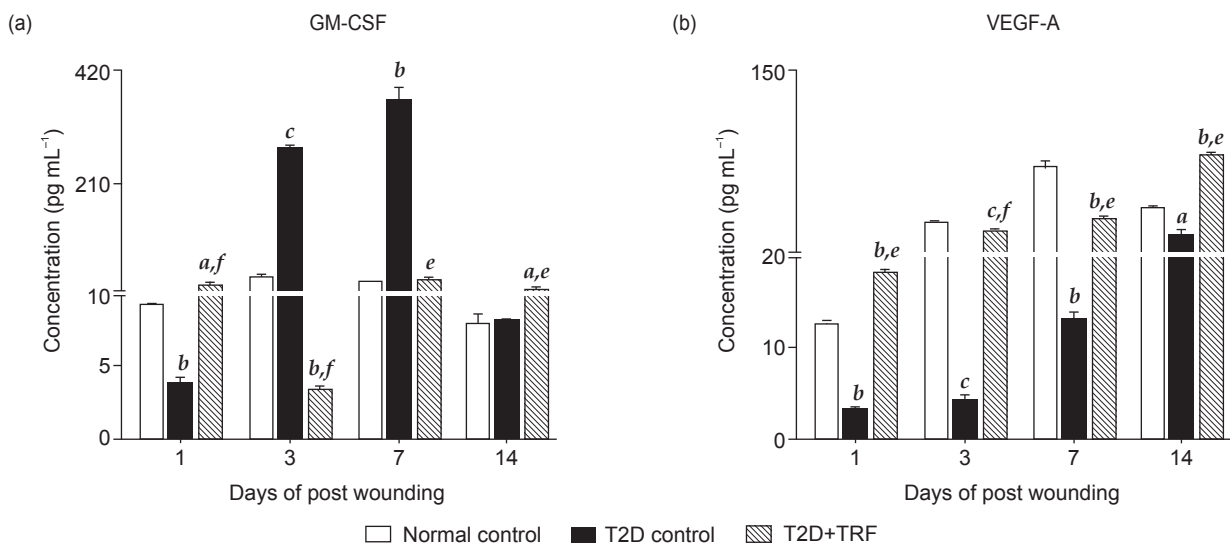

Figure 7. Effects of TRF on the levels of (a) GM-CSF, and (b) VEGF-A in skin wound tissues. GM-CSF and VEGF-A levels are represented as the mean ± SEM (n=3) and were calculated using two-way ANOVA with Tukey's multiple comparison test. ^a^p<0.05, ^b^p<0.01, ^c^p<0.001 vs. the normal control; ^e^p<0.05, ^f^p<0.01 vs. the T2D control.
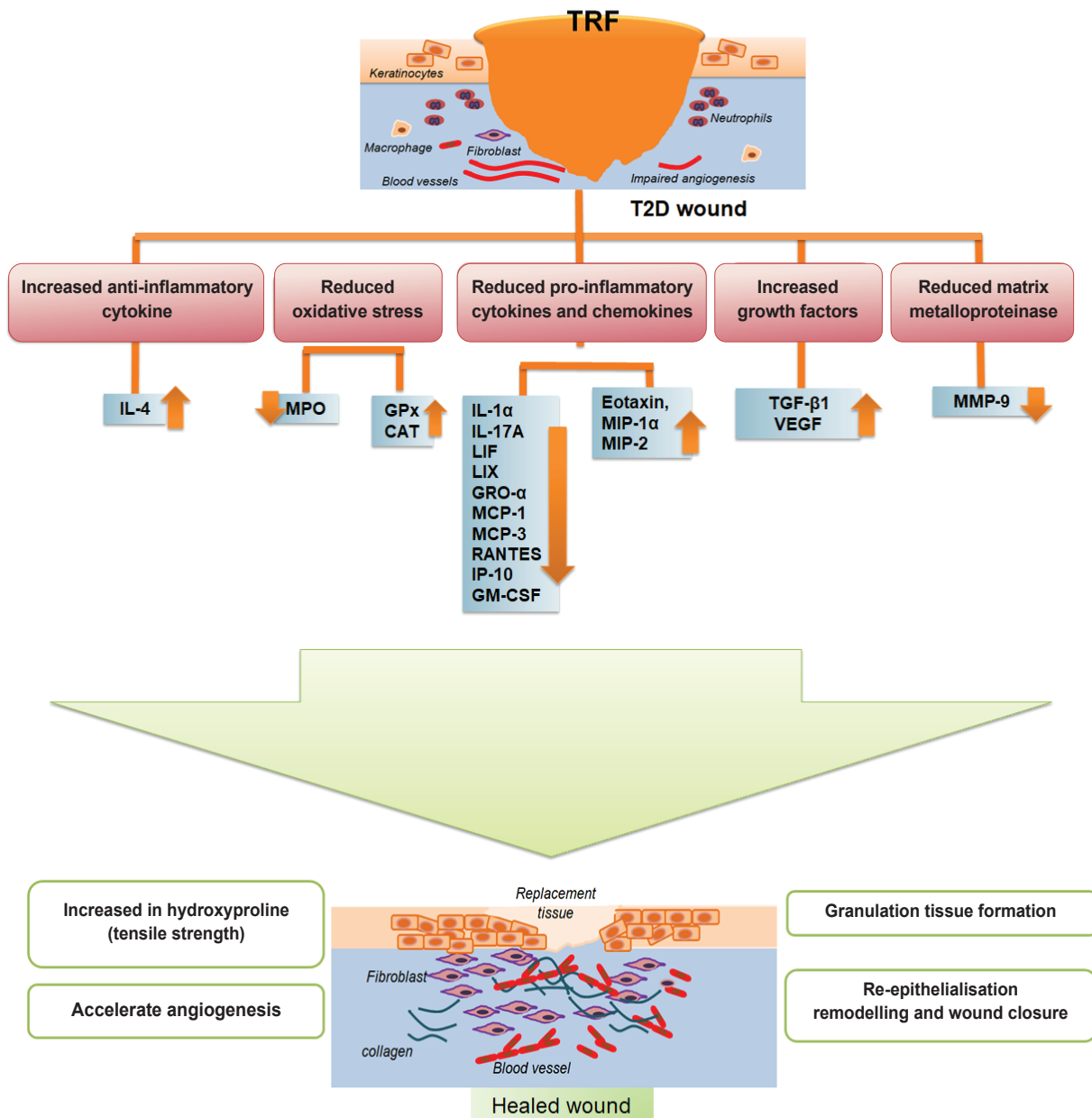
Figure 8. The suggested mechanism by which the TRF enhances wound healing under diabetic conditions.

were observed in TRF-treated diabetic wounds. These results may be due to decreased production of proinflammatory cytokines and metalloproteinases, and increased levels of growth factors released by cells to induce the proliferation and migration of keratinocytes, macrophages, and fibroblasts into the wound space (Rousselle *et al.*, 2019; Tan *et al.*, 2019; Yamakawa and Hayashida, 2019). We also observed increases in anti-inflammatory cytokines and antioxidant enzymes at the wound site in diabetic mice. Based on these findings, we proposed a schematic illustration of the potential mechanism by which TRF enables successful healing of wounds in a T2D mouse model (*Figure 8*) due to the anti-inflammatory and antioxidant potential of the TRF.

CONCLUSION

Topical application of the TRF promotes wound repair in the cutaneous wounds of T2D mice. The results of our study demonstrated that topical TRF application accelerated cutaneous wound repair in T2D mice by elevating the levels of antioxidant enzymes such as CAT and GPx and cytokines such as IL-4, reducing MPO, and modulating proinflammatory cytokines, such as IL-1α, IL-17A, and LIF, chemokines (GRO-α, MCP-1, -3, RANTES, IP-10) and GM-CSF in T2D wounds. Moreover, eotaxin, MIP-1α, -2, IL-4, VEGF and TGF-β1 levels were elevated in TRF-treated T2D wounds, which accelerated the progression of healing. Thus, the findings of this study suggest the benefits and

potential use of the TRF as a therapeutic agent to treat cutaneous wounds in T2D patients.

REFERENCES

Ahsan, H; Ahad, A; Iqbal, J and Siddiqui, W A (2014). Pharmacological potential of tocotrienols: A review. *Nutr. Metab., 11(1)*: 52.

Alghazeer, R; Alghazir, N; Awayn, N; Ahtiwesh, O and Elgahmasi, S (2018). Biomarkers of oxidative stress and antioxidant defense in patients with type 1 diabetes mellitus. *Ibnosina J. Med. Biomed. Sci., 10(6)*: 198.

Ayuk, S M; Abrahamse, H and Houreld, N N (2016). The role of matrix metalloproteinases in diabetic wound healing in relation to photobiomodulation. *J. Diabetes Res., 2016*: 2897656.

Bhattacharya, P; Thiruppathi, M; Elshabrawy, H A; Alharshawi, K; Kumar, P and Prabhakar, B S (2015). GM-CSF: An immune modulatory cytokine that can suppress autoimmunity. *Cytokine, 75(2)*: 261-271.

Brandt, S L; Wang, S; Dejani, N N; Klopfenstein, N; Winfree, S; Filgueiras, L; McCarthy, B P; Territo, P R and Serezani, C H (2018). Excessive localized leukotriene B4 levels dictate poor skin host defense in diabetic mice. *JCI Insight, 3(17)*: e120220.

Burns, B; Jackson, K; Farinas, A; Pollins, A; Bellan, L; Perdikis, G; Kassis, S and Thayer, W (2020). Eosinophil infiltration of burn wounds in young and older burn patients. *Burns, 46(5)*: 1136-1141.

Cano Sanchez, M; Lancel, S; Boulanger, E and Neviere, R (2018). Targeting oxidative stress and mitochondrial dysfunction in the treatment of impaired wound healing: A systematic review. *Antioxidants, 7(8)*: 98.

Chang, Y C; Soriano, M; Hahn, R A; Casillas, R P; Gordon, M K; Laskin, J D and Gerecke, D R (2018). Expression of cytokines and chemokines in mouse skin treated with sulfur mustard. *Toxicol. Appl. Pharmacol., 355*: 52-59.

Cheng, H S; Ton, S H; Tan, J B L and Abdul Kadir, K (2017). The ameliorative effects of a tocotrienol-rich fraction on the AGE-RAGE axis and hypertension in high-fat-diet-fed rats with metabolic syndrome. *Nutrients, 9(9)*: 984.

Daemi, A; Lotfi, M; Farahpour, M R; Oryan, A; Ghayour, S J and Sonboli, A (2019). Topical application of *Cinnamomum* hydroethanolic extract improves wound healing by enhancing re-epithelialization and keratin biosynthesis in streptozotocin-induced diabetic mice. *Pharm. Biol., 57(1)*: 799-806.

Deng, L; Du, C; Song, P; Chen, T; Rui, S; Armstrong, D G and Deng, W (2021). The role of oxidative stress and antioxidants in diabetic wound healing. *Oxid. Med. Cell. Longev., 2021*. DOI: 10.1155/2021/8852759. eCollection 2021.

DiPietro, L A (2016). Angiogenesis and wound repair: When enough is enough. *J. Leukoc. Biol., 100(5)*: 979-984.

Dwivedi, D; Dwivedi, M; Malviya, S and Singh, V (2017). Evaluation of wound healing, anti-microbial and antioxidant potential of *Pongamia pinnata* in wistar rats. *J. Tradit. Complement. Med., 7(1)*: 79-85.

Elsy, B; Khan, A A and Maheshwari, V (2017). Effect of co-administration of vitamin E isoforms d-α-tocopherol and d-δ-tocotrienol rich fraction on the healing of skin wounds in diabetic rats. *Int. J. Biomed. Eng. Clin. Sci., 3(5)*: 52-62.

Fan, S L; Lin, J A; Chen, S Y; Lin, J H; Lin, H T; Chen, Y Y and Yen, G C (2021). Effects of Hsian-tsao (*Mesona procumbens* Hemsl.) extracts and its polysaccharides on the promotion of wound healing under diabetes-like conditions. *Food and Funct., 12(1)*: 119-132.

Fatehi, F; Hassanshahi, G; Hosseini, S E; Zade, A S and Taghavi, M M (2015). Systemic effect of Angipars on regulation of wound healing is mediated by CXC in diabetes. *Trop. J. Pharm. Res., 14(1)*: 79-85.

Ferdous, M; Sonam, C R; Mudi, S R; Ali, M; Jasmin, S; Fariduddin, M; Alam, S M K; Arslan, M I and Biswas, S K (2020). Expression of neutrophil elastase and myeloperoxidase mRNA in patients with newly diagnosed type 2 diabetes mellitus. *Diabetes Metab. Syndr.: Clin. Res. Rev., 14(2)*: 83-85.

Fields, J K; Günther, S and Sundberg, E J (2019). Structural basis of IL-1 family cytokine signaling. *Front. Immunol., 10*: 1412.

Ford, J; Hughson, A; Lim, K; Bardina, S V; Lu, W; Charo, I F; Lim, J K and Fowell, D J (2019). CCL7 is a negative regulator of cutaneous inflammation

following *Leishmania* major infection. *Front. Immunol., 9*: 3063.

Hasan, Z A A; Idris, Z; Gani, S and Basri, M (2018). *In vitro* safety evaluation of palm tocotrienol-rich fraction nanoemulsions for topical application. *J. Oil Palm Res., 30*: 150-162.

Hadian, Y; Bagood, M D; Dahle, S E; Sood, A and Isseroff, R R (2019). Interleukin-17: Potential target for chronic wounds. *Mediat. Inflamm., 2019*. DOI: 10.1155/2019/1297675.

Hemmati, A A; Larki-Harchegani, A; Shahbib, S; Jalali, A; Rezaei, A and Housmand, G (2018). Wound healing property of milk in full thickness wound model of rabbit. *Int. J. Surg., 54*: 133-140.

Hutchings, G; Kruszyna, Ł; Nawrocki, M J; Strauss, E; Bryl, R; Spaczyńska, J; Perek, B; Jemielity, M; Mozdziak, P; Kempisty, B; Nowicki, M and Krasiński, Z (2021). Molecular mechanisms associated with ROS-dependent angiogenesis in lower extremity artery disease. *Antioxidants, 10(5)*: 735.

Ighodaro, O and Akinloye, O (2018). First line defence antioxidants-superoxide dismutase (SOD), catalase (CAT) and glutathione peroxidase (GPX): Their fundamental role in the entire antioxidant defence grid. *Alexandria J. Med., 54(4)*: 287-293.

Johnson, K E and Wilgus, T A (2014). Vascular endothelial growth factor and angiogenesis in the regulation of cutaneous wound repair. *Adv. Wound Care, 3(10)*: 647-661.

Jones, J I; Nguyen, T T; Peng, Z and Chang, M (2019). Targeting MMP-9 in diabetic foot ulcers. *Pharmaceuticals, 12(2)*: 79.

Karim, S; AlKreathy, H M; Ahmad, A and Khan, M I (2021). Effects of methanolic extract based-gel from Saudi-pomegranate (*Punica granatum* L.) peels with enhanced *in vivo* healing potential on excision wounds in diabetic rats. *Front. Pharmacol., 12*: 1337.

Katsuhiro, M; Teoh, S H; Yamashiro, H; Shinohara, M; Fatchiyah, F; Ohta, T and Yamada, T (2018). Effects on glycemic control in impaired wound healing in Spontaneously Diabetic Torii (SDT) fatty rats. *Med. Arch., 72(1)*: 4.

Khan, A A; Alsahli, M A and Rahmani, A H (2018). Myeloperoxidase as an active disease biomarker: Recent biochemical and pathological perspectives. *Med. Sci., 6(2)*: 33.

Khor, S C; Wan Ngah, W Z; Mohd Yusof, Y A; Abdul Karim, N and Makpol, S (2017). Tocotrienol-rich fraction ameliorates antioxidant defense mechanisms and improves replicative senescence-associated oxidative stress in human myoblasts. *Oxid. Med. Cell Longev., 2017*.

Kurahashi, T and Fujii, J (2015). Roles of antioxidative enzymes in wound healing. *J. Dev. Biol., 3(2)*: 57-70.

Liarte, S; Bernabé-García, Á and Nicolás, F J (2020). Role of TGF-in skin chronic wounds: A keratinocyte perspective. *Cells, 9(2)*: 306.

Ligi, D; Mosti, G; Croce, L; Raffetto, J D and Mannello, F (2016). Chronic venous disease-Part I: Inflammatory biomarkers in wound healing. *Biochim Biophys Acta-Mol. Basis. Dis., 1862(10)*: 1964-1974.

Lin, T S; Abd Latiff, A; Abd Hamid, N A; Wan Ngah, W Z and Mazlan, M (2012). Evaluation of topical tocopherol cream on cutaneous wound healing in streptozotocin-induced diabetic rats. *Evid. Based Complement. Alternat. Med., 2012*. DOI: 10.1155/2012/491027.

Lotfi, N; Thome, R; Rezaei, N; Zhang, G X; Rezaei, N; Rostami, A and Esmaeil, N (2019). Roles of GM-CSF in the pathogenesis of autoimmune diseases: An update. *Front. Immunol., 10*: 1265.

Manzuoerh, R; Farahpour, M R; Oryan, A and Sonboli, A (2019). Effectiveness of topical administration of *Anethum graveolens* essential oil on MRSA-infected wounds. *Biomed. Pharmacother., 109*: 1650-1658.

Matough, F A; Budin, S B; Hamid, Z A; Abdul-Rahman, M; Al-Wahaibi, N and Mohammed, J (2014). Tocotrienol-rich fraction from palm oil prevents oxidative damage in diabetic rats. *Sultan Qaboos Univ. Med. J., 14(1)*: e95.

Musalmah, M; Nizrana, M; Fairuz, A; NoorAini, A; Azian, A; Gapor, M and Ngah, W W (2005). Comparative effects of palm vitamin E and α-tocopherol on healing and wound tissue antioxidant enzyme levels in diabetic rats. *Lipids, 40(6)*: 575-580.

Nor Azman, N H E; Goon, J A; Abdul Ghani, S M; Hamid, Z and Wan Ngah, W Z (2018). Comparing palm oil, tocotrienol-rich fraction and α-tocopherol supplementation on the antioxidant levels of older adults. *Antioxidants, 7(6)*: 74.

Okonkwo, U A and DiPietro, L A (2017). Diabetes and wound angiogenesis. *Int. J. Mol. Sci., 18(7)*: 1419.

Peiseler, M and Kubes, P (2019). More friend than foe: The emerging role of neutrophils in tissue repair. *J. Clin. Invest., 129(7)*: 2629-2639.

Raziyeva, K; Kim, Y; Zharkinbekov, Z; Kassymbek, K; Jimi, S and Saparov, A (2021). Immunology of acute and chronic wound healing. *Biomolecules, 11(5)*: 700.

Rho, C R; Park, M Y and Kang, S (2015). Effects of granulocyte-macrophage colony-stimulating (GM-CSF) factor on corneal epithelial cells in corneal wound healing model. *PLoS ONE, 10(9)*: e0138020.

Ridiandries, A; Tan, J and Bursill, C A (2018). The role of chemokines in wound healing. *Int. J. Mol. Sci., 19(10)*: 3217.

Rodrigues, M; Kosaric, N; Bonham, C A and Gurtner, G C (2019). Wound healing: A cellular perspective. *Physiol. Rev., 99(1)*: 665-706.

Rousselle, P; Braye, F and Dayan, G (2019). Re-epithelialization of adult skin wounds: Cellular mechanisms and therapeutic strategies. *Adv. Drug Deliv. Rev., 146*: 344-365.

Serra, M B; Barroso, W A; da Silva, N N; Silva, S D N; Borges, A C R; Abreu, I C and Borges, M O D R (2017). From inflammation to current and alternative therapies involved in wound healing. *Int. J. Inflam., 2017*. DOI: 10.1155/2017/3406215.

Shahidi, F and De Camargo, A C (2016). Tocopherols and tocotrienols in common and emerging dietary sources: Occurrence, applications and health benefits. *Int. J. Mol. Sci., 17(10)*: 1745.

Shahrim, Z; Omar, Z; Zainal, Z and Hasan, Z A A (2016). Palm tocotrienol: A good antioxidant for skin wound healing. *Palm Oil Developments, 64*: 14-19.

Shahrim, Z; Makpol, S; Tan, G C and Azizul Hasan, Z A (2019). Clinical dermatology: Topical application of palm tocotrienol enhances cutaneous wound healing in diabetes. *Proc. of the 2019 International Palm Oil Congress - Oleo & Specialty Chemicals Conference*. MPOB, Bangi.

Sokol, C L and Luster, A D (2015). The chemokine system in innate immunity. *Cold Spring Harb. Perspect. Biol., 7(5)*: a016303.

Strang, H; Kaul, A; Parikh, U; Masri, L; Saravanan, S; Li, H; Miao, Q and Balaji, S (2020). *Wound Healing, Tissue Repair, and Regeneration in Diabetes*. Academic Press, Elsevier, Cambridge, Massachubetts, USA. p. 197-235.

Tan, W S; Arulselvan, P; Ng, S F; Taib, C N M; Sarian, M N and Fakurazi, S (2019). Improvement of diabetic wound healing by topical application of Vicenin-2 hydrocolloid film on Sprague Dawley rats. *BMC Complement. Altern. Med., 19(1)*: 1-16.

Thangavel, P; Ramachandran, B; Chakraborty, S; Kannan, R; Lonchin, S and Muthuvijayan, V (2017). Accelerated healing of diabetic wounds treated with L-glutamic acid loaded hydrogels through enhanced collagen deposition and angiogenesis: An *in vivo* study. *Sci. Rep., 7(1)*: 1-15.

Thangavel, P; Kannan, R; Ramachandran, B; Moorthy, G; Suguna, L and Muthuvijayan, V (2018). Development of reduced graphene oxide (rGO)-isabgol nanocomposite dressings for enhanced vascularization and accelerated wound healing in normal and diabetic rats. *J. Colloid Interface Sci., 517*: 251-264.

Tsalamandris, S; Antonopoulos, A S; Oikonomou, E; Papamikroulis, G A; Vogiatzi, G; Papaioannou, S; Deftereos, S and Tousoulis, D (2019). The role of inflammation in diabetes: Current concepts and future perspectives. *Eur. Cardiol., 14(1)*: 50.

Van Asten, S A; Nichols, A; La Fontaine, J; Bhavan, K; Peters, E J and Lavery, L A (2017). The value of inflammatory markers to diagnose and monitor diabetic foot osteomyelitis. *Int. Wound J., 14(1)*: 40-45.

Wang, L; Qin, W; Zhou, Y; Chen, B; Zhao, X; Zhao, H; Mi, E; Mi, E; Wang, Q and Ning, J (2017). Transforming growth factor β plays an important role in enhancing wound healing by topical application of Povidone-iodine. *Sci. Rep., 7(1)*: 991.

Weston, B R; Li, L and Tyson, J J (2018). Mathematical analysis of cytokine-induced differentiation of granulocyte-monocyte progenitor cells. *Front. Immunol., 9*: 2048.

Xiao, T; Yan, Z; Xiao, S and Xia, Y (2020). Proinflammatory cytokines regulate epidermal stem cells in wound epithelialization. *Stem Cell Res. Ther., 11(1)*: 1-9.

Yap, W N (2018). Tocotrienol-rich fraction attenuates UV-induced inflammaging: A bench to bedside study. *J. Cosmet. Dermatol., 17(3)*: 555-565.

Yamakawa, S and Hayashida, K (2019). Advances in surgical applications of growth factors for wound

healing. *Burns and Trauma, 7*. DOI: 10.1186/s41038-019-0148-1.

Yuan, Y; Das, S K and Li, M (2018). Vitamin D ameliorates impaired wound healing in streptozotocin-induced diabetic mice by suppressing NF-κB-mediated inflammatory genes. *Biosci. Rep., 38(2)*: BSR20171294.

Zadeh Gharaboghaz, M N; Farahpour, M R and Saghaie, S (2020). Topical co-administration of *Teucrium polium* hydroethanolic extract and Aloe vera gel triggered wound healing by accelerating cell proliferation in diabetic mouse model. *Biomed. Pharmacother, 127*: 110189.

Zhao, R; Liang, H; Clarke, E; Jackson, C and Xue, M (2016). Inflammation in chronic wounds. *Int. J. Mol. Sci., 17(12)*: 2085.

Zhou, J; Ni, M; Liu, X; Ren, Z and Zheng, Z (2017). Curcumol promotes vascular endothelial growth factor (VEGF)-mediated diabetic wound healing in streptozotocin-induced hyperglycemic rats. *Med. Sci. Monit., 23*: 555-562.

Zheng, Y; Ley, S H and Hu, F B (2018). Global aetiology and epidemiology of type 2 diabetes mellitus and its complications. *Nat. Rev. Endocrinol., 14(2)*: 88-98.

TOXICOLOGICAL ASSESSMENT OF REFINED PALM-PRESSED MESOCARP FIBRE OIL

**KIM-TIU TENG[1]*; RADHIKA LOGANATHAN[1]; EE LING SIEW[2,3]; HARRISON LIK NANG LAU[1]
and NOR FADILAH RAJAB[3,4]**

ABSTRACT

Refined palm-pressed mesocarp fibre oil (PMFO) is a rich source of phytonutrients, which merits further exploration as a functional food component. Current study aimed to evaluate the cytotoxicity and genotoxicity of refined PMFO using MTT [3-(4,5-dimethylthiazol-2-yl)-2,5-diphenyltetrazolium bromide] and alkaline comet assay, respectively. Acute oral toxicity assessment was performed on two groups of rats using a stepwise procedure based on OECD 423. Animals were observed for clinical effects at 30 min, hourly for 4 and 6 hr post dosing and once daily up to day 14. There were no inhibitory concentration (IC_{50}) values observed for refined PMFO treated V79-4 Chinese hamster lung cells as compared to positive control hydrogen peroxide (H_2O_2), where a concentration response effect was seen following treatment with H_2O_2 with an IC_{50} value of 1.568 mM. Refined PMFO has no capability to induce direct deoxyribonucleic acid (DNA) strand breakage in V79-4 cells. In addition, refined PMFO showed no-observed-adverse-effect level (NOAEL) up to 2000 mg/kg body weight of the animal. Taken together, our study suggests that refined PMFO has great potential to be used in functional applications such as in food, dietary supplements and pharmaceutical products.

INTRODUCTION

Palm-pressed mesocarp fibre oil (PMFO) is a residual oil extracted from palm-pressed mesocarp fibre, a by-product obtained from palm oil milling process. Crude palm oil (CPO) is typically recovered from the mesocarp of palm fruits by dry method using hydraulic press or a screw press (Obibuzor *et al.*, 2012). Following this process, 5%-6% of oil still remains as a ratio to the dry matter of mesocarp fibre (Obibuzor *et al.*, 2012). This residual oil can be recovered by several methods *e.g.*, solvent extraction (Neoh *et al.*, 2011), supercritical carbon dioxide extraction (Lau *et al.*, 2006; Putra *et al.*, 2019), enzymatic reaction (Noorshamsiana *et al.*, 2017), soxhlet method (Neoh *et al.*, 2011; Putra *et al.*, 2019), reflux method (Neoh *et al.*, 2011) and residual oil recovery system (Subramaniam *et al.*, 2013). The valuable phytonutrients in the residual oil are urged to be recovered before subjecting the mesocarp fibre as energy source for palm oil mills (Choo *et al.*, 1996).

The PMFO is richer in phytonutrients as compared to CPO (Teh and Lau, 2021). Refined PMFO was extracted from pressed mesocarp using

[1] Malaysian Palm Oil Board,
    6 Persiaran Institusi, Bandar Baru Bangi,
    43000 Kajang, Selangor, Malaysia.

[2] ASASI Pintar Unit, Pusat GENIUS@Pintar Negara,
    Universiti Kebangsaan Malaysia,
    43600 Bangi, Selangor, Malaysia.

[3] Biocompatibility and Toxicology Laboratory,
    Centre for Research and Instrumentation Management
    (CRIM), Universiti Kebangsaan Malaysia,
    43600 Bangi, Selangor, Malaysia.

[4] Center for Healthy Aging and Wellness Faculty of Health
    Sciences, Universiti Kebangsaan Malaysia,
    Kuala Lumpur, Malaysia.

* *Corresponding author e-mail: kimtiu@mpob.gov.my*

n-hexane while CPO was obtained by mechanical pressing of mesocarp. A significant quantity of carotenes (1716-2083 ppm), tocols (900-1200 ppm) (Abd Majid *et al.*, 2012), sterols (4509-8490 ppm) (Choo *et al.*, 1996) and squalene (1117-9690 ppm) (Lau *et al.*, 2008) remain in the residual oil of PMFO as compared to CPO. Inferior to PMFO, CPO contains 599-619 ppm of carotenes, 600-800 ppm of tocols (Abd Majid *et al.*, 2012), 250-620 ppm sterols (Choo *et al.*, 1996) and squalene (250-540 ppm) (Loganathan *et al.*, 2010). The tocols composition also differs between PMFO (54% of α-tocopherol, 19% of α-tocotrienol, 17% of γ-tocotrienol, and 10% of δ-tocotrienol) and CPO (21% of α-tocopherol, 25% of β-tocotrienol, 37% of γ-tocotrienol, and 17% of δ-tocotrienol) (Abd Majid *et al.*, 2012). Ninety percent of carotenoids found in CPO are in the form of α- and β-carotenes (35% and 56%, respectively) (Choo *et al.*, 1996). In the case of PMFO, α- and β-carotenes only constitute to 50% (19% and 31%, respectively). Interestingly, higher amounts of lycopene (14.10%), phytoene (11.90%), δ-carotene (7.60%), δ-carotene (6.90%), neurosporene (3.38%), and γ-carotene (2.70%) are found in PMFO as compared to CPO (Choo *et al.*, 1996). In terms of sterols, both PMFO and CPO have similar compositional profile of β-sitosterol (56%-59%), campesterol (19%-22%) and stigmasterol (18%-20%) (Choo *et al.*, 1996).

Both the PMFO and CPO contains predominantly palmitic acid (PMFO: 30.9%-32.6%, CPO: 39.5%-39.8%) and oleic acid (PPFO: 24.5%-25.1%, CPO: 35.6%-38.7%). PMFO is unique as it is rich in medium chain triglyceride namely lauric acid (20.0%-23.6%) which is trace in CPO (0.2%-0.3%) (Abd Majid *et al.*, 2012). The presence of lauric acid in PMFO is due to broken kernels trapped in mesocarp fibre (Abd Majid *et al.*, 2012; Sulihatimarsyila *et al.*, 2019).

To date, there is no scientific evidence on the safety assessment of PMFO nor refined PMFO. There is a recent publication on the blending of PMFO with CPO on oil quality and nutritional profile (Hasliyati *et al.*, 2021), yet toxicological aspects have not been investigated. Although chemically refined PMFO is proven to be safe for food application (Sulihatimarsyila *et al.*, 2019), however, there is no biological evidence to support this claim. Hence, there exists a necessity to study the toxicity aspects of refined PMFO to further exploit their functional applications in food, dietary supplements and pharmaceutical. Thus, the present study was designed to examine the safety assessment of refined PMFO based on its toxicological potential using both cell culture and animal acute study models. The terms of refined PMFO or PMFO are used throughout the manuscript to indicate the difference between refined PMFO and PMFO.

MATERIALS AND METHODS

Materials

The refined PMFO used in the current study was refined according to the published method as described by Sulihatimarsyila *et al.* (2019; 2020). The optimum conditions for the refining process comprised of water degumming using 5.0 v/v% of water at 90°C, followed by acid degumming using 1.0 weight % of phosphoric acid at 90°C, bleaching using 0.1 weight % of natural bleaching earth at 105°C and deacidification at 110°C at 0.1 mtorr (Lau *et al.*, 2006). The refined PMFO was supplied by Kim Loong Palm Oil Mills Sdn. Bhd., Johor, Malaysia.

Cell Line, Standards, Chemicals and Reagents

V79-4 Chinese hamster lung cells (*Cricetulus griseus* fibroblast, CCL-93TM) were purchased from the American Type Culture Collection (ATCC) (Montgomery, USA). Myristic acid (14:0), palmitic acid (16:0), stearic acid (18:0), and oleic acid (18:1); monopalmitin, monostearin, and monoolein; 1,2- and 1,3-dipalmitin, 1,2- and 1,3-distearin, and 1,2- and 1,3-diolein; tripalmitin and squalene; β-sitosterol, campesterol, stigmasterol, and cholesterol; low melting points agarose (LMA) and normal melting point agarose (NMA); acetone, uranyl acetate, hydrogen peroxide (H_2O_2), ethidium bromide solution and 3-(4,5-dimethylthiazol-2-yl)-2,5-diphenyltetrazolium bromide (MTT) reagent were obtained from Sigma Aldrich (Montgomery, USA). Dubelcco Modified Eagle Media (DMEM), fetal bovine serum (FBS), penicillin–streptomycin, glutaraldehyde, and phosphate buffer saline were purchased from Gibco-Thermo Fisher Scientific, Inc. (England, United Kingdom). The silylating reagent N,O-bis(trimethylsilyl) trifluoroacetamide with 1% trimethylchlorosilane (BSTFA) was purchased from Fluka Chemicals (Buchs, Switzerland). All solvents were purchased from Merck and were of chromatographic or analytical grade. A TLC plate coated with silica gel 60 F254 (20 × 20 cm; Merck 1.05715.0001) was obtained from Merck (Darmstadt, Germany).

Cell Culture

The Chinese hamster lung V79-4 fibroblast cells were cultured in DMEM supplemented with 10% FBS and maintained at 37°C in a 5% carbon dioxide (CO_2) incubator. After reaching confluency, cells were detached via trypsinisation (0.025% trypsin).

Preparation of Compound and Evaluation of Physical Characteristics

Refined PMFO was first dissolved in dimethyl

sulphoxide (DMSO) at a concentration of 50%. The solution was further diluted in DMEM to 1%(v/v) of concentration as working solution. Total carotene content in the oil sample was analysed using a UV-Vis Spectrometer, model U-2001 (Hitachi Instruments Inc., Tokyo, Japan) according to MPOB Test Method p2.6:2004 (Ainie *et al.*, 2005). Free fatty acid (FFA), monoacylglycerols (MAG), diacylglycerols (DAG), triacylglycerols (TAG), sterols and squalene were determined by using a Hewlett-Packard Series II gas chromatography, model 5890 (Hewlett-Packard, Avondale, USA), as described previously (Nang Lau *et al.*, 2005). Vitamin E content was determined by high-performance liquid chromatography with fluorescence detector (Agilent Technologies, Palo Alto, USA) as described previously (Sulihatimarsyila *et al.*, 2019).

MTT Viability Assay

The cytotoxicity of refined PMFO was determined using MTT assay to assess the amount of formazan crystals formed via a reduction process in the mitochondria (Mosmann, 1983). The cells were seeded in 96-well microplate at 5×10^4 cells/mL (based on established and published data in our laboratory) (Awang *et al.*, 2015; Siew *et al.*, 2020) and were incubated at 37°C in 5% CO_2 for 24 hr. Media was replaced with treatment medium containing highest concentration of refined PMFO (1%v/v) on the following day and the cells were incubated further for 24 hr. Then 30 µL of sterile MTT solution (5 mg/mL) was added into each well and the plate was incubated for 4 hr. Media and MTT solution were removed after 4 hr and 200 µL of DMSO was added into each well to dissolve the formazan crystals. The plate was shaken for 10 min and the optical density reading of each well was obtained using enzyme-linked immunoassay (ELISA) plate reader at 570 nm wavelength. Graph of viability was plotted against concentration.

Alkaline Comet Assay

The genotoxicity of refined PMFO was assessed using the alkaline comet assay by detecting the primary DNA damage (Tice *et al.*, 2000). The V79-4 cells were seeded in 6-well plate were treated with IC10 [0.162% (v/v)] and IC25 [0.450% (v/v)] following 24 hr of incubation. Cells were also treated with H_2O_2 (positive control, 1.0 mM) for 30 min. Then, the cells were detached, trypsinised and collected for centrifugation at 2500 rpm for 5 min. The supernatant was removed, and the pellet was washed with Ca^{2+}-/Mg^{2+}-free PBS prior to re-centrifugation. Pellets left at the bottom were mixed thoroughly with 80 mL of 0.6% LMA (w/v) and the mixture was pipetted onto hardened 0.6%

NMA (w/v) on the slide. Cover slips were placed to spread the mixture and the slides were left on ice for LMA to solidify. Following the removal of the cover slips, the embedded cells were lysed in lysis buffer containing 2.5 M sodium chloride (NaCl), 100 mM Na_2EDTA, 10 mM Tris, and 1% Triton X-100 for 1 hr at 4°C. As for DNA-unwinding procedure, slides were soaked in electrophoresis buffer solution for 20 min at 4°C prior to electrophoresis at 300 mA, 25 V, for 20 min. Subsequently, the slides were rinsed with neutralising buffer for 5 min and stained with 50 µL ethidium bromide solution. Slides were left overnight at 4°C before analysis with fluorescence microscope (Nikon E600, USA) equipped with 515 barrier filter and 560 emission filter. Tail moment (TM) of 50 cells per slide were scored and analysed using COMET assay III (Perceptive Instruments, United Kingdom).

Acute Oral Toxicity Study

Acute oral toxicity study was appropriate for the purpose to determine the adverse toxic effect and responses of a test material following oral administration of the test material in rats within a short time period. Hence, the study was performed on two groups of rats using a stepwise procedure. In the first step, three female Sprague-Dawley rats (Test Group) were administered orally with 2000 mg/kg body weight of test substance in 10 mL/kg vehicle (pre-filtered water). Three additional female rats (Control Group) used as control were administered with pre-filtered water (10 mL/kg). Animals were observed for clinical effects at 30 min, hourly up to 4 hr, at 6 hr post dosing and once daily up to day 14. Their body weights were measured on day 1, 7 and at termination (day 14). Following euthanasia, gross necropsy was performed on both the Test Group and Control Group animals. Following the no-observable-adverse-effects-level (NOAEL) findings from the previously tested group (Test Group), three female rats (Continuing Test Group) were administered orally with 2000 mg/kg body weight of test substance in 10 mL/kg vehicle pre-filtered water. Animals were observed for clinical effects at 30 min, hourly up to 4 hr, and at 6 hr post dosing and once daily up to day 2. Their body weights were measured on day 1 and at termination (day 2). On day 2 the animals were sacrificed for necropsy. This study was performed in compliance with the appropriate provision of the OECD (2002), Test No. 423: Acute Oral toxicity - Acute Toxic Class Method, OECD Guidelines for the Testing of Chemicals, Section 4. The procedures of use and care of animals were adhered to approval from Universiti Kebangsaan Malaysia's Animal Ethics Committee (BIOSERASI/UKM/2018/FAEZA/28-JUNE/931-JUNE-2018-JUNE-2019).

Statistical Analysis

All the data were presented as the mean ± standard error of mean (SEM) in at least three independent experiments. Statistical analyses using analysis of variance (ANOVA) was conducted to assess the significance between means followed by a Dunnet's t-test. A p-value of <0.05 was considered significant.

RESULTS AND DISCUSSION

Physical Characteristics of Refined PMFO

The physical characteristics of refined PMFO is presented in *Table 1*. The oil was degummed, bleached and deacidified. The phytonutrient contents of refined PMFO are as follows: carotenes (1255 ppm), tocopherols and tocotrienols (1290 ppm), sterols (591 ppm) and squalene (886 ppm). The oil contains 7.79 g/100 g DAG and 92.2 g/100 g TAG. The fatty acid composition is similar to what have been reported for palm olein, which is predominantly high in palmitic acid (C16:0, 36.9 g/100 g) and oleic acid (43.5 g/100 g), with 10.6 g/100 g linoleic acid (C18:2) (Teh and Lau, 2021). The present data is in line with what has been recently reported, where refined PMFO retains substantial amount of total

TABLE 1. PHYSICAL CHARACTERISTICS OF REFINED PALM-PRESSED MESOCARP FIBRE OIL[1]

Parameter	Weight
Free fatty acids (g/100 g)	0.2
Fatty acid composition (g/100 g)	
C10:0	0.1
C12:0	2.6
C14:0	1.5
C16:0	36.9
C16:1	0.5
C18:0	3.6
C18:1	43.5
C18:2	10.6
C18:3	0.6
C20:0	0.1
Acylglycerol composition (g/100 g)	
Monoacylglycerol	0.05
Diacylglycerol	7.79
Triacylglycerols	92.17
Phytonutrients (mg/kg)	
Carotenoids	1 255
Tocols	1 290
Sterols	591
Squalene	886

Note: [1]Results are presented in means ±SE of at least three separate experiments.

carotene, vitamin E and sterols compared to PMFO (Teh and Lau, 2021). Notably, the concentration of phytonutrients are still substantially higher than that of CPO and commercially available red palm oil as reviewed in our published data (carotenoids, 600-750 ppm and tocols, 717-863 ppm) (Loganathan *et al.*, 2017). This could be explained by the extraction methods, where refined PMFO used in the present study was extracted from pressed mesocarp using n-hexane while CPO was obtained by mechanical pressing of mesocarp. The high amount of carotenes and vitamin E in refined PMFO was due to its high content in the bi-membrane layer of the cell in the membrane and was co-extracted with the residual oil using n-hexane (Lau *et al.*, 2006). The condition subjected to the extraction of PMFO, in particular the deodorisation temperature (which is below 200°C, as compared to conventional CPO deodourisation temperature at 265°C), does not significantly degrade the phytonutrients. The extraction method however, did not modify the fatty acid composition of PMFO as compared to CPO.

MTT Viability Assay

The cytotoxic effects of refined PMFO against V79-4 fibroblast cells as assessed by MTT assay following 24 hr treatment are shown in *Figure 1*. V79-4 cells showed decrease in viability in a concentration-dependent manner following 24 hr treatment with refined PMFO. The results show that at the highest concentration of refined PMFO (1%v/v), (72.65 ± 4.1) % of viable cells were observed (*Figure 1*). A concentration response effect was seen following treatment with H_2O_2 with an inhibitory concentration (IC_{50}) value of 1.568 mM. No IC_{50} values were observed for refined PMFO treated V79-4 cells as compared to positive control (H_2O_2) (*Figure 1*). H_2O_2 was used to validate the experimental procedure. Based on the results obtained, refined PMFO has no cytotoxic effect using a widely acceptable method (MTT assay) in V79-4 fibroblast cells. Our group has previously studied the cytotoxicity of PMFO against three human cancer cell lines, namely Hep-G2, LS174T and SK-MEL-28, and no cytotoxic effect has been reported (Teh *et al.*, 2021). The results were supported by a study conducted on cytotoxic effect oil palm kernel protein hydrolysates (OPKHs) against Hep-G2 cells where no cytotoxicity was observed. The growth simulation and prolongation of cells could occur due to the presence of oleic acids in OPKHs that also present in oil palm-based oil extracts (Chang *et al.* 2014). Other than that, this could also be possibly explained by the synergistic and antagonistic effects of the components in PMFO, which warrants further investigation.

Note: [1] The results are expressed as mean ± SE of at least three independent experiment.
* Significant difference ($p<0.05$) as compared to negative control.

Figure 1. Cytotoxicity of (a) refined palm-pressed mesocarp fibre oil (PMFO), and (b) H_2O_2 against V79-4 cells with 24 hr of incubation.

Alkaline Comet Assay

The detection of primary DNA damage induced by refined PMFO in V79-4 cells was assessed by Alkaline Comet assay. Negative control cells displayed low levels of background damage. Scoring for the DNA damage was done based on TM values. As shown in *Table 2*, V79-4 negative control cells has TM of (0.432 ± 0.09). As shown in *Table 2*, there was a slight increase with no significant difference in TM at IC_{25}, (0.468 ± 0.09) of refined PMFO treated cells respectively at 24 hr as compared to negative control cells. This data showed that refined PMFO has no capability to induce direct DNA strand breakage in V79-4 cells. A significant ($p<0.05$) increase in DNA damage shown by TM was observed in H_2O_2 treatment at 1 mM, which served as positive control (*Table 2*). This data indicates that refined PMFO does not induce DNA damage, this may partly be explained by the fact that PMFO is the power house of antioxidants, with a recent published data from our group to support

TABLE 2. LEVEL OF DNA DAMAGE ON V79-4 TREATED CELL LINE WITH R REFINED PALM-PRESSED MESOCARP FIBRE OIL[1]

Item	Level of DNA damage (Arbitrary unit)
	(TM) 24 hr
Negative control	0.432 ± 0.08
Refined PMFO (IC_{10})	0.343 ± 0.04
Refined PMFO (IC_{50})	0.468 ± 0.09
	(TM) 30 min
Positive control (H_2O_2)	*9.762 ± 1.41

Note: [1]The results are the means ±SE of at least three separate experiments (*$p<0.05$ *vs.* negative control). PMFO - palm-pressed mesocarp fibre oil; TM - tail moments.

this (Teh *et al.*, 2021). It has been reported that the bouquet of phytonutrients in PMFO has free radical scavenging effects as assessed using α, α-diphenyl-β-picrylhydrazyl (DPPH), H_2O_2 and nitric oxide (NO) radicals scavenging assay when compared with extra virgin coconut oil and red palm oil (Teh *et al.*, 2021). The presence of vitamin E, particularly tocotrienols and tocopherols, are known for their potent antioxidant activity. Moreover, carotenoids and co-enzyme Q10 are proven to scavenge H_2O_2 radicals effectively. A previous study also acknowledged the antioxidant capacity of the extracts of oil palm fruit through H_2O_2 scavenging assay (Balasundram *et al.*, 2005). This finding further confirms that the oil palm-based edible oil, is rich in antioxidants that acts on radicals. Carotenoids and tocotrienols, the two most abundantly available antioxidants in PMFO have been reported to exert protective effects in various diseases using animal and human models as reviewed by our group (Fu *et al.*, 2014; Loganathan *et al.*, 2017).

Acute Oral Toxicity

There was no difference observed between female Sprague-Dawley rats treated with refined PMFO at 2000 mg/kg body weight and control (with 10 mL/kg body weight of pre-filtered water) on the behavioural observations (over the 14-day interval). General clinical observations (namely skin and fur, eyes, respiratory effect, mucous membrane, motor activity, tremor, convulsion, walking behaviours, and diarrhoea) were normal for both treated and control animals (*Table 3*). No mortality or any toxic symptoms was observed. Furthermore, necropsy results including observations in all eight separate organs (namely brain, kidneys, lungs, liver, stomach, spleen, heart, and pancreas) showed no notable abnormalities. No significant differences in body weight were

observed between rats treated with refined PMFO treatment and control (*Figure 2*). Percent of increment in rat's body weights for treated and control showed no significant difference. There was no remarkable difference in mean percentage of organ to animal body weight between rats treated with refined PMFO and control. The heart, kidneys, liver, lungs and spleens are the first organs to display metabolic responses to toxic substances. Organ weights are useful indicator of any kind of toxicity, in particular in drug administration. It is important to note that without further morphological changes in acute toxicity, differences in organ weight between treated and control animals may occur (Ara and Usmani, 2015). Taken together the data observed, the administration of refined PMFO does not exert acute oral toxicity impact in rats. This is in line with an extensive review published by our group on the toxicological and nutritional assessment of CPO and red palm oil (Loganathan *et al.* 2017). In addition, a study conducted in weanling Wistar/NIN albino rats using CPO, refined palm oil and peanut oil has shown that the vegetable oils tested using a diet containing 10% dietary fat has no adverse effects on growth rate, feed efficiency, digestibility and fat absorption after a 90-day feeding period (Manorama and Rukmini, 1991).

Limitations/Recommendations

The method for refining and processing of PMFO varies between factories. Apart from that, diversity, degree of palm fruit ripeness and geographical location of plantation could also contribute to variation in the carotene concentration (Loganathan *et al.*, 2017). In view of that, it is advisable to have a harmonised method and national standard specification for PMFO and refined PMFO to provide consistency in the nutritional properties.

TABLE 3. CLINICAL FEATURES OF THE TEST AND CONTROL ANIMALS DURING OBSERVATION PERIOD[1]

Observation-post dosing	Control group			Test group			Continuing test group (2000 mg/kg)		
	1	2	3	1	2	3	1	2	3
Sex	F	F	F	F	F	F	F	F	F
Duration	A-K	A-K	A-K	A-K	A-K	A-K	A-K	A-K	A-K
30 min	0	0	0	0	0	0	0	0	0
1 hr	0	0	0	0	0	0	0	0	0
2 hr	0	0	0	0	0	0	0	0	0
3 hr	0	0	0	0	0	0	0	0	0
4 hr	0	0	0	0	0	0	0	0	0
6 hr	0	0	0	0	0	0	0	0	0
Day 2	0	0	0	0	0	0	0	0	0
Day 3	0	0	0	0	0	0			
Day4	0	0	0	0	0	0			
Day 5	0	0	0	0	0	0			
Day 6	0	0	0	0	0	0			
Day 7	0	0	0	0	0	0			
Day 8	0	0	0	0	0	0			
Day 9	0	0	0	0	0	0			
Day 10	0	0	0	0	0	0			
Day 11	0	0	0	0	0	0			
Day 12	0	0	0	0	0	0			
Day 13	0	0	0	0	0	0			
Day 14	0	0	0	0	0	0			

Note: [1]For Test Group and Control Group, animals were observed for morbidity and mortality at 30 min, hourly up to 4 hr, at 6 hr post dosing and once daily up to day 14. Continuing Test Group animals were observed at 30 min, hourly up to 4 hr, at 6 hr post dosing and at 24 hr. Alphabetical values (A - K) denote clinical changes observed and scored following treatment, with zero ("0") denoted as "normal" (A - fur and skin changes; B - eye changes; C - respiratory effect; D - mucous membrane; E - motor activity; F - tremor; G - convulsion; H - walking backwards or ataxia, inability to coordinate body movements; I - diarrhea; J - death; K - others).
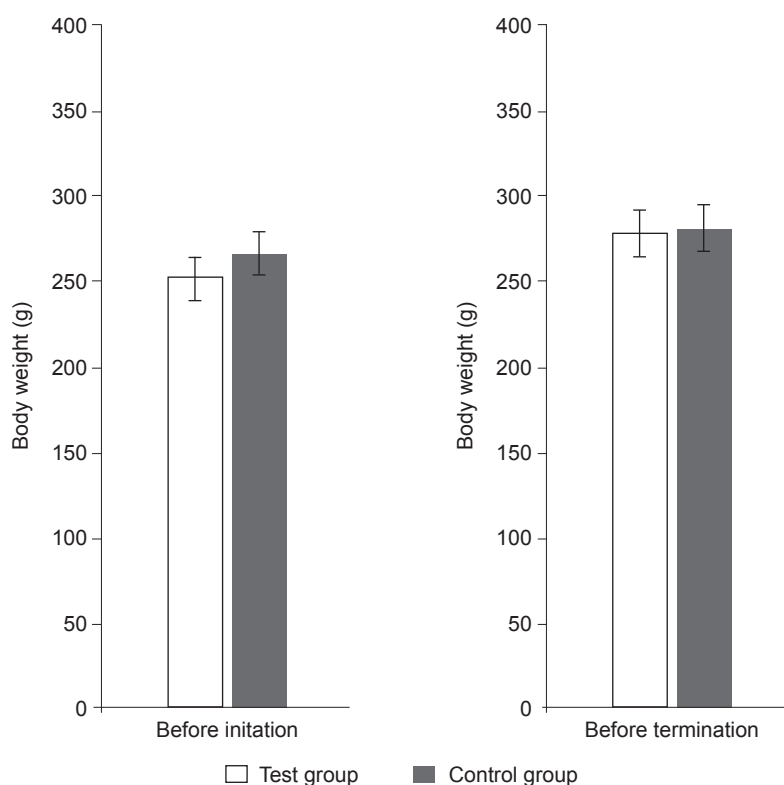
Note: [1] Results are expressed as mean ± SE of at least three independent experiments.
* No significant difference ($p>0.05$) was observed as compared to Control Group.

Figure 2. Mean body weight of Test Group and Control Group measured at two intervals of the study period.

CONCLUSION

Our toxicological assessment provides a preliminary finding on the safety usage of refined PMFO as a food component. Refined PMFO shows no cytotoxicity and did not cause any DNA damage in V79-4 cells. Acute toxicity animal testing has also shown no significant difference between groups treated. Based on toxicological study, refined PMFO showed no-observed-adverse-effect level (NOAEL) up to 2000 mg/kg body weight of the animal. Further analysis may be needed to conduct more in-depth analysis on various aspects in relation to impact to health.

ACKNOWLEDGEMENT

REFERENCES

Abd Majid, R; Mohammad, A W and Choo, Y M (2012). Properties of residual palm pressed fibre oil. *J. Oil Palm Res., 24*: 1310-1317.

Ainie, K; Siew, W; Tan, Y A; Nor Aini, I; Mohtar, Y; Tang, T and Nuzul, A (2005). *MPOB Test Methods*. MPOB, Bangi.

Ara, A and Usmani, J A (2015). Lead toxicity: A review. *Interdiscip. Toxicol., 8*: 55-64.

Awang, N; Ahlam, S N F and Chan, K M (2015). Cytotoxicity and genotoxicity assessments of Batik industrial wastewater on V79 cells. *Toxicol Inter., 22(3)*: 76-82.

Ayeleso, A; Brooks, N and Oguntibeju, O (2014). Impact of dietary red palm oil (*Elaeis guineensis*) on liver architecture and antioxidant status in the blood and liver of male Wistar rats: Peered reviewed original articles. *Med. Tech. SA., 27(2)*: 18-23.

Chang, S K; Hamajima, H; Amin, I; Yanagita, T; Mohd Esa, N and Baharuldin, M T H (2014). Cytotoxicity effect of oil palm (*Elaeis guineensis*) kernel protein hydrolysates. *Int. Food Res. J., 21(3)*: 909-914.

Choo, Y M; Yap, S C; Ooi, C K; Ma, A N; Goh, S H and Ong, A S H (1996). Recovered oil from palm-pressed fibre: A good source of natural carotenoids, vitamin E, and sterols. *J. Am. Oil Chem. Soc., 73(5)*: 599-602.

Fu, J Y; Che, H L; Tan, D M Y and Teng, K T (2014). Bioavailabilities of tocotrienols: Evidence in human studies. *Nutr. Metab. (Lond.), 11(1)*: 5.

Hasliyati, A; Rusnani, A M; Wan Hasamuddin, W H; Ng, M H; Nor Faizah, J and Rohaya, M H (2021). The effects of recylcing palm pressed fibre oil on crude palm oil quality. *J. Oil Palm Res.* DOI: 10.21894/jopr.2021.0016.

Lau, H L N; Choo, Y M; Ma, A N and Chuah, C H (2006). Quality of residual oil from palm-pressed mesocarp fibre (*Elaeis guineensis*) using supercritical CO_2 with and without ethanol. *J. Am. Oil Chem. Soc., 83(10)*: 893-898.

Loganathan Jr, R; Selvaduray, K; Nesaretnam, K and Radhakrishnan, A K (2010). Health promoting effects of phytonutrients found in palm oil. *Malays. J. Nutr., 16(2)*: 309-322.

Loganathan, R; Subramaniam, K M; Radhakrishnan, A K; Choo, Y M and Teng, K T (2017). Health-promoting effects of red palm oil: Evidence from animal and human studies. *Nutr. Rev., 75(2)*: 98-113.

Manorama, R and Rukmini, C (1991). Nutritional evaluation of crude palm oil in rats. *Am. J. Clin. Nutr., 53(4)*: 1031S-1033S.

Manorama, R; Chinnasamy, N and Rukmini, C (1993a). Effect of red palm oil on some hepatic drug-metabolizing enzymes in rats. *Food Chem. Toxicol., 31(8)*: 583-588.

Manorama, R; Chinnasamy, N and Rukmini, C (1993b). Multigeneration studies on red palm oil, and on hydrogenated vegetable oil containing mahua oil. *Food Chem Toxicol., 31(5)*: 369-375.

Manorama, R; Harishankar, N; Polasa, K and Rukmini, C (1989). Mutagenicity studies on repeatedly heated crude and refined palm oil. *J. Oil Tech. Assoc. India., 21(2)*: 29-31.

Mosmann, T (1983). Rapid colorimetric assay for cellular growth and survival: Application to proliferation and cytotoxicity assays. *J. Immunol. Methods., 65(1-2)*: 55-63.

Nang Lau, H L; Puah, C W; Choo, Y M; Ma, A N and Chuah, C H (2005). Simultaneous quantification of free fatty acids, free sterols, squalene, and acylglycerol molecular species in palm oil by high-temperature gas chromatography-flame ionization detection. *Lipids, 40(5)*: 523-528.

Neoh, B K; Thang, Y M; Zain, M Z M and Junaidi, A (2011). Palm pressed fibre oil: A new opportunity for premium hardstock? *Int. Food Res. J., 18(2)*: 769-773.

Noorshamsiana, A W; Astimar, A A; Iberahim, N I; Nor Faizah, J; Anis, M; Hamid, F A and Kamarudin, H (2017). The quality of oil extracted from palm pressed fibre using aqueous enzymatic treatment. *J. Oil Palm Res., 29(4)*: 588-593.

Obibuzor, J U; Okogbenin, E A and Abigor, R D (2012). Oil recovery from palm fruits and palm kernel. *Palm Oil.* p. 299-328.

OECD (2002). Test No. 423: Acute oral toxicity - Acute toxic class method. *OECD Guidelines for the Testing of Chemicals*. OECD Publishing, Paris. https://www.oecd-ilibrary.org/environment/test-no-423-acute-oral-toxicity-acute-toxic-class-method_9789264071001-en.

Putra, N R; Wibobo, A G; Machmudah, S and Winardi, S (2019). Recovery of valuable compounds from palm-pressed fibre by using supercritical CO_2 assisted by ethanol: Modeling and optimization. *Sep. Sci. Technol., 55(17)*: 3126-3139.

Siew, E L; Farris, A F; Rashid, N; Chan, K M and Rajab, N F (2020). *In vitro* toxicological assessment of gadolinium (III) chloride in V79-4 fibroblasts for classification of health hazard. *Genes Environ., 42*: 22.

Subramaniam, V; Menon, N R; Sin, H and May, C Y (2013). The development of a residual oil recovery system to increase the revenue of a palm oil mill. *J. Oil Palm Res., 25(1)*: 116-122.

Sulihatimarsyila, A N; Lau, H L N; Nabilah, K M and Azreena, I N (2019). Refining process for production of refined palm-pressed fibre oil. *Ind. Crops Prod., 129*: 488-494.

Sulihatimarsyila, A N; Lau, H L N; Nabilah, K and Azreena, I N (2020). Production of refined red palm-pressed fibre oil from physical refining pilot plant. *Case Stud. Chem. Environ. Eng., 2*: 100035.

Teh, S S; Lau, H L N and Mah, S H (2019). Palm-pressed mesocarp fibre oil as an alternative carrier oil in emulsion. *J. Oleo Sci., 68(8)*: 803-808.

Teh, S S and Lau, H L N (2021). Quality assessment of refined red palm-pressed mesocarp olein. *Food Chem., 340*: 127912.

Teh, S S; Mah, S H; Lau, H L N; Teng, K T and Loganathan, R (2021). Antioxidant potential of red palm-pressed mesocarp olein. *J. Oleo Sci., 70(12)*: 1719-1729.

Tice, R R; Agurell, E; Anderson, D; Burlinson, B; Hartmann, A; Kobayashi, H; Miyamae, Y; Rojas, E; Ryu, J C and Sasaki, Y F (2000). Single cell gel / comet assay: Guidelines for *in vitro* and *in vivo* genetic toxicology testing. *Environ. Mol. Mutagen., 35(3)*: 206-221.

ESTIMATING THE SHELF LIFE OF FLAVOURING OIL GRAVY CONSISTING OF RED PALM OIL

GUANGYI GONG[1]; XIAOJING WU[1]; SHIMIN WU[1, 2]*; JUNHAO YOONG[3], MIN JI[3] and MINGMING HU[3]

ABSTRACT

The nutritional quality and sensory properties of flavouring oil gravy enclosed in instant noodle products have aroused great attention. In this study, we investigated the effects of the replacement of tallow with red palm oil (RPO) on the shelf life of flavouring oil gravy between one commercial sample and two pilot samples with different ingredients. The quality of the three gravy samples during the accelerated shelf-life test was evaluated by sensory properties using a spectrophotometer for colour measurement and sensory evaluation. In addition, the acid value (AV) and peroxide value (POV) dynamic equations of flavouring oil gravy were monitored. The shelf life of the two pilot samples was predicted using Arrhenius models. The results indicated that compared with the flavouring oil gravy of commercial stewed beef (CSB), only one-third to one- half of the colour differences were observed in the other two pilot gravies. The predicted shelf lives of experimental stewed beef and experimental sour soup were 33.33% and 33.33% longer, respectively, than CSB at a storage temperature of 20°C. These results may help predict the shelf life of flavouring oil gravies and innovate the diversity of RPO in the food industry.

INTRODUCTION

Instant noodles are an important constitution of diet worldwide, especially in East and Southeast Asian countries (Gulia *et al.*, 2014). This popularity is attributed to their desirable flavour, affordable price and rapid preparation. However, great concerns also emerge with the overconsumption of instant noodles (Huh *et al.*, 2017). With the aim of meeting the health demands and reassuring the increasing health concerns of consumers, it is necessary to develop new products with novel ingredients and, more importantly, with higher quality.

Flavouring oil gravy, which accounts for 10%-20% of the total weight of the instant noodle product, has a significant impact on its sensory quality. These gravies not only provide consumers with pleasant aroma and taste but also contribute to the energy and nutritional value to a great extent. Furthermore, the oil content in flavouring oil gravy makes up to nearly 50% of the weight. Therefore, the oil used in flavouring oil gravy plays a critical role in the overall quality of instant noodles. Traditionally, animal fats rich in saturated fat are widely used in commercial flavouring oil gravy. However, with an increasing number of ethnic consumers preferring food products without animal fat, it is an emerging trend to develop an

[1] Department of Food Science and Technology,
    School of Agriculture and Biology,
    Shanghai Jiao Tong University,
    800 Dongchuan Road,
    Shanghai 200240, China.

[2] Key Laboratory of Urban Agriculture (South),
    Ministry of Agriculture,
    800 Dongchuan Road,
    Shanghai 200240, China.

[3] Palm Oil Research and Technical Service Institute of
    Malaysian Palm Oil Board (PORTSIM),
    Shanghai 201108, China.

* *Corresponding author e-mail: wushimin@sjtu.edu.cn*

alternative way to replace animal fat. In addition, a high intake of saturated fat is generally recognised as the main cause of cardiovascular diseases (Wang and Hu, 2017). Therefore, it is essential to find a sophisticated way to reduce the potential health risk of flavouring oil gravy and simultaneously maintain flavour and colour.

Palm oil with high thermal stability is considered an ideal alternative for the instant noodle frying industry. A high content of n-6 unsaturated fatty acids in palm oil also reduces the risk of cardiovascular diseases (Wang and Hu, 2017). In addition to the benefits of palm oil, red palm oil (RPO) has the further advantage of possessing more abundant natural antioxidants, including over 20 types of different carotenes. Carotenes with high content and diversity present in RPO give this refined oil a typical orange-red colour (Oguntibeju et al., 2009), which is close to those of gravies made of animal fats. Due to the abundant content of various kinds of carotenoids, RPO has been used to prevent children and women from potential vitamin A deficiency. In addition, it also helps patients with liver cirrhosis regulate their oxidative stress. Moreover, people who suffer from cystic fibrosis may also benefit from the intake of RPO since it can increase the concentrations of β-carotene and retinol (Burri, 2012; Catanzaro et al., 2016). In addition to carotene, palm oil is abundant in various kinds of vitamin E, including α-tocopherol, α-tocotrienol, γ-tocopherol, γ-tocotrienol, δ-tocopherol and δ-tocotrienol (David et al., 2000; Ng et al., 2004). A previous study indicated that the total concentration of α-tocopherol, as well as α-, γ-, and δ-tocotrienol, in RPO reached 955 mg/kg (Yi et al., 2011). Using rat model experiments, researchers observed the attenuation of cytotoxic effects as well as the increasing threshold for ventricular fibrillation with the intake of RPO (Katengua-Thamahane et al., 2014; Wergeland et al., 2011). In our previous study (Wu et al., 2018), RPO enhanced the carotenoid content of flavouring oil gravy, and delightfully, it had a negligible adverse impact on the sensory qualities. Therefore, without the loss of the original flavour, the nutritional quality and oxidation resistance of the gravy were enhanced with the replacement of RPO. However, the effects of RPO on the shelf life of flavouring oil gravies were not investigated in that study.

Shelf life has been generally recognised as an important factor of food for a long time. It can be defined as the length of time during which food products can be stored without their quality becoming unacceptable to consumers (Calligaris et al., 2016). Generally, the determination of the shelf life of food is considered time-consuming. However, with the introduction of accelerated shelf life testing (ASLT), the determination time

can be largely reduced (Mizrahi, 2000). Usually, there are three fundamental steps that constitute typical ASLT. First, a group of indicators need to be selected, which can be used to reflect product quality. Second, changes in indicators that are selected in the first step need to be observed. Third, an appropriate kinetics model needs to be set after the collection of data from step 2. Subsequently, an equation also needs to be established to predict the shelf life (Manzini et al., 2017).

In the present study, we evaluated changes in the sensory properties of flavouring oil gravy by colour differences and sensory evaluation. In addition, the acid value (AV) and peroxide value (POV) dynamic equations of flavouring oil gravy were monitored by the Arrhenius model during ASLT. We also compared the predicted shelf life with those of actual flavouring oil gravies stored at room temperature for eight consecutive months.

MATERIALS AND METHODS

Materials

The RPO used in this study was specially refined and supplied by Carotino Sdn. Bhd. (Johor, Malaysia). The two other commonly used palm oils (5°C and 8°C) were supplied by Tianjin Longwei Co., Ltd. (Tianjin, China). The slip melting point of RPO was 5°C, while the melting points of the two other palm oils were 5°C and 8°C.

Based on the survey we established previously on market data and consumer preferences, commercial stewed beef (CSB) flavouring oil gravy was chosen for experiments and bought from the market. The ingredients of CSB are tallow (60%), beef paste (15%), thick broad-bean sauce (15%), chive oil (5%), five spice powder (1%), beef extract paste (1%), soybean sauce (1%), cooking wine (1%) and salt (1%). The shelf life of CSB is 180 days, as shown by the food label. For comparison, two other flavouring oil gravies, including experimental stewed beef (ESB) and experimental sour soup (ESS), were used in this experiment. The ingredients in ESB include palm oil (60%), beef paste (15%), thick broad-bean sauce (15%), chive oil (5%), five spice powder (1%), beef extract paste (1%), soybean sauce (1%), cooking wine (1%) and salt (1%). The ingredients in ESS include palm oil (60%), beef paste (20%), thick broad-bean sauce (10%), diced needle mushroom (5%), five spice powder (1%), beef extract paste (1%), vinegar (1%), soybean sauce (1%), and salt (1%). Palm oil was first heated to 160°C and mixed with pastes and seasonings. Then, the mixture was pan-fried for

3 min and cooled to 40°C. Finally, the products were packed in polyethylene terephthalate bags.

Experimental Design for the Prediction of Shelf Life

Each type of flavouring oil gravy was prepared and packed in polypropylene bags. In total, 300 bags (100 bags of each type of gravy) of the flavouring oil gravies were stored at four temperatures: 4°C, 25°C, 37°C and 45°C (25 bags from each type of gravy stored at a specific temperature). In this study, the gravies were consecutively stored for 63 days. The quality and safety indices of the samples were monitored at 0, 7, 14, 21, 28, 35, 49 and 63 days.

The reaction constant, k_n, was calculated based on oxidation indices, *i.e.*, the AV and POV, using the Equation (1):

$$ln\ N = ln\ N_0 + k_n \cdot t \qquad (1)$$

where N_0 is the initial value of the oxidation index at different storage temperatures, N is the oxidation index value at different storage temperatures after storage, and t is the storage time.

The temperature dependence of the deterioration rate, k_n, is then modelled by the Arrhenius Equation (2):

$$ln\ k_n = ln\ k_0 - \frac{E}{RT} \qquad (2)$$

where k_0 is the change in the rate of the respective quality index at a reference temperature, T is the storage temperature (K), E is the activation energy of the studied action (J/mol), and R is the universal gas constant of 8.314 J/(mol·K).

Extraction of Oils from Commercial and Pilot Flavouring Oil Gravies

The extraction process of oils was reported in our previous study (Wu *et al.*, 2018). Briefly, 10 g of each sample was put in a glass flask before being dissolved in 100 mL of n-hexane. The mixture was sonicated for 1 hr, and then the supernatant was transferred from the flask into a Soxhlet extractor. The ultrasound extraction process was repeated three times. Subsequently, excess solvent stored in the Soxhlet extractor was removed under vacuum conditions at 45°C with the assistance of a rotary evaporator (Yuanhuai Chemical Technology Co., Ltd, Shanghai, China). Residual oil in the extractor was absorbed by a dropper and then transferred into a 15 mL plastic centrifuge tube. Samples were kept in the dark at -20°C prior to analysis.

Analysis of AV and POV

The AV and POV of oils were determined using a titrimetric method according to corresponding Chinese national standards (GB 5009.227; GB 5009.229) Chinese Standard (2016a); Chinese Standard (2016b). For AV, a 2.5 g extracted oil sample was dissolved in 50 mL of ether/isopropanol (1:1, *v*: *v*). The mixture was neutralised using KOH at a concentration of 0.1 mol/L. The result was represented in units of mg/g. For POV, a 2.5 g extracted oil sample was dissolved in 30 mL of chloroform/acetic acid (2:3, *v*: *v*). Then, 1 mL of saturated potassium iodide (KI) solution was added to the solution and stored in the dark for 3 min. Finally, 100 mL of water was added to the solution, and then, it was titrated using a $Na_2S_2O_3$ solution at a concentration of 0.002 mol/L. The result was represented in units of g/100 g.

Determination of Colour

To clearly describe the colour changes during storage, colour measurements were performed using a PilotScan spectrophotometer (Hunterpilot, Reston, VA, USA). L*, a* and b* values were used to express the result (Antonis, 2019). Measurements were repeated three times, and the mean value was calculated. Additionally, the brightness or vividness of colour was also determined, and the results were expressed using chroma (C*). The C* value can describe the colour saturation of the samples, in which the initial value is 0, and was calculated using the formula $C^* = (a^{*2} + b^{*2})^{1/2}$. In contrast, ΔE was used to describe colour differences and was calculated using the Equation (3):

$$\Delta E = [(L^* - L_{ref}^*)^2 + (a^* - a_{ref}^*)^2 + (b^* - b_{ref}^*)^2]^{1/2} \quad (3)$$

Sensory Panel Evaluation

The sensory evaluation of the samples in this study was carried out according to our previous method (Wu *et al.*, 2018). A panel of 12 judges was composed of six semi-trained students and six trained employees (seven males and five females between the ages of 20 and 50 years old). Instruction was provided at the beginning of the first evaluation session, which lasted approximately 30 min (Kwak *et al.*, 2015).

Each flavouring oil gravy sample was stored in the dark at room temperature and opened immediately before sensory analysis. Disposable coded paper cups were offered to each panellist, along with a scorecard. Five grams of each sample was placed on a transparent vessel for evaluation of appearance (presence of impurities and appearance of organisation). Additionally, 5 g samples were dissolved in 1 L of boiling water for the evaluation

of colour, and 5 g samples were added to 500 mL of boiling water for the evaluation of odour and taste. For each product, the panellists scored five perceived attributes from weak (1) to strong (10), which included colour, texture, odour, flavour and durance of fragrance.

Evaluations were performed at room temperature (18°C-20°C) under natural light. To minimise fatigue and standardise the assessment process, a rigorous tasting and rinsing procedure was established. Panellists were asked to smell and taste the flavouring oil gravy sample in the mouth for 4-5 s, spit, and then fill out the scorecard. Panellists were then asked to rinse their mouth with water, eat a piece of bread or Melba toast, rinse again with water, and wait 1 min before proceeding to the next sample.

Validation of the Predicted Shelf Life

To verify the predicted shelf life calculated using the Arrhenius equation, 50 bags each of ESS and ESB were prepared. The bags containing flavouring oil gravies were stored outside and protected from sunlight exposure to imitate the actual storage environment. It is worth mentioning that the 'room temperature' in this experiment refers to a changing external environment temperature rather than a constant temperature of 25°C. The gravies were consecutively stored for eight months. The average temperatures in Shanghai from March to December 2017 were 11°C, 18°C, 23°C, 25°C, 32°C, 31°C, 26°C, 22°C, 14°C and 8°C. The quality and safety indices of the samples were monitored every month.

RESULTS AND DISCUSSION

Colour Difference between Flavouring Gravies during Storage

The colour of edible oil is one of the most critical indicators that can be used to monitor oil quality both visually and physically (Kim *et al.*, 2015). As shown in *Table 1*, colour differences were presented using C* and ΔE, which represented brightness of colour and colour differences, respectively. The results indicated that the brightest colour in flavouring oil gravy was exhibited by ESS, while the darkest was exhibited by ESB. This result was consistent with our previous research, which might result from the thick broad-bean sauce added in the formulation of ESB (Wu *et al.*, 2018). It is worth mentioning that the brightness in ESB and ESS gradually decreased with increasing storage temperature. The reduction in brightness may be attributed to the degradation of pigments (Alvarruiz *et al.*, 2020). In contrast, a significant

decrease was witnessed between the brightness in CSB at storage temperatures of 4°C and 25°C, while no obvious change was seen between those at 25°C, 37°C and 45°C. The results indicated that oil gravies need to be kept in cold storage. Moreover, abundant carotenoids in ESB and ESS may prevent the degradation of other pigments, which leads to milder changes in brightness.

These results indicated that solid substances might disperse in the flavouring oil gravies, which resulted in a decrease in brightness. Increasing the storage temperature could also accelerate the process. However, no significant difference was found in the ΔE for all three samples.

Changes in Oxidation Indices in Flavouring Oil Gravies during Storage

The oxidation of edible oils is one of the most important quality criteria in the food industry since hydroperoxides will be formed during both processing and storage and further decrease the nutritional quality of edible oils (Huyan *et al.*, 2019). Changes in AV and POV in flavouring oil gravies during consecutive 63-day storage are shown in *Table 2*. It is predictable that both AV and POV increased with storage time and storage temperature. At the end of storage, the AVs and POVs in all gravy samples were below the Chinese regulatory limit of edible oils.

For AV, the initial values were 1.25 mg/g for ESB, 1.53 mg/g for ESS and 1.20 mg/g for CSB. The AVs for ESS were higher than those of the other two gravies during the whole storage period, which might result from the vinegar added in the ingredient panel of ESS. The other two gravies, ESB and CSB, witnessed a similar increasing trend during storage. The growth rates of ESB and ESS were 17.00% and 19.00% at 4°C and 166.7% and 152.9% at 45°C, respectively. In comparison, the growth rate of CSB was slightly higher, *i.e.*, 20% at 4°C and 170.8% at 45°C. Vegetable oils rich in unsaturated fatty acids are generally regarded as more vulnerable to oil oxidation than animal oils with abundant saturated fatty acids. Our study indicates that the high content of carotenoids in palm oil not only gives a red colour similar to animal oil but also compensates for shortcomings of the tendency to oxidise.

In addition to the gravy type, the storage temperature also had a great impact on AVs and POVs during storage. Taking AV as an example, it took 63 days for the AV in the three gravy samples to reach an AV value of 1.42-1.72 mg/g at a storage temperature of 4°C. In comparison, it took 28 days to reach a value of 1.42-1.78 mg/g at 25°C, 14 days to reach 1.48-1.64 mg/g at 37°C, and only seven days to reach 1.48-1.65 mg/g at 45°C. It is widely reported that temperature storage has a great

TABLE 1. COLOUR DIFFERENCES IN THE THREE FLAVOURING OIL GRAVIES DURING STORAGE AT FOUR DIFFERENT TEMPERATURES

Colour differences

Formula	4°C			25°C			37°C			45°C		
	C*1	C*2	ΔE	C*1	C*2	ΔE	C*1	C*2	ΔE	C*1	C*2	ΔE
ESB	29.09 ± 1.22[a]	22.26 ± 3.56[a]	8.74 ± 1.25[a]	28.36 ± 3.25[a]	17.27 ± 2.31[a]	13.71 ± 0.88[a]	28.36 ± 2.56[a]	13.60 ± 3.33[a]	16.97 ± 2.25[a]	28.36 ± 5.12[a]	8.53 ± 1.20[a]	21.02 ± 5.12[a]
ESS	56.53 ± 5.50[c]	41.18 ± 6.33[c]	17.93 ± 0.58[c]	47.00 ± 6.25[b]	32.81 ± 2.56[c]	15.42 ± 1.23[a]	47.00 ± 3.56[c]	29.68 ± 5.22[c]	21.81 ± 5.22[c]	47.00 ± 1.58[b]	29.89 ± 3.02[b]	21.60 ± 6.35[a]
CSB	45.20 ± 3.56[b]	30.85 ± 4.25[b]	29.09 ± 2.22[c]	45.87 ± 8.25[b]	20.61 ± 3.15[b]	32.40 ± 5.25[b]	45.20 ± 5.58[b]	19.76 ± 3.33[b]	34.58 ± 7.12[b]	45.20 ± 4.44[b]	23.58 ± 3.55[b]	32.74 ± 3.45[b]

Note: CSB - commercial strewed beef flavouring oil gravy; ESB - experimental strewed beef flavouring oil gravy; ESS - experimental sour soup flavouring oil gravy. C*1 - brightness or vividness of colour in flavouring oil gravy at 0 day; C*2 - brightness or vividness of colour in flavouring oil gravy at 63 days. ΔE - colour differences of flavouring oil gravy at 0 day and 63 days. Different lowercase letters within a column represent significant differences ($p<0.05$).

TABLE 2. AV AND POV CHANGES IN THE THREE FLAVOURING OIL GRAVIES DURING STORAGE AT FOUR DIFFERENT TEMPERATURES

Oxidation indices

Storage time (day)	4°C			25°C			37°C			45°C		
	ESB	ESS	CSB	ESB	ESS	CSB	ESB	ESS	CSB	ESB	ESS	CSB
AV (mg/g)												
0	1.25 ± 0.06[a]	1.53 ± 0.06[a]	1.20 ± 0.08[a]	1.25 ± 0.12[a]	1.53 ± 0.08[a]	1.20 ± 0.03[a]	1.25 ± 0.10[a]	1.53 ± 0.05[a]	1.20 ± 0.11[a]	1.25 ± 0.10[a]	1.53 ± 0.10[a]	1.20 ± 0.06[a]
7	1.28 ± 0.04[a]	1.55 ± 0.12[a]	1.22 ± 0.10[a]	1.26 ± 0.02[a]	1.58 ± 0.10[a]	1.25 ± 0.04[ab]	1.33 ± 0.11[ab]	1.60 ± 0.08[a]	1.30 ± 0.05[ab]	1.48 ± 0.05[b]	1.65 ± 0.08[ab]	1.38 ± 0.04[b]
14	1.30 ± 0.03[a]	1.65 ± 0.08[ab]	1.23 ± 0.11[a]	1.28 ± 0.10[a]	1.59 ± 0.10[a]	1.28 ± 0.04[ab]	1.48 ± 0.03[b]	1.64 ± 0.10[a]	1.38 ± 0.08[b]	1.56 ± 0.06[b]	1.84 ± 0.02[b]	1.45 ± 0.05[b]
21	1.32 ± 0.10[a]	1.58 ± 0.07[a]	1.28 ± 0.12[ab]	1.38 ± 0.07[b]	1.65 ± 0.06[ab]	1.30 ± 0.05[ab]	1.60 ± 0.05[b]	1.83 ± 0.04[b]	1.48 ± 0.04[b]	1.87 ± 0.05[c]	2.12 ± 0.11[c]	1.79 ± 0.06[c]
28	1.32 ± 0.05[a]	1.63 ± 0.05[ab]	1.25 ± 0.03[a]	1.42 ± 0.03[b]	1.78 ± 0.07[b]	1.39 ± 0.07[b]	1.87 ± 0.08[c]	1.84 ± 0.08[b]	1.65 ± 0.03[c]	2.12 ± 0.10[d]	2.35 ± 0.05[d]	2.12 ± 0.10[d]
35	1.40 ± 0.08[ab]	1.60 ± 0.11[a]	1.35 ± 0.05[b]	1.63 ± 0.05[c]	1.86 ± 0.05[b]	1.56 ± 0.04[c]	2.06 ± 0.12[d]	2.05 ± 0.04[c]	1.80 ± 0.10[cd]	2.54 ± 0.04[e]	2.87 ± 0.03[e]	2.53 ± 0.07[e]
49	1.45 ± 0.11[b]	1.70 ± 0.12[b]	1.40 ± 0.12[b]	1.77 ± 0.04[c]	1.89 ± 0.06[b]	1.75 ± 0.10[d]	2.18 ± 0.05[e]	2.40 ± 0.06[d]	2.36 ± 0.08[d]	3.06 ± 0.08[f]	3.23 ± 0.04[f]	2.78 ± 0.12[f]
63	1.42 ± 0.05[b]	1.72 ± 0.05[b]	1.44 ± 0.05[b]	1.97 ± 0.06[d]	2.06 ± 0.10[c]	1.92 ± 0.12[e]	2.33 ± 0.15[e]	2.82 ± 0.12[e]	2.60 ± 0.14[e]	3.33 ± 0.12[g]	3.87 ± 0.06[g]	3.25 ± 0.03[g]
POV (10⁻²g/100 g)												
0	1.98 ± 0.06[a]	2.26 ± 0.12[a]	1.84 ± 0.03[a]	1.98 ± 0.03[a]	2.26 ± 0.05[a]	1.84 ± 0.03[a]	1.98 ± 0.05[a]	2.26 ± 0.10[a]	1.84 ± 0.02[a]	1.98 ± 0.03[a]	2.26 ± 0.12[a]	1.84 ± 0.12[a]
7	2.01 ± 0.03[a]	2.31 ± 0.05[ab]	1.89 ± 0.07[a]	2.06 ± 0.05[a]	2.26 ± 0.07[a]	1.90 ± 0.11[ab]	2.03 ± 0.03[a]	2.56 ± 0.11[b]	1.98 ± 0.03[b]	2.35 ± 0.05[b]	2.42 ± 0.10[b]	2.26 ± 0.03[b]
14	2.18 ± 0.05[b]	2.41 ± 0.07[b]	1.93 ± 0.08[ab]	2.28 ± 0.07[b]	2.35 ± 0.15[ab]	2.09 ± 0.12[b]	2.37 ± 0.12[b]	2.51 ± 0.12[b]	2.26 ± 0.05[b]	2.90 ± 0.10[c]	2.94 ± 0.13[c]	2.40 ± 0.05[c]
21	2.22 ± 0.02[b]	2.66 ± 0.03[c]	2.06 ± 0.10[b]	2.50 ± 0.10[c]	2.40 ± 0.13[b]	2.07 ± 0.05[ab]	2.56 ± 0.10[c]	2.93 ± 0.05[c]	2.51 ± 0.10[d]	3.30 ± 0.05[d]	3.96 ± 0.05[d]	3.64 ± 0.08[e]
28	2.49 ± 0.05[c]	2.56 ± 0.15[bc]	2.42 ± 0.05[c]	2.47 ± 0.05[c]	2.54 ± 0.05[bc]	2.37 ± 0.03[c]	2.69 ± 0.11[d]	3.25 ± 0.08[d]	2.56 ± 0.11[d]	3.62 ± 0.10[e]	4.54 ± 0.04[e]	3.38 ± 0.07[d]
35	2.44 ± 0.10[c]	2.86 ± 0.12[d]	2.42 ± 0.12[c]	2.69 ± 0.09[d]	2.98 ± 0.07[c]	2.69 ± 0.05[d]	3.27 ± 0.06[e]	3.90 ± 0.07[e]	3.12 ± 0.12[e]	4.19 ± 0.06[f]	4.94 ± 0.05[f]	3.96 ± 0.05[f]
49	2.75 ± 0.08[d]	3.07 ± 0.05[e]	2.59 ± 0.08[cd]	2.98 ± 0.07[e]	3.38 ± 0.08[d]	2.83 ± 0.07[e]	3.67 ± 0.05[f]	4.39 ± 0.06[f]	3.40 ± 0.08[f]	5.27 ± 0.07[g]	5.79 ± 0.06[g]	5.23 ± 0.04[g]
63	2.89 ± 0.11[d]	3.32 ± 0.10[f]	2.91 ± 0.12[f]	3.38 ± 0.12[f]	3.67 ± 0.04[e]	3.17 ± 0.08[f]	4.20 ± 0.11[h]	5.31 ± 0.04[g]	3.81 ± 0.05[g]	6.68 ± 0.12[h]	7.04 ± 0.11[h]	6.21 ± 0.03[h]

Note: CSB - commercial strewed beef flavouring oil gravy; ESB - experimental strewed beef flavouring oil gravy; ESS - experimental sour soup flavouring oil gravy. Results are given mean ± standard deviation (n=3). Different lowercase letters within a column represent significant differences ($p<0.05$).

impact on the quality of edible oil, and high storage temperatures promote the rancidity of edible oil (Guiotto *et al.*, 2014; Zhao *et al.*, 2021). Similar effects were observed in the POV. These results remind us to prevent gravies from high-temperature storage, especially in summer.

Calculation of the Kinetic Model and Prediction of Shelf Life

AV and POV values are commonly used as indicators of oil quality. As discussed above, AV and POV changed significantly during consecutive storage. Therefore, to investigate the dynamic change of flavouring oil, we chose AV and POV to fit with the first-order kinetic equation. The results showed that all fitting coefficients were higher than 0.98, which indicated that the fitting model was reasonable and precise (*Table 3*).

The reaction constant k_n increased with storage temperature. The effects were more obvious at storage temperatures higher than 25°C. The reaction constant calculated using AV at 25°C was close to that at 4°C. In comparison, k_n doubled with an increasing storage temperature of 12°C (37°C) and increased by three times at 45°C. A similar phenomenon was observed when we used the POV fitting model. Although room temperature of 25°C is commonly considered a storage temperature in daily life, the storage temperature may reach 40°C in practical use. The results of this study indicated that storage temperatures under 25°C could prevent oil-rich foods from rancidity to a great extent, while these foods need to be cooled in summer. Moreover, the variation in k_n of the CSB samples was slightly higher than that of the other two gravy samples, which was consistent with the AV and POV results.

The Arrhenius formula indicates that there is a linear relation between lnk and 1/T. Therefore, the equation of lnk and 1/T can be calculated according to the first-order reaction rates of four storage temperatures. The shelf life of these flavouring oil gravies at three different temperatures was further calculated. The first-order reaction rate constant at 25°C can be calculated with the substitution of T = 298.15 K. *Table 4* shows the parameters of the first-order reaction kinetics equation and the predicted shelf life for each sample at three commonly used storage temperatures: 20°C, 25°C and 30°C. The predicted shelf life lasted for six to eight months, and the results were consistent with the oxidation indices. In comparison, the labelled shelf life of CSB was 180 days, which is close to our estimation. The shelf life of ESS was slightly shorter than that of the other two gravies. In addition, the shelf life is shortened by 30 days for every 5°C rise in temperature.

TALBE 3. KINETIC MODEL PARAMETERS ACCORDING TO TWO OXIDATION INDICES IN THE THREE FLAVOURING OIL GRAVIES DURING STORAGE AT FOUR DIFFERENT TEMPERATURES

Formula	Kinetic model parameters											
	4°C			25°C			37°C			45°C		
	N_0	k_n (×10⁻²)	R^2	N_0	k_n (×10⁻²)	R^2	N_0	k_n (×10⁻²)	R^2	N_0	k_n (×10⁻²)	R^2
AV (mg/g)												
ESB	1.49	0.41	0.99	1.50	0.45	0.99	1.50	0.88	0.99	1.54	1.23	0.97
ESS	1.57	0.39	0.97	1.56	0.42	0.99	1.51	0.85	0.99	1.56	1.29	0.99
CSB	1.46	0.43	0.99	1.46	0.46	0.99	1.45	0.94	0.99	1.43	1.52	0.99
POV (g/100 g)												
ESB	1.74	0.40	0.99	1.69	0.91	0.99	1.76	1.31	0.99	1.74	1.76	0.99
ESS	1.65	0.47	0.99	1.70	0.95	0.99	1.76	1.44	0.98	1.77	1.69	0.98
CSB	1.71	0.44	0.99	1.74	0.94	0.99	1.79	1.41	0.98	1.80	1.56	0.99

Note: ESB - experimental strewed beef flavouring oil gravy; ESS - experimental sour soup flavouring oil gravy; CSB - commercial strewed beef flavouring oil gravy.

TABLE 4. THE SHELF LIFE OF THE THREE GRAVIES ACCORDING TO POV AT THREE TEMPERATURES

Formula	Kinetic model parameters						
	E (kJ)	k_0	N_0	N/N_0	Temperature	$1/k_n$	t (day)
ESB	25.30	246.02	1.71	5.85	20°C / 293.15 K	131.15	236
					25°C / 298.15 K	110.20	194
					30°C / 303.15 K	93.12	164
ESS	23.33	117.68	1.67	5.99	20°C / 293.15 K	122.18	218
					25°C / 298.15 K	104.06	186
					30°C / 303.15 K	89.10	159
CSB	23.82	136.30	1.73	5.78	20°C / 293.15 K	129.04	226
					25°C / 298.15 K	109.53	192
					30°C / 303.15 K	93.47	164

Note: CSB - commercial strewed beef flavouring oil gravy; ESB - experimental strewed beef flavouring oil gravy; ESS - experimental sour soup flavouring oil gravy.

Verification of the Prediction of Shelf Life

To verify the predicted shelf life calculated using the Arrhenius equation, both ESB and ESS were consecutively stored at practical room temperature. Sensory evaluation was conducted during the whole storage process. As shown in *Figure 1*, the scores of both ESB and ESS were 47.17 and 47.67 at the beginning, respectively. The scores of colour, texture, odour were all 10 at the beginning, while the score of flavour and durance of fragrance still need improvement. The results of sensory evaluation indicated that both gravies had a bright tawny colour and moderate viscosity. In addition, ESB and ESS were abundant in soy sauce fragrance in both odour and flavour. The odour and flavour scores gradually decreased in the first four months and witnessed a dramatic decrease during the fourth to eighth months. The odour and flavour of soy sauce fragrance gradually disappeared, while the viscosity gradually increased. On the one hand, a decrease in scores might result from the loss of origin flavour and the unpleasant flavour produced by the rancidity and deterioration of oil during long-term storage (Shen *et al.*, 2018). Changes in the sensory profile may be indicators for the chemical oxidation index during storage. The formation of secondary metabolites may be the cause of unpleasant odours and flavours (Serfert *et al.*, 2010). On the other hand, the fourth to eighth months during storage referred to July to October. High storage temperature further accelerated the deterioration process, which explained the sharp decrease in score.

AV and POV were also determined during storage, as shown in *Figure 2*. The results were consistent with the sensory evaluation scores. The AV of both ESB and ESS increased from approximately 2.00 to 9.20 mg/g, while the POV increased from 0.025 to 0.180 g/100 g. AV and POV accelerated at the fifth month, and the growth rate still increased even with decreasing storage temperature. This reminded us that oil deterioration is an irreversible process and would accelerate until the end point.
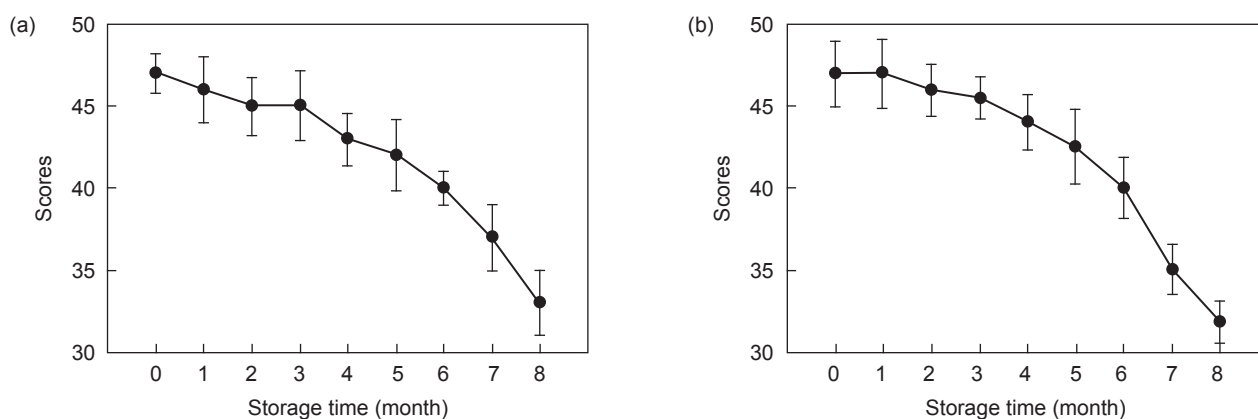

Figure 1. Changes of sensory evaluation scores in flavouring oil gravy during storage at room temperature. (a) Experimental strewed beef flavouring oil gravy; (b) experimental sour soup beef flavouring oil gravy.
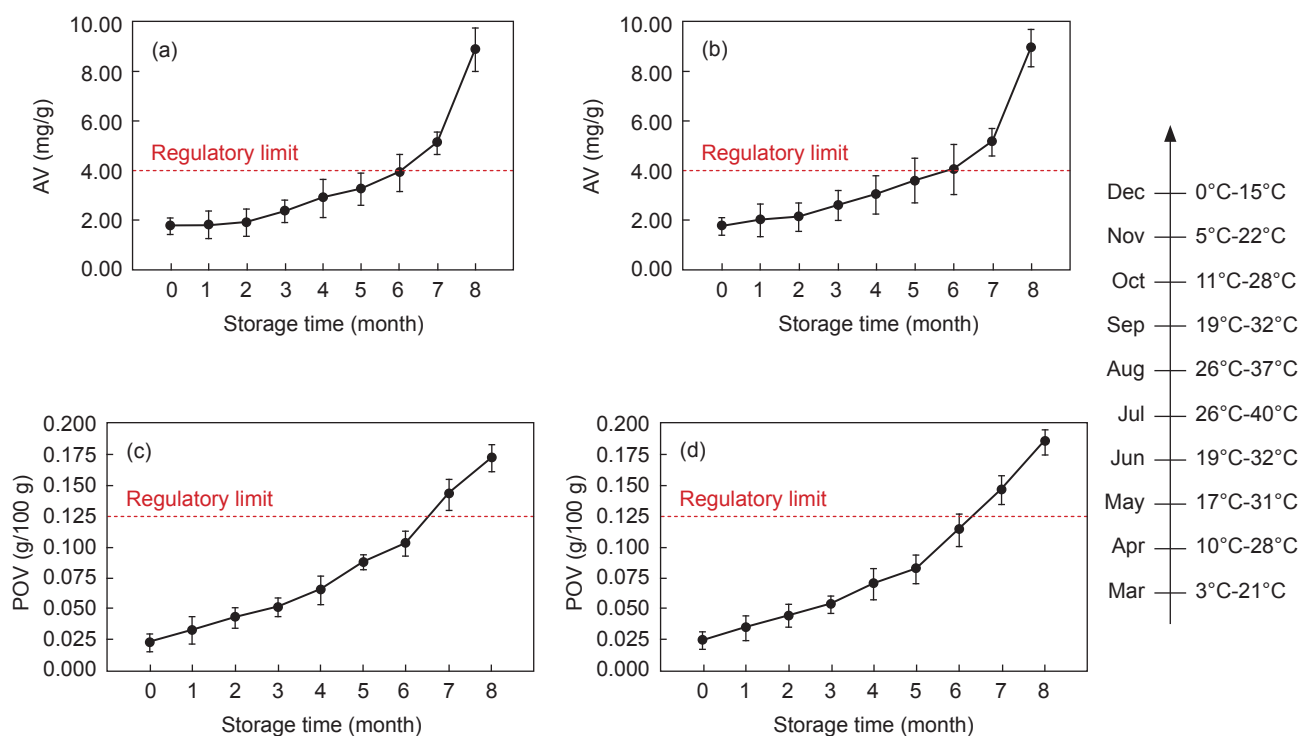
Figure 2. Changes of AV and POV in flavouring oil gravy during storage at room temperature (a) changes of AV in experimental strewed beef flavouring oil gravy, (b) changes of AV in experimental sour soup beef flavouring oil gravy, (c) changes of POV in experimental strewed beef flavouring oil gravy, and (d) changes of POV in experimental sour soup beef flavouring oil gravy.

CONCLUSION

The results of this study indicated that colour differences between pilot gravies before and after storage were less significant than those of commercial gravy, which might be favoured by consumers. In addition, the shelf life of pilot gravies was slightly longer than that of commercial gravy. The predicted shelf life was shortened by 30 days for every 5°C rise between 20°C and 30°C. The results of imitated storage indicated that AV and POV exceeded the regulatory limit after six months of consecutive storage and were close to the prediction model values. Therefore, we recommended that flavouring oil gravy made of RPO should be stored at room temperature and should be consumed within six months. Furthermore, the shelf-life model presented in this study provides a direction for selecting the storage temperature, which will be useful for shelf-life management combined with the target market.

ACKNOWLEDGEMENT

REFERENCES

Alvarruiz, A; Pardo, J E; Copete, M E; de Miguel, C; Rabadan, A; Lopez, E and Alvarez-Orti, M (2020). Evolution of virgin olive oil during long-term storage. *J. OLEO Sci., 69(8):* 809-814.

Antonis, K (2019). Alterations of PET material physical properties during storage of olive oil. *Food Packag. Shelf Life*, 21: 100336.

Burri, B J (2012). Evaluating global barriers to the use of red palm oil as an intervention food to prevent vitamin A deficiency. *Compr. Rev. Food. Sci. Food Saf.*, 11(2): 221-232.

Calligaris, S; Manzocco, L; Anese, M and Nicoli, M C (2016). Shelf-life assessment of food undergoing oxidation - A review. *Crit. Rev. Food Sci. Nutr.*, 56(11): 1903-1912.

Catanzaro, R; Zerbinati, N; Solimene, U; Marcellino, M; Mohania, D; Italia, A; Ayala, A and Marotta, F (2016). Beneficial effect of refined red palm oil on lipid peroxidation and monocyte tissue factor in HCV-related liver disease: A randomised controlled study. *Hepatobiliary Pancreat. Dis. Int.*, 15(2): 165-172.

Chinese Standard (2016a). GB 5009.227 Food safety national standards - determination of peroxide value in food samples. Standards Press, China.

Chinese Standard (2016b). GB 5009.229 Food safety national standards - determination of acid value in food samples. Standards Press, China.

David, K; Shirley, A T; Arnis, K; Scott, W and Susanne, K C (2000). Cholesterol vehicle in experimental atherosclerosis. 22. Refined, bleached, deodorized (RBD) palm oil, randomised palm oil and red palm oil. *Nutr. Res., 20(6):* 887-892.

Guiotto, E N; Ixtaina, V Y; Nolasco, S M and Tomas, M C (2014). Effect of storage conditions and antioxidants on the oxidative stability of sunflower-chia oil blends. *J. Am. Oil Chem. Soc., 91(5):* 767-776.

Gulia, N; Dhaka, V and Khatka, B (2014). Instant noodles: Processing, quality and nutritional aspects. *Crit. Rev. Food Sci. Nutr., 54:* 1386-1399.

Huyan, Z Y; Ding, S X; Mao, X H; Wu, C E and Yu, X Z (2019). Effects of packaging materials on oxidative product formation in vegetable oils: Hydroperoxides and volatiles. *Food Packag. Shelf Life, 21:* 100328.

Huh, I S; Kim, H; Jo, H K; Lim, C S; Kim, J S; Kim, S J; Kwon, O; Oh, B and Chang, N (2017). Instant noodle consumption is associated with cardiometabolic risk factors among college students in Seoul. *Nutr. Res. Pract., 11:* 232-239.

Katengua-Thamahane, E; Marnewick, J L; Ajuwon, O R; Chegou, N N; Szucs, G; Ferdinandy, P; Csont, T; Csonka, C and Van Rooyen, J (2014). The combination of red palm oil and rooibos show anti-inflammatory effects in rats. *J. Inflamm. (Lond), 11:* 41-52.

Kim, J; Shin, E C; Lim, H J; Yoon, M; Yang, H; Park, J; Park, E; Yoo, H; Baek, J and Cho, S (2015). Thermal oxidative stability of various vegetable oils used for the preparation of the seasoned laver *Pyropia* spp. *Fish. Aquatic Sci., 18(1):* 21-26.

Kwak, H S; Ahn, B H; Kim, H R and Lee, S Y (2015). Identification of sensory attributes that drive the likeability of Korean rice wines by American panelists. *J. Food Sci., 80(6):* S161-S170.

Manzini, R; Accorsi, R; Piana, F and Regattieri, A (2017). Accelerated life testing for packaging decisions in the edible oils distribution. *Food Packag. Shelf Life, 12:* 114-127.

Mizrahi, S (2000). Accelerated shelf-life tests. *The Stability and Shelf-life of Food* (Kilcast, D and Subramaniam, P eds.). Elsevier Science, Boca Raton. p. 107-125.

Ng, M H; Choo, Y M; Ma, A N; Chuah, C H and Hashim, M A (2004). Separation of vitamin E (tocopherol, tocotrienol, and tocomonoenol) in palm oil. *Lipids, 39(10):* 1031-1035.

Oguntibeju, O O; Esterhuyse, A J and Truter, E J (2009). Red palm oil: Nutritional, physiological and therapeutic roles in improving human wellbeing and quality of life. *Brit. J. Biomed. Sci., 66(4):* 216-222.

Serfert, Y; Drusch, S and Schwarz, K (2010). Sensory odour profiling and lipid oxidation status of fish oil and microencapsulated fish oil. *Food Chem., 123(4):* 968975.

Shen, L; Chen, X; Lee, D S; Zhu, X T; Chen, M and Yam, K L (2018). Effects of diffusion controlled release of tocopherol on lipid oxidation. *Food Packag. Shelf Life, 17:* 129-133.

Wang, D D and Hu, F B (2017). Dietary fat and risk of cardiovascular disease: Recent controversies and advances. *Annu. Rev. Nutr., 37:* 423-446.

Wergeland, A; Bester, D J; Sishi, B J N; Engelbrecht, A M; Jonassen, A K and Van Rooyen, J (2011). Dietary red palm oil protects the heart against the cytotoxic effects of anthracycline. *Cell Biochem. Funct., 29(5):* 356-364.

Wu, X J; Wu, S M; Ji, M and Yoong, J H (2018). Influence of red palm oil on the physicochemical and sensory qualities of flavouring oil gravy for instant noodles. *RSC Adv., 8:* 1148-1158.

Yi, J Y; Anderson, M L and Skibsted, L H (2011). Interactions between tocopherols, tocotrienols and carotenoids during autoxidation of mixed palm olein and fish oil. *Food Chem., 127(4):* 1792-1797.

Zhao, P; Zhang, X; Jin, Y and Xu, L Y (2021). Long-term stability of blends of sesame oil or soybean oil with tuna oil under daily use conditions. *J. Am. Oil Chem. Soc., 98(9):* 933-941.

MOLECULAR IDENTIFICATION AND PHYLOGENETIC ANALYSIS OF FUNGI AND BACTERIA ASSOCIATED TO COMMON SPEAR ROT DISEASE IN MALAYSIA

NUR DIYANA ROSLAN[1]; INTAN NUR AINNI MOHAMED AZNI[1] and SHAMALA SUNDRAM[1]*

ABSTRACT

Common spear rot (CSR) also known as crown disease (CD), is a disease known to affect young immature oil palm (Elaeis guineensis *Jacq.) in the field. However, there is limited information on CSR disease incidences reported in Malaysia. Hence, this study was aimed to identify possible pathogens causing CSR disease on oil palm in Malaysia. Palm showing severe lesions and rotting of unopened spear leaves was identified, and the internal tissues from healthy and infected bole sections were sampled. Five fungal and 12 bacterial isolates were recovered from the infected tissues, while three fungal and two bacterial isolates were isolated from healthy tissue. Macroscopic identification of these cultures was conducted by observing the bacterial and fungal isolates grown in nutrient agar (NA) and potato dextrose agar (PDA), respectively. Molecular identification was carried out using internal transcribed spacer (ITS), translation elongation factor (TEF 1-α) and 16S primers through polymerase chain reaction (PCR). The identity of each isolate was determined using the BLASTN program through non-redundant database nucleotide collection. The sequence analysis showed most of the fungal isolates isolated were identical to* Fusarium *genus with 96.35% to 100.00% similarity when compared to sequences deposited in the GenBank. The species* Fusarium solani *was one of the most frequently recovered fungal isolates from the infected tissues. Meanwhile, one* Erwinia *sp., nine* Klebsiella *sp., three* Dickeya *sp. and one* Enterococcus *sp. were identified from the bacterial collection. Phylogenetic analysis revealed that all isolates of* F. solani *from the diseased palm clustered together with* F. solani *belonging to other hosts, validating the identity of the isolates. Apart from that,* Klebsiella *sp. was also isolated and could also be responsible for causing CSR but requires further validation through Koch's postulate assessment. Nevertheless, this is the first study reporting the isolation of* Klebsiella *sp. in diseased CSR oil palm.*

INTRODUCTION

Common spear rot (CSR) also known as crown disease (CD) is commonly found affecting oil palm during the juvenile years especially in the first two years after field transplanting. It has been reported that CSR/CD occurs in all regions where oil palms are grown (Corley and Tinker, 2008; Duff, 1963; Turner, 1981). The disease was first reported in North Sumatera in the 1920s (Turner, 1981). There have been occasional reports of isolated cases of CSR on oil palm in Malaysia, where incidences rarely exceeded 1%. However, the disease has attracted considerable amount of attention in Malaysia due to the lack of information on potential pathogen identified as the causal agent.

[1] Malaysian Palm Oil Board,
6 Persiaran Institusi, Bandar Baru Bangi,
43000 Kajang, Selangor, Malaysia.

* Corresponding author e-mail: shamala@mpob.gov.my

The term CSR was used by Chinchilla-López (2008) to describe the disease with or without the typical characteristics of rachis bending and rotting that does not progress towards meristem. During the development of the disease, the young leaves become shorter and distorted, followed by rachis bending characteristics manifested due to the reduction in lignification process in the parenchyma's tissues and this appears especially when the disease was under favourable condition (Hartley, 1988) and the emergence of rotting and drying in some sections of the spears. Another symptom describing CSR is that the tissues at the tips of the youngest leaves appear rotting or known as wither tip (Turner, 1981). Extensive rotting may affect the meristem which leads to the death of the palm, otherwise it is possible to recover provided the rotting tissue does not progress towards meristem. Additionally, the incidences of CSR do not manifest immediately but occurs between 12 to 18 months after transplanting from the nursery in a dry season followed by rainy period after replanting (Suwandi *et al.*, 2012).

Several isolates were recovered from diseased leaf tissues of oil palms in Indonesia such as *Fusarium incarnatum*, *Fusarium sacchari* and *Ceratocystis paradoxa* (Suwandi *et al.*, 2012). Pathogenicity test revealed that *C. paradoxa* caused the rotting symptoms and upon inoculation on the leaves, the lesion enlarged rapidly. The lesion also turned from brownish to blackish which is a typical symptom of CSR in the field (Suwandi *et al.*, 2012). Considering the fact that *C. paradoxa* is a common fungus recovered from various diseases of oil palm, its association with the CSR lesion is still not well established. Another study reported that high dosages of nitrogen and poor drainage condition also promoted the oil palm's susceptibility and led to CSR (Alvarado-Vega *et al.*, 1996). This was also demonstrated in the study by Suwandi *et al.* (2012) whereby seedlings were subjected to drainage for nine days before inoculation, followed by no watering for six days before being flooded with freshly prepared fertiliser solution which resulted in the increased seedlings' susceptibility to CSR infection. Other predisposing factors that were also identified were the soil conditions including soil compaction and water saturation, imbalance of nutrients in particular nitrogen, which may contribute to the incidences of spear rot and rachis bending characteristics (Alvarado-Vega *et al.*, 1996; Breure and Soebagjo, 1991; Chinchilla-López *et al.*, 1997; Turner, 1981). However, due to the scarcity of the studies conducted, there is inadequate findings to conclude these observations. Moreover, there is also lack of studies conducted on CSR affected palms in Malaysia to verify the results reported in the previous studies. Therefore, this study was initiated with the primary objective to investigate on the possible pathogens that could be associated for the occurrence of CSR in the younger palms in Malaysia.

MATERIALS AND METHODS

Sampling of Diseased Tissue

An infected 3 year-old palm with rotting observed at the tips of younger leaves (*Figure 1*) was removed at the basal area in order to examine the degree of infection. For sampling purpose, the bole and roots of the palm were removed. Selected roots were detached while the bole was cross sectioned horizontally into smaller sections and brought into the laboratory for further analysis.
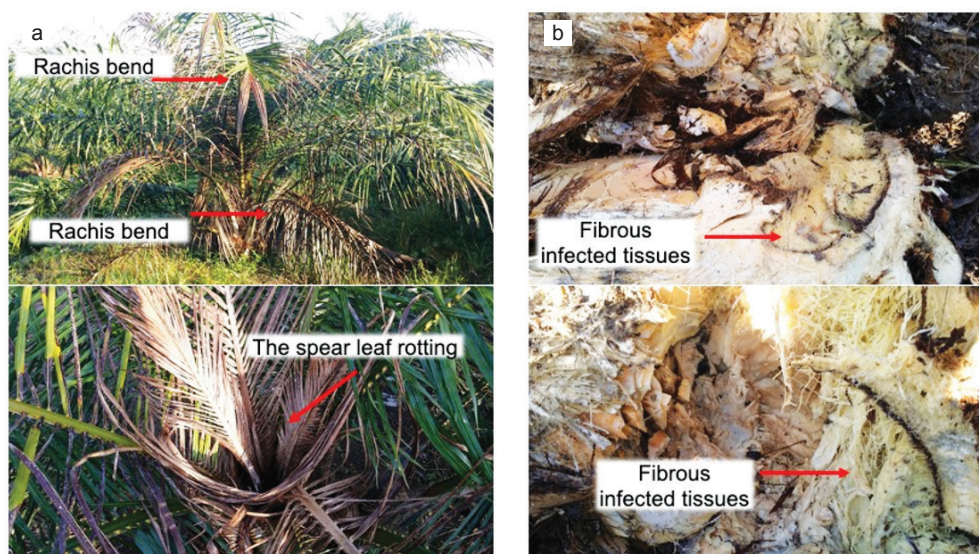

Figure 1. Symptoms of common spear rot (CSR) of oil palm. a) Emergence of spear rot on 3 year-oil palm, b) cross-section of oil palm basal area, revealing the fibrous infected tissues at the inner part.

Isolation of Fungal and Bacterial Strains

Isolation from infected bole. Large portion of infected oil palm bole was carefully removed and cut into smaller pieces for ease of handling during the isolation process. The bole pieces were then cut into even smaller pieces aseptically in a biosafety cabinet. The marginal area of actively developing lesions from diseased tissue were excised and plated onto quarter strength potato dextrose agar (¼ PDA) (Difco™, USA) for the isolation of fungal strains. Healthy/uninfected regions were identified on the infected bole were also carefully excised and plated onto the same media. Plates were incubated for three to five days at 28°C to allow for fungal growth. Isolated colonies were purified and maintained on ¼ PDA. Pure cultures of these colonies were maintained on ¼ PDA slants as well as in sterile distilled water in universal bottles and stored in incubator at 28°C. Meanwhile, nutrient agar (NA) (Oxoid, United Kingdom) was used for the isolation of bacterial colonies. The NA plates were incubated for two to three days at 37°C. The emerging bacterial colonies were purified and maintained on NA plates. The obtained pure strains were stored in sterile distilled water and stored at 4°C.

Molecular Identification of Pure Cultures

The deoxyribonucleic acid (DNA) of fungal and bacterial cultures were extracted using microLYSIS-Plus (Microzone, United Kingdom) according to manufacturer's instructions. Samples were amplified by polymerase chain reaction (PCR) using TW81: 5'-GTTTCCGTAGGTGAACCTGC-3' and AB28: 5'-ATATGCTTAAGTTCAGCGGGT-3' primer pairs to amplify ITS1 and ITS2 regions for fungal strains (Howlett *et al.*, 1992) and using TEF1 5'-ATGGGTAAGGA(A/G)GACAAGAC-3' and TEF2 5'-GGA(G/A)GTACCAGT(G/C)ATCATGTT-3' to amplify the TEF 1-α gene region (O'Donnell *et al.*, 1998) and 16S-F: 5'-GAGTTTGATCCTGGCTCAG-3' and 16S-R: 5'-CGGCTACCTTGTTACGACTT-3' for bacterial strains. The PCR reaction mixture containing 1 × Taq DNA polymerase buffer (Invitrogen, Brazil), 0.50 mm dNTPs (Biolab, USA), 1.25 mm of magnesium chloride (MgCl$_2$) (Invitrogen, Brazil), 0.50 mm of each primer, 2 μL of DNA template, 1 U/μL of recombinant Taq DNA polymerase (Invitrogen, Brazil) and sterile distilled water was added to make up a final volume of 50 μL. PCR was performed in a Vapoprotect™ Mastercycler Pro S (Eppendorf, Germany) with initial denaturation condition at 95°C for 5 min; 35 cycles of denaturation at 95°C for 30 s, annealing at 52°C for 30 s and extension at 72°C for 60 s; and a final extension at 72°C for 10 min. The PCR products were run on 1.5% gel electrophoresis at 80 V for 30 min. The amplified region was excised, extracted using QIAquick® Gel Extraction Kit (QIAGEN) and sent for sequencing.

Phylogenetic Analysis

The raw sequence was cleaned using Applied Biosystem Sequence Scanner Software by viewing the base quality value (QV) score of >20. ITS sequences of each individual isolate were compared to those in non-redundant protein database in GenBank using BLASTN program available at the NCBI website (http://www.ncbi.nlm.nih.gov) with cut-off E-value ≤1e⁻⁵. The sequence data of internal transcribed spacer (ITS), translation elongation factor 1-α (TEF 1-α) and 16S were aligned separately with other sequence data retrieved from GenBank database to determine the genetic relationship between the nucleotides as listed in *Tables 1-3*, respectively. Phylogenetic tree was constructed using MEGA 6.06 (Tamura *et al.*, 2013) and Neighbour-Joining statistical method with 1000 bootstrap replications via estimation of pairwise distances.

RESULTS AND DISCUSSION

Isolation of Fungi and Bacteria

Five fungal isolates were recovered from infected tissues (*Table 4*). The identity of the representative isolates using ITS were *F. solani* and *Fusarium* sp. *Fusarium solani* (three isolates) was most frequently isolated, whereas the *Fusarium* sp. was only isolated once. Additionally, *Fusarium* sp. (two isolates) and *Fusarium verticillioides* were found in the healthy tissue. The *Fusarium* spp. were further identified using TEF-1α (*Table 4*). Among the non-*Fusarium* species, *Cryptococcus* sp. was also retrieved from infected tissues. Meanwhile, 12 bacterial isolates were recovered from infected tissues including *Klebsiella pneumoniae* (two isolates); *Klebsiella variicola* (three isolates); *Klebsiella* sp. (three isolates); *Dickeya zeae* (two isolates); *Erwinia chrysanthemi* and *Enterococcus gallinarum* were isolated once (*Table 5*). The culture plates of the isolates recovered from healthy tissues are shown in *Figure 2* while the plates of isolates from infected tissues are shown in *Figure 3*. The morphology of each culture plate was described in the respective figures.

DNA Sequencing and Phylogenetic Analysis

A PCR based method is a popular method in microbial study to understand the evolutionary relationship of isolated cultures. This approach uses DNA sequences referred to as primers which bind at specific DNA sequences and amplify the

**TABLE 1. LIST OF INTERNAL TRANSCRIBED SPACER (ITS) SEQUENCES DATA
OF FUNGAL SPECIES RETRIEVED FROM GENBANK**

No.	GenBank accession	Species name	Strain ID	Size of rRNA ITS region (bp)	Origin	Host plant/source
1.	MK174969.1	*Fusarium verticillioides*	171779	540	Mexico	-
2.	KY495190.1	*F. verticillioides*	CGARSF	1 149	Nigeria	Rhizosphere soil
3.	MG561965.1	*Fusarium* sp.	Endophytic fungi	526	China	*Bupleurum chinense* DC.
4.	EF680757.1	*Fusarium* sp.	TN2-86032	549	India	*Saccharum officinarum* (sugarcane)
5.	GU595038.1	*F. solani*	H4470	566	China	*Rhizophoraceae* sp. (mangrove)
6.	HQ248197.1	*F. solani*	PCO.30	567	Colombia	*Elaeis guineensis* (oil palm)
7.	KF679356.1	*F. solani*	1HBF 2353	573	India	*Aquilaria agallocha* (agarwood)
8.	EU871517.1	*Cryptococcus magnus*	S22814	651	India	*Filobasidium magnum*
9.	JQ425367.1	*C. magnus*	AUMC7772	623	Egypt	*F. magnum*
10.	MH401206.1	*Phytophtora infestant*	13-A2	883	United Kingdom	*Solanum tuberosum*
11.	FJ801316.1	*P. palmivora*	WPC10213A717	786	United State	-
12.	KF939052.1	*Cerotocystis paradoxa*	BX3	497	China	*Butia capitata*

**TABLE 2. LIST OF TRANSLATION ELONGATION FACTOR 1-α (TEF 1-α) SEQUENCES DATA
OF FUNGAL SPECIES RETRIEVED FROM GENBANK**

No.	GenBank accession	Species name	Strain ID	Size of rRNA ITS region (bp)	Origin	Host plant/source
1.	MT119148.1	*Fusarium solani*	FSCS8	789	India	-
2.	HM770727.1	*F. solani*	SB 21	701	Indonesia	Leaflet, oil palm
3.	MN193859.1	*F. brevicatenulatum*	NRRL 25447	1 768	Guyana	*Xyris* spp.
4.	JF270183.1	*F. incarnatum*	Spt 017	702	USA	Sorghum
5.	JF270304.1	*F. incarnatum*	Spt 142	697	USA	Sorghum
6.	HM569630.2	*Thielaviopsis paradoxa*	C1481	1 492	USA	Oak

TABLE 3. LIST OF 16S SEQUENCES OF BACTERIAL SPECIES RETRIEVED FROM GENBANK

No.	GenBank accession	Species name	Strain ID	Size of rRNA ITS region (bp)	Origin	Host plant/source
1.	GU811708.1	*Erwinia crysanthemi*	PY-3	1 491	China	Banana
2.	GU362079.1	*E. crysanthemi*	PD2098	1 499	India	Aloe vera
3.	KJ8337551	*E. crysanthemi*	BM01	1 454	China	Banana
4.	JQ398851.1	*Klebsiella* sp.	VITC1	1 444	India	Cinnamon fed rat
5.	MK905714.1	*Klebsiella* sp.	RIB-SCM15	1 387	Nepal	Banana
6.	MN725742.1	*K. variicola*	SA002	1 411	Colombia	*Aedes aegypti* (L.)
7.	MN725749.1	*K. variicola*	SA006	1 415	Colombia	*Aedes aegypti* (L.)
8.	KJ438947.1	*Dickeye. zeae*	Dz-7	1 414	Mexico	Maize
9.	KJ438946.1	*D. zeae*	Dz-7	1 414	Mexico	Maize
10.	MH9030397.1	*Klebsiella pneumonia*	TZT-18-63	1 441	China	Banana
11.	MN749602.1	*K. pneumonia*	GMH480	1 071	Iraq	Water sample
12.	MK902672.1	*K. pneumonia*	SK1	1 406	India	-
13.	MT573855.1	*Enterococcus gallinarum*	1 465	1 385	China	-
14.	MT158593	*E. gallinarum*	G116	1 411	China	-

583

TABLE 4. FUNGAL ISOLATES RECOVERED FROM INFECTED AND HEALTHY TISSUES OF THE PALM

Isolates ID	Annotation using ITS primer	Percent identity (%)	GenBank accession no.	Annotation using TEF 1-α primer	Percent identity (%)	GenBank accession no.
Fungal Isolates						
SPEAR ROT: INFECTED TISSUES (ACTIVELY GROWING LESIONS)						
SR1fi	*Fusarium solani* (KU377470.1)	100.00	MW 314726	*F. solani* (KX497028.1)	99.86	Submitted and awaiting assignment of accession number
SR2fi	*F. solani* (KU377470.1)	100.00	MW 314727	*F. solani* (KX497028.1)	100.00	saa
SR3fi	*Cryptococcus* sp. (HQ426594.1)	100.00	MW 314728	*F. solani* (MT119148.1)	100.00	saa
SR7fi	*F. solani* (KU377470.1)	100.00	MW 314730	*F. solani* (MT119148.1)	99.73	saa
SR8fi	*Fusarium* sp. (MT636465.1)	99.56	MW 314731	*F. brevicatenulatum* (MT011005.1)	96.35	saa
SPEAR ROT: HEALTHY TISSUES						
SR1fh	*Fusarium* sp. (MT636465.1)	100.00	MW 314732	Not amplified	-	saa
SR3fh	*Fusarium* sp. (MT636465.1)	100.00	MW 314733	*F. incarnatum* (JF 270296.1)	99.19	saa
SR4fh	*F. verticillioides* (MT035918.1)	99.40	MW 314734	Not amplified	-	saa

Note: saa - same as above.

TABLE 5. BACTERIAL ISOLATES RECOVERED FROM INFECTED AND HEALTHY TISSUES OF THE PALM

Isolates ID	Accession no.	Annotation	Percent identity (%)	GenBank accession no.
Bacterial Isolates				
SPEAR ROT: INFECTED TISSUES (ACTIVELY GROWING LESIONS)				
SR1bi	GU811708.1	*Erwinia chrysanthemi*	97.58	MW334951
SR2bi	KJ42495.1	*Klebsiella pneumoniae*	100.00	MW334952
SR3bi	MN082124.1	*K. variicola*	100.00	MW334953
SR4bi	KR399998.1	*Klebsiella* sp.	100.00	MW334954
SR5bi	CP025799.1	*Dickeya zeae*	100.00	MW334955
SR6bi	MN082124.1	*K. variicola*	100.00	MW334956
SR7bi	KR399998.1	*Klebsiella* sp.	100.00	MW334957
SR8bi	MT597704.1	*Enterococcus gallinarum*	100.00	MW334958
SR9bi	MN082124.1	*K. variicola*	100.00	MW334959
SR10bi	CP025799.1	*D. zeae*	99.88	MW334960
SR11bi	MH930397.1	*K. pneumoniae*	99.82	MW3349561
SR12bi	KR399998.1	*Klebsiella* sp.	100.00	MW3349562
SPEAR ROT: HEALTHY AREA				
SR1bh	KR399998.1	*Klebsiella* sp.	100.00	MW334963
SR2bh	CP025799.1	*D. zeae*	100.00	MW334964

targeted sequences (Mitchell and Zuccaro, 2006). The primers used are conserved molecular markers such as 18S ribosomal RNA (rRNA), 28S rRNA, ITS region (Innis *et al.*, 2012) and the TEF-1α gene, which encodes an essential part of the protein translation machinery. ITS region is one of the most commonly used markers in the phylogenetic study of most fungi, however, many *Fusarium* possess non-orthologous copies of the ITS, which can lead to incorrect phylogenetic inferences (O'Donnell
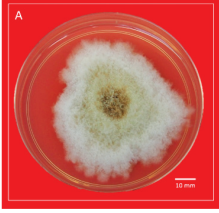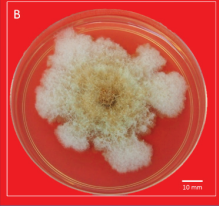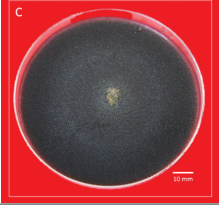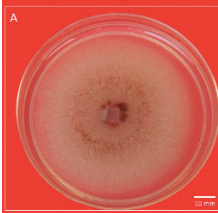
Isolates ID	Identity based on TEF 1-α	Cultures plates	Mycelium characteristics
SR1fh	unknown		Creamy with fluffy and cottony growth of mycelia. The mycelia appeared light yellowish at the centre
SR3fh	*Fusarium incarnatum*		Uneven creamy with fluffy and cottony growth of mycelia. The mycelia appeared yellowish at the centre
SR4fh	unknown		Blackish with flat and dense growth of mycelia

*Figure 2. Morphology of isolates recovered from healthy tissues. a) SR1fh (unknown), b) SR3fh (*Fusarium incarnatum*), and c) SR4fh (unknown).*

Isolates ID	Identity based on TEF 1-α	Cultures plates	Mycelium characteristics
SR1fi	*Fusarium solani*		Creamy off white with flat and fine growth of mycelia
SR2fi	*F. solani*		Creamy grey with flat but dense growth of mycelia. Mature mycelia will be observed with yellowish dense mycelia and sporulation
SR3fi	*F. solani*		Creamy, cottony with dense growth of mycelia
SR7fi	*F. solani*		Creamy, cottony with dense growth of mycelia
SR8fi	*F. brevicatenulatum*		Creamy, clumpy and thin layer growth of mycelia

*Figure 3. Morphology of fungal isolates recovered from infected tissues. a) SR1fi (*Fusarium solani*), b) SR2fi (*F. solani*), c) SR3fi (*F. solani*), d) SR7fi (*F. solani*), and e) SR8fi (*F. brevicatenulatum*).*

et al., 1997). Therefore, the TEF-1α gene was also used in this study, whereby it has high phylogenetic utility due to its highly informative at the species level in *Fusarium*. TEF-1α is a non-orthologous copy of the gene that have not been detected in the genus and it is a universal primer designed to detect the genus (O'Donnell *et al.*, 1998). Similar to 16S rRNA, the region is a portion of the 30S small subunit of a prokaryotic ribosomal that binds to the Shine-Dalgarno sequence and is used in the reconstruction of phylogenetic trees due to the slow evolution of this gene region (Schuster *et al.*, 2002).

A single band approximately 600-700 bp was amplified using ITS primer while ~716 bp was amplified using TEF-1α primer. The similarity search of BLASTN against NCBI database is shown in *Table 4*. From the BLASTN annotation, the retrieved sequences matched to that of *Cryptococcus* sp. upon using ITS primer SR3fi but matched *F. solani* when TEF-1α primer sequencing results were used. This is because identification solely based on ITS can lead to misleading identification as two non-orthologous sequences can be isolated from a single isolate. Meanwhile, isolates SR8fi and SR3fh that annotated as *Fusarium* sp. upon using ITS primer was later shared similarity with *F. brevicatenulatum* and *F. incarnatum* respectively which proved the latter primers are highly informative at species level in *Fusarium*. *Fusarium* spp. has been identified before in previous studies

as endophytes in oil palm (Rusli *et al.*, 2016) and their presence in the infected tissues is either as secondary opportunistic pathogen due to the compromised status of the affected CSR palms. Isolates SR1fh and SR3fh were not amplified when using TEF-1α primer and this could be due to the non-specific primer and may require other species - specific primers for further validation.

All the sequences were submitted to GenBank with accession number MW 314726-MW 314734 for ITS while TEF sequences were submitted and awaiting accession number assignment. The phylogenetic trees were constructed with 1000 bootstrap and Neighbour-Joining method was found to group both *C. magnum* and *Phytophtora*
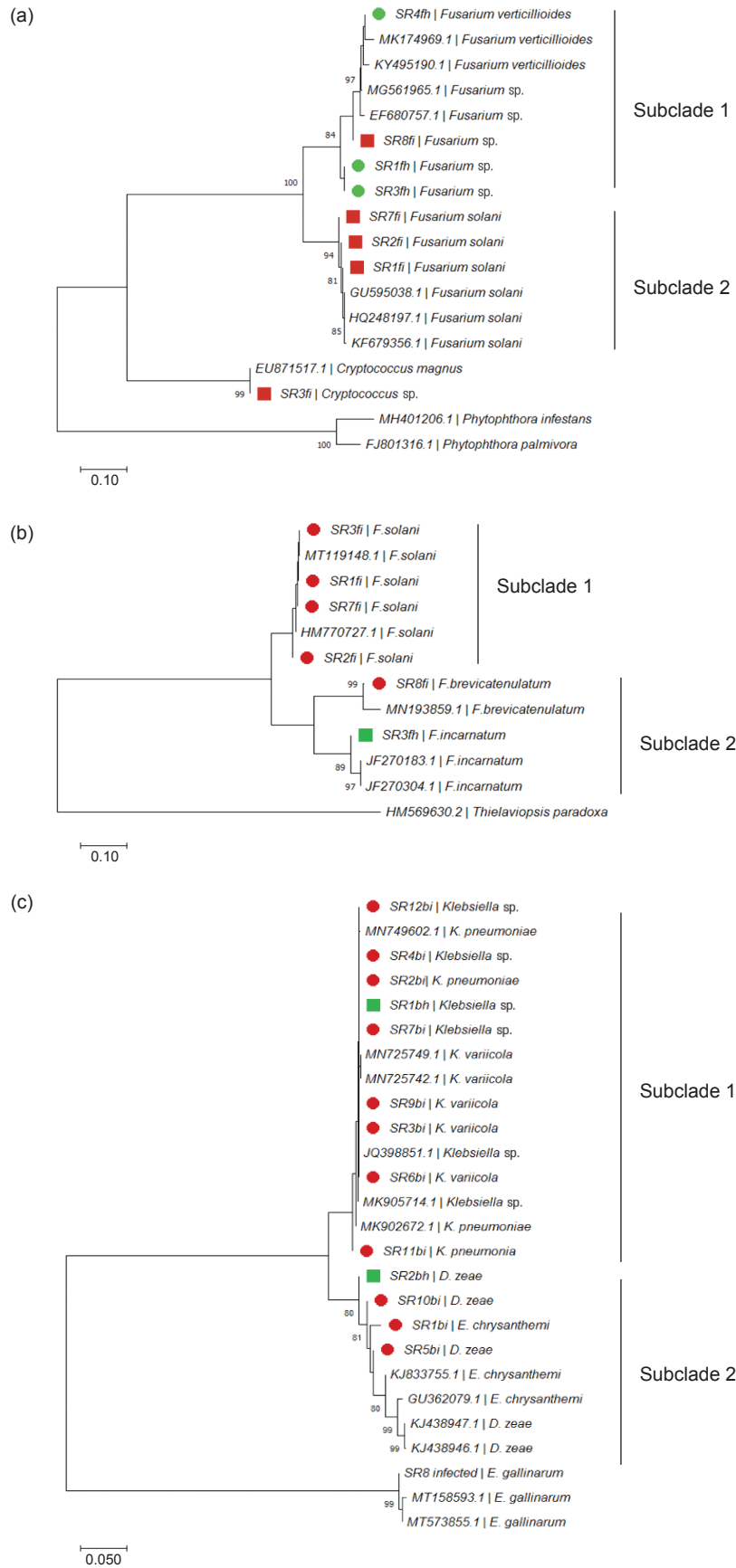
Figure 4. The evolutionary relationship of fungal isolates recovered from common spear rot (CSR) tissues were conducted in MEGA X. The phylogenetic tree was inferred using the Neighbour-Joining method from (a) ITS region, (b) TEF-1α region, and (c) 16S region obtained from NCBI, respectively. The percentage of replicate trees in which the associated taxa clustered together in the bootstrap test (1000 replicates) are shown next to the branches. The evolutionary distances were computed using the Maximum Composite Likelihood method. The green circle ● represent isolates from healthy tissue and the red square ■ represent isolates from infected tissues.

species as an outgroup clade respectively from the *Fusarium* species with ITS (*Figure 4a*) while *Thielaviopsis paradoxa* was noted as an outgroup clade for TEF (*Figure 4b*). Both phylogenetic trees of *Fusarium* were divided into two subclades supported by 100% bootstrap showing that most of the fungal isolates isolated from infected tissues falling under the *F. solani* subclades suggesting that the particular species may also be the causal agent for CSR. *Fusarium solani* causes crown and root rot on several crops such as strawberry (Pastrana *et al.*, 2014), soybean (Abood *et al.*, 2020) and potato (Falert and Akarapisan, 2019) which also appropriately elucidates the presence of the species in the infected tissues in this study. This finding is also in agreement with Turner (1981) whereby *F. solani* was reported as the predominant species isolated from CSR infected tissues. Previous studies have reported that inoculation of *Fusarium* sp. on oil palm leaves has been proven to cause wither tips symptoms of CSR affected palms (Turner and Bull, 1967).

As for bacterial isolates, approximately 1500 bp PCR product was amplified using 16S primer pairs and the sequences was submitted to GenBank with accession number of MW334951-MW334964 (*Table 5*). Phylogenetic tree showed that most of the strains recovered from infected tissue were grouped in the subclade of *Klebsiella* species (*Figure 4c*). Meanwhile, three isolates fall into the group of *Erwinia* species. *Klebsiella pneumoniae* is one of the isolates identified from infected tissues and known as an endophyte bacterium that can promote plant growth or control plant disease (Iniguez *et al.*, 2004) but it has been reported to also cause disease in maize (Huang *et al.*, 2016). The *K. pneumoniae* strain Borkar was reported to affect the root systems of *Solanaceous* plants, pomegranate or known as root bark necrosis disease. The bacterium inhibits the plant respiration mechanism creating anaerobic condition to the roots and leads to the emission of organic compounds, alcohol which results in a foul smell in the root and wilting in plants (Ajayasree and Borkar, 2018). Besides this, *K. variicola* was also reported to cause soft rot in banana (Fan *et al.*, 2016) and carrot (Chandrashekar *et al.*, 2018).

Interestingly, the remaining three isolates (SR1bi, SR5bi and SR10bi) recovered from infected tissues were segregated from the first subclade as they clustered forming a second cluster or subclade together with *Dickeya* species. Most of the *Dickeya* species has been reported to cause serious soft rot diseases in crops, fruits and ornamental plants. As a group, *Dickeya* species are considered as one of the most important bacterial phytopathogens (Mansfield *et al.*, 2012). Most species of *Dickeya* have a wide host range and infection can be initiated in dicotyledon and monocotyledon (Hussain *et al.*, 2008). Infections

of Dickeya can be characterised as invasion at the center of the rhizome, which results in maceration, rotting and vascular discoloration (Perombelon and Kelman, 1980). One of the *Dickeya* species in the cluster is *D. dadantii* or previously known as *E. chrysanthemi* can cause soft rot diseases on many crops. These bacteria have the ability to survive in soils, and the mode of transmission to plants is via water, insects, or cultural technique. The common symptom for *D. dadantii* infection, or identified as pectinolytic soft rot *Erwinia*, is characterised by the disruptions of parenchymatous tissues, caused by pectic enzymes (Hugouvieux-Cotte-Pattat *et al.*, 1996). Nevertheless, soft rot *Erwinia* that colonises plant involves a few cascading mechanism factors such as depolymerisation of cellulase that can cause degradation of plant cell wall components, assimilation of Ferum, an Hrp type III secretion system, exopolysaccharides, motility and plant defence protein (Toth *et al.*, 2003). An interesting finding from the generated phylogenetic study herein shows that apart from *Erwinia* sp. that has been reported as the most frequently isolated bacterial strains from necrotic lesion on leaves and rachises (Monge Pérez *et al.*, 1993), *Klebsiella* sp. may also be another bacterial strain potential in causing the disease. This observation and isolation of *Klebsiella* sp. is the first to be reported for CSR in oil palm.

Most of the bacterial isolates are related to soft rot disease suggesting that the isolates are highly potential in initiating CSR disease in oil palms. However, this warrants for pathogenicity tests using individual bacterial and fungal isolates.

CONCLUSION

A number of fungal and bacterial isolates were successfully isolated from the CSR oil palm infected tissues. All the isolates are expected to be associated with CSR disease as some of the fungal species have been reported earlier to cause disease in other host. This study also reports the first findings of *Klebsiella* sp. as one of the most frequently isolated bacterial strain in this study. Nevertheless, a follow up study is crucial in determining the causal agent of CSR disease in palms by conducting a Koch's postulate investigation using the isolated fungal and bacterial collection.

ACKNOWLEDGEMENT

REFERENCES

Abood, N T; Abdul-Moohsin, R G and Altaie, A H (2020). Isolation and diagnosis of *Fusarium solani* that causes root rot soybean and evaluating the efficiency of bacteria *Bacillus subtilus* and *Azotobacter* spp in controlling the disease. *Eurasia J. BioSci., 14*: 4617-4623.

Ajayasree, T S and Borkar, S G (2018). Pathogenic potentiality of the bacterium of *Klebsiella pneumoniae* strain Borkar on different plants. *J. Appl. Biotechnol. Bioeng., 5*: 233-235.

Alvarado-Vega, A; Chinchilla-López, C M; Bulgarelli-Mora, J M and Sterling-Rodríguez, F (1996). Agronomic factors associated to common spear rot/crown disease in oil palm. *ASD Oil Palm Papers, 15*: 8-28.

Breure, C J and Soebagjo, F X (1991). Factors associated with occurrence of crown disease in oil palm (*Elaeis guineensis* Jacq.) and its effect on growth and yield. *Euphytica, 54*: 55-64.

Chandrashekar, B S; Prasannakumar, M K; Puneeth, M E; Teli, K; Priyanka, K; Mahesh, H B and Desai, R U (2018). First report of bacterial soft rot of carrot caused by *Klebsiella variicola* in India. *New Dis. Rep., 37*: 21-22.

Chincilla-López, C M (2008). The many faces of spear rots in oil palm and the need for an integrated management approach. *ASD Oil Palm Papers, 32*: 1-10.

Chinchilla-López, C M; Salas, A and Castrillo, G (1997). Common spear rot/crown disease in oil palm: Effect on growth and initial yields. . *ASD Oil Palm Papers*. p. 1-17.

Corley, R H V and Tinker, P B H (2008). *The Oil Palm*. 4th edition. John Wiley and Sons. USA.

Duff, A D S (1963). The bud rot little leaf disease of the oil palm. *J. Waifor, 4*: 176-190.

Falert, S and Akarapisan, A (2019). Identification of *Fusarium* spp. causing dry rot of seed potato tubers in Northern Thailand. *Int. J. Agric. Technol., 15*: 567-578.

Fan, H C; Zeng, L; Yang, P W; Guo, Z X and Bai, T T (2016). First report of banana soft rot caused by *Klebsiella variicola* in China. *Plant Dis., 100*: 517-517.

Hartley, C W S (1988). *The Oil Palm*. Harlow, England, Longman.

Howlett, B J; Brownlee, A G; Guest, D I; Adcock, G J and Mcfadden, G I (1992). The 5S ribosomal RNA gene is linked to large and small subunit ribosomal RNA genes in the oomycetes, *Phytophthora vignae, P. cinnamomi, P. megasperma* f. sp. *Glycinea* and *Saprolegnia ferax*. *Curr. Genet., 22*: 455-461.

Huang, M; Lin, L; Wu, Y X; Honhing, H; He, P F; Li, G Z; He, P B; Xiong, G R; Yuan, Y and He, Y Q (2016). Pathogenicity of *Klebsiella pneumonia* (KpC4) infecting maize and mice. *J. Integr. Agric., 15*: 1510-1520.

Hugouvieux-Cotte-Pattat, N; Condemine, G; Nasser, W and Reverchon, S (1996). Regulation of pectinolysis in *Erwinia chrysanthemi*. *Annu. Rev. Microbiol., 50*: 213-257.

Hussain, M B B M; Zhang, H B; Xu, J L; Liu, Q; Jiang, Z and Zhang, L H (2008). The acyl-homoserine lactone-type quorum-sensing system modulates cell motility and virulence of *Erwinia chrysanthemi* pv. zeae. *J. Bacteriol., 190*: 1045-1053.

Iniguez, A L; Dong, Y and Triplett, E W (2004). Nitrogen fixation in wheat provided by *Klebsiella pneumoniae* 342. *Mol. Plant Microbe Interact., 17*: 1078-1085.

Innis, M A; Gelfand, D H; Sninsky, J J and White, T J (2012). *PCR protocols: A Guide to Methods and Applications*. Academic Press, London. 49 pp.

Mansfield, J; Genin, S; Magori, S; Citovsky, V; Sriariyanum, M; Ronald, P; Dow, M; Verdier, V; Beer, S V; Machado, M A; Toth, I; Salmond, G and Foster, G D (2012). Top 10 plant pathogenic bacteria in molecular plant pathology. *Mol. Plant Pathol., 13*: 614-629.

Mitchell, J I and Zuccaro, A (2006). Sequences, the environment and fungi. *Mycologist, 20*: 62-74.

Monge Pérez, J E; Chinchilla López, C M and Wang Wong, A (1993). Studies on the etiology of the crown disease/spear rot syndrome in oil palm. *ASD Oil Palm Papers, 7*: 1-16.

O'donnell, K; Cigelnik, E; Weber, N S and Trappe, J M (1997). Phylogenetic relationships among ascomycetous truffles and the true and false morels inferred from 18S and 28S ribosomal DNA sequence analysis. *Mycologia, 89*: 48-65.

O'donnell, K; Kistler, H C; Cigelnik, E and Ploetz, R C (1998). Multiple evolutionary origins of the fungus causing Panama disease of banana: Concordant evidence from nuclear and mitochondrial gene genealogies. *Proc. Natl. Acad. Sci., 95*: 2044-2049.

Pastrana, A M; Capote, N; De Los Santos, B; Romero, F and Basallote-Ureba, M J (2014). First report of *Fusarium solani* causing crown and root rot on strawberry crops in Southwestern Spain. *Plant Dis., 98*: 161-161.

Perombelon, M C M and Kelman, A (1980). Ecology of the soft rot erwinias. *Annu. Rev. Phytopathol., 18*: 361-387.

Rusli, M H; Idris, A S and Cooper, R M (2016). Evaluation of Malaysian soils for potential suppressiveness of *Fusarium* wilt of oil palm caused by *Fusarium oxysporum* f. sp. *elaeidis. J. Microb. Biochem. Technol., 8*: 459-464.

Schuster, E; Dunn-Coleman, N; Frisvad, J C and Van Dijck, P W (2002). On the safety of *Aspergillus niger* - A review. *Appl. Microbiol. Biotechnol., 59*: 426-435.

Suwandi; Akino, S and Kondo, N (2012). Common spear rot of oil palm in Indonesia. *Plant Dis., 96*: 537-543.

Tamura, K; Stecher, G; Peterson, D; Filipski, A and Kumar, S (2013). MEGA6: Molecular evolutionary genetics analysis version 6.0. *Mol. Biol. Evol., 30*: 2725-2729.

Toth, I K; Bell, K S; Holeva, M C and Birch, P R J (2003). Soft rot erwiniae: From genes to genomes. *Mol. Plant Pathol., 4*: 17-30.

Turner, P D (1981). *Oil Palm Diseases and Disorders*. Oxford University. Press. 280 pp.

Turner, P D and Bull, R A (1967). *Diseases and Disorders of the Oil Palm in Malaysia*. Incorporated Society of Planters. Kuala Lumpur, Malaysia.

JOURNAL OF OIL PALM RESEARCH

GUIDE FOR AUTHORS
(for more details, kindly surf http://jopr.mpob.gov.my)

Type of Articles

1. **Regular Article**
   Full-length original empirical investigations, consisting of introduction, materials and methods, results and discussion, conclusions. Original work must provide references and an explanation on research findings that contain new and significant findings. Conclusion should be brief and focus on the research output, should not be in point form. These papers should not exceed 6000 words of text (including tables, figures and references) and generally not more than a total of 10 figures and tables. After peer-review, the article word count limit can be extended to a maximum of 8000 words to better address the reviewers' and editors' comments. Any additional figures or tables can be included in the supplementary data. Please note that papers submitted to JOPR will be sent back to authors because of poor figure resolution or exceeding the number of figures permitted.

2. **Short Communication**
   Significant new information to readers of the Journal in a short but complete form. Preferably not exceeding 3000 words (including tables, figures and references), and is intended for rapid publication. They are not intended for publishing preliminary results or to be a reduced version of regular article.

3. **Review Article**
   Critical evaluation of materials about current research that have already been published by organising, integrating, and evaluating previously published materials. Re-analyses as meta-analysis and systemic reviews are encouraged. Review articles provide systemic overview, evaluation and interpretation of research in a given field. They should not exceed 12 000 words (excluding references only) and should contain no more than a total of 20 figures and tables. Any additional figures or tables can be included in the supplementary data. Please note that papers submitted to JOPR will be sent back to authors because of poor figure resolution or exceeding the number of figures permitted. The same information should not be repeated in a figure and a table.

Language
Please write your text in good English (only British English is accepted). We do not accept American English or a mixture of these.

JOPR's Template
JOPR's template, which is a standard format that facilitates the manuscript writing and copyediting process. This template is created to provide a detail and clear house style of JOPR. The template is drafted according to JOPR's house style, but in standard word version format. When writing a paper, authors need to format their papers to fit into the journal's house style. To make this easier, Word templates are available for many of other established journals, ready for them to download and apply to their research paper format. It is crucial for author to write a research paper while considering formatting. Each journal has its own guidelines for formatting; hence, the template defines how an article will look when it is published online or in print.

JOPR's Aims & Scope
This is established to provide a detail and clear aims and scope for author reference. Authors should declare in the cover letter how the research fits the aims and scope of JOPR.

JOPR's House Style
A detail listing of JOPR's house style for authors and a checklist to facilitate the copyediting process and standardise the copyediting process. The JOPR's house style remains the same and is drafted into a detail version for author's reference.

Manuscript Submission
- Manuscripts should be submitted via: https://mc04.manuscriptcentral.com/jopres
- JOPR does not permit dual submission, publication and/or any archive platform (preprint) in violation of journal ethical practices.

For more details and to download the JOPR's House Style and Template, kindly surf http://jopr.mpob.gov.my

Contents of the Coming Issue
Journal of Oil Palm Research
Vol. 34 (4) December 2022[*]

Note: * Subject to change.